

AD-781 338

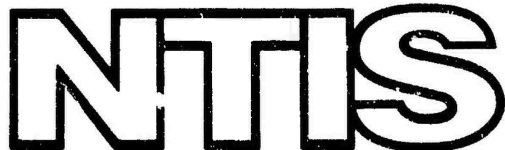
THE NONLINEAR DYNAMICS OF PLATES
AND SHELLS

A. S. Volmir

Foreign Technology Division
Wright-Patterson Air Force Base, Ohio

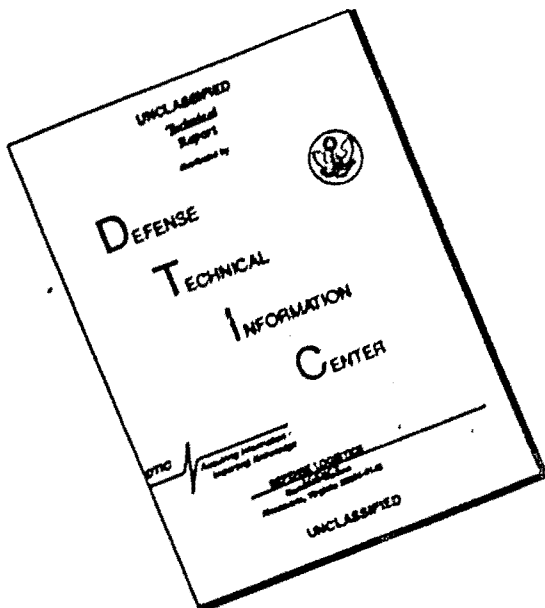
16 April 1974

DISTRIBUTED BY:



National Technical Information Service
U. S. DEPARTMENT OF COMMERCE
5285 Port Royal Road, Springfield Va. 22151

DISCLAIMER NOTICE



**THIS DOCUMENT IS BEST
QUALITY AVAILABLE. THE COPY
FURNISHED TO DTIC CONTAINED
A SIGNIFICANT NUMBER OF
PAGES WHICH DO NOT
REPRODUCE LEGIBLY.**

FTD-HC-23-851-74

EDITED TRANSLATION

FTD-HC-23-851-74

16 April 1974

THE NONLINEAR DYNAMICS OF PLATES AND SHELLS

By: A. S. Vol'mir

English pages: 540

Source: Nelineynaya Dinamika Plastinok i Obolochek,
1972, pp. 1-432

Country of Origin: USSR

Translated under: F33657-72-D-0355

Requester: FTD/PDTI

Approved for public release;
distribution unlimited.

THIS TRANSLATION IS A RENDITION OF THE ORIGINAL FOREIGN TEXT WITHOUT ANY ANALYTICAL OR EDITORIAL COMMENT. STATEMENTS OR THEORIES ADVOCATED OR IMPLIED ARE THOSE OF THE SOURCE AND DO NOT NECESSARILY REFLECT THE POSITION OR OPINION OF THE FOREIGN TECHNOLOGY DIVISION.

PREPARED BY:

TRANSLATION DIVISION
FOREIGN TECHNOLOGY DIVISION
WP-AFB, OHIO.

FTD-HC-23-851-74

Date 16 Apr 19 74

Preface

This book deals with nonlinear dynamic problems of the theory of plates and shells.

Over the course of the last three decades, the attention of authors concerned with the theory of thin plates and shells has been concentrated mainly on the problems of statics. These studies include the known work on methods of reducing static three-dimensional theory of solid deformable bodies to two-dimensional theory, on the static stability of shells in the small and large, on slowly developing creep of plates and shells, etc. Although these problems must not by any means be considered solved, the theoretical and experimental data accumulated in the literature already permit fairly reliable practical calculations of many actual structures.

At the present time, the emphasis in the study of plate and shell theory is shifting into the realm of dynamics. This is explained primarily by the demands of aviation and space engineering; let us note that these were the areas responsible for the significant progress in shell theory that we are now witnessing. However, the study of the dynamic behavior of structures is also of essential importance for ship building, engineering structures, etc.

Most unsafe for thin-walled shell-type structures is a combination of static loads with various types of dynamic actions. Such combined loads frequently result in snaps (pops) of the shell, which in many cases succeed each other and lead to the formation of fatigue cracks. Failure of the structure may then occur within a very short period.

A description of the process of snapping of a shell can be given only from the points of view of geometrically nonlinear theory. However, exhaustion of the bearing capacity of shells frequently involves accumulation of plastic strains, and therefore it is important to study physically nonlinear systems as well. Thus, nonlinear problems of plate and shell dynamics are of major practical interest.

Until recently, nonlinear dynamics of plates and shells have been given comparatively

little attention in the literature. Presented below are data of theoretical and experimental studies in this field, obtained over the course of the last few years by the authors and his collaborators. In addition, an attempt was made to systematize the existing literature and to present results that can be applied directly in practical calculations.

The book consists of ten chapters.

Chapter I contains the fundamental equations of dynamic theory of large-deflection plates and shells. Let us note that a series of fundamental studies have dealt with general nonlinear shell theory in the last thirty-years. Analysis of these studies is beyond the scope of this book. The first chapter discusses only those mathematical models that are subsequently used in the solution of specific problems.

Chapters II-V examine the various types of vibratory motions of plates and shells. Specific problems pertaining to natural and forced vibrations are apparently presented here for the first time. In some cases, we abandoned the usual model in the form of a system with one degree of freedom, characteristic of the majority of previous studies dealing with nonlinear vibrations of elastic systems. In the section pertaining to self-induced vibrations, principal attention is given to new data on panel flutter.

Chapters VI-IX describe the behavior of thin-walled systems under dynamic loading. It includes an analysis of deformation of plates and shells under rapid and very rapid impact loads of different types.

Finally, Chapter X presents some problems of shell and plate dynamics requiring a statistical approach.

This book follows the author's previous monographs, Flexible Plates and Shells (Moscow, 1956) and Stability of Deformable Systems (Moscow, 1967). The author tried to avoid repetitions as much as possible; many relations are given without derivation, with references to the 1956 and 1967 books. This applies particularly to Chapters VI-

Unclassified

Security Classification

AD 781338

DOCUMENT CONTROL DATA - R & D

(Security classification of title, body of abstract and indexing annotation must be entered when the overall report is classified)

1. ORIGINATING ACTIVITY (Corporate author) Foreign Technology Division Air Force Systems Command U. S. Air Force	2a. REPORT SECURITY CLASSIFICATION Unclassified
	2b. GROUP

3. REPORT TITLE

THE NONLINEAR DYNAMICS OF PLATES AND SHELLS

4. DESCRIPTIVE NOTES (Type of report and inclusive dates)

Translation

5. AUTHOR(S) (First name, middle initial, last name)

A. S. Vol'mir

6. REPORT DATE 1972	7a. TOTAL NO. OF PAGES 543	7b. NO. OF REPS 411
8a. CONTRACT OR GRANT NO.	8b. ORIGINATOR'S REPORT NUMBER(S) FTD-HC-23-851-74	
8c. PROJECT NO		
c.	8d. OTHER REPORT NO(S) (Any other numbers that may be assigned this report)	
d.		
10. DISTRIBUTION STATEMENT Approved for public release; distribution unlimited.		
11. SUPPLEMENTARY NOTES	12. SPONSORING MILITARY ACTIVITY Foreign Technology Division Wright-Patterson AFB, Ohio	

13. ABSTRACT

20

Reproduced by
NATIONAL TECHNICAL
INFORMATION SERVICE
U.S. Department of Commerce
Springfield VA 22151

DD FORM 1 NOV 68 1473

Unclassified
Security Classification

VIII and X, which are closely related to the corresponding sections of the monograph "Stability of Deformable Systems". The bibliography for these chapters pertains to literature published mainly after 1967.

The formulas and illustrations are numbered according to chapter; in references to formulas within the chapters, their numbers were omitted.

The manuscript of the book was carefully reviewed by L.I. Balabukh, who made a number of valuable comments. The large job of editing the manuscript was done by I.G. Kil'dibekov. The author thanks them sincerely, as well as all those who helped him in the preparation of the individual chapters of the book.

A.S. Vol'mir

Let that which floats in vacillating outline
Be secured in firm ideas

Goethe, Faust

Chapter I

General Relationships of Nonlinear Shell Theory

I. Classification of Dynamic Problems of Nonlinear Theory of Plates and Shells

During the last few decades, shell theory, which is a natural continuation and extension of plate theory, has undergone an extensive development. The monographs of V.Z. Vlasov [1.10], A.L. Gol'denveyzer [1.13], N.A. KII'chevskiy [1.15], A.I. Lur'ye [1.18], Kh.M. Mushtari and K.Z. Galimov [1.21], V.V. Novozhilov [1.22], A. Love [1.32], and S.P. Timoshenko [1.38] contain the fundamental relationships of modern shell theory; they also give the solution to many specific examples. However, these books discuss mainly static problems. However, at the present time, problems of dynamic behavior of plates and shells are becoming increasingly important. Among them are studies of periodic or nearly periodic vibrations of thin-walled structures including plates and shells and their unsteady deformation under rapid and impact loading.

The study of shell vibrations was begun by Rayleigh in his Theory of Sound. Recently, studies in this area have been published by N.A. Alumyaev, L.I. Balabukh, V.V. Bolotin, E.I. Grigolyuk, and others. The existing literature usually deals with small vibrations of elastic shells, when the relationships between the deformations and displacements on the one hand and deformations and stresses on the other can be assumed to be linear. Even in this formulation, such problems prove to be very difficult. While small vibrations of plates are associated only with the appearance of flexural stresses proper, in the case of a shell, membrane stresses add on to them. Depending on the contour of the shell and fixing conditions, we obtain a given spectrum of frequencies and vibration forms. For some types of vibrations, flexural stresses, and for others, membrane stresses are predominant. The character of the state of stress may change

markedly along the leading dimensions of the shell during the vibrations as the distance from the edge increases.

A special chapter of vibration theory is the study of nonlinear vibrations, which have important specific properties. Motions of this kind may arise in plates and shells at large displacements, when the deformations and displacements are related by nonlinear relations. On the other hand, deformations may lie beyond the range of applicability of Hooke's law and depend nonlinearly on the stresses.

In this book, we will deal with nonlinear vibrations of plates and shells. This is one of the areas of general nonlinear mechanics of deformable solids or, in a broader framework, of nonlinear mechanics of continuous media.

The second group of problems studied in this book and finding increasingly broader practical applications pertains to the behavior of plates and shells under impulsive actions. While the analysis of periodic vibrations may involve a certain steady motion of the system, in problems of dynamic loading, most of the attention is concentrated on unsteady, transient processes. Such a process usually consists in an abrupt transition, i.e., a jump of the system from steady motion of one type to some other motion. This phenomenon is particularly characteristic of shells and is termed popping or snapping. Popping of a shell is usually accompanied by substantial displacements. For this reason, the study of the behavior of plates and shells under impulsive actions will be sufficiently complete only if it is conducted for large deflections, from the points of view of nonlinear theory. However, in some examples the initial stage of a transient process can also be studied with the aid of linearized relations.

Let us turn to the initial relationships of the dynamics of plates and shells.

2. Some Background Information on Shells

Below we shall study thin shells, i.e., bodies, one of whose measurements (the shell thickness) is much smaller than the other two. As a rule, the shell thickness

will be assumed to be constant. The surface dividing the shell thickness in half is called the middle surface. If the middle surface is a plane, we obtain a thin plate.

Shells may be classified according according to the contour of the middle surface. The simplest examples are cylindrical (Figure 1.1 a) or conical (Figure 1.1 b) shells with a circular cross section. The figures show straight lines running along the length of the shell, i.e., meridians, and circles of the cross sections, i.e., parallels. We draw a normal N to the middle surface, then variously oriented planes containing N

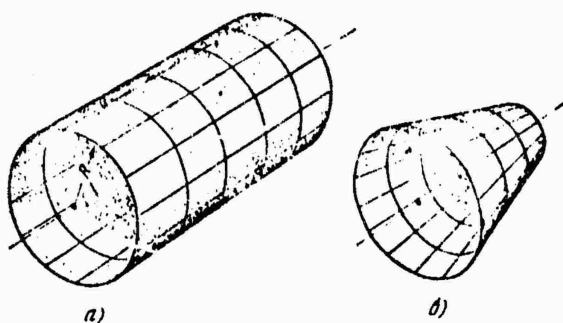


Figure 1.1. Section of closed circuit shell: a) cylindrical, b) conical.

(Figure 1.2). At the intersection of these planes with the surface we obtain curves which are normal sections of the middle surface. To characterize the surface, it is important to determine at each of its points the largest and smallest radii of curvature will be that of the meridians in both cases: the centers of curvature for them will lie at infinity. If however the planes normal to the meridional ones are drawn, the lines thus obtained will have the smallest radius of curvature. The corresponding centers of curvature will be located at the points of intersection of the normal with the axis of symmetry. For a circular cylindrical shell, the smallest radius of curvature is the same as the radius of the cross section.

A third example of a shell of the simplest shape is the spherical shell. Here the radii of curvature of all the normal sections are equal!.

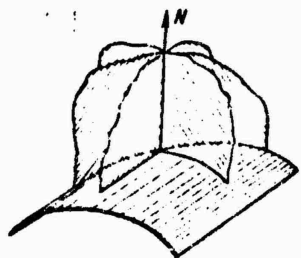


Figure 1.2. Normal sections of middle surface of shell.

The above examples of shells are special cases of shells of revolution. Figure 1.3 shows a section of the middle surface of a shell of revolution of arbitrary shape by a meridional plane. Let us also draw the normal N in this figure; the centers of curvature of the normal section will lie on this normal.

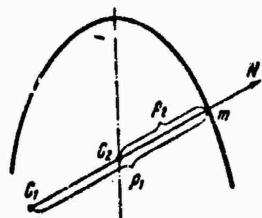


Figure 1.3. Centers of curvature of normal sections of a shell of revolution.

Let the center of curvature of the meridian line be located at point C_1 ; the center of curvature of the section by the plane normal to the meridional plane will be located at point C_2 cf intersection of the normal with the axis of symmetry. We denote the corresponding radii of curvature by p_1 and p_2 . It can be shown that one of them is the largest, and the other, the smallest in comparison with the radii of curvature of all the normal sections passing through a given point m . The directions of these two normal sections with extreme properties define the so-called principal

directions for point m. If we now draw the lines whose tangents will coincide with the principal directions at each point of the middle surface, we obtain the so-called lines of curvature. For a shell of revolution, the lines of curvature will be the meridians and parallels.

In the most general case of a shell of arbitrary configuration, the principal directions and corresponding principal radii of curvature ρ_1 and ρ_2 can be determined at each point of the middle surface in the same manner (Figure 1.4). If the centers of curvature C_1 and C_2 lie on the same side of the middle surface, we will arbitrarily assign the same sign to the radii ρ_1 and ρ_2 , and in the opposite case, different signs.

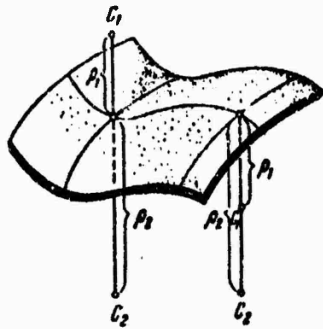


Figure 1.4. Sections of a shell of negative curvature (left) and positive curvature (right).

The product of the principal curvatures $k_1 = 1/\rho_1$ and $k_2 = 1/\rho_2$ for a given point is called the Gaussian curvature of a surface (or, more briefly, surface curvature): $r = k_1 k_2$; the half-sum is called the mean curvature: $k = 1/2(k_1 + k_2)$. A cylindrical shell and a conical shell both have a middle surface of zero curvature. A spherical shell has a positive curvature. If we consider a toroidal shell, however, (Figure 1.5), it will have a positive curvature in one part of the surface (point A), and a negative

curvature in the other (point B).

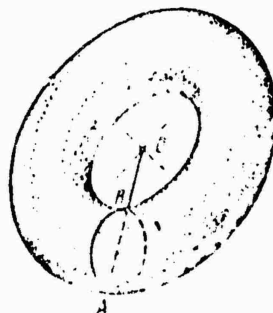


Figure 1.5. A toroidal shell of circular cross section has a positive curvature at point A and a negative one at point B.

Shells and plates have been finding increasingly wide applications in technology in the last few decades. The body of a spaceship is a structure consisting of different types of shells of revolution, i.e., cylindrical, conical, and spherical. The fuselage of an airplane as a whole, i.e., together with the stiffening ribs, may be treated as a cylindrical shell. The wing of an airplane can also be represented as a shell or plate having a different rigidity in different directions. Other shells are jet engine bodies, all-metal railroad car bodies, submarine hulls, etc. Shells are also found in engineering structures in the form of various tanks, pipes, domes, and other coverings of buildings, etc. Along with static stresses, such structures may experience rapidly changing loads. The behavior of structures acted upon by such loads has a number of characteristics. For this reason, the study of the behavior of shells and plates acted upon by dynamic factors is very essential.

3. Description of Shell Models

A series of assumptions must be made in establishing a model representing real shells in theoretical studies.

Let us begin with a characterization of the structure of a shell and its material. Shells of the most varied structure are found in the technical applications mentioned above. They include, for example, two- and three-layer shells; structures consisting of composite materials such as glass-reinforced, graphite-reinforced and boron plastics, and shells stiffened with ribs.

The description of the dynamic behavior of such shells is very complex. As the simplest model, this chapter will consider single-layer shells made of a homogeneous isotropic material. However, such a homogeneous isotropic material may possess different properties.

If we consider the effects of plastic or viscoplastic deformation, we should proceed from nonlinear relationships between the stresses, deformations, and rates of change of these quantities with time. As a rule, however, the material will be assumed to be elastic and to obey Hooke's Law.

It should be kept in mind that the mechanical characteristics of a material at high deformation rates may have values differing markedly from static ones. The modulus of elasticity increases slightly, and the elastic limit, yield point, and ultimate strength may increase by 50% or more.

Hereinafter, we will consider shells of constant thickness h .

A distinctive feature of the general relationships pertaining to thin shells is the reduction of equations of a three-dimensional problem of elasticity theory to equations for two measurements. Moreover, for a single-layer homogeneous shell, it is natural to place the coordinate system at the middle surface of the shell. For example, we can take the middle-surface lines of curvature as the principal coordinate directions.

One of the ways of reducing a three-dimensional problem to a two-dimensional one is to adopt the hypothesis of nondeformable normals (the Kirchhoff-Love hypothesis), whereby any fiber normal to the middle surface before deformation remains straight and

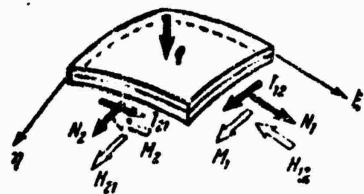


Figure 1.6. Shell element subjected to an external load and internal forces.

normal to the middle surface in its new configuration after deformation; in addition, the length of the fiber remains unchanged along the thickness of the shell. In an additional assumption, the normal stresses in the direction of the normal to the middle

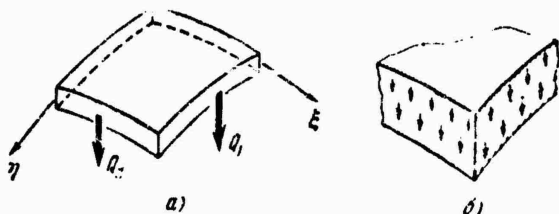


Figure 1.7. Transverse forces in shell section (a) and as resultants of tangential forces (b).

surface may be neglected in comparison with the principal stresses.

By principal stresses in shell theory are meant the normal and tangential stresses in the middle surface itself and in the shell layers parallel to it.

Let us consider a shell element defined by sections along the coordinate lines ξ , η (Figure 1.6) and acte on, generally speaking, by a transverse load of intensity q . The normal forces in each of these sections may be reduced to forces N_1 and N_2 , on the one hand, and bending movements M_1 , M_2 on the other (open arrows in the figure represent the moment vectors). The tangential forces are reduced to the shearing forces T_{12} , T_{21} and twisting moments H_{12} , H_{21} .

Let us now turn to the transverse forces Q_1 , Q_2 shown in Figure 1.7 a. They are the equivalent of the tangential forces acting in the sections ξ , η themselves (Figure 1.7 b) and directed along the normal to the middle surface*. The same type of tangential forces are set up in the cross sections of beams subjected to cross bending.

In static problems, the internal forces acting on a shell element balance an external transverse load as follows. On the one hand, equilibrium is reached thanks to the forces in the middle surface. This is illustrated in Figure 1.8 with the example of a distorted panel: the normal forces N in the sections of the panel produce an equivalent, balancing external load. If in addition, there are no bending or twisting moments in the sections of the shell, the latter may be described as being a zero-moment shell. On the other hand, in a flat plate with small deflections, equilibrium of the element can be obtained only as a result of a difference of the transverse forces Q (Figure 1.9), which in turn are related to the bending and twisting moments. In the general case of a moment shell, there is a combined action of the forces in the middle surface, transverse forces and moments.

In the dynamics problems of interest to us, using d'Alembert's principle, we must introduce the inertial forces into consideration. Let us first determine the inertial forces corresponding to displacements of the shell elements along the normal. Denoting the normal displacements, i.e., deflections, by w , we obtain the inertial force per unit volume, equal to $[-(\gamma/g)(\partial^2 w / \partial t^2)]$, where γ is the density of the material, g is the acceleration due to gravity, and t is the time. We similarly find the inertial forces corresponding to displacements u , v .

Let us now turn to deformations connected with the different types of forces. Forces N cause elongations or contractions along the coordinate lines ξ , η , and forces T cause a shift of the element in the middle surface. The effect of moments M is manifested in a change of the shell curvature, and that of moments H , in a torsion of the element. As for the shearing strains due to the shearing forces and to the corresponding tangential stresses τ , these strains are usually neglected.

*Their reciprocal tangential forces are acting in the layers parallel to the middle surface.

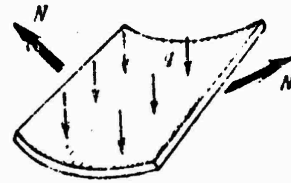


Figure 1.8. In a shell, an external transverse load is partially balanced by forces in the middle surface.

The above scheme of the stressed and strained state of a shell, based on the Kirchhoff-Love hypothesis, may be regarded as a first-approximation model. It has proven convenient in solving many static and dynamic problems; the results thus obtained are in many cases sufficiently accurate for practical applications.

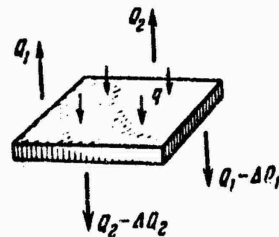


Figure 1.9. In a plate and shell, the external load is partially balanced by transverse forces.

We will now turn to an analysis of the fundamental relationships of dynamic shell theory for such a model.

4. Deformations and Displacements

Let us examine more closely the strained state of a shell of arbitrary contour,

assuming that the deflections of the points of the middle surface may be of the same order as the shell thickness. The x , y , z Cartesian coordinates will be used herein-after. We will stipulate that the x , y coordinate lines coincide with the lines of curvature of the middle surface. Line z will be directed along the normal to the middle surface toward the center of curvature. We will use the right-handed coordinate system below. The displacements of middle-surface points along the x , y , z directions will be denoted by u , v , w .

Our objective will be to express the relationships between the deformations and displacements. The displacements of the middle-layer points along the coordinate lines are functions of x , y coordinates and time t : $u = u(x, y, t)$, $v = v(x, y, t)$, and the same applies to deflections $w = w(x, y, t)$. The displacements of an arbitrary point with coordinate (prior to deformation) z , which will be denoted by $u^z(x, y, z, t)$, etc., will be assumed equal to

$$\left. \begin{aligned} u^z &= u - z \frac{\partial w}{\partial x}; \\ v^z &= v - z \frac{\partial w}{\partial y}; \\ w^z &= w. \end{aligned} \right\} (1.1)$$

The first of these relations is illustrated by Figure 1.10, which shows the section of a shell by the plane tangent to lines x and z . As the shell is deformed, the normal to line x rotates through the same angle $\partial w / \partial x$ as the tangent l to the same line. This is a consequence of the Kirchhoff-Love hypothesis. The signs in expressions (1) correspond to the frame of reference we have chosen.

Let us turn to the determination of deformations in some layer parallel to the middle surface and separated from it by a distance z . The elongation strains in the direction of lines x , y will be denoted by ϵ_x^z , ϵ_y^z , and the shear strain, by γ^z . The quantities ϵ_x^z , ϵ_y^z , γ^z depend on the displacements u^z , v^z , w^z .

We will first determine the strain components ϵ_x^z , ϵ_y^z due to displacements u^z , v^z . Consider an element ABCD of a given shell layer*, defined by sections normal to lines

*We are dealing with the projection of a layer element on the plane tangent to lines x , y at point A.

x, y (Figure 1.11). Point A, whose coordinates will be x, y , undergoes displacements

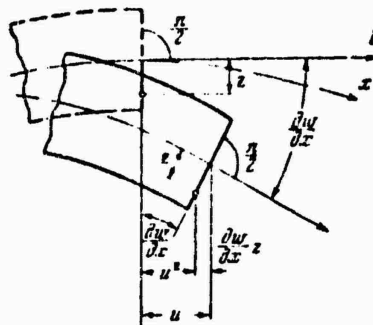


Figure 1.10. Deformation of a shell element according to the Kirchhoff-Love hypothesis.

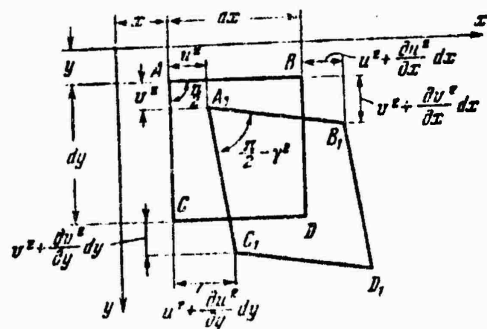


Figure 1.11. Strains in a shell layer parallel to the middle surface.

u^z, v^z ; for point B with coordinates $x + dx, y$, the displacements are $u^z + (\partial u^z / \partial x)dx, v^z + (\partial v^z / \partial x)dx$. For point C with coordinates $x, y + dy$, we obtain the quantities $u^z + (\partial u^z / \partial y)dy, v^z + (\partial v^z / \partial y)dy$.

The new length dx of the element after deformation will be

$$ds_1 = \overline{A_1 B_1} = \left[\left(dx + \frac{\partial u^z}{\partial x} dx \right)^2 + \left(\frac{\partial v^z}{\partial x} dx \right)^2 \right]^{1/2},$$

or

$$ds_1 = dx \left\{ 1 + \left[2 \frac{\partial u^z}{\partial x} + \left(\frac{\partial u^z}{\partial x} \right)^2 + \left(\frac{\partial v^z}{\partial x} \right)^2 \right] \right\}^{1/2}.$$

We will expand this expression in a series; considering the expression in square brackets to be small in comparison with unity, we obtain

$$ds_1 = dx \left\{ 1 + \frac{1}{2} \left[2 \frac{\partial u^x}{\partial x} + \left(\frac{\partial u^x}{\partial x} \right)^2 + \left(\frac{\partial v^x}{\partial x} \right)^2 \right] \right\}.$$

The elongation strain, dependent on u^z , v^z , will be

$$\epsilon_x^z = \frac{\partial u^z}{\partial x} + \frac{1}{2} \left(\frac{\partial u^x}{\partial x} \right)^2 + \frac{1}{2} \left(\frac{\partial v^x}{\partial x} \right)^2. \quad (a)$$

By analogy, the expression for the elongation strain along line y is found to be

$$\epsilon_y^z = \frac{\partial v^z}{\partial y} + \frac{1}{2} \left(\frac{\partial v^y}{\partial x} \right)^2 + \frac{1}{2} \left(\frac{\partial v^x}{\partial y} \right)^2. \quad (b)$$

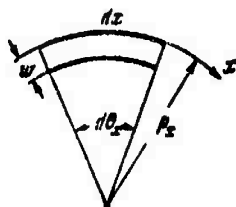


Figure 1.12. Strain components in the middle surface due to radial displacements.

Let us now determine the components of strains ϵ_x^z , ϵ_y^z due to a general displacement toward the center of curvature (or away from it) of the element in the section normal to line y (Figure 1.12). If the length of the element is initially $dx = R_x d\theta_x$,

then after the displacement it will be $(\rho_x - w)d\theta_x$. The corresponding strain of the element turns out to be

$$\epsilon_x^e = \frac{(\rho_x - w)d\theta_x - \rho_x d\theta_x}{\rho_x d\theta_x} = -\frac{w}{\rho_x} = -k_x w. \quad (a')$$

Here we took $w^z = w$. Similarly, for coordinate line y , we obtain

$$\epsilon_y^e = -k_y w. \quad (b')$$

We will subsequently assume k_x and k_y for the portion of the shell under consideration to be constant.

We then find the elongation strains arising from the change in deflection along the coordinate lines. If the deflection at point A along the z direction is equal to w (Figure 1.13), the deflections of points B and C amount to $w + (dw/dx)dx$ and $w + (dw/dy)dy$, respectively. Neglecting the distortion of a small element, we find its new length

$$ds_1 = dx \left[1 + \left(\frac{\partial w}{\partial x} \right)^2 \right]^{1/2} \quad (c)$$

Proceeding as in the derivation of expression (a), we find

$$ds_1 = dx \left[1 + \frac{1}{2} \left(\frac{\partial w}{\partial x} \right)^2 \right].$$

Hence we obtain the strain

$$\epsilon_x^e = \frac{ds_1 - dx}{dx} = \frac{1}{2} \left(\frac{\partial w}{\partial x} \right)^2. \quad (a'')$$

For line y, by analogy we have

$$\epsilon_y^* = \frac{1}{2} \left(\frac{\partial w}{\partial y} \right)^2. \quad (\text{b}''')$$

Let us now determine the shear strain γ^z . The first component of this strain, dependent on the displacements u^z , v^z , will be determined as the difference between the right angle formed by sides dx , dy before deformation and the angle formed by these sides after deformation (Figure 1.11):

$$\gamma^z = \frac{\partial u^z}{\partial y} + \frac{\partial v^z}{\partial x}. \quad (\text{d})$$

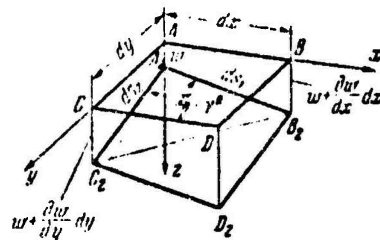


Figure 1.13. Elongation strains in the middle surface, due to large deflections.

The component of shear strain corresponding to deflection w will be found by considering Figure 1.13. The latter shows how a right-angle triangle* with sides dx , dy is distorted by the deformation. Using an expression of type (c), we determine the squares of lengths of the sides after deformation:

$$(ds_1)^2 = (dx)^2 \left[1 + \left(\frac{\partial w}{\partial x} \right)^2 \right], \quad (ds_2)^2 = (dy)^2 \left[1 + \left(\frac{\partial w}{\partial y} \right)^2 \right].$$

*The projection of the layer element is considered here as well. See previous footnote.

The square of the third side $\overline{B_2 C_2}$ will be equal to

$$\begin{aligned} (\overline{B_2 C_2})^2 &= (dx)^2 \left[1 + \left(\frac{\partial w}{\partial x} \right)^2 \right] + (dy)^2 \left[1 + \left(\frac{\partial w}{\partial y} \right)^2 \right] - \\ &\quad - 2 dx dy \cos \left(\frac{\pi}{2} - \gamma^z \right) \left[1 + \left(\frac{\partial w}{\partial x} \right)^2 \right] \left[1 + \left(\frac{\partial w}{\partial y} \right)^2 \right]. \end{aligned} \quad (e)$$

Here one can assume $ds_1 ds_2 = dx dy$ to within small terms of higher order.

On the other hand, comparing the lengths of segments BB_2 and CC_2 , we obtain

$$(\overline{B_2 C_2})^2 = (dx)^2 + (dy)^2 + \left(\frac{\partial w}{\partial y} dy - \frac{\partial w}{\partial x} dx \right)^2. \quad (f)$$

Comparing expressions (e) and (f) and assuming $\cos \left(\frac{\pi}{2} - \gamma^z \right) \approx \gamma^z$, we have

$$\gamma^z = \frac{\partial w}{\partial x} \frac{\partial w}{\partial y}. \quad (d')$$

Using the results obtained, we write the complete expressions for elongation and shear strains in a shell layer separated by distance z from the middle surface:

$$\left. \begin{aligned} e_x^z &= \frac{\partial u^z}{\partial x} - k_x w + \frac{1}{2} \left(\frac{\partial u^z}{\partial x} \right)^2 + \frac{1}{2} \left(\frac{\partial v^z}{\partial x} \right)^2 + \frac{1}{2} \left(\frac{\partial w}{\partial x} \right)^2; \\ e_y^z &= \frac{\partial v^z}{\partial y} - k_y w + \frac{1}{2} \left(\frac{\partial u^z}{\partial y} \right)^2 + \frac{1}{2} \left(\frac{\partial v^z}{\partial y} \right)^2 + \frac{1}{2} \left(\frac{\partial w}{\partial y} \right)^2; \\ \gamma^z &= \frac{\partial u^z}{\partial y} + \frac{\partial v^z}{\partial x} + \frac{\partial w}{\partial x} \frac{\partial w}{\partial y}. \end{aligned} \right\} \quad (1.2)$$

Since we are studying the deformation of thin flexible shells and plates, we can assume that the angles of rotation $\partial w^z / \partial x$, $\partial w^z / \partial y$, related to the deflection considerably exceed the values of the derivatives $\partial u / \partial x$, $\partial u / \partial y$ etc. pertaining to strains in the body of the material. We will assume that the squares of the derivatives $(\partial w^z / \partial x)^2$ are of the same order as the components $\partial u^z / \partial x$, etc; then the squares of derivatives of type $(\partial w^z / \partial x)^2$ of these expressions may be neglected. We arrive at the simpler relations

$$\left. \begin{aligned} \epsilon_x^z &= \frac{\partial u^z}{\partial x} - k_x w + \frac{1}{2} \left(\frac{\partial w}{\partial x} \right)^2, \\ \epsilon_y^z &= \frac{\partial v^z}{\partial y} - k_y w + \frac{1}{2} \left(\frac{\partial w}{\partial y} \right)^2, \\ \gamma^z &= \frac{\partial u^z}{\partial y} + \frac{\partial v^z}{\partial x} + \frac{\partial w}{\partial x} \frac{\partial w}{\partial y}. \end{aligned} \right\} \quad (1.3)$$

We make further use of expressions (1) for displacements of an arbitrary point over the thickness; we then obtain

$$\left. \begin{aligned} \epsilon_x^z &= \frac{\partial u}{\partial x} - k_x w + \frac{1}{2} \left(\frac{\partial w}{\partial x} \right)^2 - z \frac{\partial^2 w}{\partial x^2}, \\ \epsilon_y^z &= \frac{\partial v}{\partial y} - k_y w + \frac{1}{2} \left(\frac{\partial w}{\partial y} \right)^2 - z \frac{\partial^2 w}{\partial y^2}, \\ \gamma^z &= \frac{\partial u}{\partial y} + \frac{\partial v}{\partial x} + \frac{\partial w}{\partial x} \frac{\partial w}{\partial y} - 2z \frac{\partial^2 w}{\partial x \partial y}. \end{aligned} \right\} \quad (1.4)$$

We introduce the symbols ϵ_x , ϵ_y and γ for the strains in the middle surface (for $z = 0$); they will be equal to

$$\left. \begin{aligned} \epsilon_x &= \frac{\partial u}{\partial x} - k_x w + \frac{1}{2} \left(\frac{\partial w}{\partial x} \right)^2, \\ \epsilon_y &= \frac{\partial v}{\partial y} - k_y w + \frac{1}{2} \left(\frac{\partial w}{\partial y} \right)^2, \\ \gamma &= \frac{\partial u}{\partial y} + \frac{\partial v}{\partial x} + \frac{\partial w}{\partial x} \frac{\partial w}{\partial y}. \end{aligned} \right\} \quad (1.5)$$

The total strains of an arbitrary point along the thickness ϵ_x^z , ϵ_y^z and γ^z consist of strains in the middle surface ϵ_y , γ and bending strains, for which we will introduce the symbols $\epsilon_{x,b}$, $\epsilon_{y,b}$, γ_b . The bending strains are equal to

$$\epsilon_{x,b} = -z \frac{\partial^2 w}{\partial x^2}, \quad \epsilon_{y,b} = -z \frac{\partial^2 w}{\partial y^2}, \quad \gamma_b = -2z \frac{\partial^2 w}{\partial x \partial y}. \quad (1.6)$$

When (5) and (6) are taken into account, expressions (4) take the form

$$\epsilon_x^z = \epsilon_x + \epsilon_{x,b}, \quad \epsilon_y^z = \epsilon_y + \epsilon_{y,b}, \quad \gamma^z = \gamma + \gamma_b. \quad (1.7)$$

It is important to note that the strains in the middle surface according to (5) are not independent; they are expressed in terms of the same functions u , v , w . Differentiating the second of relations (5) twice with respect to x , the first relation twice with respect to y , and the third, with respect to x and y successively, after some simple transformations we arrive at the following equation of compatibility or continuity of strains in the middle surface:

$$\frac{\partial^2 \epsilon_x}{\partial y^2} + \frac{\partial^2 \epsilon_y}{\partial x^2} - \frac{\partial^2 \gamma}{\partial x \partial y} = \left(\frac{\partial^2 w}{\partial x \partial y} \right)^2 - \frac{\partial^2 w}{\partial x^2} \frac{\partial^2 w}{\partial y^2} - k_x \frac{\partial^2 w}{\partial y^2} - k_y \frac{\partial^2 w}{\partial x^2}. \quad (1.8)$$

We will now examine the stressed state of a shell.

5. Stress State. Relationship between Forces and Deformations

Within the limits of our assumptions, we can treat the stress state of a shell as a result of superposition of three states. One of them corresponds to the so-called membrane stresses; hereinafter we will frequently call them stresses in the middle surface. The second state corresponds to bending stresses, normal and tangential, changing linearly along the thickness; the "neutral" layer in which the bending stresses are zero coincides with the middle layer. These two stress states taken together determine the "classical" forces. Finally, the third state corresponds to transverse tangential stresses. In the variant of the theory under consideration, only the resultants of these stresses are taken into account; they are investigated in more detail in another variant given below (9).

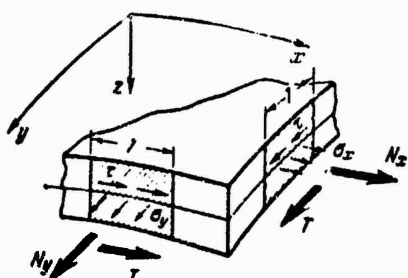


Figure 1.14. Membrane stresses in sections of a shell.

Let us isolate a shell element whose faces coincide with tangents to lines x and y . Figure 1.14 shows the membrane stresses: normal ones σ_x , σ_y and tangential ones τ . If we isolate the portions of the edges having a length equal to unity, we will be able to determine the normal forces N_x , N_y and tangential force T corresponding to these stresses:

$$N_x = \sigma_x h, \quad N_y = \sigma_y h, \quad T = \tau h. \quad (1.9)$$

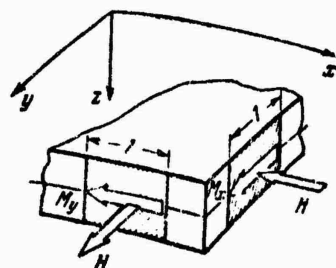


Figure 1.15. Bending and twisting moments in sections of a shell.

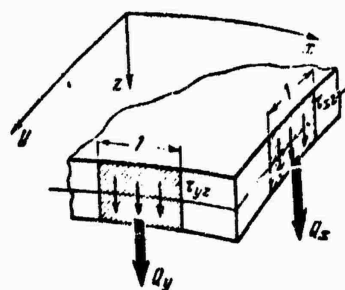


Figure 1.16. Transverse forces and corresponding tangential stresses in sections of a shell.

Let us now turn to bending stresses. We denote the normal stresses by $\sigma_{x,b}$, $\sigma_{y,b}$ and the tangential stresses by τ_b . It is evident that they will be associated with bending moments M_x , M_y and twisting moment H (Figure 1.15). These quantities,

corresponding to a unit length of the faces of the element, will be equal to

$$M_x = \int_{-h/2}^{h/2} \sigma_{x,z} z dz, \quad M_y = \int_{-h/2}^{h/2} \sigma_{y,z} z dz, \quad H = \int_{-h/2}^{h/2} \tau_{z,z} z dz. \quad (1.10)$$

The transverse stresses shown in Figure 1.16 will be denoted by τ_{xy} , τ_{yz} ; they are related to the transverse forces Q_x , Q_y per unit length of the section as follows:

$$Q_x = \int_{-h/2}^{h/2} \tau_{xz} dz, \quad Q_y = \int_{-h/2}^{h/2} \tau_{yz} dz. \quad (1.11)$$

Thus, the integral characteristics of the forces and the local stresses are related by (9)-(11).

In deriving the expressions relating the forces and moments to the strains, we will proceed from the assumption that the strains lie in the effective range of Hooke's law.

For strains in the middle surface, we can write the well-known relations

$$\epsilon_x = \frac{\sigma_x}{E} - \mu \frac{\sigma_y}{E}, \quad \epsilon_y = \frac{\sigma_y}{E} - \mu \frac{\sigma_x}{E}, \quad \gamma = \frac{\tau}{G} = \frac{2(1+\mu)}{E} \tau, \quad (1.12)$$

where G is the modulus of elasticity in shear. Hence

$$\left. \begin{aligned} \sigma_x &= \frac{E}{1-\mu^2} (\epsilon_x + \mu \epsilon_y), & \sigma_y &= \frac{E}{1-\mu^2} (\epsilon_y + \mu \epsilon_x), \\ \tau &= \frac{E}{2(1+\mu)} \gamma, \end{aligned} \right\} \quad (1.12a)$$

Considering relations (5) and (9), we find

$$\left. \begin{aligned} N_x &= \frac{Eh}{1-\mu^2} \left\{ \frac{\partial u}{\partial x} - k_x w + \frac{1}{2} \left(\frac{\partial w}{\partial x} \right)^2 + \right. \\ &\quad \left. + \mu \left[\frac{\partial u}{\partial y} - k_y w + \frac{1}{2} \left(\frac{\partial w}{\partial y} \right)^2 \right] \right\}, \\ N_y &= \frac{Eh}{1-\mu^2} \left\{ \frac{\partial v}{\partial y} - k_y w + \frac{1}{2} \left(\frac{\partial w}{\partial y} \right)^2 + \right. \\ &\quad \left. + \mu \left[\frac{\partial u}{\partial x} - k_x w + \frac{1}{2} \left(\frac{\partial w}{\partial x} \right)^2 \right] \right\}, \\ T &= \frac{Eh}{2(1+\mu)} \left(\frac{\partial u}{\partial y} + \frac{\partial v}{\partial x} + \frac{\partial w}{\partial x} \frac{\partial w}{\partial y} \right). \end{aligned} \right\} \quad (1.15)$$

We then determine the stresses at an arbitrary point with coordinate z:

$$\sigma_x^* = \frac{E}{1-\mu^2} (\epsilon_x^* + \mu \epsilon_y^*), \quad \sigma_y^* = \frac{E}{1-\mu^2} (\epsilon_y^* + \mu \epsilon_x^*), \quad \tau = \frac{E}{2(1+\mu)} \gamma^*. \quad (1.14)$$

The expressions for bending and twisting moments (10), allowing for relations (6), will take the form

$$\left. \begin{aligned} M_x &= -D \left(\frac{\partial^2 w}{\partial x^2} + \mu \frac{\partial^2 w}{\partial y^2} \right), \\ M_y &= -D \left(\frac{\partial^2 w}{\partial y^2} + \mu \frac{\partial^2 w}{\partial x^2} \right), \\ H &= -D(1-\mu) \frac{\partial^2 w}{\partial x \partial y}. \end{aligned} \right\} \quad (1.15)$$

D denotes the cylindrical rigidity of the shell

$$D = \frac{Eh^3}{12(1-\mu^2)}. \quad (1.16)$$

The dependences of transverse forces Q_x and Q_y on the displacements are not given here, since the conditions of equilibrium of the element are used for their derivation in this model; the corresponding expressions will be given in the next section.

6. Approximate Equations of Motion

We will derive the equations of motion of a shell element $h dx dy$, over the faces of which are acting forces in the middle surface, moments, and transverse forces (Figure 1.17). The intensity of specified external loads applied to the element along the x, y, z directions will be denoted by p_x , p_y , and q respectively.

We will use d'Alembert's principle and will add inertial forces to the specified forces and dynamic reactions of the neighboring shell elements (forces and moments). The components of the resultant inertial force along the x, y, z directions will be

$$\frac{\gamma}{g} h \frac{\partial^2 u}{\partial t^2} dx dy, \quad \frac{\gamma}{g} h \frac{\partial^2 v}{\partial t^2} dx dy, \quad \frac{\gamma}{g} h \frac{\partial^2 w}{\partial t^2} dx dy.$$

The rotatory inertia of element $h dx dy$ relative to the x, y directions will not be considered in this shell model.

The equation of motion of the element in projections on the direction of the tangent to line x is

$$\begin{aligned} \left(N_x + \frac{\partial N_x}{\partial x} dx \right) dy - N_x dy + Q_x \frac{\partial w}{\partial x} dy - \\ - \left(Q_x + \frac{\partial Q_x}{\partial x} dx \right) \left(\frac{\partial w}{\partial x} + \frac{\partial^2 w}{\partial x^2} dx \right) dy + \left(T + \frac{\partial T}{\partial y} dy \right) dx - \\ - T dx + p_x dx dy - \frac{N}{\mu} h \frac{\partial^2 u}{\partial x^2} dx dy = 0, \end{aligned}$$

or

$$\frac{\partial N_x}{\partial x} + \frac{\partial T}{\partial y} - \frac{\partial}{\partial x} \left(Q_x \frac{\partial w}{\partial x} \right) + p_x - \frac{N}{\mu} h \frac{\partial^2 u}{\partial x^2} = 0. \quad (1.17)$$

The term underscored by the dotted line in the equation may prove substantial only in the formation of very large depressions. However, in the problems considered below,

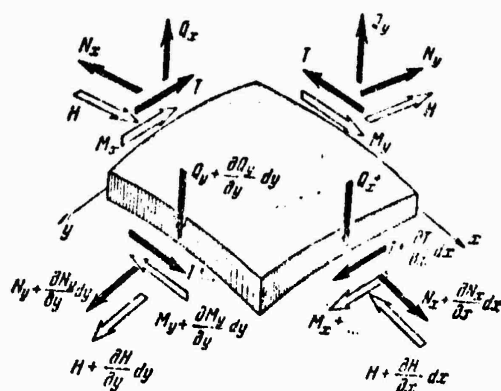


Figure 1.17. Shell element acted upon by bending and twisting moments and transverse forces.

the deformation of a shell is usually associated with the formation of comparatively

shallow depressions whose dimensions are small in comparison with the radii of curvature of the shell*. Therefore, the equation of projections on the tangent to line x may be written in the form

$$\frac{\partial N_x}{\partial x} + \frac{\partial T}{\partial y} + p_x - \frac{y}{g} h \frac{\partial^2 w}{\partial t^2} = 0. \quad (1.18)$$

Similarly, we will write the equation in projections on the direction of the tangent to line y:

$$\frac{\partial T}{\partial x} + \frac{\partial N_y}{\partial y} + p_y - \frac{x}{g} h \frac{\partial^2 w}{\partial t^2} = 0. \quad (1.19)$$

We will now construct the equation in projections of all the forces on the direction of the normal to the middle surface. After simplifications, we obtain

$$\begin{aligned} \frac{\partial Q_x}{\partial x} + \frac{\partial Q_y}{\partial y} + k_x N_x + k_y N_y + \frac{\partial}{\partial x} \left(N_x \frac{\partial w}{\partial x} + T \frac{\partial w}{\partial y} \right) + \\ + \frac{\partial}{\partial y} \left(T \frac{\partial w}{\partial x} + N_y \frac{\partial w}{\partial y} \right) + q - \frac{y}{g} h \frac{\partial^2 w}{\partial t^2} = 0. \end{aligned} \quad (1.20)$$

Let us turn to the equations of moments with respect to tangents to lines y and x. In accordance with the assumption made at the beginning of this section, these equations do not contain any terms related to the rotatory inertia of the element. The first of these equations is

$$\begin{aligned} \left(M_x + \frac{\partial M_x}{\partial x} dx \right) dy - M_x dy + \left(H + \frac{\partial H}{\partial y} dy \right) dx - \\ - H dx - q dx dy \frac{dx}{2} - \left(Q_x + \frac{\partial Q_x}{\partial x} dx \right) dy dx - \\ - \frac{\partial Q_y}{\partial y} dy dx \frac{dx}{2} + \frac{y}{g} h \frac{\partial^2 w}{\partial t^2} dx dy \frac{dx}{2} = 0. \end{aligned}$$

*This assumption is characteristic of the theory of slightly curved shells, which is not used here.

Discarding small terms of higher order, after simplifications we have

$$\frac{\partial M_x}{\partial x} + \frac{\partial M_y}{\partial y} - Q_x = 0. \quad (1.21)$$

By analogy, the second of the equations of moments is written as follows:

$$\frac{\partial H}{\partial x} + \frac{\partial M_y}{\partial y} - Q_y = 0. \quad (1.22)$$

Using relations (15), (21) and (22), we obtain the values of the transverse forces

$$\left. \begin{aligned} Q_x &= -D \frac{\partial}{\partial x} \nabla^2 w, \\ Q_y &= -D \frac{\partial}{\partial y} \nabla^2 w. \end{aligned} \right\} \quad (1.23)$$

Here $\nabla^2 = \frac{\partial^2}{\partial x^2} + \frac{\partial^2}{\partial y^2}$ — is a two-dimensional Laplacian.

Eliminating Q_x and Q_y from Eq. (20) by means of (21) and (22), and writing out (18) and (19) again, we obtain the following system of equations:

$$\frac{\partial N_x}{\partial x} + \frac{\partial T}{\partial y} + p_x - \frac{\gamma}{k} h \frac{\partial^2 w}{\partial t^2} = 0, \quad (1.24)$$

$$\frac{\partial T}{\partial x} + \frac{\partial N_y}{\partial y} + p_y - \frac{\gamma}{k} h \frac{\partial^2 v}{\partial t^2} = 0, \quad (1.25)$$

$$\begin{aligned} \frac{\partial^2 M_x}{\partial x^2} + \frac{\partial^2 M_y}{\partial y^2} + 2 \frac{\partial^2 H}{\partial x \partial y} + k_x N_x + k_y N_y + \\ + \frac{\partial}{\partial x} \left(N_x \frac{\partial w}{\partial x} + T \frac{\partial w}{\partial y} \right) + \frac{\partial}{\partial y} \left(T \frac{\partial w}{\partial x} + N_y \frac{\partial w}{\partial y} \right) + q - \frac{\gamma}{k} h \frac{\partial^2 w}{\partial t^2} = 0. \end{aligned} \quad (1.26)$$

Equations (24)-(26) describe the motion of the shell element. To these equations should be added the boundary and initial conditions.

7. Equations in Displacements

We will express the forces entering into Eqs. (24)-(26) in terms of displacements u, v, w with the aid of relations (13), (15) and (23). From Eq. (24) we find*

$$\begin{aligned} \frac{\partial^2 u}{\partial x^2} + \frac{1-\mu}{2} \frac{\partial^2 u}{\partial y^2} + \frac{1+\mu}{2} \frac{\partial^2 v}{\partial x \partial y} - (k_x + \mu k_y) \frac{\partial w}{\partial x} + \\ + \frac{\partial w}{\partial x} \frac{\partial^2 w}{\partial x^2} + \frac{1+\mu}{2} \frac{\partial w}{\partial y} \frac{\partial^2 w}{\partial x \partial y} + \frac{1-\mu}{2} \frac{\partial w}{\partial y} \frac{\partial^2 v}{\partial y^2} + \\ + \frac{1-\mu^2}{Eh} p_x - \frac{\gamma}{g} \frac{1-\mu^2}{E} \frac{\partial^2 u}{\partial t^2} = 0. \end{aligned} \quad (1.27)$$

Similarly, from Eq. (25) we obtain

$$\begin{aligned} \frac{1+\mu}{2} \frac{\partial^2 u}{\partial x \partial y} + \frac{\partial^2 v}{\partial y^2} + \frac{1-\mu}{2} \frac{\partial^2 v}{\partial x^2} - (\mu k_x + k_y) \frac{\partial w}{\partial y} + \\ + \frac{\partial w}{\partial y} \frac{\partial^2 w}{\partial y^2} + \frac{1+\mu}{2} \frac{\partial w}{\partial x} \frac{\partial^2 w}{\partial x \partial y} + \frac{1-\mu}{2} \frac{\partial w}{\partial x} \frac{\partial^2 v}{\partial x^2} + \\ + \frac{1-\mu^2}{Eh} p_y - \frac{\gamma}{\mu} \frac{1-\mu^2}{E} \frac{\partial^2 v}{\partial t^2} = 0. \end{aligned} \quad (1.28)$$

The equation of motion in projections on the normal to the median surface (26) will be as follows:

$$\begin{aligned} \frac{h^2}{12} \nabla^4 w - (k_x + \mu k_y) \frac{\partial u}{\partial x} - (\mu k_x + k_y) \frac{\partial v}{\partial y} + \\ + (k_x^2 + k_y^2 + 2\mu k_x k_y) w - \frac{k_x + \mu k_y}{2} \left(\frac{\partial w}{\partial x} \right)^2 - \frac{k_y + \mu k_x}{2} \left(\frac{\partial w}{\partial y} \right)^2 - \\ - \frac{\partial}{\partial x} \left\{ \frac{\partial w}{\partial x} \left[\frac{\partial u}{\partial x} + \mu \frac{\partial v}{\partial y} - (k_x + \mu k_y) w \right] + \right. \\ \left. + \frac{1-\mu}{2} \frac{\partial w}{\partial y} \left(\frac{\partial u}{\partial y} + \frac{\partial v}{\partial x} \right) \right\} - \frac{\partial}{\partial y} \left\{ \frac{\partial w}{\partial y} \left[\mu \frac{\partial u}{\partial x} + \frac{\partial v}{\partial y} - (\mu k_x + k_y) w \right] + \right. \\ \left. + \frac{1-\mu}{2} \frac{\partial w}{\partial x} \left(\frac{\partial u}{\partial y} + \frac{\partial v}{\partial x} \right) \right\} - \frac{1-\mu^2}{Eh} q + \frac{\gamma}{g} \frac{1-\mu^2}{E} \frac{\partial^2 w}{\partial t^2} = 0. \end{aligned} \quad (1.29)$$

*In Eqs. (27)-(29) and later in (80)-(84), certain terms of higher order of smallness were discarded.

Here

$$\nabla^4 = \nabla^2 \nabla^2 = \frac{\partial^4}{\partial x^4} + 2 \frac{\partial^4}{\partial x^2 \partial y^2} + \frac{\partial^4}{\partial y^4}.$$

If the dynamic process can be considered without taking the propagation of elastic waves into account, Eqs. (24)-(26) become simplified. It becomes possible to discard the inertial terms in the first two equations. These two equations will be satisfied (in the absence of forces p_x and p_y) if we introduce the stress function ϕ in the middle surface according to the formulas

$$\sigma_x = \frac{N_x}{h} = \frac{\partial^2 \Phi}{\partial y^2}, \quad \sigma_y = \frac{N_y}{h} = \frac{\partial^2 \Phi}{\partial x^2}, \quad \tau = \frac{T}{h} = -\frac{\partial^2 \Phi}{\partial x \partial y}. \quad (1.30)$$

Expressing in (8) the strains in the middle surface in terms of forces, then in terms of ϕ , we reduce the strain compatibility equation to the form

$$\frac{1}{E} \nabla^4 \Phi = -\frac{1}{2} L(w, w) - k_x \frac{\partial^2 w}{\partial y^2} - k_y \frac{\partial^2 w}{\partial x^2}. \quad (1.31)$$

Here the operator $L(w, w)$ has been introduced:

$$L(w, w) = 2 \left[\frac{\partial^2 w}{\partial x^2} \frac{\partial^2 w}{\partial y^2} - \left(\frac{\partial^2 w}{\partial x \partial y} \right)^2 \right]. \quad (1.32)$$

The equation of motion of the shell element will take the form

$$\frac{D}{h} \nabla^4 w = L(w, \Phi) + k_x \frac{\partial^2 \Phi}{\partial y^2} + k_y \frac{\partial^2 \Phi}{\partial x^2} + \frac{q}{h} - \frac{V}{g} \frac{\partial^2 w}{\partial t^2}, \quad (1.33)$$

where

$$L(w, \Phi) = \frac{\partial^2 w}{\partial x^2} \frac{\partial^2 \Phi}{\partial y^2} + \frac{\partial^2 w}{\partial y^2} \frac{\partial^2 \Phi}{\partial x^2} - 2 \frac{\partial^2 w}{\partial x \partial y} \frac{\partial^2 \Phi}{\partial x \partial y}. \quad (1.34)$$

We finally obtain the following equations:

$$\frac{D}{h} \nabla^4 w = L(w, \Phi) + V_k^2 \Phi - \frac{q}{h} - \frac{\gamma}{g} \frac{\partial^2 w}{\partial t^2}, \quad (1.35)$$

$$\frac{1}{E} \nabla^4 \Phi = -\frac{1}{2} [L(w, w) - V_k^2 w]. \quad (1.36)$$

Here V_k^2 represents the operator

$$V_k^2 = k_x \frac{\partial^2}{\partial x^2} + k_y \frac{\partial^2}{\partial y^2}. \quad (1.37)$$

Below, we will frequently consider shells with initial irregularities in the shape of the middle surface. We will assume that the initial deflections are small in comparison with the leading dimensions of the shell, but that they are nevertheless comparable with its thickness. We will give without derivation* the equations corresponding to (35), (36) and derived by considering the initial deflections $w_0 = w_0(x, y)$:

$$\frac{D}{h} \nabla^4 (w - w_0) = L(w, \Phi) + V_k^2 \Phi - \frac{q}{h} - \frac{\gamma}{g} \frac{\partial^2 w}{\partial t^2}, \quad (1.38)$$

$$\frac{1}{E} \nabla^4 \Phi = -\frac{1}{2} [L(w, w) - L(w_0, w_0)] - V_k^2 (w - w_0). \quad (1.39)$$

Let us consider some special cases.

For a circular cylindrical shell for $k_x = 0$, $k_y = 1/R$, where R is the radius of curvature of the middle surface, we obtain the following equations:

$$\frac{D}{h} \nabla^4 (w - w_0) = L(w, \Phi) + \frac{1}{R} \frac{\partial^2 \Phi}{\partial x^2} + \frac{q}{h} - \frac{\gamma}{g} \frac{\partial^2 w}{\partial t^2}, \quad (1.40)$$

$$\frac{1}{E} \nabla^4 \Phi = -\frac{1}{2} [L(w, w) - L(w_0, w_0)] - \frac{1}{R} \frac{\partial^2 (w - w_0)}{\partial x^2}, \quad (1.41)$$

*See the author's book [0.6], p. 505.

In studying a spherical shell of radius R for $k_x = k_y = 1/R$, we will have the equations

$$\frac{D}{h} \nabla^4(w - w_0) = L(w, \Phi) + \frac{1}{R} \nabla^2 \Phi + \frac{q}{h} - \frac{\gamma}{\mu} \frac{\partial^2 w}{\partial t^2}, \quad (1.42)$$

$$\frac{1}{E} \nabla^4 \Phi = -\frac{1}{2} [L(w, w) - L(w_0, w_0)] - \frac{1}{R} \nabla^2(w - w_0). \quad (1.43)$$

In the case of a plate, we obtain

$$\frac{D}{h} \nabla^4(w - w_0) = L(w, \Phi) + \frac{q}{h} - \frac{\gamma}{\mu} \frac{\partial^2 w}{\partial t^2}. \quad (1.42a)$$

$$\frac{1}{E} \nabla^4 \Phi = -\frac{1}{2} [L(w, w) - L(w_0, w_0)]. \quad (1.43a)$$

Another way of transforming the initial equations (24)-(26) consists in introducing the so-called dynamic stress function in the middle surface; this variant is described in the author's book [0.6], pp. 792-796.

8. Boundary and Initial Conditions

In integrating the equations of motion, we must proceed from definite boundary and initial conditions.

If the hypothesis of straight normals is used, each point of the contour must satisfy four boundary conditions. Actually, if the displacements u, v, w of the points of the contour line are known, this determines the position of this line in space after deformation. A normal drawn at any point of the contour may move progressively together with this point and rotate through some angle in the plane normal to the countour line. Consequently, the position of the normal after deformation of the shell is defined by means of four quantities [1.11].

We will enumerate certain boundary conditions typical of practical problems; it is assumed that the external conditions do not change their direction during deformation of the shell. We will write them down for the shell edge $x = \text{const}$; the conditions pertaining

to the edge $y = \text{const}$ will be obtained by substitution of y for x and v for u .

.. The points of the plate edge do not undergo normal displacements. In that case

$$w = 0. \quad (1.44)$$

2. The edge is clamped, and the tangent to the middle surface does not undergo rotation. Then we should have

$$\frac{\partial w}{\partial x} = 0. \quad (1.45)$$

3. The edge is hinged.

$$M_x = 0. \quad (1.46)$$

This condition may be rewritten in the form

$$\frac{\partial^2 w}{\partial x^2} + \mu \frac{\partial^2 w}{\partial y^2} = 0. \quad (1.46a)$$

4. The points of the unloaded edge move freely along the z axis. Then the pressure on the stiffening rib should be zero (see [1.11], p. 41):

$$R_x = Q_x + \frac{\partial H}{\partial y} + N_x \frac{\partial w}{\partial x} + T \frac{\partial w}{\partial y} = 0. \quad (1.47)$$

5. The points of the edge do not move along a normal to the boundary line. Then

$$u = 0. \quad (1.48)$$

6. The points of the unloaded edge move freely along a normal to the boundary line. In this case, it is necessary to set

$$N_x = 0. \quad (1.49)$$

7. The points of the edge do not move along the boundary line. It is necessary that

$$v = 0. \quad (1.50)$$

8. The points of the unloaded edge move freely along the boundary line. It is necessary to set

$$T = 0. \quad (1.51)$$

The boundary conditions pertaining to the displacements are geometric. At the same time, the conditions formulated for the forces and moments will be termed dynamic.

In integrating the fundamental equations, the initial conditions pertaining to the displacements and velocities of the points of the middle surface of the shell must also be satisfied.

9. Shell Model Allowing for Rotatory Shear and Inertia. Deformations and Displacements

The preceding sections gave the fundamental relationships pertaining to a shell model based on the Kirchhoff-Love hypothesis. As already noted, use of this first approximation model makes it possible to attain a sufficient accuracy in solving many practical problems.

However, in some cases, this scheme proves insufficiently complete. For instance, in the theory of three-layered shells, whose middle layer is very pliable to shear, the deformations corresponding to shearing stresses along the normal cannot be neglected. With respect to a stack of layers as a whole, the hypothesis of straight normals is no longer applicable. This also applies to shells made of composite materials with a binder having a relatively low shear stiffness.

Another example that is particularly important for further discussion pertains to

dynamic processes in shells connected with the propagation of deformation waves. We have in mind the deformation excited by impact or in any other way in some region of the shell, then transmitted in different directions along the middle surface. In this case, we must take into consideration the inertial forces corresponding to displacements u and v . By taking these inertial forces into account, we can describe the wave processes connected with elongations (contractions) in the middle surface.

However, this leaves out the description of transmission of the transverse forces connected with the local action of normal loads. Such a process may occur either independently, or together with the propagation of tension-compression waves. Of major importance in this case are the shear strains connected with transverse forces Q or stresses τ . Moreover, it is necessary to consider the rotatory inertia of the shell element; if the angles of rotation of the tangents to lines ξ , n are denoted by θ_ξ and θ_n , the moments of the inertial forces for a prism with dimensions along ξ and n equal to l , will be $(\gamma/g)l(\partial^2\theta_\xi/\partial t^2)$ and $(\gamma/g)l(\partial^2\theta_n/\partial t^2)$, where $(\gamma/g)l$ is the mass moment of inertia of the volume under consideration with respect to the corresponding axes; $l = h^3/12$.

Hence, to supplement the "classical" deformation and inertial forces, we introduce the deformations related to transverse forces and the rotatory inertia. Such a picture of the stressed and strained state may be regarded as a second-approximation model.

In the literature, this model is usually tied to the name of S.P. Timoshenko, who proposed it for use in the theory of bending of beams*. It is important to note that the equations of motion obtained for the second approximation model are of hyperbolic type; these are the equations that describe the phenomenon of wave propagation.

The disadvantage of the Kirchhoff-Love and Timoshenko theories is that they were constructed on hypotheses that, at least at first glance, are intuitive in character. Another way of setting up the fundamental relations of the theory of thin shells

*Further studies in this area were made by Ya. S. Uflyand [1.23b] with application to plates and by S.A. Ambartsumyan [1.5] and others with application to shells.

consists in expanding the displacements or stresses in series (power or functional) along the normal coordinate and keeping a certain segment of this series, depending on the accuracy required and the nature of the problem**.

Let us now examine the characteristics introduced into the analysis by the consideration of shear strain. The Timoshenko model which we are using is characterized by a distinct separation of the displacements caused by "classical" forces on the one hand, and, on the other hand, transverse tangential forces. Figure 1.18 shows the section of the middle surface of the shell by the plane tangent to lines x and z at point K .

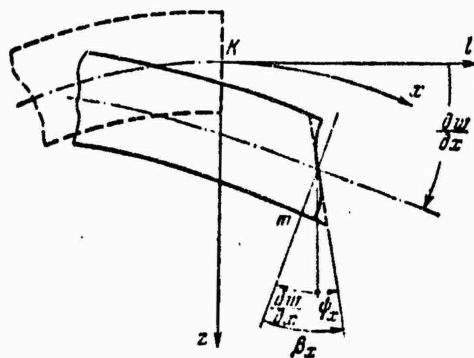


Figure 1.18. Deformation of shell element according to a Timoshenko type hypothesis.

The figure shows tangent l to line x . Upon deformation of the shell, the tangent is turned by an angle equal to $\partial w / \partial x$, (in the range of relatively small displacements) along the direction from line x to z . If the points located along the shell thickness and lying on the normal to line x before deformation remained on the rotated normal, their new position would be determined by line m . However, shear strains related to transverse forces cause the linearity to be violated. The corresponding "integral" angle of rotation of the segment of the normal will be denoted by β_x ; it will be

**A classification of the various methods of constructing a theory of thin shells is given by A.L. Gol'denvyizer [1.13a], N.A. Kli'chevskiy [1.15], L. Ya. Aynola and U.K. Nigul [1.2], and other authors.

assigned a plus sign for the positive direction of transverse forces (see Figure 1.18). Then the final angle of rotation of the segment of the normal at the middle surface will be $\Psi_x = \beta_x - (\partial w / \partial x)$. Introducing the same notation for the angles of rotation in the plane tangent to lines z and x , we finally obtain

$$\psi_x = \beta_x - \frac{\partial w}{\partial x}, \quad \psi_y = \beta_y - \frac{\partial w}{\partial y}. \quad (1.52)$$

We will arbitrarily assume that the normal to the undistorted middle surface rotates as a whole through these angles without being distorted. We will assume further that the normal does not change its length in such rotation; this assumption enters into the system of Kirchhoff-Love hypotheses. The displacements of an arbitrary point of the normal with coordinate z (before deformation) will now be equal to

$$u^* = u + z\psi_x, \quad v^* = v + z\psi_y, \quad w^* = w. \quad (1.53)$$

These relations could be given a more symmetric structure by assuming the element along the normal to be deformable according to the law $w^* = w + z\psi$; ψ being some function of x, y, t . However, this would complicate the subsequent relations.

In order to find the magnitudes of the strains in a shell layer separated by distance z from the middle surface, we will substitute relations (53) into relations (3), which also apply to the given model.

Instead of (4), we obtain

$$\left. \begin{aligned} e_x^* &= \frac{\partial u}{\partial x} - k_x w + \frac{1}{2} \left(\frac{\partial w}{\partial x} \right)^2 + z \frac{\partial \psi_x}{\partial x}, \\ e_y^* &= \frac{\partial v}{\partial y} - k_y w + \frac{1}{2} \left(\frac{\partial w}{\partial y} \right)^2 + z \frac{\partial \psi_y}{\partial y}, \\ \gamma^* &= \frac{\partial u}{\partial y} + \frac{\partial v}{\partial x} + \frac{\partial w}{\partial x} \frac{\partial w}{\partial y} + z \left(\frac{\partial \psi_x}{\partial y} + \frac{\partial \psi_y}{\partial x} \right), \end{aligned} \right\} \quad (1.54)$$

or, considering expressions (5) for strains in the middle surface,

$$\epsilon_x^s = \epsilon_x + z \frac{\partial \psi_x}{\partial x}, \quad \epsilon_y^s = \epsilon_y + z \frac{\partial \psi_y}{\partial y}, \quad \gamma^s = \gamma + z \left(\frac{\partial \psi_x}{\partial y} + \frac{\partial \psi_y}{\partial x} \right). \quad (1.55)$$

We will now examine the stresses and forces acting in the shell.

10. Stress State Allowing for Shear

As was shown in §5, the stress state of a shell corresponds in the general case to stresses in the middle surface, classical bending stresses, and transverse tangential stresses.

The bending and shearing stresses are associated with bending moments and a twisting moment (10). Considering relations (14) and (55), we obtain the following expressions for the moments from (10):

$$\left. \begin{aligned} M_x &= D \left(\frac{\partial \psi_x}{\partial x} + \mu \frac{\partial \psi_y}{\partial y} \right), \\ M_y &= D \left(\frac{\partial \psi_y}{\partial y} + \mu \frac{\partial \psi_x}{\partial x} \right), \\ H &= D \frac{1-\mu}{2} \left(\frac{\partial \psi_x}{\partial y} + \frac{\partial \psi_y}{\partial x} \right). \end{aligned} \right\} \quad (1.56)$$

Transverse tangential stresses τ_{xz} and τ_{yz} are related to transverse forces Q_x and Q_y by the expressions

$$\tau_{xz} = \frac{1}{h} Q_x f(z), \quad \tau_{yz} = \frac{1}{h} Q_y f(z). \quad (1.57)$$

Function $f(z)$ represents the law of distribution of stresses τ_{xz} and τ_{yz} over the thickness of the shell. This function is even:

$$f(z) = f(-z), \quad (a)$$

which corresponds to a distribution of stresses τ_z symmetric with respect to the middle surface. It also follows that

$$\int_{-h/2}^{h/2} f(z) z dz = 0. \quad (b)$$

Integrating (57) over the shell thickness, we should obtain relations (1).

Hence the following property of function $F(z)$:

$$\frac{1}{h} \int_{-h/2}^{h/2} f(z) dz = 1. \quad (c)$$

Finally, we introduce the notation

$$\frac{1}{k^2} = \frac{1}{h} \int_{-h/2}^{h/2} f'(z) dz. \quad (d)$$

The quantity k^2 will be discussed in more detail below.

In conformity with Hooke's Law, we should assume the relationship between stresses τ_{xz} , τ_{yz} and shearing strains β_x^z , β_y^z to be

$$\tau_{xz} = \frac{E}{2(1+\mu)} \beta_x^z, \quad \tau_{yz} = \frac{E}{2(1+\mu)} \beta_y^z. \quad (1.58)$$

Comparing these relations with expressions (57), we find

$$\beta_x^z = \frac{Q_r}{h} \frac{2(1+\mu)}{E} f(z), \quad \beta_y^z = \frac{Q_\mu}{h} \frac{2(1+\mu)}{E} f(z). \quad (1.59)$$

However, in conformity with (52), we assume the angles of transverse shear to be constant over the shell thickness and equal to

$$\beta_x = \frac{\partial w}{\partial x} + \psi_x, \quad \beta_y = \frac{\partial w}{\partial y} + \psi_y. \quad (1.60)$$

Let us take the condition of equivalence, expressed in the equality of the work of

transverse forces, found by using the hypothesis of undistortable normals, and the work of tangential forces:

$$\frac{1}{2} Q_x \beta_x = \frac{1}{2} \int_{-h/2}^{h/2} \tau_{xz} \beta_x^z dz. \quad (1.61)$$

Substituting the value of β_x from (60) into the left side and τ_{xz} from (58) and β_x^z from (59) into the right side, we find

$$\frac{Q_x}{h} \int_{-h/2}^{h/2} f^2 dz = \frac{Eh}{2(1+\mu)} \left(\frac{\partial w}{\partial x} + \psi_x \right). \quad (1.62)$$

Considering the notation introduced (d), we write Q_x and by analogy for Q_y :

$$\left. \begin{aligned} Q_x &= h^2 \frac{Eh}{2(1+\mu)} \left(\frac{\partial w}{\partial x} + \psi_x \right), \\ Q_y &= h^2 \frac{Eh}{2(1+\mu)} \left(\frac{\partial w}{\partial y} + \psi_y \right). \end{aligned} \right\} \quad (1.63)$$

The values of coefficients k^2 depend on the form of functions $f(z)$ in (57). Let us recall that in the theory of bending of beams, in the case of a rectangular section, we obtain a parabolic law of change of transverse tangential stresses with height. They turn out to be equal to zero at the extreme points of the section and maximum at the points of the "neutral" layer. A similar pattern of distribution of stresses τ_z should be obtained for the portion of the shell section in the shape of a rectangle $h \times l$. Then function $f(z)$ takes the form

$$f(z) = 6 \left[\frac{1}{4} - \left(\frac{z}{h} \right)^2 \right].$$

This relation satisfies conditions (a), (b), and (c), and k^2 according to expression (d) turns out to be equal to $5/6$. Such is the value assumed for k^2 in the refined plate theory of Ambartsumyan [1.5a] and Reissner [1.36]; Timoshenko [1.37] gives the values $k^2 = 2/3$ and $8/9$. The first of these values was also used by Uflyand [1.23b].

Mindlin [1.33] proposed to determine k^2 for a plate by equating the propagation velocity of elastic waves on the basis of the adopted model with the corresponding velocity found from three-dimensional equations of elasticity theory. Rayleigh [1.35] and Lamb [1.31] showed that the relation between the propagation velocity c of flexural waves and the velocity c_s of shear waves at wavelengths $\lambda \rightarrow 0$ has the form

$$4c_s^2 \sqrt{(c_s^2 - ac^2)(c_s^2 - c^2)} = (2c_s^2 - c^2)^2 \quad (1.64)$$

for $0 < c/c_s < 1$, where

$$c_s = \sqrt{\frac{G}{\rho}}, \quad a = \frac{1-2\mu}{2(1-\mu)}.$$

For the propagation velocity of waves in a plate, allowing for shear and rotatory inertia at $\lambda \rightarrow 0$,

$$c^2 = k^2 c_s^2. \quad (1.65)$$

From (64) and (65), we find the following equation for k^2 :

$$4 \sqrt{(1-ak^2)(1-k^2)} = (2-k^2)^2 \quad \text{npui} \quad 0 < k < 1. \quad (1.66)$$

A study of this dependence shows that k^2 should change according to a law that is very close to linear, from the value of 0.76 for Poisson's ratio $\mu = 0$ to 0.91 for $\mu = 0.5$.

We obtain a different value for k^2 by equating the frequencies of the first anti-symmetric vibration mode of an elongated rectangular plate and the frequencies obtained from exact theory ($\omega = \omega_0/h$) and from relations allowing for the effects of shear and rotatory inertia ($\omega = kc_s \sqrt{12}/h$). We then have $k^2 = \pi^2/12$, which is close to the value of 5/6 proposed by Ambartsumyan and Reissner. For $\mu = 0.176$, the value of k^2

from (66) agrees with the value ($\pi^2/12$). Generally speaking, it is advisable to choose the coefficient k^2 on the basis of precisely what mode of vibrations or wave motions is essential in the problem under consideration.

The experimental determination of the shear coefficient is due to Faylon; he obtained $k^2 = 8/9$. This value may be considered to be in good agreement with (66), since the material on which the experiments were carried out, a photoelastic coating, had a high Poisson's ratio.

II. Variational Equation

We will derive the equations of motion of a shell allowing for shear and rotatory inertia, as well as the corresponding boundary conditions, on the basis of energetic premises*.

Let us consider the process of motion during a time interval between instants t_0 and t_1 . For this time interval, we will compare different trajectories of motion of the points of the system between the initial and final positions. The true trajectories differ from other possible ones (consistent with the relations) in that for the former, the following condition must be fulfilled:

$$\int_{t_0}^{t_1} (\delta K - \delta II + \delta' W) dt = 0. \quad (I.67)$$

Here K stands for the kinetic energy of the system, II is the potential energy, and $\delta' W$ is the sum total of the elementary work done by the external forces.

When all the forces acting on the system have a potential, Eq. (67) takes the form

*Compare the book [1.11], p. 53, in which the principle of possible displacements was used to derive the fundamental differential equations of statics of flexible plates. The conclusion given below is due to M.S. Gershteyn.

$$\delta S = \delta \int_0^t (K - \Pi) dt = 0,$$

where

$$S = \int_0^t (K - \Pi) dt$$

is the Hamiltonian action. The latter equality expresses the well-known Hamilton-Ostrogradskiy principle.

First of all, let us determine the variation of the potential energy of deformation of the shell, $\delta\pi$. The quantity π represents the sum of the energies corresponding to deformation in the middle surface π_m , on the one hand, and deformation of bending and transverse shear π_b on the other:

$$\Pi = \Pi_e + \Pi_u.$$

The energy π_m is equal to

$$\Pi_e = \frac{1}{2} \iint (N_x e_x + N_y e_y + T\gamma) dx dy.$$

Introducing the expressions for strains (5), we obtain

$$\begin{aligned} \Pi_e = & \frac{1}{2} \iint \left\{ N_x \left[\frac{\partial u}{\partial x} - k_z w + \frac{1}{2} \left(\frac{\partial w}{\partial x} \right)^2 \right] + \right. \\ & \left. + N_y \left[\frac{\partial v}{\partial y} - k_z w + \frac{1}{2} \left(\frac{\partial w}{\partial y} \right)^2 \right] + T \left(\frac{\partial u}{\partial y} + \frac{\partial v}{\partial x} + \frac{\partial w}{\partial x} \frac{\partial w}{\partial y} \right) \right\} dx dy. \end{aligned} \quad (1.68)$$

The energy π_b is expressed as follows:

$$\begin{aligned} \Pi_u = & \frac{1}{2} \iint \left[M_x \frac{\partial \psi_x}{\partial x} + M_y \frac{\partial \psi_y}{\partial y} + H \left(\frac{\partial \psi_x}{\partial y} + \frac{\partial \psi_y}{\partial x} \right) + \right. \\ & \left. + Q_x \left(\frac{\partial w}{\partial x} + \psi_x \right) + Q_y \left(\frac{\partial w}{\partial y} + \psi_y \right) \right] dx dy. \end{aligned} \quad (1.69)$$

The kinetic energy of the shell is, allowing for the energy of rotation of the element, equal to

$$K = \frac{1}{2} \frac{\gamma}{g} h \int \int \left[\left(\frac{\partial u}{\partial t} \right)^2 + \left(\frac{\partial v}{\partial t} \right)^2 + \left(\frac{\partial w}{\partial t} \right)^2 + \frac{h^3}{12} \left(\frac{\partial \psi_x}{\partial t} \right)^2 + \frac{h^2}{12} \left(\frac{\partial \psi_y}{\partial t} \right)^2 \right] dx dy. \quad (1.70)$$

The elementary work done by the external forces will be

$$\delta'W = \int \int (p_x \delta u + p_y \delta v + q \delta w) dx dy. \quad (1.71)$$

Let us consider the portion of the shell bounded by coordinate lines $x = a_1$, $x = a_2$, $y = b_1$, $y = b_2$. We will determine a partial variation of the energy, assuming that only function u is variable; we then find

$$\delta_u II = \int_{b_1}^{b_2} \int_{a_1}^{a_2} \left[N_x \frac{\partial}{\partial x} (\delta u) + T \frac{\partial}{\partial x} (\delta u) \right] dx dy.$$

Integrating by parts, we obtain

$$\delta_u II = \int_{b_1}^{b_2} [N_x \delta u]_{a_1}^{a_2} dy + \int_{a_1}^{a_2} [T \delta u]_{b_1}^{b_2} dx - \int_{b_1}^{b_2} \int_{a_1}^{a_2} \left(\frac{\partial N_x}{\partial x} + \frac{\partial T}{\partial y} \right) \delta u dx dy. \quad (1.72)$$

We turn to the integral of the variation of the kinetic energy of the shell with respect to time. Again we will consider the case in which only function u varies. Then, for the time interval from t_0 to t_1 , we have

$$\int_{t_0}^{t_1} \delta_u K dt = \int_{t_0}^{t_1} \int_{b_1}^{b_2} \int_{a_1}^{a_2} \frac{\gamma}{g} h \frac{\partial u}{\partial t} \delta \left(\frac{\partial u}{\partial t} \right) dx dy dt.$$

Integrating by parts, we find

$$\int_{t_0}^{t_1} \delta_u K dt = \frac{Y}{8} h \int_{t_0}^{t_1} \int_{a_1}^{a_2} \left[\frac{\partial u}{\partial t} \delta u \right]_{a_1}^{a_2} dx dy - \frac{Y}{8} h \int_{t_0}^{t_1} \int_{b_1}^{b_2} \int_{a_1}^{a_2} \frac{\partial^2 u}{\partial t^2} \delta u dx dy dt. \quad (1.73)$$

Let the reader find similar expressions for variations in v:

$$\delta_v \Pi, \quad \int_{t_0}^{t_1} \delta_v K dt.$$

We will now vary the angular displacement function ψ_x . Then, from expression (69)

$$\delta_{\psi_x} \Pi = \int_{t_0}^{t_1} \int_{a_1}^{a_2} \left[M_x \frac{\partial}{\partial x} (\delta \psi_x) + H \frac{\partial}{\partial y} (\delta \psi_x) - Q_x \delta \psi_x \right] dx dy.$$

Again using integration by parts, we obtain

$$\begin{aligned} \delta_{\psi_x} \Pi = & \int_{b_1}^{b_2} \left[M_x \delta \psi_x \right]_{a_1}^{a_2} dy + \\ & + \int_{a_1}^{a_2} \left[H \delta \psi_x \right]_{b_1}^{b_2} dx - \int_{t_0}^{t_1} \int_{b_1}^{b_2} \int_{a_1}^{a_2} \left(\frac{\partial M_x}{\partial x} + \frac{\partial H}{\partial y} - Q_x \right) \delta \psi_x dx dy. \end{aligned} \quad (1.72a)$$

For the variation of kinetic energy, we will have

$$\begin{aligned} \int_{t_0}^{t_1} \delta_{\psi_x} K dt = & \frac{Y}{8} \frac{h^3}{12} \int_{t_0}^{t_1} \int_{b_1}^{b_2} \int_{a_1}^{a_2} \left[\frac{\partial \psi_x}{\partial t} \delta \psi_x \right]_{a_1}^{a_2} dx dy - \\ & - \frac{Y}{8} \frac{h^3}{12} \int_{t_0}^{t_1} \int_{b_1}^{b_2} \int_{a_1}^{a_2} \frac{\partial^2 \psi_x}{\partial t^2} \delta \psi_x dx dy dt. \end{aligned} \quad (1.73a)$$

The variations

$$\delta_{\psi_y} \Pi, \quad \int_{t_0}^{t_1} \delta_{\psi_y} K dt.$$

will be found in similar fashion.

When the deflection function w varies, the potential energy variation can be found from expressions (68) and (69)

$$\delta_w \Pi = \int_{a_1}^{b_1} \int_{a_2}^{b_2} \left\{ -k_x N_x \delta w - k_y N_y \delta w + N_x \frac{\partial w}{\partial x} \frac{\partial}{\partial x} (\delta w) + \right. \\ \left. + N_y \frac{\partial w}{\partial y} \frac{\partial}{\partial y} (\delta w) + T \left[\frac{\partial w}{\partial x} \frac{\partial}{\partial y} (\delta w) + \frac{\partial w}{\partial y} \frac{\partial}{\partial x} (\delta w) \right] + \right. \\ \left. + Q_x \frac{\partial}{\partial x} (\delta w) + Q_y \frac{\partial}{\partial y} (\delta w) \right\} dx dy.$$

Integrating by parts, we obtain

$$\delta_w \Pi = \int_{a_1}^{b_1} \left[\left(N_x \frac{\partial w}{\partial x} + T \frac{\partial w}{\partial y} \right) \delta w \right]_{a_2}^{b_2} dy + \\ + \int_{a_1}^{b_1} \left[\left(T \frac{\partial w}{\partial x} + N_y \frac{\partial w}{\partial y} \right) \delta w \right]_{a_2}^{b_2} dx + \int_{a_1}^{b_1} [Q_x \delta w]_{a_2}^{b_2} dy + \\ + \int_{a_1}^{b_1} [Q_y \delta w]_{a_2}^{b_2} dx - \int_{a_1}^{b_1} \int_{a_2}^{b_2} \left[k_x N_x + k_y N_y + \frac{\partial}{\partial x} \left(N_x \frac{\partial w}{\partial x} + T \frac{\partial w}{\partial y} \right) + \right. \\ \left. + \frac{\partial}{\partial y} \left(T \frac{\partial w}{\partial x} + N_y \frac{\partial w}{\partial y} \right) + \frac{\partial Q_x}{\partial x} + \frac{\partial Q_y}{\partial y} \right] \delta w dx dy. \quad (1.72b)$$

For the kinetic energy, we find

$$\int_{t_1}^{t_2} \delta_w K dt = \frac{\gamma}{g} h \int_{b_1}^{b_2} \int_{a_2}^{b_2} \left[\frac{\partial w}{\partial t} \delta w \right]_{t_1}^{t_2} dx dy - \\ - \frac{\gamma}{g} h \int_{t_1}^{t_2} \int_{b_1}^{b_2} \int_{a_2}^{b_2} \frac{\partial^2 w}{\partial t^2} \delta w dx dy dt. \quad (1.73b)$$

We substitute all the expressions obtained into Eq. (67), which corresponds to the Hamilton-Ostrogradskiy principle. We thus arrive at the following variational equation:

$$\begin{aligned}
& \int_{t_0}^{t_1} \int_{b_1}^{b_2} \int_{a_1}^{a_2} \left\{ \left(\frac{\partial N_x}{\partial x} + \frac{\partial T}{\partial y} + p_x - \frac{y}{g} h \frac{\partial^2 u}{\partial t^2} \right) \delta u + \right. \\
& \quad + \left(\frac{\partial T}{\partial x} + \frac{\partial N_y}{\partial y} + p_y - \frac{y}{g} h \frac{\partial^2 v}{\partial t^2} \right) \delta v + \\
& \quad + \left[k_x N_x + k_y N_y + \frac{\partial}{\partial x} \left(N_x \frac{\partial w}{\partial x} + T \frac{\partial w}{\partial y} \right) + \right. \\
& \quad + \frac{\partial}{\partial y} \left(T \frac{\partial w}{\partial x} + N_y \frac{\partial w}{\partial y} \right) + \frac{\partial Q_x}{\partial x} + \frac{\partial Q_y}{\partial y} + q - \frac{y}{g} h \frac{\partial^2 w}{\partial t^2} \left] \delta w + \right. \\
& \quad + \left(\frac{\partial M_x}{\partial x} + \frac{\partial H}{\partial y} - Q_x - \frac{y}{g} h \frac{\partial^2 \psi_x}{\partial t^2} \right) \delta \psi_x + \\
& \quad \left. \left. + \left(\frac{\partial H}{\partial x} + \frac{\partial M_y}{\partial y} - Q_y - \frac{y}{g} h \frac{\partial^2 \psi_y}{\partial t^2} \right) \delta \psi_y \right\} dx dy dt - \right. \\
& \quad \left. - \int_{t_0}^{t_1} \int_{b_1}^{b_2} \left\{ N_y \delta v + T \delta u + \left[T \frac{\partial w}{\partial x} + N_y \frac{\partial w}{\partial y} + Q_x \right] \delta w - \right. \right. \\
& \quad \left. \left. - M_y \delta \psi_y - H \delta \psi_x \right\}_{b_1}^{b_2} dx dt - \right. \\
& \quad \left. - \int_{t_0}^{t_1} \int_{b_1}^{b_2} \left\{ N_x \delta u + T \delta v + \left[N_x \frac{\partial w}{\partial x} + T \frac{\partial w}{\partial y} + Q_y \right] \delta w - \right. \right. \\
& \quad \left. \left. - M_x \delta \psi_x - H \delta \psi_y \right\}_{a_1}^{a_2} dy dt + \right. \\
& \quad \left. + \int_{b_1}^{b_2} \int_{a_1}^{a_2} \frac{y}{g} h \left\{ \frac{\partial u}{\partial t} \delta u + \frac{\partial v}{\partial t} \delta v + \frac{\partial w}{\partial t} \delta w + \right. \right. \\
& \quad \left. \left. + \frac{h^3}{12} \left(\frac{\partial \psi_x}{\partial t} \delta \psi_x + \frac{\partial \psi_y}{\partial t} \delta \psi_y \right) \right\}_{a_1}^{a_2} dx dy = 0. \right.
\end{aligned} \tag{1.74}$$

In this equation, the forces in the middle surface N_x , N_y , T , moments M_x , M_y , H and transverse forces Q_x , Q_y are related to the displacements by formulas (13), (56) and (63) respectively. Since the variations of δu , δv , etc., treated as functions of t , are arbitrary, the coefficients of each of the variations in the first integral should be zero. This results in the following five differential equations of motion:

$$\frac{\partial N_x}{\partial x} + \frac{\partial T}{\partial y} + p_x - \frac{y}{g} h \frac{\partial^2 u}{\partial t^2} = 0, \tag{1.75}$$

$$\frac{\partial T}{\partial x} + \frac{\partial N_y}{\partial y} + p_y - \frac{y}{g} h \frac{\partial^2 v}{\partial t^2} = 0, \tag{1.76}$$

$$\begin{aligned}
& \frac{\partial Q_x}{\partial x} + \frac{\partial Q_y}{\partial y} + k_x N_x + k_y N_y + \frac{\partial}{\partial x} \left(N_x \frac{\partial w}{\partial x} + T \frac{\partial w}{\partial y} \right) + \\
& + \frac{\partial}{\partial y} \left(T \frac{\partial w}{\partial x} + N_y \frac{\partial w}{\partial y} \right) + q - \frac{y}{g} h \frac{\partial^2 w}{\partial t^2} = 0,
\end{aligned} \tag{1.77}$$

$$\frac{\partial M_x}{\partial x} + \frac{\partial H}{\partial y} - Q_x - \frac{\gamma}{g} \frac{h^3}{12} \frac{\partial^2 \psi_x}{\partial t^2} = 0, \quad (1.78)$$

$$\frac{\partial H}{\partial x} + \frac{\partial M_y}{\partial y} - Q_y - \frac{\gamma}{g} \frac{h^3}{12} \frac{\partial^2 \psi_y}{\partial t^2} = 0. \quad (1.79)$$

The first three of the above equations are analogous to Eqs. (18)-(20), and the last two differ from Eqs. (21), (22) in that the inertia of rotational motion of the element relative to the x and y directions is now taken into account.

12. Equations in Displacements and Boundary Conditions

Having expressed the forces in terms of displacements u , v , w and angles ψ_x and ψ_y , using relations (13), (56), and (63), we obtain a new system of equations of motion in displacements.

From (75) and (76), we find equations identical to (27) and (28):

$$\begin{aligned} \frac{\partial^2 u}{\partial x^2} + \frac{1-\mu}{2} \frac{\partial^2 u}{\partial y^2} + \frac{1+\mu}{2} \frac{\partial^2 v}{\partial x \partial y} - (k_x + \mu k_y) \frac{\partial w}{\partial x} + \\ + \frac{\partial w}{\partial x} \frac{\partial^2 w}{\partial x^2} + \frac{1+\mu}{2} \frac{\partial w}{\partial y} \frac{\partial^2 w}{\partial x \partial y} + \frac{1-\mu}{2} \frac{\partial w}{\partial x} \frac{\partial^2 w}{\partial y^2} + \\ + \frac{1-\mu^2}{Eh} p_x - \frac{\gamma}{g} \frac{1-\mu^2}{E} \frac{\partial^2 u}{\partial t^2} = 0; \end{aligned} \quad (1.80)$$

$$\begin{aligned} \frac{1+\mu}{2} \frac{\partial^2 u}{\partial x \partial y} + \frac{\partial^2 v}{\partial y^2} + \frac{1-\mu}{2} \frac{\partial^2 v}{\partial x^2} - (\mu k_x + k_y) \frac{\partial w}{\partial y} + \\ + \frac{\partial w}{\partial y} \frac{\partial^2 w}{\partial y^2} + \frac{1+\mu}{2} \frac{\partial w}{\partial x} \frac{\partial^2 w}{\partial x \partial y} + \frac{1-\mu}{2} \frac{\partial w}{\partial y} \frac{\partial^2 w}{\partial x^2} + \\ + \frac{1-\mu^2}{Lh} p_y - \frac{\gamma}{g} \frac{1-\mu^2}{E} \frac{\partial^2 v}{\partial t^2} = 0. \end{aligned} \quad (1.81)$$

The equation of motion in projections on the normal to the middle surface takes the form

$$\begin{aligned} k^2 \frac{1-\mu}{2} \left(\nabla^2 w + \frac{\partial \psi_x}{\partial x} + \frac{\partial \psi_y}{\partial y} \right) + (k_x + \mu k_y) \frac{\partial u}{\partial x} + (k_y + \mu k_x) \frac{\partial v}{\partial y} - \\ - (k_x^2 + k_y^2 + 2\mu k_x k_y) w + \frac{k_x + \mu k_y}{2} \left(\frac{\partial w}{\partial x} \right)^2 + \frac{k_y + \mu k_x}{2} \left(\frac{\partial w}{\partial y} \right)^2 + \\ + \frac{\partial}{\partial x} \left\{ \frac{\partial w}{\partial x} \left[\frac{\partial u}{\partial x} + \mu \frac{\partial v}{\partial y} - (k_x + \mu k_y) w \right] + \frac{1-\mu}{2} \frac{\partial w}{\partial y} \left(\frac{\partial u}{\partial y} + \frac{\partial v}{\partial x} \right) \right\} + \\ + \frac{\partial}{\partial y} \left\{ \frac{\partial w}{\partial y} \left[\mu \frac{\partial u}{\partial x} + \frac{\partial v}{\partial y} - (k_y + \mu k_x) w \right] + \right. \\ \left. + \frac{1-\mu}{2} \frac{\partial w}{\partial x} \left(\frac{\partial u}{\partial y} + \frac{\partial v}{\partial x} \right) \right\} + \frac{1-\mu^2}{Eh} q - \frac{\gamma}{g} \frac{1-\mu^2}{E} \frac{\partial^2 w}{\partial t^2} = 0. \end{aligned} \quad (1.82)$$

We next transform the momental equations (78) and (79). The first will have the form

$$\frac{\partial^2 \psi_x}{\partial x^2} + \frac{1-\mu}{2} \frac{\partial^2 \psi_x}{\partial y^2} + \frac{1+\mu}{2} \frac{\partial^2 \psi_y}{\partial x \partial y} - 6k^2 \frac{1-\mu}{h^2} \left(\frac{\partial w}{\partial x} + i\psi_x \right) - \frac{\gamma}{g} \frac{1-\mu^2}{E} \frac{\partial^2 \psi_x}{\partial t^2} = 0. \quad (1.83)$$

The second equation is reduced to the following:

$$\frac{1+\mu}{2} \frac{\partial^2 \psi_x}{\partial x \partial y} + \frac{\partial^2 \psi_y}{\partial y^2} + \frac{1-\mu}{2} \frac{\partial^2 \psi_y}{\partial x^2} - 6k^2 \frac{1-\mu}{h^2} \left(\frac{\partial w}{\partial y} + \psi_y \right) - \frac{\gamma}{g} \frac{1-\mu^2}{E} \frac{\partial^2 \psi_y}{\partial t^2} = 0. \quad (1.84)$$

We have obtained the system of Eqs. (80)-(84) in displacements, which makes it possible to study the vibratory motions and processes of propagation of elastic waves in a shell, account being taken of the effects of shear and rotatory inertia. Buckling of a shell in the course of impact loading is also described by these equations.

Integration of the equations of motion is performed by taking the boundary and initial conditions into account. The second and third integrals in variational equation (74) permit the formulation of five boundary conditions for each edge of the shell. We will write them down for the edge $x = \text{const}$.

1. The angle of rotation of an element of the normal about the y axis or the bending moment is given:

$$\psi_x = \psi_x^0 \text{ and } M_x = M_x^0. \quad (1.85)$$

2. The angle of rotation of an element of the normal about the x axis or the twisting moment is given:

$$\psi_y = \psi_y^0 \text{ and } H = H^0. \quad (1.86)$$

3. The normal displacement of the points of the contour or the magnitude of the external transverse force is given:

$$w = w^0 \text{ или } Q_x + N_x \frac{\partial w}{\partial x} + T \frac{\partial w}{\partial y} = Q_x^0. \quad (1.87)$$

4. The displacement of the points of the middle-surface contour in the direction of the x axis or the magnitude of the external compressive force is given:

$$u = u^0 \text{ или } N_x = N_x^0. \quad (1.88)$$

5. The displacement of the points of the middle-surface contour along the y axis or the external tangential force is given:

$$v = v^0 \text{ или } T = T^0. \quad (1.89)$$

It was noted in §8 that when the Kirchhoff-Love hypotheses are used, the position of the element of the normal in the extreme section after deformation is determined by four parameters. Accordingly, four boundary conditions are formulated on each portion of the contour. When the deformation of transverse shear is introduced into consideration, the number of degrees of freedom of the element of the normal increases to five because its independent rotation about axis x is now admissible (at the boundary, $x = \text{const}$).

Let us explain the above by the use of an example. Let the end of a cylindrical shell be supported on a diaphragm that is rigid in its plane and placed inside the shell, so that the points of the inner contour are immovable. When the equations of the shear model are used, it is necessary to determine whether the points of the outer contour of the section are also immovable. If so, the condition $\psi_y = 0$, exists; otherwise, it is necessary to assume that $H = 0$. Let us note that the appearance of a twisting moment in a Timoshenko type shell is not necessarily due to torsion of the median surface.

If we neglect the transverse shear and set $\beta_x = \frac{\partial w}{\partial x} + \psi_x = 0$, $\beta_y = \frac{\partial w}{\partial y} + \psi_y = 0$, we obtain $\frac{\partial \delta w}{\partial x} = -\delta \psi_x$, $\frac{\partial \delta w}{\partial y} = -\delta \psi_y$. Eliminating $\delta \psi_x$ and $\delta \psi_y$ from the variational equation with the aid of these relations, instead of (75)-(79), we obtain equations corresponding to the Kirchhoff-Love hypotheses (see §6).

We set up the equations in displacements u , v , w by using the variational method. We then wrote down the equations containing the deflection function w and stress function ϕ in the median surface. Generally speaking, displacements, deformations, and forces in the most diverse combinations can be chosen as the desired functions. The corresponding variants of the fundamental equations and boundary conditions can be obtained uniformly, using the variation equation that we know; however, the latter should be supplemented with certain terms containing Lagrangian multipliers. For the case where the fundamental functions are w and ϕ , this was done in the author's book [1.11], p. 53.

A general method for deriving a "universal" variational equation was proposed by K. Friedrichs (K. Friedrichs, Nachrichten der Ges. d. Wiss. zu Göttingen, 1929, 13-20); this method was discussed in the book of R. Courant and D. Hilbert, Methods of Mathematical Physics, Moscow, 1963, p. 224 (R. Courant, D. Hilbert, Methoden d. Math. Physik I, Berlin, 1931). As applied to nonlinear shell theory with the use of the Kirchhoff-Love theory, this question was discussed in detail by N.P. Abovskiy in a number of works.

13. Some Variants of Dynamic Equations

We will explain how the model described by the preceding sections of this book is related to other models studied in the literature.

We will begin with a linearized problem pertaining to small deflection plates, without considering the deformations in the middle surface. In this case, Eqs. (80)-(84) take the form

$$k^2 \frac{1-\mu}{2} \left(\nabla^2 w + \frac{\partial \psi_x}{\partial x} + \frac{\partial \psi_y}{\partial y} \right) + \frac{1-\mu^2}{Eh} q - \frac{\gamma}{g} \frac{1-\mu^2}{E} \frac{\partial^3 w}{\partial t^3} = 0, \quad (1.90)$$

$$\nabla^2 \psi_x + \frac{1+\mu}{2} \frac{\partial}{\partial y} \left(\frac{\partial \psi_y}{\partial x} - \frac{\partial \psi_x}{\partial y} \right) - 6k^2 \frac{1-\mu}{h^2} \left(\frac{\partial w}{\partial x} + \psi_x \right) - \frac{y}{g} \frac{1-\mu^2}{E} \frac{\partial^2 \psi_x}{\partial t^2} = 0, \quad (1.91)$$

$$\nabla^2 \psi_y + \frac{1+\mu}{2} \frac{\partial}{\partial x} \left(\frac{\partial \psi_x}{\partial y} - \frac{\partial \psi_y}{\partial x} \right) - 6k^2 \frac{1-\mu}{h^2} \left(\frac{\partial w}{\partial y} + \psi_y \right) - \frac{y}{g} \frac{1-\mu^2}{E} \frac{\partial^2 \psi_y}{\partial t^2} = 0. \quad (1.92)$$

We introduce the functions ϕ and θ by means of the relations*

$$\psi_x = - \left(\frac{\partial \phi}{\partial x} + \frac{\partial \theta}{\partial y} \right), \quad \psi_y = \frac{\partial \theta}{\partial x} - \frac{\partial \phi}{\partial y}, \quad (1.93)$$

then obtain

$$\frac{\partial \psi_x}{\partial x} + \frac{\partial \psi_y}{\partial y} = - \nabla^2 \phi, \quad \frac{\partial \psi_x}{\partial y} - \frac{\partial \psi_y}{\partial x} = - \nabla^2 \theta. \quad (1.94)$$

Taking the derivatives of (91) with respect to x and of (92) with respect to y and summing up, we find

$$\nabla^2 \left[\nabla^2 \phi + 6k^2 \frac{1-\mu}{h^2} (w - \phi) - \frac{y}{g} \frac{1-\mu^2}{E} \frac{\partial^2 \phi}{\partial t^2} \right] = 0.$$

This equality is satisfied if we set

$$\nabla^2 \phi + 6k^2 \frac{1-\mu}{h^2} (w - \phi) - \frac{y}{g} \frac{1-\mu^2}{E} \frac{\partial^2 \phi}{\partial t^2} = 0. \quad (1.95)$$

We now differentiate (91) with respect to y and (92) with respect to x , and subtract the second equality from the first. This gives

*See V.N. Moskalenko [1.9].

$$\nabla^2\phi - \frac{12h^2}{k^2} \phi - \frac{2(1+\mu)}{E} \frac{y}{g} \frac{\partial^2\phi}{\partial t^2} = 0. \quad (1.96)$$

Finally, substitution of (94) into (90) gives

$$\nabla^2\psi - \nabla^2w - \frac{2(1+\mu)}{k^2 Eh} q + \frac{2y}{g} \frac{1+\mu}{h^2 E} \frac{\partial^2 w}{\partial t^2} = 0. \quad (1.97)$$

We have arrived at the system of Eqs. (95)-(97), which in one form or another has been frequently discussed in the literature.

Assuming in Eqs. (80)-(84) $k_x = 0$, $k_y = 1/R$, neglecting displacements v and ψ_y and discarding nonlinear terms, we arrive at the system of three equations obtained by Herrmann and Mirsky [1.28] for the case of axially symmetric wave motion of a cylindrical shell. Neglecting the influence of transverse shear, these authors obtained a system of two equations corresponding to the moment theory of shells. If the rotatory inertia is not considered, and we turn to $R \rightarrow \infty$, the displacements w and u are separated in the equations. Motion in the z direction is described by classical plate theory, and motion along x , by the longitudinal impact theory.

Further, in the case of a cylindrical shell, equations for studying axially symmetric deformation on impact can be obtained from the above equations. Equations describing an axially symmetric wave process in a cylindrical shell, allowing for shear and rotatory inertia, were obtained for a linearized problem by Naghdi and Cooper [1.34].

In deriving the equations of motion, we assumed that the parameters determining the geometry of any layer of the shell were the same as the parameters of the middle surface. Our aim will be to obtain a refined variant of the equations based on the Kirchhoff-Love hypothesis, but allowing for a change of geometric parameters from layer to layer along the thickness of the shell. This may be a factor in solving certain practically important problems of dynamic and stability.

Let us consider a shell layer separated by distance z from the middle surface ($-h/2 \leq z \leq h/2$). We will consider the change of curvature for this layer in comparison

with the curvature of the middle surface. The expressions for the strains will then be

$$\left. \begin{aligned} e_x^z &= \frac{1}{1-k_x z} \frac{\partial u^z}{\partial x} - \frac{k_x}{1-k_x z} w^z, \\ e_y^z &= \frac{1}{1-k_y z} \frac{\partial v^z}{\partial y} - \frac{k_y}{1-k_y z} w^z, \\ \gamma^z &= \frac{1}{1-k_y z} \frac{\partial u^z}{\partial y} + \frac{1}{1-k_x z} \frac{\partial v^z}{\partial x}. \end{aligned} \right\} \quad (1.98)$$

From the hypothesis of straight normals we must assume $\gamma_{yz} = \gamma_{zx} = 0$. Expanding these expressions (see the book [0.6], p. 485), we obtain

$$\left. \begin{aligned} \frac{\partial u^z}{\partial z} + \frac{k_x}{1-k_x z} u^z + \frac{1}{1-k_x z} \frac{\partial w^z}{\partial x} &= 0, \\ \frac{\partial v^z}{\partial z} + \frac{k_y}{1-k_y z} v^z + \frac{1}{1-k_y z} \frac{\partial w^z}{\partial y} &= 0. \end{aligned} \right\} \quad (1.99)$$

For the points of a straight fiber normal to the middle surface, the derivatives $\partial u^z / \partial z$ and $\partial v^z / \partial z$ should remain constant and equal to

$$\frac{\partial u^z}{\partial z} = \frac{\partial u}{\partial z} = \frac{u^z - u}{z}, \quad \frac{\partial v^z}{\partial z} = \frac{\partial v}{\partial z} = \frac{v^z - v}{z}. \quad (1.100)$$

However, on the other hand, assuming $z = 0$ in (99), we obtain

$$\left. \begin{aligned} \frac{\partial u}{\partial z} &= -\frac{k_x}{1-k_x z} u - \frac{1}{1-k_x z} \frac{\partial w}{\partial x}, \\ \frac{\partial v}{\partial z} &= -\frac{k_y}{1-k_y z} v - \frac{1}{1-k_y z} \frac{\partial w}{\partial y}. \end{aligned} \right\} \quad (1.101)$$

Comparing (100) and (101), we find

$$\left. \begin{aligned} u^z &= (1-k_x z) u - z \frac{\partial w}{\partial x}, \\ v^z &= (1-k_y z) v - z \frac{\partial w}{\partial y}, \\ w^z &= w. \end{aligned} \right\} \quad (1.102)$$

Then the expressions for the strains will take the form

$$\left. \begin{aligned} e_x^z &= \frac{\partial u}{\partial x} - \frac{k_x}{1-k_x z} w - \frac{z}{1-k_x z} \frac{\partial^2 w}{\partial x^2}, \\ e_y^z &= \frac{\partial v}{\partial y} - \frac{k_y}{1-k_y z} w - \frac{z}{1-k_y z} \frac{\partial^2 w}{\partial y^2}, \\ \gamma^z &= \frac{1-k_x z}{1-k_y z} \frac{\partial u}{\partial y} + \frac{1-k_y z}{1-k_x z} \frac{\partial v}{\partial y} - \frac{\partial w}{\partial x \partial y} \left(\frac{z}{1-k_y z} + \frac{z}{1-k_x z} \right). \end{aligned} \right\} \quad (1.103)$$

The normal and tangential forces per unit length of arc will be

$$\left. \begin{aligned} N_x &= \int_{-h/2}^{h/2} \sigma_x^z (1 - k_y z) dz, & T_{xy} &= \int_{-h/2}^{h/2} \tau^z (1 - k_y z) dz, \\ N_y &= \int_{-h/2}^{h/2} \sigma_y^z (1 - k_x z) dz, & T_{yx} &= \int_{-h/2}^{h/2} \tau^z (1 - k_x z) dz. \end{aligned} \right\} \quad (1.104)$$

In the general case, when $k_x \neq k_y$, i.e., $R_1 \neq R_2$, where $k_x = 1/R_1$, $k_y = 1/R_2$, the tangential forces T_{xy} and T_{yx} turn out to be different. Considering that for this shells $z \ll R_1$ and $z \ll R_2$, it can be assumed in expressions (104) that

$$1 - zk_z \approx 1, \quad 1 - zk_y \approx 1;$$

we then obtain $T_{xy} = T_{yx} = T$.

We write the expressions for the bending and twisting moments per unit length of the element's faces:

$$\left. \begin{aligned} M_x &= \int_{-h/2}^{h/2} \sigma_x^z (1 - k_y z) z dz, & H_{xy} &= \int_{-h/2}^{h/2} \tau^z (1 - k_y z) z dz, \\ M_y &= \int_{-h/2}^{h/2} \sigma_y^z (1 - k_x z) z dz, & H_{yx} &= \int_{-h/2}^{h/2} \tau^z (1 - k_x z) z dz. \end{aligned} \right\} \quad (1.105)$$

The transverse shear stresses shown in Figure 1.16 will be denoted by τ_{xz} , τ_{yz} . They are related to the transverse forces Q_x and Q_y by

$$Q_x = \int_{-h/2}^{h/2} \tau_{xz} dz, \quad Q_y = \int_{-h/2}^{h/2} \tau_{yz} dz. \quad (1.106)$$

We will again assume that for a certain layer of the shell located at a distance z from the middle surface, the relationship between the stresses and strains obeys Hooke's law

$$\sigma_x^z = \frac{E}{1-\mu^2} (\epsilon_x^z + \mu \epsilon_y^z), \quad \sigma_y^z = \frac{E}{1-\mu^2} (\epsilon_y^z + \mu \epsilon_x^z), \quad \tau^z = \frac{E}{2(1+\mu)} \gamma^z. \quad (1.107)$$

Then, allowing for (103) and (107), relations (104) will have the form

$$\left. \begin{aligned} N_x &= \frac{Eh}{1-\mu^2} \left[\frac{\partial u}{\partial x} + \mu \frac{\partial v}{\partial y} - (k_x + \mu k_y) w - \right. \\ &\quad \left. - \frac{h^2}{12} (k_x - k_y) \frac{\partial^2 w}{\partial x^2} - \frac{k_x^2 h^2}{12} (k_x - k_y) w \right], \\ N_y &= \frac{Eh}{1-\mu^2} \left[\frac{\partial v}{\partial y} + \mu \frac{\partial u}{\partial x} - (k_y + \mu k_x) w - \right. \\ &\quad \left. - \frac{h^2}{12} (k_y - k_x) \frac{\partial^2 w}{\partial y^2} - \frac{k_y^2 h^2}{12} (k_y - k_x) w \right], \\ T_{xy} &= \frac{Eh}{2(1+\mu)} \left[\frac{\partial u}{\partial y} + \frac{\partial v}{\partial x} + \frac{h^2}{12} (k_x - k_y)^2 \frac{\partial w}{\partial x} - \right. \\ &\quad \left. - \frac{h^2}{12} (k_x - k_y) \frac{\partial^2 w}{\partial x \partial y} \right], \\ T_{yx} &= \frac{Eh}{2(1+\mu)} \left[\frac{\partial u}{\partial y} + \frac{\partial v}{\partial x} + \frac{h^2}{12} (k_y - k_x)^2 \frac{\partial w}{\partial y} - \right. \\ &\quad \left. - \frac{h^2}{12} (k_y - k_x) \frac{\partial^2 w}{\partial x \partial y} \right]. \end{aligned} \right\} \quad (1.108)$$

The expressions for the bending and twisting moments will be

$$\left. \begin{aligned} M_x &= -D \left[\frac{\partial^2 w}{\partial x^2} + \mu \frac{\partial^2 w}{\partial y^2} + k_y \left(\frac{\partial u}{\partial x} + \mu \frac{\partial v}{\partial y} \right) + k_x (k_x - k_y) w \right], \\ M_y &= -D \left[\frac{\partial^2 w}{\partial y^2} + \mu \frac{\partial^2 w}{\partial x^2} + k_x \left(\frac{\partial v}{\partial y} + \mu \frac{\partial u}{\partial x} \right) + k_y (k_y - k_x) w \right], \\ H_{xy} &= -D \frac{1-\mu}{2} \left[2 \frac{\partial^2 w}{\partial x \partial y} + k_x \frac{\partial u}{\partial y} - (k_x - 2k_y) \frac{\partial v}{\partial x} \right], \\ H_{yx} &= -D \frac{1-\mu}{2} \left[2 \frac{\partial^2 w}{\partial y \partial x} + k_y \frac{\partial v}{\partial x} - (k_y - 2k_x) \frac{\partial u}{\partial y} \right]. \end{aligned} \right\} \quad (1.109)$$

In calculating the forces, the logarithms found as a result of integration are expanded in a series, and the first three terms are retained.

The equations of equilibrium of the element in projections on the direction of the tangent to lines x and y by analogy with (18) has the form

$$\left. \begin{aligned} \frac{\partial N_x}{\partial x} + \frac{\partial T_{xy}}{\partial y} - k_x Q_x + p_x - \frac{\gamma}{g} h \frac{\partial^2 u}{\partial t^2} &= 0, \\ \frac{\partial T_{xy}}{\partial y} + \frac{\partial N_y}{\partial y} - k_y Q_y + p_y - \frac{\gamma}{g} h \frac{\partial^2 v}{\partial t^2} &= 0. \end{aligned} \right\} \quad (1.110)$$

The equations in projections on the direction of the normal to the middle surface will be

$$\frac{\partial Q_x}{\partial x} + \frac{\partial Q_y}{\partial y} + k_x N_x + k_y N_y + \frac{\partial}{\partial x} \left(N_x \frac{\partial w}{\partial x} + T_{xy} \frac{\partial w}{\partial y} \right) + \frac{\partial}{\partial y} \left(T_{yx} \frac{\partial w}{\partial x} + N_y \frac{\partial w}{\partial y} \right) + q - \frac{\gamma}{g} h \frac{\partial^2 w}{\partial t^2} = 0. \quad (1.111)$$

The equations of the moments with respect to the tangents to lines x and y are

$$\left. \begin{aligned} \frac{\partial M_x}{\partial x} + \frac{\partial H_{yx}}{\partial y} - Q_x &= 0, \\ \frac{\partial H_{xy}}{\partial x} + \frac{\partial M_y}{\partial y} - Q_y &= 0. \end{aligned} \right\} \quad (1.112)$$

From these equations, the expressions for Q_x and Q_y are

$$\left. \begin{aligned} Q_x &= -D \left[\frac{\partial^2 w}{\partial x^2} + \frac{\partial^2 w}{\partial x \partial y} + k_y \frac{\partial^2 u}{\partial x^2} - (k_y - 2k_x) \frac{1-\mu}{2} \frac{\partial^2 u}{\partial y^2} + \right. \\ &\quad \left. + \frac{1+\mu}{2} k_y \frac{\partial^2 v}{\partial x \partial y} + k_x (k_x - k_y) \frac{\partial w}{\partial x} \right], \\ Q_y &= -D \left[\frac{\partial^2 w}{\partial y^2} + \frac{\partial^2 w}{\partial y \partial x} + k_x \frac{\partial^2 v}{\partial y^2} - \frac{1-\mu}{2} (k_x - 2k_y) \frac{\partial^2 v}{\partial x^2} + \right. \\ &\quad \left. + \frac{1+\mu}{2} k_x \frac{\partial^2 u}{\partial x \partial y} + k_y (k_y - k_x) \frac{\partial w}{\partial y} \right]. \end{aligned} \right\} \quad (1.113)$$

Substituting expressions (112) into (111), we obtain

$$\begin{aligned} \frac{\partial^2 M_x}{\partial x^2} + \frac{\partial^2 M_y}{\partial y^2} + \frac{\partial^2}{\partial x \partial y} (H_{xy} + H_{yx}) + k_x N_x + k_y N_y + \\ + \frac{\partial}{\partial x} \left(N_x \frac{\partial w}{\partial x} + T_{xy} \frac{\partial w}{\partial y} \right) + \frac{\partial}{\partial y} \left(T_{yx} \frac{\partial w}{\partial x} + N_y \frac{\partial w}{\partial y} \right) + \\ + q - \frac{\gamma}{g} h \frac{\partial^2 w}{\partial t^2} = 0. \end{aligned} \quad (1.114)$$

We then express the forces entering into Eqs. (110) in terms of displacements u , v , w by means of relations (108), (113). Neglecting certain terms containing k_x^3 , k_y^3 , etc., we obtain

$$\begin{aligned} \frac{\partial^2 u}{\partial x^2} \left(1 + \frac{h^2}{12} k_x k_y \right) + \frac{1-\mu}{2} \left[1 + \frac{h^2}{12} (k_y^2 - 3k_x k_y + 3k_x^2) \right] \frac{\partial^2 u}{\partial y^2} + \\ + \frac{1+\mu}{2} \left(1 + \frac{h^2}{12} k_x k_y \right) \frac{\partial^2 v}{\partial x \partial y} + k_y \frac{h^2}{12} \frac{\partial^2 w}{\partial x^2} + \\ + \frac{h^2}{12} \left(k_x \frac{3-\mu}{2} - k_y \frac{1-\mu}{2} \right) \frac{\partial^2 w}{\partial y^2} - (k_x + \mu k_y) \frac{\partial w}{\partial x} + \\ + \frac{1-\mu^2}{Eh} p_x - \frac{1-\mu^2}{E} \frac{\gamma}{g} \frac{\partial^2 u}{\partial t^2} = 0, \end{aligned} \quad (1.115)$$

$$\begin{aligned}
& \frac{1+\mu}{2} \left(1 + \frac{h^2}{12} k_x k_y \right) \frac{\partial^3 u}{\partial x^2 \partial y} + \left(1 + \frac{h^2}{12} k_x k_y \right) \frac{\partial^3 v}{\partial y^2} + \\
& + \frac{1-\mu}{2} \left[1 + \frac{h^2}{12} (k_x^2 - 3k_x k_y + 3k_y^2) \right] \frac{\partial^3 u}{\partial x^2} + \\
& + \frac{h^2}{12} \left(k_y \frac{3-\mu}{2} - k_x \frac{1-\mu}{2} \right) \frac{\partial^3 w}{\partial x^2 \partial y} + k_x \frac{h^2}{12} \frac{\partial^3 w}{\partial y^2} - (k_y + \mu k_x) \frac{\partial^3 w}{\partial y} + \\
& + \frac{1-\mu^2}{Eh} p_y - \frac{1-\mu^2}{E} \frac{y}{g} \frac{\partial^3 v}{\partial t^2} = 0. \tag{1.116}
\end{aligned}$$

Eliminating nonlinear terms from (114), we arrive at the equation

$$\begin{aligned}
& \frac{k_y h^2}{12} \frac{\partial^3 u}{\partial x^3} + \frac{h^2}{12} \left(k_x \frac{3-\mu}{2} - k_y \frac{1-\mu}{2} \right) \frac{\partial^3 u}{\partial x \partial y^2} + \\
& + \frac{h^2}{12} \left(k_y \frac{3-\mu}{2} - k_x \frac{1-\mu}{2} \right) \frac{\partial^3 v}{\partial x^2 \partial y} + \frac{k_y h^2}{12} \frac{\partial^3 v}{\partial y^3} - \\
& - (k_x + \mu k_y) \frac{\partial u}{\partial x} - (k_y + \mu k_x) \frac{\partial v}{\partial y} + (k_x^2 + 2\mu k_x k_y + k_y^2) w + \\
& + \frac{h^2}{12} (k_x - k_y) (k_x^2 - k_y^2) w + \frac{h^2}{12} \nabla^4 w + \frac{h^2}{6} k_x (k_x - k_y) \frac{\partial^2 w}{\partial x^2} + \\
& + \frac{h^2}{6} k_y (k_y - k_x) \frac{\partial^2 w}{\partial y^2} - \frac{1-\mu^2}{Eh} q + \frac{1-\mu^2}{E} \frac{y}{g} \frac{\partial^2 w}{\partial t^2} = 0. \tag{1.117}
\end{aligned}$$

The above equations in the case of $k_x = 0$, $k_y = 1/R$ are the same as Flügge's equations* for a cylindrical shell.

14. More Complete Relations Between Deformations and Displacements

In the preceding sections, we derived equations of motion of a shell element that were based on a Timoshenko type model. The equations proved to be nonlinear, since they considered large displacements of points of the middle surface of the shell. These equations can be used to study the process of buckling of shells that takes place when elastic waves propagate in a material subjected to dynamic loads. The main nonlinear terms necessary for solving most practical problems were introduced into the above relations. However, in certain cases, other terms which we neglected in the derivation may also prove essential. For this reason, it is desirable to obtain more complete nonlinear equations of motion of a shell so as to introduce certain simplifications

*W. Flügge, *Stresses in Shell*, Berlin (1960), 219, 233

into these equations when solving specific problems.

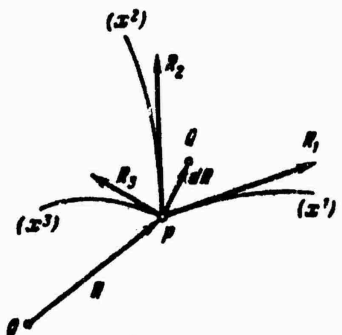


Figure 1.19. Vectors forming the basis of a curvilinear coordinate system.

To derive such refined relations, we will use the tensor formulation of the fundamental relationships of shell theory, allowing for the effect of shear and rotatory inertia.*

We will consider an elastic body to which is related a system of curvilinear coordinates x^i ($i = 1, 2, 3$). As the origin, we choose some point of space O (Figure 1.19) and denote by $R(x^i)$ the radius vector of an arbitrary point p. Considering R to be a differentiable function of variables x^i , we obtain

$$dR = \frac{\partial R}{\partial x^i} dx^i. \quad (1.118)$$

In accordance with the rule, used in tensor analysis, of summation over a twice repeated "dummy" index, expression (118) means**

*A similar derivation is given by Habip [1.27]. The equations of motion were obtained in more complete form by L. Ya. Aynol [1.1]. In the form given here, they were studied by M.S. Gershteyn.

**For more detail concerning the tensor apparatus used below, see for example I.N. Vekua's Fundamentals of Tensor Analysis, Tbilisi, 1967.

$$dR = \frac{\partial R}{\partial x^1} dx^1 + \frac{\partial R}{\partial x^2} dx^2 + \frac{\partial R}{\partial x^3} dx^3. \quad (a)$$

We will hereinafter use the following notation for each of the three vectors entering into (a):

$$\frac{\partial R}{\partial x^i} = R_i. \quad (b)$$

It is evident that each of the vectors R_i is directed along a tangent to the coordinate line x^i . For each point of the body, vectors R_i form a noncoplanar triplet which is the basis of the coordinate system. These vectors represent the change of radius vector R during displacement along the coordinate lines from a given point P. In a Cartesian system, vectors R_i will be the unit vectors of the coordinate lines.

We will denote by dR an infinitely small vector \overline{PQ} under the assumption that the position of point Q is determined by coordinates $x^i + dx^i$.

The length of vector \overline{PQ} will be denoted by ds . Using the definition of a scalar product, we find

$$ds^2 = dR dR. \quad (1.119)$$

In turn,

$$dR = R_i dx^i. \quad (1.120)$$

From (119) to (120) we obtain the following expression for the square of the distance between two infinitely close points:

$$ds^2 = R_i R_k dx^i dx^k = g_{ik} dx^i dx^k, \quad (1.121)$$

where

$$g_{ik} = g_{ki} = R_i R_k, \quad (i, k) = 1, 2, 3. \quad (1.122)$$

The right-hand side of (121) is called the metric quadratic form, and the quantities g_{ik} are the covariant components of the metric tensor.

When curvilinear coordinates are used, in addition to basis (118) of the coordinate system, its conjugate basis consisting of vectors R^i is introduced into consideration. Then

$$R_i R^k = \delta_i^k, \quad (1.123)$$

where δ_i^k is Kronecker's symbol:

$$\delta_i^k = \begin{cases} 1 & \text{if } i=k, \\ 0 & \text{if } i \neq k. \end{cases}$$

Any vector may be represented as a linear combination of vectors R_1, R_2, R_3 or R^1, R^2, R^3 .

For example, R_i will be represented as a linear combination of vectors R^1, R^2, R^3 , using relations (122) and (123):

$$R_i = g_{ik} R^k. \quad (1.124)$$

Let us recall that the expression on the right-hand side represents a sum, so that relation (124) is associated with the following relations:

$$\begin{aligned} R_1 &= g_{11} R^1 + g_{12} R^2 + g_{13} R^3, \\ R_2 &= g_{21} R^1 + g_{22} R^2 + g_{23} R^3, \\ R_3 &= g_{31} R^1 + g_{32} R^2 + g_{33} R^3. \end{aligned}$$

Solving this system of equalities with respect to vectors R^k , we obtain

$$R^k = g^{ki} R_i. \quad (1.125)$$

where the following relation holds for g^{ki} by (123):

$$g^{lk} = g^{kl} = R^l R^k. \quad (1.126)$$

The quantities g^{ki} are contravariant components of the metric tensor. They are related to the covariant components as follows:

$$g_{il} g^{ik} = \delta_{l}^k \quad (1.127)$$

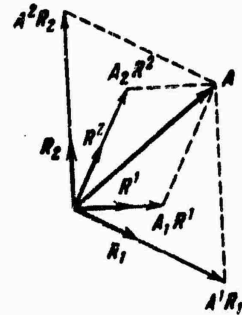


Figure 1.20. Principal and conjugate base of the coordinate system.

As an illustration, let us consider a certain vector A on a plane (Figure 1.20); R_1, R_2 are the basis of the coordinate system, and R^1, R^2 are its conjugate basis.

Vector A may be expressed in the form

$$A = A^1 R_1 \quad \text{or} \quad A = A^1 R^1. \quad (1.128)$$

Thus, the contravariant components A^1 and covariant components A^1 give two different representations of the same vector A . We multiply both parts of equalities (128) scalarly by the basis vectors R^k and R_k :

$$A^k = AR^k; \quad A_k = AR_k. \quad (1.129)$$

From these equalities, with the aid of (124) and (125), we obtain

$$A_l = g_{lk} A^k \quad \text{or} \quad A^k = g^{kl} A_l. \quad (1.130)$$

Such an operation of lowering or raising of the indices, here applied to components of vectors, is extended to tensors of any rank.

Let us return to the consideration of an elastic body whose basis vectors and metric tensor before deformation are expressed by relations (118) and (122). We will characterize the strain state of the body by means of the difference of the squares of the linear element after deformation (ds) and before deformation (ds_0). On the basis of relation (121), we obtain

$$ds^2 - ds_0^2 = 2\gamma_{ij} dx^i dx^j, \quad (1.131)$$

where

$$\gamma_{ij} = \frac{1}{2} (G_{ij} - g_{ij}); \quad (1.132)$$

quantities G_{ij} and g_{ij} being the covariant components of the metric tensor before and after deformation, respectively. Functions γ_{ij} are symmetric components of the covariant strain tensor.

We express the strain components in terms of the displacement vector. Let the radius vector of a point of the body after deformation be

$$\vec{R} = \vec{R} + \vec{u},$$

where $u(x^1, x^2, x^3, t)$ is the displacement vector. Basis vectors \vec{R} and the metric tensor after deformation G_{ij} are determined, on the basis of (b) and (122), by the

relations

$$\dot{\mathbf{R}}_i = \mathbf{R}_i + \frac{\partial \mathbf{u}}{\partial x^I}, \quad G_{ij} = \dot{\mathbf{R}}_i \dot{\mathbf{R}}_j. \quad (1.133)$$

Then the components of strain tensor (132) will have the form

$$\gamma_{ij} = \frac{1}{2} (\dot{\mathbf{R}}_i \dot{\mathbf{R}}_j - \mathbf{R}_i \mathbf{R}_j) = \frac{1}{2} [(\mathbf{R}_i + \mathbf{u}_i)(\mathbf{R}_j + \mathbf{u}_j) - \mathbf{R}_i \mathbf{R}_j] = \\ = \frac{1}{2} (\mathbf{R}_i \mathbf{u}_j + \mathbf{R}_j \mathbf{u}_i + \mathbf{u}_i \mathbf{u}_j). \quad (1.134)$$

Let us now consider a thin-walled shell. We denote by $\mathbf{r}(x^1, x^2)$ and $\mathbf{n}(x^1, x^2)$ the radius vector of some point of the middle surface of the undeformed shell and the unit vector of the normal passing through this point. The curvilinear coordinates in the middle surface are represented by x^1 and x^2 .

The radius vector of an arbitrary point of the shell, located at a distance $x^3 = z$ from the middle surface along the normal, will be

$$\mathbf{R} = \mathbf{r}(x^1, x^2) + z\mathbf{n}(x^1, x^2). \quad (1.135)$$

The basis vectors associated with the coordinate system of the shell according to (b) will be

$$\mathbf{r}_\alpha = \frac{\partial \mathbf{r}}{\partial x^\alpha}, \quad \mathbf{n}_\beta = \frac{\partial \mathbf{n}}{\partial x^\beta} \quad (\alpha, \beta = 1, 2). \quad (1.136)$$

We introduce into consideration the components of tensors of the first and second quadratic form:

$$a_{\alpha\beta} = \mathbf{r}_\alpha \mathbf{r}_\beta, \quad b_{\alpha\beta} = -\mathbf{r}_\alpha \mathbf{n}_\beta. \quad (1.137)$$

The first quadratic form (see book [0.6], pp. 472, 474) represents the lengths

of the arcs, the angles between the curves, and the areas of the regions on the surface. The second quadratic form makes it possible to determine the normal curvatures of the surface.

From Weingarten's formulas* we have

$$b_{\alpha\gamma}n = \frac{\partial r_\gamma}{\partial x^\alpha}, \quad n_\beta = -b_{\alpha\beta}r^\alpha = -b_\beta^\alpha r_\alpha. \quad (1.138)$$

Then**

$$\begin{aligned} R_\alpha &= r_\alpha + z n_\alpha = r_\alpha - z b_{\alpha\gamma} r^\gamma, \\ g_{\alpha\beta} = R_\alpha R_\beta &= (r_\alpha + z n_\alpha)(r_\beta + z n_\beta) = (r_\alpha - z b_{\alpha\gamma} r^\gamma)(r_\beta - z b_{\beta\lambda} r^\lambda). \end{aligned}$$

We will introduce the assumption of constancy of the metric along the shell thickness, i.e., will assume that $z b_{\alpha\beta} \ll 1$. Then the basis vectors and metric tensors become

$$\begin{aligned} R_\alpha &= r_\alpha, \quad R_3 = n, \quad g_{\alpha\beta} = r_\alpha r_\beta = a_{\alpha\beta}, \\ g_{\alpha 3} &= 0, \quad g_{33} = R_3 R_3 = nn = 1. \end{aligned} \quad (1.139)$$

Let us recall that vectors r_α and n are orthogonal, and $r_\alpha n = 0$.

We represent the vector of displacement of the arbitrary point in the form

$$u = u^a r_a + u^3 n = u_a r^a + u_3 n. \quad (1.140)$$

The relations representing the distribution of displacements over the shell thickness will be written in the form

*See I.N. Vekua's book mentioned above, p. 80.

**Hereinafter, the index $\gamma = 1, 2$ is used; it must not be confused with the symbol γ_{ij} for components of the strain tensor.

$$u_a = \frac{\partial u}{\partial x^a} = \frac{\partial u^\gamma}{\partial x^a} r_\gamma + u^\gamma \frac{\partial r_\gamma}{\partial x^a} + \frac{\partial u_3}{\partial x^a} n + u_3 \frac{\partial n}{\partial x^a}, \quad (1.141)$$

$$u_3 = \frac{\partial u}{\partial x^3} = \frac{\partial u^a}{\partial x^3} r_a + \frac{\partial u_3}{\partial x^3} n. \quad (1.142)$$

In tensor analysis, instead of the ordinary partial derivatives, covariant and contravariant derivatives are introduced. A characteristic feature of covariant and contravariant differentiation is that by applying these operations to a tensor, we again obtain a tensor.

The covariant derivatives of components u^γ , u_γ of vector u are related to partial derivatives as follows:

$$\nabla_a u^\gamma = \frac{\partial u^\gamma}{\partial x^a} + \Gamma_{\alpha\beta}^\gamma u^\beta, \quad (1.143a)$$

$$\nabla_a u_\gamma = \frac{\partial u_\gamma}{\partial x^a} - \Gamma_{\alpha\gamma}^\beta u_\beta. \quad (1.143b)$$

The symbol ∇_α denotes the operation of covariant differentiation. Quantities of the type $\Gamma_{\alpha\beta}^\gamma$ are called Christoffel symbols of the second kind:

$$\Gamma_{\alpha\beta}^\gamma = \Gamma_{\beta\alpha}^\gamma = r^\gamma r_{\alpha\beta} = r^\gamma r_{\beta\alpha}.$$

In orthogonal Cartesian coordinates, the Christoffel symbols are equal to zero, and the covariant derivatives are the same as ordinary partial derivatives.

The derivative of basis vector r_γ along the x^α coordinate is

$$r_{\gamma\alpha} = \frac{\partial r_\gamma}{\partial x^\alpha} = \Gamma_{\gamma\alpha}^\beta r_\beta + b_{\gamma\alpha} n. \quad (1.143c)$$

Similarly,

$$\frac{\partial r^\gamma}{\partial x^\alpha} = - \Gamma_{\alpha\beta}^\gamma r^\beta + b_{\alpha\gamma} n. \quad (1.143d)$$

Formulas (143c) and (143d) are called the Gauss derivation formulas.

Using these formulas and Weingarten's formula (138), we transform relation (141) into

$$\begin{aligned} u_a &= (\nabla_a u_\gamma) r^\gamma + u^\gamma b_{a\gamma} n + (\nabla_a u_3) n - u_3 b_{a\gamma} r^\gamma = \\ &= (\nabla_a u_\gamma - u_3 b_{a\gamma}) r^\gamma + n (u^\gamma b_{a\gamma} + \nabla_a u_3). \end{aligned} \quad (1.144)$$

We introduce the notation

$$e_{ay} = \nabla_a u_\gamma - u_3 b_{a\gamma}, \quad \theta_a = u^\gamma b_{a\gamma} + \nabla_a u_3 \quad (1.145)$$

and represent (144) in the form

$$u_a = e_{ay} r^\gamma + \theta_a n. \quad (1.146)$$

Substituting expressions (139) and (146) into (134), we arrive at the following relations (taking $e_a^Y = e_a \cdot Y$)

$$\left. \begin{aligned} \gamma_{ab} &= \frac{1}{2} (r_a u_b + r_b u_a + u_a u_b) = \frac{1}{2} (e_{ab} + e_{ba} + e_a^Y e_{bY} + \theta_a \theta_b), \\ \gamma_{a3} &= \frac{1}{2} (r_a u_3 + n u_a + u_a u_3) = \frac{1}{2} \left(\frac{\partial u_a}{\partial x^3} + \theta_a + e_{a3} \frac{\partial u_b}{\partial x^3} \right), \\ \gamma_{33} &= \frac{1}{2} (2 n u_3 + u_3 u_3) = \frac{1}{2} \frac{\partial u_a}{\partial x^3} \frac{\partial u_a}{\partial x^3}. \end{aligned} \right\} \quad (1.147)$$

The displacements u_a will be assumed to change along the shell thickness in accordance with the law

$$u_a = v_a(x^1, x^2, t) + z \psi_a(x^1, x^2, t). \quad (1.148a)$$

As far as the displacement u_3 is concerned, as we agreed earlier, we will assume

$$u_3 = w(x^1, x^2, t). \quad (1.148b)$$

We introduce expressions (148) and (145): we first obtain

$$e_{\alpha\beta} = \nabla_\alpha u_\beta - u_\beta t_{\alpha\beta} = e_{\alpha\beta} + z\nabla_\alpha \psi_\beta, \quad (1.149)$$

where

$$e_{\alpha\beta} = \nabla_\alpha v_\beta - b_{\alpha\beta} w. \quad (1.150)$$

Then

$$\left. \begin{aligned} e_{\beta\alpha} &= e_{\beta\alpha} + z\nabla_\beta \psi_\alpha, \\ e_\alpha^\gamma &= \nabla_\alpha (v^\gamma + z\psi^\gamma) - b_\alpha^\gamma w = e_\alpha^\gamma + z\nabla_\alpha \psi^\gamma. \end{aligned} \right\} \quad (1.151)$$

Finally, we have

$$\left. \begin{aligned} \theta_\alpha &= u^\gamma b_{\alpha\beta} + \nabla_\alpha u_\beta = \omega_\alpha + z b_{\alpha\gamma} \psi^\gamma, \\ \theta_\beta &= u^\gamma b_{\beta\alpha} + \nabla_\beta u_\alpha = \omega_\beta + z b_{\beta\gamma} \psi^\gamma. \end{aligned} \right\} \quad (1.151a)$$

Here we introduce the notation

$$\omega_\alpha = \nabla_\alpha w + b_{\alpha\gamma} v^\gamma. \quad (1.152)$$

Substituting the last relations into (147) and neglecting the terms containing z^2 as small ones of higher order, we obtain the following expressions for the strains:

$$\left. \begin{aligned} \gamma_{\alpha\beta} &= \frac{1}{2} [e_{\alpha\beta} + e_{\beta\alpha} + e_\alpha^\gamma e_{\beta\gamma} + \omega_\alpha \omega_\beta + z(\nabla_\alpha \psi_\beta + \nabla_\beta \psi_\alpha + \\ &\quad + r_\alpha^\gamma \nabla_\beta \psi_\gamma + e_{\beta\gamma} \nabla_\alpha \psi^\gamma + b_\beta^\gamma \omega_\alpha \psi_\gamma + b_\alpha^\gamma \omega_\beta \psi_\gamma)], \\ \gamma_{\alpha\gamma} &= \frac{1}{2} [\omega_\alpha + \psi_\alpha + \psi^\gamma e_{\alpha\gamma} + z(b_\alpha^\gamma \psi^\gamma + \psi^\gamma \nabla_\alpha \psi_\gamma)], \\ \gamma_{\alpha\alpha} &= \frac{1}{2} \psi^\gamma \psi_\gamma. \end{aligned} \right\} \quad (1.153)$$

Hooke's law in the general case may be written in the form

$$\sigma^{\alpha\beta} = E^{\alpha\beta\gamma\delta} \gamma_{\gamma\delta} \quad (\alpha, \beta, \dots = 1, 2, 3), \quad (1.154)$$

where the elasticity tensor $E^{\alpha\beta\gamma\delta}$ for isotropic bodies

$$E^{\alpha\beta\gamma\delta} = \lambda g^{\alpha\delta}g^{\gamma\beta} + 2\mu g^{\alpha\gamma}g^{\beta\delta}. \quad (1.155)$$

The forces and moments per unit length of cross section of the shell are expressed as follows:

$$N^{\alpha\beta} = \int_{-h/2}^{h/2} \sigma^{\alpha\beta} dz, \quad M^{\alpha\beta} = \int_{-h/2}^{h/2} z\sigma^{\alpha\beta} dz, \quad Q^{\alpha} = \int_{-h/2}^{h/2} \sigma^{\alpha 3} dz. \quad (1.156)$$

For an isotropic body, relation (154) also takes the form

$$\sigma^{\alpha\beta} = \lambda \theta g^{\alpha\beta} + 2\mu \gamma^{\alpha\beta}. \quad (1.157)$$

Here γ and θ are the Lame coefficients and θ is the volume expansion:

$$\theta = g^{\alpha\beta}\gamma_{\alpha\beta}. \quad (1.158)$$

In (157), we took

$$\gamma^{\alpha\beta} = g^{\alpha\gamma}g^{\beta\delta}\gamma_{\gamma\delta}.$$

Considering (139), we have: $g_{\alpha\beta} = \delta_{\alpha\beta}$; instead of (155), we find

$$E^{\alpha\beta\gamma\delta} = \lambda \alpha^{\alpha\delta}\alpha^{\gamma\beta} + 2\mu \alpha^{\alpha\gamma}\alpha^{\beta\delta} \quad (\alpha, \beta, \dots = 1, 2). \quad (1.159)$$

The expression for γ_{33} in terms of $\gamma_{\alpha\beta}$ is found from the usual condition $\delta^{33} = 0$ and is substituted into the relation for $\delta^{\alpha\beta}$. When integrating according to (156), the relations for strains (153) are used.

As we know, the Lame parameters are

$$\lambda = \frac{E\mu}{(1+\mu)(1-2\mu)}, \quad \mu = \frac{E}{2(1+\mu)}.$$

Thus, we find

$$N^{ab} = \frac{Eh}{2(1-\mu^2)} P^{ab\gamma\delta} (\epsilon_{\gamma\delta} + c_{\delta\gamma} + c_\gamma^\alpha c_{\delta\alpha} + \omega_\gamma \omega_\delta), \quad (1.160)$$

$$\begin{aligned} M^{ab} = \frac{1}{24} \frac{Eh^3}{(1-\mu^2)} P^{ab\gamma\delta} & (\nabla_\gamma \psi_\delta + \nabla_\delta \psi_\gamma + c_\gamma^\alpha \nabla_\delta \psi_\alpha + c_{\delta\alpha} \nabla_\gamma \psi_\alpha + \\ & + b_\delta^\alpha \omega_\gamma \psi_\alpha + b_\gamma^\alpha \omega_\delta \psi_\alpha), \end{aligned} \quad (1.161)$$

$$Q^a = \frac{k^2 Eh}{2(1+\mu)} (\omega_a + \psi_a + \psi^\alpha e_{\alpha\gamma}). \quad (1.162)$$

$$P^{ab\gamma\delta} = a^{\alpha\gamma} a^{\beta\delta} + \mu c^{\alpha\gamma} c^{\beta\delta}.$$

Here

c^{ab} denotes the components of the discriminant tensor and k^2 is the known coefficient of shear.

The law of stress distribution over the thickness of the shell is expressed by the relations

$$\sigma^{ab} = \frac{1}{h} N^{ab}(x^1, x^2, t) + \frac{12\mu}{h^3} M^{ab}(x^1, x^2, t), \quad (1.163)$$

$$\sigma^{a3} = \frac{1}{h} Q^a(x^1, x^2, t) f(z), \quad v^{33} = 0. \quad (1.164)$$

where f stands for the function discussed in § 10; it satisfies the conditions

$$f(-z) = f(z), \quad \frac{1}{h} \int_{-h/2}^{h/2} f dz = 1, \quad \frac{1}{h} \int_{-h/2}^{h/2} f^2 dz = \frac{1}{h^3}, \quad \int_{-h/2}^{h/2} z f dz = 0. \quad (1.165)$$

15. Equations of Motion

To derive the equations of motion, we will again use the Hamilton-Ostrogradskiy principle. The corresponding equation, analogous to (67), will be

$$\int_t^t (\delta K - \delta \Pi + \delta' W) dt = 0. \quad (1.166)$$

The potential deformation energy Π for a three-dimensional body

$$\Pi = \frac{1}{2} \int_V \sigma^{ik} \gamma_{ik} dV.$$

Here dV is the volume element. For curvilinear coordinates in the case of a shell, we have (taking $a = ||\alpha_{\alpha\beta}|| = 1$):

$$\Pi = \frac{1}{2} \int_S \int_{-h/2}^{h/2} (\sigma^{\alpha\beta} \gamma_{\alpha\beta} + 2\sigma^{\alpha\gamma} \gamma_{\alpha\gamma}) dS dz, \quad (1.167)$$

where dS is the area element of the middle surface.

We substitute the expressions for stresses (163), (164) and values of strains (153). Considering (165), we find

$$\begin{aligned} \Pi = & \frac{1}{2} \int \left\{ \frac{1}{2} N^{\alpha\beta} (\epsilon_{\alpha\beta} + \epsilon_{\beta\alpha} + \epsilon_\alpha^\gamma \epsilon_{\beta\gamma} + \omega_\alpha \alpha_\beta) + \right. \\ & + \frac{1}{2} M^{\alpha\beta} (\nabla_\alpha \psi_\beta + \nabla_\beta \psi_\alpha + \epsilon_\alpha^\gamma \nabla_\beta \psi_\gamma + \epsilon_{\beta\gamma} \nabla_\alpha \psi_\gamma + b_\beta^\gamma \omega_\alpha \psi_\gamma + \\ & \left. + b_\alpha^\gamma \omega_\beta \psi_\gamma) + Q^\alpha (\omega^\alpha + \psi_\alpha + \psi^\gamma \epsilon_{\alpha\gamma}) \right\} dS. \end{aligned} \quad (1.168)$$

We represent this expression as a sum of three functions:

$$\Pi = \Pi_c + \Pi_b + \Pi_s.$$

Component Π_m corresponds to the strain energy in the median surface; Π_b is the bending strain energy; Π_s is the strain energy of transverse shear.

Using relations (150) and (152), we rewrite the expressions for these components in the form

$$\Pi_e = \frac{1}{2} \int_s N^{ab} [v_a v_b - w b_{ab} + \frac{1}{2} c^r \nabla_b v_r + \frac{1}{2} \omega_a (\nabla_b w + b_{br} v^r)] dS, \quad (1.169)$$

$$\Pi_u = \frac{1}{2} \int_s M^{ab} [\nabla_a \psi_b + \frac{1}{2} (\nabla_b v^r \nabla_a \psi_r - b^r_b w \nabla_a \psi_r + b^r_b \psi_r \nabla_a w + b^r_b b_{ar} v^r \psi_r)] dS, \quad (1.170)$$

$$\Pi_{cas} = \frac{1}{2} \int_s Q^r [\nabla_a w + v^a b_{ar} + \psi_u + \psi^r \nabla_a v_r - \psi^r b_{ar} w] dS. \quad (1.171)$$

In the general case, the kinetic energy is determined by means of the expression

$$K = \frac{1}{2} \int_V \int \int \frac{\gamma}{g} \frac{\partial u_i}{\partial t} \frac{\partial u^i}{\partial t} dV.$$

Substituting (148), we obtain for a shell

$$K = \frac{1}{2} \frac{\gamma}{g} h \int_s (\dot{v}_a v^a + \dot{w}^2 + \frac{h^2}{12} \dot{\psi}_a \dot{\psi}^a) dS. \quad (1.172)$$

The dots denote time derivatives.

The elementary work done by external forces

$$\delta' W = \int_s (p^\alpha \delta v_\alpha + q \delta w + m^\alpha \delta \psi_\alpha) ds + \quad (1.173) \\ + \int_C (N^\alpha \delta v_\alpha + N \delta w + M^\alpha \delta \psi_\alpha) dc.$$

Here C is the contour of the undeformed shell to which are applied the components of external load N^α , N , and M^α . The symbols p^α , q and m^α denote the intensities of distributed external loads - the tangential, transverse and moment loads.

We will find the variations of total potential energy in terms of the variables v_α , w , ψ_ζ . After calculations similar to the preceding one (p. 42), we obtain

$$\begin{aligned}\delta_v \Pi = & \frac{1}{2} \int_c [N^{ab} (\delta_a^v + c_a^v) n_b + M^{ab} \nabla_a \psi^b n_b + \psi^b Q^a n_a] \delta v_b ds - \\ & - \frac{1}{2} \int_s [\nabla_a N^{ab} + \nabla_b (c_a^b N^{av}) - b_{av}^b N^{av} + \nabla_v (\nabla_a \psi^b M^{av}) - \\ & - b_{av}^b b_{av}^b \psi_a M^{av} - b_a^b Q^a + \nabla_a (\psi^b Q^a)] \delta v_b ds, \end{aligned} \quad (1.174)$$

$$\begin{aligned}\delta_w \Pi = & \frac{1}{2} \int_c [Q_a n_a + c_a N^{ab} n_b + b_a^b M^{ab} \psi_b n_b] \delta w ds - \\ & - \frac{1}{2} \int_s [\nabla_a Q^a + b_{av} N^{av} + b_{av}^b c_{av} N^{av} + \nabla_a (N^{av} \omega_p) + \\ & + \nabla_b (M^{ab} b_{av}^b \psi_v) + b_{av}^b M^{av} \nabla_a \psi_v + b_{av}^b \psi_b Q^a] \delta w ds, \end{aligned} \quad (1.175)$$

$$\begin{aligned}\delta_\psi \Pi = & \frac{1}{2} \int_c M^{ab} (\delta_a^\psi + c_a^\psi) n_b \delta \psi_b ds - \\ & - \frac{1}{2} \int_s [\nabla_a M^{ab} - Q^a - c_a^b Q^a - \nabla_v (M^{av} c_a^b) - b_a^b M^{av} \omega_v] \delta \psi_b ds. \end{aligned} \quad (1.176)$$

Here n_α is the component of the unit vector of the normal to the contour of the undeformed shell.

The kinetic energy variation is

$$\begin{aligned}\delta \int_t K dt = & \frac{\gamma h}{g} \frac{h}{2} \int_s [\delta^a \delta v_a + \dot{\psi} \delta w + \frac{h^2}{12} \dot{\psi}^a \delta \psi_a] ds - \\ & - \frac{\gamma h}{g} \frac{h}{2} \int_t \int_s [\delta^a \delta v_a + \dot{\psi} \delta w + \frac{h^2}{12} \dot{\psi}^a \delta \psi_a] ds dt. \end{aligned} \quad (1.177)$$

We will sum up the variations of potential energy (174)-(176) and together with expressions (173) and (177), substitute into (166). In view of the arbitrariness of the variations δv_α , δw , $\delta \psi_\alpha$ the condition of fulfillment of relation (166) will be the equality to zero of the coefficients of these variations. Hence the equations of motion

$$\begin{aligned}\nabla_a N^{ab} - b_a^b Q^a + \nabla_v (c_a^b N^{av}) - b_{av}^b \omega_a N^{av} + \nabla_a (\nabla_v \psi^b M^{av}) - \\ - b_{av}^b b_{av}^b \psi_a M^{av} + \nabla_a (\psi^b Q^a) - \frac{\gamma}{\mu} h \ddot{\psi}^a + p^a = 0, \end{aligned} \quad (1.178)$$

$$\begin{aligned} v_a Q^a + b_{ab} N^{ab} + v_\beta (\omega_a N^{ab}) + b_b^y v_{ay} N^{ab} + v_\beta (b_a^y \psi_y M^{ab}) + \\ + b_b^y v_a (\psi_y M^{ab}) + b_a^y \psi_\beta Q^a - \frac{y}{k} h \ddot{\omega} + q = 0, \end{aligned} \quad (1.179)$$

$$v_a M^{ab} - Q^b - c_a^b Q^a + v_y (c_a^b M^{ay}) - b_a^b \omega_y M^{ay} - \frac{y}{k} I \ddot{\psi}^b + m^b = 0, \quad (1.180)$$

where $I = h^3/12$.

The boundary conditions relate the forces and displacements on the shell contour to the loads applied along the contour. Assuming $\delta v_\beta \neq 0$, we will have

$$N^{ab} (\delta_a^y + c_a^y) n_\beta + M^{ab} v_\beta \psi^y n_a + \psi^a Q^b n_a - \eta^b = 0. \quad (1.181)$$

Then for $\delta w \neq 0$

$$Q_a n_a + \omega_a N^{ab} n_\beta + b_a^y M^{ab} \psi_y n_\beta - N = 0 \quad (1.182)$$

and for $\delta \psi_y \neq 0$

$$M^{ab} (\delta_a^y + c_a^y) n_\beta - \eta^y = 0. \quad (1.183)$$

Let us consider the case where the coordinate lines in the middle surface of the shell are lines of curvature. Then $b_1^2 = 0$. In addition, we will consider Cartesian coordinates and assume the curvatures along the coordinate lines to be constant: $b_1^1 = k_x$, $b_2^2 = k_y$. We will represent the equations of motion (178)-(180) for this case in scalar form.

As an example, we will transform the first of the terms in Eq. (178). We obtain

$$v_a N^{ab} = v_1 N^{1b} + v_2 N^{2b}.$$

For $\beta = 1$ we have

$$v_1 N^{11} + v_2 N^{21} = N_{x,x} + T_y$$

for $\beta = 2$

$$\nabla_1 N^{12} + \nabla_2 N^{21} = T_x + N_{y,y}$$

The subscript after the comma denotes the variable with respect to which the differentiation is performed.

The next term in (178) may be represented in the form

$$b_\alpha^\beta Q^\alpha = b_1^\beta Q^1 + b_2^\beta Q^2.$$

For instance, for $\beta = 1$,

$$b_1^1 Q^1 + b_2^1 Q^2 = k_x Q_x.$$

Finally, for the third term we have

$$\nabla_y (e_0^\beta N^{\alpha\gamma}) = \nabla_1 (e_1^\beta N^{11} + e_2^\beta N^{21}) + \nabla_2 (e_1^\beta N^{12} + e_2^\beta N^{22}).$$

For $\beta = 1$ we have

$$\begin{aligned} \nabla_1 (e_1^1 N^{11} + e_2^1 N^{21}) + \nabla_2 (e_1^1 N^{12} + e_2^1 N^{22}) &= \\ &= [(u_{,x} - k_x w) N_x + u_{,y} T]_{,x} + [(u_{,x} - k_x w) T + u_{,y} N_y]_{,y}. \end{aligned}$$

Performing similar operations over the remaining terms, we arrive at the following equations:

$$\begin{aligned} N_{x,x} + T_{x,y} - k_x Q_x + [N_x(u_{,x} - k_x w) + T u_{,y}]_{,x} + \\ + [T(u_{,x} - k_x w) + u_{,y} N_y]_{,y} - k_x [N_x(w_{,x} + k_x u) + \\ + T(w_{,y} + k_y v)] + [(M_x \psi_x)_{,x} + (H \psi_x)_{,y}]_{,x} + \\ + [(H \psi_x)_{,x} + (M_y \psi_x)_{,y}]_{,y} - k_x [M_x \psi_x k_x + H \psi_y k_y] + \\ + (\psi_x Q_x)_{,x} + (\psi_y Q_y)_{,y} - \frac{Y}{K} h u_{,ll} + p_A = 0, \end{aligned} \quad (1.184)$$

$$\begin{aligned}
& \underline{Q}_{x,z} + \underline{Q}_{y,y} + k_x N_x + k_y N_y + [N_x(\underline{w}_{,z} + k_x u) + \\
& + (\underline{w}_{,y} + k_y v) T]_{,z} + [\underline{T}(\underline{w}_{,z} + k_x u) + N_y(\underline{w}_{,y} + k_y v)]_{,y} + \\
& + k_x [N_x(u_{,z} - k_x w) + u_{,y} T] + k_y [v_{,z} T + (v_{,y} - k_y w) N_y] + \\
& + [M_x k_x \psi_x + H k_y \psi_y]_{,z} + [H k_x \psi_x + M_y k_y \psi_y]_{,y} + \\
& + k_x [(M_x \psi_x)_{,z} + (H \psi_y)_{,y}] + k_y [(H \psi_y)_{,z} + (M_y \psi_y)_{,y}] + \\
& + k_x Q_x \psi_x + k_y Q_y \psi_y - \frac{Y}{E} h w_{,tt} + q = 0, \tag{1.185}
\end{aligned}$$

$$\begin{aligned}
& \underline{M}_{x,z} + \underline{H}_{,y} - \underline{Q}_x - Q_x(u_{,z} - k_x w) - Q_y u_{,y} + \\
& + [H u_{,y} + M_x(u_{,z} - k_x w)]_{,z} + [M_y u_{,y} + H(u_{,z} - k_x w)]_{,y} - \\
& - k_x [M_x(w_{,z} - k_x u) + H(w_{,y} + k_y v)] - \frac{Y}{E} I \psi_{,ttt} + m_x = 0. \tag{1.186}
\end{aligned}$$

The symbols p_x , q and m_x represent the intensities of the corresponding distributed loads.

In addition, by analogy with Eq. (184) and (186), two more equations can be written down.

We obtained the equations in a more complete form as compared with those derived earlier. The terms which appeared in the preceding equations (75)-(79) are underlined here. Keeping only these terms is analogous to the assumption of smallness of the derivatives of tangential components of the displacement vector in comparison with the derivatives of normal deflection, an assumption made for slightly curved shells.

Let us turn to the boundary conditions for the edge $x = \text{const}$. Taking $n_1 = 1$, $n_2 = 0$ in (181)-(183), we obtain the following five boundary conditions:

$$N_x(1 + u_{,z} - k_x w) + T u_{,y} + M_x \psi_{x,z} + H \psi_{x,y} + Q_x \psi_x - N_x^0 = 0, \tag{1.187}$$

$$N_x v_{,x} + T(1 + v_{,y} - k_y w) + M_x \psi_{y,x} + H \psi_{y,y} + Q_y \psi_y - T^0 = 0, \tag{1.188}$$

$$\underline{Q}_x + (\underline{w}_{,z} + k_x u) \underline{N}_x + (\underline{w}_{,y} + k_y v) \underline{T} + M_x k_x \psi_x + H k_y \psi_y - Q_x^0 = 0, \tag{1.189}$$

$$\underline{M}_x(1 + u_{,z} - k_x w) + H u_{,y} - M_x^0 = 0, \tag{1.190}$$

$$M_x v_{,x} + H(1 + v_{,y} - k_y w) - H^0 = 0. \tag{1.191}$$

Here N_x^0 and T^0 represent the external forces in the middle surface applied along

the edge $x = \text{const}$, Q_x^0 is the transverse force, and M_x^0 and H^0 are the intensities of the moment loads.

We have again arrived at the five dynamic boundary conditions which correspond to the kinematic parameters u , v , w , ψ_x and ψ_y . As before, the "principal" forces N_x , T , Q_x , M_x and H participate in conditions (187)-(191); let us recall that we obtained the same result above (§ 12). However, this time the boundary conditions have been obtained in more precise form; the terms which appeared previously are underlined. The geometric boundary conditions are the same as those appearing in (81)-(89).

In the subsequent presentation, we will mostly use the Kirchhoff-Love model. With a certain approximation, this model permits us to describe the dynamic processes of interest, including those that are associated with elastic wave propagation. However, for some problems we will use the second approximation model; we will also try to determine the characteristics of both models in connection with the application of different methods of solution.

16. Shells Beyond Elastic Limits

Let us now consider the case in which the deformations of a shell are plasto-elastic. In treating this case, we must use one of the theories of plasticity. As we know, in the literature, use is made of relations based on different theories, i.e., the theory of flow, deformation, local deformations and others. The first two of these theories have been most frequently used thus far for studying dynamic problems. The present book will use both the theory of flow (Chapter VII) and deformation theory (Chapter VIII). We will now examine the relationships of deformation theory in more detail.

We will use a $\delta(\epsilon)$ diagram obtained from experiments with uniaxial extension of a sample of a given material (Figure 1.21). Under small deformations, most structural materials deform elastically. The slope of the tangent to the modulus E . We draw a tangent to the curve at some point A; in this case, the straight line AB no longer

passes through the origin, and the properties of the material at point A can be described by two parameters: tangent modulus $E_t = d\delta/d\epsilon$ and secant modulus $E_s = \delta/\epsilon$. Obviously, E_t and E_s are functions of deformation. Poisson's ratio μ in the elastic region ranges from 0.25 to 0.33 for many materials. When plastic strains arise, μ increases rapidly, approaching the limiting value $\mu = 0.5$.

In the case of compound stress, the concept of stress intensity σ_i and strain intensity ϵ_i is introduced:

$$\left. \begin{aligned} \sigma_i &= \frac{1}{\sqrt{2}} \sqrt{(\sigma_x - \sigma_y)^2 + (\sigma_y - \sigma_z)^2 + (\sigma_z - \sigma_x)^2 + 6(\tau_{xy}^2 + \tau_{xz}^2 + \tau_{yz}^2)}, \\ \epsilon_i &= \frac{\sqrt{2}}{9} \sqrt{(\epsilon_x - \epsilon_y)^2 + (\epsilon_y - \epsilon_z)^2 + (\epsilon_z - \epsilon_x)^2 + \frac{3}{2}(\gamma_{xy}^2 + \gamma_{xz}^2 + \gamma_{yz}^2)}. \end{aligned} \right\} \quad (1.192)$$

These expressions are invariant, i.e., retain their value as the orientation of the coordinate system changes. Let us assume that the strain intensity at a given point increases, and that the simple loading condition is fulfilled. The components of the stress and strain tensors are related as follows:

$$\left. \begin{aligned} \epsilon_x - \frac{1}{3}\theta &= \frac{3}{2E_c}(\sigma_x - S), \\ \epsilon_y - \frac{1}{3}\theta &= \frac{3}{2E_c}(\sigma_y - S), \\ \epsilon_z - \frac{1}{3}\theta &= \frac{3}{2E_c}(\sigma_z - S), \\ \gamma_{xy} &= \frac{3}{E_c} \tau_{xy}, \quad \gamma_{yz} = \frac{3}{E_c} \tau_{yz}, \quad \gamma_{xz} = \frac{3}{E_c} \tau_{xz}. \end{aligned} \right\} \quad (1.193)$$

θ represents the volume strain

$$\theta = \epsilon_x + \epsilon_y + \epsilon_z.$$

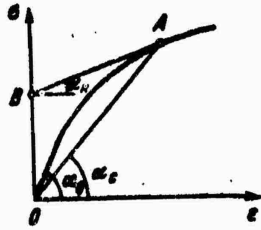


Figure 1.21. Concerning the determination of the principal, secant and tangent moduli.

and S , the average normal stress

$$S = \frac{\sigma_x + \sigma_y + \sigma_z}{3};$$

they are related as follows:

$$\theta = \frac{3(1-2\mu)}{E} S.$$

For an incompressible material, $\theta = 0$.

In conformity with the adopted model, the expressions for δ_i and ϵ_i will be different in form. Below, we will consider Timoshenko's earlier model, which allows for transverse shear; in this case, all that is necessary is to set $\epsilon_z = 0$, $\delta_z = 0$ in (192). After some obvious transformations, we obtain the expressions for the strain and stress intensities which will be used below:

$$\left. \begin{aligned} \sigma_i &= \sqrt{\sigma_x^2 - \sigma_x \sigma_y + \sigma_y^2 + 3(\tau_{xy}^2 + \tau_{xz}^2 + \tau_{yz}^2)}, \\ \epsilon_i &= \frac{2}{\sqrt{3}} \sqrt{\epsilon_x^2 + \epsilon_x \epsilon_y + \epsilon_y^2 + \frac{1}{4}(\gamma_{xy}^2 + \gamma_{xz}^2 + \gamma_{yz}^2)}. \end{aligned} \right\} \quad (1.194)$$

If however a decrease in strain intensity takes place at some point, relations (193) should be replaced with others, pertaining to load removal.

Considering that only the elastic components of strain change in the course of load removal, we can write

$$\left. \begin{aligned} \sigma_x &= \sigma_x^* + \frac{1}{3} E \left[\left(\epsilon_x + \frac{1}{2} \epsilon_y \right) - \left(\epsilon_x^* + \frac{1}{2} \epsilon_y^* \right) \right], \\ \sigma_y &= \sigma_y^* + \frac{1}{3} E \left[\left(\epsilon_y + \frac{1}{2} \epsilon_x \right) - \left(\epsilon_y^* + \frac{1}{2} \epsilon_x^* \right) \right], \\ \tau_{xy} &= \tau_{xy}^* + \frac{1}{3} E (\gamma_{xy} - \gamma_{xy}^*), \\ \tau_{xz} &= \tau_{xz}^* + \frac{1}{3} E (\gamma_{xz} - \gamma_{xz}^*), \\ \tau_{yz} &= \tau_{yz}^* + \frac{1}{3} E (\gamma_{yz} - \gamma_{yz}^*); \end{aligned} \right\} \quad (1.195)$$

where the asterisk denotes the loads and strains at the given point at the start of load removal. It is evident that in the elastic region, relations (193) and (195) are the same as generalized Hooke's law.

The regions of active plastic strains and load removal are separated by the surface $\delta e_i / \delta t = 0$.

Let us now turn to the Timoshenko-type equations obtained in 12. It is evident that the equations of motion of the shell element in forces and moments will also remain unchanged in the presence of plastic strain; only the expressions relating the forces and moments to the displacements will change.*

Keeping in mind that the strains $\epsilon_x^z, \epsilon_y^z, \dots$ are related by expressions of the type of (55)

*This problem was studied in the linear formulation by M.P. Galin (Inzh. sb. 31, 1961); the above relations were obtained by V.A. Fel'dshteyn.

$$\left. \begin{aligned} e_x^* &= e_x + z \frac{\partial \psi_x}{\partial x}, \quad e_y^* = e_y + z \frac{\partial \psi_y}{\partial y}, \\ \gamma_{xy}^* &= \gamma_{xy} + z \left(\frac{\partial \psi_x}{\partial y} + \frac{\partial \psi_y}{\partial x} \right), \quad \gamma_{xz}^* = \gamma_{xz}, \quad \gamma_{yz}^* = \gamma_{yz}, \end{aligned} \right\} \quad (1.196)$$

we rewrite the expression for the strain intensity in the form

$$c_t = \frac{2}{\sqrt{3}} \sqrt{P_2 z^2 + 2P_1 z + P_0}, \quad (1.197)$$

where

$$\begin{aligned} P_0 &= e_x^2 + e_x e_y + e_y^2 + \frac{1}{4} (\gamma_{xz}^2 + \gamma_{yz}^2 + \gamma_{xy}^2), \\ P_1 &= \frac{\partial \psi_x}{\partial x} \left(e_x + \frac{1}{2} e_y \right) + \frac{\partial \psi_y}{\partial y} \left(e_y + \frac{1}{2} e_x \right) + \frac{1}{4} \gamma_{xy} \left(\frac{\partial \psi_x}{\partial y} + \frac{\partial \psi_y}{\partial x} \right), \\ P_2 &= \left(\frac{\partial \psi_x}{\partial x} \right)^2 + \frac{\partial \psi_x}{\partial x} \frac{\partial \psi_y}{\partial y} + \left(\frac{\partial \psi_y}{\partial y} \right)^2 + \frac{1}{4} \left(\frac{\partial \psi_x}{\partial y} + \frac{\partial \psi_y}{\partial x} \right). \end{aligned}$$

It is easy to ascertain that the surface separating the regions of active plastic strains and load removal have the form

$$\frac{\partial P_2}{\partial t} z^2 + 2 \frac{\partial P_1}{\partial t} z + \frac{\partial P_0}{\partial t} = 0. \quad (1.198)$$

In the general case, both roots of polynomial (198) may be located in the range $(-h/2) < z < h/2$. The first corresponds to the boundary between the regions of primary loading A and load removal B (Figure 1.22), and the second, between the regions of load removal and secondary plastic strains C of opposite sign.

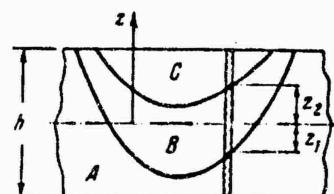


Figure 1.22. Zones of primary loading (A), load removal (B) and secondary plastic strains (C).

We will assume that at the initial stage of deformation, when the flexure of the shell is insignificant, compressive stresses predominate in the shell. As the deflections develop, the outer fibers of the shell elongate in relation to the original compressed stage, forming a region of load removal. Subsequently, the tension strains caused by bending may exceed the yield point, forming a region of secondary plastic strains. In this region the determining relations may be written down on the basis of the theory of cyclic loadings.*

However, this relationship is very difficult to use for integrating, since it is necessary to store in the computer memory the complete information on the stress state in the volume occupied by the shell over the entire duration of the integration. Therefore, two assumptions are used below. We will assume first of all that the load removal occurs in accordance with the linear law. This assumption appears to be valid in the study of transient processes in the case of loads having no well defined vibrational character with substantial amplitude. It can therefore be assumed that the vibrations are not able to develop and are associated with a change of only the elastic components of the stresses.

We will assume further that load removal in different layers along the normal begins at the instant the latter starts in some characteristic layer, for example, in the middle surface. In this case, it becomes necessary to remember only the parameters of the stress state of the middle surface.

Let us turn to the derivation of expressions for the forces and moments. Integrating the stresses and their moments over the shell thickness, we obtain the forces and moments in the region of active plastic strains (the material is considered to be incompressible, $\mu = 0.5$):

*V.V. Moskvitin, Plastichnost' pri peremennykh nagruzeniyakh (Plasticity under variable loadings), MGU, 1965.

$$\left. \begin{aligned}
N_x &= \frac{4}{3} [I_1 (\epsilon_x + \frac{1}{2} \epsilon_y) + I_2 (\chi_x + \frac{1}{2} \chi_y)], \\
N_y &= \frac{4}{3} [I_1 (\epsilon_y + \frac{1}{2} \epsilon_x) + I_2 (\chi_y + \frac{1}{2} \chi_x)], \\
T &= \frac{1}{3} [I_1 \gamma_{xy} + I_2 \left(\frac{\partial \psi_x}{\partial y} + \frac{\partial \psi_y}{\partial x} \right)], \\
Q_x &= \frac{k^2}{3} I_1 \gamma_{xx}, \quad Q_y = \frac{k^2}{3} I_1 \gamma_{yy}, \\
M_x &= \frac{4}{3} [I_2 (\epsilon_x + \frac{1}{2} \epsilon_y) + I_3 (\chi_x + \frac{1}{2} \chi_y)], \\
M_y &= \frac{4}{3} [I_2 (\epsilon_y + \frac{1}{2} \epsilon_x) + I_3 (\chi_y + \frac{1}{2} \chi_x)], \\
H &= \frac{1}{3} [I_2 \gamma_{xy} + I_3 \left(\frac{\partial \psi_x}{\partial y} + \frac{\partial \psi_y}{\partial x} \right)],
\end{aligned} \right\} \quad (1.199)$$

where

$$I_k = \int_{-h/2}^{h/2} \frac{\sigma_k}{c_i} z^{k-1} dz \quad (k = 1, 2, 3), \quad \chi_x = \frac{\partial \psi_x}{\partial x}, \quad \chi_y = \frac{\partial \psi_y}{\partial y}.$$

A characteristic feature of expressions (199) is the fact that in contrast to the elastic problem, the forces acting at the faces of the shell element depend not only on the tension strains of the median surface, but also on the deflection parameter; the moments in turn are determined by both the flexure and the tension. This is due to the nonlinearity of the stress distribution over the shell thickness, determined by the loading curve $\delta_i(e_i)$.

We similarly determine the forces and moments in the load removal zone:

$$\left. \begin{aligned}
N_x &= N_x^* + \frac{4}{3} Eh \left[\left(\epsilon_x^* + \frac{1}{2} \epsilon_y^* \right) - \left(\epsilon_x^* + \frac{1}{2} \epsilon_y^* \right) \right], \\
T &= T^* + \frac{1}{3} Eh (\gamma_{xy}^* - \gamma_{xy}^*), \\
Q_x &= Q_x^* + \frac{1}{3} Eh k^2 (\gamma_{xx}^* - \gamma_{xx}^*), \\
M_x &= M_x^* + \frac{Eh^3}{9} \left[\left(\chi_x^* + \frac{1}{2} \chi_y^* \right) - \left(\chi_x^* + \frac{1}{2} \chi_y^* \right) \right], \\
H &= H^* + \frac{Eh^3}{36} \left[\left(\frac{\partial \psi_x}{\partial y} + \frac{\partial \psi_y}{\partial x} \right)^* - \left(\frac{\partial \psi_x}{\partial y} + \frac{\partial \psi_y}{\partial x} \right)^* \right].
\end{aligned} \right\} \quad (1.200)$$

The expressions for N_y , Q_y and M_y are similarly written down; the asterisk denotes the corresponding quantities at the instant of start of load removal.

As already noted, the equations of motion, written in terms of forces and moments, are the same as (75)-(79). The complete equations of motion in displacements turn out to be very cumbersome, and will therefore be omitted here. Besides, they are not necessary in the numerical integration of the equations when the method subsequently used is employed: it is more convenient to construct the algorithm of the solution by means of a successive calculation of the derivatives of displacements, strains, stresses, forces, and moments and by substituting them into the equations obtained in II.

CHAPTER II

Natural Nonlinear Vibrations

17. Properties of Natural Nonlinear Vibrations

We will begin the discussion of specific problems pertaining to periodic motions of plates and shells with an examination of natural (free) vibrations. If the nature of the natural vibrations of a structure is known, one can evaluate its internal properties, manifested when it is acted on by external disturbances.

As we know, a plate or shell is a system with an infinitely great number of degrees of freedom. With application to the vibration problem, this means that the number of natural frequencies is infinitely great, a definite vibrational mode corresponding to each frequency.

In the case of natural linear vibrations, the amplitudes of the displacements of a given point of the system are independent of the frequency, and, when the vibrations are generated, are determined only by the initial conditions. These conditions include deviations of the elements of the plate or shell from the equilibrium position and their velocity at the initial instant of time. Such characteristics of linear vibrations are explained by the fact that the rigidity parameters of the system are assumed to be constant. However, it follows from the theory of plates and shells that the rigidity characteristics can be considered constant only for small deflections. One can then assume that the internal forces are reduced to stresses of bending proper.

If however the deflections are comparable to the thickness of the plate, membrane stresses must be taken into consideration. According to the usual classification*,

*This classification was introduced by I.G. Bubnov [0.5]. See also the book [1.11], p. 13.

we thereby switch from rigid to flexible plates. For flexible plates, the rigidity parameters are variable and depend on the deflection. This also applies to absolutely flexible plates (membranes); the bending stresses in them are neglected in comparison with the stresses in the middle surface.

For shells, as we have seen in Chapter I, the stress state generally includes bending stresses and stresses in the middle surface even for small deflections. However, in this case as well, strains at large deformations are characterized by a change in the relationship between these stresses.

However, since the frequency of natural vibrations is related to the rigidity parameters of the system, for flexible plates or shells, the frequency should depend on how much the system deviates from the equilibrium position, i.e., it should depend on the vibration amplitude. This fact is most typical of thin-walled structures experiencing large displacements.

The solution of nonlinear dynamic problems, in which the independent variables are time and the space coordinates, is comparatively complex even when modern computers are employed. For this reason, current studies are usually confined to the lower vibrational frequencies and primarily to the fundamental frequency. In the discussion of such problems, the plate or shell is frequently reduced to a system with a single degree of freedom that approximates their curved surface in some fashion.

In the case of a plate, the relation between the characteristic deflection A and the frequency, referred to the frequency of a linear system, this parameter being denoted by ν , has the form shown in Figure 2.1 a. As the amplitude increases, so does the frequency. A system with such a characteristic is called rigid. For a shell, the analogous relationship may be different (see Figure 2.1 b). The initial portion of the curve in this case deflects toward the ordinate axis, and the corresponding characteristic is defined as soft.

Line (ν, A) is called a skeletal curve. It reflects the basic properties of

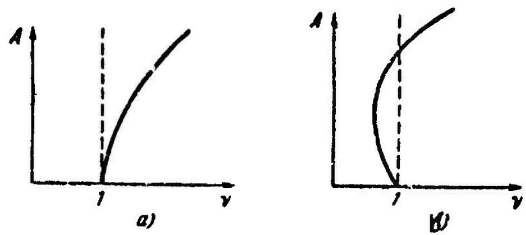


Figure 2.1. Possible variants of the relationship between the characteristic deflection and frequency of natural nonlinear vibrations.

the deformed system; as will be seen in Chapter III, different types of diagrams for forced vibrations of the system are grouped around this curve.

Let us consider some problems pertaining to natural vibrations of plates and shells. Further treatment is carried out as follows. First, "classical" problems are solved in which the plate or shell is represented as a system with one degree of freedom. This gives a general idea of the nature of the vibrations and of the influence of various factors on the amplitude-frequency characteristics. Then, more accurate solutions are given for different problems by using numerical methods. Thus, the picture of vibrations of a plate or shell becomes more complete; it becomes possible to follow the complex process of motion of different points of the system. These features show up particularly well in the case of open shells of large curvature.

For the most important problems, the initial data are provided by solving linearized variants with determination of the frequencies and modes of small vibrations.

18. Rectangular Plate Hinged at the Edges. Linear Problem

We will begin with the simplest case of a rectangular plate with hinged edges. The problem will first be examined in the linear formulation.

We denote the sides of the plate by a , b . The coordinate axes x , y are directed along the sides of the supporting contour.

We use the linear variant of basic equations (1.35), (1.36) when $k_x = k_y = 0$:

$$\frac{D}{h} \nabla^4 w + \frac{\gamma}{\rho} \frac{\partial^3 w}{\partial t^3} = 0. \quad (2.1)$$

For the deflection, we take the expression

$$w = f(t) \sin \frac{m\pi x}{a} \sin \frac{n\pi y}{b}. \quad (2.2)$$

Substituting this expression into the equality

$$\int_0^a \int_0^b \left(\frac{D}{h} \nabla^4 w + \frac{\gamma}{\rho} \frac{\partial^3 w}{\partial t^3} \right) \sin \frac{m\pi x}{a} \sin \frac{n\pi y}{b} dx dy = 0,$$

we obtain

$$\frac{d^3 \zeta}{dt^3} + \omega_{0, mn}^2 \zeta = 0; \quad (2.3)$$

where $\zeta = f_1(t)h$. The square of the frequency of natural vibrations for small deflections

$$\omega_{0, mn}^2 = \frac{\pi^4 m^4 \left(1 + \frac{n^2}{m^2} \lambda^2\right)^2 c^2 h^2}{12 \lambda^2 (1 - \mu^2) a^2 b^2}, \quad (2.4)$$

where $\lambda = a/b$, and c is the propagation velocity of longitudinal elastic waves in the plate material:*

$$c = \sqrt{Eg/\gamma}. \quad (2.5)$$

*See the book [0.6], p. 294.

Figure 2.2 shows the character of wave formation in a square plate vibrating in the first three modes. In this case, the plate executes vibrations at the lowest frequency with the formation of one half-wave along the direction of each side

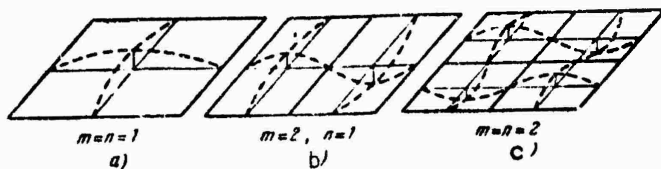


Figure 2.2. Character of wave formation in a square plate vibrating in the a) first mode, b) second mode, c) third mode.

(Figure 2.2 a); the next higher frequency is associated with two half-waves along one direction and one half-wave along the other (Figure 2.2 b), the third frequency is associated with two half-waves in each direction (Figure 2.2 c), and so on.

19. Nonlinear Problem. The Bubnov-Galerkin Method

Let us examine nonlinear vibrations with application to the above-discussed case of a rectangular plate with hinged edges.* As far as the boundary conditions for displacements and stresses in the middle surface are concerned, we will assume that the plate edges are connected to elastic ribs that do not distort in the plane of the plate and that prevent the edges from moving closer together. The limiting cases considered will be those of freely approaching linear edges on the one hand and fixed edges on the other.

It will be postulated that the ratio of the sides of the plate $\lambda = a/b$ lies in the range $1 \leq \lambda \leq 2$. The sectional area of the elastic ribs bordering the plate will be referred to the length of the corresponding side. Let the coordinate axes

*This problem was discussed by Chu and Herrmann [2.28], Greenspon [2.37], and other authors. The results cited here are those obtained by I.G. KII'dibekov.

x, y be directed along the sides a, b . The sectional areas of the ribs F_x and F_y will be assumed to correspond to the unit length of sides b and a ; we introduce the notation $h/F_x = v_x$, $h/F_y = v_y$.

We use the basic equations (1.35), (1.36) for $k_x = k_y = 0$:

$$\frac{D}{h} \nabla^4 w = L(w, \Phi) - \frac{y}{g} \frac{\partial^4 w}{\partial t^4}, \quad (2.6)$$

$$\frac{1}{E} \nabla^4 \Phi = -\frac{1}{2} L(w, w). \quad (2.7)$$

The operator $L(w, \Phi)$ is determined from (1.34).

Satisfying the equations of hinged support (1.44), (1.46 a), we choose the following expression for the deflection:

$$w = f \sin \frac{\pi x}{a} \sin \frac{\pi y}{b}. \quad (2.8)$$

Substituting (8) into the right side of Eq. (7), we obtain

$$\frac{1}{E} \nabla^4 \Phi = \frac{1}{2} f^2 \frac{\pi^4}{a^2 b^2} \left(\cos^2 \frac{\pi x}{a} \cos^2 \frac{\pi y}{b} - \sin^2 \frac{\pi x}{a} \sin^2 \frac{\pi y}{b} \right)$$

or

$$\frac{1}{E} \nabla^4 \Phi = \frac{1}{2} f^2 \frac{\pi^4}{a^2 b^2} \left(\cos \frac{2\pi x}{a} + \cos \frac{2\pi y}{b} \right). \quad (2.9)$$

The partial solution of Eq. (9) will be written in the form

$$\Phi_1 = A \cos \frac{2\pi x}{a} + B \cos \frac{2\pi y}{b}. \quad (2.10)$$

Coefficients A, B are determined by calculating $\nabla^4 \Phi$ and equating the left and right sides of (9):

$$A = E \frac{l^3}{32} \frac{a^3}{b^3}, \quad B = E \frac{l^3}{32} \frac{b^3}{a^3}.$$

Then, the solution of the homogeneous equation $\nabla^4 \Phi = 0$ will be represented as follows:

$$\Phi_2 = \frac{\bar{p}_x y^3}{2} + \frac{\bar{p}_y x^3}{2},$$

where \bar{p}_x, \bar{p}_y are the external forces applied to the plate through the edge ribs:
 \bar{p}_x and \bar{p}_y are considered to be positive in tension.

Finally,

$$\Phi = E \frac{l^3}{32} \left[\left(\frac{a}{b} \right)^2 \cos \frac{2\pi x}{a} + \left(\frac{b}{a} \right)^2 \cos \frac{2\pi y}{b} \right] + \frac{\bar{p}_x y^3}{2} + \frac{\bar{p}_y x^3}{2}. \quad (2.11)$$

The stresses in the middle surface are

$$\left. \begin{aligned} \sigma_x &= \frac{\partial^2 \Phi}{\partial y^2} = -E \frac{\pi^2}{8} \left(\frac{l}{a} \right)^2 \cos \frac{2\pi y}{b} + \bar{p}_x, \\ \sigma_y &= \frac{\partial^2 \Phi}{\partial x^2} = -E \frac{\pi^2}{8} \left(\frac{l}{b} \right)^2 \cos \frac{2\pi x}{a} + \bar{p}_y, \\ \tau &= -\frac{\partial^2 \Phi}{\partial x \partial y} = 0. \end{aligned} \right\} \quad (2.12)$$

Let us note that the tangential stresses τ turn out to be equal to zero for all the points of the plate. If the normal stresses are compressive over the entire edge (influence of the first term), they will be maximum at the edges and minimum in the middle of the sides.

We will find the mutual displacements of the edges $y = 0, y = b$. For some fiber parallel to the x axis, the closer approach of the ends will be

$$\Delta_x = - \int_0^a \frac{\partial u}{\partial x} dx. \quad (2.13)$$

Comparing formulas (1.5) for $k_x = 0$ with (1.12), we find

$$\Delta_x = -\frac{1}{E} \int_0^a \left[\frac{\partial^2 \Phi}{\partial y^2} - \mu \frac{\partial^2 \Phi}{\partial x^2} - \frac{E}{2} \left(\frac{\partial w}{\partial x} \right)^2 \right] dx. \quad (2.13 a)$$

Substituting into the above expression the values of w , Φ from (8) and (11), we obtain after integrating

$$\Delta_x = \frac{\pi^2 l^2}{8a} - \frac{\bar{p}_x - \mu \bar{p}_y}{E} a. \quad (2.14)$$

Similarly,

$$\Delta_y = \frac{\pi^2 l^2}{8b} - \frac{\bar{p}_y - \mu \bar{p}_x}{E} b. \quad (2.15)$$

These values of Δ_x and Δ_y should be equal to the elastic strains of the ribs. We denote by $\sigma_{x,p}$ and $\sigma_{y,p}$ the stresses in the braces (which are positive in compression); then

$$\Delta_x = \frac{\sigma_{x,p}}{E} a, \quad \Delta_y = \frac{\sigma_{y,p}}{E} b. \quad (2.16)$$

From the equilibrium conditions of the nodes, at which the ribs are fastened to the plate, we have

$$\sigma_{x,p} = \bar{p}_x \frac{h}{F_x} = v_x \bar{p}_x, \quad \sigma_{y,p} = \bar{p}_y \frac{h}{F_y} = v_y \bar{p}_y. \quad (2.17)$$

Then

$$\left. \begin{aligned} v_x \bar{p}_x &= E \frac{\pi^2}{8} \left(\frac{l}{a} \right)^2 - (\bar{p}_x - \mu \bar{p}_y), \\ v_y \bar{p}_y &= E \frac{\pi^2}{8} \left(\frac{l}{b} \right)^2 - (\bar{p}_y - \mu \bar{p}_x). \end{aligned} \right\} \quad (2.18)$$

Hence

$$\left. \begin{aligned} \bar{p}_x &= E \frac{\pi^2}{8b^2} \frac{\mu + \frac{b^2(1+v_y)}{a^2}}{(1+v_x)(1+v_y) - \mu^2} l^2, \\ \bar{p}_y &= E \frac{\pi^2}{8b^2} \frac{\mu \frac{b^2}{a^2} + 1 + v_x}{(1+v_x)(1+v_y) - \mu^2} l^2. \end{aligned} \right\} \quad (2.19)$$

We introduce the dimensionless parameters

$$p_x' = \frac{\bar{p}_x}{E} \left(\frac{b}{h}\right)^2, \quad p_y' = \frac{\bar{p}_y}{E} \left(\frac{b}{h}\right)^2, \quad \frac{a}{b} = \lambda, \quad \zeta = \frac{l}{h}, \quad (2.20)$$

and have

$$\left. \begin{aligned} p_x' &= \frac{\pi^2}{8} \frac{\mu + \frac{1+v_y}{\lambda^2}}{(1+v_x)(1+v_y) - \mu^2} \zeta^2, \\ p_y' &= \frac{\pi^2}{8} \frac{\mu \frac{1}{\lambda^2} + 1 + v_x}{(1+v_x)(1+v_y) - \mu^2} \zeta^2. \end{aligned} \right\} \quad (2.21)$$

We have written down the fundamental relations for the problem of natural vibrations of a rectangular plate. These relations lead to a differential equation in partial derivatives with respect to the function $w = w(x, y, t)$. An exact solution of the equation taken in its initial form is lacking. However, there are several methods that permit an approximate integration of the equation under certain boundary conditions. Using a simple example, we will present several of these approximate methods and primarily the Bubnov-Galerkin method*. The solution will be carried out in two steps. In the first step, the Bubnov-Galerkin method will be applied to Eq. (6) for some fixed instant of time t . We denote by X the expression

$$X = \frac{D}{h} \nabla^4 w - \left(\frac{\partial^4 \Phi}{\partial y^4} \frac{\partial^4 w}{\partial x^4} - 2 \frac{\partial^4 \Phi}{\partial x \partial y} \frac{\partial^4 w}{\partial x \partial y} + \frac{\partial^4 \Phi}{\partial x^4} \frac{\partial^4 w}{\partial y^4} \right) + \frac{\gamma}{g} \frac{\partial^2 w}{\partial t^2}. \quad (2.22)$$

*See I.G. Bubnov, Review of the works of Prof. Timoshenko (1913), and Structural Mechanics of Ships, pt. 2 (1914), and also B.G. Galerkin, Rods and Plates. Vestnik tekhnologov (1915).

Judging from the equation, this function should be identically equal to zero for coordinates x , y corresponding to all the points of the plate. However, we will not strive for fulfillment of this condition for all x , y , but will confine ourselves to some integral relation. In the general case, we will approximate the functions $w(x, y, t)$ in the form of the series

$$w = f_1 \eta_1 + f_2 \eta_2 + \dots + f_n \eta_n = \sum_{i=1}^n f_i \eta_i \quad (2.23)$$

where η_i are some independent functions x , y given in advance, which, when substituted for w in equalities of the type of (1.44), (1.46a), satisfy the boundary conditions of the problem; f_i are parameters dependent only on t .

According to the Bubnov-Galerkin method, we will write down n equations of the type

$$\int \int_X \chi \eta_i dx dy = 0, \quad i = 1, 2, \dots, n, \quad (2.24)$$

the integration being performed over the entire area of the plate X .

In our solution, expression (2) appears instead of series (23), and function η_i will be

$$\eta_i = \sin \frac{\pi x}{a} \sin \frac{\pi y}{b}. \quad (2.25)$$

Using the expressions for w from (8), Θ from (11), and η_i from (25), we get

$$\begin{aligned} X = & \left[\frac{D}{h} \dot{\eta}^2 \left(\frac{1}{a^2} + \frac{1}{b^2} \right)^2 + \bar{p}_x \dot{\eta} \frac{\pi^2}{a^2} + \bar{p}_y \dot{\eta} \frac{\pi^2}{b^2} - \right. \\ & \left. - E \frac{\pi^2}{b^3} \dot{\eta}^3 \left(\frac{\cos \frac{2\pi y}{b}}{a^4} + \frac{\cos \frac{2\pi x}{a}}{b^4} \right) + \frac{y}{h} \frac{d^2 \eta}{dt^2} \right] \sin \frac{\pi x}{a} \sin \frac{\pi y}{b}. \end{aligned} \quad (2.26)$$

Here it is assumed that $f = f_1$. Substituting (26) into (24) and integrating, we arrive at the equation

$$\begin{aligned} \frac{D}{h} \frac{\pi^4}{4} \left(\frac{1}{a^4} + \frac{1}{b^4} \right)^2 f + \bar{\rho}_x f \frac{\pi^2}{4a^2} + \bar{\rho}_y f \frac{\pi^2}{4b^2} + \\ + E \frac{\pi^4 h^4}{64} \left(\frac{1}{a^4} + \frac{1}{b^4} \right) + \frac{1}{4} \frac{v}{g} \frac{df}{dt} = 0. \end{aligned}$$

Switching to dimensionless parameters (20) and substituting their expressions from (21) for $\bar{\rho}_x^*$ and $\bar{\rho}_y^*$, we obtain

$$\begin{aligned} \frac{v}{g} h^2 \frac{d^2 \zeta}{dt^2} + \frac{\pi^4 E h^4}{128 \left(1 - \mu^4 \right)} \left(1 + \frac{1}{\lambda^4} \right)^2 \zeta + \left[\frac{\pi^4}{8} \frac{E h^4}{\delta^4} \frac{\mu}{\lambda^4} + 1 + v_x + \right. \\ \left. + \frac{\pi^4}{8} \frac{E h^4}{\delta^4} \frac{\mu + \frac{1+v_y}{\lambda^4}}{\left(1 + v_x \right) \left(1 + v_y \right) - \mu^4} \frac{1}{\lambda^4} + \frac{\pi^4}{16} \frac{E h^4}{\delta^4} \left(1 + \frac{1}{\lambda^4} \right) \right] \zeta^3 = 0. \end{aligned} \quad (2.27)$$

Using the initial fourth-order partial differential equation (6), we have arrived at a nonlinear equation again, but with ordinary derivatives, and of second order. It will be represented in the form

$$\frac{d^2 \zeta}{dt^2} + \omega_0^2 (1 + K \zeta^3) \zeta = 0, \quad (2.28)$$

where K stands for the expression

$$\begin{aligned} K = \frac{1.6 (1 - \mu^4)}{\left(1 + \frac{1}{\lambda^4} \right)^2 \left((1 + v_x) (1 + v_y) - \mu^4 \right)} \left[\frac{\mu}{\lambda^4} + 1 + v_x + \right. \\ \left. + \left(\mu + \frac{1+v_y}{\lambda^4} \right) \frac{1}{\lambda^4} \right] + \frac{0.76 (1 - \mu^4)}{\left(1 + \frac{1}{\lambda^4} \right)^2} \left(1 + \frac{1}{\lambda^4} \right). \end{aligned} \quad (2.29)$$

If the nonlinear term containing ζ^3 , is discarded in (28), we will arrive at Eq. (3) if we take $m = n = 1$:

$$\frac{d^2 \zeta}{dt^2} + \omega_0^2 \zeta = 0,$$

which describes small vibrations of the plate. The parameter ω_0^2 represents the square of the fundamental frequency of small natural vibrations of the plate:

$$\omega_0^2 = \frac{\pi^4 E h^3 \rho}{12b^4 (1 - \mu^2)} \left(1 + \frac{1}{\lambda^2}\right)^2. \quad (2.30)$$

or

$$\omega_0^2 = \frac{\pi^4 (1 + \lambda^2)^2}{12\lambda^4 (1 - \mu^2)} c^2 \left(\frac{h}{ab}\right)^2. \quad (2.31)$$

where c is the quantity given by (5).

Our purpose includes the study of vibrations of the plate at amplitudes comparable to the thickness; we therefore have to return to the initial nonlinear equation (28). The study of this equation is the simplest of the classical problems of general theory of nonlinear vibrations of mechanical systems.

Let us note that if Eq. (28) is represented in the form

$$\frac{d^2\zeta}{dt^2} + \omega_0^2 F(\zeta) = 0, \quad F(\zeta) = (1 + K\zeta^2)\zeta.$$

the function $F(\zeta)$ will define the elastic characteristic of the system over the entire range of the amplitudes under consideration. In our example, this characteristic is symmetric with respect to ζ , and also rigid (Figure 2.3 a). As will be shown below, the natural vibrations of such a system correspond to a rigid-type skeletal line. In the case of shells, the elastic curve may have the shape shown in Figure 2.3 b, and this explains the change in the character of the amplitude-frequency relations (see 32).

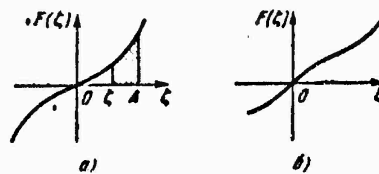


Figure 2.3. Possible variants of elastic characteristics.

Thus, we will aim at performing the integration of Eq. (28), which now contains only one independent variable, time; therein lies the second step of the solution of the problem. We will first consider the case of a plate with freely moving rectilinear edges.

1. Plate with freely moving edges.

The solution corresponding to this variant is obtained by taking $\bar{p}_x = \bar{p}_y = 0$ in the above relations. However, if one considers that the deflection is different from zero, it follows from (18) that $v_x = v_y = \infty$. From (29), we will then have

$$K = \frac{3(1-\mu^2)(1+\lambda^2)}{4(1+\lambda^2)^2}. \quad (2.32)$$

The square of the first frequency of small vibrations ω_0^2 is determined as before from (31).

We represent the deflection in the form of the function

$$\zeta = A \cos \omega t, \quad (2.33)$$

where A is a dimensionless amplitude and ω is the vibration frequency.

We denote the left side of Eq. (28) by Z :

$$Z(t) = \frac{d^2\zeta}{dt^2} + \omega_0^2(1+K\zeta^2)\zeta. \quad (2.34)$$

In the second step of the solution of the problem, we perform the integration over the total vibration period $T = 2\pi/\omega$. In other words, we write an equality of the type

$$\int_0^{2\pi/\omega} Z(t) \cos \omega t dt = 0.$$

Taking into consideration the relations

$$\int_0^{2\pi/\omega} \cos^2 \omega t dt = \frac{\pi}{\omega}, \quad \int_0^{2\pi/\omega} \cos^4 \omega t dt = \frac{3\pi}{4\omega},$$

we obtain

$$\int_0^{2\pi/\omega} Z(t) \cos \omega t dt = A(\omega_0^2 - \omega^2) \frac{\pi}{\omega} + \frac{3}{4} KA^3 \frac{\pi}{\omega} \omega_0^2 = 0.$$

We have arrived at an equation expressing the relationship between the frequency of nonlinear vibrations ω and amplitude A :

$$\omega^2 = \omega_0^2 \left(1 + \frac{3}{4} KA^2\right).$$

We introduce the notation for the ratio of ω to the corresponding frequency of linear vibrations ω_0 ; $v = \omega/\omega_0$. We then have

$$v^2 = 1 + \frac{3}{4} KA^2. \quad (2.35)$$

In the coordinates v , we obtain a rigid-type skeletal line (Figure 2.4). At very small amplitudes, we have $v \rightarrow 1$. As the amplitude increases, so does the vibration frequency, at an increasingly steeper rate.

2. Plate with immovable edges.

If the edges of the plate do not undergo displacement, it is necessary to take $v_x = v_y = 0$ in the basic relations. Then from (29) we have

$$K = \frac{0.75(1 - \mu^2)(1 + \lambda^4) + 1.5(1 + 2\mu\lambda^2 + \lambda^4)}{(1 + \lambda^2)^2}. \quad (2.32 \text{ a})$$

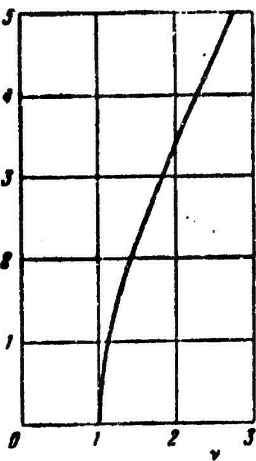


Figure 2.4. Skeletal line for an ideal square plate executing fundamental-mode nonlinear vibrations.

The square of the fundamental frequency is determined from (31). From (19), \bar{p}_x and \bar{p}_y are equal to

$$\bar{p}_x = \frac{1}{8} \frac{1+\mu\lambda^2}{1-\mu^2} \frac{\pi^2 EI^3}{a^2}, \quad \bar{p}_y = \frac{1}{8} \frac{\lambda^2 + \mu}{1-\mu^2} \frac{\pi^2 EI^3}{a^2}. \quad (2.36)$$

analyzing the problem as was done in I, we arrive at the previous equation, (35).

20. Plate Clamped at the Edges

We will consider the case of a rectangular plate clamped along the contour. As in the case of a hinged plate, we will consider the presence of rods constraining the displacement of the points of the edges $x = 0$, $x = a$. We thus assume that forces whose average values are equal to \bar{p}_x and \bar{p}_y are acting along the edges of the plate. In addition, we will stipulate that the point of each edge moves freely along the edge itself, so that the tangential forces along the contour should become zero here as well.

The ratio of the sides a/b will be assumed to lie in the range $1 \leq a/b \leq 1.5$.*

As before, we will use the basic equations in the form (6), (7). Analyzing the lower vibration mode, we approximate the deflection by means of the expression

$$w = f \sin^2 rx \sin^2 sy, \quad (2.37)$$

where $r = \pi/a$, $s = \pi/b$.

The strain compatibility equation takes the form

$$\nabla^4 \Phi = \frac{E}{2} f^2 r^2 s^2 (\cos 2rx + \cos 2sy - \cos 4rx - \cos 4sy + \cos 4rx \cos 2sy + \cos 2rx \cos 4sy - 2 \cos 2rx \cos 2sy). \quad (2.38)$$

The solution of this equation is

$$\begin{aligned} \Phi = E & \left\{ \frac{1}{32} \left(\frac{s^4}{r^4} \cos 2rx + \frac{r^4}{s^4} \cos 2sy \right) - \right. \\ & - \frac{1}{512} \left(\frac{s^2}{r^2} \cos 4rx + \frac{r^2}{s^2} \cos 4sy \right) + \frac{r^2 s^2}{32} \left[\frac{1}{4r^2 + s^2} \cos 4rx \cos 2sy + \right. \\ & \left. \left. + \frac{1}{r^2 + 4s^2} \cos 2rx \cos 4sy - \frac{r^2 s^2}{16(r^2 + s^2)^2} \cos 2rx \cos 2sy \right] \right\} + \\ & + \frac{\rho_x y^2}{2} + \frac{\rho_y x^2}{2}. \end{aligned} \quad (2.39)$$

The stresses in the middle surface will be

$$\begin{aligned} \sigma_x = \frac{\partial^2 \Phi}{\partial y^2} = -Ef^2 r^2 & \left\{ \frac{1}{8} \cos 2sy - \frac{1}{32} \cos 4sy + \right. \\ & + \frac{s^4}{8} \left[\frac{1}{(4r^2 + s^2)^2} \cos 4rx \cos 2sy + \frac{1}{(r^2 + 4s^2)^2} \cos 2rx \cos 4sy \right] - \\ & \left. - \frac{s^4}{4(r^2 + s^2)^2} \cos 2rx \cos 2sy \right\} + \bar{\rho}_x, \end{aligned} \quad (2.40)$$

*When $a/b > 1.5$, satisfactory results can be obtained by assuming the plate to be infinitely long (ef. [1.11]).

$$\sigma_y = \frac{\partial^2 \Phi}{\partial x^2} = -E f^2 s^2 \left\{ \frac{1}{8} \cos 2rx - \frac{1}{32} \cos 4rx + \right. \\ \left. + \frac{r^4}{8} \left[\frac{4}{(4r^2+s^2)^2} \cos 4rx \cos 2sy + \frac{1}{(r^2+4s^2)^2} \cos 2rx \cos 4sy \right] - \right. \\ \left. - \frac{r^4}{4(r^2+s^2)^2} \cos 2rx \cos 2sy \right\} + \bar{\rho}_y, \quad (2.41)$$

$$\tau = -\frac{\partial^2 \Phi}{\partial x \partial y} = -E f^2 \frac{r^2 s^2}{4} \left[\frac{1}{(4r^2+s^2)^2} \sin 4rx \sin 2sy + \right. \\ \left. + \frac{1}{(r^2+4s^2)^2} \sin 2rx \sin 4sy - \frac{1}{(r^2+s^2)^2} \sin 2rx \sin 2sy \right]. \quad (2.42)$$

Clearly, the condition that the tangential forces be equal to zero at the edges is fulfilled.

For the relative displacement of the edges $x = 0, x = a$, from (13a) we get

$$\Delta_x = \frac{3}{32} r^2 \bar{\rho}_a - \frac{\bar{\rho}_x - \mu \bar{\rho}_y}{E} a. \quad (2.43)$$

Similarly for the edges $y = 0, y = b$

$$\Delta_y = \frac{3}{32} s^2 \bar{\rho}_b - \frac{\bar{\rho}_y - \mu \bar{\rho}_x}{E} b. \quad (2.44)$$

Using relations (16) between displacements Δ_x, Δ_y and stresses σ_x, σ_y, τ , in elastic braces, we obtain

$$\left. \begin{aligned} \sigma_{x,p} &= v_x \bar{\rho}_x = \frac{3}{32} E r^2 f^2 - (\bar{\rho}_x - \mu \bar{\rho}_y), \\ \sigma_{y,p} &= v_y \bar{\rho}_y = \frac{3}{32} E s^2 f^2 - (\bar{\rho}_y - \mu \bar{\rho}_x). \end{aligned} \right\} \quad (2.45)$$

The notation used here is that of (17). Hence the dimensionless parameters $\bar{\rho}_x^*, \bar{\rho}_y^*$ from (20) will be

$$\left. \begin{aligned} \bar{\rho}_x^* &= \frac{3\pi^2}{32} \frac{\mu + \frac{1+v_y}{\lambda^2}}{(1+v_x)(1+v_y) - \mu^2} t^2, \\ \bar{\rho}_y^* &= \frac{3\pi^2}{32} \frac{\frac{\mu}{\lambda^2} + 1 + v_x}{(1+v_x)(1+v_y) - \mu^2} t^2. \end{aligned} \right\} \quad (2.46)$$

We will use the equation derived by means of the Bubnov-Galerkin method:

$$\iint \chi \sin^2 rx \sin^2 sy dx dy = 0. \quad (2.47)$$

We find the function χ from formula (22). Substituting expressions (37) and (39) for w and θ , we arrive at a cumbersome expression, given in the book [1.11], p. 111. Substituting this expression into (47), after integrating we get

$$\begin{aligned} & \frac{\gamma}{g} h \frac{d^2 \zeta}{dt^2} + \frac{16\pi^4 D}{9a^4} (3 + 2\lambda^2 + 3\lambda^4) \zeta + \frac{4\pi^2 h}{3a^2} (\bar{p}_x + \lambda^2 \bar{p}_y) \zeta + \\ & + \frac{2\pi^4 Eh^3}{9a^4 b^3} \left\{ \frac{17}{32\lambda^4} + \lambda^2 \left[\frac{17}{32} + \frac{1}{(1+\lambda^2)^2} + \frac{1}{4(1+4\lambda^2)^2} + \frac{1}{4(4+\lambda^2)^2} \right] \right\} \zeta = 0 \end{aligned} \quad (2.48)$$

Various special problems will be examined below.

1. Plate with freely moving edges.

For this variant, it is necessary that $\bar{p}_x = \bar{p}_y = 0$. Equation of motion (48) is reduced to the previous form (28), and K now stands for the quantity

$$K = \frac{1.5\lambda^4(1-\mu^2)}{3(1+\lambda^4)+2\lambda^2} \left\{ \frac{17}{32} \left(1 + \frac{1}{\lambda^4} \right) + \frac{1}{4} \left[\frac{1}{(1+\lambda^2)^2} + \frac{1}{(1+4\lambda^2)^2} \right] + \frac{1}{(1+\lambda^2)^2} \right\}. \quad (2.49)$$

The square of the fundamental frequency of small vibrations for a clamped plate will be

$$\omega_0^2 = \frac{4\pi^4 Eh^2 \nu}{27a^4 \gamma (1-\mu^2)} (3 + 2\lambda^2 + 3\lambda^4)$$

or

$$\omega_0^2 = \frac{4\pi^4}{27\lambda^4(1-\mu^2)} \left(\frac{ch}{ab} \right)^2 (3 + 2\lambda^2 + 3\lambda^4). \quad (2.50)$$

Comparing (31) and (50), we find the ratio of the vibration frequency of the clamped plate to the corresponding frequency of the hinged plate:

$$\frac{\omega_0^2 \cdot cl}{\omega_0^2 \cdot h} = \frac{16}{9} \frac{3 + 2\lambda^2 + 3\lambda^4}{(1 + \lambda^2)^2}. \quad (2.51)$$

For a square plate,

$$\frac{\omega_0^2 \cdot cl}{\omega_0^2 \cdot h} = \frac{32}{9} \approx 3.55. \quad (2.52)$$

The previous formula (35), where K should be found from (49), corresponds to the approximate solution of the problem.

2. Case of immovable edges.

In this case, $v = 0$. We then find from (46)

$$p_x^* = \frac{3\pi^2}{32} \frac{1 + \frac{1}{\lambda^2}}{1 - \mu^2} \zeta^2, \quad p_y^* = \frac{3\pi^2}{32} \frac{1 + \frac{1}{\lambda^2}}{1 - \mu^2} \zeta^2. \quad (2.52a)$$

Equation (48) is reduced to the form of (28). The square of the frequency is expressed according to formula (50), and the value of K in (28) is determined in the form

$$K = \frac{1.5\lambda^4(1 - \mu^2)}{3(1 + \lambda^2) + 2\lambda^2} \left\{ \frac{17}{32} \left(1 + \frac{1}{\lambda^2} \right) + \frac{1}{4} \left[\frac{1}{(1 + \lambda^2)^2} + \frac{1}{(1 + 4\lambda^2)^2} \right] + \right. \\ \left. + \frac{1}{(1 + \lambda^2)^2} + \frac{9}{16} \frac{1 + \frac{2\mu}{\lambda^2} + \frac{1}{\lambda^2}}{1 - \mu^2} \right\}. \quad (2.49a)$$

21. The Harmonic Balance Method

As we have seen, the solution of problems of nonlinear vibrations of plates consists in reducing the basic equations in partial derivatives to an ordinary differential equation in a first step, and in a second step, in integrating this last equation. The second step of the solution can be carried out together with the Bubnov-Galerkin method with the aid of several other methods. One of them is called

the harmonic balance method*.

We write Eq. (28) in the form

$$\frac{d^3\zeta}{dt^3} + \omega_0^2 F(\zeta) = 0 \quad (2.53)$$

and take

$$F(\zeta) = \zeta + K\zeta^3. \quad (2.54)$$

Since ζ is dependent on t , F is an implicit function of t as well.

We choose the solution of the equation in the form

$$\zeta = A \cos \omega t$$

and substitute this expression into (53). Thus

$$-\omega^2 A \cos \omega t + \omega_0^2 F(t) = 0. \quad (2.55)$$

We expand the function $F(t)$ in a cosine series and, wishing to compare the coefficients of $\cos \omega t$, keep the first term of the expansion

$$F(t) = B_1 \cos \omega t. \quad (2.56)$$

Then from (55) we obtain

$$\omega^2 = \omega_0^2 \frac{B_1}{A}. \quad (2.57)$$

The coefficient of the expansion, B_1 , is

*This method was substantiated in the book of N.M. Krylov and N.N. Bogolyubov [0.11].

$$B_1 = \frac{\omega}{\pi} \int_0^{2\pi/\omega} F(t) \cos \omega t dt =$$

$$= \frac{\omega}{\pi} \int_0^{2\pi/\omega} (A \cos \omega t + KA^3 \cos^3 \omega t) \cos \omega t dt = A \left(1 + \frac{3}{4} KA^2 \right).$$

We finally find

$$\omega^2 = \omega_0^2 \left(1 + \frac{3}{4} KA^2 \right). \quad (2.58)$$

This is the result obtained above by the Bubnov-Galerkin method.

22. Perturbation Method

Let us turn again to Eq. (28). It can also be solved with the aid of the so-called perturbation method, which amounts to replacing the nonlinear equation by a system of coupled differential equations.

We introduce the dimensionless time parameter $t = \omega t$ and represent Eq. (28) in the form

$$\omega^2 \frac{d^2 \zeta}{dt^2} + \omega_{00}^2 + \chi \zeta^3 = 0, \quad (2.59)$$

where $\chi = \omega_0^2 K$.

Considering that K is fairly small, we will also assume that χ is a small parameter, and expand the functions ζ and ω in powers of χ :

$$\zeta = \zeta_0 + \chi \zeta_1 + \chi^2 \zeta_2 + \dots, \quad \omega = \omega_0 + \chi \omega_1 + \chi^2 \omega_2 + \dots \quad (2.60)$$

Substituting (60) into (59) and equating to zero the coefficients of the same powers

of X, we obtain the following system of linear equations:

$$\ddot{\omega}_0 \ddot{\zeta}_0 + \omega_0^2 \zeta_0 = 0, \quad (2.61)$$

$$\ddot{\omega}_0 \ddot{\zeta}_1 + \omega_0^2 \zeta_1 = -2\ddot{\omega}_0 \omega_1 \ddot{\zeta}_0 - \zeta_0^3, \quad (2.62)$$

.....

the dots over the letters indicating differentiation with respect to t. We thus obtain a chain of successive problems consisting in the integration of Eqs. (61), (62), etc.

In addition, the periodicity condition

$$\zeta_i(\tau + 2\pi) = \zeta_i(\tau). \quad (2.63)$$

must be fulfilled.

As an example, we take the initial conditions

$$\zeta(0) = A, \quad \dot{\zeta}(0) = 0, \quad (2.64)$$

and assume

$$\left. \begin{array}{l} \zeta_0(0) = A, \quad \zeta_1(0) = \zeta_2(0) = \dots = 0, \\ \dot{\zeta}_0(0) = \dot{\zeta}_1(0) = \dots = 0, \end{array} \right\} \quad (2.65)$$

$$\zeta_i(\tau + 2\pi) = \zeta_i(\tau), \quad i = 0, 1, 2, \dots \quad (2.66)$$

We begin with the first problem, which consists in integrating Eq. (61). Its solution will be

$$\zeta_0 = B \cos \frac{\omega_0}{\omega_0} \tau + C \sin \frac{\omega_0}{\omega_0} \tau. \quad (2.67)$$

From conditions (65) and (66), we find

$$B = A, \quad C = 0, \quad \ddot{\omega}_0 = \omega_0.$$

Thus, we have

$$\zeta_0 = A \cos \tau. \quad (2.68)$$

We turn to Eq. (62). Substituting the value of ζ_0 from (68), we obtain

$$\omega_0^2(\ddot{\zeta}_1 + \zeta_1) = 2\omega_0\omega_1 A \cos \tau - A^3 \cos^3 \tau. \quad (2.69)$$

Representing $\cos^3 \tau$ approximately by the expression

$$\cos^3 \tau = \frac{3}{4} \cos \tau + \frac{1}{4} \cos 3\tau,$$

we find

$$\omega_0^2(\ddot{\zeta}_1 + \zeta_1) = \left(2\omega_0\omega_1 - \frac{3}{4}A^2\right) A \cos \tau - \frac{1}{4}A^3 \cos 3\tau. \quad (2.70)$$

When the coefficient of $\cos \tau$ is different from zero, the solution of the equation will contain a term of the type $t \sin t$. However, the function $\zeta_1(t)$ is periodic, and therefore

$$2\omega_0\omega_1 - \frac{3}{4}A^2 = 0 \quad \text{and} \quad \omega_1 = \frac{3}{8} \frac{A^2}{\omega_0}. \quad (2.71)$$

The solution of Eq. (70) takes the form

$$\zeta_1 = B_1 \cos \tau + C_1 \sin \tau + \frac{A^3}{32\omega_0^2} \cos 3\tau. \quad (2.72)$$

From initial condition (65), we find

$$B_1 = -\frac{A^3}{32\omega_0^2}, \quad C_1 = 0.$$

Finally,

$$\zeta_1 = -\frac{A^3}{32\omega_0^2} (-\cos \tau + \cos 3\tau). \quad (2.73)$$

Thus, the solution obtained after substituting the value $x = \omega_0^2 K$ takes the form

$$\zeta = A \left(1 - \frac{1}{32} KA^2 \right) \cos \tau + \frac{1}{32} KA^2 \cos 3\tau, \quad (2.74)$$

$$\omega = \omega_0 \left(1 + \frac{3}{4} KA^2 \right). \quad (2.75)$$

Then, keeping the terms containing a small parameter, we find

$$\omega^2 = \omega_0^2 \left(1 + \frac{3}{4} KA^2 \right). \quad (2.76)$$

This relation between ω^2 and A is the same as the one obtained by the previous methods. However, the expression for ζ now contains an additional term corresponding to the triple frequency.

23. Exact Solution

The solution of Eq. (28) corresponding to the initial conditions $\zeta = A$, $\dot{\zeta} = 0$ for $t = 0$ is expressed in terms of the elliptical cosine

$$\zeta = A \text{cn}(\gamma t, \chi),$$

where

$$\gamma = \omega_0 \sqrt{1 + KA^2}, \quad \chi = A \sqrt{\frac{K}{2(1 + KA^2)}}.$$

We will determine the period T for this solution.

In view of the fact that

$$\ddot{\zeta} = \frac{d\dot{\zeta}}{dt} = \frac{d\dot{\zeta}}{d\zeta} \dot{\zeta} = \frac{1}{2} \frac{d(\dot{\zeta})^2}{d\zeta},$$

Eq. (28) is reduced to the form

$$\frac{1}{2} \frac{d(\zeta)^2}{dt} + \omega_0^2 F(\zeta) = 0. \quad (2.77)$$

Let us assume that the motion of the plate at time $t = 0$ is characterized by deflection and velocity values equal to $\zeta=0=A$, $\zeta_t=0=0$. Integrating (77), we get

$$\frac{1}{2} \left(\frac{d\zeta}{dt} \right)^2 = -\omega_0^2 \int_A^\zeta F(\zeta) d\zeta = \omega_0^2 \int_\zeta^A F(\zeta) d\zeta. \quad (2.78)$$

According to (78), during the motion of a panel, the kinetic energy is equal to the difference between the potential energy corresponding to the initial position ($\zeta=A$, $\zeta=0$) and the potential energy at the given instant. This fraction of the potential energy is proportional to the area shaded in Figure 2.3 a. Expression (78) determines the velocity $\dot{\zeta}$ for any position of the panel.

Considering that the motion of the panel at the given instant of time corresponds to a decrease of the deflection, we obtain from Eq. (78)

$$dt = - \frac{d\zeta}{\sqrt{\frac{2\omega_0^2}{\zeta} \int_\zeta^A F(\zeta) d\zeta}}. \quad (2.79)$$

By integrating (79), we obtain the time necessary for the plate to get from position A to position ζ :

$$t = - \int_A^\zeta \frac{d\zeta}{\sqrt{\frac{2\omega_0^2}{\zeta} \int_\zeta^A F(\zeta) d\zeta}}. \quad (2.80)$$

In view of the symmetry of the elastic characteristic, the time required by the plate to move from position $\zeta = A$ to position $\zeta = 0$ will be equal to one-quarter of the period, and therefore the period

$$T = -4 \int_{A}^{0} \frac{d\zeta}{\sqrt{\frac{2m_0^2}{\zeta} \int F(\zeta) d\zeta}} = 4 \int_{0}^{A} \frac{d\zeta}{\sqrt{\frac{2m_0^2}{\zeta} \int F(\zeta) d\zeta}}. \quad (2.81)$$

Substituting the expression for $F(\zeta)$ from (54) into the above expression, we obtain

$$T = \frac{4}{m_0} \int_{0}^{A} \frac{d\zeta}{\sqrt{(A^2 - \zeta^2) \left(1 + \frac{K}{2} A^2 + \frac{K}{2} \zeta^2\right)}}. \quad (2.82)$$

Introducing the notation

$$r = \frac{\zeta}{A}, \quad s = KA^2,$$

we give the following form to expression (82)

$$\begin{aligned} T &= \frac{4}{m_0} \int_{0}^{1} \frac{dr}{\sqrt{(1 - r^2) \left(1 + \frac{1}{2}s + \frac{1}{2}sr^2\right)}} = \\ &= \frac{4}{m_0} \sqrt{\frac{2}{s}} \int_{0}^{1} \frac{dr}{\sqrt{(1 - r^2) \left(\frac{2+s}{s} + r^2\right)}}. \end{aligned} \quad (2.83)$$

We will reduce this expression to a form suited for calculations with the aid of tables. The elliptic integral is

$$\int_{0}^{s} \frac{d\tau}{\sqrt{(a^2 - \tau^2)(b^2 + \tau^2)}} = \frac{1}{c} F\left(\frac{a}{c}, \varphi\right). \quad (2.84)$$

Here $F(a/c, \phi)$ is an elliptic integral of the first kind. Its values as a function of $a/c, \phi$ are given in tables* in accordance with the following notation:

$$c^2 = a^2 + b^2, \quad \sin^2 \varphi = \frac{c^2 x^2}{a^2 (b^2 + x^2)}.$$

Equating (83) and (84), we obtain

$$\begin{aligned} a^2 &= 1, \quad b^2 = \frac{2+s}{s}, \quad c^2 = 1 + \frac{2+s}{s} = \frac{2(1+s)}{s}, \\ x &= 1, \quad \sin^2 \varphi = 1, \quad \varphi = \frac{\pi}{2}, \end{aligned}$$

and the final expression for the period will be

$$T = \frac{4}{\omega_0} \frac{1}{\sqrt{1+s}} F\left(\sqrt{\frac{s}{2(1+s)}}, \frac{\pi}{2}\right). \quad (2.85)$$

Setting $s = 1$, we get an expression for the period of small vibrations

$$T_0 = \frac{2\pi}{\omega_0}.$$

The ratio of the frequency of nonlinear vibrations to that of small vibrations $\nu = T_0/T$ takes the form

$$\nu = \frac{\pi \sqrt{1+s}}{2} \frac{1}{F\left(\sqrt{\frac{s}{2(1+s)}}, \frac{\pi}{2}\right)}. \quad (2.86)$$

*Cf. for example, Yanke and Emde, Tables of Functions, 3rd Edition, Fizmatgiz, Moscow, 1959.

Figure 2.5 gives the amplitude-frequency relations according to (86) for a series of boundary conditions (solid lines): 1 - hinged support for free displacement of edges; 2 - hinged support in the absence of relative displacement of edges; relations 3, 4 pertain to analogous variants of boundary conditions of a plate clamped along its contour. On the same graph, dashed lines show the corresponding relations pertaining to the above-discussed solutions (see 19, 20) in accordance with the Bubnov-Galerkin method. In Figure 2.5, use is made of the quantity v^* , equal to the ratio of the frequency of natural nonlinear vibrations to the frequency of the fundamental tone of small vibrations of the plate hinged along the contour. Therefore, $v^* = v_n$, where the values of v are found from formulas (35), (86) for the corresponding values of K from (32), (32a), (49), (49a); obviously in the case of hinged edges, $\eta = 1$. For a plate clamped along the contour, η is equal to the ratio of the frequency of the fundamental tone of small natural vibrations of the plate, clamped along the contour, to the fundamental vibration frequency in the case of hinged support of the edges, $\eta = \sqrt{3+\lambda^2} + \lambda^2/3(1+\lambda^2)$. The relations of Figure 2.5 are plotted for square plates ($\lambda=1$).

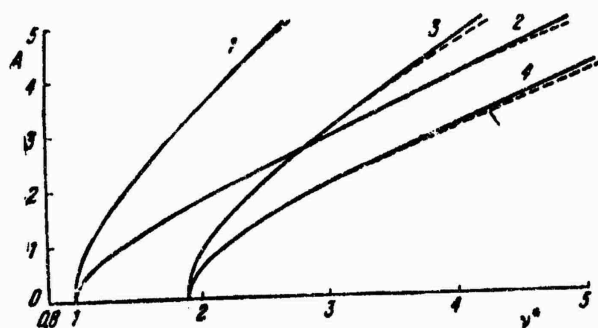


Figure 2.5. Influence of boundary conditions on the amplitude-frequency characteristics for plates according to the data of the exact solution and of the solution obtained by means of the Bubnov-Galerkin method.

24. Case of a very Long Plate. Use of the Bubnov-Galerkin Method

In conclusion, we will examine the case of a plate, one of whose dimensions

substantially exceeds the second dimension ($a \gg b$).

To study the vibrations of such a plate, we can consider a strip with a width equal to unity and a length equal to b . We thus obtain a problem with one space coordinate y . The equations of motion can then be written down in the form

$$\frac{D}{h} \frac{\partial^4 w}{\partial y^4} - \sigma \frac{\partial^2 w}{\partial y^2} - \frac{y}{g} \frac{\partial^3 w}{\partial t^3} = 0. \quad (2.87)$$

Here we replaced the derivative $\partial^2 \phi / \partial x^2$ by $\sigma_y = \sigma$; for an infinitely long plate, this quantity should be constant at all points, $\sigma = \text{const.}$ [1.11].

We will use the Bubnov-Galerkin method. Approximating the deflection by the expression

$$w = f \sin \frac{\pi y}{b}, \quad (2.88)$$

we obtain

$$\int_0^b \left(D \frac{\partial^4 w}{\partial y^4} - \sigma h \frac{\partial^2 w}{\partial y^2} + \frac{y}{g} h \frac{\partial^3 w}{\partial t^3} \right) \sin \frac{\pi y}{b} dy = 0. \quad (2.89)$$

We thus arrive at the equation

$$\frac{yh}{g} \frac{d^3 f}{dt^3} + D \frac{\pi^4}{b^4} f + \frac{\pi^3}{b^3} \sigma h f = 0. \quad (2.90)$$

The equilibrium condition of the moving edge has the form [1.11, p. 74]

$$\sigma h = \sigma_p F_{ex}, \quad (2.91)$$

where

$$\sigma = \frac{E}{1-\mu^2} \frac{1}{1+v} \frac{1}{2b} \int_0^b \left(\frac{\partial w}{\partial y} \right)^2 dy, \quad (2.91a)$$

with $v = h/F_u$. Hence

$$\sigma = \frac{E}{1-\mu^2} \frac{1}{1+v} \frac{\pi^2}{4b^2} f^2. \quad (2.92)$$

If the supports are fixed, we have $v = 0$, and in the case of absolutely movable edges, $v = \infty$.

Substituting (92) into (90), we get

$$\frac{Y}{g} h \frac{d^4 f}{dt^4} + D \frac{\pi^4}{b^4} f + \frac{\pi^4}{4} \frac{Eh}{b^4} \frac{1}{1-\mu^2} \frac{1}{1+v} f^3 = 0. \quad (2.93)$$

Equation (93) is reduced to the form

$$\frac{d^4 \zeta}{dt^4} + \omega_0^2 (1 + K \zeta^2) = 0, \quad (2.94)$$

where

$$\omega_0 = \frac{ch}{12(1-\mu^2)} \frac{\pi^2}{b^2}, \quad K = \frac{3}{1+v}. \quad (2.94a)$$

Here ω_0 , as before, is the fundamental frequency of natural vibrations of the system.

For fixed edges, $K = 3$, and in the case of absolutely movable edges, $K = 0$.

Let us consider the case of a strip with clamped edges. Representing the deflection in the form

$$w = f \sin^2 \frac{\pi y}{b}, \quad (2.95)$$

we obtain the following equation in the same manner:

$$\frac{y}{g} \frac{d^2f}{dt^2} + \frac{16}{3} D \frac{\pi^4}{b^4} f + \frac{4}{3} \frac{\pi^3}{b^3} \sigma h f = 0. \quad (2.96)$$

Determining σ from previous formulas, we find

$$\sigma = \frac{\pi^3}{4} \frac{E}{1-\mu^2} \frac{1}{1+v} \left(\frac{f}{b}\right)^2. \quad (2.97)$$

Substituting (97) into (96), we get

$$\frac{y}{g} h \frac{d^2f}{dt^2} + \frac{16}{3} D \frac{\pi^4}{b^4} f + \frac{\pi^4}{3} \frac{Eh}{b^4} \frac{1}{1-\mu^2} \frac{1}{1+v} f^3 = 0. \quad (2.98)$$

This equation is given in the form of (94), where

$$\omega_0 = \frac{2}{3} \frac{ch}{\sqrt{1-\mu^2}} \frac{\pi^3}{b^3}, \quad K = \frac{3}{4(1+v)}.$$

In the case of immovable edges, $K = 3/4$. For absolutely movable supports, $K = 0$ as before.

25. Use of the Method of Finite Differences.

Let us turn to the solution of the problem discussed in the preceding section with the aid of the method of finite differences.*

In the case of stationary edges ($v = 0$), σ is determined from Eq. (91a), and

*This solution is due to I.G. Kill'dibekov, S.V. Medvedeva and the author; they also analyzed the problems presented in 31.

Initial relation (87) acquires the form

$$\frac{D}{h} \frac{\partial^4 w}{\partial y^4} - \frac{E}{2b(1-\mu^2)} \frac{\partial^2 w}{\partial y^2} \int_0^b \left(\frac{\partial w}{\partial y} \right)^2 dy + \frac{\gamma}{g} \frac{\partial^2 w}{\partial t^2} = 0. \quad (2.99)$$

The dimensionless quantities

$$\tilde{w} = \frac{w}{b}, \quad \xi = \frac{y}{b}, \quad \tau = \frac{t}{T}, \quad (2.100)$$

where T is the period of small natural vibrations $T = 2\pi/w_0$; w_0 is determined from formula (94a). Then Eq. (99) is reduced to the form

$$\frac{\partial^4 \tilde{w}}{\partial \xi^4} - 6 \frac{\partial^2 \tilde{w}}{\partial \xi^2} \int_0^1 \left(\frac{\partial \tilde{w}}{\partial \xi} \right)^2 d\xi + \frac{\pi^2}{4} \frac{\partial^2 \tilde{w}}{\partial \tau^2} = 0. \quad (2.101)$$

We will consider the case of hinged edges; the corresponding boundary conditions are

$$\tilde{w} = 0, \quad \frac{\partial^2 \tilde{w}}{\partial \xi^2} = 0 \quad \text{for } \xi = 0, \xi = 1. \quad (2.102)$$

We take the following initial conditions:

$$\tilde{w} = A \sin \pi \xi, \quad \frac{\partial \tilde{w}}{\partial \tau} = 0 \quad \text{for } \tau = 0. \quad (2.103)$$

As we know, the corresponding solution of the linear problem for the fundamental mode of natural vibrations is

$$\tilde{w} = A \sin \pi \xi \cos \tau. \quad (2.104)$$

We will now study nonlinear vibrations with the aid of the method of finite differences.

We will represent Eq. (101) as well as the boundary and initial conditions of the problem in finite differences. The time step $s_t = 1/m$ and the coordinate step $s_\zeta = 1/n$. For the node i, j we have

$$\frac{\partial^4 \omega}{\partial \xi^4} = \frac{1}{s_\zeta^4} (\bar{\omega}_{i+2,j} - 4\bar{\omega}_{i+1,j} + 6\bar{\omega}_{i,j} - 4\bar{\omega}_{i-1,j} + \bar{\omega}_{i-2,j}), \quad (2.105)$$

$$\frac{\partial^2 \bar{\omega}}{\partial t^2} = \frac{1}{s_t^2} (\bar{\omega}_{i,j+1} - 2\bar{\omega}_{i,j} + \bar{\omega}_{i,j-1}). \quad (2.106)$$

The boundary conditions of the problem are

$$\bar{\omega}_{0,j} = 0, \quad \bar{\omega}_{n,j} = 0, \quad (2.107)$$

$$\left. \begin{aligned} \frac{1}{s_\zeta^2} (\bar{\omega}_{i,j} - 2\bar{\omega}_{0,j} + \bar{\omega}_{-1,j}) &= 0 \quad \text{для точки } \xi = 0, \\ \frac{1}{s_\zeta^2} (\bar{\omega}_{n+1,j} - 2\bar{\omega}_{n,j} + \bar{\omega}_{n-1,j}) &= 0 \quad \text{для точки } \xi = 1. \end{aligned} \right\} \quad (2.108)$$

From conditions (108) and allowing for (107), we have

$$\bar{\omega}_{-1,j} = -\bar{\omega}_{1,j}, \quad \bar{\omega}_{n+1,j} = -\bar{\omega}_{n-1,j}. \quad (2.108a)$$

Initial conditions (103) will be

$$\omega_{i,0} = A \sin \pi (s_\zeta \cdot i), \quad i = 1, 2, \dots, (n-1), \quad (2.108b)$$

$$\frac{\omega_{i,1} - \omega_{i,-1}}{s_t} = 0. \quad (2.108c)$$

Results of the calculations are given in Figures 2.6-2.9. In the calculations, the number of steps along the coordinate was taken as $n = 20$, and the ratio of steps $s_t/s_\zeta = 1/40$.

Figure 2.6b reflects the configuration of the middle surface at different instants of time, denoted on the graph by the numbers of subdivision intervals along the time axis j_1 . The value of the deflection amplitude at the center was taken as $A = 1$. The same graph shows the results of the linear problem (Figure 2.6a). It is

evident that the vibration frequency according to data of the linear approximation turns out to much lower. This fact is demonstrated even more clearly by Figure 2.7; these data reflect the motion of different points of the plate with time.

The curve of change in deflection with time is denoted by \bar{w}_{10} ; this point corresponds to the value $i = 10$. The fine line reflects the change in deflection with time according to data of the linear approximation. The ratio of the vibration frequency obtained from the method of finite differences to the frequency in the linear problem is equal to 1.8.

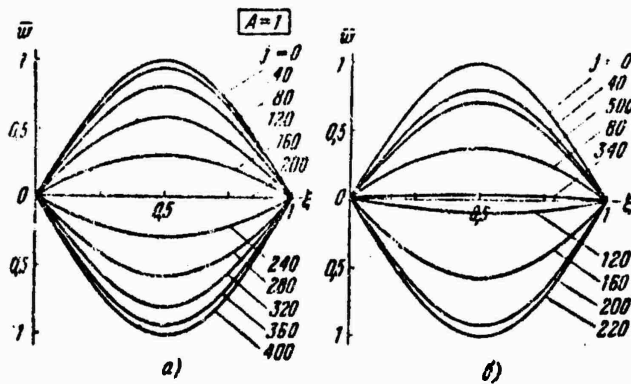


Figure 2.6. Configuration of middle surface of plate for different instants of time for deflection parameter $A = 1$: a) linear problem; b) nonlinear problem.

In Figure 2.7, the dashed line shows the dependence for the bending deflection obtained by the Bubnov-Galerkin method, and the dashed line shows it in elliptical functions.

Graphs similar to those discussed above are shown in Figures 2.8 and 2.9. These data pertain to the case of vibrations with a deflection amplitude at the center $A = 5$. In this case, the frequency of nonlinear vibrations, obtained from the method of finite differences, is approximately 7.6 times greater than the frequency obtained from data of the linear approximation. Figure 2.9 also gives data of the linear approximation and results of solutions obtained by using the Bubnov-Galerkin method

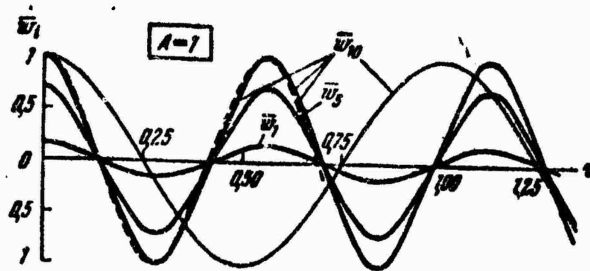


Figure 2.7. Characteristic of the motion of different points of the plate with time according to data of the solution of the linear and nonlinear problem for parameter $A = 1$.

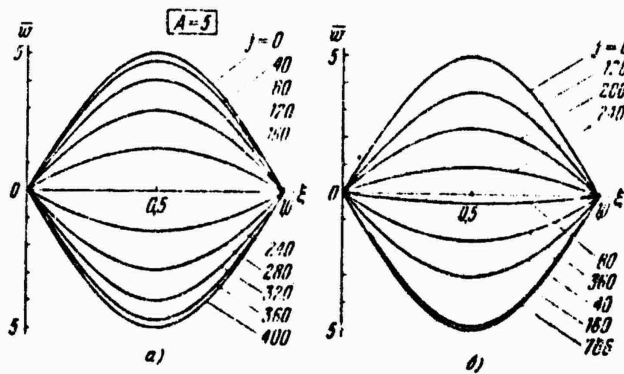


Figure 2.8. Change in the configuration of the middle surface of the plate for deflection parameter $A = 5$; a) linear problem; b) nonlinear problem.

and in elliptical functions; here, the same notation as in Figure 2.7 is adopted for the different solutions. The dashed line merges with the curve obtained by the Bubnov-Galerkin method (as in Figure 2.7).

26. Influence of Stresses in the Middle Surface on the Natural Vibrations of a Plate

We will examine the vibrations of a plate experiencing at the edges $x = 0, y = 0$

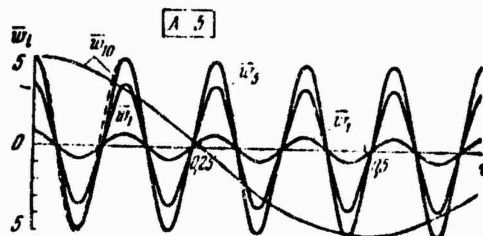


Figure 2.9. Motion of points in time according to data of the linear approximation and different solutions of the nonlinear problem for natural vibrations with deflection parameter at the center $A = 5$.

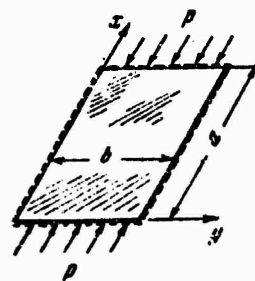


Figure 2.10. Plate acted upon by compressive stresses in the middle surface.

the action of compressive forces p_x located in the middle surface (Figure 2.10).* Let us assume that simultaneously, forces in the middle surface whose average intensity is p_y act along the plate edges $y = 0$, $y = b$ from the direction of the stiffeners. The values of p_x and p_y (without a bar) are here considered to be positive in compression. The tangential forces in the middle surface will be considered equal to zero along all four edges.

*The solution given here is due to I.G. Kill'dibekov. Also due him are the results given in 27, 29, 30, 32, 34.

I. Case of hinged edges.

First, we will consider the case in which the plate edges are hinged. Solving the problem in the first approximation by the Bubnov-Galerkin method, as was done in 19, we will adopt the previous approximating expression (8) for w . Substituting this expression into the right side of Eq. (7) and integrating, we find the stress function in the middle surface:

$$\Phi = E \frac{l^2}{32} \left[\left(\frac{a}{b} \right)^2 \cos \frac{2\pi x}{a} + \left(\frac{b}{a} \right)^2 \cos \frac{2\pi y}{b} \right] - \frac{p_x y^2}{2} - \frac{p_y x^2}{2}; \quad (2.109)$$

In comparison with (11), only the signs of p_x and p_y change here.

Then, Eq. (24) will take the form

$$\frac{\gamma}{8} h^2 \frac{d^2 \zeta}{dt^2} + \frac{\pi^2 D h}{a^4} (1 + \lambda^2)^2 \zeta - \frac{\pi^2 h^2}{a^2} (p_x + \lambda^2 p_y) \zeta + \frac{\pi^2 E h^4}{16 a^2 b^2} \left(\frac{1}{\lambda^2} + \lambda^2 \right) \zeta^3 = 0. \quad (2.110)$$

Assuming that the longitudinal edges of the plate move freely, we should set $p_y = 0$. Then the final Eq. (110) becomes

$$\frac{d^2 \zeta}{dt^2} + \omega_0^2 \left(1 - \frac{p^*}{\zeta^3} \right) (\zeta + K \zeta^3) = 0. \quad (2.111)$$

Here $p^* = p_x^* = pb^2/Eh^2$. The critical stress parameter p_{cr}^*

$$p_{cr}^* = \frac{\pi^2 (1 + \lambda^2)^2}{12 \lambda^2 (1 - \mu^2)}. \quad (2.112)$$

K (in 111) stands for the coefficient

$$K = \frac{0.75 (1 - \mu^2) (1 + \lambda^2)}{(1 + \lambda^2) \left(1 - \frac{p^*}{p_{cr}^*} \right)}. \quad (2.113)$$

The square of the fundamental frequency of natural vibrations of the plate at small deflections, allowing for compressive forces, will be

$$\omega_0^2 = \omega_0^2 \left(1 - \frac{p_x^*}{p_{cr}^*}\right), \quad (2.114)$$

where w_0^2 stands for expression (30). Formula (30) may also be rewritten in the form

$$\omega_0^2 = \pi^2 p_{cr}^* \frac{c^2 h^2}{a^2 b^2}, \quad (2.115)$$

the quantities p_{cr}^* and c being determined from (112) and (5).

The relation between the amplitude and frequency of the vibrations is determined from the formula

$$v^2 = \left(1 + \frac{3}{4} KA^2\right) \left(1 - \frac{p_x^*}{p_{cr}^*}\right), \quad (2.116)$$

by using the new expressions for w_0^2 and K (Figure 2.11); here v stands for the ratio of the vibration frequency of the plate to the natural frequency of the fundamental vibration tone without considering the compressive forces. The fine line corresponds to the case $p_x^* = 0$. It is evident that the influence of compressive forces on the amplitude-frequency characteristics of the system is significant.

If the longitudinal edges of the plate are stationary ($\Delta_y = 0$), then from Eq. (15), having changed the signs of p_x and p_y , we find

$$p_y = \mu p_x - E \frac{\pi^2}{8} \left(\frac{l}{b}\right)^2. \quad (2.117)$$

Substituting this expression into (110), we arrive at differential equation (111) having the same form as before by replacing (112) by the following:

$$p_{cr}^* = \frac{\pi^2 (1 + \lambda^2)^2}{12 \lambda^2 (1 + i \lambda^2) (1 - \mu^2)}. \quad (2.118)$$

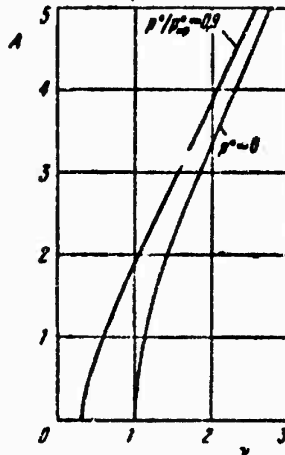


Figure 2.11. Influence of compressive forces in the middle surface of the plate on the amplitude-frequency characteristic.

The quantity K is determined from the formula

$$K = \frac{0.75(1 - \mu^2)(1 + 3\lambda^4)}{(1 + \lambda^2)^2 \left(1 - \frac{p_x}{p_{cr,1}}\right)}. \quad (2.119)$$

The expression for the square of the fundamental frequency remains (114) as before, p_{cr}^* being replaced by p_{cr}^* , i.e.

Let us note that the static variant of relation (110) leads to the following values for p_x in the supercritical region: for moving edges

$$p = D \frac{\pi^2}{hb^2} \left(\frac{1}{\lambda} + \lambda\right)^2 + \frac{E\pi^2 I}{16b^2} \left(\frac{1}{\lambda^2} + \lambda^2\right); \quad (2.120)$$

for stationary edges

$$p = D \frac{\pi^2}{hb^2} \frac{\left(\lambda + \frac{1}{\lambda}\right)^2}{1 + \mu\lambda^2} + E \frac{\pi^2 p_2}{hb^2} \frac{\frac{1}{\lambda^2} + 3\lambda^2}{1 + \mu\lambda^2}. \quad (2.121)$$

Let us turn to the variant of clamped plate edges.

2. Case of clamped edges.

Repeating the operations of I and taking the approximating expression for the deflection in the form

$$w = f \sin^2 rx \sin^2 sy, \quad r = \pi/a, \quad s = \pi/b, \quad (2.122)$$

we arrive in the case of movable longitudinal edges at the previous relations of 20, but with the introduction of the coefficient $(1 - p_{cr,2}^*/p_{cr,1}^*)$ into certain formulas, as in I. The quantity $p_{cr,2}^*$ is then equal to

$$p_{cr,2}^* = \frac{\pi^2}{9} \frac{2 + 3\left(\lambda^2 + \frac{1}{\lambda^2}\right)}{1 - \mu^2}, \quad (2.123)$$

In the case of stationary longitudinal edges, K is equal to

$$\begin{aligned} K = & \frac{1.5\lambda^4(1 - \mu^2)}{[3(1 + \lambda^4) + 2\lambda^2]\left(1 - \frac{p_x^*}{p_{cr,3}^*}\right)} \left\{ \frac{17}{32}\left(1 + \frac{1}{\lambda^2}\right) + \right. \\ & \left. + \frac{1}{4}\left[\frac{1}{(1 + \lambda^2)^2} + \frac{1}{(1 + i\lambda^2)^2}\right] + \frac{1}{(1 + \lambda^2)^2} + \frac{9}{16} \right\}, \end{aligned} \quad (2.124)$$

and the value of $p_{cr,3}^*$ will be

$$p_{cr,3}^* = \frac{\pi^2}{9} \frac{2 + 3\left(\lambda^2 + \frac{1}{\lambda^2}\right)}{(1 - \mu^2)(1 + \mu\lambda^2)}. \quad (2.125)$$

27. Effect of Initial Irregularities

The basic equations allowing for the initial imperfections in the shape of the middle surface will be taken in the form

$$\frac{D}{h} \nabla^2 \nabla^2 w_1 = L(w_1 + w_0, \Phi) - \rho h \frac{\partial^2 w}{\partial t^2} = 0, \quad (2.126)$$

$$\frac{1}{E} \nabla^2 \nabla^2 \Phi = -\frac{1}{2} L(w_1 + 2w_0, w_1), \quad (2.127)$$

operator L being determined from formula (1.34), and w_1 designating the additional deflection.

We will examine the case of a plate hinged along its contour and executing vibrations with the formation of m and n half-waves along the coordinate lines x , y^* . The following expressions will be adopted for the additional and initial deflections:

$$w_1 = f_1(t) \sin \frac{m\pi x}{a} \sin \frac{n\pi y}{b}, \quad (2.128)$$

$$w_0 = f_0 \sin \frac{m\pi x}{a} \sin \frac{n\pi y}{b}. \quad (2.129)$$

The stress function in the middle surface is found from Eq. (127) in the form

$$\Phi = \frac{E}{32} f_1 (f_1 + 2f_0) \left(\frac{n^2}{m^2} \lambda^2 \cos \frac{2m\pi x}{a} + \frac{m^2}{n^2 \lambda^2} \cos \frac{2n\pi y}{b} \right). \quad (2.130)$$

Use of the Bubnov-Galerkin method leads to the following equation of natural vibrations of the plate:

$$\frac{d^2 \zeta}{dt^2} + \omega_{0, mn}^2 (\alpha_0^2 - \beta_0^2 + K_0^2) = 0, \quad (2.131)$$

and we take the dimensionless quantities $\zeta = f_1(t)/h$, $\zeta_0 = f_0/h$. The square of the

*See article [3.11].

frequency of natural vibrations at small deflections $w_{0, mn}^2$ is determined from formula (4). The value of α in Eq. (131) will be

$$\alpha = 1 + \frac{1.5(1 - \mu^2) \left(1 + \frac{n^4}{m^4} \lambda^4 \right) \zeta_0^2}{\left(1 + \frac{n^2}{m^2} \lambda^2 \right)^2}, \quad (2.132)$$

and β and K are determined as follows:

$$\beta = - \frac{\frac{9}{4}(1 - \mu^2) \left(1 + \frac{n^4}{m^4} \lambda^4 \right) \zeta_0}{\left(1 + \frac{n^2}{m^2} \lambda^2 \right)^2}, \quad (2.133)$$

$$K = \frac{0.75(1 - \mu^2) \left(1 + \frac{n^4}{m^4} \lambda^4 \right)}{\left(1 + \frac{n^2}{m^2} \lambda^2 \right)^2}. \quad (2.134)$$

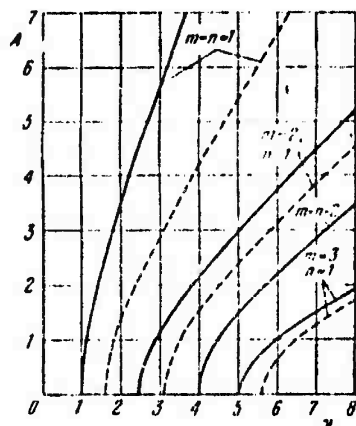


Figure 2.12. Amplitude-frequency characteristics for different modes of natural nonlinear vibrations of square and rectangular plates.

The approximate solution of Eq. (131) will be taken in the form of (33). Using the above-described method of solution, we obtain

$$v^2 - \left(\alpha + \frac{3}{4} KA^2 \right) \eta = 0. \quad (2.135)$$

In contrast to the previous notation, here v stands for the ratio of the vibration frequency to the fundamental frequency of small vibrations $w_{0,11}^*$, found for the square plate, $v = w/w_{0,11}^*$; then

$$\eta = \frac{\omega_0^2 m_n}{\omega_{0,11}^2}.$$

The relations corresponding to the motions in natural nonlinear vibrations in one of the first four modes are shown in Figure 2.12. The solid lines on this graph pertain to the case of an in-plane square panel and the dashed lines, to the case of a rectangular panel with the ratio of the sides $\lambda = 1.5$.

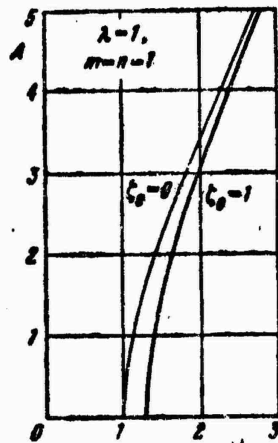


Figure 2.13. Influence of initial irregularities in fundamental-mode nonlinear vibrations of a plate.

The data reflecting the natural vibrations of a plate with initial irregularities in the shape of the middle surface at $c_0 = 1$ are shown in Figure 2.13 and 2.14. The

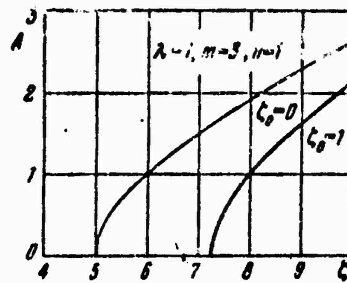


Figure 2.14. Influence of initial irregularities in fourth-mode nonlinear vibrations of a plate.

second of these graphs corresponds to fourth-mode motions of the panel. The fine lines on these graphs pertain to ideal panels. As is evident from the data cited, the higher the vibration mode, the more significant is the influence of initial deviations on the parameters of natural vibrations.

28. Closed Cylindrical Shell. Linear Problem

Let us turn to an examination of the problem of natural vibrations of a closed circular cylindrical shell (Figure 2.15). Before considering nonlinear vibrations, let us discuss the characteristics of natural vibrations for small deflections.

Let L be the length of the shell, R the radius of curvature of the middle surface, and the coordinate lines x, y will be directed along the generatrix and the arc, respectively.

Omitting the nonlinear terms in initial equations (1.40), (1.41), when $\rho = \gamma/g$, $q = 0$, we obtain for an ideal shell ($w_0 = 0$):

$$\frac{D}{h} V^4 w + \rho \frac{\partial^2 w}{\partial t^2} = \frac{1}{R} \frac{\partial^2 \Phi}{\partial x^2}, \quad (2.136)$$

$$\frac{1}{E} V^4 \Phi = \frac{1}{R} \frac{\partial^2 w}{\partial x^2}. \quad (2.137)$$

In the case of hinged support, we adopt the following expression for the deflection:

$$w = f(l) \sin \frac{m\pi x}{L} \sin \frac{ny}{R}; \quad (2.138)$$

m being the number of half-waves along the length of the shell and n , the number of full waves on the circumference. The nodal lines for different vibration modes are shown in Figure 2.16.*

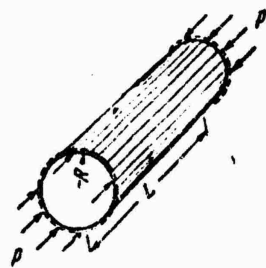


Figure 2.15. Circular cylindrical shell.

Substituting (138) into (137) and performing the integration for the case $p = 0$, we get

$$\frac{\Phi}{E} = \frac{r^2}{(r^2 + s^2)} \frac{f_l}{R} \sin rx \sin sy, \quad (2.139)$$

where

$$r = \frac{m\pi}{L}, \quad s = \frac{n}{R}. \quad (2.140)$$

We use the Bubnov-Galerkin method and set

*Hereinafter, modes with $n > 2$ are considered. The behavior of the shell when $n < 2$ is characterized by several different properties; see for example the paper of Forsberg (K. Forsberg, AIAA J. 7, No. 2, 1969).

$$\int_0^{L/2\pi R} \int_0^{2\pi R} X \sin rx \sin sy dx dy = 0, \quad (2.141)$$

where

$$X = \frac{D}{h} V^4 w + p \frac{\partial^2 w}{\partial t^2} - \frac{1}{R} \frac{\partial^2 \Phi}{\partial x^2}.$$

$$(2.142)$$

From Eq. (141) and allowing for (138), (139), we obtain the following equation:

$$\frac{d^2 \zeta}{dt^2} + \omega_0^2 \zeta = 0. \quad (2.143)$$

Here $\zeta = f(t)/h$. The quantity ω_0^2 is equal to the square of the frequency of natural vibrations of the shell for small deflections

$$\omega_0^2 = \frac{\pi^4 m^4}{\theta^2 \eta} \frac{T_1 R}{Eh} \left(\frac{h}{L^2} \right)^2 c^2, \quad (2.144)$$

T_1 being the value of the critical force for the shell, resulting from the solution of the linear problem of stability of a shell in axial compression, $T_1 = p_{cr} = \hat{\rho}_{cr} E h / R$. The dimensionless quantity in formula (144)

$$\begin{aligned} \hat{\rho}_{cr} = & \frac{1}{12(1-\mu)^2} \frac{(1+\theta)^2}{\theta^2} \eta + \\ & + \frac{\theta^2}{(1+\theta)^2 \eta}. \end{aligned} \quad (2.145)$$

The wave formation parameters are

$$\theta = \frac{l_y}{l_x} = \frac{m\pi R}{nL}, \quad \eta = \frac{n^2 h}{R}; \quad (2.146)$$

l_x, l_y are the lengths of the half-waves along the generatrix and arc, respectively.
The minimum value

$$\hat{\rho}_u = \frac{1}{\sqrt{3}(1-\mu^2)} \approx 0.605 \quad (2.147)$$

takes place when

$$\eta \left(\theta + \frac{1}{\theta} \right)^2 = \\ = \sqrt{12(1-\mu)^2} \approx 3.3. \quad (2.148)$$

The quantity c denotes the propagation velocity of longitudinal waves in the shell material according to (5).

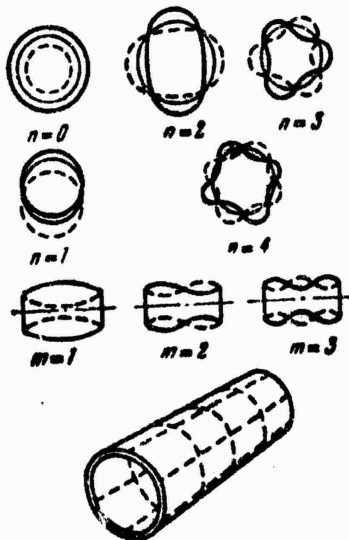


Figure 2.16. Nodal lines for different vibration modes of a circular cylindrical shell.

Results of calculations of the frequency of natural vibrations according to (144) are given in Figures 2.17-2.19a and 2.19b.* The following dimensionless frequency parameter is used here:

$$\omega_0^* = \frac{1}{\pi^2} \frac{\omega_0 L^2}{ch}. \quad (2.149)$$

*The data of Figures 2.17-2.19a and 2.19b are due to I.G. Kili'dibekov [2.12].

Reproduced from
best available copy.

The graph of Figure 2.17 gives values of this parameter plotted against the number of full waves in the circumferential direction n for $m = 1$ for a shell with parameters $L/R = 2$, $R/h = 1500$.

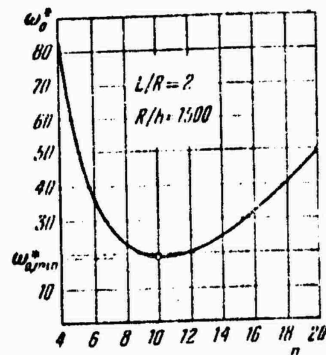


Figure 2.17. Frequency parameter of a shell for small deflections vs. number of circumferential waves.

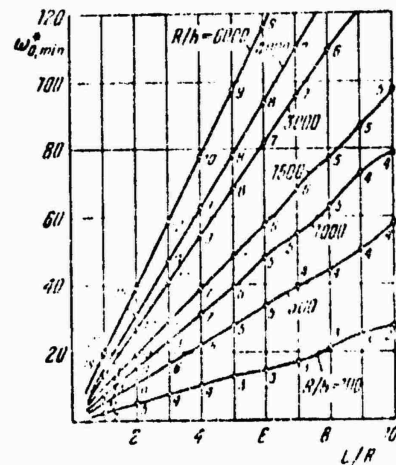


Figure 2.18. Calculated data for determining the minimum frequency of small natural vibrations of a shell.

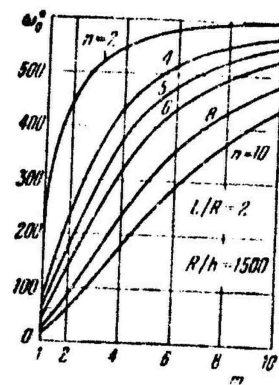


Figure 2.19a. Frequency parameter of a shell for small vibrations vs. number of half-waves along the generatrix and full waves along the circumference with small number n .

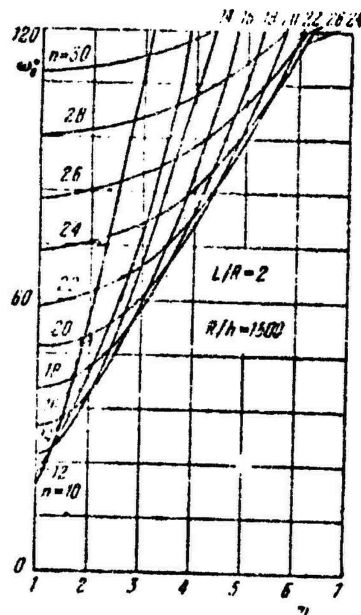


Figure 2.19b. Frequency parameter for a shell with a large number of circumferential waves n .
11-13-1962

The minimum value of the natural vibration frequency parameter w_0^* , min for the shell under consideration corresponds to the value $n = 10$.

Results of calculations of minimum values ($m = 1$) of the frequency parameter w_0^* , min for shells in a wide range of parameters L/R , R/h are given in Figure 2.18. The latter also shows the corresponding numbers of waves n for the different values of L/R .

The data of Figures 2.19a, 2.19b reflect the change of the parameter w_0^* according to (149) as a function of the number of half-waves along the length of the shell m for a series of fixed values of n ; it was assumed that $L/R = 2$, $R/h = 1500$.

Given below are the results of the improved solution of the problem.* We will use the questions of Chapter I (p. 51). For a circular cylindrical shell, they take the form

$$\begin{aligned} \frac{\partial^3 u}{\partial \xi^3} + \frac{1-\mu}{2} (1+k) \frac{\partial^3 u}{\partial \varphi^3} + \frac{1+\mu}{2} \frac{\partial^3 v}{\partial \xi \partial \varphi} + k \frac{\partial^3 w}{\partial \xi^3} - \\ - \frac{1-\mu}{2} k \frac{\partial^3 w}{\partial \xi \partial \varphi^2} - \mu \frac{\partial w}{\partial \xi} - v^2 \frac{\partial^3 u}{\partial t^3} = 0, \\ \frac{1+\mu}{2} \frac{\partial^3 u}{\partial \xi \partial \varphi} + \frac{\partial^3 v}{\partial \varphi^3} + \frac{1-\mu}{2} (1+3k) \frac{\partial^3 v}{\partial \xi^3} + \frac{3-\mu}{2} k \frac{\partial^3 w}{\partial \xi^2 \partial \varphi} - \\ - \frac{\partial w}{\partial \varphi} - v^2 \frac{\partial^3 v}{\partial t^3} = 0, \\ k \frac{\partial^3 u}{\partial \xi^3} - \frac{1-\mu}{2} k \frac{\partial^3 u}{\partial \xi \partial \varphi^2} - \mu \frac{\partial u}{\partial \xi} + \frac{3-\mu}{2} k \frac{\partial^3 v}{\partial \xi^2 \partial \varphi} - \\ - \frac{\partial v}{\partial \varphi} + w + k \left[v^2 w + 2 \frac{\partial^3 w}{\partial \varphi^3} + w \right] + v^2 \frac{\partial^3 w}{\partial t^3} = 0, \end{aligned}$$

where

$$\xi = \frac{x}{R}, \quad \varphi = \frac{\theta}{R}, \quad k = \frac{k^2}{12R^2}, \quad v^2 = \frac{\gamma R^2 (1-\mu^2)}{g E}.$$

*The results cited here are those of Forsberg (K. Forsberg, AIAA J. 2, No. 12, 1964).

The general solution of these equations will be written in the form

$$\left. \begin{aligned} u &= \left(\sum_{n=1}^{\infty} a_n A_n e^{\lambda_n x} \cos n\varphi \right) e^{i\omega t}, \\ v &= \left(\sum_{n=1}^{\infty} b_n A_n e^{\lambda_n x} \sin n\varphi \right) e^{i\omega t}, \\ w &= \left(\sum_{n=1}^{\infty} A_n e^{\lambda_n x} \cos n\varphi \right) e^{i\omega t}. \end{aligned} \right\} \quad (2.151)$$

The constants A_n are determined from the boundary conditions at each end of the shell:

$$w = 0 \quad \text{or} \quad S_t = Q_t + \frac{1}{R} \frac{\partial H_{t\varphi}}{\partial \varphi} = 0, \quad (2.152a)$$

$$\frac{\partial w}{\partial t} = 0 \quad \text{or} \quad M_t = 0, \quad (2.152b)$$

$$u = 0 \quad \text{or} \quad N_t = 0, \quad (2.152c)$$

$$v = 0 \quad \text{or} \quad T_t = N_{t\varphi} - \frac{1}{R} H_{t\varphi} = 0. \quad (2.152d)$$

Substituting expressions (151) into (150), we obtain the equation

$$\lambda_s^6 + g_{s6}\lambda_s^6 + g_{s1}\lambda_s^4 + g_{s2}\lambda_s^2 + g_{s0} = 0, \quad (2.153)$$

where

$$g_{sk} = g_{sk}\left(\frac{h}{R}, \mu, n, \omega\right).$$

The roots of Eq. (153) are

$$\lambda = \pm a, \quad \pm ib, \quad \pm (c \pm id),$$

where a, b, c, d are real numbers.

The solution becomes

$$w = [C_1 e^{at} + C_2 e^{-at} + C_3 \cos b\theta + C_4 \sin b\theta + e^{ct} (C_5 \cos d\theta + C_6 \sin d\theta) + e^{-ct} (C_7 \cos d\theta + C_8 \sin d\theta)] (\cos n\phi) e^{it}, \quad (2.154)$$

Similar expressions for u and v contain combinations of constants C_s and of real and imaginary parts of the parameters α_s, β_s . The quantities α_s, β_s depend on $\lambda_s, h/R, \mu, n, w$; they are calculated after solving Eq. (153).

Satisfying the boundary conditions, we obtain eight equations in the unknowns C_s , containing the parameters a, b, c, d . Representation of these parameters in analytical form is impossible, and the problem is solved numerically. For given parameters $R/h, L/R, \mu$, number of waves n , system of boundary conditions, taking some initial estimate for the frequency w_0 , by iteration we find those frequency values for which the determinant of the system becomes zero.

For fixed m and n , there exist three eigenfrequencies with different ratios of amplitudes u, v, w . The asymptotic values of these frequencies will be $w_{0,1}, w_{0,2}, w_{0,3}$, respectively. The value of $w_{0,1}$ corresponds to flexural motions of the ring $w_{\max} = nv_{\max}$, $u = 0$, $(w_{0,1}/w_{0,k})^2 = (h^2/12R^2)n^2(n^2 - 1)^2/(n^2 + 1)$. For longitudinal vibrations, $w = v = 0$, $(w_{0,2}/w_{0,k})^2 = (1 - \mu)n^2/2$. In the case of extension-compression vibrations of the ring, $v_{\max} = nw_{\max}$, $u = 0$, $(w_{0,3}/w_{0,k})^2 = n^2 + 1$. The quantity $w_{0,k}^2 = Eg/\gamma R^2(1 - \mu^2)$ corresponds to the square of the lower natural frequency in the case of extension-compression of the ring in plane deformation.

If the longitudinal and tangential forces of inertia are neglected, to fixed m, n there will correspond only one value of w close to the lowest of the three frequencies of the shell. The data given below were obtained by taking all three inertial terms into account.

Figures 2.20-2.24 show the minimum frequencies (envelopes of families of frequency curves plotted for constant values of n for $m = 1$). The results given here are those for boundary conditions in conformity with Table 2.1. In contrast to the value of w_0^* from (149), the following dimensionless frequency parameter was taken:

$$\bar{\omega}_0 = \frac{\omega_0}{\omega_{0,k}} = \omega_0 R \sqrt{\frac{v(1-\mu^2)}{Eg}}. \quad (2.155)$$

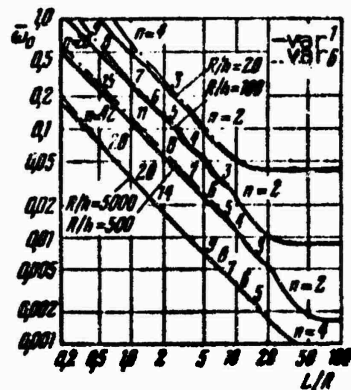


Figure 2.20. Values of minimum natural vibration frequency for small deflections for a hinged and clamped shell without longitudinal fixing.

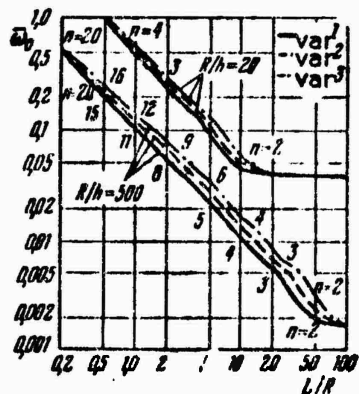


Figure 2.21. Minimum shell frequencies in the case of hinged support of the ends for different conditions fixing to prevent longitudinal displacements.

and the indicated parameters are related as follows:

$$\bar{\omega}_0 = \frac{\omega_0 n^2 \sqrt{1 - \mu^2}}{\left(\frac{R}{h}\right) \left(\frac{L}{R}\right)^2}. \quad (2.156)$$

Figure 2.20 compares values of the minimum natural frequency for a hinged (solid line) and clamped (dashed line) shell without longitudinal fixing (variants 1 and 6, Table 2.1). The increase in minimum frequency due to the fixing is very slight. This influence of fixing is manifested only for short shells ($L/R < 1$). The above results, obtained by use of the Bubnov-Galerkin method (Figure 2.18), are very close to the corresponding data of Figure 2.20 for variant 1. Thus, for $L/R = 2$, in accordance with the graph of Figure 2.18, for the minimum frequencies we obtain from (156), taking $R/h = 20$, the value $\bar{\omega}_0 = 0.264$; when $R/h = 500$, $\bar{\omega}_0 = 0.052$, and when $R/h = 5000$, $\bar{\omega}_0 = 0.016$.

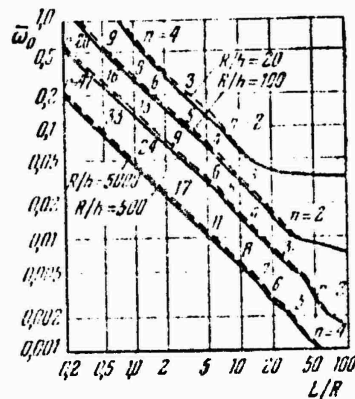


Figure 2.22. Minimum frequencies according to the data of two solutions in the case of clamping in the absence of end displacements.

Figure 2.21 gives a comparison of minimum frequencies in the case of hinged support of the ends under different conditions of longitudinal fixing. This condition has an appreciable influence even for very long shells. For the greater part

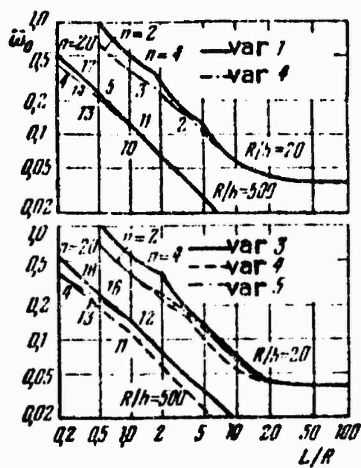


Figure 2.23. Influence of boundary conditions for tangential displacement on minimum shell vibration frequencies for hinged fixing of the ends.

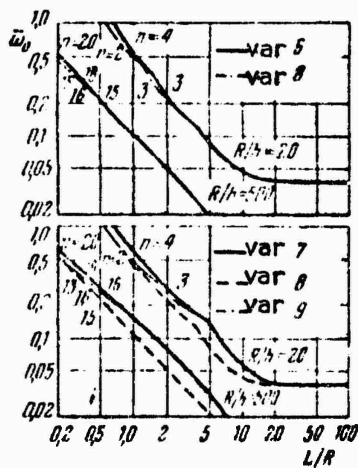


Figure 2.24. Influence of boundary conditions for tangential displacement when the ends are clamped.

Variant Number	Conditions of Support	Boundary Conditions $x = 0$ $x = L$
1	Hinged support with free displacement in the longitudinal direction and in the absence of displacement in the arc direction	$w = 0$ $w = 0$ $v = 0$ $v = 0$ $M_x = 0$ $M_x = 0$ $N_x = 0$ $N_x = 0$
2	Hinged support with free longitudinal displacement at one end and an immovable other end	$w = 0$ $w = 0$ $v = 0$ $v = 0$ $M_x = 0$ $M_x = 0$ $N_x = 0$ $u = 0$
3	Hinged support with immovable ends	$w = 0$ $w = 0$ $u = 0$ $u = 0$ $v = 0$ $v = 0$ $M_x = 0$ $M_x = 0$
4	Hinged support without fixing of the points of the end sections in the arc direction	$w = 0$ $w = 0$ $M_x = 0$ $M_x = 0$ $N_x = 0$ $N_x = 0$ $T = 0$ $T = 0$
5	Hinged support with fixing in the longitudinal direction, but without fixing in the circumferential direction	$w = 0$ $w = 0$ $u = 0$ $u = 0$ $M_x = 0$ $M_x = 0$ $T = 0$ $T = 0$
6	Clamping without longitudinal fixing	$w = 0$ $w = 0$ $\frac{\partial w}{\partial x} = 0$ $\frac{\partial w}{\partial x} = 0$ $v = 0$ $v = 0$ $N_x = 0$ $N_x = 0$
7	Clamping in the absence of displacements of end sections	$w = 0$ $w = 0$ $\frac{\partial w}{\partial x} = 0$ $\frac{\partial w}{\partial x} = 0$ $u = 0$ $u = 0$ $v = 0$ $v = 0$
8	Clamping without fixing in the circumferential direction	$w = 0$ $w = 0$ $\frac{\partial w}{\partial x} = 0$ $\frac{\partial w}{\partial x} = 0$ $N_x = 0$ $N_x = 0$ $T = 0$ $T = 0$
9	Clamping with longitudinal fixing, but without fixing in the circumferential direction	$w = 0$ $w = 0$ $\frac{\partial w}{\partial x} = 0$ $\frac{\partial w}{\partial x} = 0$ $u = 0$ $u = 0$ $T = 0$ $T = 0$
10	Hinged support without longitudinal fixing at one end, clamping with longitudinal fixing at the other end	$w = 0$ $w = 0$ $v = 0$ $v = 0$ $M_x = 0$ $\frac{\partial w}{\partial x} = 0$ $N_x = 0$ $u = 0$

Table 2.1

of the range of shell parameter values, the minimum natural frequency for variant 3 is approximately 40-60% higher than for variant 1.

Figure 2.22 shows results of the solution in comparison with the approximate solution of Arnold and Warburton (dashed line) for variant 7.* They usually exceed the exact values in the range of 2%.

The decrease in the frequency of natural vibrations as the boundary conditions change with the tangential displacement v is reflected in Figures 2.23 and 2.24.

29. Closed Cylindrical Shell, Nonlinear Problem

We will consider the problem in the nonlinear formulation, assuming that the shell is acted on by forces of axial compression p (Figure 2.15), uniformly distributed over the ends.**

We will use the basic equations in the form

$$\frac{D}{h} V^4(w - w_0) = L(w, \Omega) + \frac{1}{R} \frac{\partial^2 \Phi}{\partial z^2} - p \frac{\partial^2 w}{\partial t^2}, \quad (2.157)$$

$$\frac{1}{E} V^4 \Phi = -\frac{1}{2} [L(w, w) - L(w_0, w_0)] - \frac{1}{R} \frac{\partial^2 (w - w_0)}{\partial z^2}, \quad (2.158)$$

where w is the complete deflection, $w = w_1 + w_0$, and w_0 is the initial deflection. Operator L is determined from formula (1.34).

The additional and initial deflections will be approximated by expressions reflecting the nature of wave formation when stability is lost in a large region under axial compression in the case of hinged support [0.6]

*R.N. Arnold and G.B. Warburton, Proc. Roy. Soc., A197 (1949), 238-256; Proc. Inst. Mech. Engrs. 167 (1953), 62-80.

**See the paper [2.12].

$$w_1 = f_1 \sin rx \sin sy + f_2 \sin^2 rx, \quad (2.159)$$

$$w_0 = f_{1,0} \sin rx \sin sy + f_{2,0} \sin^2 rx, \quad (2.160)$$

where the notation used is that of (140).

Substituting (159), (160) into Eq. (158), we obtain

$$\begin{aligned} \frac{1}{E} \nabla^4 \Phi &= \frac{1}{2} r^2 s^2 f_1 (f_1 + 2f_{1,0}) (\cos 2rx + \cos 2sy) - \\ &\quad - \frac{2}{r} r^2 f_2 \cos 2rx + r^2 s^2 (f_1 f_2 + f_1 f_{2,0} + f_2 f_{1,0}) \sin 3rx \sin sy - \\ &\quad - r^2 s^2 \left(f_1 f_2 + f_1 f_{2,0} + f_2 f_{1,0} - \frac{f_1}{R s^2} \right) \sin rx \sin sy. \end{aligned} \quad (2.161)$$

Integrating (161), we determine the stress function in the middle surface

$$\begin{aligned} \frac{\Phi}{E} &= \left[\frac{1}{32} \frac{s^4}{r^4} f_1 (f_1 + 2f_{1,0}) - \frac{1}{8r^2} \frac{f_2}{R} \right] \cos 2rx + \\ &\quad + \frac{1}{32} \frac{r^4}{s^4} f_1 (f_1 + 2f_{1,0}) \cos 2sy + \frac{r^2 s^4}{(9r^2 + s^2)^2} (f_1 f_2 + f_1 f_{2,0} + f_2 f_{1,0}) \times \\ &\quad \times \sin 3rx \sin sy + \frac{1}{(r^2 + s^2)^2} \left[\frac{f_1}{R} r^2 - r^2 s^2 (f_1 f_2 + f_1 f_{2,0} + f_2 f_{1,0}) \right] \times \\ &\quad \times \sin rx \sin sy - \frac{py^2}{2E}. \end{aligned} \quad (2.162)$$

using the Bubnov-Galerkin method, we satisfy the equalities

$$\int_0^{L/2\pi R} \int_0^{2\pi R} X \sin rx \sin sy \, dx \, dy = 0, \quad (2.163)$$

$$\int_0^{L/2\pi R} \int_0^{2\pi R} X \sin^2 rx \, dx \, dy = 0, \quad (2.164)$$

$$X = \frac{D}{h} \nabla^4 (w - w_0) - L(w, \Phi) - \frac{1}{R} \frac{\partial^2 \Phi}{\partial x^2} + p \frac{\partial^2 w}{\partial t^2}. \quad (2.165)$$

Substituting expressions (159), (160), (162) into the above, and using Equations

(163), (164), we obtain the following equations of motion of the shell (for the value of T_1 , see p. 129):

$$\frac{d^2\zeta_1}{dt^2} + C_1 \left(1 - \frac{r}{T_1}\right) [(1 + a_1)\zeta_1 + \beta_1 \zeta_1^2 + \chi_1 \zeta_1^3 - \theta_1 \zeta_2] + \\ + x_1 \zeta_2^2 - \varphi_1 \zeta_2 + \psi_1 \zeta_1 \zeta_2^2] - C_1 \frac{r}{T_1} \zeta_{1,0} = 0, \quad (2.166)$$

$$\frac{d^2\zeta_2}{dt^2} + C_2 \left(1 - \frac{r}{T_2}\right) [(1 + a_2)\zeta_2 - \theta_2 \zeta_1 + x_2 \zeta_1 \zeta_2 - \varphi_2 \zeta_2^2 + \psi_2 \zeta_1 \zeta_2] - C_2 \frac{r}{T_2} \zeta_{2,0} = 0, \quad (2.167)$$

where the following dimensionless quantities were introduced:

$$\zeta_1 = \frac{f_1(t)}{h}, \quad \zeta_2 = \frac{f_2(t)}{h}, \quad \zeta_{1,0} = \frac{f_{1,0}}{h}, \quad \zeta_{2,0} = \frac{f_{2,0}}{h}. \quad (2.168)$$

C_1 stands for the square of the frequency of natural vibrations of the shell for small deflections according to (144). The wave formation parameters θ , η correspond to formulas (146). The value of C_2 , T_2 are

$$C_2 = \frac{4}{3} r^2 c^2 \frac{T_2}{E}, \quad (2.169)$$

$$T_2 = \frac{3}{4} \frac{EA^3}{r^3} \left[\frac{4r^4}{9(1-\mu^2)} + \frac{1}{3R^4 h^3} \right]. \quad (2.170)$$

The remaining quantities in Eqs. (166), (167) will be

$$a_1 = \left\{ \frac{1}{3} (r^4 + s^4) \zeta_{1,0}^2 - \frac{2r^4 s^2}{(r^2 + s^2)^2 R h} \zeta_{2,0} + \right. \\ \left. + r^4 s^4 \left[\frac{1}{(9r^2 + s^2)^2} + \frac{1}{(r^2 + s^2)^2} \right] \zeta_{2,0}^2 \right\} \Psi_1^{-1}, \quad (2.171)$$

$$a_2 = \frac{2}{3} r^4 s^4 \left[\frac{1}{(9r^2 + s^2)^2} + \frac{1}{(r^2 + s^2)^2} \right] \zeta_{1,0}^2 \Psi_2^{-1}, \quad (2.172)$$

$$\beta_1 = \frac{3}{16} (r^4 + s^4) \zeta_{1,0} \Psi_1^{-1}, \quad (2.173)$$

$$\chi_1 = \frac{1}{16} (r^4 + s^4) \Psi_1^{-1}, \quad (2.174)$$

$$\theta_1 = \left\{ \left[\frac{1}{4} \frac{s^2}{Rh} + \frac{r^4 s^2}{Rh(r^2 + s^2)^2} \right] \zeta_{1,0} - \right. \\ \left. - r^4 s^4 \left[\frac{1}{(9r^2 + s^2)^2} + \frac{1}{(r^2 + s^2)^2} \right] \zeta_{1,0} \zeta_{2,0} \right\} \Psi_1^{-1}, \quad (2.175)$$

$$\chi_2 = r^4 s^4 \left[\frac{1}{(9r^2 + s^2)^2} + \frac{1}{(r^2 + s^2)^2} \right] \zeta_{1,0} \Psi_1^{-1}, \quad (2.176)$$

$$\varphi_1 = \left\{ \frac{2r^4 s^2}{(r^2 + s^2)^2 Rh} + \frac{1}{4} \frac{s^2}{Rh} - \right. \\ \left. - 2r^4 s^4 \left[\frac{1}{(9r^2 + s^2)^2} + \frac{1}{(r^2 + s^2)^2} \right] \zeta_{2,0} \right\} \Psi_1^{-1}, \quad (2.177)$$

$$\psi_1 = r^4 s^4 \left[\frac{1}{(9r^2 + s^2)^2} + \frac{1}{(r^2 + s^2)^2} \right] \Psi_1^{-1}, \quad (2.178)$$

$$\theta_2 = \frac{2}{3} \theta_1 K, \quad \chi_2 = \frac{4}{3} \chi_1 K, \quad \varphi_2 = \frac{1}{3} \varphi_1 K, \quad \psi_2 = \frac{2}{3} \psi_1 K, \quad (2.179)$$

where $K = \psi_1/\psi_2$, and we take

$$\Psi_1 = \left[\frac{1}{12(1-\mu^2)} (r^2 + s^2)^2 + \frac{r^4}{(r^2 + s^2)^2} \frac{1}{R^2 h^2} \right] \left(1 - \frac{p}{T_1} \right), \quad (2.180)$$

$$\Psi_2 = \left[\frac{4}{9(1-\mu^2)} r^4 + \frac{1}{3R^2 h^2} \right] \left(1 - \frac{p}{T_2} \right). \quad (2.181)$$

We will cite the results of preliminary studies by assuming in the expressions obtained above that $\zeta_2=0$, $\zeta_{1,0}=\zeta_{2,0}=0$. The problem amounts to analyzing Eq. (166); in the case considered, it takes the form

$$\frac{d^2 \zeta_1}{dt^2} + \omega_0^2 \left(1 - \frac{p}{\rho_0} \right) (\zeta + \chi_1 \zeta^3) = 0. \quad (2.182)$$

The value of χ_1 from (174) may be represented in the form

$$\chi_1 = \frac{1 + \theta^4}{16} \left[\frac{(1 + \theta^4)^2}{12(1-\mu^2)} + \frac{1}{\left(1 + \frac{1}{\theta^4} \right)^2 \eta^4} \right] \left(1 - \frac{p}{T_1} \right). \quad (2.183)$$

An equation that is refined in comparison with (182) will be obtained by determining ζ_2 from static variant (167). One can then approximately assume $\zeta_2 = \phi_2 \zeta_1^2$; substituting this value into (166), we arrive in the case of an ideal shell at the equation

$$\frac{d^2 \zeta_1}{dt^2} + C_1 \left(1 - \frac{p}{T_1} \right) [\zeta_1 - (\varphi_1 \varphi_2 - \chi) \zeta_1^3 + \psi_1 \psi_2^2 \zeta_1^5] = 0. \quad (2.182a)$$

We take the solution of Eq. (182) in the form

$$\zeta = A \cos \omega t. \quad (2.184)$$

Satisfying the orthogonality condition of the result of substitution of this solution into Eq. (182), we obtain

$$v^2 = 1 + \frac{3}{4} \chi_1 A^2, \quad (2.185)$$

where

$$v = \frac{\omega}{\omega_0 \sqrt{1 - \frac{\rho}{\rho_{kp}}}}. \quad (2.186)$$

On the basis of Eq. (182a), instead of (185), we obtain the following dependence:

$$\nu^2 = 1 - \frac{3}{4}(\psi_1 \psi_2 - \chi) A^2 + \frac{5}{8} \psi_1 \psi_2 A^4. \quad (2.185a)$$

The characteristics of nonlinear vibrations of a shell according to (185) are demonstrated in Figures 2.25-2.29. Figure 2.25 gives the amplitude-frequency characteristics of natural nonlinear vibrations for a shell with parameters $L/R = 2$, $R/h = 1500$. For the shell under consideration, the minimum frequency of natural vibrations for small deflections corresponds to wave number $n = 10$ (see Figure 2.17). Subsequent higher vibration frequencies correspond to wave numbers $n = 11, 9, 12, 13, 8, 14, 15, 7$ in conformity with the left- and right-hand branches of the curve in Figure 2.17. Figure 2.25 defines the frequency dependence of the amplitude for nonlinear vibrations of a shell with wave numbers corresponding to the spectrum of frequencies of small vibrations in conformity with Figure 2.17. On this graph, instead of (186), the ratio of the vibration frequency to the minimum frequency ($n = 10$) was taken for v , i.e., $v = \omega/\omega_0, \min$. Thus, the points of intersection of the curves of Figure 2.25 with the abscissa determine the ratio of the frequency of natural vibrations of the shell for small deflections to the minimum frequency.

Figures 2.26, 2.27 show the amplitude-frequency relations from (185), (186) for wave formation corresponding to minimum frequencies of small vibrations in accordance with the data of Figure 2.18. The first of these graphs was plotted for shells with parameters $L/R = 1, 2, 3$, and $R/h = 1500$. The second graph reflects the influence of the parameter R/h for $L/R = 2$.

The influence of the character of wave formation on the amplitude-frequency relations is described in Figures 2.28 and 2.29. The graph of Figure 2.28 was plotted

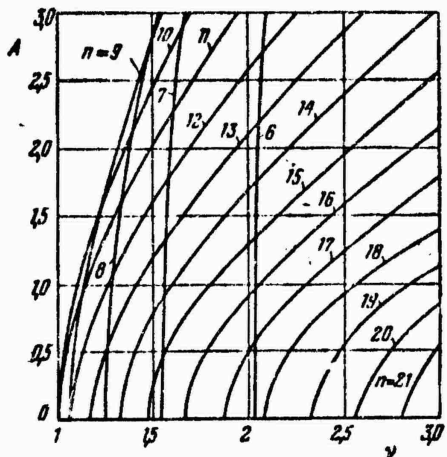


Figure 2.25. Amplitude-frequency relations for different modes of natural nonlinear vibrations of the shell.

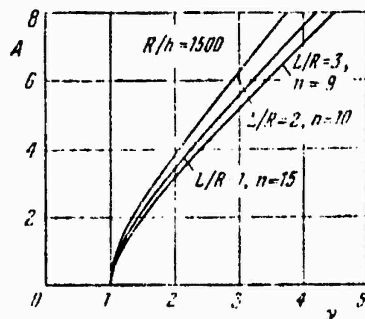


Figure 2.26. Skeletal lines for nonlinear vibrations of shells at minimum frequencies for different L/R values.

for cases in which the relation between the wave formation parameters Θ and η corresponds to the value from (148), for which the magnitude of the upper value of the critical load parameter in axial compression of the shell, $\hat{p} = 0.605$. Figure 2.29 shows the influence of the wave number over the circumference for a ratio of half-wave lengths $\Theta = 2$.

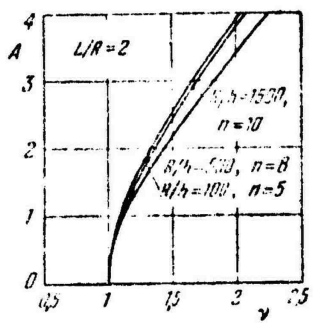


Figure 2.27. Skeletal lines for nonlinear vibrations of shells at minimum frequencies for different R/h values.

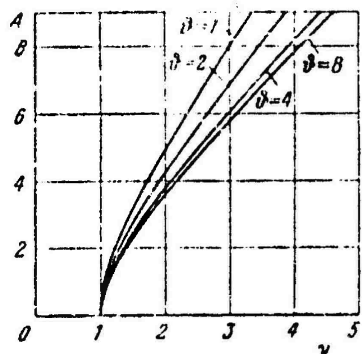


Figure 2.28. Influence of wave formation parameter on amplitude-frequency characteristics.

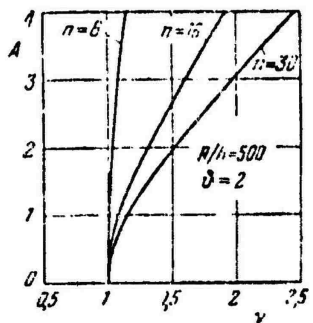


Figure 2.29. Influence of wave number in the circumferential direction on amplitude-frequency characteristics.

30. Elongated Cylindrical Panel. The Bubnov-Galerkin Method

Turning to problems of natural vibrations of panels, we will first consider the case in which the side of a slightly curved panel of radius R along the generatrix substantially exceeds the dimension b along the arc. As in the case of a flat strip, we will assume that the panel is fastened to stiffeners, and during oscillations of the stress σ_y in the middle surface is independent of the y coordinate; $\sigma_y = \sigma$. We reduce the problem to the study of the vibrations of a strip (c , unit length) and having the dimension along the arc equal to b (Figure 2.30).

Equation of motion (1.35) takes the form

$$\frac{D}{h} \frac{\partial^4 w}{\partial y^4} + \sigma \frac{\partial^2 w}{\partial y^2} + \frac{\sigma}{R} + \rho \frac{\partial^2 w}{\partial t^2} = 0. \quad (2.187)$$

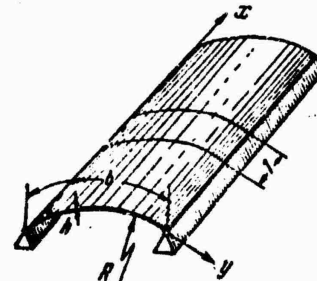


Figure 2.30. Elongated slightly curved cylindrical panel.

The expression for the deflection in the case of hinged fixing will be taken in the form

$$w = f \sin \frac{\pi y}{b}. \quad (2.188)$$

We find σ from the condition of fixing the edges. The mutual approach Δ will be

taken equal to zero:

$$\Delta := - \int_0^b \frac{\partial v}{\partial y} dy = 0. \quad (2.189)$$

From expressions (1.5) and (1.12), we have

$$\frac{\partial v}{\partial y} = - \frac{\sigma}{E} (1 - \mu^2) - \frac{1}{2} \left(\frac{\partial w}{\partial y} \right)^2 + \frac{w}{R}. \quad (2.189a)$$

Hence,

$$\frac{\sigma}{E} b (1 - \mu^2) = - \frac{1}{2} \int_0^b \left(\frac{\partial w}{\partial y} \right)^2 dy + \int_0^b \frac{w}{R} dy. \quad (2.190)$$

Substituting expression (188) for the deflection, we find

$$\sigma = - \frac{E}{1 - \mu^2} \left(\frac{\pi^2}{4} \frac{f^2}{b^2} - \frac{2}{\pi} \frac{f}{R} \right). \quad (2.191)$$

Using the Bubnov-Galerkin procedure

$$\begin{aligned} & \int_0^b \left[\frac{D}{h} \frac{\partial^4 w}{\partial y^4} - \frac{E}{1 - \mu^2} \left(\frac{\pi^2}{4} \frac{f^2}{b^2} - \frac{2}{\pi} \frac{f}{R} \right) \frac{\partial^2 w}{\partial y^2} - \right. \\ & \left. - \frac{E}{R(1 - \mu^2)} \left(\frac{\pi^2}{4} \frac{f^2}{b^2} - \frac{2}{\pi} \frac{f}{R} \right) + \frac{v}{\zeta} \frac{\partial^2 w}{\partial t^2} \right] \sin \frac{\pi y}{b} dy = 0, \end{aligned} \quad (2.192)$$

we obtain the following equation of motion:

$$\frac{d^4 \zeta}{dt^4} + \omega_0^2 (\zeta - \beta \zeta^2 + \eta \zeta^3) = 0, \quad (2.193)$$

where the magnitude of the square of the frequency for small vibrations is determined from the formula

$$\omega_0^2 = \frac{\pi^4}{12(1-\mu^2)} \cdot \frac{c^2 h^2}{b^4} \left(1 + \frac{96}{\pi^4} k^2 \right), \quad (2.194)$$

the curvature parameter being $k = b^2/Rh$, $c = \sqrt{Eg/\gamma}$. The quantities β and η are equal to

$$\beta = \frac{3k}{\frac{\pi^2}{12} + \frac{8}{\pi^2} k^2}, \quad (2.195)$$

$$\eta = \frac{1}{\frac{1}{3} + \frac{32}{\pi^4} k^2}. \quad (2.196)$$

To find the amplitude-frequency characteristic of nonlinear vibrations, we take

$$\zeta = A \cos \omega t. \quad (2.197)$$

Performing the integration over a quarter of the period [2.10], we get

$$v^2 = 1 - \frac{8}{3\pi} \beta A + \frac{3}{4} \eta A^2. \quad (2.198)$$

Examining the case of a panel with clamped edges, we take the following expression for the deflection:

$$w = f \sin^2 \frac{\pi y}{b}. \quad (2.199)$$

Similarly, we find the expression for σ :

$$\sigma = \frac{E}{(1-\mu^2)} \left(\frac{f}{2R} - \frac{1}{4} \frac{\pi^2 f^2}{b^2} \right). \quad (2.200)$$

The equation of motion is reduced to the form (193), where

$$w_0^2 = \frac{\pi^4}{12(1-\mu^2)} \frac{c^2 h^2}{b^4} \left(\frac{16}{3} + \frac{8k^2}{\pi^4} \right). \quad (2.201)$$

For β and η , we have the expressions

$$\beta = \frac{12k}{\pi^2 \left(\frac{16}{3} + \frac{8k^2}{\pi^4} \right)}, \quad (2.202)$$

$$\eta = \frac{4}{\frac{16}{3} + \frac{8k^2}{\pi^4}}. \quad (2.203)$$

31. Elongated Cylindrical Panel. Method of Finite Differences

After determining σ from expression (190) and substituting into (187), we obtain the following equation in partial derivatives:

$$\begin{aligned} \frac{D}{h} \frac{\partial^4 w}{\partial y^4} - \frac{E}{(1-\mu^2)h} \left[\frac{1}{2} \int_0^b \left(\frac{\partial w}{\partial y} \right)^2 dy - \int_0^b \frac{w}{R} dy \right] \frac{\partial^2 w}{\partial y^2} - \\ - \frac{E}{Rh(1-\mu^2)} \left[\frac{1}{2} \int_0^b \left(\frac{\partial w}{\partial y} \right)^2 dy - \int_0^b \frac{w}{R} dy \right] + \frac{\gamma}{g} \frac{\partial^2 w}{\partial t^2} = 0. \end{aligned} \quad (2.204)$$

Introducing the dimensionless quantities $\bar{w} = w/h$, $\xi = y/b$, $t = t/T$, where $T = 2\pi/w_0$, and w_0 is determined from (194), we arrive at the equation

$$\begin{aligned} \frac{\pi^2}{4} \left(1 + \frac{96}{\pi^4} k^2 \right) \frac{\partial^4 \bar{w}}{\partial \xi^4} + \frac{\partial^4 \bar{w}}{\partial \xi^4} + 12k^2 \int_0^1 \bar{w} d\xi - \\ - 6 \left[\int_0^1 \left(\frac{\partial \bar{w}}{\partial \xi} \right)^2 d\xi \right] \frac{\partial^2 \bar{w}}{\partial \xi^2} + 12k \left(\int_0^1 \bar{w} d\xi \right) \frac{\partial^2 \bar{w}}{\partial \xi^2} - 6k \int_0^1 \left(\frac{\partial \bar{w}}{\partial \xi} \right)^2 d\xi = 0. \end{aligned} \quad (2.205)$$

If the nonlinear terms are neglected in Eq. (187) and relation (189a), we obtain the following equation for studying the problem in the linear approximation:

$$\frac{\pi^2}{4} \left(1 + \frac{96}{\pi^6} k^2 \right) \frac{\partial^2 w}{\partial t^2} + \frac{\partial^4 w}{\partial \xi^4} + 12k^2 \int_0^1 w d\xi = 0. \quad (2.206)$$

In integrating Eqs. (205), (206) in finite differences, we adopted the boundary and initial conditions according to (102), (103). The number of steps along the ξ coordinate was taken as $n = 20$ as before, and the ratio of the steps $s_t/s\xi = 1/40$.

Let us analyze the results obtained. We first evaluate the influence of the magnitude of the deflections specified by the initial conditions on the natural vibrations of panels of different curvatures.

Let us consider the data of Figures 2.31-2.38. On these graphs, the time t is referred to the period of natural vibrations for small deflections, period found by considering the curvature of the corresponding panel according to formula (194).

Figure 2.31 shows the deflections of points of the middle surface of the panel with parameter $k = 10$ at different times, marked on the graph in numbers of steps j along the t coordinate according to the data of solution of the linear problem on the basis of (206) and nonlinear problem in accordance with (205), with the bending deflection amplitude $A = 0.1$. As we can see, very similar results are obtained in this case. The motion of the central point ($i = 10$) according to the two solutions is reflected in Figure 2.32; the fine line corresponds to the linear problem. This figure also shows the motion of another point ($i = 1$); this motion is consistent in frequency with the law of motion of center point. It is obvious that this value of the frequency corresponds to that calculated from formula (194).

In contrast to the case of $k = 0$ discussed in 25, the motion of the panel with parameter $k = 10$ (Figure 2.31) is characterized by a change in the mode of additional middle-surface deflections, which is specified by the initial conditions.

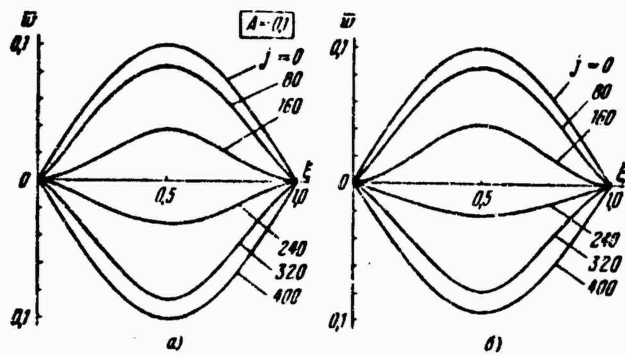


Figure 2.31. Change in the shape of deflections with time for a slightly curved shell with curvature parameter $k = 10$ at initial deflection amplitude at the center $A = 0.1$; a) from data of linear approximation, b) from data of solution of the nonlinear problem.

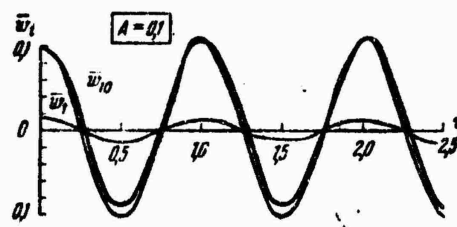


Figure 2.32. Motion of different points in time according to data of solution of the linear and nonlinear problem for shell with parameter $k = 10$ at deflection amplitude $A = 0.1$.

At amplitude $A = 5$ (Figure 2.33), the solution of the nonlinear problem leads to different results than in the case of the linear variant. In the first case, an increase in the frequency of natural vibrations of the shell is manifested for large deflections. This is demonstrated more clearly by the data of Figure 2.34, which shows the change in bending deflection with time according to the data of the linear (thin line) and nonlinear problem. The frequency of nonlinear vibration $v = 1.52$; determining the frequency from formula (198), we find $v = 1.28$.

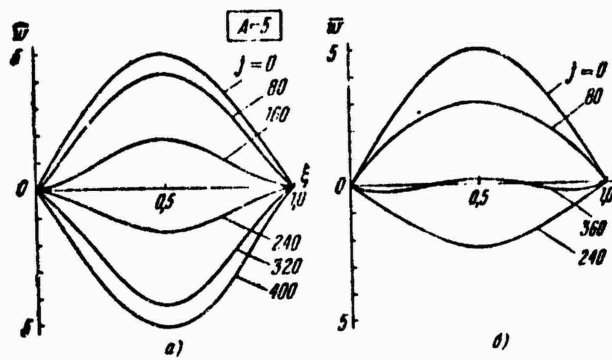


Figure 2.33. Change in the shape of deflections with time for a slightly curved shell with curvature parameter $k = 10$ at amplitude of initial mode $A = 5$; a) linear problem, b) nonlinear problem.

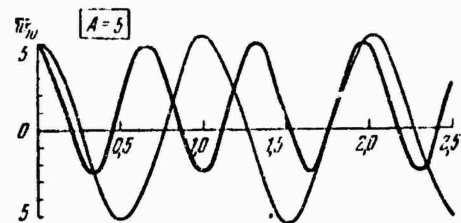


Figure 2.34. Change in bending deflection with time according to data of solution of the linear and non-linear problem for shell with parameter $k = 10$ at deflection amplitude $A = 5$.

Similar data for a panel with curvature parameter $k = 24$ are shown in Figures 2.35-2.38. In this case, even at small deflections ($A = 0, 1$) there is observed a sharp change in shape, the latter being specified as a half sine wave at instant $t = 0$ (Figure 2.35). This graph demonstrates the identical character of the motion of the shell according to the data of the two solutions. Figure 2.36 compares these solutions for the center point; it also shows the curve of motion of another point ($i = 1$). In contrast to the above-discussed case of $k = 10$, here, for small deflections, the motion of the shell has an irregular character. The characteristics also

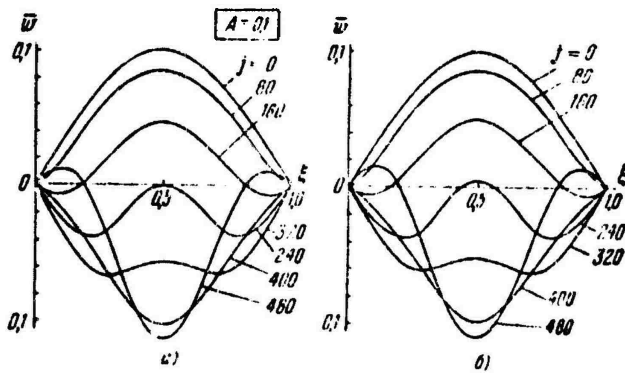


Figure 2.35. Change in the shape of deflections with time for a slightly curved shell with curvature parameter $k = 24$ at deflection amplitude at the center $A = 0.1$: a) linear problem, b) nonlinear problem.

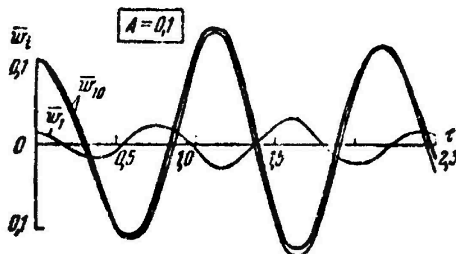


Figure 2.36. Law of motion of different points with time, based on data of two solutions for a shell with parameter $k = 24$ at deflection amplitude at the center $A = 0.1$.

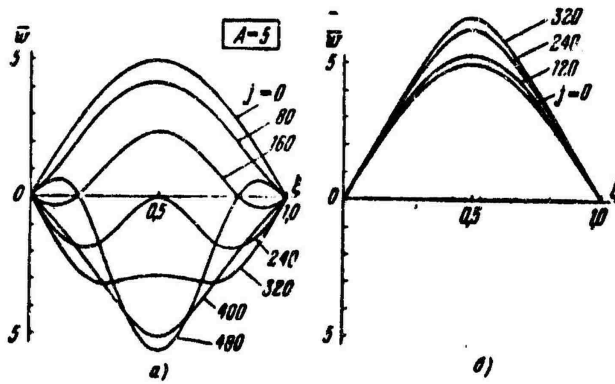


Figure 2.37. Change in the shape of deflections for shell with parameter $k = 24$ at deflection amplitude at the center $A = 5$; a) linear problem, b) nonlinear problem.

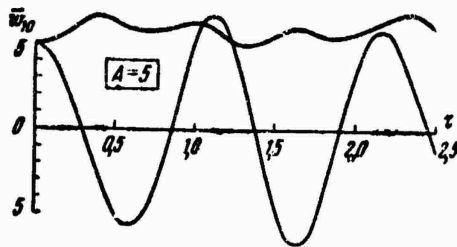


Figure 2.38. Law of motion of the central point according to two solutions for a shell with parameter $k = 24$ at deflection amplitude at the center $A = 5$.

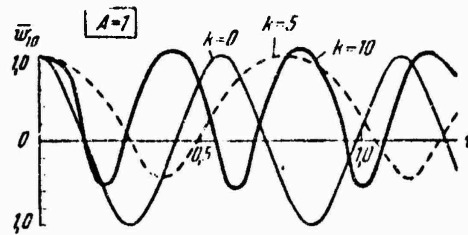


Figure 2.39. Influence of the curvature parameter of the shell on the frequency of nonlinear vibrations at deflection amplitude at the center $A = 1$.

show up in a comparative examination of the motion of different points, characterized by a different frequency. The frequency of the center point proves to be somewhat lower than the value from (194), and for the second point, substantially higher than this value.

At amplitude $A = 5$, the natural vibrations of the shell correspond to motions above the snaped equilibrium position (Figure 2.37b); this does not show up in the linear problem (Figure 2.37a). The difference in the character of the motion of the central point according to these solutions is shown in Figure 2.38.

As is evident from a comparison of Figures 2.9 and 2.34, the effect of increase in frequency for large deflections in relation to the vibration frequency of a panel

of the corresponding curvature for small deflections undergoes a significant decrease as the curvature parameter increases.

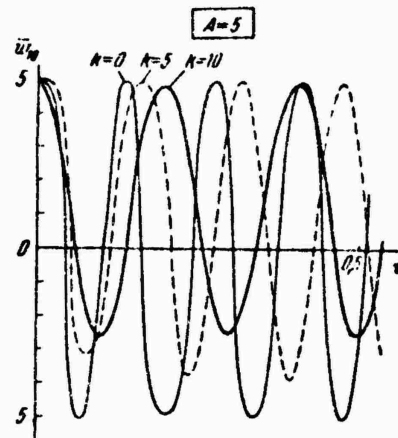


Figure 2.40. Influence of the shell curvature parameter on the frequency of nonlinear vibrations at deflection amplitude at the center $A = 5$.

On the other hand, as the deflection amplitude increases, the difference in the values of frequencies of nonlinear vibrations for panels of different curvatures levels off. This is demonstrated in Figures 2.39, 2.40 for amplitudes $A = 1$ and $A = 5$; in all these cases, the time t is referred to the period of small oscillations of a flat panel in conformity with formula (94a). For $A = 5$, an increase of the curvature parameter leads to a certain decrease in the frequency of natural nonlinear vibrations.

32. Circular Cylindrical Panel with a Finite Ratio of the Sides

Let us consider the case of vibrations of a slightly curved cylindrical panel with a finite ratio of the sides (Figure 2.41).

Let us assume that the edges of the panel are hinged and that they move freely along the arc and along the generatrix, at the same time, the edges of the panel in the middle surface remain rectilinear.

Along the curvilinear edges of the panel are acting the compressive forces p , which are uniformly distributed over the width.

Let R be the radius of the middle surface of the panel, a, b the in-plane dimensions of the sides of the supporting contour, and h , the thickness. The arrangement of the coordinate axes is shown in Figure 2.41.

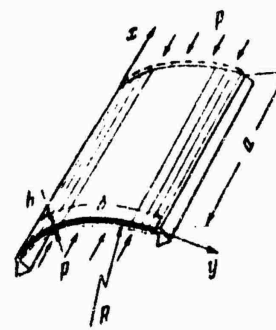


Figure 2.41. Circular cylindrical panel with a finite ratio of sides acted on by axial compressive forces.

The initial equations will be taken in the form of (1.40), (1.41).

Solving the problem in the first approximation, we approximate the deflection w in the form

$$w = f(t) \sin \frac{\pi x}{a} \sin \frac{\pi y}{b}. \quad (2.207)$$

Substituting (207) into the strain compatibility equation (1.41), we determine the stress function in the middle surface

$$\begin{aligned}\Phi = \frac{E}{32} f^2 & \left(\lambda^2 \cos \frac{2\pi x}{a} + \frac{1}{\lambda^2} \cos \frac{2\pi y}{b} \right) + \\ & + \frac{E}{R\pi^2} \frac{a^2}{(1+\lambda^2)^2} f \sin \frac{\pi x}{a} \sin \frac{\pi y}{b} - \frac{1}{2} py^2.\end{aligned}\quad (2.208)$$

where $\lambda = a/b$. Then, satisfying relation (1.40) by use of the Bubnov-Galerkin method, we obtain the following ordinary differential equation describing the natural vibrations of the panel:

$$\frac{d^2\zeta}{d\tau^2} + \frac{\omega_0^2}{\omega^2} \left(1 - \frac{p^*}{p_u^*} \right) (\zeta - \beta_n^{*2} + \eta_n^{*2}) = 0, \quad (2.209)$$

taking $\zeta = f_1(\tau)/h$, $\tau = wt$, $p^* = pb^2/Eh^2$, $p_u^* = p_u b^2/Eh^2$. The upper critical stress parameter p_u^* is

$$p_u^* = \frac{\pi^2 (1 + \lambda^2)^2}{12\lambda^2 (1 - \mu^2)} + \frac{k^2 \lambda^2}{\pi^2 (1 + \lambda^2)^2}, \quad (2.210)$$

the curvature parameter $k = b^2/Rh$. The square of the fundamental frequency of natural vibrations of an ideal panel for small deflections without considering the compressive forces is determined in the form

$$\omega_0^2 = \pi^2 p_u^* \frac{c^2 h^2}{a^2 b^2}, \quad (2.211)$$

where $c = \sqrt{Eg/\gamma}$. The quantities β and η stand for

$$\beta = \frac{16\lambda^2 k}{\pi^2} \Psi^2 \left(\frac{1}{2} + \frac{8}{(1+\lambda^2)^2} \right), \quad (2.212)$$

$$\eta = 0.75\Psi(1+\lambda^2), \quad (2.213)$$

where

$$\Psi = \sqrt{\frac{1-\mu^2}{(1+\lambda^2)^2 + \frac{16\lambda^2 k(1-\mu^2)}{\pi^2(1+\lambda^2)}}} \left(1 - \frac{p^*}{p_u} \right). \quad (2.214)$$

Under the action of axial compression forces, the panel acquires a new stable equilibrium shape in the region of large deflections. Three types of vibratory motions therefore become possible: about the main equilibrium position ζ_1 , about the snapped position ζ_3 , and abrupt displacements of the shell from one position of stable equilibrium to the other (snapping of the shell), displacements involving the crossing of the level corresponding to the unstable equilibrium position.

The possible equilibrium positions of the panel are determined by the roots of Eq. (209) in the static variant.

For $\beta < 2\sqrt{\eta}$, the shell has a single equilibrium position about which the vibrations take place; for $\beta > 2\sqrt{\eta}$, the system has three equilibrium positions.

The elastic characteristics of panels with different curvature parameters k are shown in figure 2.42 in accordance with the relation

$$f(\zeta) = \zeta - \beta \zeta^2 + \eta \zeta^3. \quad (2.215)$$

It is evident that in all these cases, the shell has a single equilibrium position.

For a panel subjected to axial compression, from Eq. (2.5) for $f(\zeta)=0$ one finds a diagram of equilibrium shapes of the ideal panel that determines the equilibrium points at an arbitrary level of axial loading; the corresponding $p^*(\zeta)$ diagram for a panel with curvature parameter $k = 24$ is shown in Figure 2.43. The parameter of the upper critical load in this case is $p_u^* = 18$; the lower critical value $p_1^* = 4.6$.

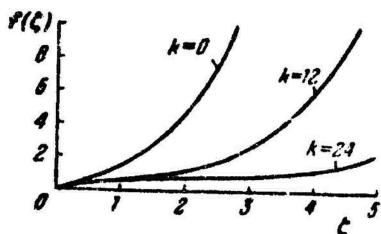


Figure 2.42. Elastic characteristics of panels with different curvature parameters.

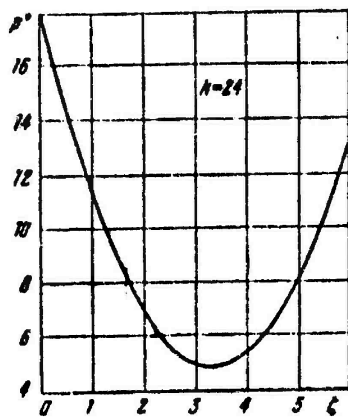


Figure 2.43. Diagram of equilibrium shapes for shell with parameter $k = 24$.

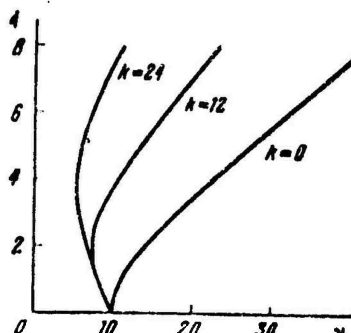


Figure 2.44. Influence of the shell curvature parameter on the amplitude-frequency relations.

Let us now consider the amplitude-frequency relations. Taking the approximate solution of Eq. (209) in the form

$$\zeta = A \cos \tau \quad (2.216)$$

and satisfying the condition of orthogonality of the result of substituting this solution into (209) to the function $\cos \tau$ in a quarter of a period, we obtain an expression of the type of (198)

$$\gamma^2 = 1 - \frac{8}{3\pi} \beta A + \frac{3}{4} \eta A^2, \quad (2.217)$$

$$\tau = \frac{\theta}{\sqrt{1 - \frac{\rho^*}{\rho_0}}}. \quad (2.218)$$

The amplitude-frequency characteristics for panels of different curvatures in the absence of initial compressive forces are shown in Figure 2.44.

33. Case of a Panel with Deforming In-Plane Edges. Refined Solution

Let us examine the solution of the same problem of a panel of finite dimensions in a slightly different formulation. We will assume that the hinged edges of a cylindrical panel distort freely while remaining in the plane of the supporting contour. The in-plane dimensions of the sides of the panel will here be denoted by $2a$ and $2b$. The origin will be placed at the center, and the x and y axes will be directed along sides $2a$ and $2b$ respectively.*

The dimensionless parameters will be introduced in the form

*The data cited here were obtained by A.A. Logvin'skaya, V.V. Rogalevich and the author, Doklady Akad. Nauk SSSR 205, No. 2 (1972), 44-46.

$$\bar{x} = \frac{x}{a}, \quad \bar{y} = \frac{y}{b}, \quad \bar{\omega} = \frac{\omega}{h}, \quad \bar{\Phi} = \frac{\Phi}{h^2}, \quad \lambda = \frac{b}{a},$$

$$\bar{k}_y = \frac{k_y (2b)^2}{h}, \quad \tau = \frac{t}{T_0}.$$

Here T_0 is the period of the fundamental tone of small vibrations of a hinged square plate. Formula (31) for the frequency of natural vibrations of the fundamental tone in the case of a square plate will be represented in the form

$$\omega_0 = \frac{2\pi^2 h}{(2b)^2 \sqrt{12(1-\mu^2)}} \sqrt{\frac{Eg}{\gamma}}. \quad (2.219)$$

Then the dimensionless time parameter will be determined as follows:

$$\tau = \frac{t}{T_0} = \frac{\omega_0}{2\pi} t = \frac{\pi h}{(2b)^2 \sqrt{12(1-\mu^2)}} \sqrt{\frac{Eg}{\gamma}} t. \quad (2.220)$$

The initial equations for a cylindrical panel in dimensionless parameters will take the form (bars over the dimensionless parameters are omitted)

$$\left. \begin{aligned} \lambda^2 \frac{\partial^4 \psi}{\partial x^4} + 2 \frac{\partial^4 \psi}{\partial x^2 \partial y^2} + \frac{1}{\lambda^2} \frac{\partial^4 \psi}{\partial y^4} &= \\ &= - \left[\frac{1}{4} k_y \frac{\partial^2 \omega}{\partial x^2} + \frac{\partial^2 \omega}{\partial x^2} \frac{\partial^2 \omega}{\partial y^2} - \left(\frac{\partial^2 \omega}{\partial x \partial y} \right)^2 \right]; \\ \lambda^2 \frac{\partial^4 \psi}{\partial x^4} + 2 \frac{\partial^4 \psi}{\partial x^2 \partial y^2} + \frac{1}{\lambda^2} \frac{\partial^4 \psi}{\partial y^4} &= 12(1-\mu^2) \left[\frac{1}{4} k_y \frac{\partial^2 \Phi}{\partial x^2} + \right. \\ &\quad \left. + \frac{\partial^2 \Phi}{\partial y^2} \frac{\partial^2 \omega}{\partial x^2} + \frac{\partial^2 \Phi}{\partial x^2} \frac{\partial^2 \omega}{\partial y^2} - 2 \frac{\partial^2 \Phi}{\partial x \partial y} \frac{\partial^2 \omega}{\partial x \partial y} \right] - \frac{\pi^2}{16\lambda^2} \frac{\partial^2 \omega}{\partial \tau^2}. \end{aligned} \right\} \quad (2.221)$$

Integration of these equations can now be performed by considering the boundary and initial conditions.

For free hinged support of the edges, the boundary conditions are

$$\begin{aligned} w = \frac{\partial^2 w}{\partial x^2} - \frac{\partial^2 \Phi}{\partial y^2} - \frac{\partial^2 \Phi}{\partial x \partial y} &= 0 \text{ for } x = \pm 1, \\ w = \frac{\partial^2 w}{\partial y^2} - \frac{\partial^2 \Phi}{\partial x^2} - \frac{\partial^2 \Phi}{\partial x \partial y} &= 0 \text{ for } y = \pm 1. \end{aligned}$$

These conditions may be represented in the form

$$\begin{aligned} w = \frac{\partial^2 w}{\partial x^2} - \Phi - \frac{\partial \Phi}{\partial x} &= 0 \text{ for } x = \pm 1, \\ w = \frac{\partial^2 w}{\partial y^2} - \Phi - \frac{\partial \Phi}{\partial y} &= 0 \text{ for } y = \pm 1. \end{aligned}$$

The initial conditions will be taken in the form

$$w = A, \quad \frac{\partial w}{\partial \tau} = 0 \text{ for } \tau = 0,$$

where A is the initial deviation from the equilibrium position at the center of the panel.

To solve the problem, we will choose a path differing somewhat from the one adopted in 32: we will apply the Bubnov-Galerkin method not only to the equilibrium equation, but also to the strain compatibility equation.

We will consider the solution of the problem in the first approximation according to both the coordinate functions and the time function.

The boundary conditions are satisfied exactly if one sets

$$\left. \begin{aligned} w(x, y, \tau) &= w_{11}(\tau) \cos \frac{\pi x}{2} \cos \frac{\pi y}{2}, \\ \Phi(x, y, \tau) &= \Phi_{11}(\tau) (1 + \cos \pi x)(1 + \cos \pi y). \end{aligned} \right\} \quad (2.222)$$

We substitute (222) into Eqs. (221) and apply the Bubnov-Galerkin procedure to each of them.

From the strain compatibility equation we obtain a relation between the stress function and the deflection

$$\Phi_{II} = \frac{16\lambda^4}{9\pi^4(3+2\lambda^2+3\lambda^4)} k_y w_{II} - \frac{\lambda^2}{8(3+2\lambda^2+3\lambda^4)} w_{II}^2, \quad (2.223)$$

and the equation of motion takes the form

$$\pi^2(\lambda^2 + 1)^2 w_{II} - 12(1 - \mu^2) \left[\frac{256}{9\pi^4} \lambda^2 k_y \Phi_{II} + 4\lambda^2 \pi^2 w_{II} \Phi_{II} \right] - \frac{d^2 w_{II}}{dr^2} = 0. \quad (2.224)$$

We substitute the values of stress function (223) into Eq. (224); we obtain an ordinary nonlinear differential equation

$$\frac{d^2 w_{II}}{dr^2} + aw_{II} - \gamma w_{II}^2 + \beta w_{II}' = 0, \quad (2.225)$$

where

$$\left. \begin{aligned} a &= \pi^2(\lambda^2 + 1)^2 + c \frac{4096\lambda^4}{81\pi^4(3+2\lambda^2+3\lambda^4)} k_y^2, \\ \gamma &= c \frac{32\lambda^4}{3\pi^2(3+2\lambda^2+3\lambda^4)} k_y, \\ \beta &= c \frac{\pi^2 \lambda^4}{2(3+2\lambda^2+3\lambda^4)}, \\ c &= 12(1 - \mu^2). \end{aligned} \right\} \quad (2.226)$$

The second step of the solution consists in integrating Eq. (225). We will give the solution in the first approximation and in terms of the time function, assuming the vibrations to be harmonic.

As was done in 19, we will represent the solution of Eq. (225) in the form

$$w(t) = A \cos \omega t, \quad (2.227)$$

which satisfies the initial conditions of the problem.

Further analysis in terms of the time function will be carried out by means of the Bubnov-Galerkin method. We thus obtain the previous formula for determining the vibration frequency of a cylindrical panel, referred to the frequency of small vibrations of a hinged square plate:

$$\nu = \sqrt{\alpha + \frac{3}{4}\beta A^2}. \quad (2.228)$$

We will examine a refined solution of the problem by approximating the curved surface of a plate or shell with the aid of several parameters. Such a solution makes it possible to follow the change in the shape of the curved surface with time. In this case, the calculations become more complex, and require the use of computers.

Given below is a solution obtained by use of the Bubnov-Galerkin method in the third approximation in coordinate functions; integration with respect to time was performed by the Runge-Kutta method.

We will represent the functions w and Φ in the form of series satisfying the above boundary conditions:

$$\left. \begin{aligned} w &= w_{11} \cos \frac{\pi x}{2} \cos \frac{\pi y}{2} + w_{12} \cos \frac{\pi x}{2} \cos \frac{3\pi y}{2} + \\ &\quad + w_{21} \cos \frac{3\pi x}{2} \cos \frac{\pi y}{2}, \\ \Phi &= \Phi_{11} (1 + \cos \pi x)(1 + \cos \pi y) + \Phi_{12} (1 - \cos 2\pi x) \times \\ &\quad \times (1 + \cos \pi y) + \Phi_{21} (1 + \cos \pi x)(1 - \cos 2\pi y). \end{aligned} \right\} \quad (2.229)$$

Applying the Bubnov-Galerkin method to both fundamental relations simultaneously, we obtain three equations of motion

$$\begin{aligned}
\frac{d^2w_{11}}{dr^2} = & \pi^2 \left\{ d_1 w_{11} - cd_4 (\Phi_{11} + 0.8\Phi_{12} + 0.8\Phi_{21}) + \right. \\
& + c\lambda^2 [2w_{11}(2\Phi_{11} + \Phi_{12} + \Phi_{21}) + 2w_{12}(3\Phi_{11} + \Phi_{12} - 4.5\Phi_{21}) + \\
& \quad \left. + 2w_{21}(3\Phi_{11} - 4.5\Phi_{12} + \Phi_{21})] \right\}, \\
\frac{d^2w_{12}}{dr^2} = & \pi^2 \left\{ d_2 w_{12} - cd_4 \left(0.2\Phi_{11} + 0.16\Phi_{12} - \frac{4}{7}\Phi_{21} \right) + \right. \\
& + c\lambda^2 [2w_{11}(3\Phi_{11} + \Phi_{12} - 4.5\Phi_{21}) + 18w_{12}(\Phi_{11} + \Phi_{21}) + \\
& \quad \left. + 25w_{21}(0.64\Phi_{11} - \Phi_{12} - \Phi_{21})] \right\}, \\
\frac{d^2w_{21}}{dr^2} = & \pi^2 \left\{ d_3 w_{21} - cd_4 \left(1.8\Phi_{11} - \frac{36}{7}\Phi_{12} + 1.44\Phi_{21} \right) + \right. \\
& + c\lambda^2 [2w_{11}(3\Phi_{11} - 4.5\Phi_{12} + \Phi_{21}) + \\
& \quad \left. + 25w_{12}(0.64\Phi_{11} - \Phi_{12} - \Phi_{21}) + 18w_{21}(\Phi_{11} + \Phi_{12})] \right\},
\end{aligned} \tag{2.230}$$

and three strain compatibility equations

$$\begin{aligned}
d_5\Phi_{11} + 2\Phi_{12} + 2\lambda^4\Phi_{21} = & d_8 \left(\frac{1}{36}w_{11} + \frac{1}{180}w_{12} + 0.05w_{21} \right) - \\
& - \frac{\lambda^2}{16}[2w_{11}(w_{11} + 3w_{12} + 3w_{21}) + 9(w_{12}^2 + w_{21}^2) + 16w_{12}w_{21}], \\
2\Phi_{11} + d_6\Phi_{12} = & d_8 \left(\frac{1}{45}w_{11} + \frac{1}{225}w_{12} - \frac{1}{7}w_{21} \right) - \\
& - \frac{\lambda^2}{16}[w_{11}(w_{11} + 2w_{12} - 9w_{21}) + 9w_{21}^2 - 25w_{12}w_{21}], \\
2\lambda^4\Phi_{11} + d_7\Phi_{21} = & d_8 \left(\frac{1}{45}w_{11} - \frac{1}{63}w_{12} + 0.04w_{21} \right) - \\
& - \frac{\lambda^2}{16}[w_{11}(w_{11} - 9w_{12} + 2w_{21}) + 9w_{12}^2 - 25w_{12}w_{21}].
\end{aligned} \tag{2.231}$$

the following notation was used:

$$\begin{aligned}
d_1 = & -(\lambda^2 + 1)^2, \quad d_2 = -(\lambda^2 + 9)^2, \quad d_3 = -(9\lambda^2 + 1)^2, \quad d_4 = \frac{256\lambda^8}{9\pi^4} k_y, \\
d_5 = & 2\lambda^4 + 2 + (\lambda^2 + 1)^2, \quad d_6 = 32\lambda^4 + 2 + (4\lambda^2 + 1)^2, \\
d_7 = & 32 + 2\lambda^4 + (\lambda^2 + 4)^2, \quad d_8 = \frac{64\lambda^2}{\pi^4} k_y.
\end{aligned}$$

Equations (230) constitute a system of ordinary differential equations, and Eqs. (231), a system of algebraic equations.

The following sequence of calculations is employed. We specify the initial deviation in the form of a half sine wave in both directions, i.e., $w_{11} = A$, $w_{12} = 0$, $w_{21} = 0$ and $t = 0$, and the value of the stress function at the initial instant is determined from formula (231). We then find the values of w_{11} , w_{12} , w_{21} at the instant Δt by integrating the system of equations (23) by the Runge-Kutta method. The time step is chosen so as to ensure the stability of the solution of Eqs. (230). The values of Φ_{11} , Φ_{12} , Φ_{21} at instant Δt is determined by solving the system of equations (231). This system is linear, since the values of $w_{11}(\Delta t)$, $w_{12}(\Delta t)$, $w_{21}(\Delta t)$ on the right sides have already been calculated in the previous step.

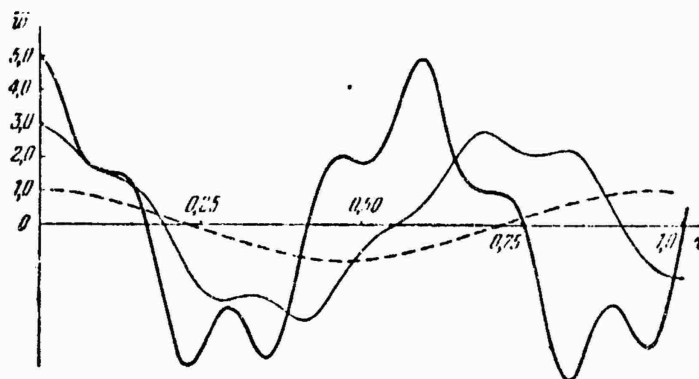


Figure 2.45. Change with time in the deflection at the center of a square plate for different initial deviations.

The values of w and Φ at an arbitrary point of the panel are calculated for a given instant of time from formulas (229).

Figure 2.45 shows the dependence of the deflection at the center of a square plate \bar{w}_0 on time for different initial deviations. For $A = 1$, the vibrations of the plate are harmonic, and the shape of the curved surface is the same as the initial shape. The solution obtained was found to be practically the same as the solution in the first approximation.

If the initial deviation exceeds the plate thickness, the vibrations differ markedly from purely harmonic ones. In addition, the vibration mode at certain times differs markedly from a half sine wave (Figure 2.46); these data were obtained at amplitude $A = 5$.

Let us note that an increase in the vibration period is observed in comparison

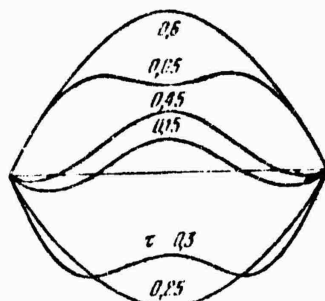


Figure 2.46. Change in
the shape of a plate
with time at amplitude
 $A = 5$.

with the first approximation. The same result was obtained by E.I. Grigolyuk [2.10] in an analysis of the solution in the second approximation in coordinate functions, but assuming that the plate executes harmonic vibrations for any initial deviation.

34. Case of a Panel of Double Curvature

Let us consider the case of a slightly curved panel with an arbitrary contour of the middle surface, rectangular in the plane (Figure 2.47).

We will assume that the panel is hinged along the contour in the presence of free displacement of the points of its edges along the x , y lines of curvature.

We will also assume that the shell has initial deviations in the middle surface that correspond to the shape of the additional deflection.

The dimensions of the sides of the supporting contour in the plane are a , b . The principal curvatures of the shell k_x , k_y are assumed to be constant.

The dynamic equations of nonlinear theory of slightly curved shells will be written in the form of (1.38), (1.39):

$$\frac{D}{h} \nabla^4(w - w_0) = L(w, \Phi) + k_x \frac{\partial^2 \Phi}{\partial y^2} + k_y \frac{\partial^2 \Phi}{\partial x^2} - \rho \frac{\partial^2 w}{\partial t^2}, \quad (2.232)$$

$$\begin{aligned} \frac{1}{E} \nabla^4 \Phi = & -\frac{1}{2} [L(w, w) - L(w_0, w_0)] - \\ & - k_x \frac{\partial^2 (w - w_0)}{\partial y^2} - k_y \frac{\partial^2 (w - w_0)}{\partial x^2}. \end{aligned} \quad (2.233)$$

For the complete and initial deflections we will take the expressions

$$w = f(t) \sin \frac{\pi x}{a} \sin \frac{\pi y}{b}, \quad w_0 = f_0 \sin \frac{\pi x}{a} \sin \frac{\pi y}{b}. \quad (2.234)$$

From Eq. (233), we determine the stress function in the middle surface

$$\begin{aligned} \Phi(x, y, t) = & \frac{E}{32} (f^2 - f_0^2) \left(\lambda^2 \cos \frac{2\pi x}{a} + \frac{1}{\lambda^2} \cos \frac{2\pi y}{b} \right) + \\ & + \frac{k_x}{\pi^2} E \frac{b^2}{\left(1 + \frac{1}{\lambda^2}\right)^2} (f - f_0) \sin \frac{\pi x}{a} \sin \frac{\pi y}{b} + \\ & + \frac{k_y}{\pi^2} E \frac{a^2}{\left(1 + \lambda^2\right)^2} (f - f_0) \sin \frac{\pi x}{a} \sin \frac{\pi y}{b}. \end{aligned} \quad (2.235)$$

Using the method employed above, we obtain the following ordinary differential equation of vibrations of the shell:

$$\frac{d^2 \zeta}{dt^2} + \omega_0^2 (\alpha_s^2 - \beta_s^2 + \gamma_s^2) = 0; \quad (2.236)$$

here $\zeta = f_1(t)/h$, $\zeta_0 = f_0/h$, $f_1 = f - f_0$; w_0^2 is the square of the fundamental frequency of natural vibrations of an ideal panel for small deflections:

$$w_0^2 = \frac{\pi^2 c^2 h^2}{a^2 b^2} \Psi, \quad (2.237)$$

where

$$\Psi = \frac{\pi^2 (1 + \lambda^2)^2}{12\lambda^2 (1 - \mu^2)} + \frac{\lambda^2}{\pi^2 (1 + \lambda^2)^2} k^2. \quad (2.238)$$

As before, c denotes the propagation velocity of longitudinal waves in the shell material; $\lambda = a/b$. The dimensionless curvature parameters of the shell are

$$k_x^* = \frac{k_x a^2}{h}, \quad k_y^* = \frac{k_y b^2}{h}, \quad k^* = k_x^* + k_y^*. \quad (2.239)$$

For the quantities α , β , η , we obtain the expressions

$$\alpha = 1 + \frac{\pi^2}{12\lambda^2 \Psi} \left\{ \frac{2}{3} (1 + \lambda^2) \zeta_0 - \frac{16\lambda^4 k_y^*}{\pi^4} \left[1 + \frac{8}{(1 + \lambda^2)^2} \right] - \right. \\ \left. - \frac{16k_x^*}{\pi^4} \left[1 + \frac{8\lambda^4}{(1 + \lambda^2)^2} \right] \right\}, \quad (2.240)$$

$$\beta = \frac{\pi^2}{12\lambda^2 \Psi} \left\{ \frac{16\lambda^4 k_y^*}{\pi^4} \left[\frac{1}{2} + \frac{8}{(1 + \lambda^2)^2} \right] + \right. \\ \left. + \frac{16k_x^*}{\pi^4} \left[\frac{1}{2} - \frac{8\lambda^4}{(1 + \lambda^2)^2} \right] - \frac{9}{4} (1 + \lambda^2) \zeta_0 \right\}, \quad (2.241)$$

$$\eta = 0.75 \frac{\pi^2}{12\lambda^2 \Psi} (1 + \lambda^2). \quad (2.242)$$

Assuming that the shell is acted on by static pressure q_0 , we obtain the elastic characteristic in the form

$$q_0(\zeta) = \alpha \zeta - \beta \zeta^2 + \eta \zeta^3, \quad (2.243)$$

where the parameter \bar{q}_0 is expressed in terms of the intensity of static pressure q_0 by the formula

$$\bar{q}_0 = \frac{16\lambda^2}{\pi^4 V} \left(\frac{b}{h} \right)^4 q_0. \quad (2.244)$$

In the special case of a spherical shell, it is necessary to take $k_x = k_y = 1/R$; from (239), $k^* = 2b^2/Rh$.

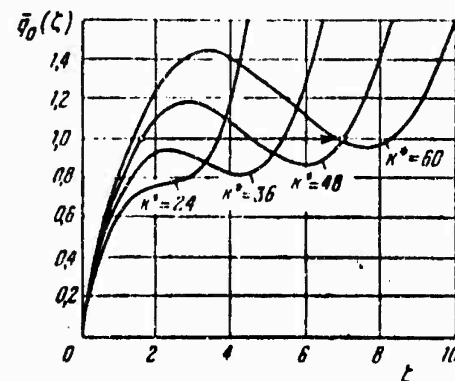


Figure 2.48. Diagrams of equilibrium shapes for ideal panels of different curvatures.

The relations $\bar{q}_0(\zeta)$ for spherical panels at $\lambda = a/b = 1$ are shown in Figures 2.48 and 2.49. The graphs of Figure 2.48, plotted for different k^* , are diagrams of equilibrium shapes for ideal panels ($\zeta_0 = 0$). We see that for values of k^* equal to 36, 48, and 60, snapping of the shell becomes possible during the action of a static transverse pressure \bar{q}_0 surpassing the lower critical value \bar{q}_l . For $k^* = 48$, $\bar{q}_l = 0.87$; the upper values of this parameter $\bar{q}_u = 1.18$.

The influence of initial camber for panels with parameter $k^* = 48$ is evident from Figure 2.49, where $\zeta_0 = 0, 0.1, 0.25$, and 0.5 .

Analyzing the natural vibrations of the shell, we take the solution of Equation (236) in the form of (197). Using the method applied above, we obtain the following

equation for determining the amplitude-frequency characteristic

$$\nu^2 = 1 - \frac{8}{3\pi^2} \beta A + \frac{3}{4} \frac{\eta}{\alpha} A^2, \quad (2.245)$$

where

$$\nu = \frac{\omega}{\sqrt{\alpha \omega_0}}. \quad (2.246)$$

The data of calculations pertaining to an ideal panel for $k_x^* = k_y^* = 24$ are indicated by solid lines in Figure 2.50. For comparison, this figure shows the case of a plate ($k_x^* = k_y^* = 0$) and cylindrical panel ($k_x^* = 0, k_y^* = 24$). The corresponding relations for panels with initial irregularities in the shape of the middle surface for $\zeta_0 = 0.5$ are denoted by dashed lines.

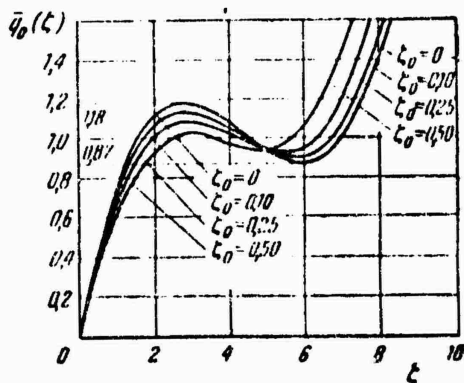


Figure 2.49. Influence of initial camber on the diagram of equilibrium shapes.

35. Slightly Curved Spherical Panel. Solution by the Method of Straight Lines.

In conclusion, let us examine the natural vibrations of a slightly curved spherical shell of circular contour.* The general equations for this case are (1.42) and (1.43). Considering linear damping, we rewrite them in the form (for $w_0 \equiv 0$)

*The results presented here were obtained by N.V. Vashishvili and V.B. Silkin (Izv. VUZ-ov, Mashinostr., No. 2, 1969, 24-28).

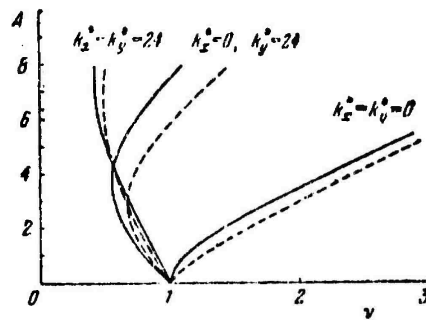


Figure 2.50. Amplitude-frequence relations for slightly curved shells of different curvatures.

$$D\nabla^4 w = \frac{1}{R} \nabla^2 F + L(F, w) + q - \frac{\gamma h}{g} \frac{\partial^2 w}{\partial t^2} - \epsilon \frac{\partial w}{\partial t}, \quad (2.247)$$

$$\frac{1}{Eh} \nabla^4 F = -\frac{1}{R} \nabla^2 w - \frac{1}{2} L(w, w), \quad (2.248)$$

where F stands for Φh . We introduce the following dimensionless parameters:

$$\begin{aligned} F^* &= v \frac{F}{Eh^3}, \quad w^* = \sqrt{v} \frac{w}{h}, \quad t^* = \omega_0 t, \quad x^* = b \frac{x}{c}, \quad y^* = b \frac{y}{c}, \\ r^* &= b \frac{r}{c}, \quad q^* = \frac{\sqrt{v}}{4} \frac{q(x, y, t)}{E} \left(\frac{R}{h}\right)^2, \quad \epsilon^* = \sqrt{\frac{g}{vE}} \frac{R}{h} \epsilon, \\ \omega_0 &= \sqrt{\frac{Eg}{vR^2}}, \quad v = 12(1 - \mu^2), \quad \rho = \sqrt{v} \frac{c^3}{Rh}, \quad b = \sqrt{\rho}. \end{aligned}$$

R and c denote the radius of curvature of the middle surface and the panel radius in the plane.

With the aid of the parameters introduced, Equations (247) and (248) will be written as follows:

$$\nabla^4 w = F^* F + L(F, w) + 4q - \frac{\partial^2 w}{\partial t^2} - \epsilon \frac{\partial w}{\partial t}, \quad (2.249)$$

$$\nabla^4 F = -\nabla^2 w - \frac{1}{2} L(w, w). \quad (2.250)$$

In Eqs. (249) and (250), the asterisks are omitted to simplify the notation.

The bending moments, forces in the middle surface, displacements and deformations are expressed in terms of the functions F and w . We will introduce the following dimensionless parameters for these functions as well:

$$\begin{aligned} M_i^* &= \nu \frac{M_i R}{Eh^3}, \quad H^* = \nu \frac{H R}{Eh^3}, \quad N_i^* = \sqrt{\nu} \frac{N_i R}{Eh^3}, \\ S^* &= \sqrt{\nu} \frac{SR}{Eh^3}, \quad e_i^* = \sqrt{\nu} \frac{R}{h} e_i, \quad \omega^* = \sqrt{\nu} \frac{R}{h} \omega, \\ u^* &= \nu^{1/2} \sqrt{\frac{R}{h}} \frac{u}{h}, \quad \sigma_x^* = \frac{\sigma_x R}{Eh}, \quad \sigma_0^* = \frac{\sigma_0 R}{Eh}, \\ \tau^* &= \frac{\tau R}{hE}, \quad \sigma_i^* = \frac{\sigma_i R}{Eh}. \end{aligned}$$

In the above expressions, σ_x , τ are the total stresses, and σ_1 , σ_0 , the principal stresses and the stress intensity at the surface of the shell, respectively. The formulas for M_2^* , N_2^* , etc. will be written similarly.

Hereinafter, we will use a cylindrical coordinate system. The length of the radius vector will be denoted by r , and the polar angle, by β . The formulas for conversion from the Cartesian to the cylindrical coordinate system can be obtained by superposing the x axis of the former system on the radius vector r .

The derivatives of w with respect to x and y are expressed in terms of the derivatives of w with respect to r and β in the following manner:

$$\begin{aligned} \frac{\partial w}{\partial x} &= \frac{\partial w}{\partial r}, \quad \frac{\partial w}{\partial y} = \frac{1}{r} \frac{\partial w}{\partial \beta}, \quad \frac{\partial^2 w}{\partial x^2} = \frac{\partial^2 w}{\partial r^2}, \\ \frac{\partial^2 w}{\partial x \partial y} &= \frac{\partial^2 w}{\partial r \partial \beta} - \frac{1}{r^2} \frac{\partial w}{\partial \beta}, \quad \frac{\partial^2 w}{\partial y^2} = \frac{1}{r} \frac{\partial w}{\partial r} + \frac{1}{r^2} \frac{\partial^2 w}{\partial \beta^2}. \end{aligned}$$

The operator

$$\begin{aligned} \nabla^2 w &= \frac{\partial^2 w}{\partial x^2} + \frac{\partial^2 w}{\partial y^2} = \frac{\partial^2 w}{\partial r^2} + \frac{1}{r} \frac{\partial w}{\partial r} + \frac{1}{r^2} \frac{\partial^2 w}{\partial \beta^2} = \\ &= \frac{1}{r} \frac{\partial}{\partial r} \left(r \frac{\partial w}{\partial r} \right) + \frac{1}{r^2} \frac{\partial^2 w}{\partial \beta^2}. \end{aligned}$$

The derivatives of the force function F are similarly expressed.

In cylindrical coordinates, Eqs. (249) and (250) take the form

$$\begin{aligned} \nabla^2 w &= \nabla^2 F + \frac{\partial^2 w}{\partial r^2} \left(\frac{1}{r} \frac{\partial^2 F}{\partial r^2} + \frac{1}{r^2} \frac{\partial^2 F}{\partial \beta^2} \right) - \\ &\quad - 2 \left(\frac{\partial^2 w}{r \partial r \partial \beta} - \frac{1}{r^2} \frac{\partial w}{\partial \beta^2} \right) \left(\frac{\partial^2 F}{r \partial r \partial \beta} - \frac{1}{r^2} \frac{\partial F}{\partial \beta^2} \right) + \\ &\quad + \frac{\partial^2 F}{\partial r^2} \left(\frac{\partial w}{r \partial r} + \frac{1}{r^2} \frac{\partial^2 w}{\partial \beta^2} \right) + 4q - \frac{\partial^2 w}{\partial t^2} - \epsilon \frac{\partial w}{\partial t}. \end{aligned} \quad (2.251)$$

$$\nabla^2 F = -\nabla^2 w - \frac{\partial^2 w}{\partial r^2} \left(\frac{1}{r} \frac{\partial w}{\partial r} + \frac{1}{r^2} \frac{\partial^2 w}{\partial \beta^2} \right) + \left(\frac{\partial^2 w}{r \partial r \partial \beta} - \frac{\partial w}{r^2 \partial \beta^2} \right)^2. \quad (2.252)$$

Hereinafter we will examine only an axially symmetric deformation of the shell. Then all the relations become considerably simplified, since the functions w and F will depend only on the variables r and t . Equation (252) becomes

$$\frac{1}{r} \frac{\partial}{\partial r} r \frac{\partial}{\partial r} \frac{1}{r} \frac{\partial}{\partial r} r \frac{\partial F}{\partial r} = -\frac{1}{r} \frac{\partial}{\partial r} r \frac{\partial w}{\partial r} - \frac{1}{r} \frac{\partial w}{\partial r} \frac{\partial^2 w}{\partial r^2}. \quad (2.253)$$

Multiplying the right and left sides of Eq. (253) by r and integrating it, we obtain the following relation:

$$r \frac{\partial}{\partial r} \frac{\partial}{r \partial r} r \frac{\partial F}{\partial r} = -r \frac{\partial w}{\partial r} - \frac{1}{2} \left(\frac{\partial w}{\partial r} \right)^2 + C(t).$$

For shells closed at the apex, the function $C(t)$ becomes zero.

We introduce a new solving function $\phi = \partial F / \partial r$. The derivatives with respect to r will hereinafter be denoted by a prime, and with respect to t , by a dot.

We finally obtain the following system of equations:

$$\begin{aligned}\theta = -\varphi''' - \frac{2w''}{r} + \frac{w'''}{r^2} - \frac{w'}{r^3} + \varphi' \left(1 + \frac{w'}{r}\right) + \\ + \frac{\varphi}{r} (1 + w'') - \varepsilon \dot{w} + 4q,\end{aligned}\quad (2.254)$$

$$\varphi'' + \frac{w'}{r} - \frac{\varphi}{r^3} = -w' \left(1 + \frac{w'}{2r}\right). \quad (2.255)$$

For the stresses and strains, we obtain the expressions

$$\begin{aligned}M_1 = -\left(w'' + \mu \frac{w'}{r}\right), \quad N_1 = \frac{\varphi}{r}, \quad N_2 = \varphi', \\ \sigma_1 = w' - w + \frac{1}{2}(w')^2 - \frac{\varphi}{r} - \mu \varphi', \\ \sigma_2 = \varphi' - \mu \frac{\varphi}{r} \text{ etc.}\end{aligned}$$

We will study the natural axially symmetric vibrations of a panel clamped along the contour (Figure 2.51), assuming that it is first acted on by a pressure of specified intensity q^* . We will assume that at the initial instant, the pressure suddenly drops to zero, and determine the subsequent motion of the shell.

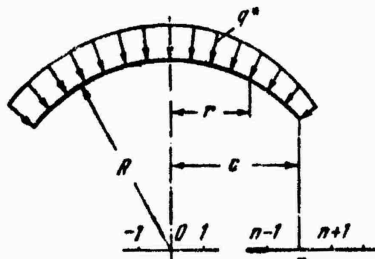


Figure 2.51. Slightly curved circular panel acted on by uniform pressure.

The initial state of the shell is determined from the solution of the static non-linear problem. In Eqs. (254) and (255), we omit the derivatives with respect to time

and integrate (254). The constant of integration for the case under consideration becomes zero. Thus, we obtain the equations

$$\theta'' + \frac{\theta'}{r} - \frac{\theta}{r^2} = \varphi \left(1 + \frac{\theta}{r} \right) + 2qr, \quad (2.256)$$

$$\varphi'' + \frac{\varphi'}{r} - \frac{\varphi}{r^2} = -\theta \left(1 + \frac{\theta}{2r} \right), \quad (2.257)$$

where $\theta = dw/dr$.

This problem can be found, for example, with the aid of the algorithm given by Valishvili*.

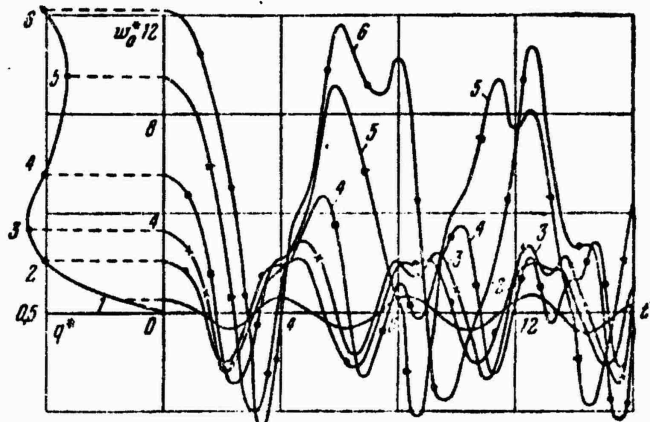


Figure 2.52. Motion of the apex of a spherical shell under different types of loading in the initial position.

Let us now consider the basic equations (254) and (255) describing the motion of an element of the shell. These equations will be transformed by means of formulas of central finite differences:

*Cf. Prikl. matem. i mekh., No. 6 (1968).

$$\begin{aligned}
\ddot{w}_i &= \frac{w_{i+1} - w_{i-1}}{2\Delta} \left(\frac{\varphi_{i+1} - \varphi_{i-1}}{2r_i} - \frac{1}{r_i^3} \right) + \\
&+ \frac{w_{i+1} - 2w_i + w_{i-1}}{r_i \Delta^2} \left(\varphi_i + \frac{1}{r_i} \right) + \frac{\varphi_{i+1} - \varphi_{i-1}}{2\Delta} + \\
&+ \frac{\varphi_i}{r_i} - \frac{w_{i+2} - 4w_{i+1} + 6w_i - 4w_{i-1} + w_{i-2}}{\Delta^4} - \\
&- \frac{w_{i+2} - 2w_{i+1} + 2w_{i-1} - w_{i-2}}{r_i \Delta^3} + 4q - \epsilon \dot{w}_i,
\end{aligned} \tag{2.258}$$

$$\begin{aligned}
\varphi_{i+1} \left(-\frac{1}{\Delta^2} - \frac{1}{2r_i \Delta} \right) + \varphi_i \left(\frac{2}{\Delta^2} + \frac{1}{r_i^2} \right) + \varphi_{i-1} \left(-\frac{1}{\Delta^2} + \frac{1}{2r_i \Delta} \right) = \\
= \frac{w_{i+1} - w_{i-1}}{2\Delta} \left(1 + \frac{w_{i+1} - w_{i-1}}{4r_i \Delta} \right),
\end{aligned} \tag{2.259}$$

where $\Delta = b/n$; n is the number of segments into which the panel radius is divided.

To formulate the boundary conditions at the apex and on the supporting contour, together with the nodal points, whose number is 0 to n , fictitious nodal points outside the segment $[0; b]$ are introduced. These points have numbers (-1) and ($n + 1$).

The conditions for $r = b$, i.e., for $r_n = b$, are determined by the nature of fixing of the supporting contour. In the case of rigid clamping of the contour for $r_n = b$, we have

$$w = 0, \quad w' = 0, \quad \epsilon_2 = 0,$$

or

$$w = 0, \quad w' = 0, \quad \varphi' - \mu \frac{\varphi}{b} = 0. \tag{2.260}$$

We then perform the integration with respect to time, using the Runge-Kutta method. In the calculations, segment b was divided into 20 equal parts. Data of the solution of the problem are given below.

36. Description of Vibrations of a Spherical Panel

The vibratory process experienced by the shell depends significantly on the intensity of the previously applied load in comparison with the critical static value.

We will assume this value to be below the upper critical value, equal to it, or above it.

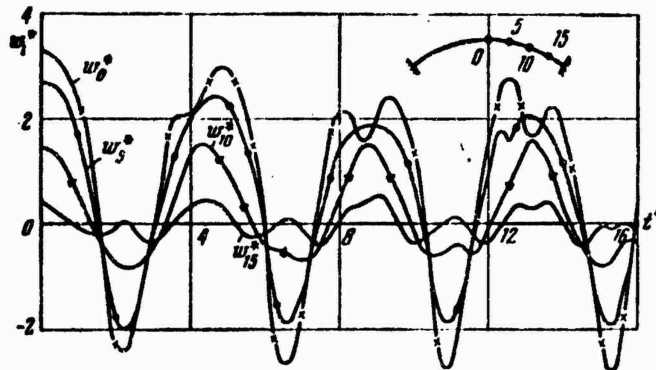


Figure 2.53. Motion of different points of a spherical shell under initial loading with pressure equal to the upper critical value.

The curvature parameter of the panel was taken as $b = 4$.

Figures 2.52 and 2.53 show the data of the calculations. In the former, the ordinate gives the parameter of the normal deflection at the apex of the shell w_0^* , and the abscissa gives the time parameter t^* to the right, and the pressure parameter q^* to the left, which determines the initial strain state of the shell. It is clear that if the initial deflections are small, the motion of the apex of the shell is close to harmonic. As an example, Figure 2.52 shows a graph of the motion of the shell apex in the initial stress and strain state, determined by point I. This point is associated with $q^* = 0.19$ and an initial value of the normal deflection parameter at the apex $w_0^* = 0.515$ or $w_0 = 0.163h$. The dimensionless vibration period $T = 4.3$. Let us note that the upper critical load for the shell under consideration $q^* = 0.56$, and the maximum period of linear free vibrations in conformity with the solution of the problem in Bessel functions* $T = 5.3$. Practically the same value of the period is obtained

*See O.D. Oinashvili's book [0.16].

from a numerical solution of the system of equations (254), (255) if their nonlinear terms are omitted.

The graphs of Figure 2.52 show that at close to critical pressure values, the motion of the shell apex is very complex.

Figure 2.53 shows graphs of the motion of individual points of the shell at an initial pressure equal to the upper critical value $q^* = 0.56$. We can see that the individual points of the middle surface of the shell move out of step.

In summary, we obtain approximately the same picture as for a cylindrical panel (see 31) when solving the problem in finite differences.

Problems of natural vibrations of plates or shells considered as systems with many degrees of freedom are awaiting further thorough study.

Chapter III

Forced Vibrations

§37. Nature of Forced Nonlinear Vibrations of Plates and Shells

The analysis of natural vibrations of plates and shells carried out in the preceding chapter enables us to turn to the study of other types of vibrations. Although natural vibrations were studied without taking damping into account, in actual systems they damp out rapidly because of internal friction in the material, resistance of the medium, etc. For this reason, the study of natural vibrations is important, as already noted, not so much in itself as for evaluating the behavior of a system in the presence of external disturbing forces of a given character. This and the next chapter will be devoted to the case of action of periodic external factors.

For elastic systems usually studied in courses on vibration theory, "ordinary" and "parametric" loads are usually distinguished. The former loads change independently of the vibrations of the system itself; they appear in equations describing the motion of a system as some functions of time and of the space coordinates. Loads of the second type enter into the equations in the form of certain parameters.

Loads of the first type are associated with forced vibrations, and those of the second type, with parametric vibrations. We will first consider the forced vibrations. It should be stated, however, that in flexible plates and shells, "ordinary" type loads such as normal pressure may cause periodically changing forces in the middle surface, giving rise to parametric-type vibrations.

In contrast to natural vibrations, forced vibrations are not damped ones. Under certain conditions, the vibration amplitudes along with the strains and stresses in the plate or shell increase sharply. Such vibrations may be dangerous for actual structures. They frequently lead to the formation of fatigue cracks even in cases where the stresses remain confined within the elastic limits.

If we regard a plate as a system with one degree of freedom, we obtain the

characteristic "displacement amplitude vs. frequency" diagrams shown in Figure 3.1 a. Ω denotes the frequency of the disturbing forces, and w_0 is the natural frequency of small vibrations of the system; $v = \Omega/w_0$. The dashes represent the skeletal line pertaining to natural vibrations. The solid lines correspond to forced vibrations.

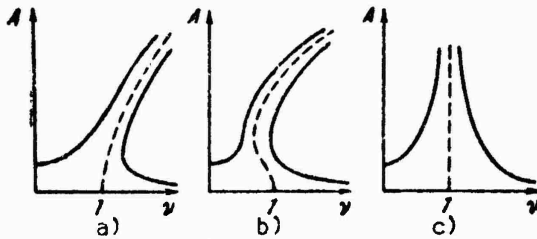


Figure 3.1. "Amplitude-frequency" relations for cases of Nonlinear Vibrations (a, b) and for a Linear System (c).

We see that the "amplitude-deflection" curves for forced vibrations follow the line corresponding to natural vibrations. As the frequency of the disturbing load gradually increases, there is a gradual increase in amplitude, this process corresponding to the left-hand branch of the curve. If however the opposite direction from high frequencies is followed, the change in amplitudes has the peculiar character described by the right-hand branch of the curve. Consequently, forced vibrations of diverse character may correspond to one and the same frequency. Under certain conditions, the representative point may shift from one branch of the curve to the other, with a simultaneous sharp change in the vibration amplitude of the system; for a real plate, such a process is in the nature of snapping; in the case of a system with many degrees of freedom, the description of the motion becomes considerably more complex.

If we are dealing with a shell having a tendency to snap, then in the simplest case, when there is a system with one degree of freedom, the skeletal line (dashes), as we have seen above (§32), has the form shown in Figure 3.1 b and contains a "falling" portion. The lines representing the vibration amplitudes now acquire a different shape (solid curves).

Figure 3.1 c shows analogous characteristics pertaining to a linear system with one degree of freedom.

Thus far, we have dealt with the results of solution of the problems without considering damping. Figure 3.2 shows similar curves, but this time in the presence of damping.

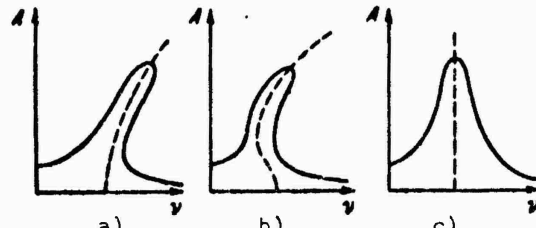


Figure 3.2. "Amplitude-frequency" curves in the presence of damping in cases of nonlinear vibrations (a, b) and for a linear system (c).

Forced vibrations in nonlinear systems are characterized by the fact that they can have additional frequencies different from the frequencies of the disturbing forces. The form of these specific vibrations depends on the initial data of the problem.

§38. Vibrations of a Plate

As our first example, we will consider the case of a hinged plate $a \times b$ with edge moving freely in the plane of the reference contour.*

Let us assume that the plate is subjected to the action of periodically changing transverse load $F \cos \Omega t$. We will also assume that the plate is compressed along side a by static forces p (Figure 3.3). Further, we will consider the initial

*The solutions of the problems given in §38 and 40 were given by I.G. Kildibekov [3.11]; see also [3.8].

deviations of the plate from the ideal plate; the initial deflections will be denoted by w_0 as before.

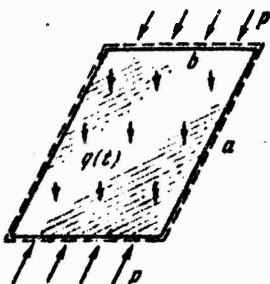


Figure 3.3. Rectangular plate acted on by a periodically changing transverse load.

We will use the system of Equations (1.42a), (1.43a). As the intensity of transverse load we will take

$$q(x, y, t) = F \cos \Omega t - 2 \frac{\gamma}{\delta} h \epsilon \frac{\partial w}{\partial t}, \quad (3.1)$$

where the second term reflects the vibration damping on the assumption that the resistance force is proportional to the velocity $\partial w / \partial t$; ϵ is the damping coefficient. It is assumed that the load is uniformly distributed over the entire area of the plate. We will take the approximating function for the complete deflection in the form

$$w = f(t) \sin \frac{m\pi x}{a} \sin \frac{n\pi y}{b}. \quad (3.2)$$

The initial deflections will be assumed to be distributed according to an analogous law:

$$w_0 = f_0 \sin \frac{m\pi x}{a} \sin \frac{n\pi y}{b}. \quad (3.3)$$

Substituting (2) and (5), as usual, into the right side of the strain compatibility equation (1.43a), we find

$$\Phi = \frac{E}{32} (f^2 - f_0^2) \left[\left(\frac{n\lambda}{m} \right)^2 \cos \frac{2m\pi x}{a} + \left(\frac{m}{n\lambda} \right)^2 \cos \frac{2n\pi y}{b} \right] - \frac{1}{2} p y^2. \quad (3.4)$$

Here $\lambda = a/b$, m denotes the number of half waves in the direction of the generatrix, and n is the number of half-waves along the arc. Then, applying the Bubnov-Galerkin method to Eq. (1.42a), we arrive at the following differential equation describing the nonlinear vibrations of the plate in the first approximation:

$$\frac{d^2\zeta}{dt^2} + 2\zeta \frac{d\zeta}{dt} + \omega_{0,mn}^2 \left(1 - \frac{p^*}{p_0} \right) (\eta\zeta^3 - \beta\zeta^2 + \alpha\zeta) - \frac{\omega_{0,mn}^2}{p_0} \zeta_0 p^* = \bar{q}(t), \quad (3.5)$$

taking

$$\zeta(t) = \frac{f_1(t)}{h}, \quad \zeta_0 = \frac{f_0}{h}, \quad f_1 = f - f_0, \quad p^* = \frac{pb^2}{Eh^2}, \quad (3.6)$$

$$\bar{q}(t) = \frac{16}{\pi^2 E} \left(\frac{c}{h} \right)^2 F \cos \omega t.$$

The quantity p_0^* is equal to the value of the compressive force parameter p^* resulting from the solution of the linear problem of stability of the plate under compression

$$p_0^* = \frac{\pi^2 m^2 \left(1 + \frac{n^2}{m^2} \lambda^2 \right)^2}{12 \lambda^2 (1 - \mu^2)}. \quad (3.7)$$

In this formula, in determining the critical compressive force proper, it is necessary to set $n = 1$ and find the number m which gives (7) its lowest value. The square of the natural vibration frequency at small deflections for a linear system

$$\omega_{0,mn}^2 = \frac{\pi^4 m^4 \left(1 + \frac{n^2}{m^2} \lambda^2 \right)^2}{12 \lambda^2 (1 - \mu^2)} \left(\frac{ch}{ab} \right)^2, \quad (3.8)$$

where c is the propagation velocity of longitudinal waves in the shell material: $c = \sqrt{Eg/\gamma}$ and γ is the specific gravity of the material. Further, the following parameters enter into (5):

$$\left. \begin{aligned} \alpha &= 1 + \frac{\frac{3}{2}(1-\mu^2)\left[1 + \left(\frac{n}{m}\lambda\right)^2\right]\zeta_0^2}{\left[1 + \left(\frac{n}{m}\lambda\right)^2\right]^2\left(1 - \frac{p^2}{p_0^2}\right)}, \\ \beta &= -\frac{\frac{9}{4}(1-\mu^2)\left[1 + \left(\frac{n}{m}\lambda\right)^2\right]\zeta_0}{\left[1 + \left(\frac{n}{m}\lambda\right)^2\right]^2\left(1 - \frac{p^2}{p_0^2}\right)}, \\ \eta &= \frac{\frac{3}{4}(1-\mu^2)\left[1 + \left(\frac{n}{m}\lambda\right)^2\right]}{\left[1 + \left(\frac{n}{m}\lambda\right)^2\right]^2\left(1 - \frac{p^2}{p_0^2}\right)}. \end{aligned} \right\} \quad (3.9)$$

Let us note that for "ideal" plates for $\zeta_0 = 0$, the coefficient α is equal to 1, and $\beta = 0$.

If we consider a quasi-static problem and omit the terms dependent on t in Eq. (5), we arrive at the following equation:

$$\eta_p^2 - p_0^2 + \alpha_0^2 = \frac{\zeta_0}{\frac{p_0}{p^2} - 1} + q^*, \quad (3.10)$$

where

$$q^* = \frac{16}{\pi^2 \omega_{0,mn}^2 E} \left(\frac{c}{h}\right)^2 \left(1 - \frac{p^2}{p_0^2}\right)^{-1} F. \quad (3.11)$$

On the basis of (11), we can determine the static states around which the natural vibrations of the plate take place.

The next step in the solution of the dynamic problem consists in integrating Eq. (5). We represent the approximate solution in the form

$$\zeta = A \cos \Omega t. \quad (3.12)$$

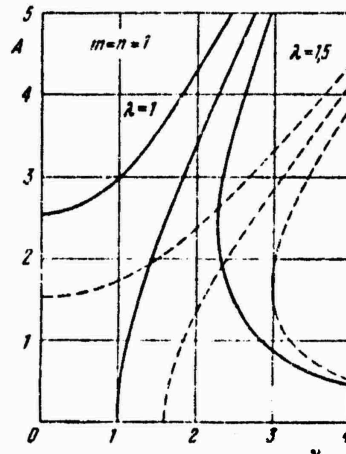


Figure 3.4. Amplitude-frequency curves for fundamental-type vibrations in cases of a square and rectangular plate.

We substitute (12) into Eq. (5) and write the condition of orthogonality of the substitution results to the function $\cos \Omega t$ for a full period:

$$\int_0^{2\pi} L(t) \cos \Omega t dt = 0, \quad (3.13)$$

where

$$L(t) = \frac{d^2 \zeta}{dt^2} + \frac{2\zeta}{\Omega} \frac{d\zeta}{dt} + \omega_{0, mn}^2 \left(1 - \frac{\rho^*}{\rho_0}\right) \times \\ \times (\eta \zeta^3 - \beta \zeta^2 + a \zeta) - \omega_{0, mn}^2 \frac{\rho^*}{\rho_0} \zeta_0 - \dot{q}(t). \quad (3.13a)$$

Performing the calculations, we obtain the following relation between the deflection amplitude and frequency:^{*}

*A result of this type occurs for odd values of m and n .

$$v^2 - \left(\frac{3}{4} \eta A^2 + a \right) K + \frac{q^* K}{A} = 0, \quad (3.14)$$

where K is a coefficient dependent on the method of determination of the dimensionless frequency v .

We obtain relations similar to those found in Figure 3.1a. Figure 3.5 corresponds to one of the higher vibration modes for $m = 3, n = 1$. As the basis of calculating v we always took the frequency of the fundamental mode of linear vibrations of a square plate without considering the compressive forces; then $v = \Omega/w_0, \text{II}$, $K = (w_0, mn/w_0, \text{II})^2 (1 - p^*/p_0^*)$. As we can see, the nonlinear character of the vibrations is expressed more clearly for the higher modes than for the fundamental one.

The influence of static compressive forces on the forced vibrations of a square plate is reflected in Figure 3.6. The level of compressive forces was chosen as 0.9 of the static critical value.

The results of calculations using Eq. (14) are given below. Figure 3.4 shows amplitude-frequency curves pertaining to cases of panels with ratio of the sides $\lambda = 1$ and 1.5 for half-wave numbers $m = n = 1$, i.e., for the fundamental vibration mode. It shows the skeletal lines pertaining to natural vibrations and the characteristics of forced vibrations for a definite transverse load level ($q^* = 8.9$).

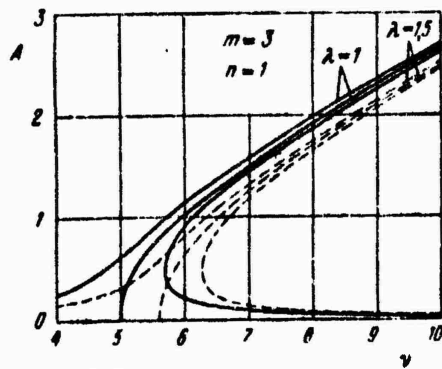


Figure 3.5. Amplitude-frequency curves for one of the higher vibration modes of a square and a rectangular plate.

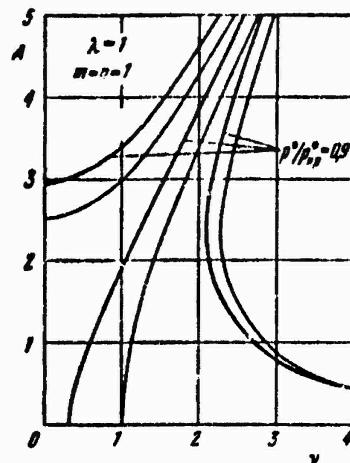


Figure 3.6. Influence of compressive forces on forced vibrations of a square plate in the fundamental mode.

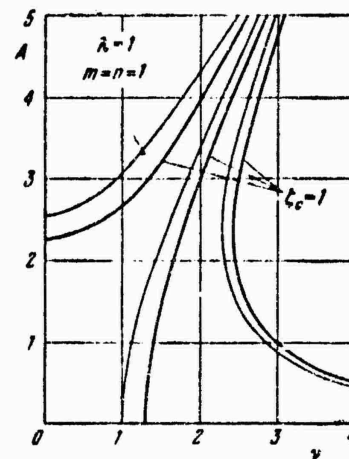


Figure 3.7. Influence of initial imperfections on forced vibrations of a square plate in the fundamental mode.

The effect of initial imperfections for $m = n = 1$ is illustrated in Figure 3.7. The initial bending deflection was chosen as $\zeta_0 = 1$. The next graph, that of Figure

3.8, pertains to a higher vibration mode. Other lines in Figures 3.7 and 3.8 pertain to ideal panels. Judging from these data, an initial camber leads to a shift in the amplitude-frequency characteristics. The higher the vibration mode, the more significant is the influence of nonideality.

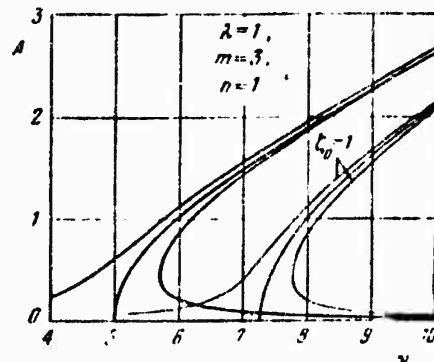


Figure 3.8. Effect of initial imperfections in the case of forced vibrations of a square plate in one of the higher modes.

§39. Closed Cylindrical Shell

Let us now turn to the case of a closed circular cylindrical shell hinged at the ends.*

On the basis of general equations (1.40) and (1.41), the disturbing load will be taken in the form

$$q(x, y, t) = Q_{mn} \sin \frac{m\pi x}{L} \cos \frac{ny}{R} \cos \Omega t. \quad (3.15)$$

Thus, we are here considering a load distributed nonuniformly over the shell surface. The coordinates x and y are measured along the generatrix and the arc. The number of half-periods of change of the load along the length of the shell L is denoted by m , and the number of full periods of change of the load along the

*The solution of the problem as given below is due to Evensen and Fulton [3.22].

circumference is denoted by n . The peak load corresponding to the given indices m and n is denoted by Q_{mn} .

We will consider flexural type vibrations of the shell and take $n \geq 2$. The deflection of the shell will be approximated by the expression

$$w(x, y, t) = A_n(t) \sin \frac{m\pi x}{L} \cos \frac{n\pi y}{R} + \frac{n^2}{4R} A_n^2(t) \sin^2 \frac{m\pi x}{L}. \quad (3.16)$$

The same type of relation was used in §29 in the study of natural vibrations. The difference lies in the choice of the coefficient of the second term. In this case, it will be specified in advance as dependent on the wave number n and on the first parameter. Comparing (2.159) and (16), we find the ratio

$$\frac{I_2}{I_1} = \frac{1}{4} \left(\frac{n^2 h}{R} \right) \left(\frac{A_n}{h} \right).$$

It is assumed that for $n = 2$, the role of this second term in (16) is minor, and that it is significant when n^2 is of the order of R/h .

We substitute (16) into the right side of Eq. (2.158). We integrate this equation and determine the function ϕ . We then apply the procedure of the Bubnov-Galerkin method to Eq. (2.157). We thus arrive at the following relation:

$$\frac{d^2\zeta}{dt^2} + \zeta + \frac{3\eta^2}{8} \zeta \left[\zeta \frac{d^2\zeta}{dt^2} + \left(\frac{d\zeta}{dt} \right)^2 \right] - s\eta^2\zeta^3 + \eta^4\delta\zeta^5 = G_{mn} \cos \nu\tau. \quad (3.17)$$

The following dimensionless parameters were introduced here:

$$\zeta = \frac{A_n}{h}, \quad \tau = \omega_0 t, \quad G_{mn} = \frac{Q_{mn} g}{\gamma h^2 \omega_0^2}. \quad (3.18)$$

v stands for the dimensionless frequency

$$v = \frac{\Omega}{\omega_0}, \quad (3.19)$$

ω_0 being the vibration frequency for the corresponding linear system and being determined from (2.144); this expression will be represented in the form

$$\omega_0 = \left\{ \frac{E_R}{\gamma R^3} \left[\frac{\theta^4}{(\theta^2 + 1)^2} + \frac{\eta^2 (\theta^2 + 1)^2}{12(1 - \mu^2)} \right] \right\}^{1/2}. \quad (3.20)$$

The main parameters determining the behavior of a nonlinear system, are the quantities

$$\left. \begin{aligned} \eta^2 &= \left(\frac{n^2 h}{R} \right)^2, \quad s = \frac{\theta^4 \left[\frac{1}{(\theta^2 + 1)^2} - \frac{1}{16} - \frac{\eta^2}{12(1 - \mu^2)} \right]}{\left[\frac{\theta^4}{(\theta^2 + 1)^2} + \frac{\eta^2 (\theta^2 + 1)^2}{12(1 - \mu^2)} \right]}, \\ \theta &= \frac{3\theta^4}{16} \left[\frac{1}{(\theta^2 + 1)^2} + \frac{1}{(9\theta^2 + 1)^2} \right]. \end{aligned} \right\} \quad (3.21)$$

The coefficient θ characterizes the form of wave formation:

$$\theta = \frac{\pi R/n}{L/m} \quad (3.22)$$

and is the ratio of the half-wavelength in the direction of the arc to the half-wavelength along the generatrix. The quantities n , θ , analogous to those used here, were used in Chapter II in the study of natural vibrations. We will assume further

$$\zeta = A' \cos v\tau. \quad (3.23)$$

Then Eq. (17) is reduced to

$$(1 - v^2) A - \frac{3\eta^2}{16} v^2 A^3 - \frac{3s\eta^2}{1} A^3 + \frac{5}{8} \eta^4 \theta A^5 = G_{mn}. \quad (3.24)$$

We have obtained the amplitude-frequency characteristic $A(\Omega)$ of forced vibrations, which is dependent on the amplitude of the disturbing load G_{mn} . When $G_{mn} = 0$, we arrive at the relation $A(v)$, corresponding to natural vibrations. In §29, we obtained a similar equation by examining the problem in a different formulation. We then considered two independent parameters in the expression for the deflection, reflecting the character of buckling of the shell in the large; one of these parameters was determined from the static variant of the corresponding equation of motion.

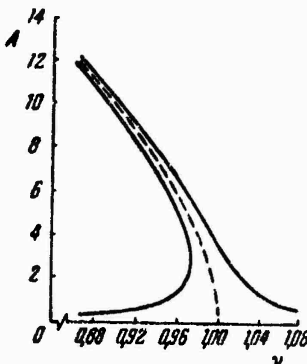


Figure 3.9. Soft-type amplitude-frequency curves in the case of a closed cylindrical shell.

Figure 3.9 shows the curves corresponding to (24) for $G_{mn} = 0.1$, $n^2 = 0.01$, $\theta = 0.1$. Dashes represent the skeletal line corresponding to $G_{mn} = 0$. We see that for the selected shell parameters, the natural vibration amplitudes increase with decreasing frequency, in contrast to the case of a flat plate. Consequently, the nonlinearity involved here is of a different type than for a plate; the entire curve obtained is "falling", as on one of the portions of the curve in Figure 3.1b. The slight nonlinearity characteristic of Figure 3.9 pertains to relatively long cylinders with thin walls. In other cases, the nonlinearity may be manifested more clearly.

Figures 3.10 and 3.11 show the character of the skeletal curves as a function of the parameters n and θ . These graphs attest to a significant influence of n on the behavior of the system.

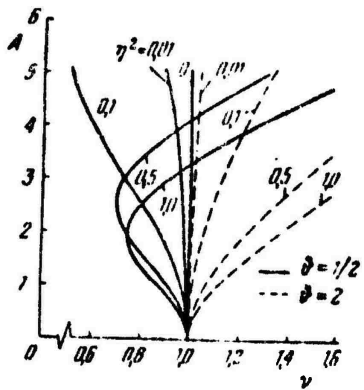


Figure 3.10. Influence of wave formation parameters on amplitude-frequency curves in the case of a closed cylindrical shell.

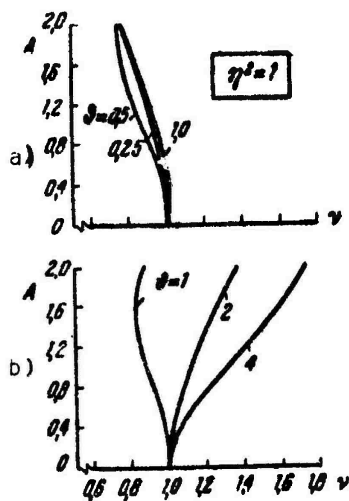


Figure 3.11. Effect of the ratio of half-wavelengths on the amplitude-frequency curves of non-linear vibrations for a cylindrical shell.

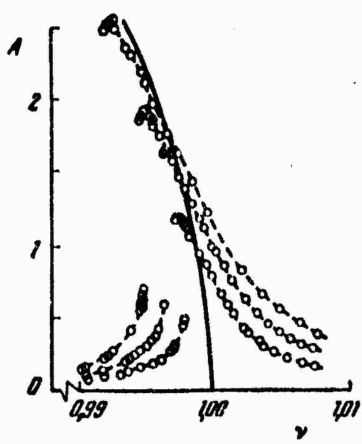


Figure 3.12. The "deflection amplitude vs. frequency" curve for a circular cylindrical shell in comparison with experimental data.

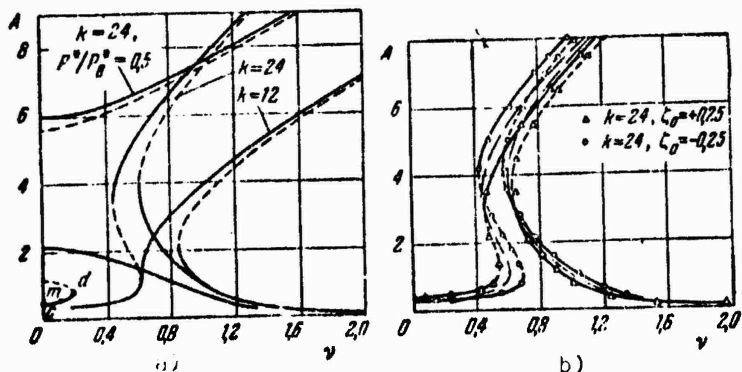


Figure 3.13. Amplitude-frequency curves for circular cylindrical panels of different curvatures: a) ideal panel, b) shell with initial camber.

Finally, Figure 3.12 illustrates the experimental data obtained by Olson [3.22] for forced vibrations. The solid line corresponds to the skeletal curve according to (24) for the parameter values taken for Olson's models. We see that the character of the relations for forced vibrations, shown in Figure 3.9, is confirmed.

It should be noted, however, that for shells of a different type, the solution of the problem can lead to graphs of the type of Figures 3.1b and 3.13.

§40. Case of a Cylindrical Panel.

Let us now examine the case of a slightly curved cylindrical panel; the natural vibrations of such a system were discussed in §32. It will again be assumed that the panel is compressed by static forces p along the generatrix.

The ordinary equations (1.40), (1.41) will be used; for the load intensity q we will choose expression (1), which takes account of the damping effect. We will approximate the complete and initial deflection in the form of (2) and (3), assuming that buckling of the panel takes place with the same half-wave in the direction of the generatrix and along the arc ($m = n = 1$).

The supplemented expression for Φ takes the form $\lambda = a/b$

$$\begin{aligned}\Phi = & \frac{E}{32} (f^2 - f_0^2) \left(\lambda^2 \cos \frac{2\pi x}{a} + \frac{1}{\lambda^2} \cos \frac{2\pi y}{b} \right) + \\ & + \frac{E}{R\pi^2} \frac{a^2}{(1+\lambda^2)^2} (f - f_0) \sin \frac{\pi x}{a} \sin \frac{\pi y}{b} - \frac{1}{2} py^2.\end{aligned}\quad (3.25)$$

After applying the Bubnov-Galerkin method to Eq. (1.40), we again arrive at relation (5). However, p_0^* should be replaced by the upper critical stress parameter p_u^* , which according to (2.210)

$$p_u^* = \frac{\pi^2 (1+\lambda^2)^2}{12\lambda^2 (1-\mu^2)} + \frac{b^2 \lambda^2}{\pi^2 (1+\lambda^2)^2}; \quad (3.26)$$

k stands for the curvature parameter $k = b^2/Rh$. The quantities α , β , η turn out to be

$$\left. \begin{aligned}\alpha &= 1 + \Psi \left\{ \frac{3}{2} (1+\lambda^2) \zeta_0^2 - \frac{16\lambda^4 k}{\pi^4} \left[1 + \frac{8}{(1+\lambda^2)^2} \right] \zeta_0 \right\}, \\ \beta &= \Psi \left\{ \frac{16\lambda^4 k}{\pi^4} \left[\frac{1}{3} + \frac{8}{(1+\lambda^2)^2} \right] - \frac{9}{4} (1+\lambda^2) \zeta_0 \right\}, \\ \eta &= \frac{3}{4} \Psi (1+\lambda^2).\end{aligned} \right\} \quad (3.27)$$

By (2.214), the expression for ψ will be

$$\Psi = \frac{1 - \mu^2}{\left[(1 + \lambda^2)^2 + \frac{12\lambda^4 k^2 (1 - \mu^2)}{\pi^4 (i + \lambda^2)^2} \right] \left(1 - \frac{p^*}{p_0} \right)}, \quad (3.28)$$

The frequency of natural vibrations w_0 is defined by expression (2.211).

The second stage of the solution of the problem will conform to the scheme employed in the case of a plate (§38). Taking $\zeta(t)$ from (12), we write the condition of orthogonality by analogy with c §32 and for $\varepsilon = 0$ arrive at the amplitude-frequency characteristic

$$v^2 = a - \frac{8}{3\pi} \beta A + \frac{3}{4} \gamma A^2 - \frac{4}{\pi A} \frac{\zeta_0}{\left(\frac{p_0}{p^*} - 1 \right)} - \frac{q^*}{A}. \quad (3.29)$$

The value of q^* is calculated as in (11).

Figure 3.13 shows curves of $A(v)$ plotted from (29) for cylindrical panels of different curvature. Figure 3.13 a pertains to cases of ideal panels for two values of the curvature parameter; we took $q^* = 0.3$. For the panel with parameter $k = 24$, we consider two cases: absence of axial compression, and parameter of axial forces p^* amounting to one-half of the upper critical value. In the latter case, the amplitude-frequency characteristics consist of several isolated segments, reflecting the presence of a second stable equilibrium position in the system. The cmd branch corresponds to vibrations about the main equilibrium position, and the upper branches correspond to vibrations with considerable amplitudes.

The data of Figure 3.13b demonstrate the influence of the initial deflection on the amplitude-frequency curves for curvature parameter $k = 24$ in the case of $p^* = 0$; for comparison, dot-dash lines in this figure indicate curves for an ideal panel. Initial irregularities directed toward the center of curvature seem to "rectify" the amplitude-frequency curves; initial camber directed away from the center of curvature causes a reinforcement of nonlinear effects.

§41. Experimental Data on Nonlinear Vibrations and Stability of Reinforced Panels in an Acoustic Field.

The results cited in the preceding section reflect the characteristic features of the behavior of structural elements undergoing vibrations under the action of pressures in a field of acoustic radiation.*

As experimental data show, deformations of shells under intensive acoustic loading are essentially nonlinear in character. This refers particularly to structural elements which, in addition to acoustic loads, are simultaneously subjected to forces of the type of axial compression or external pressure, whose influence may lead to buckling of the structure. In such cases of loading, in addition to the problem of fatigue failure, a no less important problem is that of the influence of acoustic loads on the bearing capacity of a reinforced structure.

Let us turn to the results of experimental studies of acoustic strength and bearing capacity of reinforced cylindrical Duralumin panels. We will examine data on fatigue strength, stress state characteristics, and the nature of failure of panels under conditions of acoustic loading at different levels of static axial compression.**

The specimens were cylindrical panels reinforced in the longitudinal direction with three ribs (two along the edges and one at the center). The ratio of the sides for cells of the smooth part after fastening along the curved edges $\lambda = 2$ for a curvature parameter $k = b^2/Rh \approx 10$ (see §30).

At first, static tests involving the action of only axial compression forces were performed. The results of experiments on three samples were used to establish the average critical loads of local stability loss of the skin and to determine the

*These problems are investigated in a statistical formulation in Chapter X.

**The experimental data cited were obtained by I.G. Kii'dibekov in collaboration with A.A. Mitsyuk [3.11a].

static bearing capacity.

Dynamic tests were performed by using a siren and acoustic camera, which generated a pressure field having a well-defined narrow-band energy spectrum with a marked predominance of the fluctuation level of the first harmonic. Resonance tests were carried out first. By changing the frequency smoothly at a low sound-pressure level, the frequency of the fundamental tone of natural vibrations $f_0 = 370$ Hz was established. This frequency was determined from a sharp increase in the readings of strain gauges.



Figure 3.14. Shell after loss of bearing capacity in axial compression in an acoustic field:
a) view of smooth part of skin; b) view of stiffening ribs.

The bearing capacity of the panels acted on by the acoustic load was determined as follows. The panels were first loaded with an axial compression force corresponding



Figure 3.15. Character of the fatigue failure of a specimen following an acoustic load, simultaneously acted on by axial compressive forces: a) view of skin side, b)-e) zones of failure.

to 0.7 of the average value of the static bearing capacity, then the axial force was slowly increased further in the course of the acoustic loading up to the instant of loss of bearing capacity. The character of the axial load increase corresponded to the static tests. The instant of loss of bearing capacity was recorded by analogy with static tests. The critical loads were determined at a sound pressure level of 164-168 dB and for a fluctuation spectrum concentrated around the 300 Hz frequency. The decrease in bearing capacity in relation to the results of static tests amounted to an average of 7%.

A photograph of one of the specimens at the time of loss of bearing capacity under acoustic loading is shown in Figure 3.14. The difference of these cases of loading from static tests was manifested in greater buckling of the skin and a weakening of the rivet joints.

A specimen of another series was subjected to acoustic loading at a level of 164-168 dB with a predominant frequency of 370 Hz and the simultaneous action of a static axial compression force P ; the chosen value of P corresponded to the critical load of local stability loss. The resource, i.e., the time preceding the appearance of the first crack, was 7 min. Subsequent 4-min loading of the panel caused fatigue failure with an appreciable propagation of cracks along the rivet joints and damage to the part of the skin that included the stress raisers. A view of the specimen after a total acoustic action lasting 11 min is presented in Figure 3.15, which also shows the zones of fatigue failure.



Figure 3.16. View of the specimen after a test with acoustic loading in another regime under the simultaneous action of axial compressive forces: a) photograph of specimen on the skin side; b), c) zones of fatigue failure.

Figure 3.16 shows a photograph of the specimen after acoustic loading tests under floating frequency conditions in the 10 to 500 Hz range for 8 min at the same sound pressure level. The axial compression force in this case was also equal to the critical skin-buckling load. A considerable damage to the skin (Figure 3.16, zone A) occurred in the zone of a raiser; a second failure zone is concentrated along a rivet joint.

Analysis of the oscillograms corresponding to stresses in the specimens shows that acoustic stress of the panels in the absence of axial compression leads to the formation in the structure of variable stresses with a peak cycle value in the range $\sigma_a = 200$ to 400 kg/cm^2 ; the highest value of σ_a in the tests performed was found to be 765 kg/cm^2 .

A significant increase in stresses takes place during acoustic loading and the simultaneous action of an axial compression force equal to the critical value of local stability loss. For one of the specimens (Figure 3.15), the value of σ_a reached 1000 kg/cm^2 for an average cycle value $\sigma_m = 250 \text{ kg/cm}^2$. This increase in stress level is apparently related to the snapping of the panel from one position of stable equilibrium to another, and also to vibrations around a second position of stable equilibrium. In one of the experiments, the maximum value of the stresses was close to the yield point of the material and amounted to $\sigma_{\max} = 2500 \text{ kg/cm}^2$, for a peak cycle value $\sigma_a = 1050 \text{ kg/cm}^2$.

On the basis of results of frequency analysis of the oscillograms, stress change frequencies twice as high as the frequency of acoustic action were recorded. This is explained by a characteristic of nonlinear vibrations related to the development of deflections amounting to five shell thicknesses.

§42. Spherical Panel

Let us return to the case of a spherical panel, whose natural vibrations were discussed in §35 and 36. We are dealing with a panel circular in the plane with a rigidly clamped reference contour. Axisymmetric forced vibrations of the panel will be studied. It will be assumed that the intensity of the external pressure,

constant along the radius, changes according to one of the following laws (in dimensionless parameters, §35):

$$\begin{aligned} 1. q^* &= 0.1 \sin 0.5t; & 2. q^* &= 0.4 \sin 0.5t; \\ 3. q^* &= 0.1 \sin 2t; & 4. q^* &= 0.4 \sin 2t. \end{aligned} \quad \left. \right\} \quad (3.30)$$

In these expressions, the peak load values were assumed, on the one hand, to be lying appreciably below the upper critical load ($q_u^* = 0.56$), and on the other hand, close to it. The period of the external action in the first two cases exceeds the period of free linear vibrations of the shell, and in the third and fourth cases is below this value.

Figure 3.17 and 3.18 give the results of calculations* for a shell of curvature parameter $k = 4$ (see §35). In a numerical solution of the problem carried out by using the algorithm described in §35, the initial values of the displacements and velocities were considered to be zero. Damping was not considered; it was assumed that $b = 0$.

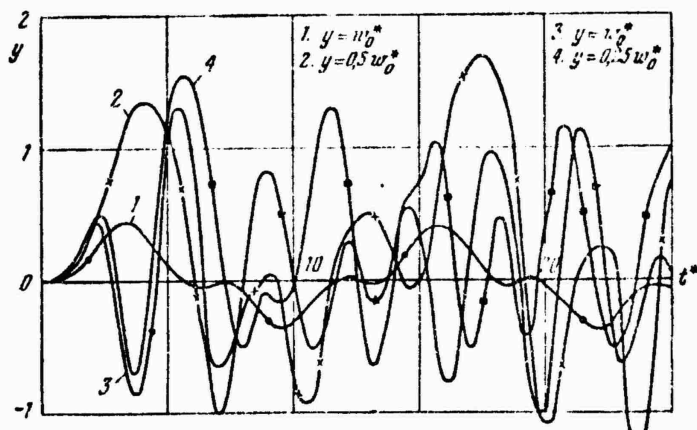


Figure 3.17. Motion of the pole of a shallow spherical shell for different laws of change in external load intensity.

Figure 3.17 shows graphs of the motion of a shell apex in time. The numbers

*These data are due to N.V. Vallishvili and V.B. Silkin.

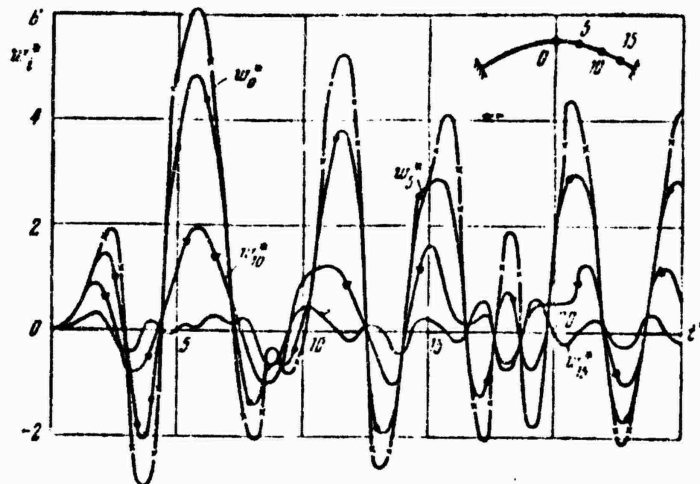


Figure 3.18. Laws of motion of different points of a shallow spherical shell.

of the curves on the graphs correspond to the number of the law governing the change of load according to (30).

The results given in Figure 3.17 indicate that the solution is periodic in character only for the first problem, and that the vibration period of the shell apex is close to the period of change of the disturbing load 4π . For the remaining laws of load change, the solutions obtained are not strictly periodic, i.e., it is difficult to establish definite values of the vibration period and amplitude. The determination of periodic solutions of the problems under consideration is possible in different ways. First of all, one can appropriately select the initial values of the displacements and velocities. However, this method is complex. Apparently, it is advisable to determine periodic solutions by considering the damping effect in the equations of motion.

Judging from the solution obtained, individual points of the middle surface of the shell execute a motion that is not synchronous with the motion of the apex. Figure 3.18 shows graphs of motions of characteristic points of the shell for the fourth problem. We can see that the points considered execute a complex motion, and that at certain times they are in antiphase. This indicates that for finite displacements, treatment of shallow shells as systems with one degree of freedom may lead to appreciable errors.

Chapter IV

Parametric Vibrations

§43. Characteristics of Parametric Vibrations

As we already know from Chapter III, parametric vibrations arise from a periodic change of "particular" loads. The quantities characterizing such loads enter as parameters into the basic differential equations of the problem.

Let us consider as an example a plate fixed along the edges in some manner. Let this plate be subjected along one of the sides to the action of compressive forces that changes periodically with time; parametric vibrations can then take place. The principal state of a structure in the presence of such vibrations is characterized by displacements of middle-surface points in this surface alone. For certain ratios of the frequency of load fluctuations to the frequency of natural vibrations, such a principal state becomes unstable, and increasing normal displacements take place.

When the problem is solved in the linear formulation, it turns out that such unstable zones of the principal state are associated with deflections increasing from one cycle to the next. It is important to note that the first zone of such a dynamic instability lies near the fluctuation frequency of the load, which is twice the frequency of natural vibrations of the structure; we are concerned here with a system with one degree of freedom.

Figure 4.1 a shows approximate boundaries of dynamic instability zones. The ratio of twice the frequency of natural vibrations 2Ω to the frequency of load fluctuations θ is laid off along the abscissa axis, a system with one degree of freedom being considered. The quantity k , dependent on the character of load fluctuations, is laid off along the ordinate axis; it represents the ratio of the amplitude of the variable part of the load to its average value. The first region of dynamic instability, corresponding to the point on the abscissa axis with coordinate $2\Omega/\theta=1$, and the second and third zone, at $2\Omega/\theta = \sqrt{2}$, 3, are shaded. This graph refers to

the case in which damping factors are not considered.

The next figure, 4.1b, was plotted by taking damping into account. For the second and the subsequent zones, the instability region moves far from the abscissa axis, so that the instability phenomenon in this case is manifested only for very sharp load changes. Practically for this reason, the highest value is in the first zone; we will be dealing with this zone in the discussion below.

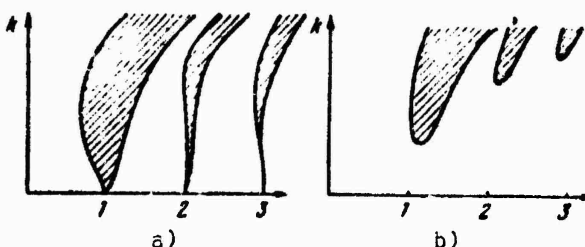


Figure 4.1. Zones of dynamic instability for small deflections: a) without consideration of damping, b) with consideration of damping.

All these considerations pertain to small deflections. For appreciable deflections, the rigidity of a shell or plate changes according to a very complex law in many cases. We thus come to the problem of nonlinear parametric vibrations of a system. Like the cases of natural and forced vibrations, they are characterized by a change in vibration amplitude as a function of frequency. If the problem is solved in the linearized formulation, we can find the outlines of dynamic instability zones; concerning the process itself, it can be stated only that the vibration amplitudes steadily increase. On the contrary, the solution of the problem from nonlinear points of view makes it possible to determine the vibration amplitude for a given frequency of fluctuations of the parameter.

Practical applications of the theory of parametric vibrations of plates and shells pertain to the most diverse areas of engineering. For example, the body of a vehicle may undergo parametric vibrations during fluctuations of the tractive force transmitted by the engines.

§44. Parametric Vibrations of Plates

Let us turn to certain specific problems involving parametric vibrations. In accordance with the general scheme adopted in this book, we will begin with the case of a rectangular plate*.

Let the compressive forces p_x , changing with time according to the law

$$p_x = p_0 + p_t \cos \Omega t. \quad (4.1)$$

be applied to the plate along sides b. Here p_0 stands for the constant part of the load, and p_t , for the amplitude of the variable part. Thus, those forces p which according to Figure 3.3 were passive and only promoted the deformation of the plate acted on by a periodic transverse load, now in turn independently set the system vibrating.

We will consider the plate to be hinged along the edges and will assume that sides a remain fixed. As for sides b, we will assume that one of the sides ($x = a$) moves freely relative to the other side ($x = 0$), which is fixed in plane xy; both of these sides continue to be rectilinear during the motion of the plate.

If the plate is considered to be a system with one degree of freedom, and the curved surface is approximated by the expression

$$w = f(t) \sin \frac{\pi x}{a} \sin \frac{\pi y}{b}, \quad (4.2)$$

we can use all the operations of Chapter II to solve the problem. Considering the natural vibrations of a rectangular plate, we used the Bubnov-Galerkin method, and finally, taking into consideration the forces in the middle surface, arrived at Eq. (2.110)

*The solution of this problem was given by V.V. Bolotin [4.2, 1954].

$$\frac{Y}{h} h^3 \frac{d^2\zeta}{dt^2} + \frac{\pi^2 D h}{a^4} (1 + \lambda^2)^2 \zeta - \frac{3^2 h^2}{a^2} (p_x + \lambda^2 p_y) \zeta + \frac{\pi^2 h^4}{16 a^2 b^2} \left(\frac{1}{\lambda^2} + \lambda^2 \right) \zeta^3 = 0; \quad (4.3)$$

where ζ stands for the ratio f/h as before, and $\lambda = a/b$. Considering that the longitudinal edges remain fixed ($\Delta y = 0$), for p_y we obtain the expression (2.117)

$$p_y = \mu p_x - E \frac{\pi^2}{h} \left(\frac{f}{h} \right)^2. \quad (4.4)$$

Equation (3) for the case under consideration will take the form

$$\frac{d^2\zeta}{dt^2} + \omega_0^2 \left(1 - \frac{p_x^*}{p_{kp}} \right) \zeta + \frac{0.75 (1 - \mu^2) (1 + 3\lambda^2)}{(1 + \lambda^2)^2} \omega_0^2 \zeta^3 = 0. \quad (4.5)$$

By (2.31)

$$\omega_0^2 = \frac{\pi^2 (1 + \lambda^2)^2}{12 \lambda^2 (1 - \mu^2)} \left(\frac{ch}{ab} \right)^2, \quad (4.6)$$

c being the sound velocity in the plate material, as before. Denoting the coefficient of ζ^3 by η

$$\eta = \frac{0.75 (1 - \mu^2) (1 + 3\lambda^2)}{(1 + \lambda^2)^2} \omega_0^2, \quad (4.6a)$$

we arrive at the equation

$$\frac{d^2\zeta}{dt^2} + \omega_0^2 \left(1 - \frac{p_x^*}{p_{kp}} \right) \zeta + \eta \zeta^3 = 0. \quad (4.7)$$

As usual, p_x^* in (5) and (7) stands for the dimensionless load parameter

$$p_x^* = \frac{p_x}{E} \left(\frac{h}{a} \right)^2. \quad (4.8)$$

The critical stress p_{cr} is determined from (3), neglecting the inertial and nonlinear terms; then, assuming $p_y = \mu p_x$, we find

$$p_{cr} = \frac{\pi^2 D}{b^2 h^2} \frac{(1+\lambda^2)^2}{1+\mu\lambda^2}. \quad (4.9)$$

By (2.118), the parameter p_{cr}^* will be

$$p_{cr}^* = \frac{\pi^2}{12\lambda^2(1-\mu^2)} \frac{(1+\lambda^2)^2}{1+\mu\lambda^2}. \quad (4.10)$$

Switching to dimensionless parameters in (1), we get

$$\dot{p}_x = \dot{p}_0 + \dot{p}_t \cos \Omega t. \quad (4.11)$$

Thus, Eq. (7) should contain compressive forces changing with time according to law (11). We finally arrive at the equation

$$\frac{d^2\zeta}{dt^2} + \omega_0^2 \left(1 - \frac{\dot{p}_0 + \dot{p}_t \cos \Omega t}{p_{cr}} \right) \zeta + \eta \zeta^3 = 0. \quad (4.12)$$

We introduce the symbol Ω for the frequency of natural vibrations of the plate as a system with one degree of freedom subjected to the static action of the constant component p_0^* :

$$\Omega^2 = \omega_0^2 \left(1 - \frac{\dot{p}_0}{p_{cr}^*} \right). \quad (4.13)$$

Further, we will refer to the quantity

$$k = \frac{\frac{\dot{p}_t}{p_{cr}}}{1 - \frac{\dot{p}_0}{p_{cr}}}, \quad (4.14)$$

as the excitation coefficient, which represents the ratio of the variable component of the load to the average value (more accurately, the difference between the Euler and the average value, cf. Figure 4.2). Using this notation, we represent (12) in the form

$$\frac{d^2\zeta}{dt^2} + \Omega^2(1 - k \cos \theta t) \zeta + \eta \zeta^3 = 0. \quad (4.15)$$

We have thus arrived at a classical equation describing the parametric vibrations of a system with one degree of freedom with a single nonlinearity parameter η . Discarding the term containing η , we obtain the usual Mathieu equation corresponding to a linear system. The properties of this equation are well known. As already noted in §43, for a linear system, a gradual increase in amplitude will take place in the region of instability. We will be interested in the first instability zone near $\theta = 2\Omega$. For such a region, like those shaded in Figure 4.1a, the vibration amplitudes will increase indefinitely.

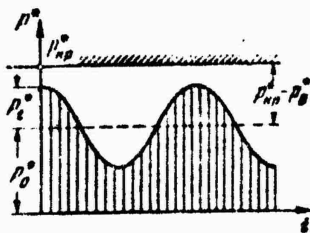


Figure 4.2. In reference to the determination of the excitation coefficient of the system.

If however we are dealing with a nonlinear system, the amplitudes prove to be limited. They can be determined in the following manner. We introduce a new time parameter

$$t_1 = \omega_0 \sqrt{1 - \frac{P_0^*}{P_{cr}^*}} t = \Omega t \quad (4.16)$$

and write

$$\delta = \frac{\eta}{\Omega^2}. \quad (4.17)$$

Then by (15), the equation will take the form

$$\frac{d^2\zeta}{dt_1^2} + \left(1 - k \cos \frac{\theta}{\Omega} t_1\right) \zeta + \delta_s^2 = 0. \quad (4.18)$$

We take the function ζ for frequencies near $\theta/\zeta = 1/2$ in the form

$$\zeta = A_1 \cos \frac{\theta t_1}{2\Omega} + B_1 \sin \frac{\theta t_1}{2\Omega}. \quad (4.19)$$

We use the formulas

$$\begin{aligned}\sin^3 x &= \frac{1}{4}(3 \sin x - \sin 3x), & \cos^3 x &= \frac{1}{4}(3 \cos x + \cos 3x), \\ \sin x \cos^2 x &= \frac{1}{4}(\sin x + \sin 3x), & \sin^2 x \cos x &= \frac{1}{4}(\cos x - \cos 3x).\end{aligned}$$

Then, discarding the terms with triple frequency, we get

where

$$(A_1 \cos x + B_1 \sin x)^3 = A^3(A_1 \cos x + B_1 \sin x),$$

$$A^3 = A_1^3 + B_1^3.$$

Consequently,

$$\zeta^3 = A^3 \left(A_1 \cos \frac{\theta t_1}{2\Omega} + B_1 \sin \frac{\theta t_1}{2\Omega} \right).$$

On the other hand, we use the relations

$$\cos 2x \cos x = \frac{1}{2} (\cos x + \cos 3x);$$

$$\cos 2x \sin x = \frac{1}{2} (-\sin x + \sin 3x).$$

Here again we keep only the first terms. Then Eq. (18) may be rewritten in the form

$$A_1 \left(1 - \frac{\theta^2}{4Q^2} - \frac{k}{2} + \frac{3}{4} \delta A^2 \right) \cos \frac{\theta_1}{2\pi} +$$

$$+ B_1 \left(1 - \frac{\theta^2}{4Q^2} + \frac{k}{2} + \frac{3}{4} \delta A^2 \right) \sin \frac{\theta_1}{2\pi} = 0. \quad (4.20)$$

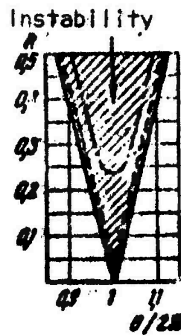


Figure 4.3.
Boundaries of
the first in-
stability
zone for
linear para-
metric vi-
brations of
a rectangular
plate.

Taking $A_1 \neq 0$ and $B_1 \neq 0$, we equate the expressions in parentheses to zero; we thus have

$$\left. \begin{aligned} 1 - \frac{\theta^2}{4Q^2} - \frac{k}{2} + \frac{3}{4} \delta A^2 &= 0, \\ 1 - \frac{\theta^2}{4Q^2} + \frac{k}{2} + \frac{3}{4} \delta A^2 &= 0. \end{aligned} \right\} \quad (4.21)$$

If the nonlinear term in (18) is absent ($\sigma = 0$), from (21) we obtain the boundaries of the first instability zone

$$\frac{\theta}{2\Omega} = \sqrt{1 - \frac{k}{2}}, \quad \frac{\theta}{2\Omega} = \sqrt{1 + \frac{k}{2}} \quad (4.22)$$

or

$$\frac{\theta}{2\Omega} \approx 1 - \frac{k}{4}, \quad \frac{\theta}{2\Omega} \approx 1 + \frac{k}{4}. \quad (4.22a)$$

For all $\theta/2\Omega$, values located within these limits, the vibration amplitudes increase indefinitely; the corresponding lines are represented in Figure 4.3, solid lines correspond to (22), and dashed lines, to (22a).

However, in the case at hand, $\sigma \neq 0$. Hence, we find for A the definite values

$$A = \left[\frac{4}{3\delta} \left(\frac{\theta^2}{4\Omega^2} - 1 \pm \frac{k}{2} \right) \right]^{\frac{1}{4}}. \quad (4.23)$$

dependent on the nonlinearity parameter σ and the excitation coefficient. The graph of $A^2(\theta^2/4\Omega^2)$, corresponding to (23), is shown in Figure 4.4; we obtain straight lines forming an angle of 45° with the abscissa axis, and the "corridor" between them has width k.

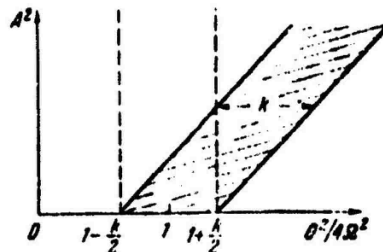


Figure 4.4. "Amplitude-frequency" curves for parametric vibrations of a plate.

Solving the problem in the linear formulation, we obtain a band of width k , shown by dashed lines: here the amplitudes increase indefinitely.

We will now determine the effect of linear damping. Introducing the corresponding term in (15), we arrive at the equation

$$\frac{d^2\zeta}{dt^2} + 2\delta \frac{d\zeta}{dt} + \Omega^2(1 - \kappa \cos \Omega t)\zeta + \eta_0^2 = 0. \quad (4.24)$$

Introducing the variable t_1 from (16), we obtain

$$\frac{d^2\zeta}{dt_1^2} + 2\frac{\sigma}{\Omega} \frac{d\zeta}{dt_1} + \left(1 - k \cos \frac{\theta}{\Omega} t_1\right) \zeta + \delta_0^2 = 0, \quad (4.25)$$

where σ is determined from (17). Expressing ζ in the form of (19) as before, we arrive at the equations (for $A = A_1^2 + B_1^2$)

$$\begin{aligned} & \left[A_1 \left(1 - \frac{\theta^2}{4\Omega^2} - \frac{k}{2} + \frac{3}{4} \delta A^2 \right) + B_1 \frac{\theta\sigma}{\Omega^2} \right] \cos \frac{\theta t_1}{2\Omega} + \\ & + \left[B_1 \left(1 - \frac{\theta^2}{4\Omega^2} + \frac{k}{2} + \frac{3}{4} \delta A^2 \right) - A_1 \frac{\theta\sigma}{\Omega^2} \right] \sin \frac{\theta t_1}{2\Omega} = 0. \end{aligned} \quad (4.26)$$

Conditions $A_1 \neq 0$, $B_1 \neq 0$ now lead to the equation

$$\begin{vmatrix} 1 - \frac{\theta^2}{4\Omega^2} - \frac{k}{2} + \frac{3}{4} \delta A^2 & \frac{\theta\sigma}{\Omega^2} \\ -\frac{\theta\sigma}{\Omega^2} & 1 - \frac{\theta^2}{4\Omega^2} + \frac{k}{2} + \frac{3}{4} \delta A^2 \end{vmatrix} = 0. \quad (4.27)$$

In the absence of the nonlinear term in (24), when $\sigma = 0$, the boundaries of the first instability zone would now be determined by the equation

$$\frac{\theta^4}{16\Omega^4} - 2\frac{\theta^2}{4\Omega^2} \left(1 - \frac{\theta^2}{\Omega^2} \right) + 1 - \frac{k^2}{4} = 0$$

or approximately

$$\frac{\theta}{2\Omega} = \sqrt{1 \mp \sqrt{\frac{k^2}{4} - \frac{4e^2}{\Omega^2}}}. \quad (4.28)$$

The curve found from (28) for some value of ϵ is represented by a dashed line in Figure 4.3.

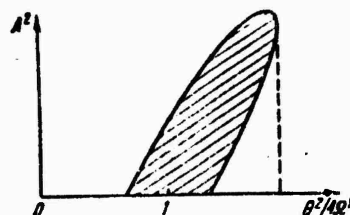


Figure 4.5. Influence of damping on parametric vibrations of a plate.

Let us return to the nonlinear problem. On the basis of the complete equation (27), A is determined as follows:

$$A = \left[\frac{1}{36} \left(\frac{\theta^2}{4\Omega^2} - 1 \pm \sqrt{\frac{k^2}{4} - \frac{4e^2}{\Omega^2}} \right) \right]^{\frac{1}{2}}. \quad (4.29)$$

The new graph for A^2 is shown in Figure 4.5. Assuming $A = 0$, we find the width of the band along the abscissa; it is now equal to $2\sqrt{k^2/4 - 4e^2/\Omega^2}$. As we see, the instability boundaries come closer together in the presence of damping. Instead of a continuous corridor as in Figure 4.4, a loop is obtained. The right-hand boundary k of the zone of stable vibrations is determined by the abscissa (dashed line):

$$\frac{\theta^2}{4\Omega^2} = \frac{k^2\Omega^2}{16e^2}.$$

§45. Closed Cylindrical Shell under Fluctuating External Pressure

Let us turn to the problem of the behavior of a closed cylindrical shell subject to a fluctuating normal pressure. This problem has important applications in modern engineering.*

The general plane of the solution of the problem will remain the same as in the discussion of forced vibrations. The deflection will be approximated by the expression ($\alpha = \pi/L$, $\beta = n/R$):

$$w = f(t)(\sin \alpha x \sin \beta y + \psi \sin^2 \alpha x + \phi). \quad (4.30)$$

Repeating the operations given in the book [0.6], p. 764, we arrive at the following equation analogous to (12):

$$C_4 \frac{d^4 \zeta}{dt^4} + [C_0 - q(t)]\zeta - C_3 \psi \zeta^2 + (C_1 + C_2 \psi^2)\zeta^3 = 0. \quad (4.31)$$

Here

$$\begin{aligned} C_0 &= \frac{\xi^4}{\pi^2(1+\xi^2)^2 s} + \frac{\pi^2}{12(1-\mu^2)} \frac{(1+\xi^2)^2}{\xi^2} s, \quad C_1 = \frac{\pi^2}{16} \frac{1+\xi^4}{\xi^2} s, \\ C_2 &= \pi^2 s^2 \left[\frac{1}{(1+\xi^2)^2} + \frac{1}{(1+\xi^2)^2} \right] s, \quad C_3 = \frac{1}{4} \left[1 + \frac{8\xi^4}{(1+\xi^2)^2} \right], \\ C_4 &= \frac{\gamma R^2}{g E \eta}. \end{aligned}$$

we further introduce the parameters

$$\zeta = \frac{f}{h}, \quad \xi = \frac{\pi R}{nL}, \quad s = \frac{Rh}{L^2}.$$

*The results given here are due to V. Ts. Gnuni [4.3].

The quantity ψ can be found with a certain approximation from the solution of the nonlinear static problem (see [0.0], p. 790). We then let $q(t) = q^0 \cos \theta t$. Then Eq. (31) can be rewritten in the form

$$\frac{d^2\zeta}{dt^2} + 2\epsilon \frac{d\zeta}{dt} + \Omega^2(1 - k \cos \theta t)\zeta - a_0^2 + \beta_0^2 = 0, \quad (4.32)$$

where

$$\Omega^2 = \frac{C_0}{C_4}, \quad k = \frac{q^0}{C_0}.$$

For the case $\pi R/nL < 2.66$, we find a relationship between the square of the amplitude of steady vibrations A^2 and the square of the ratio θ^2/Ω^2 , shown in Figure 4.6. The loop on this graph is similar to the one we obtained for a plate (Figure 4.5), but has a "falling portion". Obviously, snaps of the shell from some stable steady-state positions to others are possible in this case. For example, in going from the region of low frequencies to higher ones, one can observe the jumps shown by arrows in Figure 4.7a. On the contrary, when the frequency decreases, we obtain the jumps shown in Figure 4.7b.



Figure 4.6. The "amplitude-frequency" curve for parametric vibrations of a circular cylindrical shell.

Of interest is the study of parametric vibrations of cylindrical shells filled with liquid. Such a problem is discussed in [4.6] from points of view close to the ones described above; this work also cites data on some experiments.

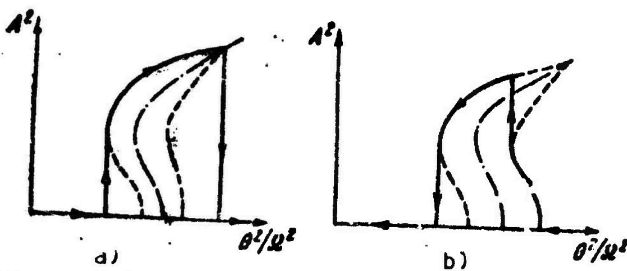


Figure 4.7. Concerning the behavior of a circular cylindrical shell for parametric vibrations related to the stall effect: a) as the frequency increases, b) as the frequency decreases.

§46. Behavior of a Cylindrical Panel under a Fluctuating Compressive Load

In conclusion, we will extend the results obtained in §44 for a plate to the case of a cylindrical panel compressed along the generatrix.*

We will assume that the edges of the panel are hinged, and that uniformly distributed compressive forces $p = p_0 + p_t \cos \theta t$ are acting along the curved edge. We will also assume that on the average, the normal and tangential forces acting along the longitudinal edges become zero.

We write the basic equations in the usual form, (1.40), (1.41). The deflection is approximated by the expression

$$w = f(l) \sin \frac{\pi x}{a} \sin \frac{\pi y}{b}, \quad (4.33)$$

assuming as a first approximation that for a slightly curved panel, one half-wave is formed in the directions of each of the sides a, b . Substituting (33) into Eq. (1.41), we find the function Φ . Then, applying the procedure of the Bubnov-Galerkin method to Eq. (1.40), we obtain the following equation ($w_0 \equiv 0, \lambda = a/b$):

*This problem was discussed by G.V. Mishchenkov [4.4].

$$\frac{d^2f}{dt^2} + 2\zeta \frac{df}{dt} + \omega_0^2 f - \frac{8}{\sqrt{\pi^4}} \left\{ \frac{\pi^2}{a^4} (\rho_0 + \rho_t \cos \Omega t) f - \frac{4Eh}{3Rb^4} \left[\frac{1}{2} + \frac{8}{(1+\lambda^2)^2} \right] f^2 + \frac{Eh}{16} \frac{\pi^4}{a^4} (1+\lambda^2) f \right\} = 0. \quad (4.34)$$

As before, ω_0 denotes the frequency of natural vibrations, which according to (2.211) is equal to

$$\omega_0^2 = \frac{Dg}{\gamma h} \frac{\pi^4}{a^4} F(\lambda, K). \quad (4.35)$$

Here K and F stand for the quantities

$$K = \frac{b^2 \lambda^2}{Rh}, \quad F = (1 + \lambda^2)^2 + \frac{12(1 - \mu^2)K^2}{\pi^4(1 + \lambda^2)^2}. \quad (4.36)$$

We then introduce the notation

$$p^* = \frac{\pi^2 D}{a^2 h} F(\lambda, K), \quad \Omega^2 = \omega_0^2 \left(1 - \frac{\rho_0}{\rho_*} \right), \quad \hat{k} = \frac{\frac{\rho_t}{\rho_*}}{1 - \frac{\rho_0}{\rho_*}}, \quad (4.37)$$

$$\eta_0 = \frac{3}{4} \frac{(1 - \mu^2)}{F} \frac{1 + \lambda^2}{1 - \frac{\rho_0}{\rho_*}}, \quad \beta_0 = \frac{16}{\pi^4} \frac{(1 - \mu^2)}{F} \frac{K \lambda^2}{1 - \frac{\rho_0}{\rho_*}} \left[\frac{1}{2} + \frac{8}{(1 + \lambda^2)^2} \right]. \quad (4.38)$$

The quantities appearing here were dealt with in §32 in connection with the discussion of natural vibrations. When $\zeta = f/h$, we arrive at the equation

$$\frac{d^2\zeta}{dt^2} + 2\zeta \frac{d\zeta}{dt} + \Omega^2 (1 - \hat{k} \cos \Omega t) \zeta - \beta_0 \Omega^2 \zeta^2 + \eta_0 \Omega^2 \zeta^3 = 0. \quad (4.39)$$

In the case $K = 0$, we obtain the case of a plate; the coefficient β_0 will be equal to zero.

If the dynamic terms are eliminated from (39), we have the equation

$$(1 - \hat{k}) \zeta - \beta_0 \zeta^2 + \eta_0 \zeta^3 = 0. \quad (4.40)$$

The roots of this equation correspond to three possible equilibrium positions. When $\beta_0 > 2n_0^{1/2}$, vibrations are possible around the initial state of equilibrium, relative to the snatched state, and covering these two states (see §32).

Let us now turn to the dynamic problem. As before, we will be interested in the main instability zone and will take the expression for ξ in the form

$$\xi = A_0 + A_1 \cos \frac{\theta t}{2} + B_1 \sin \frac{\theta t}{2}.$$

In the usual manner, we arrive at the equations

$$\left. \begin{aligned} A_0 + n_0 A_0 \left(A_0^2 + \frac{3}{2} A^2 \right) - \beta \left(A_0^2 + \frac{1}{2} A^2 \right) &= 0, \\ A_1 \left(\frac{n_0^2 - n^2}{4} - \frac{k}{2} \right) + B_1 n \frac{\Delta}{2} &= 0, \\ - A_1 n \frac{\Delta}{2} + B_1 \left(\frac{n_0^2 - n^2}{4} + \frac{k}{2} \right) &= 0, \end{aligned} \right\} \quad (4.41)$$

where $n = \theta/\Omega$, $\Delta = 2\varepsilon/\Omega$, and n_0 is the dimensionless frequency of natural vibrations, determined from the equation

$$\frac{n_0^2}{4} = 1 + \frac{3}{4} n_0 A^2 + A_0 (3n_0 A_0 - 2\beta_0);$$

as before, A stands for the amplitude of steady state vibrations. From the first equation of (41) we find

$$A^2 = 2A_0 \frac{\beta_0 A_0 - 3n_0 A_0^2 - 1}{3n_0 A_0 - \beta}. \quad (4.42)$$

The other two equations for $A_1 \neq 0$, $B_1 \neq 0$ give

$$\left| \begin{array}{cc} \frac{n_0^2 - n^2}{2} - k & n\Delta \\ - n\Delta & \frac{n_0^2 - n^2}{2} + k \end{array} \right| = 0. \quad (4.43)$$

Hence

$$n^2 = (n_0^2 - 2\Delta^2) \pm 2\sqrt{k^2 - n_0^2\Delta^2 + \Delta^4}. \quad (4.44)$$

In the absence of damping

$$\frac{n^2}{4} = 1 \approx \frac{k}{2}, \quad (4.45)$$

which agrees with (22).

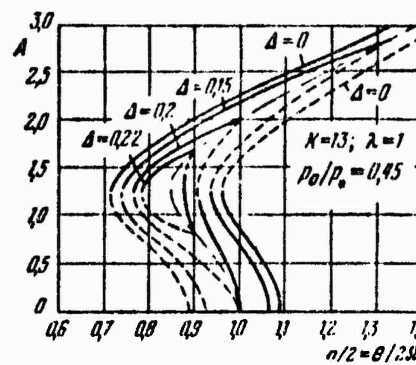


Figure 4.6. Amplitude-frequency curves in the case of parametric vibrations of a cylindrical panel.

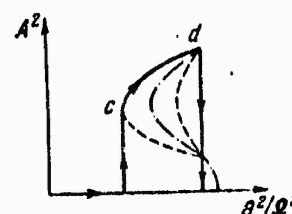


Figure 4.9. Behavior of a shell in parametric vibrations in the case of appreciable damping.

Figure 4.8 shows amplitude-frequency curves plotted on the basis of the above relations for a square panel with $K = 13$ and $p_0/p_* = 0.45$; the coefficient η_0 and β_0 , calculated from (38), will then be $\eta_0 = 0.26$, $\beta_0 = 0.8$. In this case, vibrations around only one equilibrium position take place. Figure 4.8 contains curves plotted by assuming the absence of damping ($\Delta = 0$) and its presence ($\Delta = 0.15, 0.2, 0.22$). Solid lines show stable branches of the curves, and dashed lines, unstable ones. At small damping ratios, graphs whose general form was given in Figure 4.7 are obtained. In the case of considerable damping, a different response is possible, as in Figure 4.9. Here the jumps can take place only in the presence of sufficiently low disturbances, which throw the system over to the cd branch.

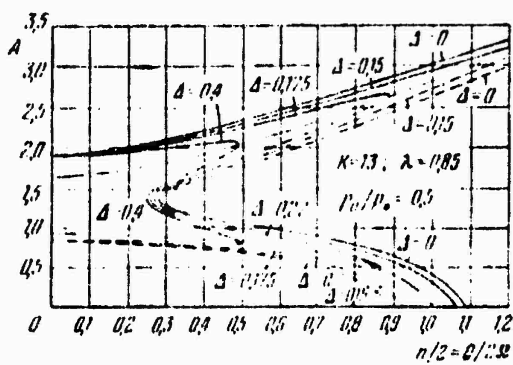


Figure 4.10. "Deflection amplitude-frequency" curves for parametric vibrations of a panel having three equilibrium positions.

Figure 4.10 shows a case in which there are three equilibrium positions; the following values were taken: $\lambda = 0.85$, $K = 13$, $p_0/p_* = 0.5$. The calculations give $\eta_0 = 0.26$; $\beta_0 = 1.1$, so that $\beta_0 > 2\sqrt{\eta_0}$. In this case, some of the curves have different branches separated along the ordinate axis. We have already encountered a similar example in the discussion of forced vibrations of cylindrical panels.

§47. Resonances in Nonlinear Systems

To conclude the chapter of the book dealing with periodic actions of loads on

shells or plates, let us recall certain definitions pertaining to the phenomenon of resonance in nonlinear systems.

In analyzing a vibratory process, we are interested in the zones where the vibration amplitudes increase, and do so in such a way that this phenomenon affects the way in which the structure is used. The phenomenon of increase in vibration amplitudes is related to the concept of resonance.

When the nonlinear components in the equations of vibrations are expanded in a Fourier series, and the equations are reduced to the solving form, terms with combination frequencies of the type $n\theta \pm m\Omega$ appear, where θ is the load change frequency (external frequency), Ω is the fundamental frequency of natural vibrations, and n and m are certain integers. Therefore, in contrast to linear systems, in nonlinear problems resonances are set up at different combinations of frequencies: Ω , where r and q are coprime integers [0.21]; these combinations depend on the characteristics of the system.

The case $r\Omega \approx q\theta$ is known as main or ordinary resonance; we were interested in it for forced vibrations.

On the contrary, for parametric vibrations, of greatest importance is the case in which the frequency of natural vibrations is equal to a fraction of the external frequency ($\Omega = \theta/2$); such resonance is called parametric.

Vibrations with the frequency relation $\Omega = q\theta$ may also be of practical importance. These vibrations pertain to overtones of the external frequency.

Complex problems of various resonances in nonlinear systems pertaining to plates and shells have been inadequately treated and are of considerable theoretical and practical interest.

Chapter V

Self-Excited Vibrations

§48. Basic Concepts

The next important type of vibrations which we will now consider are self-excited vibrations. These are undamped vibrations excited by forces dependent on the deformation of the vibrating system itself: hence the term self-excited. The energy to sustain such vibrations is supplied by some external source.

One of the most important types of self-excited vibrations in engineering are flutter type vibrations. They are set up as a result of the action of a gas flow on a deformed system. As it moves past the structure, the flow exerts different forces on it, depending on the position of the system. For example, the wing of an aircraft undergoing deformation in certain given flight regimes is subjected to different pressures from the incident gas flow. The change in wing geometry due to the deformation leads in turn to an increase or decrease of the pressure at various points of the wing. Thus, a coupled "elastic structure - gas flow" system is obtained whose characteristics change continuously. For certain parameters of this system, the amplitudes of wing displacements that are vibratory in character increase sharply. The deformations arising from flutter are very dangerous for the structure, since they quickly lead to a loss of stability and to the development of fatigue cracks.

It is necessary to distinguish the so-called "classical" flutter, associated with a general flexural-torsional deformation of the wing or combined displacements of the wing and ailerons, and deformation of the fuselage and tail assembly, from "panel" flutter, characterized by local buckling of parts of the skin of the wing or fuselage between the stiffeners. Panel flutter may involve the skin of various types of aircraft structures. This type of flutter assumes a particular importance at supersonic and hypersonic flying speeds.

At the present time, the problem of flutter is particularly pressing in aircraft

construction in connection with the increased dimensions of aircraft and higher flying speeds.

§49. Nonlinear Flutter of a Plate

Let us first consider the problem of flutter of a flat rectangular plate with length a along the flow and width b , hinged along all the edges. It will be assumed that a supersonic gas flow characterized by velocity U flows past the plate on one side (Figure 5.1). The coordinate lines x, y, z will be placed, respectively, along sides a, b and a normal to the surface of the plate.*

The equations describing the behavior of the plate will be written in the form of (1.42a), (1.43a), assuming $w_0 \equiv 0$:

$$\left. \begin{aligned} \frac{\rho}{h} \nabla^4 w &= L(\Phi, w) - \frac{\gamma_0}{\gamma} \frac{\partial^2 w}{\partial t^2} + \frac{\gamma}{\gamma h} \left(\frac{\partial \Phi}{\partial t} + U \frac{\partial \Phi}{\partial x} \right), \\ \frac{1}{E} \nabla^4 \Phi &= -\frac{1}{2} L(w, w); \end{aligned} \right\} \quad (5.1)$$

where γ_0 denotes the specific gravity of the plate material. The first equation contains a term characterizing the pressure exerted on the plate by the gas flow; γ is the specific gravity of the gas, and Φ is the velocity potential. Equations (1) were set up by using the linearized theory of nonviscous potential flow. The function Φ must satisfy the equation

$$\nabla^2 \Phi = \frac{1}{c^2} \left(\frac{\partial}{\partial t} + U \frac{\partial}{\partial x} \right)^2 \Phi; \quad (5.2)$$

and the solution must conform to the boundary condition

$$\left. \frac{\partial \Phi}{\partial z} \right|_{z=0} = \frac{\partial w}{\partial t} + U \frac{\partial w}{\partial x} \quad (5.3a)$$

*See E.N. Dowell, Nonlinear Oscillations of a Fluttering Plate, AIAA Paper No. 67-13, 1967.

at the plate surface and to the condition

$$\frac{\partial \psi}{\partial z} \Big|_{z>0} = 0 \quad (5.3b)$$

outside the plate; c denotes the sound velocity in the undisturbed gas flow.

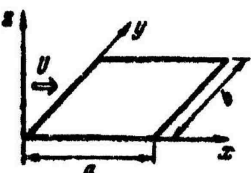


Figure 5.1. Plate
in a flow.

We will now use the Bubnov-Galerkin method. The deflection function is approximated by the series

$$w = \sum_m A_m(t) \sin \frac{m\pi x}{a} \sin \frac{m\pi z}{b}. \quad (5.4)$$

It is assumed that in the direction of the width of the plate, one half-wave is always formed; the number of half-waves along the length is m . Substituting (4) into Eqs. (1) and taking (2) and (3) into account, we arrive at the following system of equations, which here are written in the dimensionless form:

$$\begin{aligned} \frac{d^4 I_m}{dt^2} &= -f_m \pi^4 (m^4 + \lambda^2)^2 - 3\pi^4 (1 - \mu^2) \left[\frac{I_m}{2} (m^2 A + \lambda^2 B) + C \lambda^4 \right] + \\ &+ 4 \frac{\lambda}{\mu} \frac{U^2 a^3}{D} \sum_r Q_{rm}, \quad m = 1, 2, \dots \end{aligned} \quad (5.5)$$

f_m denotes the dimensionless amplitude of the m -th component of the deflection, and τ is the dimensionless time; $\lambda = a/b$. The coefficients A, \dots, C depend on the parameters of the plate and characteristics of the material. Q_{rm} stands for expressions of the type

$$Q_{rm} = \frac{1}{ab} \int_0^a \int_0^b \theta_f - p_\infty \sin \frac{m\pi x}{a} \sin \frac{n\pi y}{b} dx dy,$$

where p_f is the pressure arising from the appearance of the deflection component

$$w_r = A_r \sin \frac{r\pi x}{a} \sin \frac{r\pi y}{b},$$

p_∞ is the pressure in the incident flow, $\rho = \gamma/g$.

The coefficients Q_{rm} are

$$Q_{rm} = f_r(s) S_{rm} + \frac{df_r(s)}{ds} D_{rm} + \int_0^s f_r(\bar{s}) H_{rm}(s - \bar{s}) d\bar{s} + \int_s^\infty \frac{df_r(\bar{s})}{d\bar{s}} f_{rm}(s - \bar{s}) d\bar{s}, \quad (5.6)$$

where

$$s = Ua \sqrt{\frac{\lambda h}{Dg}} \tau;$$

S_{rm} , D_{rm} , H_{rm} , f_{rm} are some functions of M and λ . If the integrals entering into Eq. (6) are omitted, the remaining terms give values of Q_{rm} corresponding to the piston theory.

Thus, the problem reduces to solving the system of equations (5), which determine the change in deflection amplitude with time. These equations were solved by a numerical method with the aid of a computer. The character of change in the amplitudes of the limiting cycle as a function of the velocity head is illustrated by the graph of Figure 5.2. It was assumed that $\lambda = 1$. Amplitudes of dimensionless deflection w/h are laid off along the ordinate axis, and the velocity head parameter $q^* = \rho U^2 a^3 / D$ along the abscissa axis. The different curves correspond to a series of Mach numbers M from 1 to 1.6.

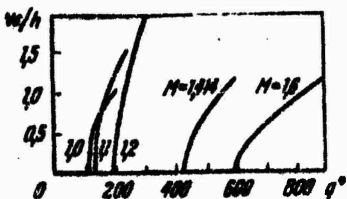


Figure 5.2. Change in the amplitudes of the limiting cycle as a function of the velocity head.

§50. Experimental Studies of Plate Flutter

We will describe some experimental studies of flutter pertaining to flat panels.

In the majority of experiments conducted by various authors, the plates tested were fixed on a rigid model with a sharp leading edge; the gas jet flowed past the plate at a zero angle of incidence. In this case, it may be assumed that the supersonic flow past the panel is undisturbed. The cavity under the panel is usually connected with the atmosphere of the wind tunnel. In other variants, the cavity is sealed, and a given pressure may be maintained in it [5.30, 5.23, 5.35, 5.13, 5.24].

In addition, in a series of experiments, the plates were loaded with longitudinal compressive forces in the plane of the plate [5.35, 5.24]. In some experiments, the temperature of the incident flow was varied; thermal stresses causing buckling were set up in the plate.

Figure 5.3 shows computed flutter limits for a freely supported square plate in a supersonic flow under conditions of uniform temperature rise by an amount ΔT . Here ΔT_{cr} denotes the temperature at which static buckling of the plate takes place, and $\eta = \frac{h}{a} \sqrt{\frac{2EI}{\rho_0 U^2}}$. It is evident from Figure 5.3 that self-excited vibrations are absent for a plate in a flat or buckled state (regions K and N respectively) for high values of the aerodynamic parameter and a uniform temperature increase; however, at lower values of the aerodynamic parameter, the representative point will move from the region of static stability (point A) into the flutter region S (point B), where

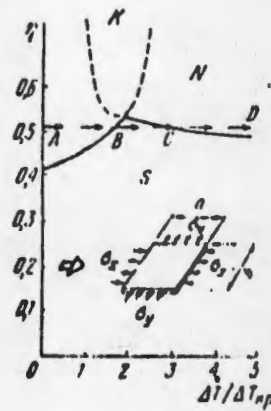


Figure 5.3. Stability limits of a plate.

self-excited vibrations will be set up. As the temperature rises further, the "plate-flow" system will leave the flutter region (point C), and a static loss of stability will take place (point D); the buckled panel will then by dynamically stable.

§51. Quasi-Static Problem for a Closed Cylindrical Shell

Let us consider the behavior of a closed circular cylindrical shell in a supersonic gas flow moving on the outside of the shell; the undisturbed jet velocity U will be considered directed along the generatrix. In addition, it will be assumed that the shell is subjected to the static action of uniform compressive stresses σ_0 along its length (Figure 5.4.*).

The phenomenon of panel flutter, which is the subject of this chapter, is frequently manifested together with monotonic shell buckling, which has no vibratory character and may be treated as a quasi-static process. In aviation literature,

*This problem was solved by E.D. Skurlatov [5.16]. He also obtained the theoretical and experimental results presented below in §§52-55, 57, 60; see the collection Transitional Processes of Deformation of Shells and Plates, Tartu, 1967.

such a process is known as divergence. In certain cases, the phenomena of divergence and flutter may alternate as the velocity of the gas jet or the magnitude of the compressive stresses changes. For this reason, we will first study the phenomenon of divergence. The aerodynamic forces will be determined in accordance with the piston theory (see the book [0.6] §225).

We will first treat this problem as a geometrically linear one; considering the shell deflections to be small in comparison with the thickness. The basic equations will be taken in the form (see [0.6], p. 858):

$$\left. \begin{aligned} \frac{\partial}{\partial x} \nabla^4 w &= \frac{1}{R} \frac{\partial^2 \Phi}{\partial x^2} - \sigma_0 \frac{\partial^2 w}{\partial x^2} + \frac{q}{h}, \\ \frac{1}{E} \nabla^4 \Phi &= - \frac{1}{R} \frac{\partial^2 w}{\partial x^2}. \end{aligned} \right\} \quad (5.7)$$

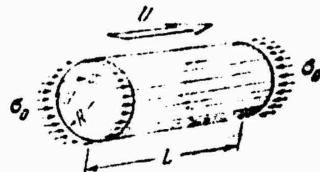


Figure 5.4. Cylindrical shell acted on by a gas flow and axial stresses.

It is easy to see that these equations constitute a linearized variant of Eqs. (1.40), (1.41) for $\sigma_0 = -\partial^2 \Phi / \partial y^2$; the quantity q will be taken according to the formula of the piston theory (also in linearized form) as

$$q = -\kappa p_\infty M \frac{\partial w}{\partial x}.$$

The solution will be sought in the form [0.6]:

$$w(x, y, t) = f_{m,n}(t) \sin \alpha x \sin \beta y + f_{m+1,n} \sin \gamma x \sin \beta y, \quad (5.8)$$

where $\bar{\alpha} = m\pi/L$, $\gamma = (m+1)\pi/L$, $\beta = n/R$; m is the number of half-waves along the generatrix, and n is the number of waves in the circumferential direction*. Substituting (8) into the second of Eqs. (7), we find an expression for the stress function in the middle surface:

$$\Phi(x, y, t) = l_1 \sin \bar{\alpha}x \sin \beta y + l_2 \sin \gamma x \sin \beta y, \quad (5.9)$$

$$l_1 = \frac{\bar{\alpha}^4 E}{R(\bar{\alpha}^2 + \beta^2)^2} f_{m, n}, \quad l_2 = \frac{\gamma^4 E}{R(\gamma^2 + \beta^2)^2} f_{m+1, n}.$$

where

Using (8) and (9) in the first equation of system (7) and applying the Bubnov-Galerkin method, we arrive at a system of two algebraic equations in $f_{m, n}$ and $f_{m+1, n}$. We introduce the dimensionless quantities under

$$\begin{aligned} \zeta_{m, n} &= \frac{f_{m, n}}{h}, \quad \zeta_{m+1, n} = \frac{f_{m+1, n}}{h}, \quad a = \frac{Mh}{L}, \\ K &= \frac{m(m+1)}{1+2m} \frac{48\pi p_m L^4}{Eh^4} \frac{(1-\mu^2)}{\pi^4}, \quad K_1 = \frac{12(1-\mu^2)}{\pi^2} \frac{L^4}{Rh} m^2, \\ K_2 &= \frac{12(1-\mu^2)}{\pi^2} \frac{L^2}{Rh} (m+1)^2, \quad \delta_0 = \frac{\sigma_0 R}{Eh}, \\ \omega_{m, n}^2 &= \left[m^2 + \left(\frac{nL}{\pi R} \right)^2 \right]^2 + \frac{12(1-\mu^2)m^4 L^4}{R^2 h^2 \pi^4 \left[m^2 + \left(\frac{nL}{\pi R} \right)^2 \right]^2}. \end{aligned}$$

Then the system of equations takes the form

$$\left. \begin{aligned} \omega_{m, n}^2 \zeta_{m, n} - \delta_0 K_1 \zeta_{m, n} - K a \zeta_{m+1, n} &= 0, \\ \omega_{m+1, n}^2 \zeta_{m+1, n} - \delta_0 K_2 \zeta_{m+1, n} + K a \zeta_{m, n} &= 0. \end{aligned} \right\} \quad (5.9a)$$

Setting to zero the determinant of the system of equations (9a), we find the upper critical compressive stress as the minimum root of the following equation:

*The quantity $\bar{\alpha}$ must not be confused with the parameter α which occurs below.

$$\delta_0 = \frac{1}{2K_1 K_2} \left[(\omega_{m+1,n}^2 K_1 + \omega_{m,n}^2 K_2) \pm \right. \\ \left. \pm \sqrt{(\omega_{m+1,n}^2 K_1 - \omega_{m,n}^2 K_2)^2 - 4K^2 a^2 K_1 K_2} \right]. \quad (5.10)$$

If no flow is present ($\alpha = 0$), relation (10) is the same as the expression for the upper critical value of the parameter of axial compressive stresses. Analysis of relation (10) leads to the conclusion that a gas flow may stabilize a shell compressed in the longitudinal direction (Figure 5.5).

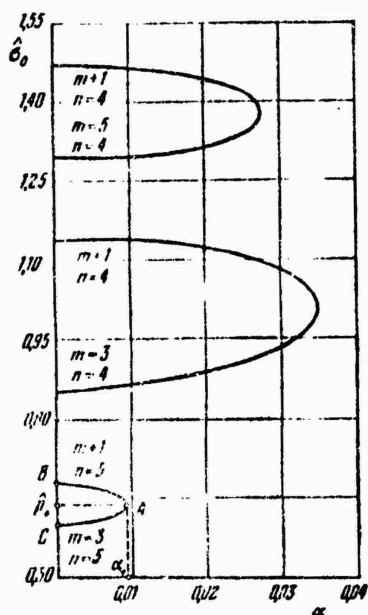


Figure 5.5. Axial compressive stress parameter vs. flow velocity.

We will examine the same problem in the nonlinear formulation, for which we will use general equations of type (1.40), (1.41). Since both the deflections and their derivatives enter into these equations in a degree no higher than third, the aerodynamic forces will be determined from the third approximation formula (see [0.6], p. 835). The expression for the deflection will be given in the form of the series

$$w(x, y, t) = f_1(t) \sin \alpha x \sin \beta y + \\ + f_2(t) \sin \gamma x \sin \beta y + f_3(t) \sin^2 \alpha x. \quad (5.11)$$

Further calculations are similar to those made for the linear problem, but are very cumbersome. Omitting the intermediate operations, we finally write the equations in the dimensionless form

$$\left. \begin{aligned} a_{100}\xi_1 + a_{010}\xi_2 + a_{101}\xi_1\xi_2 + a_{001}\xi_1^2 + a_{120}\xi_1\xi_2^2 + \\ + a_{102}\xi_1\xi_2^2 + a_{020}\xi_2^3 + a_{210}\xi_1^2\xi_2 + a_{011}\xi_2\xi_1^2 = 0, \\ b_{100}\xi_1 + b_{000}\xi_1^2 + b_{002}\xi_2^2 + b_{210}\xi_1^2\xi_2 + b_{120}\xi_1\xi_2^2 + \\ + b_{102}\xi_1\xi_2^2 + b_{011}\xi_2\xi_1^2 = 0, \\ c_{001}\xi_3 + c_{200}\xi_1^2 + c_{020}\xi_2^2 + c_{002}\xi_1^2 + c_{210}\xi_1^2\xi_2 + \\ + c_{011}\xi_2\xi_1^2 + c_{111}\xi_1\xi_2\xi_3 = 0. \end{aligned} \right| \quad (5.12)$$

The coefficients a_{ijk} , b_{ijk} , c_{ijk} depend on the parameters L , R , h , m , n , δ_0 , K , α [5.16]. On the basis of Eqs. (12), one can determine the equilibrium shape of a shell for different values of the axial load parameter $\hat{\sigma}_0$ and different flow velocities. For a steel shell having the dimensions $L/R = 6$, $R/h = 500$, Figure 5.6 shows the envelopes of branches of equilibrium shapes in stationary air ($\alpha = 0$) and in a flow at a velocity equal to one-half of this critical value α_{cr}^* , which is determined from the solution of the linear problem (see formula (24) below). The critical compressive stress for a shell in a flow turns out to be higher in this case than in a stationary medium*. The form of wave formation also changes: numbers m and n for a compressed shell in a gas flow are higher than for the same shell in a stationary medium.

§52. Dynamic Linear Problem for a Closed Cylindrical Shell

Let us consider the dynamic problem of flutter of a closed circular cylindrical shell. As before, a gas will be assumed to flow outside the shell. In addition, it will be assumed that the shell contains an incompressible liquid of density ρ_L . We will consider a linearized problem as the introductory one.

The expression for the normal component of the load q will be made to include the

*This phenomenon was observed in experiments conducted by E.I. Grigolyuk, R. Ye. Lamper, and L.G. Shandarov (Theory of Shells and Plates, Yerevan, 1964, pp. 407-411) and in the experiments of E.D. Skurlatov [5.16].

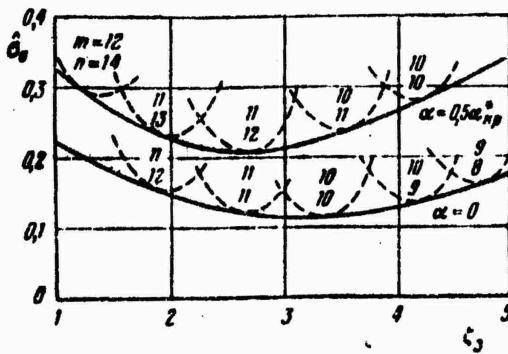


Figure 5.6. Equilibrium shapes of a shell with and without consideration of flow.

inertia forces, dissipative forces, gas pressure and pressure of the liquid filling the shell:

$$q = -\frac{\gamma_0}{g} i_r \frac{\partial^2 w}{\partial t^2} - \frac{\gamma}{g} h \epsilon \frac{\partial w}{\partial t} + p_i + \frac{\gamma_L}{g} \frac{\partial \phi_L}{\partial t}, \quad (5.13)$$

where ϵ is the damping coefficient, p_i is the external gas pressure, ϕ_L is the velocity potential, γ_L is the specific gravity of the liquid filling the shell, and γ_0 and γ are, as before, the specific gravities of the shell material and gas.

We will switch to cylindrical coordinates x , θ , r .

The velocity potential ϕ_L of the liquid contained in the shell must satisfy the equation

$$\frac{\partial^2 \phi_L}{\partial r^2} + \frac{1}{r} \frac{\partial \phi_L}{\partial r} + \frac{\partial^2 \phi_L}{\partial x^2} + \frac{1}{r^2} \frac{\partial^2 \phi_L}{\partial \theta^2} = 0. \quad (5.14)$$

One of the boundary conditions is

$$\frac{\partial \phi_L}{\partial r} = -\frac{\partial w}{\partial t} \quad \text{for } r = R; \quad (5.15)$$

the other conditions refer to the edges $x = 0$, $x = L$; in addition, the function ϕ_L must be finite when $r = 0$.

Substituting the function w , characterizing the vibration mode of the shell, in the form

$$w = f_{m,n}(t) \sin \frac{m\pi x}{L} \cos n\theta, \quad (5.16)$$

we find the following solution of Eq. (14):

$$\varphi_L = A_{m,n}(t) I_n\left(\frac{m\pi r}{L}\right) \sin \frac{m\pi x}{L} \cos n\theta. \quad (5.17)$$

Here I_n is a modified Bessel function of the first kind with index n , and $f_{m,n}$ and $A_{m,n}$ are the desired time functions. Using condition (15), we determine $A_{m,n}$:

$$A_{m,n} = - \frac{L}{m\pi I_n'(\alpha R)} \frac{df_{m,n}}{dt}. \quad (5.18)$$

Substituting (18) into (17), we find the expression for the velocity potential

$$\varphi_L = - \frac{R I_n(\lambda_m)}{\lambda_n I_n'(\lambda_m)} \frac{\partial w}{\partial t}, \quad (5.19)$$

where $\lambda = m\pi R/L$. The transient pressure of the liquid on the wall of the shell will be defined by the formula

$$p_L = - \rho_L \frac{\partial \varphi_L}{\partial t} = \frac{\rho_L R}{\lambda_m} \frac{I_n'(\lambda_m)}{I_n(\lambda_m)} \frac{\partial^2 w}{\partial t^2} = m_L \frac{\partial^2 w}{\partial t^2}, \quad (5.20)$$

where m_L is the apparent mass of the liquid, corresponding to vibrations of the shell with the formation of n waves in the circumferential direction and m half-waves along the generatrix. Thus, the inertial term of the type $(\gamma_0/g)h(\partial^2 w/\partial t^2)$ will be replaced by

where

$$\frac{y_0}{g} h K_{m,n} \frac{\partial^2 w}{\partial t^2},$$

$$K_{m,n} = 1 + \frac{m_L g}{h y_0}.$$

Following the same procedure as in §51, we obtain the following equations of motion:

$$\left. \begin{aligned} \ddot{\zeta}_{m,n} + g_{m,n} \dot{\zeta}_{m,n} + \frac{1}{K_{m,n}} \{ (1 - \delta_0 m^2 a) \zeta_{m,n} - Q \zeta_{m+1,n} \} &= 0, \\ \ddot{\zeta}_{m+1,n} + g_{m+1,n} \dot{\zeta}_{m+1,n} + \\ + \frac{1}{K_{m+1,n}} \{ (\bar{\omega}_{m+1,n}^2 - \delta_0 (m+1)^2 a) \zeta_{m+1,n} + Q \zeta_{m,n} \} &= 0, \end{aligned} \right\} \quad (5.21)$$

where

$$Q = \frac{48 \times p_m M}{E \omega_{m,n}^2} \frac{L^3}{h^3} \frac{1 - \mu^2}{\pi^4} \frac{m(m+1)}{1+2m},$$

$$a = \frac{12(1-\mu^2)}{\pi^2} \frac{1}{\omega_{m,n}^2} \frac{L^2}{Rh}, \quad \bar{\omega}_{n+1,n} = \frac{\omega_{m+1,n}}{\omega_{m,n}};$$

where the dots denote derivatives with respect to time. Damping coefficients corresponding to the different vibration modes are denoted by $g_{m,n}$ and $g_{m+1,n}$. We further assume $g_{m,n} = g_{m+1,n} = g$. Representing the solution of (21) in the form

$$\zeta_{m,n} = F_{m,n} e^{\lambda t}, \quad \zeta_{m+1,n} = F_{m+1,n} e^{\lambda t}, \quad (5.22)$$

we obtain a system of homogeneous linear algebraic equations in $F_{m,n}$ and $F_{m+1,n}$. Setting to zero the determinant of the system, we find the characteristic equation

$$\lambda^4 + 2g\lambda^3 + (b_1 + b_2 - b_3 - b_4 + g^2)\lambda^2 + g(b_1 + b_2 - b_3 - b_4)\lambda + \\ + b_1 b_2 - b_2 b_3 - b_1 b_4 + b_3 b_4 + b_5 = 0; \quad (5.23)$$

where

$$b_1 = \frac{1}{K_{m,n}}, \quad b_2 = \frac{\bar{\omega}_{m+1,n}^2}{K_{m+1,n}}, \quad b_3 = \frac{\delta_0 m^2 a}{K_{m,n}},$$

$$b_4 = \frac{\delta_0 (m+1)^2 a}{K_{m+1,n}}, \quad b_5 = \frac{Q^2}{K_{m,n} K_{m+1,n}} \frac{(1+m)^2 m^2}{(1+2m)^2}.$$

The undisturbed equilibrium form of the shell will be stable if all the real parts of the characteristic indices are negative, and will become unstable if among the characteristic indices there will be at least one with a positive real part. Using the Routh-Hurwitz criterion, we determine the parameter α^* corresponding to the critical flutter velocity:

$$\alpha^* = \frac{1+2m}{2m(1+m)} \frac{\sqrt{K_{m,n} K_{m+1,n}}}{S} \sqrt{(\theta_{m+1,n}^2 - \theta_{m,n}^2)^2 + 2g^2(\theta_{m+1,n}^2 + \theta_{m,n}^2)}, \quad (5.24)$$

where

$$S = \frac{48\pi\rho_\infty}{\pi^4 E \omega_{m,n}^2} \frac{L^4}{h^4} (1 - \mu^2), \quad \theta_{m,n}^2 = \frac{1 - \delta_0 m^2 a}{K_{m,n}},$$

$$\theta_{m+1,n}^2 = \frac{\hat{\omega}_{m+1,n}^2 - (m+1)^2 \delta_0 a}{K_{m+1,n}}.$$

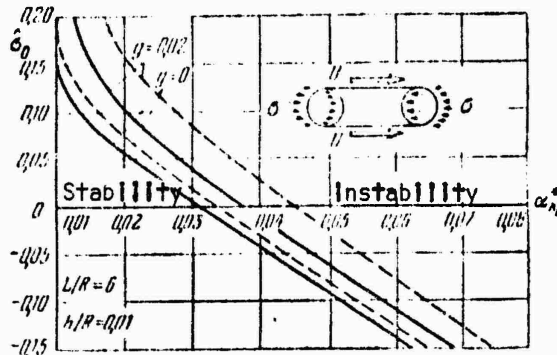


Figure 5.7. Graph for critical flow velocities in the course of a cylindrical shell, with consideration of damping and apparent mass of the liquid.

We then minimize α^* with respect to the number of waves in the circumferential direction n , considering n to be sufficiently large. Results of the calculations are presented in Figure 5.7. The latter gives the critical numbers α_{cr}^* for different values of compressive ($\hat{\sigma}_0 > 0$) and tensile ($\hat{\sigma} < 0$) stresses, and also with (dashed lines) and without (solid lines) consideration of the effects of apparent mass of the liquid and vibration damping. Figure 5.8 shows the stability limits for shells having different L/R and h/R values, either hollow (dashed lines) or filled with liquid (solid lines). It follows from Figures 5.7 and 5.8 that damping stabilizes the shell in this case. In

the presence of axial and compressive stresses changing within the limits considered, the critical flutter velocity is sharply reduced, while in tension, on the contrary, it increases. Consideration of the apparent mass of the liquid leads here to a certain increase in critical velocity; let us note that the vibration mode also changes.

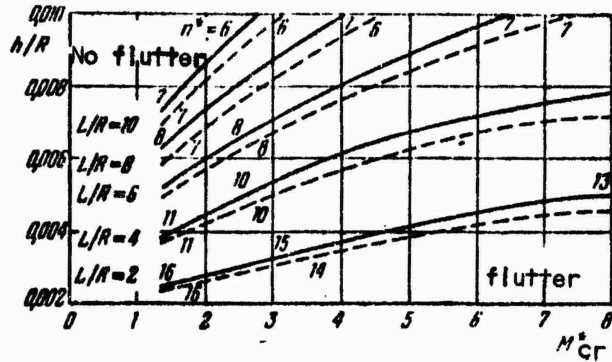


Figure 5.8. Stability limits of hollow and liquid-filled cylindrical shells.

Examination of the function $\alpha_{cr}^*(n)$ reveals that it has two minima, the first minima being characteristic of long shells, and the second, of short ones. As the shell length decreases, the number of waves along the generatrix decreases; at the same time, the number of waves in the circumferential direction increases. On the basis of the assumption that $n \gg m$, from relation (24) one can obtain an approximate dependence for determining the number of waves in the circumferential direction corresponding to the minimum critical flutter velocity:

$$n^4 = 5\pi^2 \left(\frac{R}{L}\right)^2 \left(\frac{12\mu^2 R^3}{h^2} + 1\right), \quad (5.25)$$

the minimum critical velocity being described by the relation

$$\frac{R}{h} \left[\frac{\rho U^2}{2E \sqrt{M^2 - 1}} \right]^{1/4} = 0.91 \left[n^2 \frac{R}{L} \right]^{1/4}. \quad (5.26)$$

Example. Determine the critical parameters for a copper shell with a radius of 204 mm, a length of 408 mm, and wall thickness of 0.1 mm. Using relations (25) and (26), we obtain

$$n^2 = 20, \quad \frac{R}{h} \left[\frac{\gamma U^2}{2Eg \sqrt{M^2 - 1}} \right]^{1/2} = 7.1.$$

In experiments with such shells [5.24], fairly close values were obtained:

$$14 < n^2 < 24 \text{ and } \frac{R}{h} \left[\frac{\gamma U^2}{2Eg \sqrt{M^2 - 1}} \right]^{1/2} \approx 7.$$

It should be recalled that relations (25) and (26) were obtained on the basis of a two-term approximation of the shell deflection. Considering the data obtained from calculations with a large number of degrees of freedom, one can find the following estimates of critical velocity valid for $L/R > 3(h/R)^{1/2}$ and a slight compression of the shell along its axis.* For the first minimum

$$\frac{\kappa p_{\infty} M}{E} \approx 19.3 \left(\frac{h^2}{L^2 R^2} \right)^{1/2} - 8.0 \frac{h}{L} \frac{\sigma_x}{E}, \quad (5.27)$$

$$\frac{\kappa p_{\infty} M}{E} \approx 16 \left(\frac{h^2}{L^2 R^2} \right)^{1/2} - 13 \frac{h}{L} \frac{\sigma_x}{E}, \quad (5.28)$$

where σ_x is the axial stress.

§53. Refined Solution of the Linear Dynamic Problem

For a refined solution of the linear problem, it is necessary to consider a larger number of terms of the series in expansion (4). Because of the cumbersomeness of the

*These data are due to E.I. Grigolyuk, R. Ye. Lamper and L.G. Shandarov [5.10, 1969].

calculations, it becomes necessary to use a computer in determining the stability limits. We will consider an algorithm permitting the determination of the stability limit in the plane of the two parameters h/R and M when many terms are considered in series (4), which approximates the deflection, and when the damping is different from zero [5.16]*. The solution of a system of equations of the type of (21), determinable in the form of (22), leads to the characteristic determinant (the values of R and C are given on p. 243):

$$\left| \left(\lambda^2 + g\lambda + \frac{\omega_{m,n}^2}{K_{m,n}} - \frac{m\dot{\alpha}_n}{K_{m,n}} \right) \delta_{m,l} + \frac{R\alpha C_{m,n,l,l}}{K_{m,n}} \right| = 0, \quad m = 1, 2, 3, \dots, \quad (5.29)$$

$$n = 0, 1, 2, \dots,$$

which is associated with the characteristic polynomial

$$b_{11}\lambda^l + b_{12}\lambda^{l-1} + b_{13}\lambda^{l-2} + b_{22}\lambda^{l-3} + \dots = 0. \quad (5.30)$$

We will now adopt the Routh criterion, which is very convenient for use on a computer, since it calls for operations of the same type. The following sequence of operations was adopted. Polynomial (30) is used to construct the Routh scheme

$$\begin{array}{cccccc} b_{11} & b_{12} & b_{13} & \dots \\ b_{21} & b_{22} & b_{23} & \dots \\ \dots & \dots & \dots & \dots \\ b_{l1} & b_{l2} & b_{l3} & \dots \\ b_{l+1,1} & b_{l+1,2} & b_{l+1,3} & \dots \end{array}$$

Here the elements of the first and second rows are the coefficients of the polynomial. The elements of the subsequent rows are computed from the formula

$$b_{ij} = b_{i-2,j+1} - \frac{b_{i-2,j}}{b_{i-1,j}} b_{i-1,j+1}.$$

*See also the papers [5.16], 1967.

In order that all the roots of polynomial (30) have negative real parts, it is necessary and sufficient that all $b_{ij}(\hat{\alpha})$ in the Routh scheme be different from zero and have the same sign.

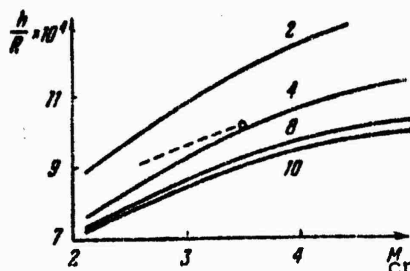


Figure 5.9. Stability limits of cylindrical shells determined by considering different numbers of terms of the series approximating the deflection.

An example of the determination of the stability regions, carried out by considering 2, 4, 8, and 10 terms of the series approximating the deflection, is shown in Figure 5.9; the corresponding number of terms of the series is indicated for each curve. A dashed line indicates the data of an experimental study described by Fung [5.24]. A certain divergence of the calculated and experimental data is explained by the fact that the analysis takes no account of various factors, the most important of which is the influence of the boundary layer.

§54. Transient Flutter of a Cylindrical Shell

The motion of aircraft under actual conditions involves a simultaneous change in flying speed, density of the ambient medium, temperature, stresses in the middle surface of the skin elements, etc. Depending on the relative magnitudes of these parameters, the skin elements may experience flutter or divergence; also possible is the alternation of self-excited vibrations of different modes with states of dynamic

stability.* To study the behavior of shells under such conditions, it is convenient to use the concept of the representative point. We will consider the plane of two parameters characterizing the axial load ($\hat{\sigma}$) and flow velocity (α). The representative point with coordinates $\hat{\sigma}$ and α will move in the plane $\hat{\sigma}, \alpha$ as the axial longitudinal stresses and the flow velocity change. Some idea of the behavior of a shell for a sufficiently slow change of any given parameter can be obtained by analyzing the relative positions of the limits of steady flutter and divergence, shown in Figure 5.10. Let us suppose that the compressive stresses are small and below the critical value $\hat{\sigma} = 0.6$. As the velocity parameter α increases and $\hat{\sigma} = \text{const}$, the representative point moves in the plane of the graph on the level of line ab. The shell will remain stable up to the value of α corresponding to point b, where flutter is set up. Let α now remain constant, and compressive stresses be set up in the shell. Then, following line cd, we come to the point corresponding to the divergence of the shell. For a higher value of $\alpha = \text{const}$ and increasing compression, the representative point moves along line fe, which successively intersects the regions of flutter corresponding to vibrations with different modes and regions of dynamic stability.

In real systems possessing structural damping, a certain time is necessary to establish the vibration amplitudes corresponding to flutter. For instance, if the time during which the critical value $\hat{\sigma}_u$ is reached (motion along line lk) is comparable with several periods of natural vibrations of the shell, flutter motions may be unable to develop, and a quasi-static stability loss will occur. For this reason, in studying transient flutter, it is necessary to consider the time spent by the representative point in the flutter region. Let us note that we are considering loading during a time longer than the period of several natural vibrations (or several tens of natural vibrations) of the unloaded shell, so that the process differs only slightly from a static one and does not result in an increase of the upper critical load parameter $\hat{\sigma}_u$.

*This problem was discussed in the paper [5.16]; see Strength Calculations 15, Mashinostroyeniye, Moscow, 1971; also E.D. Skurlatov and A.S. Vol'mir, Theory of Plates and Shells, Nauka, Moscow, 1971, pp. 29-33.

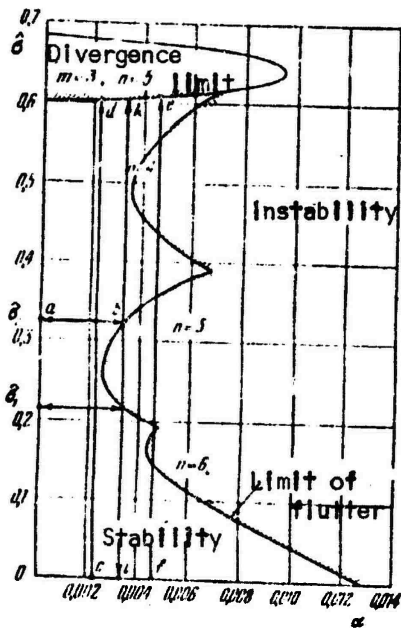


Figure 5.10. Limits of steady flutter and divergence for a cylindrical shell.

The transient flutter of a cylindrical shell in the linear formulation will be described by equations of the type of (21) with variable coefficients:

$$\frac{d^2\zeta_{m,n}}{d\tau^2} + g_{m,n} \frac{d\zeta_{m,n}}{d\tau} + \omega_{m,n}^2 \zeta_{m,n} - \alpha [\delta(\tau) m^2 + Q(\tau)] \zeta_{m,n} + \tilde{K}(\tau) \alpha(\tau) \sum_{i=1}^{\infty} \sum_{j=0}^{\infty} C_{m,n,i,j} \zeta_{i,j} = 0, \quad (5.31)$$

where

$$\begin{aligned} \zeta_{m,n} &= \frac{f_{mn}}{h}, \quad \delta(\tau) = \frac{R}{Eh} \sigma(\tau), \quad \alpha = \frac{h}{L} M(\tau), \\ Q(\tau) &= \frac{\kappa}{2\pi^2 E} \frac{L^2}{h^2} p_{\infty}(\tau), \quad \omega_{m,n}^2 = A + \frac{12m^4 L^4 (1-\mu^2)}{R^2 h^2 \pi^4 A}, \\ A &= [m^2 + (\frac{nL}{\pi R})^2]^2, \quad \tilde{K} = \frac{48(1-\mu^2)L^4 \kappa}{Eh^4 \pi^4} p_{\infty}(\tau), \end{aligned} \quad (5.32)$$

$$C_{m,n,i,j} = \begin{cases} \frac{ml}{m^2 - l^2}, & \text{if } n=j, m \pm 1 - \text{ odd} \\ 0, & \text{if } n=j, m \pm 1 - \text{ even} \\ 0, & \text{if } n \neq j. \end{cases}$$

To study Eqs. (31), use is made of the method of numerical integration, principal attention being given to various laws of change with time of the longitudinal load parameter $\hat{\sigma}$ for fixed values of the flow velocity α . The prepared computer program applied the Runge-Kutta method with a variable, automatically selectable integration step. Some results of the computations are shown in Figure 5.11. We considered a shell with parameters $L/R = 6$, $R/h = 100$, $n = 6$ for $g = 0.001$ and initial conditions

$$\zeta_1 = \zeta_2 = 0.4, \dot{\zeta}_1 = \dot{\zeta}_2 = 0 \text{ for } \tau = 0.$$

Envelopes of the vibration amplitudes and lines corresponding to the different loading laws $\hat{\sigma} = \hat{\sigma}(\tau)$ are plotted on Figure 5.11. Motions with exponentially increasing amplitudes may be considered as flutter motions. The dashed lines in Figure 5.11 delineate the zones corresponding to the region of steady flutter in Figure 5.10 as the representative point moves along the trajectory ik.

At a subcritical flow velocity, the loading and unloading rate and the time spent by the representative point in the flutter zone were varied. Comparison of curves of the transient process for different loading laws leads to the conclusion that a change in longitudinal compression may lead both to vibrations with increasing amplitude (Figure 5.11a, d) if the representative point stays long enough in the flutter region, and to damped motions (Figure 5.11 b, c) if the flutter region is crossed rapidly. Thus, an increase in the compression stresses of the shell may lead to the discontinuation of flutter that has already started. As the load increases during a time commensurate with several vibration periods of the shell, flutter motions are unable to develop (Figure 5.11c), and snapping of the shell sets in.

Let us note that structural damping leads to a sharp increase in the time necessary to reach some definite vibration amplitude (Figure 5.11a).

A more complete investigation should be carried out on the basis of nonlinear theory, which permits the description of the snapping phenomenon and the determination of limiting cycles.

§55. Nonlinear Flutter of a Closed Cylindrical Shell

Let us turn to the solution of the dynamic problem of flutter in the nonlinear formulation of [5.16]. Supplementing Eqs. (12) with terms corresponding to inertia forces and damping, we obtain a system of three nonlinear differential equations relating the deflection parameters ξ_1 , ξ_2 , ξ_3 with time. An integration of this system,

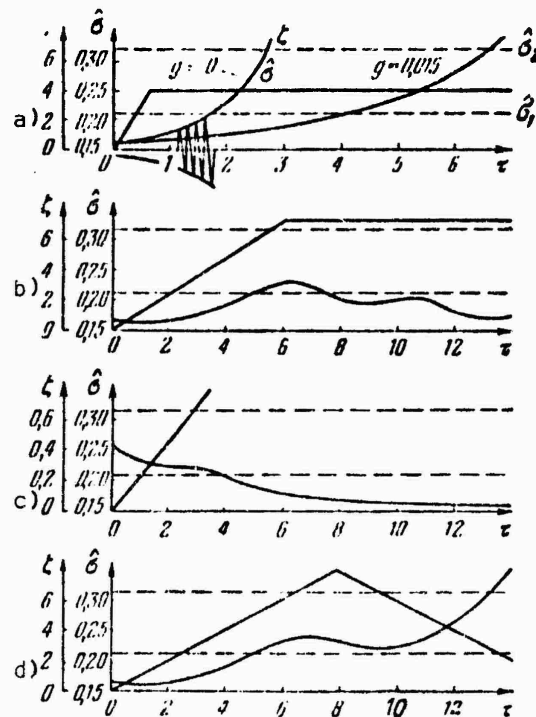


Figure 5.11. Change of vibration amplitudes of a cylindrical shell for different laws of loading by axial forces with time.

carried out with a computer for a shell with parameters $L/R = 6$, $R/h = 100$, $n = 7$ for $g = 0.005$, is reflected in Figure 5.12. The latter gives the dependence of the relative deflection ξ_1 on the flow velocity parameter $\alpha = Mh/L$ referred to the

critical value resulting from the solution of the linear problem. From the point $a/a^* = 1$ there diverge two branches which determine the vibration amplitudes for different stable limiting cycles (the dashed line represents the unstable limiting cycle). Judging from these data, for a closed shell, rigid excitation of flutter at large disturbances becomes possible: self-excited oscillations with finite amplitudes appear at flow velocities smaller than the critical velocities obtained from linear theory. Let us note that the solution of the problem in the linear formulation makes it possible to find the critical flow velocity at which the undisturbed velocity of the shell ceases to be stable in relation to small disturbances and enables one to estimate only the initial tendency of the vibrations. However, this does not permit one to predict the further development of the process, whereas nonlinear theory permits one to determine the characteristics of both the transient process and limiting cycle, which are necessary for estimating the fatigue strength of a thin-walled structure in a gas flow. In the nonlinear formulation, one can also estimate more exactly the influence on the amplitudes of self-excited vibrations of such factors as structural damping and internal pressurization, and also to describe flutter with a wave traveling in the circumferential direction, observed in experiment and not described by linear treatment. These questions will be discussed below.

§56. Flutter of a Cylindrical Shell with a Wave Traveling in the Circumferential Direction

It was shown above that by treating the dynamic problem in the nonlinear formulation, one can determine the "lower" critical velocity of flutter, which cannot be found with the aid of linear theory. We will consider below the problem of formation of flutter with a wave traveling in the circumferential direction, flutter that also cannot be described in nonlinear terms [5.22]. Waves traveling in the circumferential direction were observed in the experiments described in [5.32]. This is sometimes referred to as a "pseudo-traveling" wave, since, at first glance, no factors causing it are present in the external flow. It may be postulated that the traveling wave is produced by the nonlinear character of the vibrations of the cylindrical shell. A phenomenon of this type has been observed in a study of forced nonlinear vibrations

of a thin ring. Since nonlinear vibrations of a cylindrical shell with long wavelengths in the axial direction are similar phenomenon arises in the flutter of a closed shell. If resonance vibrations with a mode of type $\cos n\theta$ are excited in a thin ring, and the vibration amplitude is gradually increased by increasing the amplitude of the exciting force, then at some critical value of the amplitude, a mode of type $\sin n\theta$ will be suddenly excited. The latter mode is superposed on the mode of $\cos n\theta$ in such a way that a pseudo-traveling wave is formed. The critical value of the amplitude decreases as the number of circumferential waves n increases and the dissipation effect in the ring decreases. It can be expected that qualitatively similar results can be obtained with vibrations of a cylindrical shell in the case of large values of n for small m .

We will use equations of the type of (1.40), (1.41) in the form (N_x , N_θ being the forces in the axial and circumferential directions):

$$D\nabla^4 w + \beta \frac{\partial w}{\partial t} + \rho_0 h \frac{\partial^2 w}{\partial t^2} + p = N_x \frac{\partial^2 w}{\partial x^2} + \frac{N_\theta}{R^2} \frac{\partial^2 w}{\partial \theta^2} + \frac{1}{R} \frac{\partial^3 \Phi}{\partial x^2} + \frac{1}{R^2} \left(\frac{\partial^2 \Phi}{\partial \theta^2} \frac{\partial^2 w}{\partial x^2} - 2 \frac{\partial^3 \Phi}{\partial x \partial \theta} \frac{\partial^2 w}{\partial x \partial \theta} + \frac{\partial^2 \Phi}{\partial x^2} \frac{\partial^2 w}{\partial \theta^2} \right), \quad (5.33)$$

$$\frac{1}{E} V^4 \Phi = - \frac{1}{R} \frac{\partial^2 w}{\partial x^2} + \frac{1}{R^2} \left[\left(\frac{\partial^2 w}{\partial x \partial \theta} \right)^2 - \frac{\partial^2 w}{\partial x^2} \frac{\partial^2 w}{\partial \theta^2} \right], \quad (5.34)$$

where the aerodynamic pressure p is approximated by the linear approximation of the piston theory.

The deflections of a shell vibrating with the formation of a wave traveling in the circumferential direction will be approximated by the following expression containing four terms:

$$w(x, \theta, t) = \left[A_1(t) \sin \frac{\pi x}{L} + A_2(t) \sin \frac{2\pi x}{L} \right] \cos n\theta + \\ + \left[B_1(t) \sin \frac{\pi x}{L} + B_2(t) \sin \frac{2\pi x}{L} \right] \sin n\theta + \\ + \frac{n^2}{4R} \left[A_1(t) \sin \frac{\pi x}{L} + A_2(t) \sin \frac{2\pi x}{L} \right]^2 + \\ + \frac{n^2}{4R} \left[B_1(t) \sin \frac{\pi x}{L} + B_2(t) \sin \frac{2\pi x}{L} \right]^2. \quad (5.35)$$

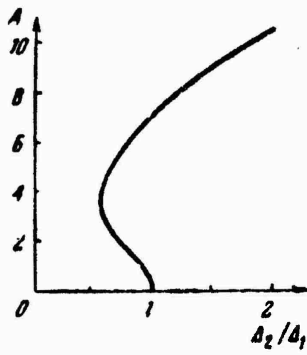
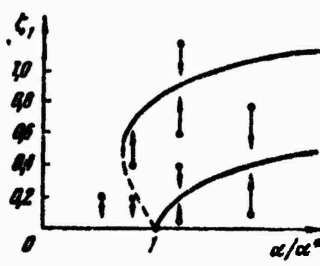


Figure 5.13. Amplitudes of limiting cycles for flutter with a wave traveling in the circumferential direction.

Relation (35) includes terms containing $n^2/4R$, so that the solution satisfies the condition of periodic continuity of circumferential displacement v . Applying the procedure of the Bubnov-Galerkin method, we obtain a system of four nonlinear ordinary differential equations. These equations were solved by the harmonic balance method, and were also integrated numerically. As in §55, integration with respect to time was continued until the amplitudes either fell off to zero, or one of the steady limiting cycles was reached; the stability of the limiting cycles was also studied.

Figure 5.13 shows the results of computations performed for certain characteristics of the shell and flow. It shows the character of change in the amplitude of the limiting cycle, obtained by assuming that damping is absent. It can be shown that structural damping causes only a slight change in the amplitude of the limiting cycle for flutter with a travelling wave. The values of Δ_1 and Δ_2 are listed below on p. 202.

Let us note that the minimum values of the amplitude of limiting cycles of flutter, listed in the figure, amount to approximately 4-5 shell thicknesses. At the same time, the deflections observed in experiments with such shells are of the order of one to two thicknesses. It should be expected that the magnitude of the deflection obtained theoretically will decrease if the shell is assumed to be not hinged, but clamped along the edges, as was the case in the experiment. Moreover, by keeping a large number of the terms of the series in the expression approximating the deflection, one can obtain a more accurate solution. Such a study will be made below.

§57. Divergence and Flutter of a Cylindrical Shell with Consideration of the Boundary Layer

To elucidate the role of the boundary layer in the divergence and panel flutter of a closed circular cylindrical shell, we will use the idealized scheme proposed by Fung [5.24]. The boundary layer will be represented as an annular region of uniform subsonic flow, located between the shell and a homogeneous supersonic flow. The thickness of the subsonic region will be denoted by σ , and the flow velocity by U_σ (Figure 5.14). It will also be assumed that the elastic cylindrical shell under consideration, of finite length L , is a portion of an infinitely long cylinder. The problem consists in finding the aerodynamic pressure on the surface of the shell arising as a result of small deviations of the shell from the undisturbed shape. The disturbances of the flow generated by the shell deformations will be considered slight. For the disturbed velocity potential within the boundary layer we will write the linearized equation (see [5.24])

$$\frac{1}{c_0^2} \frac{\partial^2 \Phi_\Lambda}{\partial t^2} + 2 \frac{M_\Lambda}{c_0} \frac{\partial \Phi_\Lambda}{\partial x \partial t} - \beta_\Lambda^2 \frac{\partial^2 \Phi_\Lambda}{\partial x^2} = \frac{\partial^2 \Phi_\Lambda}{\partial r^2} + \frac{1}{r} \frac{\partial \Phi_\Lambda}{\partial r} + \frac{1}{r^2} \frac{\partial^2 \Phi_\Lambda}{\partial \theta^2}$$

for $R \leq r \leq R + \delta$, (5.36)

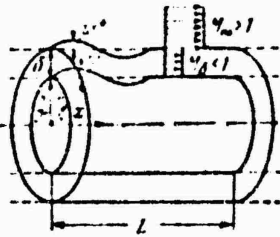


Figure 5.14. Boundary layer on the surface of a cylindrical shell in a gas flow.

where c_σ is the sound velocity in the boundary layer, Φ_σ is the velocity potential in the region of the boundary layer, $M_\sigma = U_\sigma/c_\sigma$ is the Mach number in the boundary layer, and $\beta = \sqrt{1 - M_\sigma^2}$.

The potential Φ_σ is related to the normal deflection function by the condition of impermeability of the walls

$$\left. \frac{\partial \Phi_\sigma}{\partial r} \right|_{r=R} = \frac{\partial w}{\partial t} + U_\delta \frac{\partial w}{\partial x}. \quad (5.37)$$

In addition, at the interface between the subsonic and supersonic flows (for $r = R + \delta$), the values of the pressure and velocity normal to the surface should be continuous. Denoting by w^* the small radial displacement of the interface, we write the condition of radial velocity continuity

$$\left. \frac{\partial \Phi_\sigma}{\partial r} \right|_{r=R+\delta} = \frac{\partial w^*}{\partial t} + U_\delta \frac{\partial w^*}{\partial x}. \quad (5.38)$$

The condition of pressure continuity at the boundary surface will be written in the form (Φ and p_∞ pertain to the external flow):

$$-\rho_\delta \left(\frac{\partial \Phi_\delta}{\partial t} + U_\delta \frac{\partial \Phi_\delta}{\partial x} \right) = -\rho_\infty \left(\frac{\partial \Phi}{\partial t} + U \frac{\partial \Phi}{\partial x} \right) \quad \text{for } r = R + \delta. \quad (5.39)$$

Representing the shell wall displacements in the form

$$w(x, 0, t) = w_0 e^{i\omega t} \cos n\theta \sin \alpha x, \quad (5.40)$$

where $\alpha = m\pi/L$, and m is the number of half-waves in the longitudinal direction, we write the solution of Eq. (36) in the form

$$\begin{aligned} \Phi_\theta(x, r, \theta, t) = & e^{i\omega t} \cos n\theta \left\{ \exp \left[i(K_0 M_0 - \lambda_1) \frac{M_0 x}{B_0 R} \right] \left[B_1 I_n \left(\mu_1 \frac{M_0 r}{B_0 R} \right) + \right. \right. \\ & \left. \left. + C_1 Y_n \left(\mu_1 \frac{M_0 r}{B_0 R} \right) \right] - \exp \left[i(K_0 M_0 + \lambda_2) \frac{M_0 x}{B_0 R} \right] \left[B_2 I_n \left(\mu_2 \frac{M_0 r}{B_0 R} \right) + \right. \right. \\ & \left. \left. + C_2 Y_n \left(\mu_2 \frac{M_0 r}{B_0 R} \right) \right] \right\}, \end{aligned} \quad (5.41)$$

where I_n , Y_n are Bessel functions. The arbitrary constants entering into (41) are determined from the boundary conditions. Omitting the intermediate operations, we write the final expression for the disturbed pressure on the cylinder wall:

$$\bar{p}(x, r, 0, t) = \frac{w_0 x \rho_\infty M}{R} e^{i\omega t} \cos n\theta (\bar{A}_{mn} \cos \alpha x + \bar{B}_{mn} \sin \alpha x), \quad (5.42)$$

where the coefficients \bar{A}_{mn} , \bar{B}_{mn} depend on the parameters of the boundary layer and incident flow. In the absence of the boundary layer ($\sigma = 0$), the aerodynamic pressure according to (42) is the same as the expression obtained from the piston theory.

It was established in §51 that the static loss of stability of shells placed in a supersonic gas flow takes place at greater axial stresses than in the absence of the flow. We will attempt to determine the role of an idealized boundary layer in such a problem. The expression for the aerodynamic load (42) after some obvious transformations will take the form

$$\bar{p}(x, R, 0) = \frac{w_0 x \rho_\infty M}{R} \cos n\theta [\bar{B}_{mn} \cos \alpha x + \bar{B}_{mn} \sin \alpha x], \quad (5.43)$$

where

$$\begin{aligned}\bar{B}_{mn} &= \frac{n_1 + n_2 n_3}{1 + n_1^2} q, \quad \bar{B}_{nm} = -\frac{n_1 n_3 - n_2}{1 + n_1^2} q, \\ q &= \frac{\sqrt{1 - M_0^2} x_0 \rho_0 M_0}{x_0 \rho_0 M}, \quad n_1 = (\alpha R)^2 \Theta \left(1 - \frac{\delta}{\eta_0}\right), \\ n_2 &= (\alpha R)^2 \delta, \quad n_3 = \Theta \delta \left(\mu_1^2 - \frac{n_1^2}{\eta_0^2}\right), \\ \delta &= \frac{M_0 \delta}{R \sqrt{1 - M_0^2}}, \quad \eta_0 = \frac{M_0}{\sqrt{1 - M_0^2}}, \quad \Theta = \frac{x_0 \rho_0 M}{\sqrt{1 - M_0^2} x_0 \rho_0 M_0 \alpha R}.\end{aligned}$$

Reducing system (7) to a single equation, we get

$$DV^4 w + \frac{Eh}{R^2} \frac{\partial^4 w}{\partial x^4} + \sigma h V^4 \frac{\partial^2 w}{\partial x^2} + V^4 p = 0. \quad (5.44)$$

Let us consider the case of hinged support. The shell deflection will be approximated by two terms of the series:

$$w = f_{mn} \sin \alpha x \cos \eta \theta + f_{m+1,n} \sin \alpha x \cos \eta \theta. \quad (5.45)$$

Applying the Bubnov-Galerkin method to (44) and performing certain transformations, we arrive at a system of two algebraic equations similar to (9a):

$$\left. \begin{aligned} (\omega_{m,n}^2 - \delta_0 \alpha m^2 + \Psi \bar{B}_{mn}) \zeta_{m,n} - \eta_m \Psi \bar{B}_{m+1,n} \zeta_{m+1,n} &= 0, \\ (\omega_{m+1,n}^2 - \delta_0 \alpha (m+1)^2 + \Psi \bar{B}_{m+1,n}) \zeta_{m+1,n} + \\ + \eta_{m+1} \Psi \bar{B}_{m,n} \zeta_{m,n} &= 0, \end{aligned} \right\} \quad (5.46)$$

where

$$\Psi = \frac{x_0 \rho_0 M / \alpha}{DR^2 \Theta}.$$

Setting the determinant of the system of equations (46) to zero, we solve it for the longitudinal stress parameter $\hat{\sigma}_0$:

$$\begin{aligned}\hat{\sigma}_0 &= \frac{1}{2am(m+1)} \left[(\Omega_{m+1,n}^2 m + \Omega_{m,n}^2 (m+1)) \pm \right. \\ &\quad \left. \pm \sqrt{[\Omega_{m+1,n}^2 m - \Omega_{m,n}^2 (m+1)]^2 - 4m(m+1)\bar{\varphi}\bar{B}_{m,n}\bar{B}_{m+1,n}} \right].\end{aligned}\quad (5.47)$$

Relation (47) has the same form as relation (10) obtained earlier, but the quantities entering into it have different values:

$$\begin{aligned}\Omega_{m,n}^2 &= \omega_{m,n}^2 + q\bar{B}_{m,n}, \quad \Omega_{m+1,n}^2 = \omega_{m+1,n}^2 + q\bar{B}_{m+1,n}, \\ \bar{\varphi} &= \frac{16m(m+1)}{\pi^2(2m+1)^2} q^2.\end{aligned}$$

It can be shown that in the absence of the boundary layer ($\delta = 0$), relation (47) becomes equality (10).

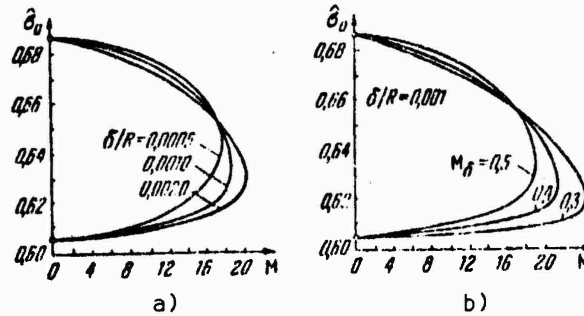


Figure 5.15. Divergence limits of cylindrical shell: a) for different values of the boundary layer thickness, b) for different Mach numbers in the boundary layer.

Figure 5.15 presents in graphical form the results of calculations for $L/R = 6$, $R/h = 100$, $E = 2 \times 10^6 \text{ kg/cm}^2$, $M_f = 0.5$, $m = 3$, $n = 5$, carried out in accordance with (47). The thickness of the boundary layer and the flow velocity in the subsonic zone were varied [5.16].

Analysis of results of computations performed for shells with dimensions changing over wide limits leads to the conclusion that increasing the thickness of the boundary layer or decreasing the flow velocity in the subsonic region leads to values of upper critical stresses δ_u that are somewhat lower than for $\delta = 0$. These data indicate that, to a first approximation, the boundary layer model under consideration reflects the physical conditions characteristic of a real boundary layer.

Let us consider the problem of flutter of a circular cylindrical shell in the presence of a boundary layer. We will use the linearized equation (1.40); the aerodynamic load \bar{p} will be taken into consideration in accordance with (42):

$$DV^2w + \frac{Eh}{R^2} \frac{\partial^4 w}{\partial x^4} + \nabla^4 \left(\alpha h \frac{\partial^2 w}{\partial x^2} + \rho_0 h \frac{\partial^2 w}{\partial t^2} + \rho_0 h c \frac{\partial w}{\partial t} + \bar{p} \right) = 0. \quad (5.48)$$

The displacement of the shell walls is approximated by the following series:

$$w = e^{i\omega t} \cos n\theta \sum_{m=1}^{\infty} a_m \sin mx. \quad (5.49)$$

Substituting (49) into (48) and using the Bubnov-Galerkin method, we obtain a system of algebraic equations homogeneous and linear with respect to a_m . The determinant of this system

$$\Delta = \begin{vmatrix} \omega_{1,n}^2 - D\omega - \alpha a + \sigma \tilde{A}_{1,n} & -\frac{f}{3n} \sigma \tilde{A}_{2,n} & 0 & \dots \\ \frac{f}{3n} \sigma \tilde{A}_{1,n} & \omega_{2,n}^2 - D\omega - \alpha a + \sigma \tilde{A}_{2,n} & -\frac{f}{3n} \sigma \tilde{A}_{3,n} & \dots \\ 0 & \frac{f}{3n} \sigma \tilde{A}_{2,n} & \omega_{1,n}^2 - D\omega - \alpha a + \sigma \tilde{A}_{1,n} & \dots \\ \dots & \dots & \dots & \dots \end{vmatrix} \quad (5.50)$$

has complex elements. The values of the number M and vibration frequency ω at which the real and imaginary parts of the determinant simultaneously becomes zero correspond to the neutral state of the shell. Exceeding this velocity leads to vibrations with an amplitude increasing with time.

Determination of the critical values of M and w is usually carried out by using a very tedious graphical method [5.19]. A different technique of solving the problem will be used here requiring a much smaller number of operations for the calculation of each variant, this being particularly important in the study of the influence of many parameters. In this approach, a system of two algebraic equations nonlinear with respect to M and w , obtained by setting to zero the real and imaginary parts of determinant (50), was solved by Newton's method. Results of the solution of the problem discussed in §52 were used as the first approximation in the case of a very thin boundary layer. The process usually converged quickly, and the new values of M and w obtained were used as the initial approximation in the problem with a new value of the boundary layer thickness $\delta + \Delta\delta$.

The boundary layer parameters δ and U_δ can also be determined in the following manner.* It is necessary that an energy correspondence exist between the approximate model used and an "exact" model. By "exact" is meant a model describable either theoretically on the basis of viscous equations, or experimentally. Thus, to determine the parameters δ and U_δ , one can consider two problems of stationary flow past a boundary, i.e. flow of, an ideal fluid with a piecewise-constant velocity profile, and viscous flow. If the approximate or exact solutions $u_u(y)$ of the latter problem are known, the parameters U_δ and δ in these two problems are uniquely determined from the conditions of conservation of the total vortex and momentum.

In the case of a piecewise-constant velocity profile, the expression for the total vortex has the form ($0 < \delta < y_1$):

$$\int_0^{y_1} \text{curl}_2 \mu dy = - \int_0^{y_1} (U - U_\delta) \delta_0(y - \delta) dy = -(U - U_\delta); \quad (a)$$

where $\delta_0(y - \delta)$ is the Dirac delta-function. The quantity y_1 should be chosen in accordance with the condition

*These results are due to L.V. Selezova (Candidate's dissertation, Kiev State University, 1969); they pertain to flow past a flat boundary.

$$\int_{y/L}^{\infty} \left(1 - \frac{y}{L}\right) d\left(\frac{y}{L}\right) = \varepsilon \ll 1.$$

For the momentum we have

$$K = U_\delta \rho_\delta \delta + U \rho (y_1 - \delta). \quad (b)$$

Considering expressions (a) and (b), the conditions of conservation of the vortex and momentum are written in the form

$$\int_0^{y_1} \frac{\partial u_0}{\partial y} dy = U - U_\delta, \quad (c)$$

$$\int_0^{y_1} u \rho u_0 dy = U_\delta \rho_\delta \delta + U \rho (y_1 - \delta). \quad (d)$$

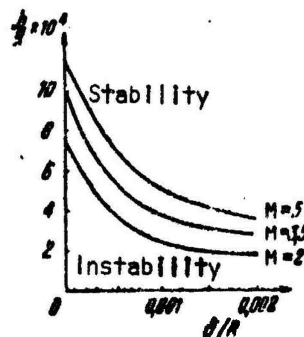


Figure 5.16. Relative shell thickness necessary for preventing flutter vs. boundary layer thickness and Mach number of incident flow.

From Eqs. (c) and (d) we obtain expressions determining U_δ and δ (for $\rho_u \approx \rho_\delta \approx \rho$):

$$\frac{U_f}{U} \approx 1 - \frac{1}{U} \int_0^L \frac{\partial u_y}{\partial y} dy,$$

$$\frac{\delta}{L} \approx \frac{\frac{n}{L} U - \frac{1}{L} \int_0^L u_y dy}{\int_0^L \frac{\partial u_y}{\partial y} dy}. \quad (e)$$

(f)

Some results of determination of flutter limits taking into account four terms of the series for cylindrical shells having boundary layers of different thicknesses are shown in Figure 5.16, assuming that $L/R = 2$, $E = 1.1 \times 10^6 \text{ kg/cm}^2$, $n = 22$, $M_\infty = 0.5$, $p_\infty = p_\delta = 0.12 \text{ kg/cm}^2$. The data obtained confirm the conclusion reached in the studies of Fung [5.24] and Anderson [5.19] on the stabilizing influence of a subsonic idealized boundary layer. It may be postulated that the stabilizing effect obtained by using an idealized boundary layer scheme is exaggerated. This question ought to be studied further.

§58. Flutter of a Cylindrical Shell in the Presence of Changing Pressure in the Incident Flow

It was assumed earlier that the pressure and velocity of a supersonic flow incident on a shell are constant. However, a problem of practical interest is that of the behavior of shells in a flow with time-varying parameters such as pressure (see also §103).

We will use Eqs. (33), (34) describing the behavior of a closed cylindrical shell [5.32]. The solution of the equations of motion is represented in the more complex form

$$w = [f_1(t) \sin \alpha x + f_2(t) \sin 2\alpha x] \sin \beta y + \frac{n^2}{4R} [f_1(t) \sin \alpha x + f_2 \sin 2\alpha x]^2, \\ \alpha = m\pi/L, \beta = n/R, \quad (5.51)$$

assuming that $m = 1$. The factor $n^2/4R$ was chosen so as to satisfy the periodicity condition of the circumferential displacement v . Using the procedure of the Bubnov-Galerkin method, we arrive at the following system of equations:

$$\begin{aligned} \frac{d^2\zeta_1}{dt^2} + \Delta_1 \frac{d\zeta_1}{dt} + \omega_{in}^2 \zeta_1 + \\ + \frac{c}{8} \left\{ \zeta_1 \left[3 \left(\frac{d\zeta_1}{dt} \right)^2 + 2 \left(\frac{d^2\zeta_1}{dt^2} \right) \right] + \left(\frac{d^2\zeta_1}{dt^2} + \Delta_1 \frac{d\zeta_1}{dt} \right) (3\zeta_1^2 + 2\zeta_2^2) + \right. \\ \left. + 4\zeta_2 \left(\zeta_1 \frac{d^2\zeta_2}{dt^2} + \frac{d\zeta_1}{dt} \frac{d\zeta_2}{dt} \right) + 4\Delta_1 \zeta_1 \zeta_2 \frac{d\zeta_2}{dt} \right\} - \\ - c\zeta_1 (a\zeta_1^2 + b\zeta_2^2) - \Delta_2 \eta \left[1 + \frac{c}{5} \left(\zeta_1^2 + \frac{4}{7} \zeta_2^2 \right) \right] = 0, \end{aligned} \quad (5.52a)$$

$$\begin{aligned} \frac{d^2\zeta_2}{dt^2} + \Delta_1 \frac{d\zeta_2}{dt} + \omega_{in}^2 \zeta_2 + \frac{c}{8} \left\{ \zeta_2 \left[3 \left(\frac{d\zeta_2}{dt} \right)^2 + 2 \left(\frac{d^2\zeta_2}{dt^2} \right) \right] + \right. \\ \left. + \left(\frac{d^2\zeta_2}{dt^2} + \Delta_1 \frac{d\zeta_2}{dt} \right) (3\zeta_2^2 + 2\zeta_1^2) + 4\zeta_1 \left(\zeta_2 \frac{d^2\zeta_1}{dt^2} + \frac{d\zeta_1}{dt} \frac{d\zeta_2}{dt} \right) + \right. \\ \left. + 4\Delta_1 \zeta_1 \zeta_2 \frac{d\zeta_1}{dt} \right\} - c\zeta_2 (16c\zeta_2^2 + b\zeta_1^2) + \\ + \Delta_2 \zeta_2 \left[1 + \frac{c}{5} \left(\zeta_2^2 + \frac{4}{7} \zeta_1^2 \right) \right] = 0, \end{aligned} \quad (5.52b)$$

where

$$\begin{aligned} \zeta_1 &= \frac{l_1}{h}, \quad \zeta_2 = \frac{l_2}{h}, \quad c = \left(\frac{n^2 h}{R} \right)^2, \\ \Delta_1 &= \frac{\kappa p_{\infty} \alpha}{\gamma_0 h c_{\infty}}, \quad \Delta_2 = \frac{8 \times M p_{\infty} \alpha}{3 \gamma_0 l_1 h}; \end{aligned}$$

a, b, c being some coefficients dependent on the shell parameters.

Equations (52) were integrated numerically with a computer and were also solved by the harmonic balance method. The computations were carried out for a copper shell with the parameters given in the preceding section for different values of the pressure in the incident flow and a constant Mach number equal to 3. As is evident from Figure 5.17, for the chosen deflection approximation, the change in the amplitudes of limiting cycles with increasing pressure in the flow is more complex in character, but it also turns out that the portions of the curves having a negative slope angle correspond to unstable limiting cycles. Despite the continuous pressure increase in the incident flow, the amplitudes of limiting cycles may change abruptly.

Let us examine the behavior of the shell when the pressure in the incident flow increases smoothly. When the aerodynamic parameter Δ_2 reaches a value of 1.41×10^5 , a disturbance of the shell (for example, caused by noise in the turbulent boundary layer) will give rise to self-excited vibrations with mode $n = 23$. For a small increase of Δ_2 , the vibration amplitudes will begin to increase exponentially up to the values corresponding to the limiting cycle with $n = 23$. As the aerodynamic parameter

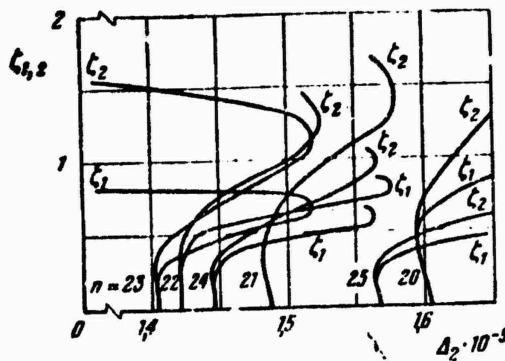


Figure 5.17. Change in the amplitudes of limiting cycles of a shell as a function of pressure in the incident flow.

increases further to the value $\Delta_2 = 1.52 \times 10^5$, there is the possibility of an abrupt transition to vibrations with another mode, for example, with $n = 22$, since this curve is closest to the original curve. At the same time, if the pressure increase is continuous, the representative point may also move to other curves (Figure 5.17), corresponding to vibrations with a markedly different vibration frequency and amplitude (for example, transition from vibrations with mode $n = 21$ to mode $n = 25$ for $\Delta_2 = 1.58 \times 10^5$). A sharp, abrupt transition to vibrations with another mode and amplitude may lead to failure of the structure.

§59. Experimental Study of the Flutter of Closed Cylindrical Shells

The experiments described below [5.24, 5.32] were carried out with closed cylindrical copper shells with a radius of 204 mm, length of 408 mm, and thickness of 0.081 and 0.102 mm; hence, the ratio R/h was 2500 and 2000.

In the experiments, purely sinusoidal vibrations corresponding to shell flutter in one mode, beats corresponding to flutter in two or a large number of modes, as well as complex large-amplitude vibrations arising from a zero or negative pressure

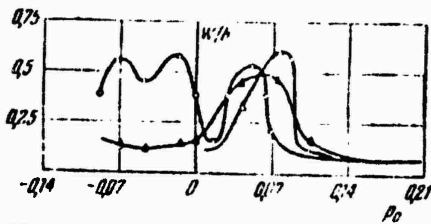


Figure 5.18. Vibration amplitudes vs. magnitude of internal pressure in the shell.

differential in the cavity under the shell and in the free flow were observed. The amplitude and mode of the vibrations during the flutter were found to be a very complex function of the parameters of the incident flow, pressure in the cavity under the shell p_0 , and axial compressive forces (see Figure 5.18 and §58). In the figures, the open triangles correspond to shells loaded with an axial force of 90.8 kg; black triangles, to a force of 40.9 kg; and circles, to shells free of longitudinal forces. It is important to note that at high values of internal pressure p_0 (in Figure 5.18 in technical atmospheres), the shell becomes completely stabilized even in the presence of axial load.

Data on the determination of vibration modes during the flutter were obtained.

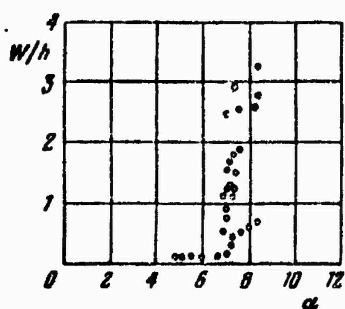


Figure 5.19. The "deflection vs. aerodynamic load" relation obtained in the experiments.

The mode in the longitudinal direction corresponds to vibrations with 1, 2 or 3 half-sine waves, the nodal circles being irregularly arranged. The presence of waves

traveling in the circumferential direction was noted; a theoretical substantiation of this phenomenon was given earlier in §56,

In experiments with shells that buckled when subjected to axial compression with the formation of diamond-shaped depressions, intensive flutter on smooth areas of the shell began. At the same time, the shell was not subject to flutter, having lost its stability under the action of external pressure.

Figure 5.19 shows the experimentally obtained dependence of the amplitude of flutter of a cylindrical shell on the parameter

$$a = \left(\frac{\rho U^2}{2E\sqrt{M^2 - 1}} \right)^{1/4} \frac{R}{h}$$

At the same time, the pressure inside the shell changed over wide limits. Assume as the pressure in the free flow exceeds a definite critical value, a fairly sharp increase of amplitude is observed.

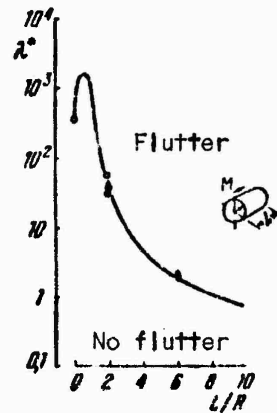


Figure 5.20. Semi-empirical limit of flutter for cylindrical shells.

Figure 5.20 shows the dependence of the flow parameter on L/R, with The solid curve was drawn through the mean values of the calculated λ^* ; it represents

the flutter limit in the region $L/R > 0.75$. The open symbols denote the results of calculations obtained by other authors; it is evident that they are in good agreement with the semiempirical curve. The black circle represents an experimental point of the flutter limit. The experimental value of the dynamic pressure differs from the value of the point of the semiempirical curve by 22%; for flutter, such agreement is considered good. Thus, the semiempirical flutter limit appears useful for rapid estimates of the conditions giving rise to flutter. The dashed line indicates the flutter limit in the range $L/R \leq 0.75$. It is obvious from Figure 5.20 that the flutter velocity depends strongly on the shell length. Therefore, the large number of studies dealing with the theoretical solution for infinitely long shells is of interest mainly from the standpoint of the methods employed.

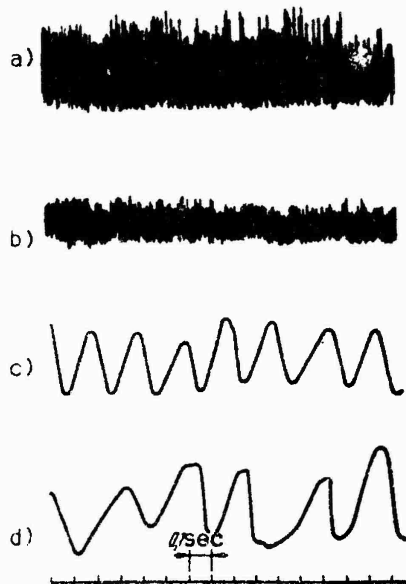


Figure 5.21. Oscillograms of vibrations of a panel excited by a) a close-to-supersonic flow ($M < 1$), b) noise in the boundary layer ($M > 1$); c, d) flutter vibrations.

§60. Experimental Study of the Behavior of Cylindrical Panels in a Supersonic Gas Flow

We will cite the results of a series of experiments conducted in a supersonic wind tunnel.* Cylindrical steel panels with a length (along the generatrix) of 360 mm, a radius of 250 mm, and thicknesses of 0.1, 0.2, and 0.3 mm were fastened to a special model.

The experiments recorded the dynamic deformations of the panel by means of gauges placed on the inner surface of the specimen, and high-speed motion pictures were taken. The thickness of the boundary layer was determined with a shadow instrument.

The experiments were conducted at M numbers equal to 1.78, 2.2, 2.5, and 3. The observed motions of the panels may be divided into three types. Figure 5.21 shows samples of oscillograms for each of these vibration types. During the time interval from the start of the wind tunnel to the onset of the supersonic regime, the panel undergoes high frequency vibrations of large amplitude (Figure 5.21a). Let us note that vibrations of such type have been recorded on thin-walled aircraft crossing the transonic region; they are excited by pulsating shock waves and stalls [9.22]. The triggering shock, which is a pressure wave moving in the direction of the flow, usually leads to snapping of the panel being tested (Figure 5.22) if special steps (introduction of tensile forces) aimed at preserving it are not taken.

After the establishment of supersonic flow at a flow velocity below the critical flutter velocity for the panel being tested, random vibrations with a relatively low amplitude level were observed, caused by noise in the boundary layer (Figure 5.21b). If the flow velocity was higher than the flutter velocity, vibrations with higher amplitudes were set up. The magnitude of the amplitudes depends on the degree to which the flow velocity surpasses the critical flutter velocity. These motions are the result of superposition of two or more vibrations (Figure 5.21, c, d).

*See the paper [5.16], 1971.



Figure 5.22. Characteristic shape of undulation under the action of a moving pressure wave.

When compressive forces are acting, the walls of the panel past which the gas flows at a subflutter velocity, initially execute high-frequency vibrations invisible to the eye, as discussed above; then, in the case of panels having initial shape irregularities, individual zones are formed which execute weak vibrations. A further slow increase of compression results in vibrations covering the region adjacent to the rear wing frame support. The amplitude of these vibrations is small, but it increases substantially with increasing intensity of axial compression, then the entire surface of the panel is set in motion. The vibrations are in the form of standing waves with a single circumferential nodal line located approximately at the midsection of the panel, and with maximum amplitudes at the trailing edge. Further increase of the compressive forces leads to large-amplitude vibrations; typical cross-shaped cracks develop at the trailing edge (Figure 5.23). The flow tears out individual pieces of the shell; subsequently, failure propagates rapidly toward the leading edge.

In several experiments, a phenomenon whose theoretical explanation was attempted in §54 was observed; the intense vibrations of the panel ceased abruptly after a certain slight increase in compressive forces. A subsequent increase of the compressive forces led to vibrations with a different amplitude and frequency; when the stresses were reduced, vibrations of the former type set in. Qualitatively, the behavior of the panel in this case may be illustrated by Figure 5.10. The character of the motions

depends on the location of the representative point, which determines the state of the "shell-flow" system in different regions of stability or instability. As the compressive load is increased further, static loss of stability of the shell takes place, characterized by the formation of a series of diamond-shaped bulges located in the region adjacent to the rear wing frame support. Static loss of stability of the panel in a gas flow (divergence) always took place at a somewhat greater magnitude of axial forces than for the same panels without a flow (see §51).



Figure 5.23. Typical pattern of failure of a panel undergoing flutter vibrations in a supersonic flow (direction of the flow, from the bottom up).

Figure 5.24 shows some results obtained in the above-described tests for panels 0.2 mm thick at $M = 3$; theoretical data corresponding to calculations employing two (curve 1) and six (curve 2) terms of series (4) are also presented. Here

$$\beta = \frac{R}{h} \sqrt{\frac{\rho_\infty U^2}{2E(M^2 - 1)^{1/2}}} = \alpha.$$

The circles correspond to the start of small-amplitude vibrations covering the region at the trailing edge of the panel, and the points correspond to intense large-amplitude motions of the entire panel (the amplitudes reached 5-6 mm at the edge). The conditions under which static loss of stability occurs are denoted by triangles, and the square corresponds to Fong's experimental criterion (see §59, Figure 5.19).

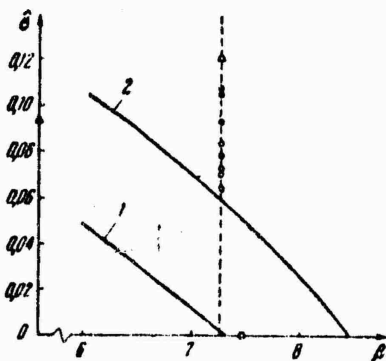


Figure 5.24. Comparison of experimental and theoretical data for a panel compressed in the axial direction and located in a supersonic gas flow.

Under actual conditions, a viscous boundary layer exists between the skin surface of the aircraft and the supersonic flow around it; the thickness of this layer depends on the flow parameters and the configuration of the structure. As we have seen, the presence of a boundary layer is an important cause of the discrepancy between the theoretical and experimental data. It was found that the thickness of the turbulent boundary layer is 6-7 mm at $M = 3$ and somewhat smaller at $M = 2.5$. However, when $M = 2.5$, more intense vibrations of the panel are observed; failure occurs faster than at $M = 3$, indicating a considerable influence of the boundary layer on the character of the process. Let us note for comparison that in the experiments of Olson and Fong [5.32], the boundary layer thickness slightly exceeded 10 mm, and the flutter vibrations did not result in failure of the shell walls during the entire experiment. Apparently, the boundary layer affects not only the magnitude of the critical flutter velocity but

also the vibration amplitudes; therefore, when the results of experiments are used, it is necessary to consider the characteristics of the flow in the region adjacent to the skin surface.

Let us consider some results of a study of transient flutter arising from the action of longitudinal axial forces changing with time in accordance with different laws. Loads of this type may arise in aircraft structures buffeted by the wind or subjected to thermal and other factors. In flight at close to-flutter velocity, small loads that are not dangerous to static strength may give rise to vibrations that lead to fatigue failure of the skin.

Tests have shown that during a change in axial forces, the character of the motion of an elastic surface depends on the law of change of these forces with time. This conclusion was qualitatively confirmed by the calculations carried out in §54.

An increase in the axial compression parameter leads to a decrease in critical flutter velocity; if however the system stays in the critical region for a short time, failure of the shell will not necessarily result from self-excited vibrations.



Figure 5.25. Shape of undulation and typical damage done to a panel compressed by continuously increasing longitudinal forces and located in a supersonic gas flow.

Figure 5.23 shows a panel loaded with axial compression forces according to a law similar to the one pictured in Figure 5.11a. At a certain value of the longitudinal forces corresponding to the migration of the representative point into the instability region, flutter vibrations are set up. Subsequently, the longitudinal forces remained constant up to the failure. Failure of the panel began 2 to 3 sec after the onset of violent flutter vibrations with the formation of cross-shaped cracks at the trailing edge, and it propagated in the direction of the leading edge.

The panel shown in Figure 5.25 was loaded with monotonically increasing compression forces (Figure 5.11 b, c), and the flutter zones were crossed in two seconds. When the magnitude of the axial forces exceeded the critical value, static loss of stability occurred. During the crossing of the flutter region, as a result of intense vibrations, cracks were formed at the trailing edge, caused by axial compression, stopped the flutter motions. Stabilization of the shell may be explained by the fact that the part of the panel adjacent to the trailing edge behaves as if it were corrugated, while for the remaining smooth part the critical velocity will be considerably higher because of the decrease in length. Let us note that at the end of the experiment, fields of shallow wavy bulges remained on all the panels that had undergone flutter vibrations for a certain period of time. An explanation of this phenomenon is given below in §103 in Chapter IX.



Figure 5.26. Bulging of a panel in the course of a faster increase of longitudinal compressive forces, the panel being simultaneously placed in a supersonic flow.

The panel shown in Figure 5.26 was subjected to a faster loading by axial compression forces. The lower critical force was reached 0.3 sec after the loading started; at the same time, in the region of the rear ring frame support, high bulges were formed that increased its stability toward the action of the flow. In addition, the panel retains a certain bearing capacity. Flutter vibrations were not recorded in this experiment, either in the course of loading or after the formation of large depressions, although as the axial forces increased, the representative point characterizing the state of the system evidently crossed the same flutter zones as in the preceding test.

Thus, in certain flight regimes, a small compression force may lead to flutter vibrations of the skin with the formation of cracks, so that under supersonic flight conditions, a complete failure of the skin may take place. At the same time, forces exceeding the critical value and giving rise to bulges may be less dangerous.

In the preceding sections of this chapter we discussed the behavior of plates and shells in a supersonic gas flow and made use primarily of the piston theory.

However, the means at the disposal of modern aerodynamics for the solution of aeroelasticity problems are much more extensive.

For supersonic flows, if one deals with linearized relations, the solution may be given with the aid of numerical methods. Their substantiation and development are given in the known works of Ye. A. Krasil'shchikova Finite-Span Wing in a Compressible Fluid (Moscow, Gostekhizdat, 1952), J. Miles Potential Theory of Transient Supersonic Flows (Moscow, Fizmatgiz, 1963), S.M. Belotserkovskiy, N.A. Kudryavtseva, B.N. Fedotov (Izv. AN SSSR, MZhG, No. 2, 1969), S.M. Belotserkovskiy, S.A. Popytalov (ibid., No. 2, 1970) and are summarized in the monograph of S.M. Belotserkovskiy, B.K. Skripach, and V.G. Tabachnikov, The Wing in a Transient Gas Flow (Nauka, Moscow, 1971). The solution is based on the general equation for the perturbation potential, treated from the standpoint of the method of sources. The aerodynamic characteristics pertaining to each element of a carrying surface are determined by taking into account the influence of all the remaining elements during the motion of the structure. Of particular importance is the fact that the previous history of the process is thus taken into consideration.

For the case of subsonic flow velocity, the original methods of solution of problems of intransient aerodynamics were developed by S.M. Belotserkovskiy in the book A Thin Supporting Surface in a Subsonic Gas Flow (Nauka, Moscow, 1965); see also the papers of S.M. Belotserkovskiy (Izv. AN SSR, MZhG, No. 1 and 6, 1966), G.A. Kolesnikov (Ibid., No. 6, 1967), and S.M. Belotserkovskiy and G.A. Kolesnikov (Ibid., No. 5, 1969). These methods are based on the theory of adjacent and free vortices; they are also systematically presented in the above-indicated monograph of S.M. Belotserkovskiy, B.K. Skripach, and V.G. Tabachnikov.

The use of the relationships given in the above works for supersonic and sonic flows is advisable not only in the case of self-excited oscillations, but also in the study of transient processes, discussed in the subsequent chapters of this book.

Chapter VI

Criteria of Dynamic Stability of Shells and Plates

§61. Basic Definitions

We will examine the process of buckling of shells and plates subjected to aperiodic actions. In the beginning of Chapter I, we discussed problems, taken as examples from aviation practice which are related to the study of periodic vibrations of thin-walled structures. Of no less importance are problems related to a rapidly occurring transient process leading to buckling of a shell or plate.

Some examples will be given here as well. The body of a flying vehicle is subjected on take-off to a thrust force causing significant longitudinal compressive stresses over a short period of time. This involves the risk of buckling of the structure. The structure of an aircraft is also subjected to dynamic loads when the flight regime undergoes abrupt changes. In some cases, elements of the body of an aircraft engine are subjected to short-term changes in external pressure.

The nature of buckling of a plate or shell under rapid loading may be completely different from the behavior of a structure experiencing a static loss of stability.* This is explained by the influence of the forces of inertia corresponding to the displacements involved in the buckling. The structure "does not have the time" to receive the displacements corresponding to an abruptly changing load. Such a "lag" causes a change in the load under which severe buckling of the load or plate takes place in comparison with Euler's static value. In addition, as will be seen below, for a shell, the supporting capacity of the structure may surpass in various degrees not only the "nearest" lower critical static load**, but also the upper critical value.

*This was first pointed out by M.A. Lavrent'yev and A. Yu. Ishlinskii [6.7].

**This concept is explained below in §69.

Below, we will conventionally distinguish between a dynamic load and an impact load. We will assume that the load is dynamic if only the forces of inertia corresponding to normal displacements (deflections) can be taken into consideration in solving the problem. At the same time, we leave out the mechanism of transfer of the load along the structure, assuming that for practical purposes, the stresses generated in the middle surface by this load are set up instantaneously. The "lag" of the buckling process is manifested with particular clarity in this case. For metal structures, the time of application of the pulse turns out to be of the order of 10^{-2} to 10^{-3} sec. For slower processes, the dynamic effect is manifested very weakly.

In the case of an impact load, however, in addition to the forces of inertia corresponding to the deflections, we will also consider the effect of the forces of inertia along certain directions in the middle surface of the shell or plate. In other words, the buckling phenomenon will be studied together with the process of transfer of the principal stresses. The characteristic load application time in this case is 10^{-4} - 10^{-6} sec for metal structures.

Let us examine in more detail a typical diagram representing the dependence of the deflection (displacement) parameter characterizing the buckling process on the load parameter. We will assume that the load increases monotonically with time. In Figure 6.1, the load parameter p (or time parameter t) is laid off along the abscissa axis, and the characteristic displacement f is laid off along the ordinate axis.

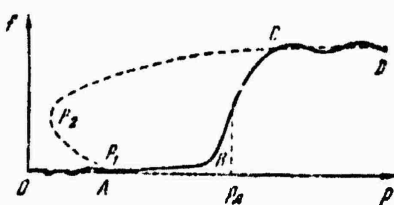


Figure 6.1. Relationship between the deflection and load parameters under dynamic (solid line) and static loading (dashed curve).

The shape of the f-p or f-t diagram depends on whether the shell or plate is ideal, or whether it has initial imperfections. We will proceed from the model of a nonideal system. Then the f-p graph will reflect the vibratory motion of the structure up to the instant when the load parameter reaches the upper static critical value. Let this portion correspond to segment OA. Starting with point A, the diagram acquires a different shape: the characteristic deflection increases monotonically with time (or with increasing load). Of greatest interest here is the rate of increase in deflection. At first, the deflections increase slightly, and the f-p diagram is close to the abscissa axis. However, at some instant corresponding to a certain load, a rapid increase in deflection takes place; segment BC corresponds to this stage on the diagram of Figure 6.1. For shells, snapping to a new, bent equilibrium shape is observed on segment BC. In Figure 6.1, the dashed curve corresponds to the static behavior of the structure and includes the upper and lower critical points p_1 , p_2 ; the supercritical segment p_2C corresponds to stable equilibrium shapes of the shell with large deflections. We can see that the dynamic process consists in a transition of the structure to new stable static shapes; subsequently nonlinear vibrations around these equilibrium states should occur on the CD segment.

Dynamic snapping of a shell may occur in different ways depending on the buckling form. From a practical point of view, we are interested in those wave formulation forms that are associated with the earliest buckling. Let us assume that we are dealing with different wave formation forms. It is necessary to find, on a diagram such as that of Figure 6.1, curves for which the deflection buildup front is the earliest.

In such a study, what we are most interested in is the nonstationary, transient process of motion of a shell or plate of segment BC. Experiments show that as a rule, dynamic snapping of the shell is produced by the appearance of plastic strains along the lines separating the bulges, and under lasting loading, by the formation of cracks along these lines. For composite materials, characterized by a linear law of deformation up to failure, the buckling pattern is different. In this case, dynamic buckling under relatively weak pulses does not cause residual strains. However, under sufficiently intense impact loads, cracks running along the ribs of the vanished dents appear in shells made of such materials.

Judging from experimental data, the general character of wave formation in dynamic buckling is similar to that in the case of static loss of stability of a shell or plate. For example, in a cylindrical shell under axial compression, rhombic dents of the same shape as in slow loading are formed. However, the dimensions of the dents change: they depend on the type of pulse applied to the shell. In addition, the narrow areas separating the dents show up less clearly in a dynamic process.

Thus far, we have discussed the case in which the structure has initial shape irregularities. The problem is thus reduced to determining the functions characterizing the strained and stressed state of a system as a function of time. The problem to be dealt with here is one in which it is necessary to determine the displacements of the middle-surface points of the shell and the quantities dependent on them for specified boundary and initial conditions. One can also visualize a case in which the structure is ideal, but subjected to certain initial velocities. Finally, a combined variant may also occur, i.e., in the presence of initial shape irregularities and initial velocities. Moreover, individual pulses may also be applied at other times, in the course of deformation of a structure.

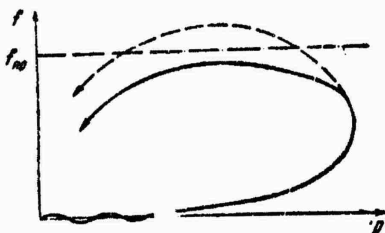


Figure 6.2. Conventional determination of a pulse that is safe (solid lines) and unsafe (dotted line) for a structure.

The question arises, how can one estimate the degree of danger posed to a structure by a given pulse with a falling segment? This author proposed [0.6] that the complete f - p diagram for a shell or plate be studied in this case. Its general form may be of the type shown in Figure 6.2. The characteristic deflection increases at

first,,then, as the load decreases, begins to fall. We will assume that during the application of the pulse, the structure was subjected to dangerous deformations if the characteristic deflection parameter f reached a certain limiting value f_{lim} . As f_{lim} , one can take, for example, the deflection corresponding to the appearance of plastic strains in the static process, or, say, a value equal to the thickness of the shell or plate. If such a criterion is used, and the level f_{lim} is denoted by the dot-dash line of Figure 6.2, the dynamic process corresponding to the dashed line should be considered dangerous, and that corresponding to the solid line, safe.

§62. Different Types of Impulsive Loads

Thus far, we have discussed the case in which the load changes monotonically with time. However, the real dynamic forces with parameter p acting on structures may vary with time t in accordance with a great variety of laws. Figure 6.3 shows different variants of the $p-t$ diagram.

Figure 6.3 a corresponds to a linear law of increase in p ; this case will be frequently discussed in Chapter VII. In talking about a continuous load increase, we bear in mind that the case of shell snapping that is important to us takes place on the ascending portion of the loading diagram; we are not interested in the subsequent behavior of the structure. Other things being equal, a decisive influence on the location of the severe buckling front of a plate or shell is exerted by the rate s of load increase, described by the angle made by curve OA with the abscissa axis. As s increases, the lag effect is reinforced. The diagram of Figure 6.3 b consists of two portions: in the first, the load increases linearly, and in the second, it remains constant.

Let us examine more closely the shape of the pulse according to Figure 6.3 c. Here the load first rises to some level at a rate s_1 , then falls at some other rate s_2 . The behavior of the structure turns out to be dependent on both quantities. Let us suppose that for a sufficiently large s_1 , the structure did not undergo snapping in the first of these portions. If the rate in the second portion decreases comparatively slowly, i.e., the rate s_2 is low, this is precisely where the snapping may take place. Therefore, the character of the "falling" portion is just as important as that of the "rising" portion.

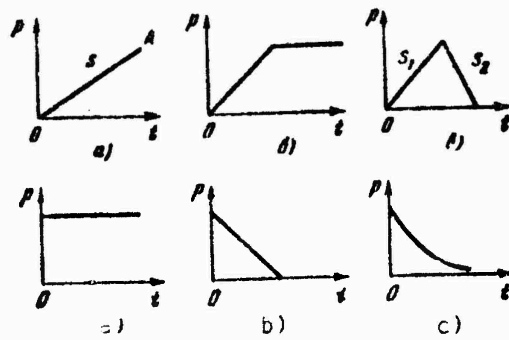


Figure 6.3. Possible diagrams representing the relationship between the load and time parameters.

Similar assumptions may be made with regard to the following variants of the p-t dependence according to Figure 6.3. The nature of the behavior of the shell can be tied to the general outline of the p-t curve and to the magnitude of the pulse, determined by the area of the diagram, as will be done in Chapter VII.

§63. The Concepts of Dynamic Critical Load and Dynamic Coefficient

In discussing the process of dynamic buckling of a structure, we will turn our attention first of all to the location of the zone of severe buckling of a plate or shell. The term "dynamic loss of stability" is frequently applied to this portion of the f-p diagram. However, one must be careful here. The question of the nature of stability of the motion of a shell in different portions of the diagram requires a special study. Judging from calculation data, slight changes in the initial displacements and initial velocities will be associated with ever-so-slight changes in the outline of f-p curves. We will subsequently treat the snapping portion as a process of onset of dynamic instability, since it involves an abrupt change in the nature of wave formation of the shell or plate.

In the same arbitrary sense one can speak of the concept of the dynamic critical load, determined by the location of segment BC in Figure 6.1. However, this segment can be defined in different ways; it is therefore natural to try to define the "critical" force or "critical" time interval more specifically. One of the possible approaches

consists in establishing the location of the inflection point of the characteristic f-p curve on this segment and in defining the critical dynamic load as the abscissa of this point. Another proposal consists in defining the abscissa of some "middle" point of segment BC.

Some authors consider the critical dynamic load reached at the instant when the deflection reaches a value equal to the thickness of the plate or shell. This assumption is based on the fact that this point approximately corresponds to the attainment of the yield point by the reduced stress.

One can determine the largest value of the intensity of stresses in the middle surface or intensity of total stresses by taking the bending stresses into consideration, and compare this value with the yield point.

If the dynamic "critical" load has been determined in some manner, it can be compared with the corresponding static value. Below, we will use the concept of the dynamic coefficient K_d . This quantity stands for the ratio of the dynamic "critical" load to the upper static critical load calculated for an ideal shell or plate with the same parameters, or for a structure with the same initial imperfections. If experimental data are compared, it is appropriate, in our view, to find the dynamic coefficient as the ratio of the experimentally obtained dynamic load, associated with sharp buckling, to the critical load for the same kind of shell, found in static tests. Let us note that the theoretically calculated upper static critical load can also be taken as the basic quantity in this case.

§64. Other Possible Approaches to the Problem

Thus, we have agreed to refer to imperfect structures all the concepts pertaining to dynamic snapping. It is natural to ask the following question: should the dynamic critical load be also defined for an ideal system by considering the latter as the limiting case of a structure with initial imperfections? To this one can only reply that in the framework of the adopted mathematical model, an ideal structure cannot be considered: additional deflections will be absent in the course of the entire process

of rapid loading. It is true that when the problem is solved by means of computers, the errors of the computational process could be expected to serve as the disturbances. However, in the examples analyzed by the author and his collaborators, it was found that such "pulses" have no appreciable effect on the shape of the f-p diagram.



Figure
6.4.
Char-
acter
of
block-
ling
of a
com-
pres-
sed
bar:
under
im-
pact.

In the literature, however, other approaches to the problem have been proposed, but they pertain to ideal structures. One such approach* is most conveniently described with application to the problem of the behavior of a bar with one fixed end A when a longitudinal impact load is applied to the other end B (Figure 6.4). Let us assume that at the instant of impact, the element of the bar at the B end is subjected

*See G. Gerard and H. Becker, J. Aeron. Sci. 19, No. 1 (1952), 58-62, 65.

to some compressive deformation which then propagates along the bar as a wave. At different times, the compressive deformation covers different parts of the bar. It may be postulated that on impact, loss of stability takes place in the same portion of bar BC that corresponds to Euler's static load. The question arises, what boundary conditions should be adopted for the portion under consideration? This is answered by saying that one of the ends (B) should be considered hinged, and the other (C), for example, elastically clamped. The question whether the bar loses stability in the course of propagation of a longitudinal elastic wave can be answered affirmatively if the calculated length of segment BC turns out to be smaller than the full length of the bar AB.

Such an approach is intuitive; it can be evaluated only by analyzing a dynamic buckling process. Studies made on a bar with an initial camber show (see the book [0.6], p. 304) that indeed following impact, one half-wave is formed in the portion of the bar covered by the elastic wave. However, the actual process of buckling of the bar is much more complex than in the model under discussion. The elastic wave reflects from the fixed end, then, after some successive reflections, the bar is divided into a certain number of sections with an increasing additional deflection. The length of such a section depends on the circumstances of the impact; it is interesting to note that under certain assumptions, this length turns out to be approximately equal to the length corresponding to the Euler static critical force. However, this result appears to be accidental.

A similar method of reducing a dynamic problem to a quasi-static one has also found application to shells. Let us assume that the subcritical stresses in the middle surface of the shell are determined by taking into account the forces of inertia from the dynamic relationships. As for the buckling process itself, the influence of the forces of inertia is excluded from consideration in this variant of the analysis. Unexpected results can be obtained in this manner. For example, when an instantaneous pulse is applied, the system, as we know, is subjected to strains that are twice as high as static strains. Hence, a system in such an interpretation of the problem should lose stability in a dynamic process at the instant when its strains reach one-half of the maximum value. If the dynamic coefficient is calculated according to the method proposed previously, it will be found to be 0.5. However, numerous experiments

show that for dynamic application of a load, the supporting capacity of the structure is usually higher than in the case of slowly increasing stresses; the dynamic coefficient should exceed unity. Thus, in an approach of this kind, the subcritical stresses are determined from the solution of the dynamic problem, whereas the buckling process itself is analyzed from static points of view.

Another approach consists in analyzing the problem of buckling of a structure under dynamic application of a load in terms of the parametric resonance theory. As we know from Chapter IV, when a load having a periodic component is applied to an elastic structure, the system may turn out to be dynamically unstable. It begins to execute vibrations of increasing amplitude: several instability zones are formed; the greatest danger is posed by the first zone, corresponding to the lowest frequency. In this and the following chapters, the expression "dynamic instability" is not related to the theory of parametric vibrations.

Apparently, the parametric resonance theory can be used to describe the process of transfer of the energy of longitudinal motion of the elements of a structure, in the case of axial compression, to the energy of transverse vibrations. Essentially, we should observe such a phenomenon of energy transfer in dynamic buckling as well. This idea requires a further study.

The next two chapters of the book will discuss the behavior of shells and plates under dynamic and impact loading. We will follow the line defined in this chapter. We are dealing with imperfect systems; they are studied from the points of view of nonlinear theory in accordance with the equations given in Chapter I. Because of the difficulties involved in the application of any analytical methods, emphasis will be placed on various numerical methods with extensive use of computers.

Chapter VII

Buckling of Shells and Plates under Dynamic Loading

§65. Statement of the Problem. Initial Equations

The present chapter will discuss cases of dynamic buckling in which the wave character of propagation of the principal stresses over the volume of the structure can be neglected. These stresses will be assumed to penetrate the structure instantaneously, changing with time in accordance with a specified law. The problem is to follow the behavior of a shell or plate acted on by such loads, assuming that, as rule, the structure has initial imperfections.

The fundamental relationships for such a problem will be written on the basis of the equations of Chapter I. Introducing the stress function $\Phi(x, y, t)$, from relations (1.30) we arrive at the following system of equations according to (1.38) and (1.39):

$$\frac{D}{h} V^4(w - w_0) = L(w, \Phi) + k_x \frac{\partial^2 \Phi}{\partial y^2} + k_y \frac{\partial^2 \Phi}{\partial x^2} + \frac{q}{h} - \frac{y}{g} \frac{\partial^2 w}{\partial t^2},$$
$$\frac{1}{E} V^4 \Phi = -\frac{1}{2} [L(w, w) - L(w_0, w_0)] -$$

$$- k_x \frac{\partial^2 (w - w_0)}{\partial y^2} - k_y \frac{\partial^2 (w - w_0)}{\partial x^2}. \quad (7.1)$$

Here the operators $L(w, \Phi)$ and $L(w, w)$ correspond to expressions (1.32) and (1.34). Let us recall that k_x and k_y denote the principal middle-surface curvatures, which are considered constant, w and w_0 denote the complete and initial deflections, and q is the transverse pressure.

§66. Behavior of Plates under Dynamic Compression

As the first example, let us consider the case of a plate $a \times b$ compressed in one direction (see Figure 2.10) along side a . We will first assume that the compressive stresses p increase in proportion to time according to the law $p = st$ (Figure 6.3a).

We will solve this problem with the aid of the Bubnov-Galerkin method.* The fundamental equations (1) and (2) will take the form

$$\frac{D}{h} \nabla^4(w - w_0) = L(w, \Phi) + \frac{q}{h} - \frac{\gamma}{E} \frac{\partial^3 w}{\partial t^3}, \quad (7.3)$$

$$\frac{1}{E} \nabla^4 D = \frac{1}{2} [L(w_0, w_0) - L(w, w)]. \quad (7.4)$$

Considering the plate to be nearly square and assuming it to be hinged along all the edges, we take the following expressions as the approximating functions:

$$w = f \sin \frac{m\pi x}{a} \sin \frac{n\pi y}{b}, \quad w_0 = f_0 \sin \frac{m\pi x}{a} \sin \frac{n\pi y}{b}, \quad (7.5)$$

where m and n are the numbers of half-waves along a and b . Substituting relations (5) into (4), we find (the edges a approach each other freely):

$$\Phi = E \frac{l^2 - l_0^2}{32} \left[\left(\frac{n}{m} \right)^2 \left(\frac{a}{b} \right)^2 \cos \frac{2m\pi x}{a} + \left(\frac{m}{n} \right)^2 \left(\frac{b}{a} \right)^2 \cos \frac{2n\pi y}{b} \right] - \frac{py^3}{2}. \quad (7.6)$$

Then, applying the Bubnov-Galerkin method to Eq. (3), we obtain the following relation:

$$\begin{aligned} & \left\{ p \cdot \left(\frac{m}{\lambda} \right)^2 - (\zeta^2 - \zeta_0^2) \frac{\pi^2}{16} \left[\left(\frac{m}{\lambda} \right)^4 + n^4 \right] \right\} \zeta - \\ & - \frac{\pi^2}{12(1-\mu^2)} \left[\left(\frac{m}{\lambda} \right)^2 + n^2 \right]^2 (\zeta - \zeta_0) + \frac{16a}{nm\pi} q^* - \frac{\gamma}{Egn^3} \frac{b^4}{h^3} \frac{d^3 \zeta}{dt^3} = 0. \end{aligned} \quad (7.7)$$

Here the following notation is used (concerning α , see p. 335):

$$\zeta = \frac{l}{h}, \quad \zeta_0 = \frac{l_0}{h}, \quad \lambda = \frac{a}{b};$$

*The solutions of the problems for a plate and a cylindrical panel as given in §66, 67, 76 are due to Ye. A. Vol'mir (Dokl. Akad. Nauk SSSR 201, No. 6, 1971, 46-48); previously, one special example was discussed in the book [0.6].

with

$$p^* = \frac{p}{E} \left(\frac{b}{h}\right)^2, \quad q^* = \frac{q}{E} \left(\frac{b}{h}\right)^3.$$

Omitting the nonlinear and inertial terms in (7), we arrive at the well-known formula for the dimensionless critical stress for $\lambda = 1, 2, 3\dots$

$$\rho_{cr}^* = \frac{\rho_{cr} b^2}{E} = \frac{\pi^2}{3(1-\mu^2)}. \quad (7.8)$$

On the other hand, rejecting the nonlinear terms, we obtain an equation for small vibrations of an unloaded plate; for $\zeta_0 = 0$,

$$\rho_{cr}^* \frac{\left[\left(\frac{m}{\lambda}\right)^2 + n^2\right]^2}{4} \zeta + \frac{\psi b^4}{E g \pi^2 h^2} \frac{d^2 \zeta}{dt^2} = 0.$$

The square of the fundamental frequency for a square plate

$$\omega_0^2 = \frac{\pi^2 E \rho h^2}{\psi b^4} \rho_{cr}^*. \quad (7.9)$$

Introducing the symbol t^* for the time parameter

$$t^* = \frac{t}{\rho_{cr}} = \frac{\rho^*}{\rho_{cr}}, \quad (7.10)$$

we arrive at an ordinary differential equation for the deflection

$$\begin{aligned} \frac{1}{s} \frac{d^2 \zeta}{dt^{*2}} + (\zeta - \zeta_0) \left\{ \frac{1}{4} \left[\left(\frac{m}{\lambda}\right)^2 + n^2 \right]^2 + \zeta \frac{\zeta + \zeta_0}{16} \frac{\pi^2}{\rho^*} \left[\left(\frac{m}{\lambda}\right)^2 + n^2 \right] \right\} - \\ - \zeta \left(\frac{m}{\lambda}\right)^2 t^* - 16 \frac{\omega_0^2}{\rho_{cr}^* m n \pi^2} = 0. \end{aligned} \quad (7.11)$$

where

$$S = \rho_{cr}^2 \left(\frac{\pi c l / h^3}{s b^2} \right)^2. \quad (7.12)$$

c being the velocity of sound in the plate material, determinable from (2.5). Comparing expressions (9) and (12), we find that $\sqrt{S} = (\omega_0 p^* / s) E(h/b)^2$.

The Integration of Eq. (11) was performed by means of the Runge-Kutta method. The results of the computations, carried out with a BESM-2M computer, are reflected in the graphs shown in Figure 7.1-7.3. Below, we will determine the dynamic "critical" load from the data of Chapter VI, on the basis of the criterion of severe buckling of the system.

Figure 7.1 pertains to the case of a square plate ($\lambda = a/b = 1$) with an initial deflection $\zeta_0 = 1 \times 10^{-4}$; we assume that the transverse load is absent, $q = 0$. Solid lines represent the $\zeta(\tau^*)$ curves, corresponding to $S = 1$ and $m = 1, 2, 3$. We can see that the development of sharp deflections begins most rapidly when $m = 2, n = 1$. Thus, in this case one should expect the development of dynamic deflections for two half-waves along the length. Let us recall that the static loss of stability of a square plate takes place when $m = n = 1$. The dynamic coefficient, equal to the ratio of the dynamic "critical" load to the static load, turns out to be $K_d = 5$ in the case under consideration. In the case of $S = 10$ (dashed lines), the buckling shape according to these two half-waves ($m = 2$) turns out to be "critical", but the coefficient K_d will be about 3 in this case.

The dot-dash line in Figure 7.1 shows the quasi-static dependence between the stress and the deflection in supercritical deformation.

Figure 7.2 shows a similar graph for $S = 0.5, 0.2$, and 0.1 ; in these cases, the "critical" value of K_d is equal to 6, 7.5, and 8.5, respectively.

The influence of an additional static transverse load on the behavior of a square plate was studied. For the case $S = 1$ and $q^* = 1$, the "critical" number of half-waves m was found to be $m = 1$, while for $q^* = 0$, it was $m = 2$.

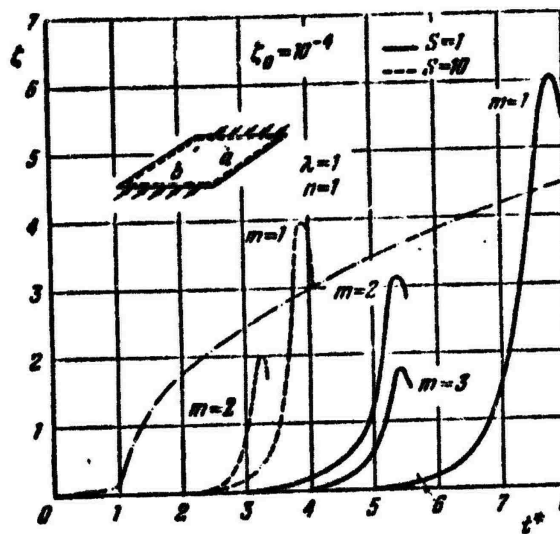


Figure 7.1. "Deflection-time" diagram for a compressed plate in dynamic loading; solid lines pertain to the faster load increase.

Thus, in the presence of transverse load, the effect of occurrence of higher buckling shapes attenuates. The corresponding value of K_d for $q^* = 1$ is 4.25, whereas for $q^* = 0$, it was $K_d = 5$.

We analyzed the case of an elongated plate for which $\lambda = 2$. As was shown by the calculations, the static form of the stability loss then corresponds to $m = 2$, $n = 1$; the critical load coefficient K_d was the same as the value for $\lambda = 1$. In the dynamic process, for $S = 1$ and $S = 0.5$, we obtained $m = 5$, and for $S = 0.1$, we found $m = 6$. The corresponding K_d values were 4.9, 5.8 and 8.4. If these values are compared with the same coefficients at $\lambda = 1$, approximately the same values are obtained. Hence we can draw the preliminary conclusion that the dynamic response factors found for a square plate can be extended with little error to rectangular plates of a different configuration.

In Figure 7.3, one can follow the effect of initial deflection on the behavior of a plate. It gives the "critical" curves $\xi(t^*)$ for $S = 1$ for gradually decreasing ξ_0 , from 1 to 1×10^{-6} .

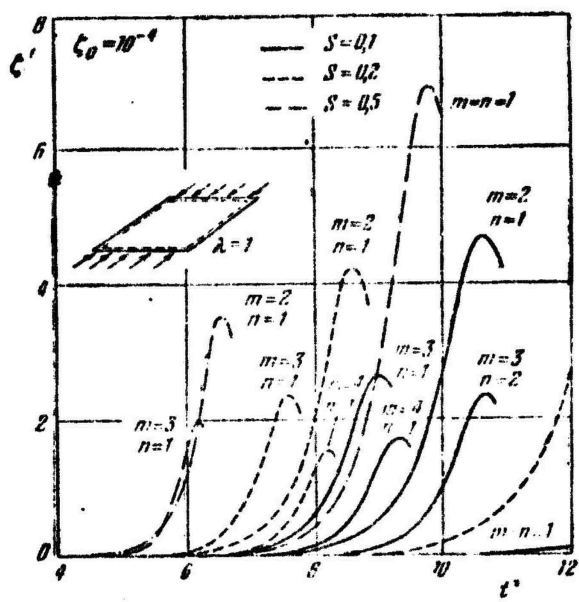


Figure 7.2. Behavior of a compressed plate under very rapid loading; the fastest load increase is reflected by the solid lines.

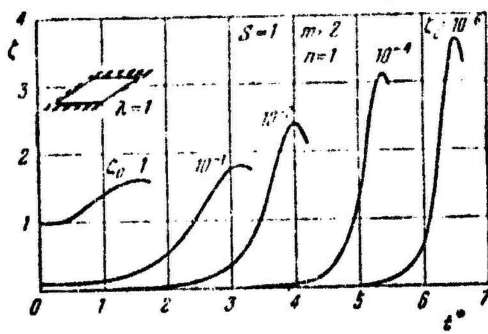


Figure 7.3. Effect of initial deflections on the behavior of a compressed plate under dynamic loading.

§67. Effect of Pulse Shape on the Behavior of a Plate

We will now turn to a problem similar to the one discussed in §66, but different in that we will not limit the character of change in axial compressive load to the law $p = st$, but will assume that it can be given by an arbitrary function of time $p = \phi(t)$. It is convenient at this point to introduce another dimensionless time parameter $\tau = w_0 t$; w_0 denotes the lowest frequency of natural vibrations of an unloaded plate according to (9). Taking into consideration the relation

$$p = \varphi(t) = \varphi(\tau) \frac{\delta^2 [3(1-\mu^2)]^{1/2}}{c h n^2},$$

we reduce (11) to the form (for $q^* = 0$)

$$\begin{aligned} \frac{d^2\zeta}{d\tau^2} - \left(\frac{m}{\lambda}\right)^2 \tilde{S}\varphi(\tau)\zeta + \\ + (\zeta - \zeta_0) \left\{ \frac{1}{4} \left[\left(\frac{m}{\lambda}\right)^2 + n^2 \right]^2 + \right. \\ + \frac{3}{16} (1-\mu^2) \left[\left(\frac{m}{\lambda}\right)^4 + n^4 \right] \zeta (\zeta + \\ \left. + \zeta_0) \right\} = 0; \end{aligned} \quad (7.13)$$

where

$$\bar{S} = \frac{h^4 [3(1-\mu^2)]^{1/2}}{g^4 h^2 e L},$$

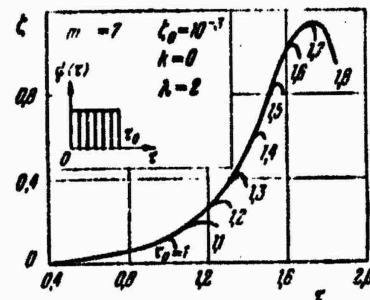


Figure 7.4. Character of "deflection-time" curves for a step-shaped pulse.

We will now use the dimensionless function of time $\psi(\tau) = \tilde{S}\phi(\tau)$.

Using (13), we will study the case of the step pulse

$$\psi(\tau) = \begin{cases} \psi_0 & \text{for } 0 \leq \tau \leq \tau_0, \\ 0 & \text{for } \tau > \tau_0. \end{cases}$$

Figure 7.4 gives data of computations for the same parameter $\psi_0 = 5$, but for pulses of different duration; we took $\zeta_0 = 1 \times 10^{-3}$, $\lambda = 2$. The "critical" number of half-waves n_{cr} in this case was found to be independent of the pulse duration and equal to 7; n_{cr} was 1 as before.

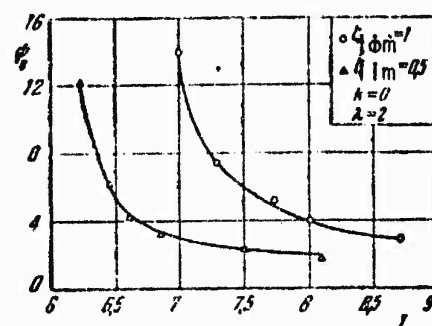


Figure 7.5. Regions of safe step pulses for a compressed plate.

Below, we will use the criterion of an "unsafe" value of the pulse $J = \psi_0 \tau_0$, on the basis of a given maximum deflection. We will find those combinations of values of the load ψ_0 and pulse J for which some limiting deflection amplitude is reached for the first time. Figure 7.5 shows the corresponding curves for these cases, when the deflections $\zeta = 1$ and $\zeta = 0.5$ are considered to be the limiting ones. As we can see, the pulses that are unsafe are smaller, the higher the higher the load level. It is interesting to note that in the left-hand portion, the "limiting" pulse values remain almost unchanged.

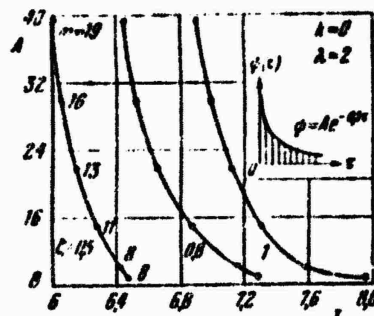


Figure 7.6. Regions of safe exponential pulses for a compressed plate.

Figure 7.6 shows the same type of data for the case of an exponential pulse according to Figure 6.3 f, given by the law $\psi(\tau) = Ae^{-0.5\tau}$. The curves plotted in Figure 7.6 correspond to the limiting values of the deflection $\xi = 0.5, 0.8, 1$; also, the magnitude of the pulse J , whose application is necessary to achieve a given deflection, decreases here as the load amplitude A increases.

§68. Dynamic Buckling of Plates in Shear

We will consider a case in which a rectangular plate is subjected to the dynamic action of shearing forces uniformly distributed over its edges.* Problems of this type are encountered, for example, in ship building, when the hull of the ship is acted on by dynamic loads produced by the impact of waves, the passage of an acoustic wave, etc. Similar loads may take place in the skin panels of a flying vehicle.

We will take a plate hinged along the edges and assume that the edges approach each other freely. As before, the Bubnov-Galerkin method will be used.

In accordance with the solution of the static problem (see [1.11], p. 157), we will choose the approximating expression for the deflection in the form**

*This problem was studied by M.S. Gershteyn [7.9 a].

**For the sake of simplicity, in the equations, we do not cite the terms related to the initial irregularities.

$$w = f_{11} \sin \frac{\pi x}{a} \sin \frac{\pi y}{b} + f_{22} \sin \frac{2\pi x}{a} \sin \frac{2\pi y}{b}. \quad (7.14)$$

This formula pertains to the case in which the sides a and b of the plate differ little in magnitude. Further procedure is the same as in §66. By integrating Eq. (2), we find the function ϕ in the form

$$\begin{aligned} \Phi = E \left\{ f_{11}^2 \frac{1}{32a^2b^2} \left(a^4 \cos \frac{2\pi x}{a} + b^4 \cos \frac{2\pi y}{b} \right) + \right. \\ \left. + f_{22}^2 \frac{1}{32a^2b^2} \left(a^4 \cos \frac{4\pi x}{a} + b^4 \cos \frac{4\pi y}{b} \right) + \right. \\ \left. + f_{11}f_{22} 4a^2b^2 \left[\frac{\cos \frac{\pi x}{a} \cos \frac{3\pi y}{b}}{(9a^2 + b^2)^2} + \frac{\cos \frac{3\pi x}{a} \cos \frac{4\pi y}{b}}{(a^2 + 9b^2)^2} \right] \right\} + sxy; \end{aligned} \quad (7.15)$$

where s denotes the intensity of tangential forces. Then, applying the Bubnov-Galerkin procedure to (3), we arrive at a system of nonlinear differential equations

$$\begin{aligned} \frac{\gamma}{Eg} \frac{\lambda^2 b^4}{\pi^2 h^2} \frac{d^2 \zeta_1}{dt^2} + \frac{\pi^2}{6} \left(\lambda^2 + \frac{1}{\lambda^2} \right) \zeta_1^3 + \\ + 16\pi^2 \lambda^2 \frac{(\lambda^2 + 9)^2 + (9\lambda^2 + 1)^2}{(9\lambda^2 + 1)^2 (\lambda^2 + 9)^2} \zeta_1 \zeta_2^2 + \frac{\pi^2}{12(1 - \mu^2)} \frac{\lambda^2 + 1}{\lambda^2} \zeta_1 - \frac{128}{9\pi^2} s^* \zeta_2 = 0, \end{aligned} \quad (7.16)$$

$$\begin{aligned} \frac{\gamma}{Eg} \frac{\lambda^2 b^4}{\pi^2 h^2} \frac{d^2 \zeta_2}{dt^2} + \pi^2 \left(\lambda^2 + \frac{1}{\lambda^2} \right) \zeta_2^3 + \\ + 16\pi^2 \lambda^2 \frac{(\lambda^2 + 9)^2 + (9\lambda^2 + 1)^2}{(9\lambda^2 + 1)^2 (\lambda^2 + 9)^2} \zeta_1^2 \zeta_2 + \frac{4\pi^2}{3(1 - \mu^2)} \frac{(\lambda^2 + 1)}{\lambda^2} \zeta_2 - \frac{128}{9\pi^2} s^* \zeta_1 = 0. \end{aligned} \quad (7.17)$$

The following notation was introduced above:

$$s^* = s \frac{ab}{Eh^2}, \quad \lambda = \frac{a}{b}, \quad \zeta_1 = \frac{f_{11}}{h}, \quad \zeta_2 = \frac{f_{22}}{h}.$$

If the inertial terms and nonlinear components are discarded in the above equations, an approximate value of the critical static shear stress can be determined:

where

$$\tau_{cr}^* = \frac{3\pi^4}{128(1 - \mu^2)} \frac{(\lambda^2 + 1)^2}{\lambda},$$

$$\tau_{cr} = \tau_{cr}^* \frac{ah}{Eh^2}.$$

Let us now consider a dynamic problem, assuming that the relative displacement of the edges in the direction of side a takes place at a constant rate. The shear corresponding to this displacement will be

$$0 = \frac{1}{b} (u_{y=b} - u_{y=0}) = \Omega' \quad (7.17a)$$

Here $u_{y=b}$ — the "average" displacement of side $y = b$,

$$u_{y=b} = \frac{1}{a} \int_0^a u \Big|_{y=b} dx;$$

is also determined by $u_{y=0}$.

The displacement u is found by analogy with the solution of the static problem ([1.11], p. 159). We now determine the "average" displacements of sides $y = 0$ and $y = b$, which we substitute into (17a). After some simple transformations and reduction to the dimensionless form, we get

$$\frac{s^*}{\tau_{kp}^*} = \frac{t^*}{1+\mu} - \frac{10\lambda^3}{(1+\mu)\tau_{kp}^*} \frac{(\lambda^2 - 9\mu)(9\lambda^2 + 1)^2 + 9(9 - \mu\lambda^2)(\lambda^2 + \mu)^2}{9(\lambda^2 + \mu)^2(9\lambda^2 + 1)^2} \xi_1 \xi_2, \quad (7.18)$$

where $t^* = \Omega ab/h^2 \tau_{cr}^*$ is the dimensionless time parameter. Introducing (18) into (16) and (17), we arrive at a system of ordinary nonlinear equations in ξ_1 , ξ_2 .

Assuming that the plate under consideration has an initial deflection described by the expression

$$w_0 = f_0 \sin \frac{\pi x}{a} \sin \frac{\pi y}{b},$$

Instead of the system (16), (17), it is necessary to write down new equations of motion. For a square ($\lambda = 1$) plate of material with Poisson's ratio $\mu = 0.32$, after some simplifications, these equations take the form

$$\left. \begin{aligned} \frac{d^2\zeta_1}{dt^2} + S [0.124(\zeta_1^2 - \zeta_0^2)\zeta_1 + 0.469\zeta_1\zeta_2^2 + 0.368(\zeta_1 - \zeta_0) - \\ - 1.091t\zeta_2] = 0, \end{aligned} \right\} \quad (7.19)$$

$$\left. \begin{aligned} \frac{d^2\zeta_2}{dt^2} + S (1.98\zeta_2^3 + 0.469\zeta_1^2\zeta_2 + 5.89\zeta_2 - 1.09t\zeta_1) = 0, \end{aligned} \right\}$$

где

where

$$S = \pi^2 r_{cr}^2 \left(\frac{V}{W} \right)^2 \left(\frac{h}{a} \right)^6, \quad c = \sqrt{\frac{Eg}{\gamma}}.$$

The numerical integration of the equations of system (19) was performed by using the Runge-Kutta method.

Results of the calculations are presented in Figure 7.7 and 7.8 for a case in which the initial deflection $\zeta_0 = 0.01$ for different values of S . The solid lines represent plots of $\zeta_1(t^*)$; for one variant ($S = 2$), the function $\zeta_2(t^*)$ is also shown. The dashed curves indicate the corresponding static relationships. The general character of the curves corresponds to the case of compression described in §66.

In Figure 7.9, the solid lines indicate the theoretical values of the dynamic coefficient K_d as a function of the initial deflection. The figure also shows the results of experiments*. Crosses mark the data pertaining to plates 0.75 mm thick, and circles, to 0.95 mm; the models were made of AMG-6 aluminum alloy. Triangles correspond to data for Duralumin plates 1 mm thick.

*Carried out by M.S. Gershteyn and V.P. Blagoveshchenskiy.

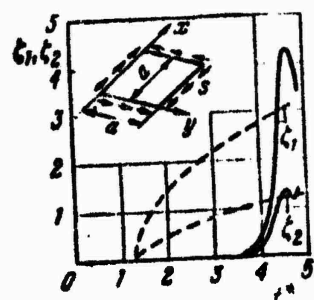


Figure 7.7. "Deflection-time" curves for a square plate subjected to dynamic shear ($S = 2$).

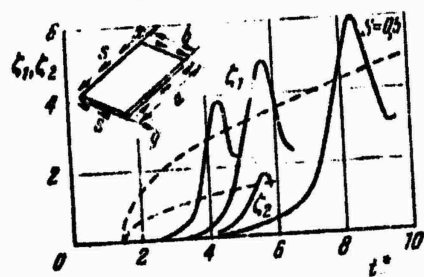


Figure 7.8. Amplitudes of different wave formation shapes for an elongated plate in dynamic shear ($S = 0.5, 2, 6$).

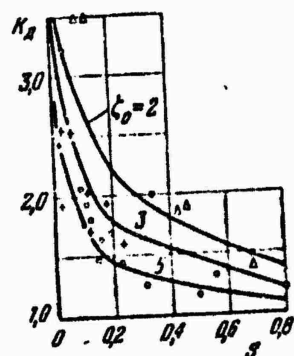


Figure 7.9. Comparison of theoretical (solid lines) and experimental values of the dynamic coefficient for a plate in shear.

The experiments were conducted at various loading rates. The process of buckling of the plate began in the elastic stage, as a rule, with the formation of a single diagonal crimp. Let us note that this form of bending corresponds to the approximation of the type of (14). Oscillographic analysis of the shear strains in the middle surface was performed during the experiments. The buildup of this strain with time conformed to a law that was close to linear. After the shear strain reached a certain value θ^* , a sharp buckling of the plate began. Qualitatively, the experimental data agreed with the theoretical ones.

Let us note that in very rapid loading, buckling of the plate during the experiments took place with the formation of not one but two or three crimps. In other words, this involved buckling in higher forms of stability loss or vibrations. This fact should be taken account in subsequent studies of dynamic shear, as was done in the case of compression.

§69. Buckling of Cylindrical Shells Under Dynamic Loading. Basic Concepts

Let us turn to dynamic buckling of closed circular cylindrical shells under different types of loads. First, we will consider the case of axial compression. However, before dealing with the dynamic problem, let us recall the data available in the literature on the buckling of axially compressed cylindrical shells in the case of quasi-static loading.

It is well known that thin-walled metallic shells subjected to axial compression lose stability, as a rule, with the formation of rhombic dents. These dents usually form two to three bands; in some experiments, however, it is possible to obtain dents covering almost the entire surface of the shell. This phenomenon can be explained from geometric points of view*. The shell buckles chiefly inward, toward the center of curvature, since the middle surface is not subjected to any substantial tension-compression strains in such deformation.

*For more detail, see the book [0.6], p. 534, and A.V. Pogorelov's monograph, Geometric Methods in Nonlinear Theory of Elastic Shells, Moscow, 1967.

Bending of the shell is not continuous and takes place in the course of sharp snapping. However, if we imagine that the equilibrium forms of the shell follow each other continuously, we obtain, to a first approximation, the "deflection parameter-load" diagram shown in Figure 6.1 by a dashed curve. Actually, the buckling pattern of the shell turns out to be much more complex. The snapping phenomenon is associated with a transformation of the buckling forms. If this phenomenon is investigated by means of high speed motion pictures, one finds that the number of waves along the circumference decreases, then begins to increase again in certain cases. Thus, instead of the single smooth curve of Figure 6.1, we obtain a series of curves corresponding to different numbers of waves. In the literature on the static stability of shells in the large, the practice has been to plot the envelope of these curves; then, the lower critical load is determined at the point corresponding to the minimum p for the lowest of the curves. However, recent data have forced a revision of this procedure, at least as applied to practical calculations. It was found that a refinement of the calculations leads to a substantial decrease of the lower critical load, and in the limit, this quantity approaches zero. However, the distant $p(f)$ curves correspond to very significant deflections exceeding the shell thickness by tens and hundreds of times. On the other hand, it can be shown that the transition to these distant equilibrium branches requires the overcoming of a very high energy barrier.* On the basis of these data, the author of the book proposed the introduction of the concept of the nearest lower critical load.** If one examines the experimental data pertaining to real shells, one finds that they fall chiefly into a region located between the upper critical load and the value corresponding to the nearest lower critical load.

Let us now return to the dynamic problem. As was stated in Chapter VI, the character of the $p(f)$ curve under impulsive loading may differ sharply from the static branches. Here again the problem amounts to the integration of equations of the type of (1) and (2) by means of certain approximate methods. As a rule, we will approximate the deflection and stress function with expressions that correspond to static solutions of the first approximation, but allowing for a possible change in

*This was pointed out by L.I. Balabukh in 1952.

**See also the paper of Jones (AIAA Journ. 5, No. 9, 1966).

the number of nodal lines in different directions.

§70. Cylindrical Shells Acted on by Dynamic Axial Compression

Let us consider the case of a closed circular cylindrical shell fastened at the ends by rigid ring frame supports. The shell will be assumed to be subjected to a rapid application of an axial load uniformly distributed over its ends. Our purpose will be to determine the behavior of the shell in time, assuming, as agreed previously, that the forces applied to the ends "instantaneously" penetrate the entire shell.

We will adopt the following plan for solving the problem. Using the variational method and approximating the expression for the deflection, we reduce the problem to finding the time dependence of the deflection parameters. In other words, we will proceed along the same lines as in the case of a plate.

The expression for the complete deflection will be taken in the form

$$w = f \left(\sin \frac{m\pi x}{L} \sin \frac{ny}{R} + \psi \sin^2 \frac{m\pi x}{L} + \varphi \right). \quad (7.20)$$

Here L and R denote the length of the shell and radius of curvature of the middle surface. The number of half-waves along the length is denoted by m, and the number of waves along the circumference, by n.

We will assume below that in its form, the initial deflection is effectively in "resonance" with the form of the additional deflection, and we will approximate the initial deviations by the expression

$$w_0 = f_n \left(\sin \frac{m\pi x}{L} \sin \frac{ny}{R} + \psi \sin^2 \frac{m\pi x}{L} + \varphi \right). \quad (7.21)$$

Let us note that expressions (20) and (21) correspond to the solution of the static problem of shell stability in the first approximation (see [0.6], p. 526). The first of the terms in parentheses corresponds to the form of stability loss of the shell in the small, and also to the form of small flexural vibrations. The second term takes into account the predominant direction of buckling of the shell toward the center of curvature. The third terms reflects the radial displacements of the points of the end sections.

We substitute expressions (20) and (21) into the right-hand side of Eq. (2) for $k_x = 0$, $k_y = 1/R$. After integrating, we find

$$\Theta = B \left(K_1 \cos \frac{2m\pi s}{L} + K_2 \cos \frac{2ny}{R} + K_3 \sin \frac{2m\pi s}{L} \sin \frac{ny}{R} + K_4 \sin \frac{2m\pi s}{L} \sin \frac{np}{R} \right) - \frac{py^2}{2}. \quad (7.22)$$

The coefficients K_1, \dots, K_4 are

$$K_1 = \frac{1}{16a_m^2} \left[\frac{(l-l_0)\beta^2}{2} + (l-l_0)f_0\beta^2 - \frac{2(l-l_0)\psi}{R} \right],$$

$$K_2 = \frac{n\beta^2}{8^2 f_m} (f^2 - f_0^2), \quad K_3 = \frac{a_m^2 \beta^2}{(0a_m^2 + \beta^2)^2} (f^2 - f_0^2) \psi,$$

$$K_4 = \frac{a_m^2 (l-l_0)}{R(a_m^2 + \beta^2)} - \frac{a_m^2 \beta^2 (f^2 - f_0^2)}{(a_m^2 + \beta^2)^2} \psi,$$

where $a_m = m\pi/L$; $\beta = n/R$. The average intensity of the compressive forces applied to the ends of the shell is denoted by p .

The condition of closure of the shell for a displacement v is:

$$\int_0^{2\pi R} \frac{\partial v}{\partial y} dy = 0. \quad (7.22a)$$

Equating the expressions for ϵ_y written in terms of the deflection and stress function, we find

$$\frac{\partial \psi}{\partial y} = \frac{1}{E} \left(\frac{\partial^2 w}{\partial x^2} - \mu \frac{\partial^2 \Phi}{\partial y^2} \right) - \frac{1}{2} \left(\frac{\partial w}{\partial y} \right)^2 + \frac{1}{2} \left(\frac{\partial^2 w}{\partial y^2} \right)^2 + \frac{w}{R} - \frac{w_0}{R}.$$

Substituting (20)-(22) into the above equation and taking the previous relations into account, we find

$$\phi = -\frac{\gamma}{2} + \frac{R}{8}(f + f_0)\theta^2.$$

Thus, ϕ is found to be expressed in terms of the parameter ψ , f and f_0 .

We now apply the Bubnov-Galerkin method to Eq. (1). The fundamental equations are

$$\int_0^{L/2\pi R} \int_{-\pi R}^{\pi R} X \sin a_m x \sin b_n y dx dy = 0. \quad (7.23)$$

$$\int_0^{L/2\pi R} \int_{-\pi R}^{\pi R} X \sin^2 a_m x dx dy = 0; \quad (7.24)$$

and X will be

$$X = \frac{D}{h} \nabla^4(w - w_0) - L(w, \Phi) - \frac{1}{R} \frac{\partial^2 \Phi}{\partial x^2} + \frac{\gamma}{8} \frac{\partial^4 w}{\partial x^4}. \quad (7.24a)$$

After integrating Eq. (23), we find

$$\begin{aligned} \beta = C_0 &\left(1 - \frac{\zeta_0}{\zeta} \right) + C_1 (\zeta^2 - \zeta_0^2) + C_2 (\zeta^2 - \zeta_0^2) \psi^2 - \\ &- C_3 (\zeta - \zeta_0) \psi + C_4 \frac{1}{\zeta} \frac{d^2 \zeta}{dt^2} - C_5 \frac{\zeta^2 - \zeta_0^2}{\zeta} \psi, \end{aligned} \quad (7.25)$$

where

$$C_0 = \frac{\xi_m^2}{(1+\xi_m^2)^2 \eta} + \frac{1}{12(1-\mu^2)} \frac{(1+\xi_m^2)^3}{\xi_m^2} \eta,$$

$$C_1 = \frac{1}{16} \frac{1+\xi_m^2}{\xi_m^2} \eta,$$

$$C_2 = \xi_m^2 \left[\frac{1}{(1+\xi_m^2)^2} + \frac{1}{(1+2\xi_m^2)^2} \right] \eta,$$

$$C_3 = \frac{1}{4\xi_m^2} \left[1 + \frac{4\xi_m^2}{(1+\xi_m^2)^2} \right],$$

$$C_4 = \frac{\gamma R^2}{Eg\eta} \frac{1}{\xi_m^2}, \quad C_5 = \frac{\xi_m^2}{(1+\xi_m^2)^2}.$$

The dimensionless parameters introduced are

$$\zeta = \frac{l}{h}, \quad \xi_0 = \frac{l_0}{h}, \quad \xi_m = \frac{m\pi R}{nL} = \frac{a_m}{\beta},$$

$$\hat{\rho} = \frac{\rho}{E} \frac{R}{h}, \quad \eta = n^2 \frac{h}{R}.$$

If the inertial term is eliminated from Eq. (25) and we set $\xi_0 = 0$, we arrive at the solution of the static problem for a shell of ideal shape. Taking into account only the terms linear in ζ , we find the parameter $\hat{\rho}$

$$\begin{aligned} \hat{\rho} = C_0 &= \frac{1}{12(1-\mu^2)} \frac{(1+\xi_m^2)^2}{\xi_m^2} \eta + \frac{\xi_m^2}{(1+\xi_m^2)^2 \eta} = \\ &= \frac{x}{12(1-\mu^2)} + \frac{1}{x}. \end{aligned} \quad (7.26)$$

This corresponds to formula (13.39) of the book [0.6]. Minimizing $\hat{\rho}$ with respect to the parameter $x = (1 + \xi_m^2)^2 \eta / \xi_m^2$, we obtain

$$\hat{\rho}_u = \frac{1}{\sqrt{3}(1-\mu^2)} \quad \text{or for } \mu = 0.3, \hat{\rho}_u \approx 0.605. \quad (7.27)$$

If however the nonlinear terms are considered in the static problem, this variant of the solution leads to a lower critical stress parameter $\hat{\beta}_1 = 0.15\beta_u = 0.09$; it corresponds to the value $\zeta_m = 0.6$. This means that when the compressive stress reaches the "nearest" lower critical value, the ratio of the arc dimension of the dent $\pi R/n$ to the axial dimension L/m is 0.6; in other words, dents of rhomboidal shape turn out to be stretched out along the arc. Let us note that we are dealing here with the lower point of the envelope of a series of $p(\zeta)$ curves which are determinable for various m and n .

Let us now turn to the dynamic problem again. We will assume, as in the case of a plate, that the external forces increase according to the law $p = st$; we introduce the dimensionless parameters

$$r = \frac{sR}{Eh\beta_u} = \frac{p}{p_u}, \quad s = A_0 n \zeta_m^2 \left(\frac{h}{R} \right)^2 \left(\frac{cE}{Rs} \right)^2, \quad c = \sqrt{\frac{E\kappa}{\gamma}}.$$

Then Eq. (25) takes the form

$$\begin{aligned} \frac{1}{s} \frac{d^2\zeta}{dr^2} - & \left\{ \left(r - \frac{\zeta - \zeta_0}{\zeta} \right) \zeta - \frac{1}{16\beta_u} n^2 \frac{1 + \zeta_m^2}{\zeta_m^2} (\zeta^2 - \zeta_0^2) \zeta - \right. \\ & - \frac{\zeta_m^2 \gamma}{\beta_u} \left[\frac{1}{(1 + \zeta_m^2)^2} + \frac{1}{(1 + \zeta_m^2)^2} \right] (\zeta^2 - \zeta_0^2) \zeta \psi^2 + \\ & + \frac{1}{\zeta_m^2 \beta_u} \left[1 + \frac{\zeta_m^2}{(1 + \zeta_m^2)^2} \right] \psi (\zeta - \zeta_0) \zeta + \\ & \left. + \frac{\zeta_m^2}{(1 + \zeta_m^2)^2} \frac{1}{A_0} (\zeta^2 - \zeta_0^2) \psi \right\} = 0. \end{aligned} \quad (7.28)$$

Equation (28) was integrated by the Runge-Kutta method with the aid of a computer. A shape of the dents was adopted that corresponded to the lowest upper critical stress; we are dealing here with the limiting values of the wave formation shape parameters, found from the solution of the nonlinear problem for $\zeta_0 = 0$, when $\zeta \rightarrow 0$. The parameter ψ , characterizing the proportion of the "unsymmetric" component of the deflection in (20), was assumed to be the same as in the corresponding static problem for a shell of perfect shape, and therefore the second of Eqs. (23),

(24) was not considered in the solution. The results are presented in Figure 7.10 and pertain to a shell with $R/h = 180$, $L/R = 2.2$. Values of

$$t^* = \frac{p}{p_u} = \frac{p}{p_{u*}}$$

were plotted along the abscissa axis, where p_u is the smallest upper critical stress, and the deflection parameter ζ is plotted along the ordinate axis. The different series of curves pertain to dynamic loading taking place at a constant rate of load increase $s = 1 \times 10^6$, 2×10^6 , and $5 \times 10^6 \text{ kg/cm}^2 \text{ sec}$. Each curve is characterized by a certain number of waves n indicated on the graph. We see that a rapid increase takes place the earliest in the first case at $n = 11$, in the second case at $n = 12$, and in the third case at $n = 13$.

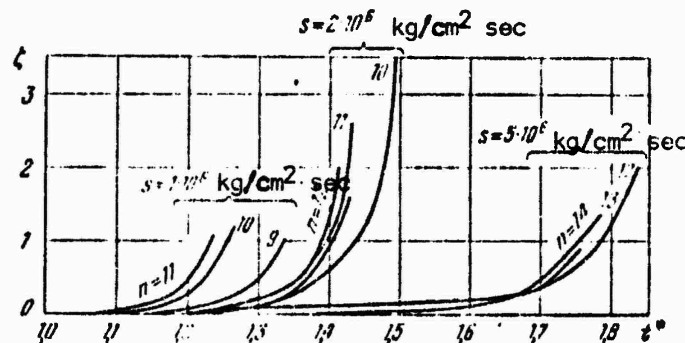


Figure 7.10. "Characteristic deflection-time" diagrams for a closed cylindrical shell under a axial compression.

In Figure 7.11, depending on the loading rate s , the theoretical values of K_d are compared with the experimental ones.* The dynamic overload coefficient K_d was obtained by dividing the load at which dynamic buckling occurred by the static value, also found experimentally. A continuous curve was drawn through the points obtained by integrating Eq. (28) for $\xi_0 = 0.001$. Inspection of the graph shows

*The experiments were performed by S.N. Kiryushina, and the calculations given above are due to her.

that the test data are characterized by a considerable scatter, but generally follow the theoretical curve. Let us note that in other cases, a fairly good agreement of the experimental data for carefully prepared shells with theoretical data exists if the initial deflection parameter in the calculations is taken approximately as

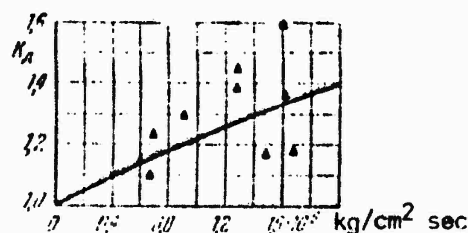


Figure 7.11. Theoretical values of the dynamic coefficient for a compressed cylindrical shell (solid line) in comparison with experimental data ($R/h = 180$, $L/R = 2.2$).

$\zeta_0 = 0.001$. In the dynamic process, the tested shells obviously buckled under a load 10 to 60% greater than the static load, depending on the loading rate. Although the smaller of these values is low and lies in the range of spread of the experiments, the upper limit characterizes a significant increase in the supporting capacity of the shell.

Other authors who have dealt with the same problem* have approximated the deflection by means of a somewhat different expression:

$$w = f \left(\sin \frac{m\pi x}{L} \sin \frac{n\pi y}{R} + \phi \sin^2 \frac{m\pi x}{L} \sin^2 \frac{n\pi y}{R} \right).$$

In the calculations performed in this manner, it was assumed that the waves were square.

*See V.L. Agamirov and the author [7.1], and also O.I. Terebushko [7.22].

§71. Cylindrical Shells under External Pressure

Let us consider another important problem, the behavior of a closed circular cylindrical shell under dynamic application of a uniformly distributed external pressure. As was done in §70, we consider the shell to be fastened at the ends to ring frame supports whose shape remains circular as the structure is deformed. In the operations carried out below, we will actually consider a somewhat more general problem for the case of uniform pressure. In other words, the shell will be assumed to be provided with a bottom, and the pressure to act with equal intensity on the lateral surface and bottom.

The case of rapid loading by external pressure is characteristic, for example, of shells in the structures of aircraft engines.

Solving the problem along the same lines as in §70, we will take the following approximating expressions for the complete and initial deflections:

$$\left. \begin{aligned} w &= f \left(\sin \frac{\pi x}{L} \sin \frac{ny}{R} + \psi \sin^2 \frac{\pi x}{L} + \varphi \right), \\ w_0 &= f_0 \left(\sin \frac{\pi x}{L} \sin \frac{ny}{R} + \psi \sin^2 \frac{\pi x}{L} + \varphi \right). \end{aligned} \right\} \quad (7.29)$$

These expressions were set up like (20), (21), and differ from them only in that the number of half-waves along the length is taken to be $m = 1$; this corresponds to the data from the study of the static problem and experimental data. Substituting (29) into an equation of the type of (2) and integrating it, we obtain

$$\Phi = E \left(K_1 \cos \frac{2\pi x}{L} + K_2 \cos \frac{2ny}{R} + K_3 \sin \frac{\pi x}{L} \sin \frac{ny}{R} + \right. \\ \left. + K_4 \sin \frac{3\pi x}{L} \sin \frac{ny}{R} \right) - \frac{qR}{2h} x^2 - \frac{qR}{4h} y^2. \quad (7.30)$$

The coefficients K_1, \dots, K_4 are determined by the previous expressions (see p. 297) but with the replacement of α_m by α , where $\alpha = \pi/L$; here again, $\beta = n/R$. The intensity of external pressure is denoted by q ; the last but one term in (30) corresponds to the stress $\sigma_1 = qR/h$ in the middle surface, caused by the pressure on the

lateral surface, and the last term, to the stress $\sigma_2 = qR/2h$, caused by the pressure on the bottom.

Using the closure condition as in §70, we obtain

$$\psi = -\frac{\Phi}{2} + \frac{R}{8}(I + I_0)\beta^2 + \frac{R^2}{8(I - I_0)} \frac{q}{E} \left(1 - \frac{\mu}{2}\right). \quad (7.31)$$

The equations of the Bubnov-Galerkin method will be written as before in the form

$$\left. \begin{aligned} \int_0^{L/2\pi R} \int_{-\pi}^{\pi} X \sin \alpha x \sin \beta y dx dy &= 0, \\ \int_0^{L/2\pi R} \int_{-\pi}^{\pi} X \sin^2 \alpha x dx dy &= 0, \end{aligned} \right\} \quad (7.32)$$

where X stands for expression (24a).

Performing the integration of the first of Eqs. (32), we have

$$\begin{aligned} \psi &= C_0 \left(1 - \frac{\xi_0}{\xi}\right) + C_1 (\xi^2 - \xi_0^2) + C_2 (\xi^2 - \xi_0^2) \psi^2 - \\ &\quad - C_3 (\xi - \xi_0) \psi - C_4 \left(1 - \frac{\xi_0}{\xi}\right) \xi \psi + C_5 \frac{d^2 \psi}{d\xi^2}. \end{aligned} \quad (7.33)$$

The coefficients C_0, C_1, C_5 are

$$\begin{aligned} C_0 &= \frac{2}{2 + \xi^2} \left[\frac{\xi^2}{\pi^2 (1 + \xi^2)^2 \delta} + \frac{\pi^2}{12 (1 - \mu^2)} \frac{(1 + \xi^2)^2}{\xi^2} \delta \right], \\ C_1 &= \frac{\pi^2}{8(2 + \xi^2)} \frac{1 + \xi^2}{\xi^2} \delta, \quad C_2 = \frac{2\pi^2 \xi^2}{2 + \xi^2} \left[\frac{1}{(1 + \xi^2)^2} + \frac{1}{(1 + \xi^2)^2 \delta} \right] \delta, \\ C_3 &= \frac{1}{2(2 + \xi^2)} \left[1 + \frac{8\xi^2}{(1 + \xi^2)^2} \right], \\ C_4 &= \frac{2\xi^4}{(1 + \xi^2)^2 (2 + \xi^2)}, \quad C_5 = \frac{2\pi^2 \xi^2}{Eg\eta} \frac{1}{2 + \xi^2}, \quad \delta = \frac{Rh}{L^2}. \end{aligned}$$

Here, in addition to the notation of §70, we will use the dimensionless parameters

$$q = \frac{q}{E} \left(\frac{R}{h} \right)^2, \quad \xi = \frac{\pi R}{nL} = \frac{a}{b}. \quad (7.34)$$

Excluding the inertial term from (33) and taking $\zeta_0 = 0$, we arrive at an equation corresponding to the solution of the linear static problem

$$\hat{q}_{cr} = C_0 = \frac{2}{2 + \xi^2} \left[\frac{\xi'}{(1 + \xi^2)\eta} + \frac{(1 + \xi^2)^2}{12(1 - \mu^2)} \eta \right]. \quad (7.35)$$

Minimizing \hat{q}_{cr} with respect to η (or, in other words, with respect to the number of waves n), we determine the upper critical pressure \hat{q}_u (see p. 545 of the book [0.6], where only the case of radial pressure is discussed).

We will return to the dynamic problem, assuming further that the parameter ψ is by agreement considered to be the same as in the static solution. Again, the pressure intensity will be assumed to increase according to the law $q = st$, and we will introduce the time parameter

$$\hat{t} = \frac{stR^2}{Eh^2q_u} = \frac{q}{q_u} = \frac{q}{\hat{q}_u};$$

then Eq. (33) takes the form

$$\frac{d^2\zeta}{dt^2} - S \left[\left(\hat{t} - \frac{\zeta - \zeta_0}{\xi} \right) \zeta - B_1 (\zeta^2 - \zeta_0^2) \zeta - B_2 \frac{(\zeta^2 - \zeta_0^2) \zeta^3}{N_1 \zeta^2 + N_3} + B_3 \frac{(\zeta - \zeta_0) \zeta^2}{N_1 \zeta^2 + N_1} + B_4 \frac{(\zeta - \zeta_0) \zeta \zeta_0}{N_2 \zeta^2 + N_1} \right] = 0, \quad (7.36)$$

where the values N_1 , N_2 , N_3 are given in [0.6], p. 766;

$$\begin{aligned} \delta &= \frac{Rh}{L^2}, \quad I_{11} = C_1 \frac{\xi^2}{\pi^2} \frac{1}{\delta q_u}, \quad R_1 = C_2 \frac{\delta N_1^2}{4q_u}, \quad R_2 = \frac{C_1 N_1}{2q_u}, \\ B_1 &= \frac{C_1 N_1 \eta \left(1 + \frac{1}{2} \xi^2 \right)}{2q_u}, \quad S = \left(1 + \frac{\xi^2}{2} \right) q^4 \left(\frac{cE}{sK} \right)^2 \left(\frac{h}{R} \right)^4 \eta. \end{aligned}$$

Equation (36) for the dimensionless deflection was integrated numerically for the following initial data:

$$\zeta = \zeta_0, \quad \frac{d\zeta}{dt} = 0 \text{ for } t=0.$$

The computations were carried out with application to Duralumin shells for the initial data $c = 5 \times 10^5 \text{ cm/sec}$, $\mu = 0.3$, $E = 7.75 \times 10^5 \text{ kg/cm}^2$. In addition, we took $R/L = 0.45$, $R/h = 112$, $\delta = 1.8 \times 10^{-3}$.

Figure 7.12 represents the graph of the relationship between the complete deflection and the loading (or load) time for the case $\zeta_0 = 1 \times 10^{-3}$. The first line on the left corresponds to the solution of the static problem for $s \rightarrow 0$. The graph shows the envelope of different curves corresponding to a given wave number n . The upper critical pressure takes place at a wave number $n = 6$, and the lower, at $n = 5$. The same Figure 7.12 shows curves plotted for cases of dynamic loading at rates $s = 0.2 \times 10^4$, 1×10^4 , and $2 \times 10^4 \text{ at/sec}$. The figure again shows the curves for three wave numbers at which a rapid increase of deflections corresponds to the smallest parameter f . As is evident from the figure, the dynamic effect is manifested in a gradual increase in the number of waves and a significant increase of the critical pressure.

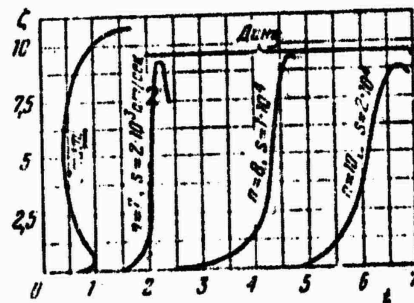


Figure 7.12. "Characteristic deflection-time" dependence for a closed cylindrical shell under external pressure. Key: 1) stat., 2) at/sec, and 3) Dyn.

Comparasion of the data pertaining to the case of dynamic application of axial compression (see Figure 7.11) and uniform pressure shows that in the second of these cases, the dynamic effect is manifested more clearly. This may be explained by the characteristics of wave formation: when the external pressure predominates, one half-wave is usually formed along the length of the shell, whereas the case of compression is characterized by the presence of shallow dents both along the circumference and along the length. In the former case, the shell elements apparently are subjected to relatively large accelerations, and the effect of inertial forces is more perceptible.

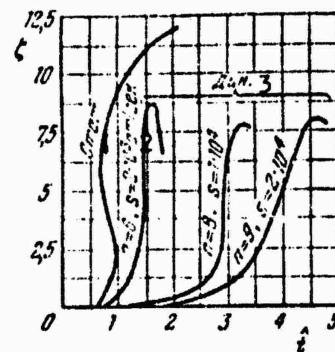


Figure 7.13. Graph which together with the preceding figure reflects the effect of initial camber on the behavior of the shell. Key: 1) Stat., 2) at/sec, and 3) Dyn.

The graph shown in Figure 7.13 contains curves analogous to those pictured in Figure 7.12, but for the case of a large initial camber ($\zeta_0 = 0.1$). At comparable values of the rate s , lower forms of stability loss are manifested in this case than when $\zeta_0 = 0.001$; the critical pressures are also lower (by a factor of approximately 1.5). The general shape of the curves is slightly different: the front of rapid increase in deflection is not as well defined as when $\zeta_0 = .001$.

Let us now consider a more complex program of loading of the shell. We will

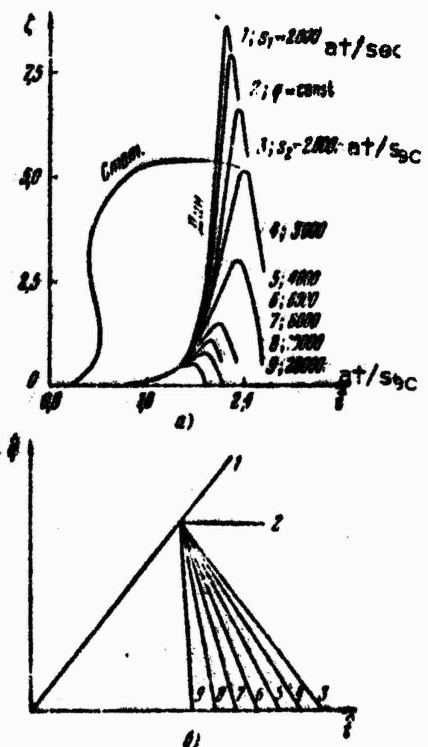


Figure 7.14. Behavior of the shell characterized by graphs a) for the different pulse shapes shown in b).

assume that the system is subjected to loading by a pressure increasing at a rate $s = 2000 \text{ at/sec}$ and reaching a value equal to 80% of the critical dynamic value. Moreover, the shell does not experience any appreciable deflections in the course of loading. Subsequently, the load will be assumed to vary in accordance with different laws (Figure 7.14b). Variant 1 is the same as the one discussed earlier: here the load continues to increase at the former rate. In variant 2, the load remains constant at the second stage. In the remaining variants (3-9), the load decreases linearly; the rate of load decrease is denoted by s_2 and changes from 2×10^3 to $2 \times 10^4 \text{ at/sec}$. Figure 7.14 a shows graphs of the deflection change with time. Despite the fact that in variants 3-9 the load decreases, the deflection increases up to a certain limit, then begins to decrease.

The behavior of a shell during unloading is characterized by the magnitude of the maximum deflection. In Chapter VI, we assumed that the shell buckles during unloading if the maximum deflection exceeds the static deflection corresponding to the highest pressure; the static curve is shown in Figure 7.14 a on the left. If this assumption is accepted, the unsafe load-decrease rates are below the value $s_2 = 3000$ at/sec. In Figure 7.15, these curves are represented in different coordinates. The magnitude of the load is laid off along the abscissa axis, and the deflection, along the ordinate axis.

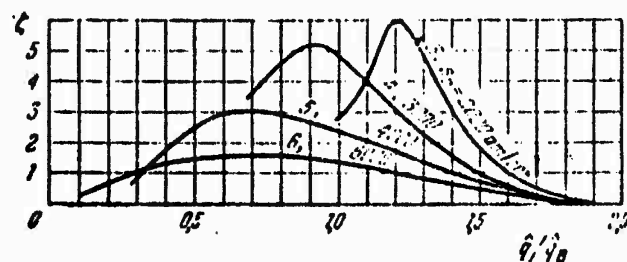


Figure 7.15. Character of the dependence between the deflection and load parameters for different pulse shapes.

A somewhat different approach to the solution of the problem was used by Yu. I. Kadashevich and A.K. Pertsev [7.11]. They obtained certain characteristic curves of the behavior of shells under an abruptly applied transverse load which then remained constant in magnitude during a given period of time; loads increasing linearly with time were also considered. These authors showed that under very rapid loading, the effect of a lag in the axisymmetric compression of the shell must be considered. In addition, it was found that the parameters ψ and ϕ in (29) will be different for dynamic problems than in the static solution. M.A. Shumik [7.25] proposes that one should consider unsafe a load at which the maximum stress reaches the yield point.

§72. Experimental Data

Let us turn to the results of several series of experiments dealing with the dynamic buckling of shells under uniform pressure.

We will first consider the experiments conducted on a series of carefully prepared (machined) Duralumin specimens with $R/h = 220$ and $L/R = 2.2$.* A specially designed installation consisted of two tanks placed one inside the other and filled with oil. The specimen, in the shape of a circular cylindrical shell, was placed in the inner tank; the upper end of the specimen remained open. The opening in the bottom of the inner tank was closed with a valve connected to a system of springs. A higher pressure in the range from 5 to 15 atm was produced in the outer tank, and the gas "cushion" located in the upper part of the tank was suddenly opened, a hydraulic impact occurred which was transmitted to the specimen; it may be assumed with a certain approximation that the specimen was thus subjected to dynamic loading by a uniform external pressure. The change of pressure with time at several points of the tank was measured with special gauges whose signals were recorded on the tape of a loop oscillograph. Ohmic resistance gauges stuck to the outer and inner surface of the specimen permitted the determination of elongation strain at the corresponding point; the readings of the gauges were also fed to an oscillograph. During the test, the pressure difference between the outer and inner tank was varied, as was the time of opening of the valve, so that it was possible to obtain various rates of pressure increase in the range from 2×10^3 to 6.5×10^3 atm/sec.

It was found that in dynamic loading, the general character of deep dents directed mainly toward the center of curvature was the same as in static loading; however, the configuration of the dents changes slightly: under dynamic application of pressure, their outline is close to rectangular.

In Figure 7.16, the experimental data are compared with the results obtained in §71 for shells of the same dimensions. The rate s in atm/sec is laid off along the abscissa axis, and the dynamic overload coefficient K_d is laid off along the

*The experiments were conducted by V. Ye. Mineyev with the participation of V.S. Smirnov.

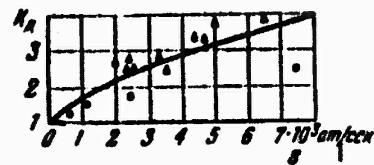


Figure 7.16. Comparison of theoretical data on dynamic buckling of cylindrical shells under uniform compression with experimental results.

ordinate axis. A solid line connects the points obtained by calculation for $\xi_0 = 0.001$. The triangles represent the experimental data for initially perfect shells, and the circles, for shells with initial camber. Judging from the graph, the experiments confirmed the theoretical conclusions, at least qualitatively. Some deviations of the experimental values of the critical pressure for shells of "ideal shape" upward from the theoretical curve may be explained by the fact that the edges of the shells were clamped in the experiments, and that the forces of inertia of the adjacent liquid layer were added to those of the shell mass.

Experiments on steel shells were performed by V.V. Sorokin (see [0.6], p. 775); the shell parameters $R/h = 200$, $L/R = 2.9$. The shells, equipped with inserted bottoms, were placed in a tank filled with liquid. The free surface of the liquid was hit by a dropping load. Changing the drop height of the load made it possible to vary the rate of increase of the uniform pressure transmitted to the shell. As was shown by the test results, under static loading, the shell received six dents along the circumference, and under dynamic loading at different rates, eight and nine dents.

Figure 7.17 gives the results of studies made by Wood and Koval [7.61]. A cylindrical shell clamped at the ends was loaded at one end by a constant axial force, then subjected to an axisymmetric hydrostatic pressure that rose rapidly to a constant value. The rise time of the pressure to the maximum value was 0.003 sec. The unsafe deformation of specimens in static and dynamic tests was characterized by the appearance of large dents and the exhaustion of the supporting capacity

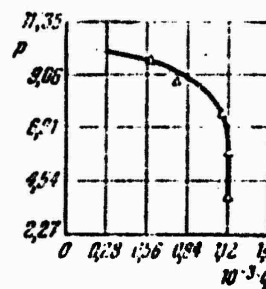


Figure 7.17. Unsafe values of the dynamic hydrostatic pressure parameter for the simultaneous action of static axial forces.

with respect to the axial load. The specimen then returned to the stable position (at a zero pressure differential), after which the magnitude of the axial load changed, and a series of external pressure jumps were reapplied. The pressure gradually increased until unsafe deformation of the specimen took place. Thus were determined the maximum values of pressure increasing in jumps, during the action of which unsafe deformation was absent. Figure 7.17 shows the $P-q$ dependence, where P is the axial load in kg, and q is the maximum value of the pressure differential in atm. These data pertain to a shell with parameters $L/R = 2$, $R/h = 800$, $h = 0.13$ mm.

Under laboratory conditions, it is difficult to obtain a given law of change of the external load. Let us examine certain devices which permit one to carry out such loading.* Figure 7.18 shows a general view of the pressure chamber of an experimental device that makes it possible to obtain different loading laws. Cavity 8 of chamber 1 is filled with liquid. The pressure on specimen 2 is produced by moving piston 4 downward in cylinder 3. The motion of the piston is determined by the velocity of mass M at the instant of contact with crusher 8, by the rigidity of the crusher, and by the resistance of gasket 6 to the displacement of the piston.

*These data are due to Yu.K. Bivin and A.A. Nayda, Prikl. mekh., No. 10 (1970), 28-34.

If cavity A is filled with air, the start of the pressure drop in cavity B may be regulated by selecting the thickness of membrane 5. The pressure measurement in the chamber is made with gauges 7.

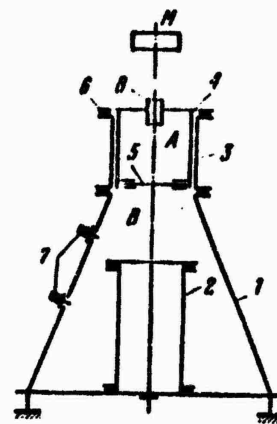


Figure 7.18. Sketch of device for testing models of cylindrical shells (2) for uniform dynamic compression.

We will now consider the electrohydraulic method of producing uniform pressure. Its use permits an easy regulation of the magnitude of the pressure pulse by means of the electrohydraulic effect. A general view of the chamber for testing the models for the action of an impulsive load is shown in Figure 7.19. One of electrodes 2 of chamber 1 is grounded, and the other is connected to a discharger. A spark is formed when there is a breakdown between the electrodes of the discharger. As a result, the pressure rises sharply in this zone. A pressure wave is formed which then travels along the chamber at the speed of sound. The magnitude and character of the change in the load on the structure 3 being tested with time depends on many factors, chief of which are the energy accumulated in the capacitors, distance between the electrodes, density of the medium occupying the chamber, distance from the discharge zone, rigidity of the chamber, electrical characteristics of the discharge circuit, etc. Other things being equal, the pressure in the wave will be higher if a conductor is exploded between the electrodes. If the compression wave destroys diaphragm

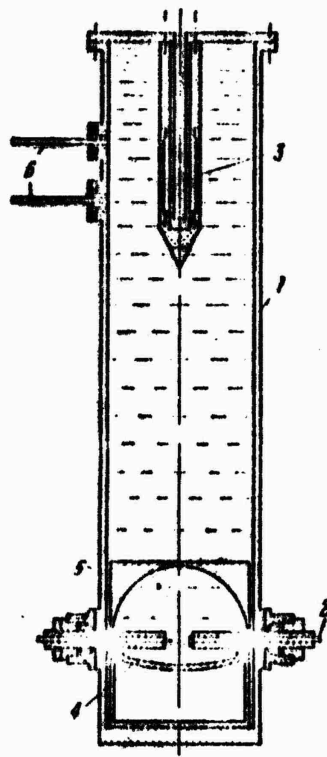


Figure 7.19. Use of electrohydraulic method in experiments on uniform dynamic compression of shells (3).

4, the pulse of the load on the model will be smaller. By using inserts 5 of various configurations, one can appreciably alter the character of the load with time.

§73. Effect of Internal Pressure

Let us now consider a case in which in addition to a dynamic axial compressive load, a closed circular cylindrical shell is subjected to a statically applied internal pressure of variable intensity.

Let us first recall the results produced by the study of this problem in the quasi-static formulation.* If we consider the case of combined loading from linear points of view, we will find that the internal pressure relative to a low intensity should not affect the upper critical load of axial compression. If however one starts from nonlinear equations and uses the procedure of determination of the nearest lower critical loads (see §69), one finds that the internal pressure has an appreciable effect on the supporting capacity of the shell. As the internal pressure parameter increases, the nearest lower critical load increases and at a certain pressure intensity approaches the upper value. These results are confirmed by experimental data.

To solve the corresponding dynamic problem,** it is necessary to supplement an equation of the type of (28) by a term corresponding to the internal pressure of intensity q . As before, we assume that the compressive load changes according to the law $p = st$. Then, instead of (28), we obtain

$$\begin{aligned} \frac{1}{S} \frac{d^2\zeta}{dt^2} - \left[\left(t^* - \frac{\zeta - \zeta_0}{\zeta} \right) \zeta - \frac{1}{11\rho h} \eta \frac{1 + \xi_m^4}{\xi_m^2} (\zeta^3 - \zeta_0^2) \zeta - \right. \\ \left. - \frac{\xi_m \eta}{\rho_h} \left[\frac{1}{(1 + \xi_m)^2} + \frac{1}{(1 + \xi_m^2)^2} \right] (\zeta^3 - \zeta_0^2) \zeta \psi + \right. \\ \left. + \frac{1}{4\xi_m^2 \rho_h} \left[1 + \frac{4\xi_m}{(1 + \xi_m)^2} \right] \psi (\zeta - \zeta_0) \zeta + \right. \\ \left. + \frac{\xi_m^2}{(1 + \xi_m^2)^2} \frac{1}{\rho_h} (\zeta^3 - \zeta_0^2) \psi + \frac{\eta \zeta}{\rho_h \xi_m} \right] = 0 \end{aligned} \quad (7.37)$$

In addition to the notation of §70, the quantity $\hat{q} = qR^2/Eh^2$ was introduced above.

Equation (37) was integrated by using the Runge-Kutta method as before. The initial conditions chosen were the same as in §70: $\zeta = \zeta_0$ and $\dot{\zeta} = 0$ for $t^* = 0$. In the course of the calculations, the ratio R/h was varied from 100 to 1000, and

*For more detail see the book [0.6], p. 573.

**A similar problem was discussed by A.V. Sevast'yanov (Mekh. tv. tela, No. 3, 1968). The results cited here were obtained by B.A. Kiladze and the author [7.6a].

the intensity of internal pressure \hat{q} , from zero to two. The initial deflection parameter ξ_0 was chosen as 1×10^{-3} in all cases. The loading rate s was varied from 1×10^6 kg/cm² sec to 5×10^6 kg/cm² sec. The parameter ξ characterizing the form of wave formation during snapping of the shell varied from 0.4 to 3. Let us note that the increase in ξ is due to an elongation of the dents along the arc. In each variant of the calculations, $\xi - t^*$ relationships were found that corresponded to different numbers of waves n along the arc. That number of waves was determined for which a rapid increase of deflections occurred the earliest.

As an example, the data of the calculations are presented in the form of graphs in Figure 7.20. The values chosen were $R/h = 200$ and $s = 2 \times 10^6$ kg/cm² sec. All the curves were rearranged so that the upper critical static stress $\hat{\rho}_u$ was taken as the base. The first of the graphs (Figure 7.20 a) pertains to the case of absence of internal pressure. Here a rapid increase of deflections takes place the earliest for $\xi = 0.8$ and $n = 14$, and the "critical" time parameter $t_{cr}^* = 1.006$. In other words, the excess over the upper critical value in dynamic buckling is 0.6%. From the next graph (Figure 7.20 b) pertaining to the case of $\hat{q} = 0.1$, it is evident that dynamic snapping takes place at another parameter $\xi = 1.2$, and wave number $n = 12$. The static critical value is exceeded here by 2.5%. Finally, Figure 7.20 c shows the $\xi - t^*$ relationship for the case $\hat{q} = 0.02$. Sharp buckling should take place in this example when the parameter $\xi = 1.2$ and $n = 12$. The excess over the upper static "critical" load is 4.5%.

We will now cite the data pertaining to higher values of \hat{q} . When $\hat{q} = 0.2$, the dynamic "critical" load proves to be higher than the upper static load 10.3%; when $\hat{q} = 0.5$, by 12.1%, when $\hat{q} = 1$, by 23% when $\hat{q} = 2$, by 34%.

Figure 7.21 compares the final results pertaining to the cases $\hat{q} = 0, 0.01, 0.02$. It indicates the "critical" parameters ξ and n when $R/h = 200$ and $s = 2 \times 10^6$ kg/cm² sec.

Thus, in the presence of static internal pressure, the character of wave formation of the shell changes sharply in comparison with the case of pure dynamic

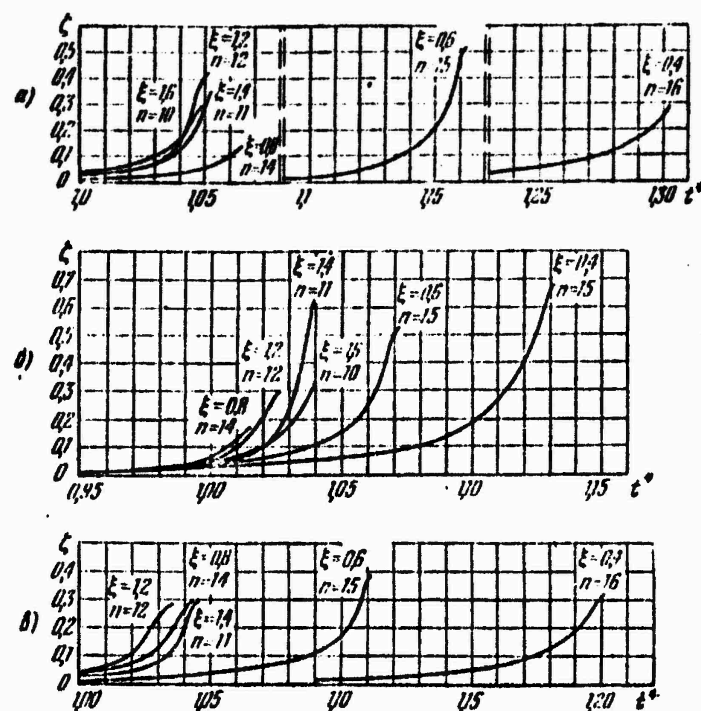


Figure 7.20. "Deflection-time" diagram for dynamic compression in the absence of internal pressure (a) and presence of static pressure of low (b) and high (c) intensity.

compression. The higher the internal pressure, the more elongated are the dents along the arc. The parameter of the dynamic "critical" compressive load increases in the presence of internal pressure in comparison with the static value. For the internal pressure values encountered in practice, this excess ranges from 5 to 10%. It should be noted that for real shells, static buckling takes place at stresses considerably below the upper static "critical" value. For this reason, this dynamic effect of the load is actually much greater than would follow from the above results.

The theoretical conclusions obtained have been qualitatively confirmed by a series of steel shells.* Specimens filled to different degrees with a loose material

*Performed by B.A. Kiladze.

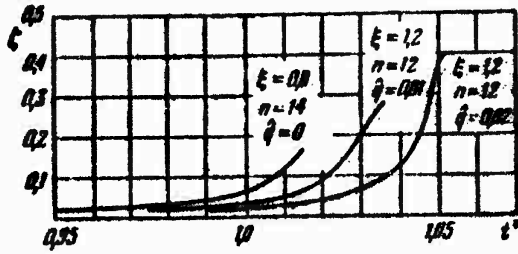


Figure 7.21. Effect of static internal pressure in the presence of dynamic application of axial compression.

were subjected to the action of a dynamic compressive load. The signals from gauges placed in one of the sections of the shell were fed to an oscilloscope. One could thus compare the dynamic stresses in the shell wall, set up at different intensities of internal pressure. The character of wave formation changed in accordance with the results given above.

§74. Anisotropic Cylindrical Shells Under External Pressure

We will now consider the case of an orthotropic shell. Various types of shells can be reduced to such a model of orthotropic structure. Included here are shells stiffened with ribs, i.e., structural variants in which the ribs are arranged at fairly frequent intervals and they can be "smoothered out" along the basic dimensions of the skin (Figure 7.22 a). Another class of such structures are one- or many-layer shells of composite materials with continuous fibers of glass, boron, carbon, graphite, beryllium, etc. (Figure 7.22 b).

We will study the behavior of a closed circular cylindrical orthotropic shell* subjected to the dynamic action of an external normal pressure uniformly distributed over the lateral surface and changing with time according to the law $q = q(t)$. As in the previous variants of the solution of the problems, we will assume that the

*This solution is due to L.N. Smetanina.

shell is hinged to ring frame supports whose points may undergo certain radial displacements while the frames remain circular. It is assumed that the principal



Figure 7.22. Circular cylindrical shell:
a) reinforced with stringers and ring
frame supports; b) smooth.

directions of rigidity coincide with the generatrix of the cylinder and with the arc of the cross section. The elastic properties of orthotropic shells are characterized by moduli E_1 and E_2 along the x and y directions, by the shear modulus G , and by Poisson's ratios μ_1 , μ_2 . Let us note the relation $E_2\mu_1 = E_1\mu_2$. The equation of motion of a shell element has the form (see the book [0.6], p. 580)

$$D_1 \frac{\partial^4(w - w_0)}{\partial x^4} + 2D_3 \frac{\partial^4(w - w_0)}{\partial x^2 \partial y^2} + D_2 \frac{\partial^4(w - w_0)}{\partial y^4} = \\ = h \frac{\partial^2 w}{\partial x^2} \frac{\partial^2 \Phi}{\partial y^2} + h \frac{\partial^2 w}{\partial y^2} \frac{\partial^2 \Phi}{\partial x^2} - 2h \frac{\partial^2 w}{\partial x \partial y} \frac{\partial^2 \Phi}{\partial x \partial y} + \\ + \frac{h}{R} \frac{\partial^3 \Phi}{\partial x^3} + q - \frac{\gamma h}{g} \frac{\partial w}{\partial t}; \quad (7.38)$$

where w and w_0 are the complete and initial deflections; γ is the specific gravity of the shell material; D_1 , D_2 are the bending rigidities in the axial and annular directions; D_3 is the reduced rigidity; D_G is the torsional rigidity:

$$D_1 = \frac{E_1 h^3}{12(1-\mu_1\mu_2)}, \quad D_2 = \frac{E_2 h^3}{12(1-\mu_1\mu_2)}, \quad D_3 = D_1\mu_2 + 2D_G, \\ D_G = \frac{G h^3}{12}.$$

We now write the strain compatibility equation:

$$\begin{aligned} & \delta_1 \frac{\partial^4 \Phi}{\partial x^4} + 2\delta_2 \frac{\partial^4 \Phi}{\partial x^2 \partial y^2} + \delta_3 \frac{\partial^4 \Phi}{\partial y^4} - \\ & = - \frac{\sigma_{xy}}{\delta x} \frac{\sigma_{yy}}{\delta y} + \left(\frac{\sigma_{xy}}{\delta x \delta y} \right)^2 + \frac{\partial^2 \sigma_{xx}}{\partial x^2} \frac{\partial^2 \sigma_{yy}}{\partial y^2} - \left(\frac{\partial^2 \sigma_{xy}}{\partial x \partial y} \right)^2 - \frac{1}{R} \frac{\partial^2 (\omega - \omega_0)}{\partial x^2}, \end{aligned} \quad (7.39)$$

where

$$\delta_1 = \frac{1}{E_1}, \quad \delta_2 = \frac{1}{E_2}, \quad 2\delta_3 = \frac{1}{G} - \frac{2\mu_1}{E_1}.$$

The boundary condition for the deflection w will be $w = 0, \frac{\partial^2 w}{\partial x^2} = 0$ for $x = 0, L$.

The approximating expressions for the complete and initial deflections will be chosen as before in the form

$$w = f(\sin ax \sin by + \psi \sin^2 ax + \phi), \quad (7.40)$$

$$w_0 = f_0(\sin ax \sin by + \psi \sin^2 ax + \phi), \quad (7.41)$$

where

$$a = \frac{m\pi}{L}, \quad \phi = \frac{n}{R}.$$

Again we assume that the form of the initial wave formation, characterized by parameters ψ and ϕ , is in "resonance" with the wave formation of the shell in the course of deformation, and let the only parameter specified in advance is f_0 . As we already know, under external pressure, the shell buckles along the generatrix in one half-wave, and therefore we will hereinafter assume that $m = 1$. We substitute expressions (4) and (41) into the right-hand side of (39). After integrating the equation obtained, we arrive at the following expression for the stress function:

$$\begin{aligned} \Phi = & C_1 \cos 2ax + C_2 \cos 2by + C_3 \sin 3ax \sin by + \\ & + C_4 \sin ax \sin by - \frac{qR}{2h} x^2; \end{aligned} \quad (7.42)$$

the following notation being used:

$$\begin{aligned}
C_1 &= B_1(l^2 - l_0^2) + B_5(l - l_0)\psi, & C_2 &= B_2(l^2 - l_0^2), \\
C_3 &= B_1(l^2 - l_0^2)\psi, & C_4 &= B_4(l - l_0) - B_6(l^2 - l_0^2)\psi, \\
B_1 &= \frac{\alpha^2 E_1}{32\alpha^4}, & B_3 &= \frac{\alpha^2 \beta^2}{8l \left[\frac{\alpha^2}{E_1} + \alpha \beta^2 \left(\frac{1}{a} - \frac{2\mu_1}{E_1} \right) + \frac{\beta^2}{E_1} \right]}, \\
B_2 &= \frac{\alpha^2 E_1}{32l^3}, & B_4 &= \frac{\alpha^2}{R \left[\frac{\alpha^2}{E_1} + \alpha \beta^2 \left(\frac{1}{a} - \frac{2\mu_1}{E_1} \right) + \frac{\beta^2}{E_1} \right]}, \\
B_5 &= -\frac{E_1}{8ka^3}, & B_6 &= \frac{\alpha \beta^2}{\frac{\alpha^2}{E_1} + \alpha \beta^2 \left(\frac{1}{a} - \frac{2\mu_1}{E_1} \right) + \frac{\beta^2}{E_1}}.
\end{aligned}$$

The last term in expression (42) corresponds to stresses in the middle surface determined from zero-moment theory.

The displacement v must satisfy the closure condition (22a). Comparing the expressions for ϵ_y in terms of displacements, on the one hand, and in terms of the function Φ on the other, we find

$$\frac{\partial v}{\partial y} = \frac{1}{E_1} \left(\frac{\partial^2 \Phi}{\partial x^2} - \mu_1 \frac{\partial^2 \Phi}{\partial y^2} \right) - \frac{1}{2} \left(\frac{\partial w}{\partial y} \right)^2 + \frac{1}{2} \left(\frac{\partial w_0}{\partial y} \right)^2 + \frac{w - w_0}{R}.$$

Using the expressions written above (40-(42)), we find

$$\psi = \frac{\eta R^3}{E_1 h (l - l_0)} + \frac{l + l_0}{8} R \beta^2 - \frac{\Psi}{2}.$$

Thus, the parameter ϕ turns out to be expressed in terms of f and ψ .

To find the dependence between the deflection parameters and a time-dependent load, we will write Lagrange equations of the type

$$\frac{d}{dt} \left(\frac{\partial \hat{T}}{\partial \dot{q}_I} \right) - \frac{\partial \hat{T}}{\partial q_I} = \hat{Q}_I. \quad (7.43)$$

As generalized coordinates, we will choose the deflection parameters $q_1 = \xi_1$, $q_2 = \xi_2$; as the generalized forces, the quantities

$$\hat{Q}_1 = -\frac{\partial^3}{\partial z_1^3} \text{ and } \hat{Q}_2 = -\frac{\partial^3}{\partial z_2^3}.$$

The following dimensionless parameters are introduced here:

$$\zeta_1 = \frac{l - l_0}{h}, \quad \zeta_2 = \frac{(l - l_0)\psi}{h},$$

$$\hat{\delta} = \delta \frac{4R}{\pi L h^3 \sqrt{E_1 E_2}}, \quad \hat{q} = \frac{q}{\sqrt{E_1 E_2}} \left(\frac{R}{h} \right)^3.$$

The kinetic energy T of the system is

$$T = \frac{1}{2} \int_0^L \int_0^{2\pi R} \frac{y^4}{8} \left(\frac{\partial w}{\partial t} \right)^2 dx dy; \quad (7.44)$$

in dimensionless form

$$\hat{T} = T \frac{4R}{\pi L h^3 \sqrt{E_1 E_2}}.$$

The total potential energy of the system \mathcal{E} is defined as the sum of the strain energy of the middle surface and potential energy of bending minus the work done by external forces. We find

$$\hat{Q}_1 = \frac{\eta(\xi^4 + \zeta^2) \zeta_1 (\zeta_1 + 2\zeta_2)}{164} + \frac{(\lambda_1 + \lambda_2) \Delta \xi^4 \eta (\zeta_1 + 2\zeta_2) \zeta_2^2}{\zeta_1 + \zeta_2} -$$

$$-\frac{\zeta_2 \Delta}{4} (1 + 8\xi^2 \lambda_2) + \frac{\Delta \xi^4 \lambda_2}{\eta (\zeta_1 + \zeta_2)} - 4 + \frac{\eta \xi^2 \lambda_2}{\zeta_1 + \zeta_2}, \quad (7.45)$$

$$\hat{Q}_2 = 2\zeta_2 \Delta \xi^4 \eta^2 (\zeta_1 + 2\zeta_2)^2 (\lambda_1 + \lambda_2) - \frac{\Delta \eta \zeta_1}{4} (\zeta_1 + 2\zeta_2) (1 + 8\xi^2 \lambda_2) +$$

$$+ \zeta_2 \Delta + 160 \Delta \zeta_2 \xi^4 \eta^2. \quad (7.46)$$

The following notation was introduced above:

$$\begin{aligned}\zeta_0 &= \frac{L}{\pi}, \quad \xi = \frac{\pi R}{nL}, \quad \delta = \frac{R^2}{L^2}, \quad \eta = \frac{n^2 h}{R}, \\ \Delta &= \sqrt{\frac{E_1}{E_2}}, \quad \theta = \frac{a}{\sqrt{E_1 E_2}}, \quad Q = \frac{E_1}{\sqrt{E_1 E_2}}, \quad \Theta = \frac{1}{12(1-\mu_1 \mu_2)}, \\ \lambda_1 &= \frac{1}{81\xi^4 + 9\xi^2 \left(\frac{1}{\theta} - 2\mu_1 \lambda\right) \Delta + \Delta^2}, \\ \lambda_2 &= -\frac{1}{\xi^4 + \xi^2 \left(\frac{1}{\theta} - 2\mu_1 \lambda\right) + \Delta^2}, \\ \lambda_3 &= \xi^4 \Omega + \left(2\mu_2 \Omega + \frac{\theta}{30}\right) \xi^2 + \Delta.\end{aligned}$$

Let us assume that the pressure q changes with time according to the law $q = st$; we will also assume that the buckling of the shell takes place on the rising branch of the pressure pulse. We introduce the dimensionless time parameter \hat{t} , then the Lagrange equation for the variable ζ_1 takes the form

$$\begin{aligned}\frac{d^2\zeta_1}{dt^2} + \frac{\eta^2(\zeta_1 + \zeta_0)}{4 + \eta^2(\zeta_1 + \zeta_0)^2} \left(\frac{d\zeta_1}{dt} \right)^2 - \frac{4S_1(\zeta_1 + \zeta_0)}{4 + \eta^2(\zeta_1 + \zeta_0)^2} \times \\ \times \left\{ \hat{t} - \frac{\eta(\xi^4 + \Delta^2)\zeta_1(\zeta_1 + \zeta_0)}{16\Delta q_0} - \frac{(\lambda_1 + \lambda_2)\Delta E^4 \eta(\zeta_1 - 2\zeta_0)\zeta_2^2}{q_0(\zeta_1 + \zeta_0)} + \right. \\ \left. + \frac{\lambda(1 + 8\xi^2 \lambda_2)\zeta_2}{4q_0} - \frac{\zeta_1}{\zeta_1 + \zeta_0} \right\} = 0,\end{aligned}\tag{7.47}$$

where

$$S_1 = \left(\frac{E_1}{E_2} \right)^{1/2} \eta M_0^2 \left(\frac{1}{\pi R} \right)^2 E_1^2 \left(\frac{h}{R} \right)^4 E_2^2 \frac{a}{\gamma}, \quad \hat{t} = \frac{t}{q_0}.$$

The second Eq. (43) for ζ_2 will be

$$\begin{aligned}\frac{d^2\zeta_2}{dt^2} + \frac{S_1}{M_0^2} \left\{ 2\zeta_0 \Delta \xi^4 \eta^2 (\zeta_1 + 2\zeta_0)^2 (\lambda_1 + \lambda_2) - \right. \\ \left. - \frac{\lambda \eta \zeta_1}{4} (\zeta_1 + 2\zeta_0)(1 + 8\xi^2 \lambda_2) + \zeta_0 \Delta + 160 \Omega \zeta_0 \xi^4 \eta^2 \right\} = 0.\end{aligned}\tag{7.48}$$

Equations (47) and (48) were integrated by the Runge-Kutta method with the aid of a BESM-2M computer for the following initial data:

$$\zeta_1 = 0, \frac{d\zeta_1}{dt} = 0,$$

$$\zeta_1 = 0, \frac{d\zeta_i}{dt} = 0 \text{ for } i=0.$$

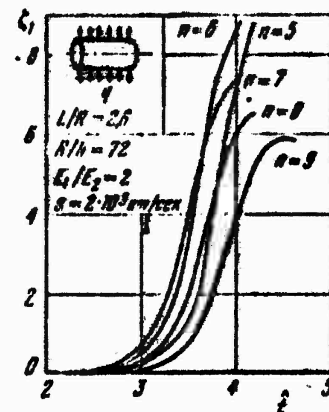


Figure 7.23. "Deflection-time" diagram for a shell of composite material under dynamic loading.
Key: 1) at/sec .

The calculation involved the use of various values of u_1 , u_2 , E_1 and E_2 for different brands of glass-reinforced plastic for the following shell parameters: $L/R = 2.6$, 3.5 and $R/h = 72$; we took $\xi = 0.001$. Figure 7.23 shows a series of $\zeta_1 = \zeta_1(t)$ curves for shells with $E_1/E_2 = 2$ and a loading rate $s = 2 \times 10^3 \text{ at/sec}$ for different wave numbers n . We see that the curve for which $n = 7$ deviates from the abscissa axis the earliest. A rapid increase of deflections takes place for parameter t ranging from 2.7 to 3.9. Thus, the critical pressure here is approximately three times as high as the upper critical load. Figures 7.24 and 7.25 show $\zeta_1 - t$ curves reflecting the dependence between the complete deflection and loading time at rates $s = 0.2 \times 10^4$, 0.5×10^4 , 2×10^4 , $5 \times 10^4 \text{ at/sec}$ for $E_1/E_2 = 2$ and $E_1/E_2 = 5$, respectively. The figures show the curves for wave numbers n at which a rapid increase of deflections corresponds to the smallest parameter t . We see that the dynamic effect is also manifested here in a gradual increase of the wave number and a significant increase of critical pressure.

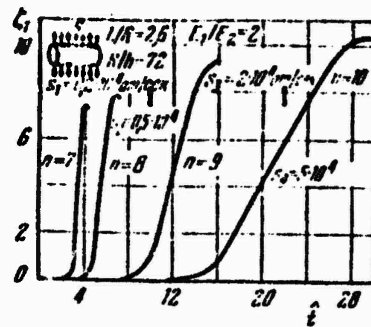


Figure 7.24. Effect of loading rate on the behavior of a shell of composite material for $E_1/E_2 = 2$.

Figure 7.26 shows $\xi_1 = \xi_1(\hat{t})$ curves for different ratios E_1/E_2 at a loading rate $s = 5 \times 10^3$ at/sec. The first curve on the left reflects the dependence $\xi_1 = \xi_1(\hat{t})$ for isotropic shells, and the remaining curves, for shells with different degrees of anisotropy. As the degree of anisotropy increases, the entire curve shifts to the right, toward higher \hat{t} values. Figure 7.27 gives curves which establish the dependence between the dynamic overload coefficient and loading rate

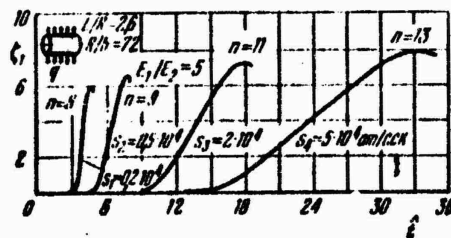


Figure 7.25. Effect of loading rate in the case of the ratio $E_1/E_2 = 5$.

s for different ratios E_1/E_2 when $E_1 \geq E_2$. It is evident from the graphs that the coefficient K_d increases as the loading rate and degree of anisotropy increase. We bear in mind that the direction of the fibers corresponding to a large modulus E coincides with the direction of the generatrix.

§75. Anisotropic Conical Shells Under Axial Loading

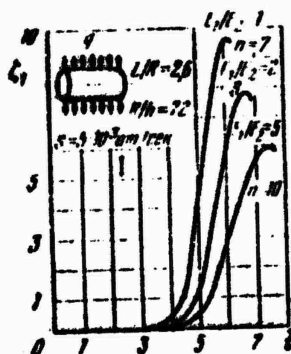


Figure 7.26. Effect of the ratio of moduli E_1/E_2 on the behavior of a shell under dynamic loading. Key:
1) at/sec.

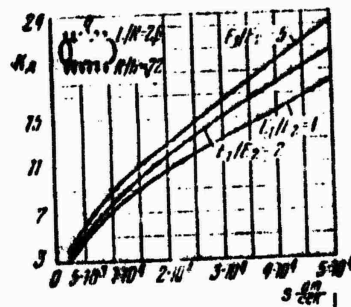


Figure 7.27. Dynamic coefficient for a shell of composite material for different loading rates.

Circular conical shells enter into the structure of jet engines, flying vehicles, tanks, etc. The study of the stability of conical shells is more difficult than in the case of cylindrical shells, since the structure of the initial equations is more complex. We will give a solution* to the problem of dynamic stability of a structurally orthotropic truncated conical shell loaded along the generatrices by

*This solution was obtained by A.A. Solomonenko.

stresses p_1 , p_2 uniformly distributed over the contour (Figure 7.28). It is assumed that the law of change of the external force with time is known. The reinforcing ribs are assumed to be symmetric with respect to the middle surface of the shell. If the ribs are considered to be located at sufficiently frequent intervals, their rigidity can be distributed over the length of the step and the model of an orthotropic shell can be employed.

We write the equations of compatibility and motion of an element of such a shell in projections on the normal, first using linearized relations (see [0.6], p. 643):

$$\frac{h}{h_1} \left(\frac{1}{s^4} \frac{\partial^4 \varphi}{\partial \theta_1^4} + \frac{2}{s^3} \frac{\partial^2 \varphi}{\partial \theta_1^2} - \frac{1}{s^2} \frac{\partial^2 \varphi}{\partial s^2} + \frac{1}{s^3} \frac{\partial \varphi}{\partial s} \right) + \frac{h}{h_2} \left(\frac{\partial^4 \varphi}{\partial s^4} + \frac{2}{s} \frac{\partial^3 \varphi}{\partial s^3} \right) - \\ - \mu \frac{h}{h_1} \left(\frac{1}{s^2} \frac{\partial^4 \varphi}{\partial s^2 \partial \theta_1^2} - \frac{1}{s} \frac{\partial^3 \varphi}{\partial s^3} \right) - \mu \frac{h}{h_2} \left(\frac{1}{s^2} \frac{\partial^4 \varphi}{\partial s^2 \partial \theta_1^2} - \frac{2}{s^3} \frac{\partial^3 \varphi}{\partial s \partial \theta_1^2} + \right. \\ \left. + \frac{2}{s^4} \frac{\partial^2 \varphi}{\partial \theta_1^2} + \frac{1}{s} \frac{\partial^2 \varphi}{\partial s^3} \right) + 2(1+\mu) \left(\frac{1}{s^2} \frac{\partial^4 \varphi}{\partial s^2 \partial \theta_1^2} - \frac{1}{s^3} \frac{\partial^3 \varphi}{\partial s \partial \theta_1^2} + \frac{1}{s^4} \frac{\partial^2 \varphi}{\partial \theta_1^2} \right) + \quad (7.49)$$

$$+ Eh \frac{\partial^2 w}{\partial s^2} \frac{\lg a}{s} = 0; \quad (7.50)$$

$$DV^4 w + C_1 L_1(w) + C_2 L_2(w) = \frac{\partial^2 \varphi}{\partial s^2} \frac{\lg a}{s} - p \frac{\partial^3 w}{\partial s^3} - \rho h \frac{\partial^2 w}{\partial t^2} +$$

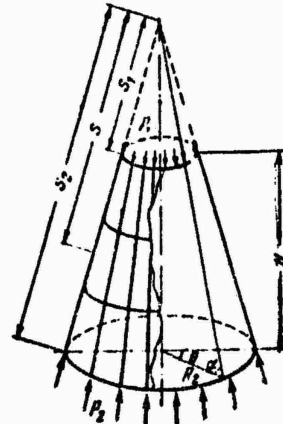


Figure 7.28. Circular conical shell reinforced with stringers and ring frame supports.

The following notation is used; $\theta_1 = \theta \cdot \cos \alpha$; α is the slope angle of the generatrix to the base of the cone; h is the shell thickness; h_1, h_2 are the reduced thicknesses of the reinforced shell in the direction of the coordinates s and θ , respectively; I_1, I_2 are the moments of inertia of the stringers and ring frame supports, calculated with respect to the axes lying in the middle surface of the shell; b_1, b_2 are the distances between the stringers and ring supports; ϕ is the force function in the middle surface; w is the additional deflection;

$$D = \frac{Eh^3}{12(1-\mu^2)}, \quad C_1 = \frac{EI_1}{b_1}, \quad C_2 = \frac{EI_2}{b_2},$$

$$\nabla^4 w = \frac{\partial^4 w}{\partial s^4} + \frac{2}{s} \frac{\partial^3 w}{\partial s^3} - \frac{1}{s^2} \frac{\partial^2 w}{\partial s^2} + \frac{1}{s^3} \frac{\partial w}{\partial s} + \frac{2}{s^2} \frac{\partial^4 w}{\partial s^2 \partial \theta_1^2} -$$

$$- \frac{2}{s^3} \frac{\partial^3 w}{\partial s \partial \theta_1^2} + \frac{4}{s^4} \frac{\partial^2 w}{\partial \theta_1^2} + \frac{1}{s^3} \frac{\partial^4 w}{\partial \theta_1^4};$$

$$L_1(w) = \frac{\partial^4 w}{\partial s^4} + \frac{2}{s} \frac{\partial^3 w}{\partial s^3};$$

$$L_2(w) = \frac{1}{s^1} \frac{\partial^4 w}{\partial \theta_1^4} + \frac{2}{s^1} \frac{\partial^3 w}{\partial \theta_1^3} + \frac{1}{s^1} \frac{\partial^2 w}{\partial \theta_1^2} - \frac{1}{s^2} \frac{\partial^4 w}{\partial \theta_1^2}.$$

The function of the deflection arising in the shell on buckling will be represented in the form

$$w = f_1 e^z \sin \beta_1 z \cdot \sin \beta_2 \theta_1, \quad (7.51)$$

where

$$\beta_1 = \frac{m\pi}{z_0}, \quad \beta_2 = \frac{n}{\cos \alpha}, \quad z_0 = \ln \frac{s_2}{s_1}, \quad z = \ln \frac{s}{s_1}; \quad (7.52)$$

m being the number of half-waves along the generatrix of the shell, n the number of waves along the circumference, s_1 the distance from the apex of the cone to the smaller base, and s_2 , the distance from the apex to the larger base. We introduce the new variables

$$s = s_1 e^z; \quad \varphi = \phi_1 e^{2z}. \quad (7.53)$$

Then, (51) being taken into account, the compatibility equation assumes the following form:

$$\begin{aligned} r_1 \frac{\partial^4 \varphi_1}{\partial z^4} + r_2 \frac{\partial^3 \varphi_1}{\partial z^3} + r_3 \frac{\partial^2 \varphi_1}{\partial z^2} + r_4 \frac{\partial \varphi_1}{\partial z} + r_5 \frac{\partial^4 \varphi_1}{\partial z^2 \partial \theta_1^2} + r_6 \frac{\partial^3 \varphi_1}{\partial z \partial \theta_1^3} + \\ + r_7 \frac{\partial^2 \varphi_1}{\partial \theta_1^2} + r_8 \frac{\partial \varphi_1}{\partial \theta_1^3} = E \cdot h \cdot s_1 \cdot f_1 \cdot \lg \alpha \times \\ \times \beta_1 (\beta_1 \sin \beta_1 z - \cos \beta_1 z) \sin \beta_2 \theta_1. \end{aligned} \quad (7.54)$$

Here r_1, r_2, \dots, r_8 are some functions of μ, h, h_1 and h_2 . The solution of Eq. (54) will be written in the form

$$\varphi_1 = K_1 \sin \beta_1 z \sin \beta_2 \theta_1 + K_2 \cos \beta_1 z \sin \beta_2 \theta_1. \quad (7.55)$$

Here

$$\begin{aligned} K_1 &= Ehs_1 f_1 \frac{\beta_1 (\beta_1 \rho_1 + \rho_2)}{\rho_1^2 + \rho_2^2} \lg \alpha, \\ K_2 &= Ehs_1 f_1 \frac{\beta_1 (\beta_1 \rho_2 - \rho_1)}{\rho_1^2 + \rho_2^2} \lg \alpha, \\ \rho_1 &= r_1 \beta_1^2 - r_2 \beta_1^2 + r_3 \beta_1^2 \beta_2^2 - r_4 \beta_2^2 + r_5 \beta_2^2, \\ \rho_2 &= \beta_1 (r_2 \beta_1^2 - r_4 + r_5 \beta_2^2). \end{aligned}$$

After relations (51) and (53) are introduced into the equation of motion, the latter will be rewritten as

$$\begin{aligned} DV_1^4 w + C_1 L_1^*(w) + C_2 L_2^*(w) - s_1 \lg \alpha \left(\frac{\partial^2 \varphi_1}{\partial z^2} + 3 \frac{\partial \varphi_1}{\partial z} + 2 \varphi_1 \right) e^{2z} + \\ + s_1^2 \cdot \mu \left(\frac{\partial^2 w}{\partial z^2} - \frac{\partial w}{\partial z} \right) e^{2z} + s_1^2 e^{4z} \rho h \frac{\partial^2 w}{\partial t^2} = W = 0, \end{aligned} \quad (7.56)$$

$$V_1^4 w = \frac{\partial^4 w}{\partial z^4} - 4 \frac{\partial^3 w}{\partial z^3} + 4 \frac{\partial^2 w}{\partial z^2} +$$

$$+ 2 \frac{\partial^2 w}{\partial z^2 \partial \theta_1^2} - 4 \frac{\partial^3 w}{\partial z_1 \partial \theta_1^3} + 4 \frac{\partial^2 w}{\partial \theta_1^2} + \frac{\partial^4 w}{\partial \theta_1^4},$$

$$L_1^*(w) = \frac{\partial^4 w}{\partial z^4} - 4 \frac{\partial^3 w}{\partial z^3} + 5 \frac{\partial^2 w}{\partial z^2} - 2 \frac{\partial w}{\partial z},$$

$$L_2^*(w) = \frac{\partial^4 w}{\partial \theta_1^4} + 2 \frac{\partial^3 w}{\partial \theta_1^3} + 2 \frac{\partial^2 w}{\partial z^2} - \frac{\partial^3 w}{\partial z^3}.$$

We now use the Bubnov-Galerkin method, assuming the parameter f_1 to be variable; the corresponding equation has the form

$$\int_0^{2\pi} \int_{r_1}^{r_2} W e^z \sin \beta_1 z \sin \beta_1 \theta_1 dz d\theta_1 = 0.$$

After integrating, we obtain the equation relating the deflection parameter and the time-dependent load:

$$\frac{\partial^2 \zeta}{\partial t^2} = \frac{3}{2} \frac{E \beta_2 \theta^2 (\beta_1^2 + \beta_2^2) \zeta}{\rho (s_1^4 + s_2^2 + s_3^2)} (p^* - p_s^*); \quad (7.57)$$

where the following notation was introduced:

$$p^* = \frac{p}{Eh}, \quad \zeta = \frac{f_1}{h}, \quad \theta = \frac{m\pi \cos \alpha}{ns_0} = \frac{\beta_1}{\beta_2},$$

p_u^* being the parameter of the upper critical stress for static loading of the conical shell. If the shells studied satisfy the conditions

$$\beta_1^2 \gg 1 \text{ and } \beta_2^2 \gg 1$$

then

$$p_s^* = \frac{2h \lg a}{\sqrt{6(1-\mu^2)(s_1^2 + s_2^2)}} \sqrt{\frac{r_3 \theta^4 + 2\theta^2 + r_{10}}{r_1 \theta^4 + r_3 \theta^2 + r_9}},$$

where

$$r_9 = 1 + 12(1-\mu^2) \frac{I_1}{\beta_1 h^3}, \quad r_{10} = 1 + 12(1-\mu^2) \frac{I_2}{\beta_2 h^3}.$$

If we now use nonlinear equations, the function approximating the additional deflection may be chosen in the form

$$w = f e^z (\sin \beta_1 z \sin \beta_2 \theta_1 + \psi \sin^2 \beta_1 z). \quad (7.58)$$

Carrying out the operations in the same sequence as above, we obtain equations which establish the dependence between the deflection parameters and a time-dependent load:

$$\frac{\partial^2 \zeta}{\partial t^2} = \frac{3}{2} \frac{E}{\rho} \beta_2^2 \theta^2 \frac{s_1^2 + s_2^2}{s_1^2 + s_1^2 s_2^2 + s_2^4} \left\{ p^* \zeta - p_s^* (\zeta - \zeta_0) - \right. \\ \left. - \frac{h^3}{s_1^2 \beta_2^2 \theta^2} [K_1^* (\zeta^3 - \zeta \zeta_0^2) + K_2^* (\zeta^3 - \zeta \zeta_0^2) \psi^2 - \right. \\ \left. - K_3^* (\zeta^3 - \zeta_0^3) \psi - K_4^* (\zeta^3 - \zeta \zeta_0) \psi] \right\}; \quad (7.59)$$

$$\frac{\partial^2 \zeta}{\partial t^2} \psi + 2 \frac{\partial \zeta}{\partial t} \frac{\partial \psi}{\partial t} + \frac{\partial^2 \psi}{\partial t^2} \zeta = 2 \frac{E}{\rho} \frac{s_1^2 + s_2^2}{s_1^2 + s_1^2 s_2^2 + s_2^4} \left\{ p^* \left(\beta_2^2 \theta^2 \psi \zeta - \frac{s_1}{h} \lg a \right) - \right. \\ \left. - \frac{2h^3 \beta_2^2 \theta^2}{s_1^2 + s_2^2} \left[\frac{\beta_2^2 \theta^2}{3(1-\mu^2)} + \frac{4\mu \beta_2^2 \theta^2}{\delta_1 h^3} + \frac{\delta_2}{\delta_2 h^3} \right] (\zeta - \zeta_0) \psi - \right. \\ \left. - \frac{h^3}{s_1^2} \left[K_5^* (\zeta^3 - \zeta \zeta_0^2) \psi^3 + K_6^* (\zeta^3 - \zeta \zeta_0^2) \psi + K_7^* (\zeta^3 - \zeta \zeta_0^2) \psi^2 \frac{s_1}{h} \lg a + \right. \right. \\ \left. \left. + K_8^* (\zeta^3 - \zeta \zeta_0^2) \psi^2 \frac{s_1}{h} \lg a + K_9^* (\zeta - \zeta_0) \psi \frac{s_1^2}{h^2} \lg^2 a + \right. \right. \\ \left. \left. + K_{10}^* (\zeta^3 - \zeta \zeta_0^2) \frac{s_1}{h} \lg a + K_{11}^* (\zeta^3 - \zeta \zeta_0^2) \frac{s_1}{h} \lg a \right] \right\}, \quad (7.60)$$

where K_1^* , K_2^* , K_3^* , K_4^* , K_5^* , K_6^* , K_7^* , K_8^* , K_9^* , K_{10}^* , K_{11}^* are functions of B_1 , B_2 , μ , h , h_1 , h_2 . The dimensionless parameter of complete deflection is denoted by ζ .

If the shell is acted on by a load changing linearly with time $p = St$, then after the introduction of the dimensionless time parameter into Eq. (59), we arrive at the following equation:

$$t^* = \frac{St}{Eh\rho_s} = \frac{p^*}{p_s^*},$$

$$\frac{d\zeta}{dt^2} = Q \left[(\zeta - (\zeta - \zeta_0) - Q_1(\zeta^3 - \zeta_{10}^3) - Q_2(\zeta^3 - \zeta_{11}^3)) \frac{\psi'}{\zeta^2} + Q_3(\zeta^3 - \zeta_{12}^3) \frac{\psi}{\zeta^3} + Q_4(\zeta^3 - \zeta_{13}^3) \frac{\psi}{\zeta^3} \right]; \quad (7.61)$$

where

$$Q = \frac{3}{2} \beta_2^2 \theta^2 \frac{h^2(s_1^2 + s_2^2)}{s_1^2 + s_1^2 s_2^2 + s_2^4} \left(\frac{cE}{s} \right)^2 p_0^{-2},$$

$$Q_1 = \frac{h^2}{s_1^2 \beta_2^2 \theta^2} \cdot \frac{K_1^*}{p_0^2}, \quad Q_2 = \frac{h^2}{s_1^2 \beta_2^2 \theta^2} \cdot \frac{K_2^*}{p_0^2},$$

$$Q_3 = \frac{h \lg a}{s_1 \beta_2^2 \theta^2} \cdot \frac{K_3^*}{p_0}, \quad Q_4 = \frac{h \lg a}{s_1 \beta_2^2 \theta^2} \cdot \frac{K_4^*}{p_0},$$

$$K_1^* = \frac{\beta_2^4}{4} \left[\frac{r_1 \beta_2^2 \theta^2 + r_2}{4r_1^2 \beta_2^2 \theta^2 + r_2^2} + \frac{\alpha^4}{4r_3} \right],$$

$$K_2^* = \beta_2^2 \theta^4 \left[\frac{r_1 \theta^4 + r_3 \theta^2 + r_6}{\beta_2^2(r_1 \theta^4 + r_3 \theta^2 + r_6)^2 + \theta^2(r_2 \theta^2 + r_6)^2} + \frac{s_1 r_1 \theta^4 + s_3 r_3 \theta^2 + r_6}{\beta_2^2(3s_1 r_1 \theta^4 + 3s_3 r_3 \theta^2 + r_6)^2 + 9\theta^2(s_2 r_2 \theta^2 + r_6)^2} \right].$$

$$K_3^* = \frac{\beta_2^2 \theta^4 (r_1 \theta^4 + r_3 \theta^2 + r_6)}{\beta_2^2(r_1 \theta^4 + r_3 \theta^2 + r_6)^2 + \theta^2(r_2 \theta^2 + r_6)^2},$$

$$K_4^* = \beta_2^2 \left[\frac{r_1 \beta_2^2 \theta^2 + r_2}{4r_1^2 \beta_2^2 \theta^2 + r_2^2} + \frac{\beta_2^2 \theta^4 (r_1 \theta^4 + r_3 \theta^2 + r_6)}{\beta_2^2(r_1 \theta^4 + r_3 \theta^2 + r_6)^2 + \theta^2(r_2 \theta^2 + r_6)^2} \right].$$

The parameter ψ :

$$\frac{h^2}{s_1^2} (K_3^* - K_0^*) \zeta^3 \psi^3 - \frac{h}{s_1} \lg a \left(\frac{1}{\beta_2^2 \theta^2} K_2^* + K_3^* + K_4^* + K_{10}^* + K_{11}^* \right) \zeta^2 \psi^2 +$$

$$+ \left\{ \beta_2^2 \theta^2 p_0^2 - \frac{2h^2 \beta_2^2 \theta^2}{s_1^2 + s_2^2} \left[\frac{\beta_2^2 \theta^2}{3(1 - \mu^2)} + \frac{4r_1 \beta_2^2 \theta^2}{b_1 h^2} + \frac{r_2}{b_2 h^2} \right] + \right.$$

$$+ \left. \left[\frac{1}{\beta_2^2 \theta^2} (K_3^* + K_4^*) - K_0^* \right] \lg^2 a + \frac{h^2}{s_1^2} (K_3^* - K_0^*) \zeta^2 \right\} \zeta \psi -$$

$$- \frac{h}{s_1} \lg a \left(\frac{1}{\beta_2^2 \theta^2} K_{10}^* + K_{11}^* + K_{12}^* \right) \zeta^3 - \frac{s_1}{4} \lg a \cdot p_0^2 = 0. \quad (7.62)$$

In conformity with N.A. Alfutov's proposition, it may be assumed that the parameter of the "unsymmetric" component of the deflection ψ is proportional to the "symmetric" component, $\psi = a\zeta$; the coefficient a is determined from the formula

$$a = \frac{\left(\frac{1}{\beta_2^2 \theta^2} K_2^* + K_{10}^* + K_{11}^* \right) \frac{h}{s_1} \lg a}{\beta_2^2 \theta^2 \left\{ p_0^2 - \left[\frac{\beta_2^2 \theta^2}{3(1 - \mu^2)} + r_1 \beta_2^2 \theta^2 + r_{12} \right] \frac{2h^2}{s_1^2 + s_2^2} \right\} + \left[\frac{1}{\beta_2^2 \theta^2} (K_3^* + K_4^*) - K_0^* \right] \lg^2 a}.$$

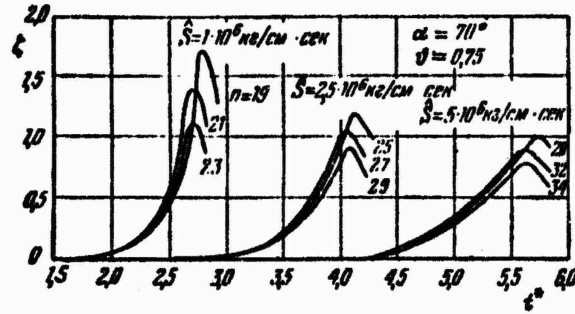


Figure 7.29. Time dependence of the deflection parameter for a conical shell under axial compression.

resulting from (62). The following notation is used:

$$K_0 = \frac{r_1 \beta_2^2 \theta^2 + r_2}{\beta_1^2 \beta_2^2 \theta^2 + r_2^2}, \quad K_{10} = -\frac{\beta_2^2 (r_1 \beta_2^2 \theta^2 + r_2)}{4(r_1 \beta_2^2 \theta^2 + r_2^2)},$$

$$K_{11} = \frac{\beta_2^2 \theta^4 (r_1 \theta^4 + r_2 \theta^2 + r_3)}{\beta_1^2 (r_1 \theta^4 + r_2 \theta^2 + r_3)^2 + \theta^2 (r_1 \theta^2 + r_3)^2},$$

$$r_{11} = \frac{I_1}{b_1 h^3}, \quad r_{12} = \frac{I_2}{b_2 h^3}.$$

Equation (61) is finally written in the form

$$\frac{d^2\zeta}{dt^{*2}} - Q \left([t^* - (Q_1 - Q_3 \cdot a)(\zeta^2 - \zeta_0^2)] \zeta - (\zeta - \zeta_0) - Q_2 (\zeta^3 - \zeta^2 \zeta_0) a^2 + Q_4 (\zeta^3 - \zeta^2 \zeta_0) a \right) = 0.$$

This equation was integrated numerically. The initial conditions were chosen in the form $d\zeta/dt^* = 0$, $\zeta = \zeta_0$ at $t^* = 0$. Figure 7.29 shows $\zeta(t^*)$ curves obtained with the following data: $\alpha = 70^\circ$, $s_1 = 19.9$ cm, $s_2 = 73.1$ cm, $R_2 = 25$ cm, $H = 50$ cm, $h = 0.05$ cm. Reinforcement parameters: $r_1 = 0.954$, $r_2 = 3.53$, $r_3 = 2.054$,

$r_6 = 4.16$, $r_8 = 0.866$, $r_9 = 2.69$, $r_{10} = 1.57$, $r_{11} = 1.05$, $r_{12} = 0.135$. Cromansil was used as the material of the shells. The amplitude of the initial deflection $\xi_0 = 1 \times 10^{-3}$. The wave formation shape parameter was taken to be $\theta = 0.75$.

The loading rates used were $\dot{S} = 1 \times 10^6$, 2.5×10^6 , and 5×10^6 kg/cm sec. Each curve corresponds to a definite number of waves indicated on the graphs. We see that a rapid increase of deflections takes place in the first case when $n = 21$, in the second when $n = 27$, and in the third when $n = 32$. Thus, as the loading rate increases, the number of circumferential waves n also increases. There is a simultaneous increase in critical loading time.

§76. Cylindrical Panel Under Dynamic Compression

Let us consider a cylindrical panel subjected to dynamic compressive stresses along the generatrix. We will solve the problem in the first approximation, using the Bubnov-Galerkin method. We will first consider the case in which the compressive stress p increases with time according to the law $p = st$, and will assume that dynamic buckling of the panel takes place before the load reaches its maximum value. As the approximating functions for the complete and initial deflections we will choose the expressions

$$w = f \sin \frac{m\pi x}{a} \sin \frac{n\pi y}{b}, \quad w_0 = f_0 \sin \frac{m\pi x}{a} \sin \frac{n\pi y}{b}. \quad (7.63)$$

Sides a and b are oriented along the generatrix and the arc of the panel, respectively. The number of half-waves along side a is denoted by m, and along b, by n. Substituting expressions (63) into the right-hand side of an equation of the type of (2) and integrating it, we find the function Φ in the form

$$\begin{aligned} \Phi = & \frac{E}{32} (f^2 - f_0^2) \left[\left(\frac{m}{n} \frac{a}{b} \right)^2 \cos \frac{2m\pi x}{a} + \left(\frac{m}{n} \frac{b}{a} \right)^2 \cos \frac{2n\pi y}{b} \right] + \\ & + \frac{E}{\pi^2 R} (f - f_0) \left(\frac{m}{a} \right)^2 \frac{1}{\left[\left(\frac{m}{a} \right)^2 + \left(\frac{n}{b} \right)^2 \right]^2} \sin \frac{m\pi x}{a} \sin \frac{n\pi y}{b} - \frac{pp^2}{2}. \end{aligned} \quad (7.64)$$

We now apply the Bubnov-Galerkin method to Eq. (1). Integration yields

$$\begin{aligned} & \left\{ \bar{\rho} - \frac{\pi^2}{16} \left[\left(\frac{m}{\lambda} \right)^2 + \left(\frac{n^2 \lambda}{m} \right)^2 \right] (\zeta^2 - \zeta_0^2) + \right. \\ & + \alpha \frac{32}{3} \frac{k n m}{\pi^3} \left[\frac{\lambda}{m^2 + (\lambda n)^2} \right]^2 (\zeta - \zeta_0) \left. \right\} \zeta - \left\{ \frac{\pi^2}{12(1-\mu^2)} \left(\frac{m}{\lambda} + \frac{n^2 \lambda}{m} \right)^2 + \right. \\ & + \left(\frac{b m}{\pi} \right)^2 \left[\frac{\lambda}{m^2 + (\lambda n)^2} \right]^2 - \alpha \frac{2}{3} \frac{k n \lambda^2}{\pi^2 m^2} (\zeta + \zeta_0) \left. \right\} (\zeta - \zeta_0) + \\ & \left. + \alpha \frac{16 \lambda^2}{\pi^2 m^2 n} \bar{q} - \frac{\gamma}{E h} \left(\frac{b^2}{h} \frac{\lambda}{\pi m} \right)^2 \frac{d^2 \zeta}{dt^2} = 0. \right. \end{aligned} \quad (7.65)$$

The following dimensionless parameters are used above: $\zeta = f/h$, $\zeta_0 = f_0/h$, $\lambda = a/b$, $k = b^2/Rh$, $\bar{\rho} = pb^2/Eh^2$, $\bar{q} = qb^4/Eh^4$, R being the radius of curvature of the middle surface. The coefficient α is equal to 1 if m and n are odd; if however at least one of these parameters is even, $\alpha = 0$.

Discarding the inertial and nonlinear terms in Eq. (65) and taking $\zeta_0 = 0$, we arrive at the following expression for the dimensionless upper critical stress under quasi-static loading at $\lambda = 1$:

$$\bar{\rho}_{kp} = \frac{\pi^2}{3(1-\mu^2)} + \frac{k^2}{4\pi^2}. \quad (7.66)$$

We introduce the notation t^* for the dimensionless time parameter according to the formula

$$t^* = \frac{st}{\rho_{kp}} = \frac{s}{\bar{\rho}_{kp}}. \quad (7.67)$$

Equation (65) takes the form

$$\begin{aligned} & \frac{1}{3} \frac{d^2 \zeta}{dt^{*2}} + \frac{(\zeta - \zeta_0)}{\bar{\rho}} \left\{ \pi^4 \left[\left(\frac{m}{\lambda} \right)^2 + n^2 \right]^2 + 12(1-\mu^2) \left[\frac{m^2 k}{m^2 + (\lambda n)^2} \right]^2 + \right. \\ & + \zeta (\zeta + \zeta_0) \frac{3}{4} \pi^4 (1-\mu^2) \left[\left(\frac{m}{\lambda} \right)^4 + n^4 \right] - \alpha \zeta \cdot 128 \frac{(1-\mu^2) k n m^2}{[m^2 + (\lambda n)^2]^3} - \\ & \left. - \alpha (\zeta + \zeta_0) 8 \frac{n k}{m} (1-\mu^2) \right\} - \frac{\alpha}{\bar{\rho}} 192 \frac{1-\mu^2}{\pi^2 n m} \bar{q} - \left(\frac{m}{\lambda} \right)^2 U^* = 0; \end{aligned} \quad (7.68)$$

where B denotes $b = 4\pi^4 + 3(1-\mu^2)k^2$, and S stands for

$$S = \bar{p}_{cr}^2 \left(\frac{\pi c E}{s} \frac{h^3}{b^4} \right)^2, \quad (7.69)$$

c being the speed of sound in the panel material. In the case of a flat plate, the expression for the critical stress will be written in the form of (8)

$$\bar{p}_{cr} = \frac{\pi^2}{3(1-\mu^2)}, \quad (7.70)$$

and the equation of motion reduces to the form of (11)

$$\begin{aligned} \frac{1}{S} \frac{d^2\zeta}{dt^2} + (\zeta - \zeta_0) \left\{ \frac{1}{4} \left[\left(\frac{m}{\lambda} \right)^2 + n^2 \right]^2 + \right. \\ \left. + \frac{3}{16} \zeta (\zeta + \zeta_0) (1 - \mu^2) \left[\left(\frac{m}{\lambda} \right)^4 + n^4 \right] \right\} - \\ - n \frac{18}{\pi^2 m n} (1 - \mu^2) \dot{\zeta} - \zeta \left(\frac{m}{\lambda} \right)^2 \ddot{\zeta} = 0. \end{aligned} \quad (7.71)$$

The integration of Eq. (65) was performed with the aid of the Runge-Kutta method on a BESM-2M computer; the step with respect to dimensionless time was taken equal to 0.01. A preliminary study of the practical convergence of the solution was made; a further decrease of the step had no appreciable effect on the results of the calculations.

The algorithm described above was used for the solution of several specific problems. First, the behavior of the panel was studied as a function of its geometrical characteristics. Figure 7.30 shows the results of calculations for elongated panels and square panels in the plane. In both cases, the initial deflection parameter $\zeta_0 = 10^{-3}$, and the loading rate parameter $S = 0.1$. This value of S in the case of a Duralumin panel having thickness h of the order of 0.1 cm and parameter $k = 6$ is associated with a rate of increase of the "physical" stress $s = 2.2 \times 10^5$ kg/cm² sec. Let us note that each curve in Figure 7.30 b has its own scale along the abscissa axis; in the expression for the parameter $t^* = \bar{p}/\bar{p}_{cr}$, for each value of the curvature k , \bar{p}_{cr} denotes the value of the upper critical static stress according to (66). This makes it possible to use the plotted diagrams for a direct determination of the dynamic coefficient K_d , equal to the ratio of the conventional critical load to the upper static value.

Figure 7.30 shows only the curves corresponding to the "critical" number of half-waves m_{cr} , i.e., curves whose portion characterizing the front of sharp buckling lies closest to the ordinate axis.* As expected, the values of m_{cr} corresponding to an elongated panel with a side ratio $\lambda = 2$ were twice as high as the values of m_{cr} for a panel square in the plane ($\lambda = 1$). It follows from these data that the length of the panel has practically no effect on the value of the dynamic coefficient. In addition, the dynamic coefficient decreases with increasing curvature parameter of the panel. This can be explained by the fact that a warped panel has a tendency to snap, as reflected in a decrease of its supporting capacity in comparison with a plate or panel of smaller curvature.

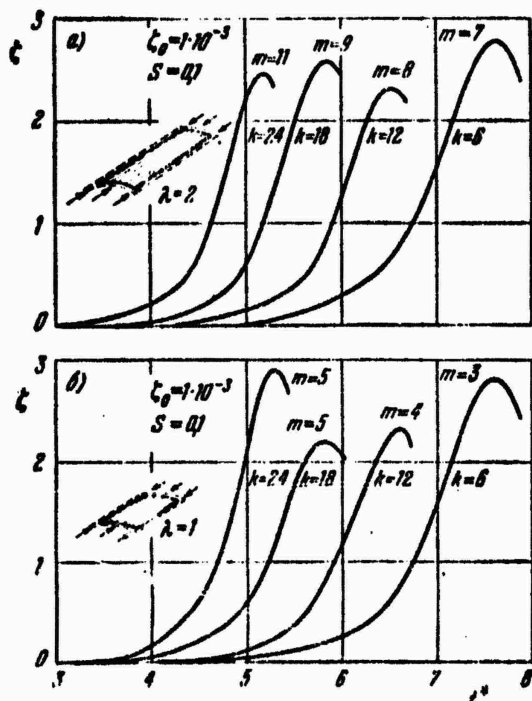


Figure 7.30. "Deflection-time" plot for a slightly curved circular cylindrical panel under dynamic application of axial compression in the cases a) $\lambda=2$ & b) $\lambda=1$.

*The entire series of calculations showed that the "critical" number of half-waves along the arc $n = 1$.

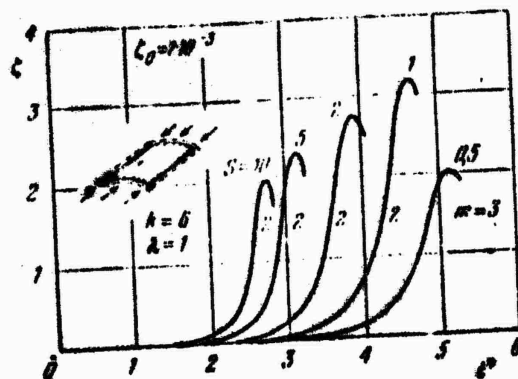


Figure 7.31. Effect of loading rate on the behavior of a cylindrical panel under axial compression.

We then studied the effect of initial deflection on the behavior of the panel. As ξ_0 changes, the dynamic coefficient changes sharply, amounting to approximately 2.6 in the case of $\xi_0 = 10^{-1}$, and to about 5.2 when $\xi_0 = 10^{-5}$ (we took $s = 1$).

The calculations made for a flat plate in §66 yielded a pattern very similar to the one described above.

Figure 7.31 shows data of calculations for a panel square in the plane with parameter $k = 6$ and initial deflection $\xi_0 = 10^{-3}$ for different S . Let us recall that a smaller S is associated with a higher rate of load increase s .

We then studied the effect of transverse statically applied load q , both positive, directed toward the center of curvature of the panel, and negative (away from the center).

It was found that the application of a relatively small "positive" transverse load had no appreciable effect on the process of buckling of the panel.

If however there is a load applied away from the center of curvature, then as a rule, the panel "prefers" to buckle in the opposite direction.

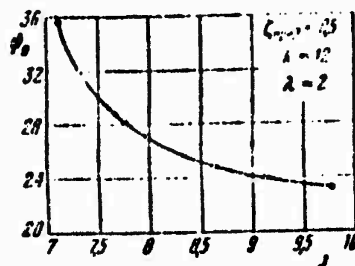


Figure 7.32. Effect of pulse shape in dynamic loading of a cylindrical panel.

Figure 7.32 shows the relationship between the parameter of a step pulse J and load amplitude ψ_0 for a panel characterized by the values $k = 12$, $\lambda = 2$. These data may be compared with the results obtained in §67 for a flat plate; see also §102.

The above results make it possible, with a certain degree of confidence, to perform practical calculations of warped panels with a small curvature parameter (up to $k = 12$). Subsequently, it will be of interest to examine the problem in higher approximations; this is particularly important for panels of large curvature.

577. Spherical Panel Under Dynamic Application of External Pressure

Let us now consider the case of a slightly curved spherical panel subjected to a dynamically applied normal external pressure. We will study only the case of axisymmetric deformation. Here, use may be made of the equations given in Chapter III in the notation of §35.

Let us turn first of all to the law of pressure change that was studied in detail in the preceding sections of the chapter: we will assume that the intensity of uniformly distributed pressure q^* changes with time according to the linear law $q^* = at^*$. We will find out how the buckling of the shell will occur at different loading rates. We adopted the same method of integration of the fundamental equation as in §35.

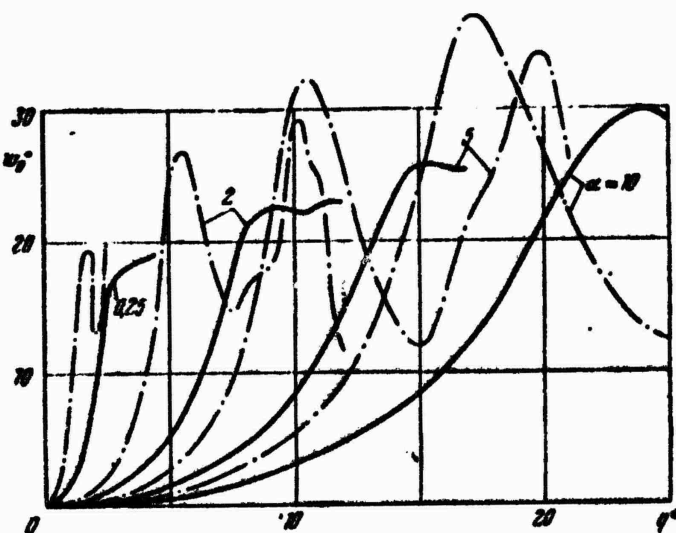


Figure 7.33. Graph of the motion of the apex of a spherical panel under dynamic application of external pressure.

The calculations were carried out* for a shell with a rigidly clamped support contour having a shallowness parameter $b = 4$ (see §35). Some results of the calculations are given in Figure 7.33. The solid lines represent graphs of the motion of the shell apex at different loading rates of the shell, determined by α . The load parameter is laid off along the abscissa axis, but it may be assumed that the graphs were plotted on an altered scale for the time parameter. The forces of viscous drag of the medium are considered here. The dot-dash lines represent the same kind of plots, but in the absence of drag forces.

The above results attest to the fact that at a certain value of the load, the shell crosses over to a distant equilibrium branch, whereupon nonlinear vibrations begin. In the presence of forces of viscous drag of the medium, these vibrations

*The data given below were obtained by N.V. Vashishvili.

damp out rapidly. As was shown in the preceding paragraphs, an increase in loading rate leads to a delay of the crossover process; therefore, as the loading rate increases, the load corresponding to the instant of the crossover also increases. The presence of forces of viscous drag of the medium leads to a similar effect.

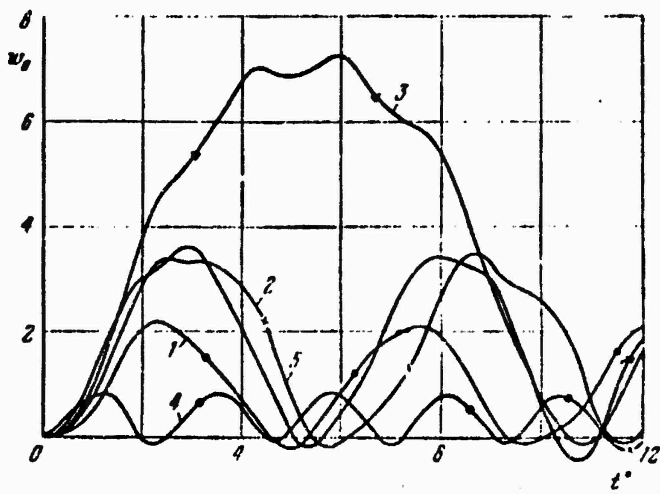


Figure 7.34. Displacements of the apex of a spherical panel for various shapes of the step pulse.

Naturally, in the presence of forces of viscous drag, the spread of the vibrations around the new state of equilibrium is smaller than in their absence.

Let us turn to the case where at $t^* = 0$, a uniform pressure which subsequently remains constant with time is applied to the panel. The problem is solved with the aid of a system of equations in which we take $q^* = \text{const}$, and the initial displacements and rates are considered to be zero. Some results of the calculations are given in Figure 7.34. The parameter of normal displacement of the shell apex is laid off along the abscissa axis. The first three curves were plotted for a shell with shallowness parameter $b = 3.5$ and the following values of the pressure parameter: $q^* = 0.4$ (curve 2), $q^* = 0.5$ (curve 3). Let us note that for the shell under consideration, the upper critical pressure $q_u^* = 0.6$.

The above results indicate that if the pressure is small in comparison with the critical value, the motion of the shell apex takes place in accordance with a law that is close to harmonic (curve 1). Near the critical pressure, the vibration period of the shell increases sharply, and the motion assumes a complex character; simultaneously with the slow basic process, a motion with a small period takes place around the position determined by the principal state of the system (curve 3).

Curves 4 and 5 were plotted, respectively, for shells with parameters $b = 2$ and $b = 3$ when $q^* = 0.5$. It is obvious that as the parameter b decreases, the vibration period decreases (if the processes are considered for the same load).

It should be noted that in all the problems considered, the vibrations are executed around a position displaced from the initial undeformed state of the shell toward the center of curvature of the shell.*

§78. Reinforced Shallow Shells of Positive Curvature

Of practical importance is the study of the behavior of a shallow shell of positive curvature reinforced with elastic ribs (Figure 7.35) under dynamic loading by normal pressure. For the sake of generality, it will be assumed that the ribs are located either on the inside or outside,** unsymmetrically with respect to the middle surface.

The expressions for the forces per unit length of the contour and reduced to the middle surface of the shell may be represented as follows:

*These problems were solved with both automatic selection of the step as a function of a given accuracy, and with a constant step $\Delta t = 10^{-3}$. In the solution of each of the problems, more than 13000 steps were performed, and the count was stable.

**This problem has been discussed earlier by O.I. Terebushko for a cylindrical shell. The data given here are due to S.A. Timashev; Eqs. (72) and (73) are also his; see the collection "Stroitel'naya mekhanika," 158, Sverdlovsk, 1968.

$$N_x = B_1 e_x + \mu H_1 e_y - A_1 \frac{\partial^2 \omega}{\partial x^2},$$

$$T = \frac{1-\mu}{2} B_1 \gamma_1,$$

$$M_x = -D \left(\frac{\partial^3 \omega}{\partial x^3} + \mu \frac{\partial^3 \omega}{\partial y^3} \right) - C_1 \frac{\partial^2 \omega}{\partial x^2} + A_1 e_x + \mu A_2 e_y,$$

$$H = -[D(1-\mu) + H_1] \frac{\partial^2 \omega}{\partial x \partial y};$$

the expressions for N_y and M_y can be similarly written.

The following parameters are used:

$$B_1 = \frac{Eh}{1-\mu^2} + \frac{EF_1}{I_1} = \frac{Eh}{1-\mu^2}, \quad A_1 = \frac{ES_1}{I_1}, \quad C_1 = \frac{EJ_1}{I_1}, \quad H_1 = \frac{EK_1}{I_1},$$

where F_1 , S_1 , J_1 , K_1 denote the sectional area, static moment, and bending and twisting moments of inertia of the rib section of the first direction. The distances between the ribs of the first and second directions are denoted by I_1 and I_2 .

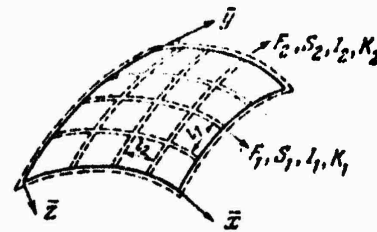


Figure 7.35. Reinforced shallow panel of positive curvature.

The strains in the middle surface will be

$$\epsilon_x = \frac{1}{B_1(1-\mu^2)} \left(N_x - \mu N_y + A_1 \frac{\partial^2 \omega}{\partial x^2} - \mu A_2 \frac{\partial^2 \omega}{\partial y^2} \right),$$

$$\epsilon_y = \frac{1}{B_1(1-\mu^2)} \left(N_y - \mu N_x + A_2 \frac{\partial^2 \omega}{\partial y^2} - \mu A_1 \frac{\partial^2 \omega}{\partial x^2} \right),$$

$$\gamma = \frac{2T}{(1-\mu)B} \quad \text{for} \quad B = \frac{Eh}{1-\mu^2}.$$

The fundamental nonlinear equations in the deflection functions and stress function in the middle surface take the form (in dimensionless parameters)

$$D_1 \frac{\partial^4 (w - w_0)}{\partial x^4} + 2D_1 \lambda^2 \frac{\partial^4 (w - w_0)}{\partial x^2 \partial y^2} + D_1 \lambda^4 \frac{\partial^4 (w - w_0)}{\partial y^4} = \\ = \frac{\partial^4 \Phi}{\partial y^4} \frac{\partial^2 w}{\partial x^2} \lambda^2 + \frac{\partial^2 \Phi}{\partial x^2} \frac{\partial^2 w}{\partial y^2} \lambda^2 - 2 \frac{\partial^2 \Phi}{\partial x \partial y} \frac{\partial^2 w}{\partial x \partial y} \lambda^2 + \\ + \lambda^2 k_x^* \frac{\partial^4 \Phi}{\partial y^4} + \lambda^2 k_y^* \frac{\partial^4 \Phi}{\partial x^2} + \frac{\partial^4 \Phi}{\partial x^2 \partial y^2} \lambda^2 (\gamma_1 + \gamma_2) (1 - \mu^2) + \\ + \frac{\partial^4 \Phi}{\partial x^4} \mu (\gamma_2 - \gamma_1) + \frac{\partial^4 \Phi}{\partial y^4} \lambda^4 \mu (\gamma_1 - \gamma_2) + \lambda^2 q^*, \quad (7.72)$$

$$\lambda^4 \delta_1 \frac{\partial^4 \Phi}{\partial y^4} + 2\delta_1 \lambda^2 \frac{\partial^4 \Phi}{\partial x^2 \partial y^2} + \delta_2 \frac{\partial^4 \Phi}{\partial x^4} = \frac{\partial^4 (w - w_0)}{\partial x^4} \mu \gamma_1 \frac{\delta_1}{\delta_1} + \\ + \left(\frac{\partial^4 w}{\partial x \partial y} \right)^2 \lambda^2 - \lambda^2 \left(\frac{\partial^4 w}{\partial x \partial y} \right) + \frac{\partial^2 w}{\partial x^2} \frac{\partial^2 w}{\partial y^2} \lambda^2 - \\ - \frac{\partial^2 w_0}{\partial x^2} \frac{\partial^2 w_0}{\partial y^2} \lambda^2 - \frac{\partial^4 w}{\partial x^2 \partial y^2} \lambda^2 (\gamma_1 + \gamma_2) - \lambda^2 k_x^* \frac{\partial^2 (w - w_0)}{\partial y^2} - \\ - \lambda^2 k_y^* \frac{\partial^2 (w - w_0)}{\partial x^2} - \frac{\partial^4 (w - w_0)}{\partial y^4} \lambda^4 \mu \gamma_2 \frac{\delta_1}{\delta_1}. \quad (7.73)$$

The forces N_x , N_y , T are related to the dimensionless stress function as follows:

$$N_x = \frac{\partial^4 \Phi}{\partial y^4} \frac{Eh^3}{\delta_1^3}, \quad N_y = \frac{\partial^4 \Phi}{\partial x^4} \frac{Eh^3}{\delta_1^3}, \quad T = - \frac{\partial^2 \Phi}{\partial x \partial y} \frac{Eh^3}{\delta_1^3}.$$

In the above relations, we took:

$$x = \bar{x}/a, \quad \lambda = a/b, \quad w = \bar{w}/h, \\ \delta_1 = E/E_1, \quad \delta_2 = E/E_2, \quad 2\delta_3 = 2(1 + \mu) - \mu(\delta_1 + \delta_2), \\ k_x^* = \frac{k_x a^2}{h}, \quad k_x = \frac{1}{R_1}, \\ q^* = \frac{q}{E} \left(\frac{ab}{h^2} \right)^2 - \frac{1}{c_0^2} \frac{a^4}{h^2} \frac{\partial^2 w}{\partial t^2}, \quad D_1 = \frac{D + C_1}{Eh^3} \frac{\gamma_1}{\delta_1} (\gamma_1 - \mu^2 \gamma_2), \\ 2D_3 = 2 \frac{D + H}{Eh^3} - \mu \left[\frac{\gamma_1^2}{\delta_1} + \frac{\gamma_2^2}{\delta_2} - \left(\frac{1}{\delta_1} + \frac{1}{\delta_2} \right) \gamma_1 \gamma_2 \right], \\ c_0 = \sqrt{\frac{Eh}{\gamma}}, \quad \gamma = \gamma_0 \left(1 + \frac{F_1}{t_1 h} + \frac{F_2}{t_2 h} \right);$$

the expressions for y , k_y^* , k_y^* , D_2 will be written in similar fashion. The specific gravity of the shell material is denoted by γ_0 .

For ribs arranged symmetrically with respect to the middle surface, $\gamma_1 = \gamma_2 = 0$, and an ordinary system of equations for shells with structural anisotropy is obtained from (72), (73).

We will now turn to the solution of the problem of the buckling process of a shell. Let us assume that the additional and initial deflections are approximated by the expressions

$$\left. \begin{aligned} w_1 &= w - w_0 = \zeta_1 \sin n\pi x \sin ny + \zeta_2 \sin^2 n\pi x \sin^2 ny, \\ w_0 &= \zeta_{10} \sin n\pi x \sin ny + \zeta_{20} \sin^2 n\pi x \sin^2 ny. \end{aligned} \right\} \quad (7.74)$$

We now set up Lagrange equations of the type of (43)

$$\frac{d}{dt} \left(\frac{\partial T}{\partial q_I} \right) - \frac{\partial T}{\partial q_I} = - \frac{\partial \mathcal{S}}{\partial q_I}, \quad (7.75)$$

where as before, \mathcal{S} denotes the potential energy of the system.

The stress function Φ is determined from (73):

$$\begin{aligned} \Phi = & C_1 \sin ax \sin \beta y + C_2 \cos 2ax + C_3 \cos 2ax \cos 2\beta y + \\ & + C_4 \cos 2\beta y + C_5 \cos 4ax + C_6 \cos 4\beta y + C_7 \cos 4ax \cos 2\beta y + \\ & + C_8 \cos 2ax \cos 4\beta y + C_9 \sin 3ax \sin \beta y; \end{aligned} \quad (7.76)$$

where C_1, \dots, C_9 are certain coefficients dependent on the parameters of the system.

Equation (75) takes the form

$$\begin{aligned} \frac{d^2 \zeta_1}{dt^2} = & - \frac{2 \lambda^4 \pi^4}{c_1 \psi^2} [2M_1 (\zeta_1 (\zeta_1 + \zeta_{10}) (\zeta_1 + 2\zeta_{10}) + \\ & + \zeta_{20} (\zeta_{10}\zeta_2 - \zeta_1 \cdot \zeta_{20})) + M_{16} \zeta_1 \zeta_2 + M_5 \zeta_1 + \\ & + M_7 (\zeta_2 + \zeta_{20}) (\zeta_1 \zeta_{20} + \zeta_{10}\zeta_2 + \zeta_1 \zeta_2) + M_{66} \zeta_{20} + \frac{1}{2} M_9 \zeta_{10} \zeta_2], \end{aligned} \quad (7.77)$$

$$\begin{aligned} \frac{d^2 \zeta_2}{dt^2} = & - \frac{2 \lambda^4 \pi^4}{c_2 \psi^2} [2M_1 \zeta_{10} (\zeta_1 \zeta_{20} - \zeta_{10}\zeta_2) + \\ & + 2M_6 \zeta_2 (\zeta_2 + \zeta_{20}) (\zeta_2 + 2\zeta_{20}) + \frac{1}{2} M_1 \zeta_1^2 + \frac{1}{2} M_4 \zeta_2 (3\zeta_2 + 4\zeta_{20}) + M_6 \zeta_2 + \\ & + M_7 (\zeta_1 + \zeta_{10}) (\zeta_2 \zeta_{10} + \zeta_1 \zeta_{20} + \zeta_1 \zeta_2) + \frac{1}{2} M_9 \zeta_1 \zeta_{10}] - \frac{q^*(t) \lambda^2}{4}, \end{aligned} \quad (7.78)$$

where $\psi = \lambda/m^2$, M_1, \dots, M_9 are certain new parameters.

Equations (77), (78) were represented in finite differences and were integrated with the aid of the M-20 computer for the conditions

$$(\zeta_1)_0 = (\zeta_2)_0 = \left(\frac{d\zeta_1}{dt} \right)_0 = \left(\frac{d\zeta_2}{dt} \right)_0 = 0.$$

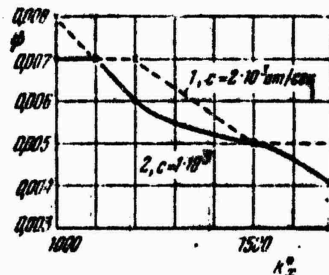


Figure 7.36. Effect of the curvature parameter on the behavior of a slightly curved reinforced panel. Key: 1) at/sec.

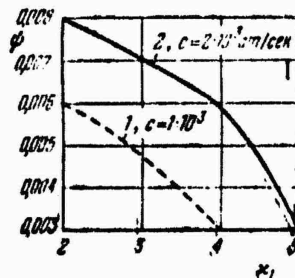


Figure 7.37. An increase in the rigidity of the reinforcing ribs causes an increase of the "critical" time.

For q , we took the expression ct , where c is the loading rate, assumed to be 1000 and 2000 at/sec. As an example, square sections ($\lambda = 1$) with dimensions $a = 6000$ mm and thickness $h = 3$ mm were considered. It was assumed that $E = 7.1 \times 10^5$ kg/cm², $\mu = 0.3$. The integration step was taken equal to 1×10^{-5} sec. The curvature parameters varied in the range 1000-1700. The dimensionless time parameter is denoted by t .

Calculations showed that the parameter $\theta = \lambda n/m$ has little effect on the critical time, and may be taken equal to unity; in other words, it may be assumed with a certain approximation that square waves are formed during buckling. Thus, the parameter $\psi = \lambda/m^2$ represents the wave formation shape during buckling.

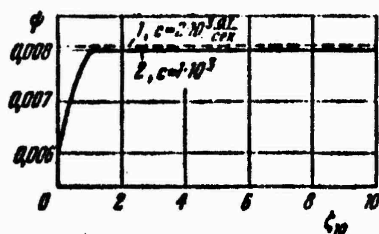


Figure 7.38. Effect of the amplitude of initial camber on the wave formation shape of a slightly curved panel.

Increasing the curvature parameter k_x^* (or k_y^*) leads to an increase in the number of half-waves (Figure 7.36). Increasing the parameter characterizing the rigidity of the reinforcing ribs is associated with a sharp decrease of ψ and increase of the "critical" time. This is evident from Figure 7.37.

The plots of Figures 7.38, 7.29 demonstrate the effect of the amplitude of initial camber on the wave formation shape. The shells considered were found to be more stable to the "unsymmetric" component of the initial camber. Thus, increasing the amplitude of the "symmetric" camber from 0.1 to 1 caused a decrease of the number m from 13 to 11; the same change in the amplitude of "unsymmetric" camber was associated with a decrease in the number of half-waves from 13 to 9 ($\psi = 0.012$).

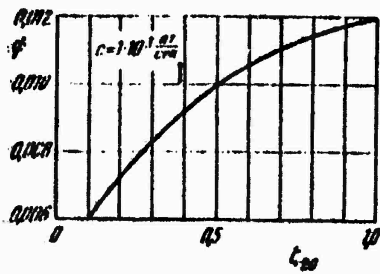


Figure 7.39. Effect of one of the parameters of initial camber on the behavior of a slightly curved panel. Key:
1) at/sec.

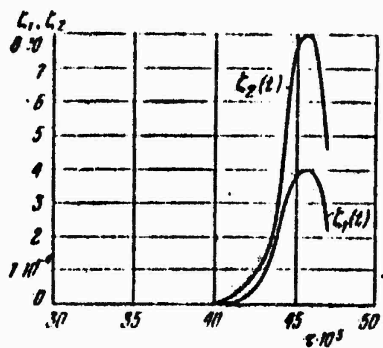


Figure 7.40. Change in wave formation parameters with time for a slightly curved panel.

It is interesting that according to the data of Figure 7.40, the shell has a tendency to bulge toward the center of curvature: the deflection component ξ_2 increases sharply much earlier than ξ_1 .

The results obtained in this paragraph are preliminary in character. It is desirable to analyze in more detail the effect of reinforcements and initial imperfections on the magnitude of the "critical" time and buckling shape.

§79. Cylindrical Shell Under Rapid Heating

Let us now turn to the problem of the behavior of a closed cylindrical isotropic shell subjected to a thermal action increasing rapidly with time.*

We will write the fundamental relations of thermal conductivity of nonlinear theory of shallow shells, taking into account the initial shape irregularities, and supplementing them with the inertial term corresponding to normal displacements:**

$$\begin{aligned} & \frac{1}{1-\mu^2} \left\{ M_3 N^4 (w - w_0) + 2 \frac{\partial M_2}{\partial x} \left[\frac{\partial^3 (w - w_0)}{\partial x^3} + \frac{\partial^3 (w - w_0)}{\partial x \partial y^2} \right] + \right. \\ & + 2 \frac{\partial M_3}{\partial y} \left[\frac{\partial^3 (w - w_0)}{\partial x^3} + \frac{\partial^3 (w - w_0)}{\partial x^2 \partial y} \right] + \left[\frac{\partial^2 M_3}{\partial x^2} \frac{\partial^2 (w - w_0)}{\partial x^2} + \right. \\ & + 2 \frac{\partial^2 M_3}{\partial x \partial y} \frac{\partial^2 (w - w_0)}{\partial x \partial y} + \left. \frac{\partial^2 M_3}{\partial y^2} \frac{\partial^2 (w - w_0)}{\partial y^2} \right] + \mu L [M_3, (w - w_0)] \} + \\ & = L(w, \Phi) + L(\Phi, M_2) + \frac{1}{R} \frac{\partial^2 \Phi}{\partial x^2} + \frac{1}{1-\mu} \frac{\partial^2}{\partial x^2} (N_0 M_2 - M_0) + \end{aligned} \quad (7.79)$$

$$\begin{aligned} & + \frac{1}{1-\mu} \frac{\partial^2}{\partial y^2} (N_0 M_2 - M_0) + q - \frac{Y}{k} \frac{\partial^2 (w - w_0)}{\partial t^2}, \\ & \frac{1}{D_0} V^2 \nabla^2 \Phi + 2 \frac{\partial M_1}{\partial x} \left(\frac{\partial^4 \Phi}{\partial x^3} + \frac{\partial^4 \Phi}{\partial x \partial y^2} \right) + 2 \frac{\partial M_1}{\partial y} \left(\frac{\partial^4 \Phi}{\partial y^3} + \frac{\partial^4 \Phi}{\partial x^2 \partial y} \right) + \\ & + \frac{\partial^2 \Phi}{\partial x^2} \frac{\partial^2 M_1}{\partial x^2} + 2 \frac{\partial^2 \Phi}{\partial x \partial y} \frac{\partial^2 M_1}{\partial x \partial y} + \frac{\partial^2 \Phi}{\partial y^2} \frac{\partial^2 M_1}{\partial y^2} - \mu L(\Phi, M_1) + \\ & + \frac{\partial^2}{\partial x^2} (M_1, N_0) + \frac{\partial^2}{\partial y^2} (M_1, N_0) = -\frac{1}{2} [L(w, w) - L(w_0, w_0)] + \\ & + \frac{\partial^2 (w - w_0)}{\partial y^2} \frac{\partial^2 M_1}{\partial x^2} + 2 \frac{\partial^2 M_2}{\partial x \partial y} \left(\frac{\partial^2 w}{\partial x \partial y} - \frac{\partial^2 w_0}{\partial x \partial y} \right) + \\ & + \frac{\partial^2 (w - w_0)}{\partial x^2} \left(\frac{\partial^2 M_2}{\partial y^2} - \frac{1}{R} \right), \end{aligned} \quad (7.80)$$

where M_1 , M_2 , etc. are determined with the aid of the expressions

$$\begin{aligned} M_1 &= \frac{1}{D_0}, \quad M_2 = \frac{D_1}{D_0}, \quad M_3 = \frac{D_1^2 - D_2 D_0}{D_0}, \\ N_0 &= \int_{-h/2}^{h/2} k^2 0^2 E^2 dz, \quad M_0 = \int_{-h/2}^{h/2} k^2 0^2 E^2 z dz; \end{aligned} \quad (7.81)$$

*This problem was solved by A.T. Ponomarev.

**See V.L. Bazhanov, I.I. Gol'denblat, N.L. Nikolayenko, and A.M. Sinyukov, Design of Structures Subjected to Thermal Action, Mischnostroyeniye, Moscow, 1969, p. 286.

where

$$D_0 = \int_{-h/2}^{h/2} E^z dz, \quad D_1 = \int_{-h/2}^{h/2} E^z z dz, \quad D_2 = \int_{-h/2}^{h/2} E^z z^2 dz;$$

E^z is the modulus of elasticity at a point with coordinate z , calculated for a given temperature, θ is the temperature, and k^z is the coefficient of linear expansion. We will assume further that the temperature, while remaining constant along the generatrix of the shell and in the circumferential direction, changes only along the thickness: $\theta = \theta(z)$. At the same time, the quantities D_0 , D_1 , D_2 , N_θ and M_θ will be constant: Eqs. (79) and (80) in the case of $q = 0$ will take the form

$$-\frac{M_1}{1-\mu^2} \nabla^2 \nabla^2 (w - w_0) = L(\Phi, w) + \frac{1}{R} \frac{\partial^2 \Phi}{\partial x^2} - \frac{1}{g} \frac{\partial^2 (w - w_0)}{\partial t^2}, \quad (7.82)$$

$$M_1 \nabla^2 \nabla^2 \Phi = -\frac{1}{2} [L(w, w) - L(w_0, w_0)] - \frac{1}{R} \frac{\partial^2 (w - w_0)}{\partial x^2}. \quad (7.83)$$

As an example, let us examine the behavior of a shell hinged on supports immovable in the longitudinal direction; the shell is heated nonuniformly along its thickness by a heat flow changing rapidly with time. In addition, we will assume that the points of the shell ends move freely in the radial direction.

As before, we will choose the expressions for the complete and initial deflections in the form of (40) and (41). Substituting them into Eq. (83), we will determine the function Φ as usual:

$$\begin{aligned} \Phi = & D_0 (K_1 \cos 2ax + K_2 \cos 2by + K_3 \sin ax \sin by + \\ & + K_4 \sin 3ax \sin by) + \frac{N_\theta \theta^2}{2}, \end{aligned} \quad (7.84)$$

where $N_x^0 = -p$ is the equivalent compressive force, determinable from the adopted condition

$$e = \frac{1}{L} \int_0^L \frac{\partial u}{\partial x} dx = 0. \quad (7.85)$$

The coefficients $K_1 - K_4$ are determined as was done in §70.

Using Lagrange equations of the type of (75), we will set up the basic relationships between the deflection parameters and the time-dependent equivalent compressive forces. We introduce the notation

$$\begin{aligned} \bar{N}_0 &= \frac{N_0}{D_0} \frac{R}{h}, \quad \bar{N}_x^0 = \frac{N_x^0}{D_0} \frac{R}{h}, \quad \eta = \frac{n^2 h}{R}, \\ \zeta_1 &= \frac{L - l_0}{h}, \quad \zeta_{10} = \frac{l_0}{h}, \quad \zeta_2 = \zeta_1 \psi, \quad \xi = \frac{m \pi R}{n L}, \end{aligned}$$

We now write the expression for the total energy of the system:

$$E = U_m + U_b - W \quad (7.86)$$

where U_m is the strain energy of the middle surface; U_b is the potential energy of bending, and W is the work done by the external forces. The components U_m , U_b and W are found from the expressions

$$\begin{aligned} U_e &= \frac{M_1}{2} \int_0^L \int_0^{2\pi R} \left\{ \left(\frac{\partial^2 \Phi}{\partial y^2} + \frac{\partial^2 \Phi}{\partial x^2} \right)^2 + 2(1+\mu) \left[\left(\frac{\partial^2 \Phi}{\partial x \partial y} \right)^2 - \right. \right. \\ &\quad \left. \left. - \frac{\partial^4 \Phi}{\partial y^4} \frac{\partial^2 \Phi}{\partial x^2} \right] \right\} dx dy + \frac{N_0}{D_0} \int_0^L \int_0^{2\pi R} \left(\frac{\partial^2 \Phi}{\partial y^2} + \frac{\partial^2 \Phi}{\partial x^2} \right) dx dy, \end{aligned} \quad (7.87)$$

$$\begin{aligned}
U_1 = & -\frac{M_1}{2(1-\mu^2)} \int_0^{L/2\pi R} \int_0^{L/2\pi R} \left\{ \left(\frac{\partial^2 w}{\partial x^2} + \frac{\partial^2 w}{\partial y^2} \right)^2 + \right. \\
& \left. + 2(1-\mu) \left[\left(\frac{\partial^2 w}{\partial x \partial y} \right)^2 - \frac{\partial^2 w}{\partial x^2} \frac{\partial^2 w}{\partial y^2} \right] \right\} dx dy - \\
& - M_1 \int_0^{L/2\pi R} \int_0^{L/2\pi R} \left(\frac{\partial^2 \Phi}{\partial y^2} \frac{\partial^2 w}{\partial x^2} + \frac{\partial^2 \Phi}{\partial x^2} \frac{\partial^2 w}{\partial y^2} + 2 \frac{\partial^2 \Phi}{\partial x \partial y} \frac{\partial^2 w}{\partial x \partial y} \right) dx dy - \\
& - \frac{M_1 N_0}{(1-\mu)} \int_0^{L/2\pi R} \int_0^{L/2\pi R} \left(\frac{\partial^2 w}{\partial x^2} + \frac{\partial^2 w}{\partial y^2} \right) dx dy - \\
& - \frac{M_0}{1-\mu} \int_0^{L/2\pi R} \int_0^{L/2\pi R} \left(\frac{\partial^2 w}{\partial x^2} + \frac{\partial^2 w}{\partial y^2} \right) dx dy, \tag{7.88}
\end{aligned}$$

$$W = -N_0 M_1 \int_0^{L/2\pi R} \int_0^{L/2\pi R} \left(\frac{\partial^2 \Phi}{\partial y^2} \right)_{x=0, L} dx dy. \tag{7.89}$$

Then, considering the symbols introduced, the equations in dimensionless form will be written as

$$\begin{aligned}
Q_1 = & -\frac{M_1}{1-\mu^2} \eta_1^2 \frac{(k^2+1)^2}{\xi_1^2} + \frac{1}{16} \eta_1^2 (\zeta_1 + 2\zeta_0) (\zeta_1 + \zeta_0) \frac{k^4+1}{\xi_1^4} + \\
& + \zeta_1 \frac{k^2}{\eta_1(k^2+1)} - \zeta_1 (\zeta_1 + \zeta_0) \left[1 + \frac{8\zeta_0^2}{(1+\xi_1^2)^2} \right] - \\
& - N_0 \frac{1}{\xi_1^2} (\zeta_1^2 + \zeta_0 \zeta_1^2 - 2\zeta_0 \zeta_1^2) + \eta_1^2 \zeta_0^2 (\zeta_1 + 2\zeta_0) \left[\frac{1}{(\eta_1^2+1)} + \frac{1}{(k^2+1)^2} \right] + \\
& + \frac{1}{8} \eta_1^2 (\zeta_1^2 + 2\zeta_0^2) \left(\zeta_1 + 3\zeta_0 + 2 \frac{\zeta_0^2}{\xi_1^2} - 2 \frac{\zeta_1 \zeta_0^2}{\xi_1^2} - 4 \frac{\zeta_0^2 \zeta_1^2}{\xi_1^4} \right), \tag{7.90}
\end{aligned}$$

$$\begin{aligned}
Q_2 = & -\frac{4M_1}{1-\mu^2} \eta_1^2 \zeta_0 + \frac{1}{2} \eta_1^2 \zeta_0 (\zeta_1 + 2\zeta_0)^2 \left[\frac{1}{(1+\xi_1^2)^2} + \frac{1}{(k^2+1)^2} \right] + \\
& + \frac{1}{4} \frac{\zeta_1}{\xi_1^2} - \frac{\zeta_1 (\zeta_1 + 2\zeta_0)}{16\eta_1^2} \left[1 + \frac{\eta_1^2}{(1+\xi_1^2)^2} \right] - N_0 \frac{(\zeta_1 + 2\zeta_0)}{\xi_1^2} \zeta_0 + \\
& + \frac{1}{8} \eta_1^2 \frac{2(\zeta_1 + 2\zeta_0)^2}{\xi_1^2} (\zeta_1^2 + 2\zeta_0^2) \zeta_0, \tag{7.91}
\end{aligned}$$

We now represent the dependence for the additional deflection in dimensionless form

$$\psi - \psi_0 = \zeta_1 \sin \alpha x \sin \beta y + \zeta_2 \sin^2 \alpha x + \lambda, \tag{7.92}$$

where

$$\lambda = \frac{(1-f_0)\varphi}{h} - \zeta_1 \varphi.$$

Using a shell closure condition of the type of (22a), we find the deflection parameter λ

$$\lambda = -\mu \bar{N}_x^0 - \frac{1}{2} \zeta_2 + \frac{1}{8} \eta \dot{\zeta}_1 (\zeta_1 + 2\zeta_0). \quad (7.93)$$

Introducing relation (92) with the consideration of (93) in (44), we obtain a dimensionless expression for the kinetic energy

$$\begin{aligned} \bar{T} = & \frac{M_1}{2} \frac{v}{R^2} \left[\frac{1}{2} \dot{\zeta}_1^2 + \frac{1}{4} \dot{\zeta}_2^2 + \frac{1}{8} \eta^2 \dot{\zeta}_1^2 (\zeta_1 + \zeta_0)^2 + \right. \\ & \left. + \frac{1}{2} \mu \bar{N}_x^0 - \mu \bar{N}_x^0 \eta \dot{\zeta}_1 (\zeta_1 + \zeta_0) \right], \end{aligned} \quad (7.94)$$

where

$$\bar{T} = \frac{RM_1}{\pi L h^3} T;$$

as usual, the dots over the letters denote derivatives with respect to time. We now write the first Lagrange equation in the form

$$\begin{aligned} \ddot{\zeta}_1 + & \frac{\eta^2 (\zeta_1 + \zeta_0)}{1 + \frac{1}{4} \eta^2 (\zeta_1 + \zeta_0)^2} (\dot{\zeta}_1)^2 - S \left\{ \bar{N}_0 \frac{1}{\zeta_1^2} (\zeta_1^2 + \zeta_0 \dot{\zeta}_1^2 + 2\zeta_0 \dot{\zeta}_2^2) + \right. \\ & + \frac{M_1}{1 - \mu^2} \eta \frac{(\xi^2 + 1)^2}{\xi^2} - \frac{1}{16} \frac{(\xi^2 + 1)}{\xi^2} \eta \dot{\zeta}_1 (\xi_1^2 + 3\zeta_0 \dot{\zeta}_1^2 + 2\dot{\zeta}_0^2) - \\ & - \eta \dot{\zeta}_1^2 \dot{\zeta}_2 (\zeta_1 + 2\zeta_0) \left[\frac{1}{(\xi_1^2 + 1)^2} + \frac{1}{(\xi_1^2 + 1)^2} \right] + \frac{1}{(\xi_1^2 + 1)^2} \frac{\dot{\zeta}_1}{\eta} + \\ & + \frac{1}{4\xi^2} \dot{\zeta}_2 (\zeta_1 + \zeta_0) \left[1 + \frac{\dot{\zeta}_1^2}{(\xi_1^2 + 1)^2} \right] - \\ & \left. - \frac{1}{8} \eta \dot{\zeta}_1^2 \left[(\zeta_1 - 2\zeta_0) (\zeta_1 + 2\zeta_0) - \frac{\zeta_0}{\zeta_1^2} \right] \right\} = 0. \end{aligned} \quad (7.95)$$

Here the following parameters are used:

$$\tau = \frac{xl}{h^2}, \quad s = \left(\frac{c}{\pi R} \right)^2 \frac{2h^4}{\left[1 + \frac{1}{4} \eta^2 (\zeta_1 + \zeta_0)^2 \right]},$$

where χ is the thermal diffusivity, and c is the velocity of propagation of sound in the material. We will assume that to a first approximation, the parameter ζ_2 in Eq. (95) will be the same for a dynamic process as for a static process in the case of an ideal shell ($\zeta_0 = 0$) and will be found from the relation

$$\text{where } \zeta_2 = -\frac{L_1 \zeta_1^2}{L_1 + L_2 \zeta_1^2}, \quad (7.96)$$

$$L_1 = \frac{\zeta_1}{10\xi^2} \left[1 + \frac{8\xi^4}{(\xi^2 + 1)^2} \right],$$

$$L_2 = \frac{1}{10} \frac{(\xi^2 + 1)}{\xi^2} \eta - \frac{1}{2} \eta \nu^2 \left[\frac{1}{(9\xi^2 + 1)^2} + \frac{1}{(\xi^2 + 1)^2} \right],$$

$$L_3 = -\frac{M_1 \eta}{(1 - \mu^2)} \frac{(\xi^2 + 1)^2}{\xi^2} + \frac{\xi^2}{(\xi^2 + 1)^2} \eta + 4 \frac{M_1}{1 - \mu^2} \eta \xi^2 - \frac{1}{10\xi^2}.$$

We have again arrived at the ordinary nonlinear second order differential equation (95), which relates the deflection parameters ζ_1 , ζ_2 , thermal stress \bar{N}_θ and time t . To find the dependence $\zeta_1 = \zeta_1(t)$, it is also necessary to find the change in thermal stress with time $\bar{N}_\theta = \bar{N}_\theta(t)$ with the aid of formula (81). For this purpose, to supplement expression (95), it is necessary to solve a thermal problem.

Since the shell is considered to be thin-walled and is subjected to the uniform action of a heat flow, we will hereinafter neglect the propagation of heat in the one-dimensional formulation. Then the heat conduction equation will be written in the form ([0.6], p. 309)

$$\frac{\partial \theta}{\partial t} = \chi \frac{\partial^2 \theta}{\partial z^2}; \quad (7.97)$$

it will be integrated for the following boundary and initial conditions:

$$\frac{\partial \theta}{\partial z} = 0, \quad \left(z = \frac{h}{2} \right), \quad \frac{\partial \theta}{\partial z} = \text{const} \quad \left(z = -\frac{h}{2} \right), \quad t > 0,$$

$$\theta = 0 \quad \text{for} \quad t = 0.$$

To find the temperature field along the shell thickness, a known solution was employed. The integration of relation (95) was carried out by means of the method of finite differences for the initial conditions

$$\zeta_1 - \zeta_0 = \dot{\zeta}_1 = 0 \text{ for } \tau = 0.$$

It was assumed that the temperature along the shell thickness is distributed in accordance with the linear law

$$\theta = a_0 - b_0 z,$$

where $a_0 = \frac{\theta_1 + \theta_2}{2}$, $b_0 = \frac{\theta_1 - \theta_2}{h}$.

Here θ_1 and θ_2 denote the temperature of the outer and inner surface, respectively. The modulus of elasticity will also be a function of the coordinate z :

$$E^z = a_E z + b_E z,$$

where $a_E z = a_E - b_E a_0$, $b_E z = b_E b_0$. For example, for D16T Duralumin, we can assume that

$$a_E = 7,29 \cdot 10^5 \text{ kg/cm}^2, b_E = 551 \text{ kg/cm}^2 \text{ }^\circ\text{C}.$$

The same type of dependence will be written for the coefficient of linear expansion k :

$$k = a_k + b_k z,$$

We then have $k^z = a_k z + b_k z$, $a_k z = a_k + a_0 b_k$.

The reduced thermal rigidity of a shell heated nonuniformly along the thickness has the form

$$\frac{D_2 D_0 - D_1^2}{(1 - \mu^2) D_0} = \frac{h^3 (12\alpha_E^2 s - b_g^2 h^2)}{144\alpha_g^2 (1 - \mu^2)}.$$

The calculations were carried out by using the example of Duralumin shells for various combinations of the geometric characteristics and heat flow parameters, for an initial deflection $\zeta_0 = 0.001$. For different parameters, ζ_1 was calculated, and the temperature distribution over the shell thickness was determined for an argument step Δt equal to 0.01. Then the values of ξ and n were found, for which the deflection front corresponded to the lowest value of t , and the coefficient of thermal overload K_d was determined equal to

$$K_d = \frac{N_0}{(N_{\theta_u})_{\min}}.$$

N_{θ_u} stands for the upper thermal critical static stress corresponding to the smallest wave number n for a given ξ .

In Figure 7.41, three groups of $\zeta_1(t)$ curves for different heat fluxes are shown for $R/h = 180$. Analysis of the data of Figure 7.41 shows that the most probable buckling shape of the shell, for example for $q = 2 \text{ kcal/cm}^2 \text{ sec}$, will correspond to wave number $n = 12$ instead of $n = 10$ for static loading. Figure 7.42 reflects the relationship between K_d and the ratio h/R for different $q(t)$. We see that the dynamic effect is manifested most clearly in the case of thinner shells.

§80. Plastic Flow in Dynamic Buckling of a Shell

Thus far, we have assumed that the buckling of shells takes place in the range of elastic deformation of the material. However, in many cases, the buckling of a shell is associated with the appearance of plastic strains. We will assume that plastic deformation is predominant in the buckling process, so that the elastic

component may be considered negligibly small in comparison with the plastic component. Thus, we can use a model similar to that of a plastic-rigid material; we

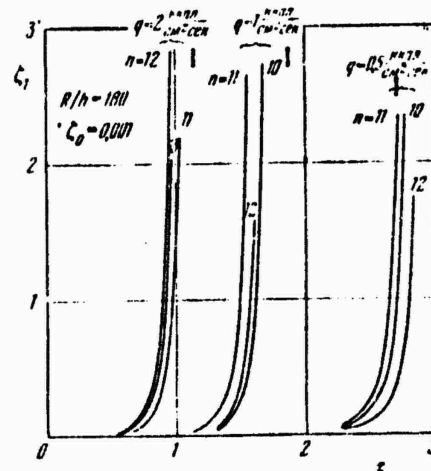


Figure 7.41. "Deflection-time" diagrams for a cylindrical shell subjected to various heat flows.
Key: 1) $\text{kcal}/\text{cm}^2 \text{ sec.}$

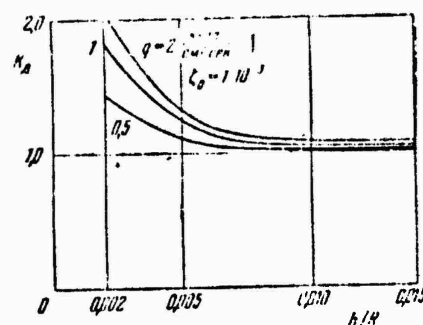


Figure 7.42. Effect of relative shell thickness in rapid heating on values of the dynamic coefficient. Key: 1) $\text{kcal}/\text{cm}^2 \text{ sec.}$

will assume the presence of hardening in the course of plastic flow. In such a treatment, it is suggested that the usual $\sigma(\epsilon)$ diagram of type I (Figure 7.43) be replaced by a line of form 2. On the plastic segment, the dependence is determined

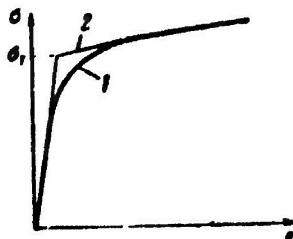


Figure 7.43. Stress-strain diagram used as the basis of the study.

by the tangent modulus E_t .

Let us consider a circular cylindrical shell, to all the elements of which are communicated appreciable radial velocities.* The shell length is considered to be so large that it is possible to confine the study to the motion of a ring of unit width.

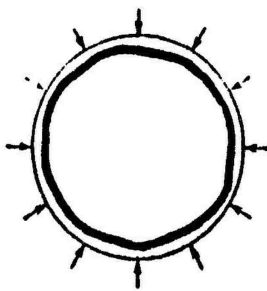


Figure 7.44. Character of plastic buckling of a ring shell.

The deformation process of such a ring shell can be divided into preliminary axisymmetric deformation and subsequent buckling, as shown in Figure 7.44. We will

*This problem was studied by Abrahamsen and Goodier [7.26], Goodier and McIvor [7.37], Lindberg [7.46], Stuiver [7.55], and others.

assume accordingly that membrane plastic flow predominates at the start of the motion, and therefore small bending strains will be proportional to the tangent modulus. The bending moment

$$M = E_k I x,$$

where x denotes the change of curvature (see [0.6], p. 507):

$$x = \frac{1}{R^2} \left(\frac{\partial^2 w}{\partial \theta^2} + w \right). \quad (7.98)$$

The moment of inertia of the cross section is denoted by $I = h^3/12$; θ is the angular coordinate. Considering a ring element (Figure 7.45), we obtain

$$Q = \frac{\partial M}{\partial y},$$

where Q is the transverse force and dy is an arc element.

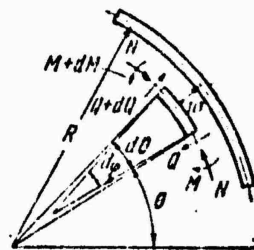


Figure 7.45. Forces applied to a ring element.

The equation describing the transverse displacement will be

$$\frac{\partial Q}{\partial y} + N \frac{\partial w}{\partial \theta} = p - \frac{y}{h} h \frac{\partial^2 w}{\partial \theta^2}, \quad (7.99)$$

where $\partial\phi/\partial y$ denotes the variable curvature

$$\frac{\partial p}{\partial y} = \frac{1}{R} + \kappa; \quad (7.100)$$

p is the pressure intensity, and $N = \sigma_y h$ is the circumferential membrane force. Substituting (100) into (99) and excluding Q and M with the aid of the preceding relations, we arrive at the equation

$$\begin{aligned} \frac{E_k I}{R^4} \left(\frac{\partial^4 w}{\partial \theta^4} + \frac{\partial^2 w}{\partial \theta^2} \right) + N \left[\frac{1}{R} + \frac{1}{R^2} \left(\frac{\partial^2 w}{\partial \theta^2} + w \right) \right] = \\ = p - \frac{\gamma}{g} h \frac{\partial^2 w}{\partial \theta^2}. \end{aligned} \quad (7.101)$$

Introducing the dimensionless parameters

$$\left. \begin{aligned} w^* &= \frac{w}{R}, \\ \tau &= \sqrt{\frac{E_k I g}{h \gamma R^4}} t = \frac{1}{V^{1/2}} \sqrt{\frac{E_k g}{\gamma}} \frac{h}{R^2} t = \frac{1}{V^{1/2}} \frac{c h}{R^2} t, \\ s^* &= -\frac{N R^2}{E_k I} = 12 \frac{N R^2}{E_k h^3} = 12 \frac{\sigma}{E_k} \left(\frac{R}{h} \right)^2, \\ \left(c = \sqrt{\frac{E_k g}{\gamma}}, \quad \sigma = \frac{N}{h} \right), \end{aligned} \right\} \quad (7.102)$$

we arrive at the following equation at $p = 0$ (the asterisk of w is omitted)

$$\frac{\partial^2 w}{\partial \tau^2} + \frac{\partial^4 w}{\partial \theta^4} + (s^2 + 1) \frac{\partial^2 w}{\partial \theta^2} + s^2 (w + 1) = 0. \quad (7.103)$$

This equation pertains to an ideal ring; the effect of initial imperfections will not be considered here.

Let us assume that certain initial radial velocities close to v_0 are communicated to all points of the ring. We will specify their magnitude by means of the series

$$\left(\frac{\partial w}{\partial \theta} \right)_{\theta=0} = v_0 \left[1 + \sum_{n=2}^{\infty} (\alpha_n \cos n\theta + \beta_n \sin n\theta) \right]. \quad (7.104)$$

where

$$v_0 = V_0 \frac{R}{h} \sqrt{\frac{12\gamma}{\pi E_k}}. \quad (7.104a)$$

The solution of Eq. (103) for initial conditions (104) will be written as

$$w = w_1(\tau) + w_2(\tau, 0); \quad (7.105)$$

where

$$w_1(\tau) = -1 + \cos s\tau + \frac{v_0}{s} \sin s\tau, \quad (7.106)$$

$$w_2(\tau, 0) = v_0 \sum_{n=2}^{n=r} (\alpha_n \cos n\theta + \beta_n \sin n\theta) \frac{\sin p_n \tau}{p_n} + \\ + v_0 \sum_{n=r+1}^{\infty} (\alpha_n \cos n\theta + \beta_n \sin n\theta) \frac{\sin p_n \tau}{p_n}. \quad (7.107)$$

The largest number smaller than s is denoted by r :

$$\text{for } n \leq r \quad p_n^2 = (n^2 - 1)(s^2 - n^2), \\ \text{for } n \geq r + 1 \quad p_n^2 = (n^2 - 1)(n^2 - s^2).$$

Let us note that Eq. (103) does not take into account the change of the circumferential force in the course of compression of the ring (see [0.6], p. 164).

The first term of solution (105) defines the axisymmetric deformation of the ring at any instant of time. If the initial velocities at any point of the ring were the same, the strains of the ring would be axisymmetric and would be determined from Eq. (106). According to Eq. (106), the process of compression of the ring continues until the instant of time given by the smallest root of the equation

$$\tau = \frac{1}{s} \operatorname{arctg} \frac{v_0}{s}. \quad (7.108)$$

The second term of (108) characterizes the magnitude of expected deviations from the circular shape of the ring. The possibility of formation of appreciable waves is related to the fact that the terms of the first line of Eq. (107) include the hyperbolic functions $\sinh p_n t$, which reach large values in the range of duration of deformation of the ring.

However, the harmonic functions $\sin p_n t$ entering into the terms of the second line of expression (107) had no appreciable influence on the growth of the waves. It may be assumed, therefore, that

$$w_2(\tau, \theta) \approx v_0 \sum_{n=1}^{n=\infty} (\alpha_n \cos n\theta + \beta_n \sin n\theta) \frac{\sin p_n \tau}{p_n}, \quad (7.109)$$

If the initial velocity v_0 and the law of its deviation from uniformity according to (104) are known, then for any instant of time one can find from (106) the magnitude of axisymmetric strains w_1 , and from Eqs. (107) or (109), the magnitude w_2 of the expected deviations of the cross section from circular shape.

If the limiting strain of the ring is given

$$s = \frac{R_0 - R}{R_0} = w_1,$$

by comparing expressions (106) and (108), one can find the minimum initial velocity necessary to achieve this strain

$$v_0 = s \sqrt{w_1^2 + 2w_1} = s \sqrt{\left(\frac{R}{R_0}\right)^2 - 4 \frac{R}{R_0} + 3}. \quad (7.110)$$

If however the character of the distribution of initial velocities according to (104) is also known, then by substituting the values of v_0 and t obtained from (108) and (110) into Eq. (107) or (109), one can determine the expected deviations

of the ring from the circular shape after its compression at the minimum initial velocity required (to obtain a given strain).

Let us consider the effect of a change in the initial velocity on the magnitude of the limiting axisymmetric strain. Using (106) and (109), we write the ratio $w_1(t)/w_2(t, 0)$ in the form

$$\frac{w_1(\tau)}{w_2(\tau, 0)} = \frac{\frac{1}{v_0} (\cos s\tau - 1) + \frac{1}{s} \sin s\tau}{\sum_{n=1}^{\infty} (\alpha_n \cos n\theta + \beta_n \sin n\theta) \frac{\sin p_n \tau}{p_n}}. \quad (7.111)$$

Since the product $s\tau$ is always smaller than $\pi/2$, then $0 < \cos s\tau < 1$, and $\frac{1}{s} \sin s\tau > 0$. Consequently, the numerator of expression (111) and hence the ratio $\frac{w_1(t)}{w_2(t, 0)}$ increase with rising v_0 .

This means that a given permissible deviation of the cross section from circular shape, $w_{2, \text{perm}}$, is associated with a greater maximum degree of axisymmetric deformation $w_{1, \text{perm}}$ the higher the initial velocity. As the initial velocity v_0 rises, $w_1(t)$ and $w_2(t, 0)$ increase. However, the growth of the function $w_1(r)$ is faster than that of the deflection amplitude $w_2(t, 0)$.

§81. Analysis of the Process of Plastic Buckling. Experimental Results

The pattern of plastic buckling described in the preceding paragraph pertains to the case in which the deformation of axisymmetric compression of a shell ring is appreciable and in the 6-8% range.

Let us note that we are dealing with a shell to all of whose points are communicated certain initial radial velocities differing little from the given value of v_0 . It is necessary to determine the limiting displacement $w_{1,\text{lim}}$ for which the axisymmetric form of the motion becomes unsymmetric, with the formation of many dents. The determination of the limiting strain of a ring shell may be carried out in the following

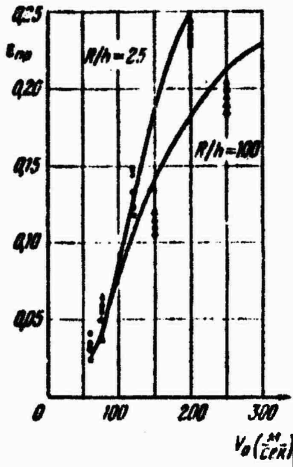


Figure 7.46. Diagrams for limiting strain as a function of radial velocity. Comparison of theoretical (solid lines) and experimental data. Key: 1) m/sec.

sequence.*

We first find the total time of compression of the ring from (108). This value can be adopted as a first approximation, and will be denoted by t_1 . Then, from (109) we find the peak value of w_2 corresponding to the instant of time t_1 and the given initial velocity. If w_2 is below the given value of w_2 , lim, the limiting strain is calculated directly. Otherwise, we take a second approximation $t_2 < t_1$ and repeat the calculations. To determine the value of t for which $w_2 \approx w_2$, lim, four to five approximations are usually sufficient.

Figure 7.46 shows two curves for the limiting strain ϵ_{lim} as functions of V_0 , found by the above described method for $R/h = 100$ and 25 . The following values of the basic parameters were taken (for D16 Duralumin): $\sigma_y = 1500 \text{ kg/cm}^2$, $E_f = 8 \times 10^4 \text{ kg/cm}^2$,

*This approach to the solution of the problem was proposed by A.I. Gorokhovich. The experimental data given below are also due to him.

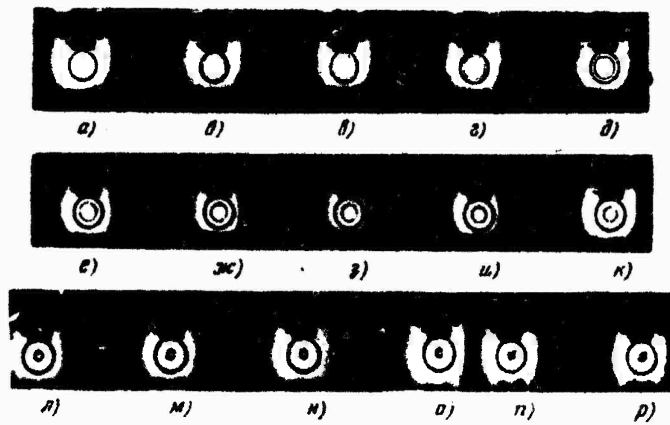


Figure 7.47. High-speed motion picture frames of the process of plasto-elastic buckling.

The law of deviation of the velocities of the individual points from the fundamental velocity was taken in the form

$$\left(\frac{\partial w}{\partial r} \right)_{r=0} = v_0 \left(1 + \frac{0.8}{\pi^3} \sum_{n=1}^{\infty} \frac{1}{n^3} \sin n\theta \right) \quad (7.112)$$

with a maximum deviation of $\pm 2.5\%$.

The same Figure 7.47 shows the experimental points for models of the same material. The experiments were conducted on a device for stamping the articles with a pulsed magnetic field. In such devices, the pressure acting on the blank is 1000-4000 kg/cm². The time of action of an external pressure pulse is measured in tens of microseconds. The experiments were carried out on rings having the following dimensions: R = 37 mm, h = 1.5 mm and R = 50 mm, h = 1 mm.

In Figure 7.46, the points pertain to the ratio R/h = 25, and the triangles, to the ratio R/h = 100. The solid lines correspond to the theoretical solution. We see that the agreement of the theoretical and experimental data is satisfactory.

Of interest are the results of high-speed motion-picture photography. Figure

7.47 a)-e) shows frames corresponding to the first stage of deformation, i.e., axisymmetric compression of the ring. Frames f)-g) reflect the second stage of wave formation and the process of increase in their amplitude. Finally, in frames k)-p), only the third stage, i.e., failure of the rings, can be observed.

Chapter VIII

Behavior of Shells Under Impact

§82. Characteristics of the Problem of the Behavior of Shells under Impact Loading

We will turn our attention to a second class of problems pertaining to dynamic buckling of thin-walled structures. As was stated in Chapter VI, we will consider here the wave character of the propagation of deformations.

Such problems are formulated most clearly when a structure of elongated outline is subjected to longitudinal impact. It is true that in the operation of structures containing shells, this type of loading occurs rather infrequently in pure form. However, its study is of practical importance for the following reasons. Under sharp overloads, massive structural elements fastened to the shell exert close-to-impact loads on the latter. In addition, in model experiments, dynamic longitudinal loading is most simply achieved precisely in the form of impact. For this reason, a study of the characteristics of shell behavior during impact is necessary in order to permit one to set up the experiments correctly.

Finally, the study of impact is very interesting from a theoretical standpoint, since the dynamic character of the deformation process, which may be described by a minimum number of parameters, is most clearly manifested in this case.

Longitudinal impact with a high deformation rate is associated with a number of complex physical phenomena: manifestation of the rheological properties of the material, temperature and chemical changes, etc. Detailed information on the physical aspect of impact processes is given

Goldsmith's monograph [8.16]. In addition, in the immediate vicinity of the end, the stressed state is essentially three-dimensional. Therefore, it is necessary to specify at the very outset precisely what aspects of the phenomenon will be subsequently studied.

To begin with, considering that the velocities of longitudinal impact to which shells in structures may be subjected, for example in flying vehicles, are relatively low, it is permissible to use the model of an elastic or elastoplastic body that is not sensitive to the deformation rate. Moreover, local effects related to the three-dimensionality of the stressed state will be neglected. In this formulation, the impact is determined by imparting a certain velocity to one of the ends of the bar or shell and by the ratio of the masses of the shell and load.

Thus, the cases of impact which will be examined in this chapter differ substantially from those arising, for example, in the study of the puncture problem, where the above-mentioned physical effects and considerations of the structure of the material are decisive.

As examples of sharp loading pertaining to the structures of flying vehicles, we can cite the action of a pressure wave, impact on landing, the mutual influence of fastened members in short-term overloads, etc. In regard to ship structures, the action of pressure waves, collision with a hard barrier, etc. are also possible. Analogous examples can also be given for shells of ground transportation structures.

Some general principles characteristic of impact problems in the formulation adopted below will be presented by using the simplest example of longitudinal deformation of an elastic bar subjected to impact loading.

§83. Bar under Longitudinal Impact

We will cite the elementary relationships pertaining to the dynamics of ideal bars under longitudinal impact. Let us consider a bar whose one end is fixed, and whose other end is subjected to collision with an absolutely hard body of mass m moving at velocity U until it hits the bar. Assuming that the bar and load touch along parallel planes and neglecting local deformations at the site of contact, we will study the change of compressive stresses in the bar during impact up to the time of separation of the load from the bar.

The differential equation for the displacements of the bar along the x axis (Figure 8.1) has the form

$$\frac{\partial^2 u}{\partial x^2} = \frac{1}{c^2} \frac{\partial^2 u}{\partial t^2}, \quad (8.1)$$

where

$$c = \sqrt{\frac{Eg}{\gamma}}.$$

The solution of this equation must satisfy the conditions

$$\left. \begin{array}{l} u(x, 0) = 0, \quad \frac{\partial u}{\partial t}(x, 0) = U \text{ for } x = 0, \quad \frac{\partial u}{\partial t} = 0 \text{ for } x > 0, \\ \frac{\partial^2 u}{\partial t^2}(0, t) = \frac{c^2}{m} \frac{\partial u}{\partial x}(0, t), \quad u(l, t) = 0. \end{array} \right\} \quad (8.2)$$

Here x is the ratio of the mass of the load to the mass of the bar. The time is measured from the instant of impact. It is known that the solution of Eq. (1) may be taken in the form

$$u(x, t) = f_1(ct - x) + f_2(ct + x), \quad (8.3)$$

where f_1 and f_2 are arbitrary twice differentiable functions of their arguments. This solution gets a clear interpretation if one assumes that the instrument recording the displacements and strains determined by function f_1 moves at velocity c from the movable to the clamped edge. In

this case, at the points where the instrument is located, $x=ct$, $f_1=\text{const}$; for this reason, the readings of the instrument will not change. Consequently, f_1 determines the deformation wave propagating in the bar in the direction from the point of impact to the fixed end, and c is the propagation velocity of the wave front, which from the standpoing of acoustics is the velocity of sound in the bar. The meaning of the function f_2 , which represents a wave reflected from the immovable edge, is established in the same manner. The local velocity of the bar particles and the strain are determined by the derivatives

$$\left. \begin{aligned} v &= \frac{\partial u}{\partial t} = c f'_1(ct-x) + c f'_2(ct+x), \\ e &= \frac{\partial u}{\partial x} = -f'_1(ct-x) + f'_2(ct+x); \end{aligned} \right\} \quad (8.4)$$

where the primes denote differentiation with respect to the arguments within the parentheses.

Let us consider the initial deformation period $0 < t < 1/c$. Setting $f_2 = 0$ and $x = 0$, we obtain an equation for determining the displacements of the loaded end

$$f''_1(t') + \frac{1}{M} f'_1(t') = 0, \quad \text{where } t' = ct. \quad (8.5)$$

Using the boundary conditions, we obtain the following expressions for the velocity of the movable end of the bar and the corresponding strain:

$$\left. \begin{aligned} v(0, t) &= \frac{\partial u(0, t)}{\partial t} = U e^{-t'/ct}, \\ e(0, t) &= -\frac{U}{c} e^{-t'/ct}. \end{aligned} \right\} \quad (8.6)$$

It follows that at the instant of impact, the bar element adjacent to the end subjected to impact receives a strain equal to the ratio of the local velocity of the upper point of the bar to the velocity of sound in the latter.

The displacement of the extreme point of the bar is determined by the relation

$$u(0, t) = U \frac{w}{c} (1 - e^{-t/c}). \quad (8.7)$$

If the mass of the load substantially exceeds the mass of the bar and one can assume $x = \infty$, then for $U = \text{const}$, from (6) there is obtained

$$u(0, t) = Ut.$$

In order to switch to the period of time $1 < ct < 2l$, it is necessary to use the function f_2 and the boundary condition at the immovable edge. Thus, direct integration of Eq. (1) leads to functions whose form changes after a time interval has elapsed that is equal to the period of transmission of the elastic wave along the length of the bar. The method of setting up these functions is given in the book of A.I. Lur'ye [8.10]. Other methods of solution are also used, the most common of which is the method of characteristics.

A typical curve for strain at a fixed point of the bar under longitudinal impact has the form of an exponential function decreasing with time, on which jumps are superimposed at times that are multiples of l/c . The exponential index is determined by the mass ratio x . The contact time depends on the quantities U and x . Separation occurs at the instant when the strain at the end becomes zero; this corresponds to the crossing of the equilibrium position.

§84. Buckling of a Bar with Initial Camber

The relationships given in the preceding section pertain to a bar deforming without bending. Let us now consider a bar in which bending strains can arise in addition to compressive strains.

Below, we will deal the behavior of a bar, one of whose ends is subjected to the impact of an absolutely hard body.

The classical theory of the strength of bars compressed by a static longitudinal force is based on the elementary theory of bending using the hypotheses of plane sections normal to the neutral axis.

The equation of transverse vibrations is a fourth order equation and the propagation velocity of disturbances determinable by its solution increases indefinitely with decreasing wavelength. This nonconformity to the physical interpretations of the finite propagation velocity of disturbances is explained by the imperfection of the model adopted in the elementary theory of bending for bars. In the study of buckling under impact, such a contradiction may prove substantial; we will therefore use a refined model of bending allowing for the transverse shear and rotatory inertia of the bar element. In Chapter I, we referred to such equations as Timoshenko type equations. In addition, we will discard the hypothesis of nonextensibility of the neutral axis and will add the equation of longitudinal vibrations derived in the preceding section.

Assuming that the deflections may be commensurate with the typical dimension of the cross section, we will use nonlinear relations to set up the expressions relating the strains with the displacements.*

*The data cited here are due to I.G. Kil'dibekov and the author, see DAN SSSR 167, No. 4, 1966.

Let us assume that the total deflection v of the bar consists of three components - the initial deflection v_0 and the deflections \bar{v} and \tilde{v} corresponding to bending and transverse shear, respectively. Then the elongation strains of the fibers, shear strain and change in curvature x will be

$$\begin{aligned}\epsilon &= \frac{\partial u}{\partial x} + \frac{1}{2} \left(\frac{\partial v}{\partial x} \right)^2 - \frac{1}{2} \left(\frac{\partial v_0}{\partial x} \right)^2, \\ \gamma &= \frac{\partial v}{\partial x}, \quad \chi = - \frac{\partial^2 v}{\partial x^2}.\end{aligned}\quad (8.8)$$

Let us consider the "equilibrium" of a bar element cut out by two close planes perpendicular to an undeformed neutral axis (Figure 8.2). Projecting the forces acting on the element in the longitudinal direction, we obtain the equation (γ_0 being the specific gravity of the material)

$$\frac{\partial P}{\partial x} + \frac{\gamma_0}{g} F \frac{\partial^2 u}{\partial t^2} = 0, \quad (8.9)$$

which essentially agrees with the equation discussed in §83. The equation of motion of the element in the normal direction is

$$\frac{\partial Q}{\partial x} - \frac{\partial}{\partial x} \left(P \frac{\partial v}{\partial x} \right) - \frac{\gamma_0}{g} F \frac{\partial^2 v}{\partial t^2} = 0, \quad (8.10)$$

where the second term must not be written in the form $P \partial^2 v / \partial x^2$, since the compressive stresses are variable over the length of the bar. The points in the figure correspond to derivatives with respect to time.

We will now set up the equation of rotation of the element in the plane xy around the transverse axis passing through the centroid:

$$\begin{aligned}\frac{\partial M}{\partial x} - Q + \\ + \frac{\gamma_0}{g} I \frac{\partial^2}{\partial t^2} \left(\frac{\partial \tilde{v}}{\partial x} \right) = 0.\end{aligned}\quad (8.11)$$

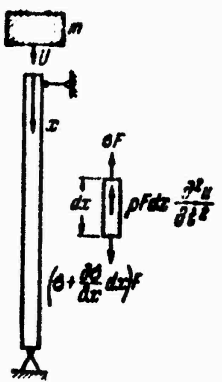


Figure 8.1.
Concerning the
problem of long-
itudinal impact
for a recti-
linear bar.

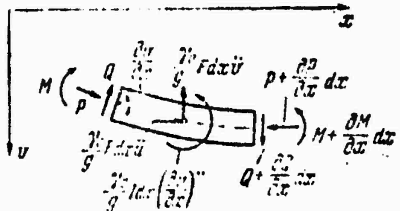


Figure 8.2. Concerning
the derivation of equations
for longitudinal-transverse
motion of the bar.

In (9)-(11), the following symbols are used: longitudinal force $P = -EFe$, transverse force $Q = k^2 FGy$, bending moment $M = E/I \cdot \frac{du}{dx}$. Concerning the coefficient k^2 , see Chapter I. Substituting relations (8) into (9)-(11) and neglecting third-order terms, we arrive at the following system of nonlinear equations in the longitudinal and normal displacement:

$$\left. \begin{aligned}
 & \frac{\partial}{\partial \tau} \left[\frac{\partial u}{\partial x} + \frac{1}{2} \left(\frac{\partial v}{\partial x} \right)^2 \right] - \frac{1}{c^2} \frac{\partial^2 u}{\partial t^2} = \frac{1}{2} \frac{\partial}{\partial x} \left[\left(\frac{\partial v_0}{\partial x} \right)^2 \right], \\
 & \frac{\partial^2 v}{\partial x^2} - \left(\frac{1}{c^2} + \frac{1}{c_i^2} \right) \frac{\partial^2 v}{\partial x^2 \partial t^2} + \frac{1}{c^2 c_i^2} \frac{\partial^2 v}{\partial t^2} = \\
 & \quad - \frac{1}{t^2} \frac{\partial}{\partial x} \left\{ \left[\frac{\partial u}{\partial x} + \frac{1}{2} \left(\frac{\partial v}{\partial x} \right)^2 - \frac{1}{2} \left(\frac{\partial v_0}{\partial x} \right)^2 \right] \frac{\partial v}{\partial x} \right\} + \\
 & \quad + \frac{1}{t^2 c^2} \frac{\partial^2 v}{\partial t^2} = \frac{\partial^2 v_0}{\partial x^2}. \quad | \tag{8.12}
 \end{aligned} \right.$$

The following notation was introduced:

$$c_1 = \sqrt{k^2 \frac{Gg}{\gamma_0}}$$

the velocity of propagation of shear waves in the bar, and $i = \sqrt{1/F}$, the radius of inertia of the section.

Introducing the dimensionless parameters

$$\begin{aligned}
 \xi &= \frac{x}{L}, \quad \tau = \frac{ct}{L}, \quad V^* = \frac{U}{c}, \quad u^* = \frac{uc}{LU}, \\
 \epsilon^* &= \frac{\epsilon}{V^*}, \quad v^* = \frac{v}{L}, \quad v_0^* = \frac{v_0}{L}, \quad \lambda = \frac{L}{t}, \quad m = \frac{E}{k^2 G}.
 \end{aligned}$$

we reduce Eqs. (12) to the dimensionless form

$$\left. \begin{aligned}
 & \frac{\partial^2 u^*}{\partial \xi^2} = \frac{\partial^2 u^*}{\partial \tau^2}, \\
 & \frac{\partial^2 v^*}{\partial \xi^2} - (1+m) \frac{\partial^2 v^*}{\partial \xi^2 \partial \tau^2} + m \frac{\partial^2 v^*}{\partial \tau^4} - \lambda^2 V^* \frac{\partial}{\partial \xi} \left(\frac{\partial u^*}{\partial \xi} \frac{\partial v^*}{\partial \xi} \right) + \\
 & \quad + \lambda^2 \frac{\partial^2 v^*}{\partial \tau^2} = \frac{\partial^2 v_0^*}{\partial \xi^2}. \quad | \tag{8.13}
 \end{aligned} \right.$$

If the ends of the bar swing freely, the boundary and initial conditions are

$$\left. \begin{array}{l} \frac{\partial^2 u^*}{\partial \tau^2}(0, \tau) = \frac{1}{x} \frac{\partial u^*}{\partial \xi}(0, \tau), \quad u^*(1, \tau) = 0, \\ u^*(0, \tau) = 0, \quad v^*(1, \tau) = 0, \\ \frac{\partial^2 v^*}{\partial \xi^2}(0, \tau) = 0, \quad \frac{\partial^2 v^*}{\partial \xi^2}(1, \tau) = 0; \end{array} \right\} \quad (8.14)$$

$$\left. \begin{array}{l} u^*(\xi, 0) = 0, \quad \frac{\partial u^*}{\partial \xi}(\xi, 0) = V^* \text{ при } \xi = 0, \quad \frac{\partial u^*}{\partial \xi} \neq 0 \text{ при } \xi \neq 0, \\ v^*(\xi, 0) = v_0^*, \quad \frac{\partial v^*}{\partial \xi}(\xi, 0) = 0. \end{array} \right\} \quad (8.15)$$

Considering that during the period in which we are interested of transient bending of the bar, the deflections are comparatively small, in (13) we neglected the nonlinear terms in the first equation, as well as terms of third-order smallness relative to the derivatives of displacements. Thus, the problem reduces to the integration of nonlinear system (13) for initial and boundary conditions (14), (15). The equations will be integrated by using the net-point method in the form of an explicit difference scheme approximateing the initial equations to within the order of the square of the step.

It is well known that the algorithm of an explicit difference scheme reduces the problem to calculating the values of the desired functions for each consecutive time layer from known values of the functions during the preceding instants of time with the aid of recurrence relations. In carrying out the calculations on a digital computer, particular attention was given to the ratio of the ξ and τ steps. It was found that when the number of length division intervals ranged from 16 to 60, the step along normalized time t should amount to 0.2-0.9 of the step along the axial coordinate ξ .

We will give the results of computations carried out on the BESM-2M computer. Figure 8.3 shows the elastic lines of a bar initially curved in one half-wave of a sinusoid. The illustrated curves pertain to different instants of time t . It is evident that during the initial period, the elastic line of the bar has the well-defined character of a traveling wave. The impact is followed by the formation of two half-waves

whose amplitudes increase. During the subsequent period, "stabilization" of the nodal points takes place, and the deflections of the bar acquire the form of a standing wave. Let us examine the process of establishment of the latter.

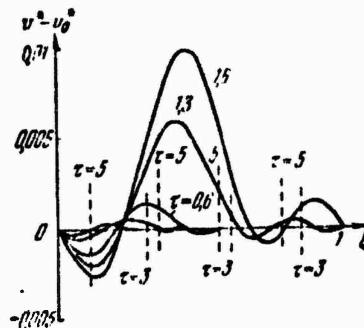


Figure 8.3. Configuration of an elastic line corresponding to additional deflections of the bar during buckling.

The functions $l_i(t)$ (Figure 8.4) for different half-waves are different, but in all cases one can define a "critical length" $l_{i \text{ cr}} = \max l_i(t)$ which is maximum during the entire duration of buckling. The computations showed that these half-wave lengths are practically unrelated to the magnitude of the initial camber, i.e., remain almost unchanged as v_0 varies over wide limits.

It is important to note that the start the decrease in the length of the first half-wave pertains to the instant of formation of a new "zero" half-wave adjacent to the end, when the bar seems to snap to the opposite side.

After reaching their maximum, the half-wavelengths begin to converge toward the same value. This ends the transient stage of buckling of the bar. Several studies published after the above-mentioned work

of M. A. Lavrent'yev and A. Yu. Ishlinskiy* pertain only to the stage of steady buckling. However, the phenomenon of transverse bending caused by the longitudinal impact is actually considerably complicated by transient processes.

§85. Various Approaches to the Problem. Experimental Data

The studies [8.15, 8.9, 8.11, 8.12] developed a criterion of stability of bars to impact, based on an intuitive interpretation of the existence of a certain portion of the bar for which the compressive stresses in the direct wave are Euler critical stresses. We will assume that in the entire portion of possible buckling, the strain $\epsilon = V/c$. Considering that the left edge of this portion is hinged and that the right edge is rigidly clamped, the critical strain given by the familiar Euler formula $E_E = \pi^2 i^2 / (vL)^2$ ($v = 0.7$), where L is the half-wavelength to be determined. Hence, one can readily obtain the critical flexibility of the bar

$$\Lambda = \pi \sqrt{c/v} \quad (8.16)$$

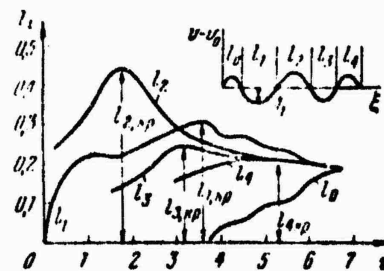


Figure 8.4. Packet of critical half-wavelengths.

*See footnote on p. 271].

and the critical length of the buckling portion

$$L_{cr} = \frac{\pi}{0.7} i \sqrt{\frac{c}{v}}. \quad (8.17)$$

Buckling begins at the instant of time called critical:

$$\tau_{cr} = \frac{\pi i}{0.7 V_r v} \text{ or } \xi_{cr} = \frac{\pi}{0.7 \lambda} \sqrt{\frac{c}{v}}. \quad (8.18)$$

where $\lambda = l/i$ is the flexibility of the entire bar, which is hinged.

According to this concept, buckling should take place if $l \geq 0.7 L_{cr}$ or $\lambda > \Lambda$.

Another possible approach to the problem follows from the results of M. A. Lavrent'yev and A. Yu. Ishlinskii, according to which the number of buckling half-waves is expressed by the integer closest to $m = \sqrt{\epsilon/2\epsilon_E}$, where $\epsilon_E = n^2/\lambda^2$. Hence, the critical flexibility within the confines of one half-wave turns out to be

$$\Lambda = \pi \sqrt{2} \sqrt{c/v}. \quad (8.19)$$

the half-wavelength

$$L_{cr} = \frac{\pi i}{\Lambda} \sqrt{\frac{c}{v}}. \quad (8.20)$$

and the critical time parameter

$$\tau_{cr} = \frac{\pi \sqrt{2}}{\Lambda} \sqrt{\frac{c}{v}}. \quad (8.21)$$

Let us note that if in the above-described approximate solution one takes $v = 0.7$, both approaches lead to the same numerical results.

Let us now return to our problem and compare the data obtained with the above relations. If we find the mean geometric value of critical lengths of the principal half-waves (first and second), then at $v = 0.75$

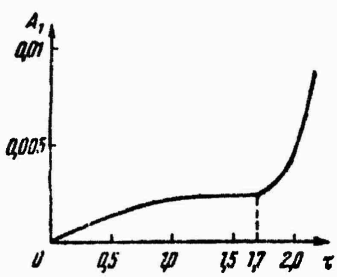
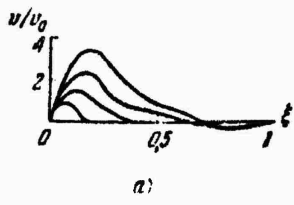
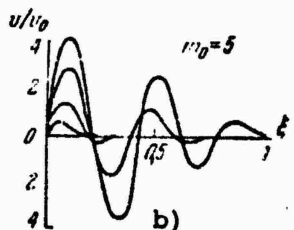


Figure 8.5. Increase in the amplitude of the critical half-wave during dynamic buckling.

it will be close to L_{cr} according to (17) and (20). However, the above data show that in the transient stage, we should be dealing, not with one half-wave, but with a whole series of half-waves.



a)



b)

Figure 8.6. Elastic line of a bar under impact: a) initial stage of buckling, b) development of deflections according to the shape of initial camber.

Of what practical use are the results pertaining to the lengths of critical half-waves? Figure 8.5 (see also Figure 8.4) shows the amplitude of the first half-wave A_1 as a function of time t . It is obvious that as long as its length $l_1(t)$ increases, the amplitude increases slowly and the $A_1 - t$ curve is convex upward. At the instant when the distance between the nodal points reaches the critical value, a rapid increase in the amplitude of the principal half-wave begins. Obviously, this instant may be interpreted as the critical time, dependent on the circumstances of the impact.

A further study of the buckling of an elastic bar under longitudinal impact was made by B.A. Gordiyenko [8.6a]. He used equations of motion similar to (13). The equations were also integrated by using the method of finite differences.

Analysis of results of computations made for different impact rates showed that the buckling process of the bar has three characteristic stages. Immediately following the impact the bar begins to bend in one half-wave, whose length of the bar, if the initial camber has more than one half-wave (in Figure 8.6, the case in which the number of half-waves $m_0=5$ was chosen), new half-waves are formed. The lengths of these half-waves change, but the displacement of the nodal points takes place in the immediate vicinity of the nodes in the form of the initial deflection. This makes it possible to consider the waves as being close to standing waves. The second stage ends in a uniform increase of the deflections, which repeat the form of the initial imperfections. Starting at some instant of time t_{cr} , a transformation of the modes of motion takes place which ends in the following. If the number of half-waves of the initial camber m_0 is smaller than $m^* = 1/\pi \cdot \sqrt{V\lambda^2/2c}$, the bar abruptly changes to a form containing a greater number of half-waves than the initial deflection. In cases where $m_0 > m^*$, the opposite phenomenon takes place, i.e., the disappearance of "excess" half-waves. In both the first and second case, after the transformation, the elastic line acquires the

same number of half-waves, determined by the parameters of the impact rate, and independent of the form and amplitude of the initial camber (Figure 8.7). The process of rearrangement of the buckling form is clearly evident from Figure 8.8, which shows the dependence of the half-wavelengths on time.

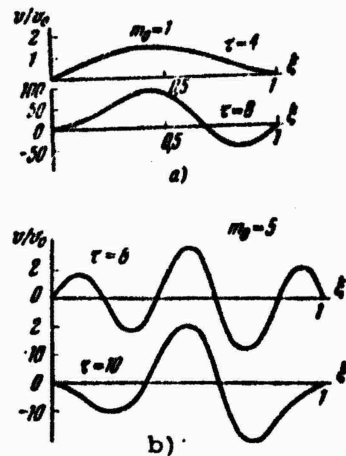


Figure 8.7. Transformation of dynamic modes: a) formation of new half-waves, b) disappearance of "excess" half-waves.

It is characteristic that an intense development of deflections takes place in the third stage, and therefore the start of rearrangement of the shape of the elastic line can be taken as the "critical time". Figure 8.9 shows the dependence of critical time on the impact velocity parameter. The points correspond to the results of numerical integration of Eqs. (13), and the straight line corresponds to the expression

$$\xi_r = 0.2\pi \sqrt{\frac{c}{V}}.$$

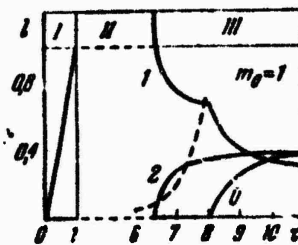


Figure 8.8. Variation of half-wavelengths during buckling.

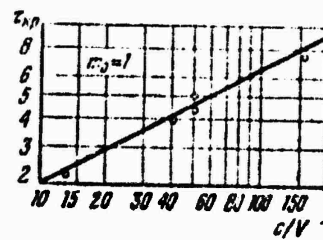


Figure 8.9. "Critical time" versus impact velocity.

Summarizing the above, for practical calculations we can recommend a comparison of the flexibility of the bar with the critical flexibility given by formula (19): buckling will occur if the flexibility exceeds the critical value.

We will cite some results of experiments on the impact loading of bars [8.6a]. The experimental loading was carried out on a device using a falling load. This made it possible to obtain impact velocities in the range of $(0.9-7.2) \times 10^{-3}$ of the velocity of sound in the material. The relative values of the weight of the specimens (ratio to the weight of the load) used in the experiments amounted to 0.01-0.48. Bars made

D16T Duralumin, spring steel, as well as wooden bars were tested.

The strains were measured with strain gauges and a loop oscillograph. High-speed motion pictures were used to record the configuration of the bar during buckling.

The experiments showed that as the impact velocity increases, a large number of half-waves are formed along the bar, with the predominant buckling taking place in the portion adjacent to the loaded end. Also observed was the phenomenon of rearrangement of dynamic modes, consisting in a change in the number of half-waves during buckling.

Thus, the experiments are in qualitative agreement with the theoretical data pertaining to the rearrangement of the wave formation shape.

§86. Cylindrical Shell under Longitudinal Impact

Let us turn to an examination of the stability of an elastic cylindrical shell undergoing collision with an absolutely hard body moving in the axial direction [8.6a].

We will use for the analysis the equations of motion obtained in Chapter I. These equations take into account the transverse shears and rotatory inertia. In its structure, the system of equations describes the propagation, compression-tension and bending-shear waves.

We will first consider the problem in a simplified formulation: the wave processes in the middle surface as well as the shears and rotatory inertia will be neglected.

Considering in (1.29) $v = 0$ and $\partial u / \partial x = -V$, we obtain a conditional relation describing the bending vibrations of the shell:

$$-\frac{h^2}{12} V^4 w - V \left(\frac{\partial^2 w}{\partial x^2} + \mu \frac{\partial^2 w}{\partial y^2} \right) - \mu \frac{V}{R} - \frac{w}{R^2} = \frac{\partial^2 w}{\partial t^2}; \quad (8.22)$$

where the dimensionless coordinates and time are referred, respectively, to the length of the shell and time of transmission of the deformation wave along the length, V is the ratio of the impact velocity to the velocity of sound in the shell, and the quantities w , h and R are also referred to the length of the shell.

Approximation of the deflection function by the series

$$w = \sum_{m=1}^{\infty} \sum_{n=1}^{\infty} f_{mn} \sin m\pi x \sin \frac{n\pi y}{2R} \quad (8.23)$$

and application of the Bubnov-Galerkin procedure leads to an infinite system of independent ordinary equations

$$f_{mn} + \left[\frac{h^2}{12} m^4 n^4 (1 + \xi^2)^2 - V m^2 n^2 (1 + \mu \xi^2) + \frac{1}{R^2} \right] f_{mn} = 0, \quad (8.24)$$

where $\xi = n/2\pi Rm$ is a parameter determining the ratio of the dimension of the dent along the generatrix to the dimension in the circular direction.

The boundary of the zones of "stable" and "unstable" solutions of each of Eqs. (24) is determined from the condition

$$\frac{h^2}{12} m^4 n^4 (1 + \xi^2)^2 - V m^2 n^2 (1 + \mu \xi^2) + \frac{1}{R^2} = 0, \quad (8.25)$$

whence the expression for the "critical" impact velocity V^* :

$$V^* = \frac{\frac{1}{12} m^2 h^2 \pi^2 (1 + \xi^2)^2 + \frac{1}{m^2 \pi^2 R^2}}{1 + \mu \xi^2}, \quad (8.26)$$

or

$$V^* = \frac{\frac{h^2}{12 R^2} (1 + \xi^2)^2 z^2 + \frac{1}{z^2}}{1 + \mu \xi^2}, \quad (8.27)$$

where $z = mwr$. The terms "stability" and "instability" are used conditionally; see Chapter VI.

In the region of "unstable" solutions, the rate of increase of the deflections is given by the expression

$$\begin{aligned}\Omega^2 &= Vm^2\pi^2(1 + \mu\xi^2) - \frac{k^2}{12}m^4\pi^4(1 + \xi^2)^2 - \frac{1}{R^2} = \\ &= -\frac{1}{R^2} \left[Vz^2(1 + \mu\xi^2) - \frac{k^2}{12R^2} z^4(1 + \xi^2)^2 - 1 \right].\end{aligned}\quad (8.28)$$

greater Ω^2 correspond to a faster rate of development of deflections. A study of Ω^2 for the extremum in z shows that the most rapid development of deflections corresponds to the value

$$z^* = \frac{R}{k(1 + \xi^2)} \sqrt{6V(1 + \mu\xi^2)}. \quad (8.29)$$

The results obtained can be refined by considering the transverse shear and rotatory inertia. In the axisymmetric case, we have the equations

$$\left. \begin{aligned} k^2 \frac{\partial}{\partial x} \left(\frac{\partial w}{\partial x} + \psi \right) - V \frac{\partial^2 w}{\partial x^2} - \mu \frac{V}{R} - \frac{w}{R^2} &= \frac{\partial^2 w}{\partial t^2}, \\ \frac{\partial^2 \psi}{\partial x^2} - \frac{12k^2}{h^2} \left(\frac{\partial w}{\partial x} + \psi \right) &= \frac{\partial^2 \psi}{\partial t^2} \end{aligned} \right\} \quad (8.30)$$

(concerning the choice of the coefficient k^2 analogous to v on p. 397 see Chapter I). Taking an approximation of the form

$$\left. \begin{aligned} w &= \sum_{m=1}^{\infty} f_m \sin mx, \\ \psi &= \sum_{m=1}^{\infty} \varphi_m \cos mx \end{aligned} \right\} \quad (8.31)$$

and making a similar study, we obtain the "critical" impact velocity

$$V^* = \frac{k^2 m^2 \pi^2}{m^2 \pi^2 + \frac{12k^2}{h^2}} + \frac{1}{m^2 \pi^2 R^2}, \quad (8.32)$$

or

$$V^* = \frac{k^2 z^2}{z^2 + \frac{12k^2}{R^2}} + \frac{1}{z^2}. \quad (8.33)$$

For $R \rightarrow \infty$, the criterion for an equivalent bar is obtained.

Figure 8.10 shows the dependence of the "critical" velocity V^* on the parameter z for a fixed value of h/R (in our case, $h/R = 1.385 \times 10^{-2}$) in axisymmetric buckling ($\xi = 0$). Figure 8.11 gives the functions $V^*(z)$ for different values of the parameter ξ . It is characteristic that as the number of half-waves decreases in the circular direction, the region of "unstable" solution expands. It is evident from the illustrated graphs that the "instability" limit - V^* as a function of z - has a minimum equal to V^{**} . A study of the extremum showed that the minimum values of "critical" velocities, determined from formulas (27) or (33), are, respectively,

$$\left. \begin{aligned} V^{**} &= \frac{h(1+\xi^2)}{\sqrt{3} R(1+\mu\xi^2)} \\ \text{for } z^2 &= \frac{2\sqrt{3} R}{h(1+\xi^2)} \end{aligned} \right\} \quad (8.34)$$

and

$$\left. \begin{aligned} V^{**} &= \frac{h(4\sqrt{3}\mu^2 - \frac{h}{R})}{12R\xi^2} \\ \text{for } z^2 &= \frac{12k^2 R}{h(2\sqrt{3}\mu^2 - \frac{h}{R})} \end{aligned} \right\} \quad (8.35)$$

It is characteristic that no deflection takes place when $V < V^{**}$. From the relation

$$\frac{dV^{**}}{d(\xi^2)} = \frac{h(1-\mu)}{R\sqrt{3}(1+\mu\xi^2)^2} > 0$$

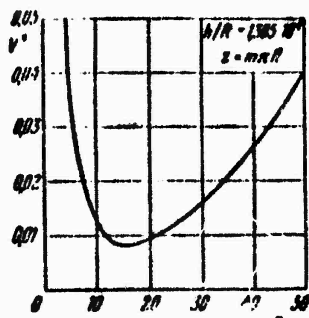


Figure 8.10. Relationship between the "critical velocity" and the wave formation parameter.

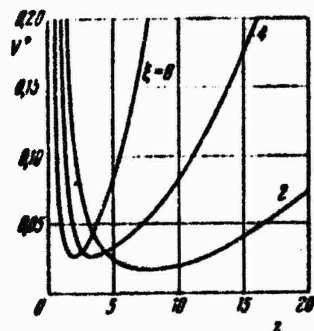


Figure 8.11. Relationship between the "critical velocity" and the wave formation parameter for different relations of the circumferential and longitudinal dimensions of dents.

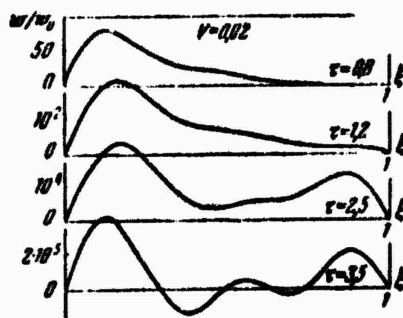


Figure 8.12. Deflections of a shell at different instants of time.

the "critical" velocity minimum decreases with decreasing parameter ξ ; the lowest value of V^{**} corresponds to axisymmetric buckling of the shell.

Let us turn to an analysis of axisymmetric buckling of the shell on the basis of the more complete equations of Chapter I. Their integration was carried out by using the method of finite differences (see [0.6]).

Figure 8.12 shows the characteristic deflections of a cylindrical

shell at different instants of time. Analysis of the results showed that the buckling process of the shells also consists of three characteristic stages analogous to those described previously for bars.

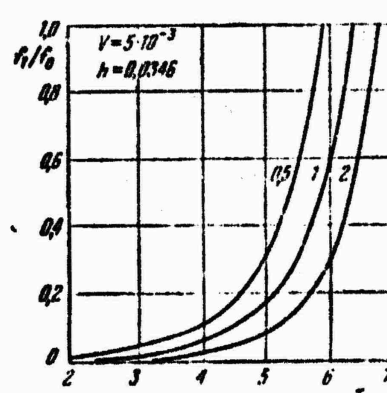


Figure 8.13. Development of the amplitude of the first half-wave.

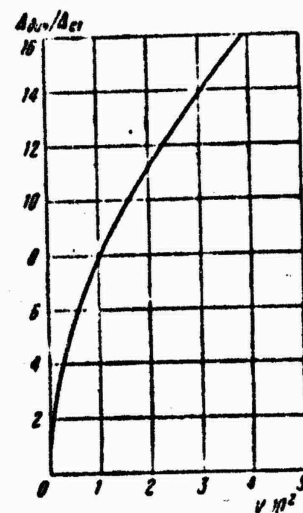


Figure 8.14. Dependence of the dynamic coefficient on the impact velocity.

Let us consider certain characteristics of the behavior of shells during impact. Figure 8.13 shows the development of the amplitude of the first half-wave with time for different values of R . It is evident that as the shell radius increases, the rate of increase of the deflections decreases. Apparently, a substantial contribution to the development of deflections, particularly in the initial stage, is made by the term $(\mu/R)(\partial u/\partial x)$ corresponding to axial compression. As R increases, its influence diminishes; the rate of development of the deflections decreases. If one follows the change in the magnitude of closer approach Δd of the shell ends which corresponds to the start of buckling as a function of the impact velocity, one finds that this magnitude increases with increasing velocity. Figure 8.14 shows the dependence of the dynamic coefficient on the relative impact velocity V .

§87. Case of Nonaxisymmetric Buckling

In the preceding section, the calculations pertained to an axisymmetric problem of longitudinal impact. This formulation is acceptable only for relatively thick shells whose buckling shape is close to axisymmetric. If the shell is sufficiently thin, however, the buckling is associated with the formation of waves in the circumferential direction.

Let us turn to the nonaxisymmetric problem of stability of an elastic circular cylindrical shell under longitudinal impact. We will assume that the phenomenon of stability loss can be divided into two stages: a first stage during which a buildup of membrane stresses takes place in the middle surface, and a second stage during which buckling occurs. On the basis of this hypothesis, we will neglect the bending of the shell in the determination of the compressive forces: at this stage, the longitudinal component of the inertial forces is the main one. On the contrary, as the deflections rapidly increase in the second stage, the normal component of inertial forces will be of decisive importance.*

In order to determine the dynamic compression tension, it is necessary to use the equation (1)

$$\frac{d^2u}{dx^2} = \frac{1}{c^2} \frac{d^2u}{dt^2}, \quad (8.36)$$

where $c = \sqrt{Eg/\gamma(1 - \mu^2)}$ is the speed of sound in the shell.

Equation (36) may be interpreted, for example, by using the method of characteristics, after which the law of change of compressive forces along the shell length will be determined. The derived law of change of the forces will be assumed to a certain region near the section under

*A similar statement of the problem was formulated by I.G. Kil'dibekov and the author [8.5, 1964].

consideration, and for each instant of time will determine the compressive forces for the selected "narrow zone" along the length [8.1].

These values of membrane stresses will be introduced into the equations of bending of the shell, which will be taken in the form

$$\left. \begin{aligned} \frac{D}{h} \nabla^4(w - w_0) &= L(w, \Phi) + \frac{1}{R^2} \frac{\partial^2 \Phi}{\partial x^2} - \frac{y}{h} \frac{\partial^2 w}{\partial t^2}, \\ \frac{1}{E} V^4 \Phi &= -\frac{1}{h} [L(w, w) - L(w_0, w_0)] - \frac{1}{R} \frac{\partial^2 (w - w_0)}{\partial x^2}, \end{aligned} \right\} \quad (8.37)$$

where as before w is the total deflection, w_0 is the initial deflection of the shell, and Φ is the stress function in the middle force, corresponding to the zone near the chosen section.

Let us consider the equations describing the second stage of stability loss. Assuming that during the buckling of the shell, the dents are rhomboidal in character, we will take the expression for the total and initial deflection in the form*

$$\left. \begin{aligned} w &= f(\sin \alpha x \sin \beta y + \psi \sin^2 \alpha x \sin^2 \beta y), \\ w_0 &= f_0(\sin \alpha x \sin \beta y + \psi \sin^2 \alpha x \sin^2 \beta y), \end{aligned} \right\} \quad (8.38)$$

where $\alpha = \pi m/L$, $\beta = n/R$. Substituting (38) into the second Eq. (37), as usual, we find the stress function in the middle surface, to which we add the term $(-py^2/2E)$, $p = p(t)$ being determined for a certain region of the shell, as was mentioned above.

The subsequent solution reduces to an application of the Bubnov-Galerkin procedure, leading to an ordinary differential equation in the amplitude of the given buckling shape (U being the impact velocity):

*This solution of the problem is due to V.L. Agamirov and the author [8.1]; the experiments were carried out by V.L. Agamirov.

$$\xi - S_0 \left\{ \left[\frac{R}{A_1} - \frac{A_1}{A_2} (\xi^2 - \xi_0^2) \right] \xi - (\xi - \xi_0) - \right. \\ \left. - \frac{A_3}{A_2} \frac{L_1^2}{(L_1 + L_2 R)^2} (\xi^3 - 27\xi\xi_0^2 + 27\xi^2\xi_0 - 10\xi^3\xi_0^2 + 9\xi_0^3) - \right. \\ \left. - \frac{A_1}{A_2} \frac{L_1}{(L_1 + L_2 R)} (\xi^3 - \xi\xi_0^2) \right\} = 0, \quad (8.39)$$

where

$$S_0 = A_1 \xi^2 \left(\frac{h}{R} \right)^2 \left(\frac{L_1}{R} \right)^2 \left(\frac{c}{h} \right)^2, \quad c = \frac{UR}{L_1 h A_1}, \\ p^* = \frac{PR}{EA}, \quad A_1 = \frac{(1+\xi^2)^2 \eta}{12(1-\mu^2)\xi^2} + \frac{\xi^2}{(1+\xi^2)^2 \eta}, \quad A_2 = \frac{1+\xi^2}{16\xi^2}, \\ A_3 = \frac{\eta}{16\xi^2} \left[1 + \xi^4 + 64 \frac{\xi^2}{(1+\xi^2)^2} + \frac{30\xi^4}{(1+9\xi^2)^2} + \frac{30\xi^4}{(9+16\xi^2)^2} \right], \\ A_4 = \frac{1}{8\xi^2} \left[1 + \frac{10\xi^2}{(1+\xi^2)^2} \right], \quad \psi = \frac{L_1 \xi}{L_1 + L_2 R}, \quad L_1 = \frac{1}{12\eta} \left[1 + \frac{10\xi^2}{(1+\xi^2)^2} \right], \\ L_2 = \frac{1+\xi^2 + \frac{2}{9}\xi^2}{4(1-\mu^2)} + \frac{1}{64\xi^2} \left[1 - \frac{11\xi^2}{2(1+\xi^2)^2} \right], \\ L_3 = \frac{1}{48} \left[1 + \xi^4 + 64 \frac{\xi^2}{(1+\xi^2)^2} + \frac{110\xi^4}{(1+9\xi^2)^2} + \frac{110\xi^4}{(9+16\xi^2)^2} \right], \\ \eta = n^2 \frac{h}{R}, \quad \xi = \frac{m n R}{n L}, \quad \zeta = l/h, \quad \xi_0 = l_0/h$$

In order to solve the problem, the parameters ψ , ξ and n must be determined. The first parameter may be chosen as in the static problem; the parameter ξ specifies the shape of the dent.

Let us examine the results of numerical integration of Eq. (39) for a shell with geometric parameters $h/R = 1/180$, $L/R = 2.2$ in the case of impact with an infinitely large mass at an initial camber amplitude of $0.001h$. Figure 8.15 shows diagrams of increase of the deflection with time. The curves have three characteristic segments. In the initial stage, the deflections show almost no increase; this corresponds to the stage of buildup of membrane stresses, followed by intensive buckling.

As is evident from the graphs, the fastest growth takes place for the curve corresponding to $n = 11$. Hence it must be concluded that the most probable buckling of the shell in this example is buckling in a form with a wave number along the circumference equal to 11. It was assumed that the impact velocity is 0.001 of the sound velocity in the shell. Judging from the results of the computations, the change in

deflection with time has the same character for all the regions along the length of the shell; hence, the critical value of the parameter t^* characterizes the behavior of the shell as a whole.

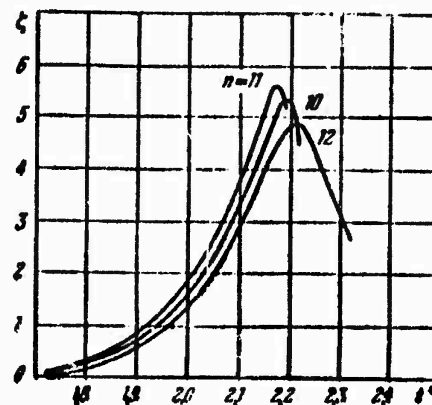


Figure 8.15. Increase in deflection during buckling of the shell.

Thus, we arrive at results similar to those described in the preceding chapter.

The computations showed that an increase in the impact velocity leads to an increase in the number of circumferential half-waves and in the critical value of the time parameter t^* .

It is of interest to find out what effect the mass has on the character of the stability loss. For an infinitely large mass, the dents turn out to be highly stretched along the arc. If however $x = 5$, the dents are nearly square.

§88. Data of Experiments on Impact Loading of Shells

The above-discussed study of nonaxisymmetric buckling of shells under

impact was based on a series of assumptions whose validity can be verified experimentally. We will consider the results of a series of experiments with cylindrical shells subjected to the longitudinal impact of a falling load. The deformations in the shell during impact were recorded with wire strain gauges whose signals were fed to a double cathode-ray oscilloscope and photographed.



Figure 8.16.
Shape of rhom-
boidal dents
formed during
longitudinal
impact.

In the experiment performed, the dents were usually located at the shell end subjected to impact, and at the immovable end, forming one or two bands in each of these zones. Figure 8.16 shows rhomboidal dents located near the loaded end. In some cases (comparatively thick shells), the impact was associated with the appearance of a continuous circular fold, probably due to the migration of deformations into the elastoplastic region.

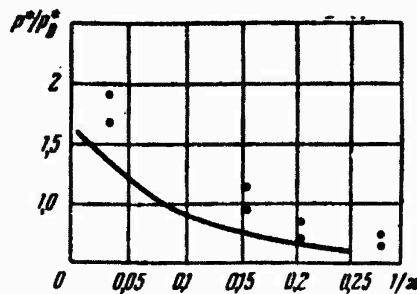


Figure 8.17. Dependence of critical stress on the shell-to-load mass ratio.

Figure 8.17 compares the experimental data on critical stress with theoretical results. The curve in the figure shows the dependence of the dynamic critical stress parameter corresponding to the "critical" value t^* on the ratio of the mass of the shell to the mass of the load. The points denote the experimental stress values determined from experiments with $R/h = 180$. The impact velocity parameter $U/c = 10^{-3}$, where U is the impact velocity and c is the propagation velocity of longitudinal elastic waves in the shell. As is evident from the figure, all the experimental points are fairly close to the theoretical curve and above it.

The dependence of the critical load parameter on the dent shape, characterized by the quantity ξ , is shown in Figure 8.18 by a solid curve. This diagram was obtained for $x = 5$ and $U/c = 10^{-3}$ (x designates the ratio of the mass of the load to the mass of the shell). The triangles indicate the experimental data for the dynamic tests, when $x = 3.85-5$ and $U/c = (0.8-1) \times 10^{-3}$. The dashed curve was obtained from the solution of the corresponding nonlinear static problem. Closed circles indicate the data of experiments on static longitudinal loading. It is obvious that the dynamic character of the process is manifested in an increase of the load parameter, by a factor of two in the case under consideration.

A series of experiments were carried out with a gradual increase of the impact velocity for the purpose of determining the minimum critical velocity. Figure 8.19 shows the test results. Triangles denote the

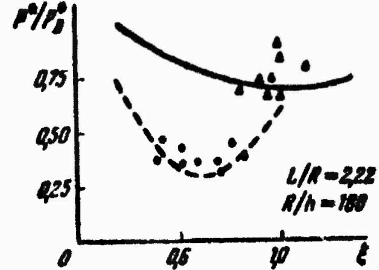


Figure 8.18. Dependence of critical stress on dent shape.

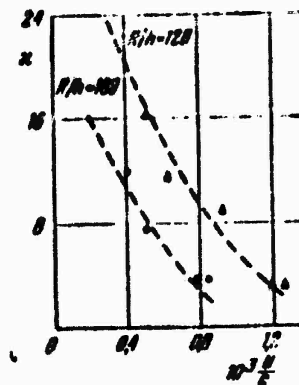


Figure 8.19. Impact velocity at which buckling of the shell takes place.

experimental data obtained on shells having $R/h = 120$, and circles, for $R/h = 180$. The curves were plotted from the experimental data. The values of compressive stresses found here are in satisfactory agreement with the results of the solution of the wave equation.

§89. Elastoplastic Buckling of Shells under Impact

The equations given in §16 will be used to study the behavior of a circular cylindrical shell during longitudinal impact (Figure 8.20). We will consider the case of axisymmetric deformation.* Equations of motion (1.75)-(1.78) will be written

$$\left. \begin{aligned} \frac{\partial \bar{N}_x}{\partial t} &= \frac{\partial^2 u}{\partial r^2}, \\ v \frac{\partial \bar{Q}_x}{\partial t} + \lambda \bar{N}_v + \frac{\partial}{\partial t} \left(\bar{N}_x \frac{\partial w}{\partial r} \right) &= \frac{\partial^2 w}{\partial r^2}, \\ \frac{\partial \bar{M}_x}{\partial t} - \frac{v}{a^2} \bar{Q}_x &= \frac{\partial^2 \psi}{\partial r^2}. \end{aligned} \right\} \quad (8.40)$$

*The solution of the problem given in §§89, 90 is due to V.A. Fel'dshteyn [8.14].

The following dimensionless parameters were introduced above:

$$\begin{aligned} \bar{u} &= \frac{u}{L}, & \bar{w} &= \frac{w}{L}, & \xi &= \frac{x}{L}, & \tau &= \frac{t}{T} \sqrt{\frac{Eg}{\gamma(1-\mu^2)}}, \\ v &= \frac{v}{L}, & \lambda &= \frac{L}{R}, & u' &= \frac{u}{12L^2}, & \bar{N}_x &= \frac{N_x}{B}, \\ \bar{Q}_x &= \frac{Q_x}{Bv}, & V &= \frac{U}{v}, & M_x &= \frac{M_x L}{D}, & (B &= \frac{Ih}{1-\mu^2}, \\ D &= \frac{Eh^3}{12(1-\mu^2)}). \end{aligned}$$

The bar over the dimensionless quantities will hereinafter be omitted.

Let us suppose that at time $t = 0$, the shell, hinged at the ends, is subjected to impact with an absolutely hard body of mass m_{lim} moving in the longitudinal direction at velocity U . The solution of Eqs. (40) must obey the following boundary and initial conditions:

$$\left. \begin{array}{l} w(0, \tau) = 0, \quad w(1, \tau) = 0, \\ M_x(0, \tau) = 0, \quad M_x(1, \tau) = 0, \\ \frac{1}{\kappa} N_x(0, \tau) = \frac{\partial^2 u}{\partial \tau^2}(0, \tau), \quad u(1, \tau) = 0; \end{array} \right\} \quad (8.41)$$

$$\left. \begin{array}{l} u(\xi, 0) = 0, \quad \frac{\partial u}{\partial \tau}(\xi, 0) = V \quad \text{for } \xi = 0, \quad \frac{\partial u}{\partial \tau} = 0 \quad \text{for } \xi > 0, \\ w(\xi, 0) = 0, \quad \frac{\partial w}{\partial \tau}(\xi, 0) = 0, \\ \psi(\xi, 0) = 0, \quad \frac{\partial \psi}{\partial \tau}(\xi, 0) = 0. \end{array} \right| \quad (8.42)$$

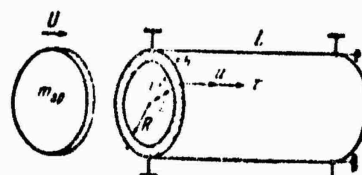


Figure 8.20. Diagram of loading of the shell.

where as before x is the ratio of the mass of the load to the mass of the shell.

To integrate Eqs. (40), we will use the net-point method in the form of an explicit difference scheme. Replacing the differential operators by symmetric differences, we obtain the approximating algebraic system

$$\left. \begin{aligned} u_k^{n+1} &= 2u_k^n - u_k^{n-1} + \Delta\tau^2 F_k^n(u), \\ w_k^{n+1} &= 2w_k^n - w_k^{n-1} + \Delta\tau^2 P_k^n(w), \\ \psi_k^{n+1} &= 2\psi_k^n - \psi_k^{n-1} + \Delta\tau^2 R_k^n(\psi). \end{aligned} \right\} \quad (8.43)$$

($k = 0, 1, \dots, K-1$; $n = 0, 1, \dots$; F_k^n are the left-hand sides of system (40), computed at the nodes of the difference grid).

For linearized Eqs. (40), the necessary stability conditions of the explicit difference scheme can be obtained by using the Lax-Richtmyer criterion.* Figure 8.21 shows a family of curves which determine the maximum permissible steps $\Delta\tau$ as a function of the steps used along the space coordinate [8.1]. As follows from the illustrated graphs, the stability condition strongly depends on the shell thickness: the smaller the ratio R/h , the weaker the constraint imposed on the step ratio.

The step ratio necessary for integrating nonlinear equations is established empirically, and the criterion obtained can be used as a first approximation. It was found that the presence of nonlinear terms makes it necessary to reduce $\Delta\tau$ determined from the graphs of Figure 8.21 by a factor of 2-3. As $\Delta\tau$ varies within these limits, the discrepancy of the results turns out to be of the same order as the approximation error. It is obvious that a scheme of the type of (43) requires a fairly small time step, and this causes certain difficulties in its application.

The paper [8.4] proposed a method for considerably increasing $\Delta\tau$. To this end, it is necessary to make the substitution

*See R.D. Richtmyer, Difference Methods of Solving Boundary Value Problems, Izd.-vo inostr. Lit., 1960.

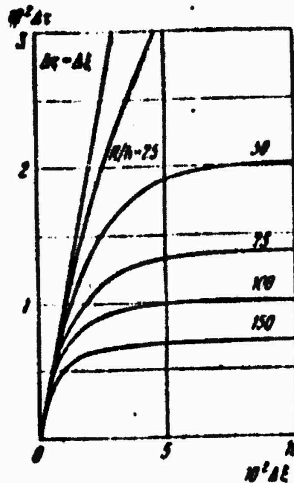


Figure 8.21. Concerning the choice of the step ratio of the difference grid.

$$\psi_k^n = \frac{1}{2} (\psi_k^{n+1} + \psi_k^{n-1}),$$

which, following substitution into the equations, makes it possible to express the values of ψ_k^{n+1} in terms of the values of the functions in the preceding time steps. However, this method automatically excludes the rotatory inertia from the equations of motion, and this, as will be shown below, may frequently lead to a substantial error.

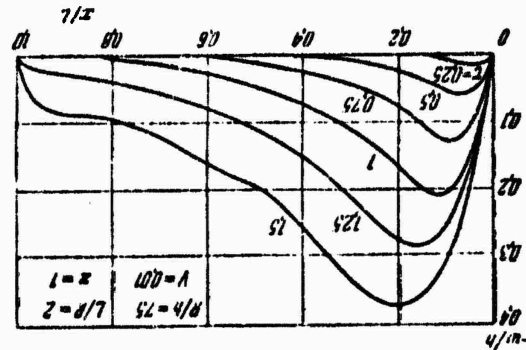


Figure 8.22. Deflections of a shell at different instants of time.

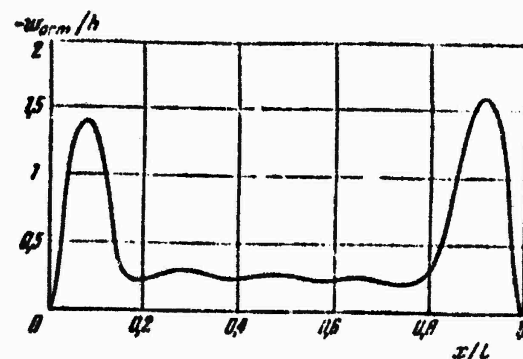


Figure 8.23. Characteristic shape of dynamic buckling beyond the elastic limit.

Let us turn to the results of computations. Our objective will be to elucidate the character of bending of the shell at different impact velocities. A series of computations carried out on the compute revealed the following regularities in the buckling process.

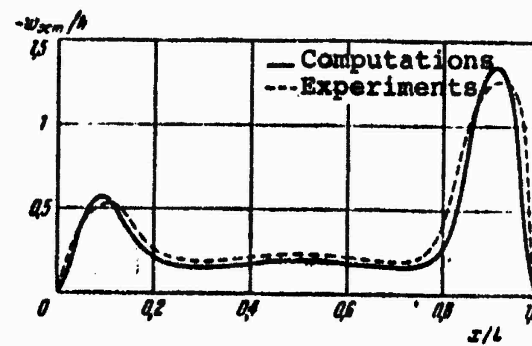


Figure 8.24. Residual deflections of a shell, theory and experiment.

In the initial stage, the deflections of the shell have the well-defined shape of a traveling wave (Figure 8.22). By the time $t = 2.5-3$, a stable bending shape begins to take form which remains unchanged until the onset of maximum deformation values (in the case of a finite mass of the striking body). Similar to this shape is that of the residual deflection at the end of the impact.

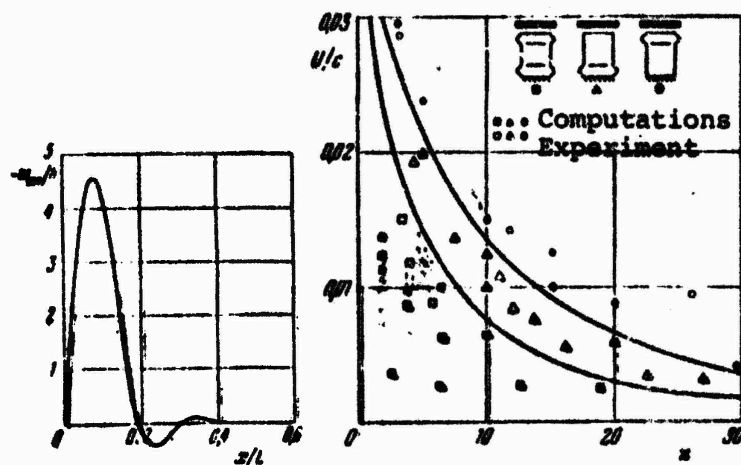


Figure 8.25. Local buckling in the impact zone.

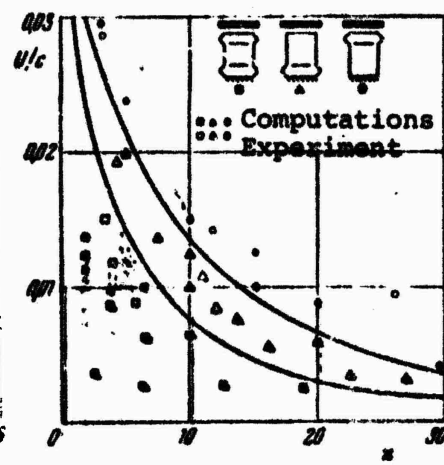


Figure 8.26. Dependence of buckling shape on impact-loading parameters.

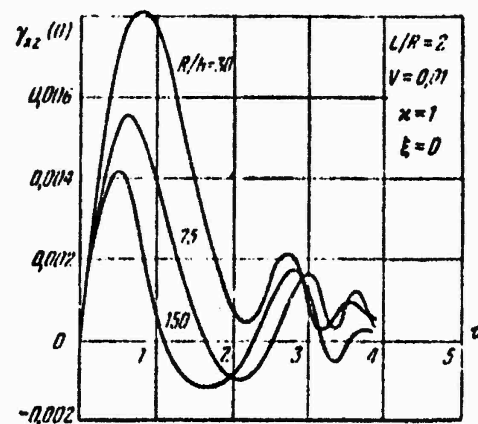


Figure 8.27. Strain of transverse shear in shells of different thicknesses.

The shells for which the computations were made are divided into three groups according to their bending character. The first group includes shells having folds of similar size near the ends (Figure 8.23), and the third, shells in which the bending is localized in a narrow zone adjacent to the point of impact (Figure 8.25). In Figure 8.26, in the plane of the parameters determining the impact conditions, squares indicate the points when the residual deflections pertain to the first

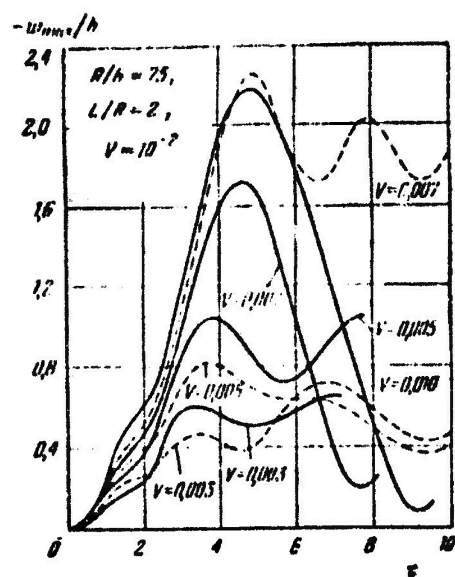


Figure 8.28. Effect of rotatory inertia on the development of deflections.

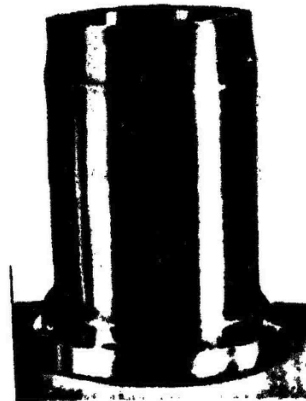


Figure 8.29. Ring folds during buckling beyond the elastic limit.

of the enumerated groups, triangles, to the second group, and circles, to the third group.

It is of interest to determine how important are the effects introduced by allowing for transverse shear and rotatory inertia. Figure 8.27 shows the development of transverse shears with time in the end section of shells of different thicknesses. We see that the shear strains reach an appreciable magnitude, and as the thickness increases, their role becomes more appreciable.

The effect of rotatory inertia on the development of deflections of the shell is illustrated by the graphs of Figure 8.28. The latter shows the development of maximum deflections with time at various impact velocities. Solid lines represent curves pertaining to solutions obtained by allowing for shear and rotatory inertia, and dashed lines represent those obtained without considering rotatory inertia. It is evident that at low velocities, the curves are similar, but as the impact velocity increases, neglecting the rotatory inertia leads to excessive values of maximum and residual deflections. Analysis of other deformation parameters also leads to the conclusion that at impact velocities amounting to more than 0.5% of the sound velocity, the influence of "secondary effects" is substantial.

The experiments performed confirmed the conclusion that the plane has a decisive influence on the buckling character. In Figure 8.26, the open symbols indicate the impact parameters achieved in the test. The residual deflections which the specimens assumed after impact had the above-described characteristic shape. In Figure 8.24, the dashed curve shows the configuration of deflections obtained experimentally. As is evident from the above graph, the theoretical and experimental data are in good agreement. The appearance of the shell after the test is shown in Figure 8.29.

§90. Conical Shell under Longitudinal Impact

Let us consider the behavior of circular conical shells under axial impact.

We will examine the problem in the same formulation as in § 89 [8.14]. In view of the great similarity between the problems, we will introduce the geometry of the cone as follows: we define a certain "basic" cylinder of length L and radius R_0 and consider the conical surfaces whose generatrices pass through the middle section of the shell at an angle α to the generatrix of the cylinder (Figure 8.30).

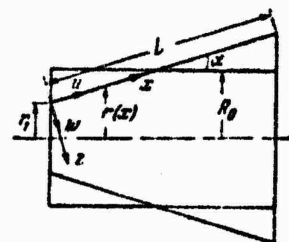


Figure 8.30. Geometry of conical shell.

We will confine the discussion to the axisymmetric case. The equations of motion are [8.14]:

$$\left. \begin{aligned} \frac{1}{r} \frac{\partial}{\partial \xi} (r N_x) + N_y \frac{\sin \alpha}{r} &= \frac{\partial^2 u}{\partial \tau^2}, \\ \frac{1}{r} \frac{\partial}{\partial \xi} \left[r \left(v Q_x + N_x \frac{\partial w}{\partial x} \right) \right] + N_y \frac{\cos \alpha}{r} &= \frac{\partial^2 w}{\partial \tau^2}, \\ \frac{1}{r} \frac{\partial}{\partial \xi} (r M_x) + M_y \frac{\sin \alpha}{r} - \frac{v}{a^2} Q_x &= \frac{\partial^2 \psi}{\partial \tau^2}; \end{aligned} \right\} \quad (8.44)$$

here

$$\begin{aligned} \xi &= x/L, \quad \tau = \frac{t}{L} \sqrt{\frac{Eg}{\gamma(1-\mu)^2}}, \quad t = \frac{\tau}{L}, \quad u = \frac{u}{L}, \quad \psi = \frac{\psi}{L}, \\ a^2 &= \frac{h^2}{12L^2}, \quad \bar{N}_x = \frac{N_x}{B}, \quad \bar{Q}_x = \frac{Q_x}{Bv}, \quad \bar{M}_x = \frac{M_x L}{B}, \quad v = \frac{\kappa'(1-\mu)}{2}. \end{aligned}$$

the bar over dimensionless quantities being omitted in (44) and everywhere hereinafter. Assuming that the edge of the shell $\xi = 1$ is hinged on a rigid immovable support, and that the other end of radius r_1 is fastened to a rigid diaphragm moving freely along the axis, we write the boundary conditions as follows:

$$\left. \begin{aligned} w(0, \tau) &= u(0, \tau) \operatorname{iga}, & u(1, \tau) &= 0, \\ M_s(0, \tau) &= 0, & M_s(1, \tau) &= 0, \\ \frac{1}{m} \left[N_s(0, \tau) + vQ_s(0, \tau) \operatorname{iga} + N_s(0, \tau) \frac{\partial w}{\partial \xi}(0, \tau) \operatorname{iga} \right] &= \\ &= \frac{\partial^2 u}{\partial \xi^2}(0, \tau), & u(1, \tau) &= 0, \\ x_1 &= x \frac{R_1}{r_1 \cos^2 \alpha}. \end{aligned} \right| \quad (8.45)$$

where x as before is the ratio of the mass of the load to the mass of the shell. The initial conditions take the form

$$\left. \begin{aligned} u(t, 0) &= 0, & \frac{\partial u}{\partial t}(t, 0) &= \frac{U}{c} \cos \omega \cdot \text{fort} = 0 \\ w(t, 0) &= 0, & \frac{\partial w}{\partial t}(t, 0) &= \frac{U}{c} \sin \omega \cdot \text{fort} = 0 \\ \psi(t, 0) &= 0, & \frac{\partial \psi}{\partial t}(t, 0) &= 0. \end{aligned} \right| \quad (8.46)$$

To integrate system (44), we will use the method of finite differences in the same form as before in the case of a cylindrical shell. Omitting the details of the computational algorithm, which is completely analogous to (43), we will consider the results of the computations.

The computations showed that the stable bending shape stabilizes after the deformation waves pass two to three times along the length of the generatrix. The bending is characterized by the formation of several half-waves, the largest of which is the first, adjacent to the loaded end

(Figure 8.31). At very high impact velocities amounting to more than 36 of the sound velocity in the shell, a half-wave is formed near the loaded end, since the remaining portion of the shell is virtually undisturbed. The formation of the dominant half-wave takes place before the deformation wave is reflected from the opposite edge; this explains the independence of the deflection amplitude from the shell length.

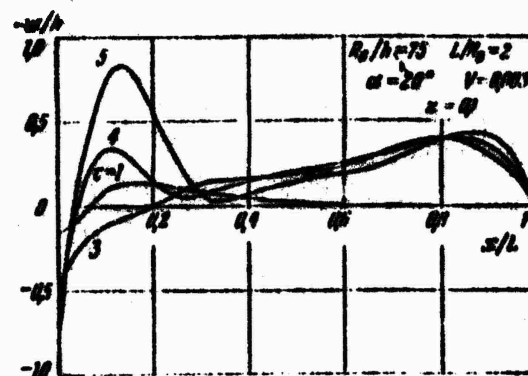


Figure 8.31. Buckling of conical shell during impact.

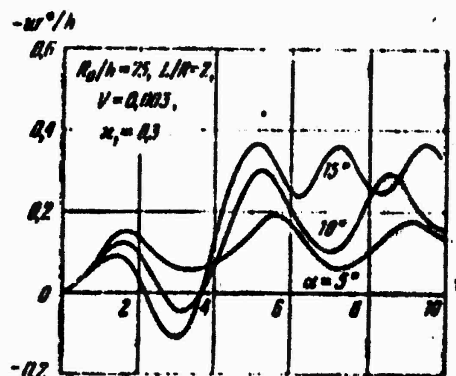


Figure 8.32. Development of fundamental half-wave at different cone angles.

Let us examine in more detail the process of formation of the dominant half-wave of banding. Figure 8.32 shows the maximum values of deflections w^* as a function of time at different half-angles α . As was

shown above, at the initial stage of buckling of a cylindrical shell, its deflections consist of one rapidly increasing half-wave with its convexity directed outward. In a conical shell, the deflections at the end are not zero by virtue of boundary condition (45).

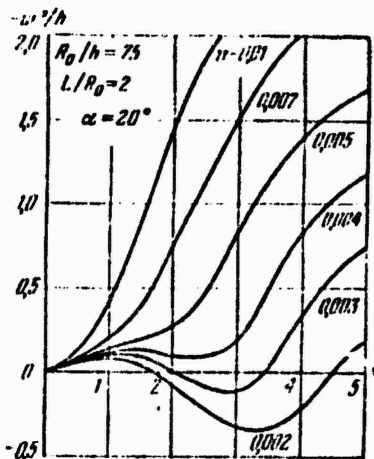


Figure 8.33. Development of fundamental half-wave as a function of impact velocity.

As follows from Figure 8.32, in slightly conical shells, the formation of the fundamental half-wave takes place without a change in the sign of the deflection, whereas with increasing α , the first half-wave is formed as a result of a marked change in the sign of the deflection w^* . At substantial impact velocities, even at large α , w^* does not change sign, so that there is no snapping (Figure 8.33).

§91. Two-Layer Shell. General Relationships

Multilayer shell-type structures find extensive applications in engineering. A very common structural element is a two-layer shell whose inner layer is the supporting one and whose outer layer, which plays an auxiliary role, is made of a material having much lower mechanical characteristics. However, the thickness of the outer layer may be significant,

So that on the whole, it is necessary to consider its influence on the strength properties of the pack.

Certain well-known theories of shells consisting of two or more different layers use the Kirchhof-Love model, applied either to the entire pack as a whole [1.5], or separately to the supporting layers connected by a light filler, to which the straight-line hypothesis is applicable [8.7].

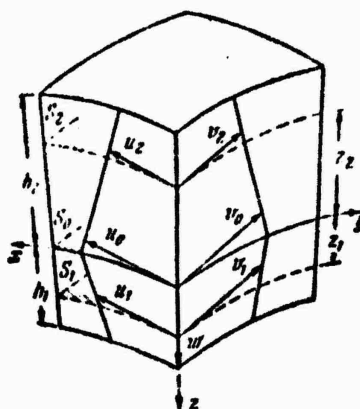


Figure 8.34. Concerning the selection of generalized coordinates of a volume element.

Let us consider the model of a shell of elastoplastic material allowing for transverse shears and rotatory inertia.* If one assumes the continuity of tangential displacements on the surface of contact and the constancy of shears over the thickness of each of the layers, one finds that the tangential stresses undergo a break when they cross the surface of contact. In real structures, this discontinuity is absorbed by a very thin bonding layer.

The surface of contact S_0 between the layers will be referred to the orthogonal coordinates x, y , coinciding with the lines of curvature k_x, k_y . As the generalized coordinates characterizing the location

*This solution was given by V.A. Fel'dshteyn (Izv. AN SSSR, MTT, 1972).

of the element in space, we will take the normal displacement w common to both layers and the tangential displacements u_0, v_0 , in the surface S_0 as well as u_k, v_k in the surfaces S_k , separated from the interface by distances z_k (Figure 8.34). The index $k = 1, 2$ denotes the number of the layer. Let us suppose that external normal stresses p_{xx}^+, p_{zz}^- are applied to the surface of the shell. The signs (+) refer to the surfaces $z = -h_2, z = h_1$, respectively. The stresses $p_{\alpha\beta}^{(k)}$, $\alpha, \beta = x, y, z$ act on the ends $x = a_1, 2, y = b_1, 2$.

According to the adopted assumptions, the displacements of the layers are distributed as follows:

$$\left. \begin{aligned} w^{(k)} &= w, \\ u^{(k)} &= u_0 - \frac{z}{z_k} (u_0 - u_k), \\ v^{(k)} &= v_0 - \frac{z}{z_k} (v_0 - v_k). \end{aligned} \right\} \quad (8.47)$$

The strains, determined from the theory of shallow shells, are

$$\left. \begin{aligned} e_x^{(k)} &= \frac{\partial u_0}{\partial x} - k_x w + \frac{1}{2} \left(\frac{\partial w}{\partial x} \right)^2 - \frac{z}{z_k} \left(\frac{\partial u_0}{\partial x} - \frac{\partial u_k}{\partial x} \right) = e_x + z \frac{\partial \psi_x^{(k)}}{\partial x}, \\ e_y^{(k)} &= \frac{\partial v_0}{\partial y} - k_y w + \frac{1}{2} \left(\frac{\partial w}{\partial y} \right)^2 - \frac{z}{z_k} \left(\frac{\partial v_0}{\partial y} - \frac{\partial v_k}{\partial y} \right) = e_y + z \frac{\partial \psi_y^{(k)}}{\partial y}, \\ \gamma_{xy}^{(k)} &= \frac{\partial u_0}{\partial y} + \frac{\partial v_0}{\partial x} + \frac{\partial w}{\partial x} \frac{\partial w}{\partial y} - \frac{z}{z_k} \left(\frac{\partial u_0}{\partial y} + \frac{\partial v_0}{\partial x} - \frac{\partial u_k}{\partial y} - \frac{\partial v_k}{\partial x} \right) = \\ &\quad = e_{xy} + z \left(\frac{\partial \psi_x^{(k)}}{\partial y} + \frac{\partial \psi_y^{(k)}}{\partial x} \right), \\ \beta_x^{(k)} &= \frac{\partial w}{\partial x} + \psi_x^{(k)} = e_{xz}^{(k)}, \quad \beta_y^{(k)} = \frac{\partial w}{\partial y} + \psi_y^{(k)} = e_{yz}^{(k)}, \end{aligned} \right\} \quad (8.48)$$

where

$$\psi_x^{(k)} = \frac{u_k - u_0}{z_k}, \quad \psi_y^{(k)} = \frac{v_k - v_0}{z_k}.$$

We now obtain the equations of motion of the shell on the basis of the Hamilton-Ostrogradskiy principle:

$$\int_4^6 (\delta K - \delta \Pi + \delta' W) dt = 0; \quad (8.49)$$

K and Π are the kinetic and potential energy, and W is the work done by the external forces. Considering (47), we write the expression for the kinetic energy (ρ_k being the density of the layer material):

$$K = \frac{1}{2} \sum_{k=1}^2 \iiint_{(V_k)} \rho_k \left[\left(\frac{\partial u}{\partial t} \right)^2 + \left(\frac{\partial u^{(k)}}{\partial t} \right)^2 + \left(\frac{\partial v^{(k)}}{\partial t} \right)^2 \right] dx dy dz; \quad (8.50)$$

V_k being the volume occupied by the shell layers. Expression (50) takes account of the energy of rotary motion. The coordinates z_k will be chosen so that after integrating with respect to z in (50), the integrand contains only square of generalized velocities. In this case, the kinetic energy will be written

$$K = \frac{1}{2} \sum_{k=1}^2 \iint_{(S_k)} \rho_k \left\{ m^{(k)} \left(\frac{\partial u}{\partial t} \right)^2 + m_0^{(k)} \left[\left(\frac{\partial u_0}{\partial t} \right)^2 + \left(\frac{\partial v_0}{\partial t} \right)^2 \right] + m_1^{(k)} \left[\left(\frac{\partial u_k}{\partial t} \right)^2 + \left(\frac{\partial v_k}{\partial t} \right)^2 \right] \right\} dx dy, \quad (8.51)$$

with the following notation:

$$m^{(k)} = \rho_k h_k, \quad m_0^{(k)} = \rho_k h_k x_k, \quad m_1^{(k)} = \frac{\rho_k h_k^3}{3x_k^2},$$

$$x_k = 1 : \left(\frac{h_k}{x_k} + \frac{h_k^2}{3x_k^2} \right).$$

The variation in potential energy

$$\delta H = \sum_{k=1}^2 \int \int \int \left[\sigma_x^{(k)} \delta e_x^{(k)} + \tau_{xy}^{(k)} \delta v_{xy}^{(k)} + \right. \\ \left. + \sigma_y^{(k)} \delta e_y^{(k)} + \tau_{xz}^{(k)} \delta v_{xz}^{(k)} + \tau_{yz}^{(k)} \delta v_{yz}^{(k)} \right] dx dy dz. \quad (8.52)$$

Integrating with respect to z and introducing the notation

$$\left. \begin{aligned} \int_{(h_k)} \sigma_x^{(k)} dz &= N_x^{(k)}, & \int_{(h_k)} \tau_{xy}^{(k)} dz &= T^{(k)}, & \int_{(h_k)} \tau_{xz}^{(k)} dz &= Q_x^{(k)}, \\ \int_{(h_k)} \sigma_y^{(k)} z dz &= M_y^{(k)}, & \int_{(h_k)} \tau_{yz}^{(k)} z dz &= H^{(k)}, \end{aligned} \right\} \quad (8.53)$$

we obtain

$$\delta H = \sum_{k=1}^2 \int \int \left[N_x^{(k)} \delta e_x + T^{(k)} \delta v_{xy} + N_y^{(k)} \delta e_y + Q_x^{(k)} \delta v_{xz} + Q_y^{(k)} \delta v_{yz} + \right. \\ \left. + M_y^{(k)} \delta \left(\frac{\partial \psi_x^{(k)}}{\partial x} \right) + H^{(k)} \delta \left(\frac{\partial \psi_x^{(k)}}{\partial y} + \frac{\partial \psi_y^{(k)}}{\partial x} \right) + M_y^{(k)} \delta \left(\frac{\partial \psi_y^{(k)}}{\partial y} \right) \right] dx dy. \quad (8.54)$$

The elementary work done by external forces

$$\delta' W = \sum_{k=1}^2 \left\{ \int_{a_1}^{a_2} \left[\left(P_{xy}^{(k)} - \frac{1}{z_k} Q_{xy}^{(k)} \right) \delta u_0 + \left(P_{yy}^{(k)} - \frac{1}{z_k} Q_{yy}^{(k)} \right) \delta v_0 + \right. \right. \\ \left. + \frac{1}{z_k} (Q_{xy}^{(k)} \delta u_k + Q_{yy}^{(k)} \delta v_k) + P_{yz}^{(k)} \delta w \right]_{b_{1,k}} dx + \\ \left. + \int_{b_1}^{b_2} \left[\left(P_{xx}^{(k)} - \frac{1}{z_k} Q_{xx}^{(k)} \right) \delta u_0 + \left(P_{xy}^{(k)} - \frac{1}{z_k} Q_{xy}^{(k)} \right) \delta v_0 + \right. \right. \\ \left. + \frac{1}{z_k} (Q_{xx}^{(k)} \delta u_k + Q_{xy}^{(k)} \delta v_k) + P_{xz}^{(k)} \delta w \right]_{d_{1,k}} dy \right\} + \\ + \int \int p_{xx}^+ \delta u (-h_2) dx dy + \int \int p_{xx}^- \delta u (h_1) dx dy + \\ + \int \int p_{yy}^+ \delta v (-h_2) dx dy + \int \int p_{yy}^- \delta v (h_1) dx dy + \\ + \int \int p_{zz} \delta w dx dy,$$
(8.55)

where $\delta u(h_k)$, $\delta v(h_k)$ are the variations in displacements, calculated on the surfaces of the shell. The following notation is used:

$$P_{\text{ap}}^{(1)} = \int_{(h_k)} p_{\text{ap}}^{(1)} dz, \quad Q_{\text{ap}}^{(1)} = \int_{(h_k)} p_{\text{ap}}^{(1)} z dz.$$

Substituting the variations δK , $\delta \Pi$ and $\delta' W$ into the Hamilton integral and carrying out the usual operations, we obtain the equations of motion

$$\begin{aligned} \frac{\partial N_x}{\partial x} + \frac{\partial T}{\partial y} - \frac{\partial M_y}{\partial x} - \frac{\partial H}{\partial y} + \frac{1}{z_1} Q_x^{(1)} + \frac{1}{z_2} Q_x^{(2)} + \\ + p_{xx}^+ \left(1 - \frac{h_2}{z_2}\right) + p_{xx}^- \left(1 + \frac{h_1}{z_1}\right) = (m_v^{(1)} + m_v^{(2)}) \frac{\partial^2 u_0}{\partial t^2}, \\ \frac{\partial N_y}{\partial y} + \frac{\partial T}{\partial x} - \frac{\partial M_x}{\partial y} - \frac{\partial H}{\partial x} + \frac{1}{z_1} Q_y^{(1)} + \frac{1}{z_2} Q_y^{(2)} + \\ + p_{yy}^+ \left(1 - \frac{h_2}{z_2}\right) + p_{yy}^- \left(1 + \frac{h_1}{z_1}\right) = (m_v^{(1)} + m_v^{(2)}) \frac{\partial^2 v_0}{\partial t^2}. \end{aligned} \quad (8.56)$$

$$\begin{aligned} \frac{\partial Q_x}{\partial x} + \frac{\partial Q_y}{\partial y} + k_x N_x + k_y N_y + \frac{\partial}{\partial x} \left(N_x \frac{\partial \omega}{\partial x} + T \frac{\partial \omega}{\partial y} \right) + \\ + \frac{\partial}{\partial y} \left(N_y \frac{\partial \omega}{\partial y} + T \frac{\partial \omega}{\partial x} \right) + p_{zz} = (m_v^{(1)} + m_v^{(2)}) \frac{\partial^2 \omega}{\partial t^2}, \\ \frac{\partial M_x^{(1)}}{\partial x} + \frac{\partial H^{(1)}}{\partial y} - Q_x^{(1)} - p_{xx}^- h_1 = m_1^{(1)} z_1 \frac{\partial^2 u_1}{\partial t^2}, \end{aligned} \quad (8.56a)$$

$$\begin{aligned} \frac{\partial M_y^{(1)}}{\partial y} + \frac{\partial H^{(1)}}{\partial x} - Q_y^{(1)} - p_{yy}^- h_1 = m_1^{(1)} z_1 \frac{\partial^2 v_1}{\partial t^2}, \\ \frac{\partial M_x^{(2)}}{\partial x} + \frac{\partial H^{(2)}}{\partial y} - Q_x^{(2)} + p_{xx}^+ h_1 = m_1^{(2)} z_2 \frac{\partial^2 u_2}{\partial t^2}, \\ \frac{\partial M_y^{(2)}}{\partial y} + \frac{\partial H^{(2)}}{\partial x} - Q_y^{(2)} + p_{yy}^+ h_2 = m_1^{(2)} z_2 \frac{\partial^2 v_2}{\partial t^2}. \end{aligned} \quad (8.56b)$$

Here and below, the following notation is used for brevity:

$$\begin{aligned}
 N_x &= N_x^{(1)} + N_x^{(2)}, \quad N_y = N_y^{(1)} + N_y^{(2)}, \quad Q_x = Q_x^{(1)} + Q_x^{(2)}, \quad Q_y = Q_y^{(1)} + Q_y^{(2)}, \\
 M_x &= \frac{1}{z_1} M_x^{(1)} + \frac{1}{z_2} M_x^{(2)}, \quad M_y = \frac{1}{z_1} M_y^{(1)} + \frac{1}{z_2} M_y^{(2)}, \\
 H &= \frac{1}{z_1} H^{(1)} + \frac{1}{z_2} H^{(2)}, \\
 P_{\alpha\beta} &= P_{\alpha\beta}^{(1)} + P_{\alpha\beta}^{(2)}, \quad Q_{\alpha\beta} = \frac{1}{z_1} Q_{\alpha\beta}^{(1)} + \frac{1}{z_2} Q_{\alpha\beta}^{(2)}, \quad \alpha, \beta = (x, y, z).
 \end{aligned}$$

Depending on the fixing conditions of the shell, the following variants of the boundary conditions for the edge $x = a_1$ can be formulated:

$$\begin{aligned}
 N_x - M_x + P_{xx} - Q_{xx} &= 0 \quad \text{or } u_0 = 0, \\
 T - H + P_{xy} - Q_{xy} &= 0 \quad " \quad v_0 = 0, \\
 \frac{1}{z_1} (M_x^{(1)} + Q_{xx}^{(1)}) &= 0 \quad " \quad u_1 = 0, \\
 \frac{1}{z_2} (M_x^{(2)} + Q_{xx}^{(2)}) &= 0 \quad " \quad u_2 = 0, \\
 \frac{1}{z_1} (H^{(1)} + Q_{xy}^{(1)}) &= 0 \quad " \quad v_1 = 0, \\
 \frac{1}{z_2} (H^{(2)} + Q_{xy}^{(2)}) &= 0 \quad " \quad v_2 = 0, \\
 N_x \frac{\partial w}{\partial x} + T \frac{\partial w}{\partial y} + Q_x + P_{xz} &= 0 \quad " \quad w = 0.
 \end{aligned} \tag{8.57}$$

The conditions at the edge $y = b_1$ are obtained from (57) by replacing subscripts x and y .

In the case of physical and geometric symmetry of the layers, setting $2u_0 = u_1 + u_2$, $2v_0 = v_1 + v_2$ and regrouping the terms in the expression for action according to Hamilton, we obtain the equations for a one-layer shell. The decrease in the number of equations corresponds to an additional hypothesis on the absence of a break in the normal on the surface of contact; this reduces the number of degrees of freedom of the element.

All that remains is to derive the expressions relating the forces and moments with the displacements. The intensity of deformations in each of the layers will be written by using expression (1.197), in which $p_0^{(k)}$, $p_1^{(k)}$ and $p_2^{(k)}$ now denote the following:

$$p_0^{(k)} = e_x^2 + e_x e_y + e_y^2 + \frac{1}{4} (e_{xx}^{(k)} + e_{yy}^{(k)} + e_{xy}^{(k)}),$$

$$p_1^{(k)} = \frac{\partial \psi_x^{(k)}}{\partial x} \left(e_x + \frac{1}{2} e_y \right) + \frac{\partial \psi_y^{(k)}}{\partial y} \left(e_y + \frac{1}{2} e_x \right) + \frac{1}{4} e_{xy} \left(\frac{\partial \psi_x^{(k)}}{\partial y} + \frac{\partial \psi_y^{(k)}}{\partial x} \right),$$

$$p_2^{(k)} = \left(\frac{\partial \psi_x^{(k)}}{\partial x} \right)^2 + \frac{\partial \psi_x^{(k)}}{\partial x} \frac{\partial \psi_y^{(k)}}{\partial y} + \left(\frac{\partial \psi_y^{(k)}}{\partial y} \right)^2 + \frac{1}{4} \left(\frac{\partial \psi_x^{(k)}}{\partial y} + \frac{\partial \psi_y^{(k)}}{\partial x} \right)^2.$$

We will use the assumptions made in §16 on the nature of unloading, the only difference being that the state of the element will be determined, not from the sign of $\partial e_i / \partial t$ at the corresponding point of the middle surface, but from the sign of $\partial e_i^{(k)} / \partial t$ at the points of z_k (on the surfaces S_k). Calculating the stresses from the relations of strain theory and integrating over the thicknesses of the layers, we obtain the expressions for the internal forces and moments. In the region of active plastic strains (see p.),

$$N_x^{(k)} = \frac{4}{3} \left[I_1^{(k)} \left(e_x + \frac{1}{2} e_y \right) + I_2^{(k)} \left(\frac{\partial \psi_x^{(k)}}{\partial x} + \frac{1}{2} \frac{\partial \psi_y^{(k)}}{\partial y} \right) \right],$$

$$N_y^{(k)} = \frac{4}{3} \left[I_1^{(k)} \left(e_y + \frac{1}{2} e_x \right) + I_2^{(k)} \left(\frac{\partial \psi_y^{(k)}}{\partial y} + \frac{1}{2} \frac{\partial \psi_x^{(k)}}{\partial x} \right) \right],$$

$$T^{(k)} = \frac{1}{3} \left[I_1^{(k)} e_{xy} + I_2^{(k)} \left(\frac{\partial \psi_x^{(k)}}{\partial y} + \frac{\partial \psi_y^{(k)}}{\partial x} \right) \right],$$

$$Q_x^{(k)} = \frac{k^2}{3} I_1^{(k)} e_{xx}^{(k)}, \quad Q_y^{(k)} = \frac{k^2}{3} I_1^{(k)} e_{yy}^{(k)},$$

$$M_x^{(k)} = \frac{4}{3} \left[I_2^{(k)} \left(e_x + \frac{1}{2} e_y \right) + I_1^{(k)} \left(\frac{\partial \psi_x^{(k)}}{\partial x} + \frac{1}{2} \frac{\partial \psi_y^{(k)}}{\partial y} \right) \right],$$

$$M_y^{(k)} = -\frac{4}{3} \left[I_2^{(k)} \left(e_y + \frac{1}{2} e_x \right) + I_1^{(k)} \left(\frac{\partial \psi_y^{(k)}}{\partial y} + \frac{1}{2} \frac{\partial \psi_x^{(k)}}{\partial x} \right) \right],$$

$$H^{(k)} = \frac{1}{3} \left[I_2^{(k)} e_{xy} + I_3^{(k)} \left(\frac{\partial \psi_x^{(k)}}{\partial y} + \frac{\partial \psi_y^{(k)}}{\partial x} \right) \right].$$
(8.58)

where

$$I_n^{(k)} = \int_{(h_k)}^{\frac{a_1^{(k)}}{c_1^{(k)}}} z^{n-1} dz \quad (n = 1, 2, 3).$$

In the region of unloading

$$\left. \begin{aligned} N_x^{(k)} &= N_x^{(k)*} + \frac{4}{3} E_k h_k \left[\left(c_x^0 + \frac{1}{2} c_y^0 \right) \mp \frac{h_k}{2} \left(\frac{\partial \psi_x^{(k)*}}{\partial x} + \frac{1}{2} \frac{\partial \psi_y^{(k)*}}{\partial y} \right) \right], \\ N_y^{(k)} &= N_y^{(k)*} + \frac{4}{3} E_k h_k \left[\left(c_y^0 + \frac{1}{2} c_x^0 \right) \mp \frac{h_k}{2} \left(\frac{\partial \psi_y^{(k)*}}{\partial y} + \frac{1}{2} \frac{\partial \psi_x^{(k)*}}{\partial x} \right) \right], \\ T^{(k)} &= T^{(k)*} + \frac{1}{3} E_k h_k \left[c_{xy}^0 \mp \frac{h_k}{2} \left(\frac{\partial \psi_x^{(k)*}}{\partial y} + \frac{\partial \psi_y^{(k)*}}{\partial x} \right) \right], \\ Q_x^{(k)} &= Q_x^{(k)*} + \frac{1}{3} E_k h_k h^2 c_{xx}^{(k)*}, \quad Q_y^{(k)} = Q_y^{(k)*} + \frac{1}{3} E_k h_k h^2 c_{yy}^{(k)*}, \\ M_x^{(k)} &= M_x^{(k)*} + \frac{4}{3} E_k h_k^2 \left[\mp \frac{1}{2} \left(c_x^0 + \frac{1}{2} c_y^0 \right) + \right. \\ &\quad \left. + \frac{h_k}{3} \left(\frac{\partial \psi_x^{(k)*}}{\partial x} + \frac{1}{2} \frac{\partial \psi_y^{(k)*}}{\partial y} \right) \right], \\ M_y^{(k)} &= M_y^{(k)*} + \frac{4}{3} E_k h_k^2 \left[\mp \frac{1}{2} \left(c_y^0 + \frac{1}{2} c_x^0 \right) + \right. \\ &\quad \left. + \frac{h_k}{3} \left(\frac{\partial \psi_y^{(k)*}}{\partial y} + \frac{1}{2} \frac{\partial \psi_x^{(k)*}}{\partial x} \right) \right], \\ H^{(k)} &= H^{(k)*} + \frac{1}{3} E_k h_k^2 \left[\mp \frac{1}{2} c_{xy}^0 + \frac{h_k}{3} \left(\frac{\partial \psi_x^{(k)*}}{\partial y} + \frac{\partial \psi_y^{(k)*}}{\partial x} \right) \right]. \end{aligned} \right\} \quad (8.59)$$

Here the parameters marked by zero represent differences of the type $f^0 = f - f^*$, where f^* are the values of the corresponding quantity at the start of unloading. Substituting (58) or (59) into the system of Eqs. (56), one can obtain the equations of motion of the shell in displacements. This will not be done, however, in view of the extreme cumbrousness of the expressions obtained. Moreover, in a numerical integration of the equations, it is not necessary to write them in displacements; it is more convenient to construct the computational algorithm by successively determining the strains, stresses, internal forces, and moments, then substituting them into system (56).

The equations obtained are hyperbolic ones. Analysis of the coefficients of the system shows that the solutions corresponding to it in elastic strains constitute compression-tension waves propagating in the surfaces S_k at velocities

$$c_k = \sqrt{\frac{E_{k\bar{k}}}{v_k(1-\mu_k^2)}}, \quad (8.60)$$

and in S_0 , at velocity

$$c_0 = \sqrt{\frac{c_1^2}{1+\alpha} + \frac{c_2^2}{1+\alpha^{-1}}}, \quad (8.61)$$

as well as bending-shear waves having velocity

$$v = c_0 \sqrt{\frac{v_1}{1+\beta} + \frac{v_2}{1+\beta^{-1}}}, \quad (8.62)$$

the following notation being used:

$$\alpha = \frac{\rho_2 h_2}{\rho_1 h_1}, \quad \beta = \frac{E_2(1-\mu_2^2)h_2}{E_1(1-\mu_1^2)h_1}, \quad v_k = \frac{k^2(1-\mu_k)}{2}.$$

If the strains of the layers exceed the yield point, formulas (60)-(62) remain valid if their moduli of elasticity are replaced by secant moduli averaged over the layer thicknesses:

$$E_c^{(k)} = \frac{1}{h_k} \int_{h_k}^{h_k} \frac{\sigma_i^{(k)}}{c_i^{(k)}} dz.$$

§92. Solution of the Problem of Behavior of a Two-Layer Shell

An analytical solution of the equations obtained above is very difficult. For this reason, as before, the method of finite differences will

be used here.

Let us consider the axisymmetric deformation of a cylindrical shell during longitudinal impact. The equations of motion in this case will be

$$\begin{aligned}
& \frac{1}{1+\beta} \frac{\partial N_x^{(1)}}{\partial x} + \frac{1}{1+\beta^{-1}} \frac{\partial N_x^{(2)}}{\partial x} - \frac{\delta_1}{z_1(1+\beta)} \left(\frac{\partial M_x^{(1)}}{\partial x} - \frac{v_1}{\delta_1} Q_x^{(1)} \right) - \\
& - \frac{\delta_2}{z_2(1+\beta^{-1})} \left(\frac{\partial M_x^{(2)}}{\partial x} - \frac{v_2}{\delta_2} Q_x^{(2)} \right) = \left(\frac{x_1}{1+a} + \frac{x_2}{1+a^{-1}} \right) \frac{\partial^2 u^1}{\partial \tau^2}, \\
& - \frac{\partial M_x^{(1)}}{\partial x} + \frac{v_1}{\delta_1} Q_x^{(1)} = \frac{1+\beta}{2(1+a)} \frac{\partial^2 u_1}{\partial \tau^2}, \\
& \frac{\partial M_x^{(2)}}{\partial x} - \frac{v_2}{\delta_2} Q_x^{(2)} = \frac{1+\beta^{-1}}{2(1+a^{-1})} \frac{\partial^2 u_2}{\partial \tau^2}, \\
& \frac{v_1}{1+\beta} \frac{\partial Q_x^{(1)}}{\partial x} + \frac{v_2}{1+\beta^{-1}} \frac{\partial Q_x^{(2)}}{\partial x} + \\
& + \frac{\partial}{\partial x} \left[\frac{\partial w}{\partial x} \left(\frac{1}{1+\beta} N_x^{(1)} + \frac{1}{1+\beta^{-1}} N_x^{(2)} \right) \right] + \\
& + \lambda \left(\frac{1}{1+\beta} N_y^{(1)} + \frac{1}{1+\beta^{-1}} N_y^{(2)} \right) = \frac{\partial^2 w}{\partial \tau^2}; \quad | \quad (8.63)
\end{aligned}$$

where the dimensionless parameters $\bar{x} = x/L$, $\tau = c_s t/L$, $\bar{u}_k = u_k/L$, $w = w/L$, $\bar{h}_k = h_k/L$, $\bar{z}_k = z_k/L$, $\lambda = L/R$, $\bar{N}_x^{(k)} = N_x^{(k)}/B_k$, $\bar{Q}_x^{(k)} = Q_x^{(k)}/v_k B_k$, $\bar{M}_x^{(k)} = M_x^{(k)}/L D_k$, were introduced; in (63) and below, the bar over the letter is omitted for the sake of brevity.

Let us suppose that the ends of the shell over the entire surface are "bonded" to rigid diaphragms, one of which is immovable, while the other can move freely in the direction of the generatrices. In this case, the boundary conditions will be written as

$$\left. \begin{aligned} w(0, \tau) &= 0, & w(1, \tau) &= 0, \\ u_1(0, \tau) &= u_0(0, \tau), & u_1(1, \tau) &= 0, \\ u_2(0, \tau) &= u_0(0, \tau), & u_2(1, \tau) &= 0, \\ \frac{1}{\kappa(1+\beta)} N_s^{(1)}(0, \tau) + \frac{1}{\kappa(1+\beta^{-1})} N_s^{(2)}(0, \tau) &= -\frac{\partial^2 u_0}{\partial \tau^2}, \\ u_0(1, \tau) &= 0, \end{aligned} \right\} \quad (8.64)$$

where x is the ratio of the mass of the load to the mass of the shell. The initial conditions are

$$\left. \begin{aligned} w(x, 0) &= 0, \quad \frac{\partial w}{\partial t}(x, 0) = 0, \\ u_0(x, 0) &= 0, \quad \frac{\partial u_0}{\partial t}(x, 0) = \frac{U}{c_0} \quad \text{for } x = 0, \\ u_1(x, 0) &= 0, \quad \frac{\partial u_1}{\partial t}(x, 0) = \frac{U}{c_0} \quad \text{for } x = 0, \\ u_2(x, 0) &= 0, \quad \frac{\partial u_2}{\partial t}(x, 0) = \frac{U}{c_0} \quad \text{for } x = 0, \end{aligned} \right| \quad (8.65)$$

We will divide the region of determination of the problem $0 < x < 1, t > 0$ with a rectangular grid $x_n = n\Delta x, t_k = k\Delta t$ ($n = 0, 1, \dots, N - 1$; $k = 1, 2, \dots$); then, replacing the differential operators by central difference operators, we obtain the approximating algebraic system

$$I_n^{k+1} = 2I_n^k - I_n^{k-1} + \Delta t^2 P_n^k; \quad (8.66)$$

where f are the functions being determined, and F are the left-hand sides of Eqs. (63), solved for the second derivatives with respect to time.

In analyzing the stability of the difference scheme, the criterion observed in [8.14] was used as a first approximation. The basis for this is the natural limiting transition to a one-layer shell for very small thicknesses of the outer layer. As was shown by a series of examples, this criterion gives satisfactory results.

Let us turn to the results of the computations. They were carried out for a shell whose inner layer was made of a material having a loading curve with linear hardening, and the outer layer, of an infinitely elastic material whose modulus of elasticity was taken to be equal to the modulus of hardening of the base layer. Figure 8.35 shows the shape of the shell deflections under longitudinal impact. Qualitatively, the

curves were similar to those obtained earlier (see §89) for a one-layer shell. It was found that the addition of an outer elastic layer

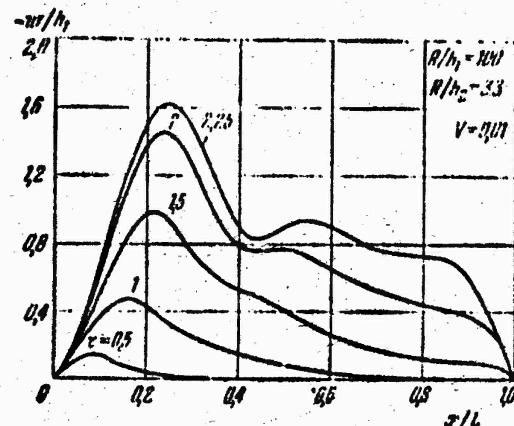


Figure 8.35. Deflections of a two layer shell under longitudinal impact.

has comparatively little effect on the shape and maximum values of the deflection. Figure 8.36 shows curves of the development of maximum deflection with time for different ratios of layer thicknesses. As follows from the graphs, the outer layer, whose thickness is three times that of the base layer, reduces the maximum deflection values by approximately 20%.

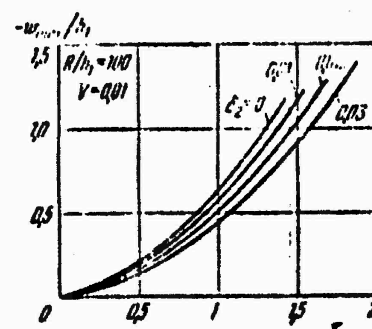


Figure 8.36. Effect of the ratio of layer thicknesses on the rate of development of deflections.

The propagation of the deformation wave $\epsilon_1(x, t)$ in a plastic layer is shown in Figure 8.37. In the case at hand, the plastic strains are strongly developed, and their front is quite removed from the front of the elastic component. On being reflected from the opposite edge, the elastic strains become superimposed on the direct wave, and form a wave of plastic strains. A redistribution of the compressive forces in the layers is characterized during the formation of plastic strains (Figure 8.38).

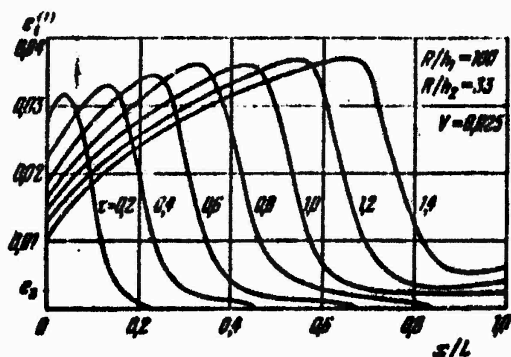


Figure 8.37. Intensity of strains of the inner layer at different instants of time.

As long as the shell is deformed in the elastic region, the forces are distributed in proportion to the compressive rigidities of the layers. After plastic strains are set up in the supporting layer, a redistribution of the compressive forces begins: a decrease in the rigidity of the inner layer leads to an increase of the loads on the outer layer.

§93. Buckling of Cylindrical Shells Under Thermal Impact

In conclusion, we will examine the problem of the behavior of a thin circular cylindrical shell of finite length acted on by an axisymmetric thermal pulse in a zone located near one of the ends.*

*This problem was studied by A.T. Ponomarev and the author, see DAN SSSR 192, No. 4 (1970), 757-759.

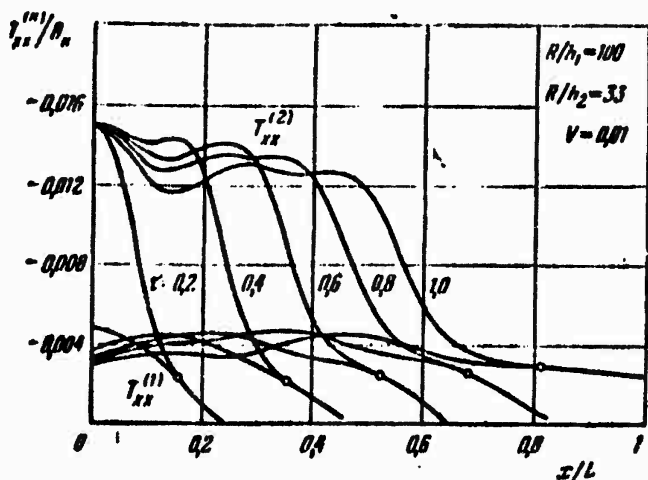


Figure 8.38. Longitudinal forces in the layers.

During the propagation of heat flow along the structure, part of the length of the shell will be subjected to dynamic compression. Under certain conditions, this will lead to the formation in the compressed zone of the shell of deep dents very dangerous for thin-walled structures.* If the period of heat inflow is much shorter than the time of propagation of the elastic wave along the length of the structure, the effect of longitudinal thermal impact may be assumed to be analogous to the action of an impact load.

To describe the behavior of a shell in fundamental equations, it is necessary to consider the inertial forces corresponding not only to the deflection but also to the displacements in the middle surface. Since a problem of this type is very complex, we will assume that the change in thermoelastic strain along the length of the shell is independent of the deflection and is determined from the solution of the corresponding one-dimensional problem for an elastic bar.** As for the buckling phenomenon, we will assume that the deflections thus formed are comparable to the

*For example, Nuclear Engineering and Design 7, No. 2 (1968).

**For example, I.N. Sneddon, Proc. Roy. Soc. of Edinburgh A65, No. 2 (1969).

shell thickness and are determined from the solution of a geometrically nonlinear problem.

Before going on to the thermodynamic relationships describing the elastic behavior of the shell in time, we will write the fundamental relations pertaining to the propagation of thermal stresses in a bar. We will assume that an element of the bar is heated from a certain absolute temperature Θ to the temperature $\Theta + \theta$, whereupon the stresses σ are set up in the bar. The total elastic linear strain will be

$$\epsilon = \frac{\partial u}{\partial x} = \frac{\sigma}{E} + k\theta, \quad (8.67)$$

where k is the coefficient of linear expansion. The parameters E and k generally depend on temperature. However, in the problem discussed below and in many other examples, when structural members are subjected to sharp surface heating, these coefficients may be assumed constant. From relation (67) we have

$$\sigma = E \left(\frac{\partial u}{\partial x} - k\theta \right). \quad (8.68)$$

If θ is small in comparison with Θ , the relation for entropy per unit volume of elastic bar is

$$S = C_v \frac{v}{g} \frac{\theta}{\Theta} + kE\epsilon, \quad (8.69)$$

where C_v is the specific heat of the material.

The second term on the right-hand side of (69) reflects the influence of deformation on the course of the thermodynamic process. Then the amount of heat absorbed by a unit volume may be considered equal to

$$h = S\theta = C_v \frac{\gamma}{\epsilon} \theta + kE\theta. \quad (8.70)$$

On the other hand, from the law of conservation of thermal energy, we should have

$$\frac{\partial q}{\partial x} dx + \frac{\partial h}{\partial t} dt = 0, \quad (8.71)$$

where $q = -a \frac{\partial \theta}{\partial x}$ is the amount of heat flowing through the section in one second; a is the thermal conductivity coefficient.

Using expressions (70) and (71), we obtain the following equation:

$$\frac{\partial \theta}{\partial t} = \kappa \frac{\partial^2 \theta}{\partial x^2} - \beta' \frac{\partial^2 u}{\partial x \partial t}. \quad (8.72)$$

The following notation was introduced above:

$$\kappa = \frac{aG}{C_v \gamma}, \quad \beta' = \frac{kE\theta_R}{C_v \gamma}. \quad (8.73)$$

Adding to (68) and (72) the equation of motion of the element

$$\frac{\partial \sigma}{\partial x} = \frac{\gamma}{\epsilon} \frac{\partial^2 u}{\partial t^2} \quad (8.74)$$

and eliminating σ from this system, we arrive at the so-called coupled problem of thermoelasticity for a bar:

$$\frac{\partial \theta}{\partial t} - \kappa \frac{\partial^2 \theta}{\partial x^2} + \beta' \frac{\partial^2 u}{\partial x \partial t} = 0, \quad (8.75)$$

$$\frac{\partial^2 u}{\partial t^2} - k \frac{\partial \theta}{\partial x} - \frac{1}{\epsilon^2} \frac{\partial^2 u}{\partial t^2} = 0, \quad (8.76)$$

where $c = \sqrt{Eg/\gamma}$, as before, is the velocity of propagation of compressive strain in the material.

We now write the fundamental dynamic relations of thermoelasticity of the theory of shallow shells [0.6]:

$$\frac{D}{h} \nabla^4 (w - w_0) = L(w, \Phi) + \frac{1}{R} \frac{\partial^2 \Phi}{\partial x^2} - \frac{kEh}{12(1-\mu^2)} \nabla^2 M_0 - \frac{\gamma}{E} \frac{\partial^2 w}{\partial t^2}, \quad (8.77)$$

$$\frac{1}{E} \nabla^4 \Phi = - \frac{1}{2} [L(w, w) - L(w_0, w_0)] - \frac{1}{R} \frac{\partial^2 (w - w_0)}{\partial x^2} - kV^2 N_0, \quad (8.78)$$

Here N_0 , M_0 designate, respectively, the equivalent thermal force and thermal moment of a section of the shell, determined by means of the expressions

$$N_0 = \int_{-h/2}^{h/2} k' \theta^* E^* dz, \quad M_0 = \int_{-h/2}^{h/2} k' \theta^* E^* z dz.$$

As before, the initial and total deflections will be chosen in the form of (38). Substituting expression (38) into the right-hand side of Eq. (78) and integrating it, we find the stress function Φ . The term $(-py^2/2)$ enters into the expression for Φ , where $p = p(t)$ is the intensity of compressive forces in the chosen section of the shell, determined from the formula

$$p = E \left(\frac{\partial u}{\partial x} - k\theta \right). \quad (8.79)$$

To find the relationship between the deflection parameters of the shell and the compressive forces changing with time, we will apply the Bubnov-Galerkin method to Eq. (77). We thus arrive at a nonlinear

second-order ordinary differential equation in deflection f .

As an example, we will study a case involving sharp local heating of one of the ends of the shell; the remaining surface will be assumed to be thermally insulated. The solution of the problem reduces to the integration of the following system of dimensionless solving equations:

$$\frac{\partial \psi^*}{\partial \tau} - d \frac{\partial^2 \psi^*}{\partial x^* \partial \tau} + kp' \frac{\partial^2 u^*}{\partial x^* \partial \tau} = 0, \quad (8.80)$$

$$\frac{\partial^2 u^*}{\partial x^* \partial \tau} - \frac{\partial^2 u^*}{\partial \tau^2} - \frac{\partial \psi^*}{\partial x^*} = 0, \quad (8.81)$$

$$\begin{aligned} \xi - S \left\{ \left[p^* - \frac{1}{16} \eta (\zeta^2 - \zeta_0^2) \frac{1 + \xi^2}{\xi^2} \right] \zeta - \right. \\ - \frac{1}{12(1-\mu^2)} \eta (\zeta + \zeta_0) \frac{(1+\xi^2)^2}{\xi^2} - \psi^* \eta \zeta \xi^2 (\zeta^2 - \zeta_0^2) \left[\frac{1}{(1+\xi^2)^2} + \frac{1}{(1+\eta \xi^2)^2} \right] + \\ + \frac{1}{4\xi^2} \psi^* (\zeta + \zeta_0) \left[1 + \frac{4\xi^2}{(1+\xi^2)^2} \right] + \psi^* \frac{\xi^2}{(1+\xi^2)^2} (\zeta^2 - \zeta_0^2) - \\ \left. - \frac{\xi^2}{\eta(1+\xi^2)^2} (\zeta - \zeta_0) \right\} = 0. \end{aligned} \quad (8.82)$$

The following new dimensionless parameters have been introduced above in addition to the notation of 587:

$$\begin{aligned} x^* &= \frac{x}{L}, \quad \tau = \frac{ct}{L}, \quad 0^* = k0, \quad u^* = \frac{u}{L}, \\ d &= \frac{\kappa}{cl}, \quad \lambda = \frac{L}{i}, \quad S = \left(\frac{L}{R} \right)^2 \lambda \xi^2, \end{aligned}$$

where $i = R/\sqrt{2}$ is the inertial radius of the section of the shell, and λ is the total flexibility of the shell, treated as a rod of circular cross section. The value of ψ is adopted conditionally on the basis of the solution of the static problem for an ideal shell. The solution of Eqs. (80) and (81) was obtained in closed form by successively applying to them integral Fourier transforms with respect to x^* and Laplace transformations with respect to t for the following boundary and initial conditions:

$$\frac{\partial \theta^*}{\partial x} = u^* = 0 \quad \text{for } x^* = 0; 1.$$

$$\frac{\partial u^*}{\partial t} = u^* = 0, \quad \theta^* = \frac{h_0}{C_{0,V}} \text{ for } t = 0, \quad x^* = 0,$$

where h is the amount of thermal energy supplied.

Equation (82) was integrated by the Runge-Kutta method with the aid of a BESM-2M digital computer, assuming that the additional deflection and the velocities of the points of the shell at the initial instant of time are equal to zero:

$$\zeta - \zeta_0 = \zeta = 0 \text{ for } t = 0.$$

In solving the problem, we determined the dynamic coefficient, which represents the ratio of the maximum compressive stress to the upper critical value p^*/p_u^* , and the number of waves for which a rapid buckling process sets in.

The results of the computations are presented in Figure 8.39 in the form of curves describing the rates of increase of the deflection ζ in the shell for the section $x = L/2$, as a function of dimensionless time t , for a thermal pulse parameter $\theta^* = 0.3$. They pertain to a shell with a ratio $R/h = 300$, an initial camber amplitude $\zeta_0 = 0.001$, and a wave formation parameter $\xi = 3$. The instant t_{cr} corresponding to the front of rapid deflection increase was taken to be the critical time. As is evident from Figure 8.39, the most probable buckling shape of the shell corresponds to the wave number $n = 27$. Similar results were obtained for shells with different combinations of geometrical relations and loading parameter. Here again, the computations showed that the dynamic effect is manifested more strongly the greater the ratio R/h (see p.).

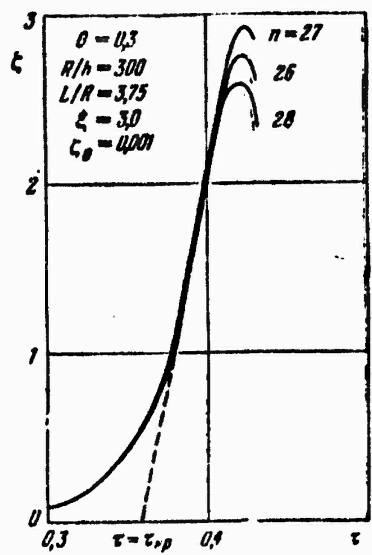


Figure 8.39. Buckling of a shell during thermal impact.

Chapter IX

Behavior of Plates and Shells Acted on by a Moving Load

§94. General Principles. The Concept of Critical Velocity of a Load

The behavior of elastic beams acted on by moving loads was discussed as early as the beginning of the twentieth century by many authors, with application to problems of railroad transportation.* A velocity of travel of the load along the beam was defined at which the deflections of the beam increased sharply. This critical velocity for a railroad track was around 500 m/sec, which considerably exceeded and still exceeds the velocity of rolling stock. Later, more complex problems were solved pertaining to the motion of a load over bridges and other constructions.

Early in the 1950's, a problem of this type arose in connection with the description of the behavior of thin-walled shells, for example, shells that were parts of aircraft structures. In this case, the pressure wave was considered to be the moving load.

In the majority of studies in this area published thus far, such problems have been studied in the linear formulation. In the solution of the linear problem for cylindrical shells, several values of the critical velocity of the load are determined which correspond to propagation velocities of elastic waves of different types, i.e., longitudinal waves associated with radial vibrations, longitudinal waves proper, and shear waves.

The effect of a moving load on the behavior of a cylindrical shell of finite length L is illustrated by the graph shown in Figure 9.1 [9.18]. This figure gives values of the dynamic coefficient K_d , which is the ratio of the amplitude of the dynamic deflection caused by the incident wave to the maximum deflection arising from

*See the book of S.P. Timoshenko [0.36], p. 341; it also gives an extensive bibliography.

the static application of the same load to the entire surface of the shell. Along the abscissa axis is laid off the dimensionless velocity parameter

$$V^* = \frac{\pi V_f}{L} \frac{1}{\sqrt{\frac{D}{\rho_0 h} \left(\frac{\pi}{L}\right)^4 + \frac{E}{\rho_0 R^2}}}. \quad (9.1)$$

where V_f is the velocity of travel of the load front, and ρ_0 is the density of the shell material.

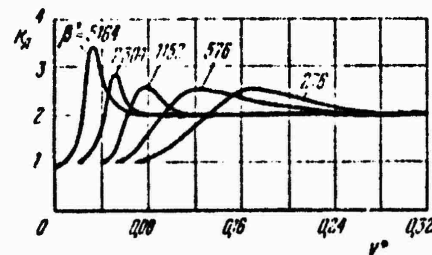


Figure 9.1. Concerning the determination of the dynamic coefficient under a moving load.

The various curves pertain to shells having different parameters $\beta^* = L^2/Rh$. We see that for shells with different parameters, the motion of the load causes a sharp increase in deflections; their magnitude reaches a maximum at a velocity that is critical. The value of the first critical velocity $V_{cr,1}$ is here equal to

$$V_{cr,1} = \sqrt{\frac{Eh}{\rho_0 R} \frac{1}{\sqrt{3(1-\mu^2)}}}. \quad (9.2)$$

When the shell is additionally acted on by static longitudinal stresses p distributed over the ends, the first critical velocity is determined by [9.25]

$$V_{cr,p,1} = \sqrt{\frac{Eh}{\rho_0 R} \left(\frac{1}{\sqrt{3(1-\mu^2)}} - \frac{p}{E} \right)}. \quad (9.2a)$$

where $\beta = pR/Eh$ (here $\beta > 0$ in compression).

The critical velocity values written above were obtained from the solution of the linearized problem. However, for thin shells with relatively large deflections, the nonlinear effects are important. For systems having a soft response, a sharp increase in deflections may take place at a lower approach velocity of the front than the value determined from (9.2) or (9.2a). On the contrary, in the case of a system having a rigid response, the maximum deflections develop at a moving velocity of the load slightly exceeding the values cited.

The second critical velocity turns out to be

$$V_{kp.2} = \sqrt{\frac{E}{\rho_0}}. \quad (9.3)$$

The third critical velocity $V_{cr,3} = k \sqrt{G/p_0}$ and corresponds to bending-shear waves, see Eq. (1.82); this velocity will not be considered below.

The problem of a load moving at a variable velocity is discussed in §100.

One of the forms of a moving load are shock waves whose front executes vibrations along the generatrix of the shell; moreover, the shock waves may move along the flow at a certain velocity [9.22]. When the vibration frequency of the front is the same as the natural vibration frequencies of the shell, intensive vibrations of the structure may arise, and the dynamic coefficient may reach a substantial value.

§95. Solution of Linearized Problems

Let us consider in more detail the solution of the linearized problem described in general outline in the preceding section.* We will study the behavior of a closed circular cylindrical shell along whose axis a pressure wave moves at constant velocity.

*This problem is discussed in the book of P.M. Ogibalov and M.A. Koltunov [0.15]. The discussion given here is patterned after the article [9.25].

Timoshenko type equations will be used for the axisymmetric case; in the presence of specified longitudinal forces $N_x = \bar{N} = \text{const}$, they can be represented in the form

$$\left. \begin{array}{l} L_{11}u + L_{12}w + L_{13}\psi_x = 0, \\ L_{21}u + L_{22}w + L_{23}\psi_x = \frac{1-\mu^2}{Eh} q(x, t), \\ L_{31}u + L_{32}w + L_{33}\psi_x = 0, \end{array} \right\} \quad (9.4)$$

where L_{ij} are linear operators:

$$\begin{aligned} L_{11} &= \left(1 + \frac{1-\mu^2}{Eh} \bar{N}\right) \frac{\partial^2}{\partial x^2} - \frac{\rho_0(1-\mu^2)}{E} \frac{\partial^2}{\partial t^2}, \\ L_{21} &= -\left(\frac{1-\mu}{2} k^2 + \frac{1-\mu^2}{Eh} \bar{N}\right) \frac{\partial^2}{\partial x^2} + \frac{1}{R^2} \left(1 + \frac{h^2}{12R^2}\right) + \frac{\rho_0(1-\mu^2)}{E} \frac{\partial^2}{\partial t^2}, \\ L_{31} &= \frac{h^2}{12} \frac{\partial^2}{\partial x^2} - k^2 \frac{1-\mu}{2} - \frac{\rho_0(1-\mu^2)h^2}{12ER} \frac{\partial^2}{\partial t^2}, \\ L_{12} &= L_{21} = -\frac{\mu}{R} \frac{\partial}{\partial x}, \\ L_{13} &= L_{31} = -\frac{h^2}{12R} \frac{\partial^2}{\partial x^2} + \frac{\rho_0(1-\mu^2)h^2}{12ER} \frac{\partial^2}{\partial t^2}, \\ L_{23} &= L_{32} = -k^2 \frac{1-\mu}{2} \frac{\partial}{\partial x}. \end{aligned} \quad (9.5)$$

In contrast to (1.80)-(1.84), terms of the order of $(h/R)^2$ were retained above.

A circular load q moving at a constant velocity c may be represented in the form

$$q(x, t) = q_1 \delta(x - ct), \quad (9.6)$$

where $\delta(x - ct)$ is Dirac's function, and q_1 is the intensity of the applied load.

We will examine the solution in axes moving together with the load. Let us suppose that the cylinder has infinite length and that the steady state of motion has been reached. Then, the following transformation of the coordinates may be introduced:

$$a = x - ct. \quad (9.7)$$

We introduce the dimensionless quantities

$$\left. \begin{aligned} U &= \frac{u}{R}, \quad W = \frac{w}{R}, \quad \eta = \frac{u}{R}, \quad \lambda^2 = \frac{c^2 \rho R (1 - \mu^2)}{Eh}, \quad \epsilon = \frac{h}{R}, \\ E_0 &= 1 + \frac{r^2}{12}, \quad K = k^2 \frac{1 - \mu}{2}, \quad q_0 = q_1 \frac{1 - \mu^2}{Eh}, \quad N = \bar{N} \frac{1 - \mu^2}{Eh}. \end{aligned} \right\} \quad (9.8)$$

Then Eqs. (4) take the form

$$\left. \begin{aligned} (1 + N - \epsilon \lambda^2) \frac{d^2 U}{d \eta^2} - \mu \frac{d W}{d \eta} - \frac{r^2}{12} (1 - \epsilon \lambda^2) \frac{d^2 \Psi_x}{d \eta^2} &= 0, \\ \mu \frac{d U}{d \eta} + \left[(K + N - \epsilon \lambda^2) \frac{d^2}{d \eta^2} - E_0 \right] W + K \frac{d \Psi_x}{d \eta} &= -q_0 \delta(\eta), \\ \frac{r^2}{12} (1 - \epsilon \lambda^2) \frac{d^2 U}{d \eta^2} + K \frac{d W}{d \eta} - \left[\frac{r^2}{12} (1 - \epsilon \lambda^2) \frac{d^2}{d \eta^2} - K \right] \Psi_x &= 0. \end{aligned} \right\} \quad (9.9)$$

To find the solution of system (9), we will use integral Fourier transforms of the type

$$\overline{U}(s) = \int_{-\infty}^{\infty} U(\eta) e^{-is\eta} d\eta, \quad (9.10)$$

$$U(\eta) = \frac{1}{2\pi} \int_{-\infty}^{\infty} \overline{U}(s) e^{is\eta} ds. \quad (9.11)$$

Multiplying system (9) by $e^{-is\eta}$, performing the integration, and solving the equations obtained for \overline{U} , \overline{W} , $\overline{\Psi}_x$, we obtain

$$\left. \begin{aligned} \frac{\overline{U}}{q_0} &= \frac{(\mu + K) \frac{r^2}{12} (1 - \epsilon \lambda^2) s^2 + i s K}{i s C(s)}, \\ \frac{\overline{W}}{q_0} &= \frac{\frac{r^2}{12} (1 - \epsilon \lambda^2) \left(1 + N - \frac{r^2}{12} + \frac{r^2}{12} \lambda^2 - \epsilon \lambda^2 \right) s^2 + K (1 + N - \epsilon \lambda^2)}{C(s)}, \\ \frac{\overline{\Psi}_x}{q_0} &= \frac{i s K (1 + N - \epsilon \lambda^2) + \mu \frac{r^2}{12} (1 - \epsilon \lambda^2)}{C(s)}. \end{aligned} \right\} \quad (9.12)$$

Here

$$\begin{aligned}
 C(s) &= e_2 s^4 + e_1 s^2 + e_0, \\
 e_2 &= (K + N - \alpha \lambda^2) \frac{e^2}{12} (1 - \alpha \lambda^2), \\
 e_1 &= \frac{e^2}{12} (1 - \alpha \lambda^2) (E_i \rho - \mu^2 - 2\mu K) + K(1 + N - \alpha \lambda^2)(N - \alpha \lambda^2), \\
 e_0 &= KE_0(1 + N - \alpha \lambda^2) - K\mu^2, \\
 e &= 1 + N - \alpha \lambda^2 - \frac{e^2}{12} (1 - \alpha \lambda^2).
 \end{aligned} \tag{9.13}$$

The displacements u , w and the angle of rotation of the normal ψ_x will be found by changing from expressions (12) to inverse transforms in accordance with formulas of the type of (11). To carry out this change, it is necessary to find the roots of the characteristic equation

$$C(s) = 0. \tag{9.14}$$

If this equation has multiple roots lying on the real axis, there is no integral of the inverse transform. Therefore, resonance takes place in the sense that the displacements increase indefinitely.

Values of the dimensionless velocity parameter at which unlimited values of the displacements are reached will be termed critical.

We write the expression

$$\Delta = e_2 e_0 \left(e_2 e_0 - \frac{1}{4} e_1^2 \right)^2. \tag{9.15}$$

The conditions of existence of a multiple root are (for $e_2 \neq 0$):

$$4e_2 e_0 - e_1^2 = 0 \tag{9.16}$$

and

$$e_0 = 0. \tag{9.17}$$

Considering (13), one can note that Eq. (16) is of eighth degree with respect to λ . If we confine ourselves to the region of actually possible parameter values of the system, we find that the forces of inertia for u and ψ_x have very little effect on the values of the two lower roots of Eq. (16). If these factors are neglected, Eq. (16) takes the form

$$e_3\lambda^4 + e_4\lambda^2 + e_5 = 0, \quad (9.18)$$

where e_3, e_4, e_5 are functions of dimensionless parameters (8):

$$\begin{aligned} e_3 &= K^2 \mu^2, \\ e_4 &= 2Ke \left\{ \frac{\mu^4}{12} \left[1 + N - \frac{\mu^2}{12} \right] (E_0 - 2\mu^2 + 2N) + \mu^2 \right\} - K \left(N - 2\mu \frac{\mu^2}{12} \right), \\ e_5 &= \left\{ \frac{\mu^4}{12} \left[E_0 \left(1 + N - \frac{\mu^2}{12} \right) - \mu^2 - 2\mu K \right] + KN \right\}^2 - \\ &\quad - \frac{\mu^4}{3} K (K + N) [E_0 (1 + N) - \mu^2] \left(1 + N - \frac{\mu^2}{12} \right). \end{aligned}$$

The roots of Eq. (18) are

$$\begin{aligned} \lambda_1^2 &= \frac{1}{e} \left[-2 \left(\frac{\mu^2}{12} \right)^{1/2} (E_0 - \mu^2)^{1/2} \left(1 + \frac{2\mu}{K} \frac{\mu^2}{12} \right)^{1/2} + N - \right. \\ &\quad \left. - \frac{\mu^2}{12K} (E_0 - \mu^2 + 2\mu K) \right], \quad (9.19) \end{aligned}$$

$$\begin{aligned} \lambda_2^2 &= \frac{1}{e} \left[2 \left(\frac{\mu^2}{12} \right)^{1/2} (E_0 - \mu^2)^{1/2} \left(1 + \frac{2\mu}{K} \frac{\mu^2}{12} \right)^{1/2} + N - \right. \\ &\quad \left. - \frac{\mu^2}{12K} (E_0 - \mu^2 - 2\mu K) \right]. \quad (9.20) \end{aligned}$$

The terms having the order of e^2 and N were omitted above in comparison with unity.

Expressions (19) and (20) show that as K diminishes, λ_1^2 and λ_2^2 decrease. The parameter K for which these values are approximately equal to zero may be found from the equation

$$e_4 = 0. \quad (9.21)$$

Hence

$$K_1 = \frac{\frac{e^2}{12} (E_0 - \mu^2)}{N - 2\left(\frac{e^2}{12}\right)^{1/2} (E_0 - \mu^2)^{1/2}}, \quad (9.22)$$

$$K_2 = \frac{\frac{e^2}{12} (E_0 - \mu^2)}{N + 2\left(\frac{e^2}{12}\right)^{1/2} (E_0 - \mu^2)^{1/2}}. \quad (9.23)$$

Here again, terms of the order of e^2 and N have been omitted in comparison with unity.

Of practical interest is the case where $K > K_1$; expression (20) has meaning only when $K > K_2$. Considering these restrictions and neglecting the terms e and N in comparison with unity, we rewrite (19) and (20) in the form:

$$\lambda_1^2 = \frac{1}{e} \left[-2\left(\frac{e^2}{12}\right)^{1/2} (E_0 - \mu^2)^{1/2} + N - \frac{e^2}{12K} (E_0 - \mu^2) \right], \quad (9.24)$$

$$\lambda_2^2 = \frac{1}{e} \left[2\left(\frac{e^2}{12}\right)^{1/2} (E_0 - \mu^2)^{1/2} + N - \frac{e^2}{12K} (E_0 - \mu^2) \right]. \quad (9.25)$$

If terms of the order of e are also neglected in Eq. (14) in comparison with unity, it can be shown that this equation should have identical real roots when the conditions $\lambda_1^2 = \lambda_2^2$ and $K > (\epsilon^2/12)^{1/2} (E_0 - \mu^2)^{1/2}$ are fulfilled. Therefore, the parameter of the first critical velocity

$$\lambda_{kp, 1}^2 = \frac{1}{e} \left[2\left(\frac{e^2}{12}\right)^{1/2} (E_0 - \mu^2)^{1/2} + N - \frac{e^2}{12K} (E_0 - \mu^2) \right]. \quad (9.26)$$

It corresponds to the lower critical velocity.

If $e_0 = 0$, i.e., equality (17) is fulfilled, Eq. (14) has equal roots provided $s = 0$. Solving the equation $e_0 = 0$, we obtain

$$\lambda_{kp, 2}^2 = \frac{E_0 - \mu^2}{E_0 e}, \quad (9.27)$$

where N as before is considered to be small in comparison with unity. The multiple zero root lies on the real axis, and there is no inverse Fourier transform. Therefore, the quantity $\lambda_{cr, 2}^2$ corresponds to the critical velocity.

Returning to the previous notation and, as usual, neglecting quantities of the order of e^2 in comparison with unity, we obtain the following values of critical velocities:

$$c_{sp, 1}^2 = \frac{Eh}{\rho_0 R \sqrt{3(1-\mu^2)}} + \frac{N}{\rho_0 h},$$

$$c_{sp, 2}^2 = \frac{E}{\rho_0}.$$

Thus, we have arrived at formulas (2a) and (3) for critical velocities, given in the preceding section; let us recall that in expression (2a), the stresses p are considered to be positive in compression, and it is necessary to set $p = -N/h$.

Given below are the results of theoretical and experimental studies of certain nonlinear problems of the behavior of shells acted on by moving and pulsating loads.

§96. Closed Cylindrical Shell Acted on by a Moving Pressure Wave. Application of the Bubnov-Galerkin Method

Let us first consider the problem in the case of a closed cylindrical shell loaded by a uniform external pressure and subjected to the action of an incident pressure wave.* The motion of the shell will be described by ordinary nonlinear equations of the type of (1.40), (1.41), bearing in mind that the action of the load may give rise to large deflections and snapping of the structure.

The hydrodynamic pressure associated with the arrival of a longitudinal wave is

*This problem was discussed by E.D. Skurlatov [9.13]; see also the book of Ye. N. Mnev and A.K. Pertsev [5.14].

composed of the pressure in the incident wave and of the radiation pressure. In the acoustic approximation, the latter pressure in turn is composed of two parts, the pressure obtained by assuming that each point of the shell surface is a point of the plane, and the load, which is the correction (in one form or another) for the curvature of the cylinder. We will assume the load intensity in the general case to be

$$q = q_f e^{-\eta(ct-x)} H(ct-x) - pc \frac{\partial w}{\partial t} + \frac{pc^2}{2H} w, \quad (9.28)$$

where q_f is the pressure at the wave front, η is an exponent determining the law of change of pressure behind the front, c is the propagation velocity of the wave in the medium surrounding the shell, p is the density of the medium, and H is the Heaviside function. The coordinate x is measured from the leading edge of the shell; thus, the pressure at every given instant is distributed over a portion of the shell with length $(ct - x)$. The last term in (28) is the correction for the curvature of the shell, as discussed above [5.9].

For the case of hinged fastening of the ends, we approximate the deflection function of the shell in the form

$$W(x, y, t) = f_1(t) \sin \alpha x \sin \beta y + f_2 \sin^2 \alpha x, \quad (9.29)$$

where $\alpha = m\pi/L$, $\beta = n\pi r$, m is the number of half-waves in the direction of the generatrix, and n is the number of waves along the circumference.

Using the Bubnov-Galerkin method, we arrive at a system of two ordinary differential equations, which after the introduction of the dimensionless parameters

$$\tau = \frac{ct}{L}, \quad \zeta_1 = \frac{x}{L}, \quad \zeta_2 = \frac{y}{r}$$

take the form

$$\left. \begin{aligned} \frac{d^2\zeta_1}{dt^2} + g \frac{d\zeta_1}{dt} + a_{10}\zeta_1 + a_{11}\zeta_1\zeta_2 + a_{12}\zeta_1\zeta_2^2 + a_{13}\zeta_1^2 + Q_1(t)\zeta_1 &= 0, \\ -\frac{d^2\zeta_2}{dt^2} + g \frac{d\zeta_2}{dt} + b_{10}\zeta_2 + b_{11}\zeta_1\zeta_2 + b_{12}\zeta_1^2 + Q_2(t)\zeta_2 &= 0, \end{aligned} \right\} \quad (9.30)$$

where $a_{10}, a_{11}, a_{12}, \dots$ are certain coefficients. The numerical integration of the equations of motion was carried out on a digital computer for different values of the parameters of the shell and pressure wave. The computations carried out for shells at different velocities of the incident wave front lead to the conclusion that each pair of values of m and n corresponding to the wave formation shape of the shell in the longitudinal and circumferential directions has its own "critical velocity;" at the same time, the dynamic deflection has the highest value in comparison with deflections developing at other velocities.

Figure 9.2 and 9.3 show curves characterizing the change in the dynamic deflection component ζ_1 with time for a shell with parameters $L/R = 2$, $R/h = 200$, $q_f = 10$ at, $\eta = 2$. Figure 9.2 pertains to the case $m = 3$, $n = 20$, and Figure 9.3, to the case $m = 1$, $n = 10$. In the first example, the critical velocity is 100 m/sec, and in the second, 700 m/sec. Having plotted such relations for different possible combinations of q_f and n , we determine that incident velocity of the load at which there takes place the greatest response of the shell to the wave with fixed m and n , and also the corresponding wave formation shape of the shell. This velocity will apparently be the most dangerous for the shell under consideration.

Figure 9.4 presents the results for the case where a uniform pressure is applied over the entire surface of the shell, and in addition, a pressure wave begins to impinge on the shell. Even if each of these loads, taken separately, is not dangerous, they may lead to snapping of the shell when they act simultaneously.

When the damping coefficient is substantial, an aperiodic transient process may take place; here the amplitude maximum is reached later and is smaller than in a system without damping.

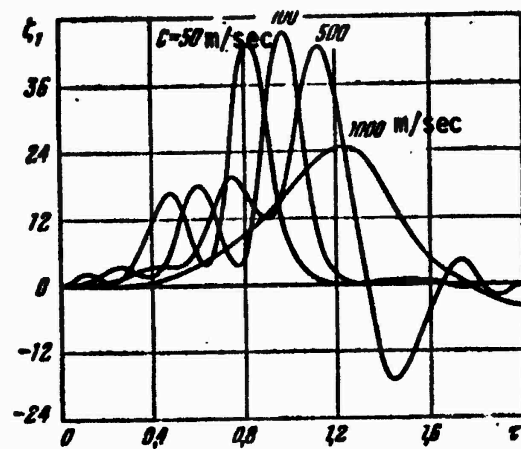


Figure 9.2. Change in the dynamic deflection of the shell with time when $m = 3$, $n = 20$ for different incident velocities of the load.

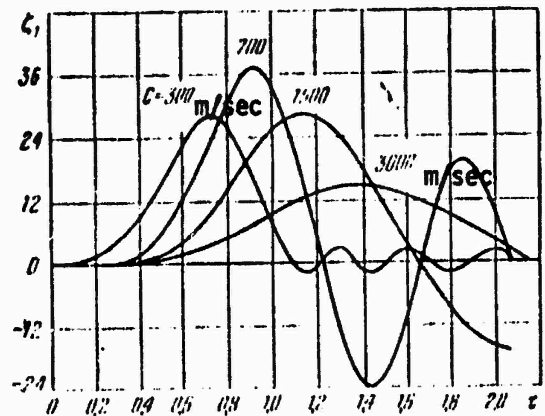


Figure 9.3. Change in the dynamic deflection of the shell for $m = 1$, $n = 10$ and different incident velocities of the load.

This is illustrated in Figure 9.5, which also shows deflection-time curves allowing for damping for different media - air (curve 1) and water (curve 2).

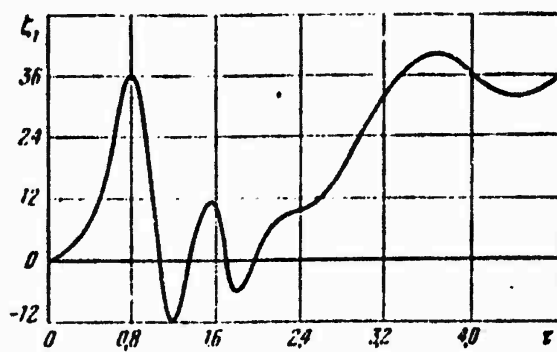


Figure 9.4. Change in dynamic deflection with time for a shell under combined loading.

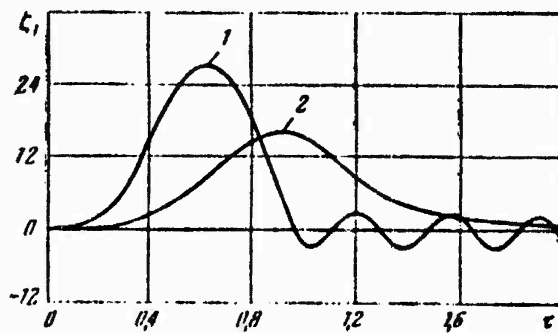


Figure 9.5. Deflection-time curves for a shell surrounded by air (1) and water (2).

597. Solution of the Problem with the Aid of the Method of Finite Differences

In applying the Bubnov-Galerkin method, we had to approximate the deflection of the shell with a series, and the error of the result depended on how successfully the expression for the deflection was chosen. A more accurate solution of the problem can be obtained by representing the initial equations in finite differences. One can thus follow the change in the character of the curved surface of the shell during

the action of the incident load.*

We will assume that the shell is subjected to the action of compressive static stresses p along the axis. In determining the pressure intensity, in addition to (28), we will introduce a term allowing for structural damping, and thus obtain

$$q = q_f e^{-\eta(\tau l - x)} / (\tau l - x) - pc \frac{\partial w}{\partial l} + \frac{pc^3}{2R} w - p_0 h \epsilon \frac{\partial w}{\partial l}, \quad (9.31)$$

where p_0 as before is the density of the shell material.

We use the dimensionless parameters

$$\left. \begin{aligned} \tau &= \frac{cl}{L}, & w' &= \frac{w}{h}, & x' &= \frac{x}{L}, & y' &= \frac{y}{2\pi R}, \\ \eta' &= \eta l, & \Phi' &= \frac{\Phi}{Lh^2}, \end{aligned} \right\} \quad (9.32)$$

where initial Eqs. (1.40) and (1.41) may be represented as follows (the primes are omitted):

$$\begin{aligned} \frac{\partial^2 w}{\partial \tau^2} + g \frac{\partial w}{\partial \tau} + a_1 \frac{\partial^4 w}{\partial x^4} + a_2 \frac{\partial^4 w}{\partial x^2 \partial y^2} + a_3 \frac{\partial^4 w}{\partial y^4} + a_4 \frac{\partial^2 w}{\partial y^2} \frac{\partial^2 \Phi}{\partial x^2} + \\ + a_5 \frac{\partial^2 w}{\partial x^2} \frac{\partial^2 \Phi}{\partial y^2} + 2a_6 \frac{\partial^2 w}{\partial x \partial y} \frac{\partial^2 \Phi}{\partial x \partial y} - a_7 \frac{\partial^2 \Phi}{\partial x^2} - \\ - a_7 c^{-\eta(\tau-x)} / (\tau - x) - a_8 w = 0, \end{aligned} \quad (9.33)$$

$$\begin{aligned} b_1 \frac{\partial^2 \Phi}{\partial x^2} + 2 \frac{\partial^4 \Phi}{\partial x^2 \partial y^2} + \frac{1}{b_1} \frac{\partial^4 \Phi}{\partial y^4} - \left(\frac{\partial^2 w}{\partial x \partial y} \right)^2 + \\ + \frac{\partial^2 w}{\partial x^2} \frac{\partial^2 w}{\partial y^2} + b_2 \frac{\partial^2 w}{\partial x^2} = 0. \end{aligned} \quad (9.34)$$

In the above equations, as the coefficients $a_1, a_2, \dots, b_1, b_2, \dots$, we introduce certain dimensionless quantities dependent on the shell dimensions, Poisson's ratio, and the parameters p and q_f .

*This problem was discussed by L.I. Dolgikh, E.D. Skurlatov, V.R. Solonenko and the author (Proceedings of the Seventh All-Union Conference on the Theory of Shells and Plates, Nauka, Moscow, 1970, 133-155).

Let us note that in selecting the parameters according to (32), the development of the shell corresponds to a square area with a side length equal to unity.

The boundary conditions will be considered constant in time; the initial conditions may, for example, have the form

$$w = w_0, \quad \frac{\partial w}{\partial t} = 0 \quad \text{at } t = 0.$$

The derivatives with respect to the space coordinates and time will be replaced by symmetric difference operators with an error having the order of the square of the step. Substituting them into Eqs. (33) and (34), we obtain two equations in finite differences at each current point of the three-dimensional grid region of space of variables x , y and t . To solve large systems of linear algebraic equations, use was made of the methods of conjugate gradients and random search.

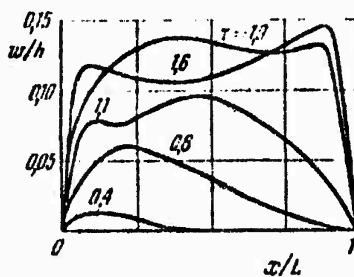


Figure 9.6. Distribution of normalized deflections over the shell length for different instants of time.

We will cite some results of solving the derived difference equations with a computer for different values of the axial load parameter $\beta = pR/Eh$ and different incident pressure wave velocities. The transient deformation process was studied on a shell with dimensions $R = 50$ mm, $L = 200$ mm, $h = 0.8$ mm, compressed by prior application of static axial force ($\beta = 0.1$) and subjected to the action of an exponential pressure wave incident at different velocities in the longitudinal directions. The critical traveling

velocity of the wave for the shell compressed in the axial direction was found to be much lower than for the unstressed shell and equal to 350 m/sec; the critical velocity of a shell of this type free from longitudinal stresses is 500 m/sec. The dynamic deflections arising at an incoming pressure wave front velocity different from the critical value of 350 m/sec are smaller and develop more slowly than at the critical velocity. At a velocity equal or close to the critical value, the deflection is maximum at the trailing edge of the shell. This is illustrated in Figure 9.6, which shows dimensionless deflections w/h for various sections of the shell with relative coordinates x/L at different instants of time t .

Preliminary axial tension causes an increase in critical velocity; in a certain range of velocities of the moving load, the extended shell may have greater dynamic deflections than a shell free from longitudinal stresses or compressed along the axis.

These characteristics of the behavior of shells acted on by longitudinal static forces and incident pressure waves are in qualitative agreement with the experimental data.

§98. Application of the Method of Finite Differences to Equations in Displacements

We will study the above-discussed problem of the behavior of a closed shell in more general form by considering the effect of initial camber; equations in displacement will be employed. As before, we will assume that at the initial instant, a pressure wave having a straight front and an exponential pressure change behind the front is incident in the direction of the generatrix; the shell may also be loaded by static longitudinal stresses p and a uniform external pressure q .* The behavior of the shell will be described by the following equations analogous to (1.24)-(1.26):

$$\begin{aligned} \rho_0 h \frac{\partial^2 u}{\partial t^2} &= \frac{\partial N_x}{\partial x} + \frac{\partial T}{\partial y}, \quad \zeta_0 h \frac{\partial^2 v}{\partial t^2} = \frac{\partial T}{\partial x} + \frac{\partial N_y}{\partial y}, \\ \rho_0 h \frac{\partial^2 w}{\partial t^2} + p_0 h e \frac{\partial w}{\partial t} &= -D V^4 (w - w_0) + \frac{1}{R} N_y + N_x \frac{\partial^2 w}{\partial x^2} + \\ &+ N_y \frac{\partial^2 w}{\partial y^2} + \left(\frac{\partial N_x}{\partial x} + \frac{\partial T}{\partial y} \right) \frac{\partial w}{\partial x} + \left(\frac{\partial T}{\partial x} + \frac{\partial N_y}{\partial y} \right) \frac{\partial w}{\partial y} + \\ &+ 2T \frac{\partial^2 w}{\partial x \partial y} - p \frac{\partial^2 w}{\partial x^2} - q(x, y, t). \end{aligned} \quad (9.35)$$

*See the footnote on p. 441).

Introducing the dimensionless parameters

$$\left. \begin{aligned} \xi &= \frac{x}{R}, \quad 0 = \frac{\theta}{R}, \quad \tau = \frac{c_0 t}{R}, \quad v = \frac{L}{R}, \quad a^2 = \frac{h^2}{12E}, \\ g &= \frac{u}{h}, \quad \theta = \frac{\theta}{h}, \quad \psi = \frac{w}{h}, \quad w_0 = \frac{w_0}{h}, \end{aligned} \right\} \quad (9.36)$$

where c_0 is the velocity of sound in the shell material,

$$c_0 = \sqrt{\frac{B}{\rho_0(1-\mu^2)}}.$$

We write the equations in dimensionless form (the bars are omitted):

$$\begin{aligned} \frac{\partial^2 u}{\partial \tau^2} &= \frac{\partial N_x}{\partial \xi} + \frac{\partial f}{\partial \theta}, \\ \frac{\partial^2 v}{\partial \tau^2} &= \frac{\partial T}{\partial \xi} + \frac{\partial N_y}{\partial \theta}, \\ \frac{\partial^2 w}{\partial \tau^2} + c \frac{\partial w}{\partial \tau} &= -a^2 v^4 (w - w_0) + N_y + \frac{h}{R} N_x \frac{\partial^2 w}{\partial \xi^2} + \\ &+ \frac{h}{R} N_y \frac{\partial^2 w}{\partial \theta^2} + \frac{h}{R} \left(\frac{\partial N_x}{\partial \xi} + \frac{\partial T}{\partial \theta} \right) \frac{\partial w}{\partial \xi} + \frac{h}{R} \left(\frac{\partial T}{\partial \xi} + \frac{\partial N_y}{\partial \theta} \right) \frac{\partial w}{\partial \theta} + \\ &+ 2 \frac{h}{R} \frac{\partial^2 w}{\partial \xi \partial \theta} - \bar{\rho} \frac{\partial^2 w}{\partial \xi^2} + q(\xi, \theta, \tau), \end{aligned} \quad (9.37)$$

where

$$q(\xi, \theta, \tau) = \frac{q_0}{E} \left(\frac{R}{h} \right)^2 (1 - \mu^2) e^{-\eta \left(\frac{v_0}{c} \tau - \xi \right)} H \left(\frac{v_0}{c} \tau - \xi \right),$$

$$\bar{\rho} = \frac{\rho}{J_h} (1 - \mu^2).$$

We will represent these equations in finite differences. Let us consider the plane ξ, θ with variables $0 \leq \xi \leq v$, $0 \leq \theta \leq 2\pi$, corresponding to the $m - 1$ time layer. Having selected the step $\Delta \tau$ along the coordinate t , we will arrange the following time layers: $m, m + 1, m + 2$, and so on. On the plane ξ, θ , we will apply a grid with the aid of straight lines $i\xi$ and $i\theta$, parallel to the coordinate axes, and this grid will subsequently be referred to as the grid area with a step along the coordinates $\Delta \xi = v/N - 1$ and $\Delta \theta = 2\pi/M - 1$, where N is the number of nodes in the ξ direction,

and M is the number of nodes in the θ direction. Then for each inner node of the grid area, the differentiation operators can be approximated by difference operators (see for example [0.6]). Thus, we arrive at a system of nonlinear algebraic equations that is solved jointly with the relations corresponding to the condition of closure of the shell and to the boundary conditions. The equations have a recurrent form, which from given values of u , v and w on $m - 1$ and m layers makes it possible to calculate the displacements on the $m + 1$ layer.

The stability of the computational scheme is achieved by an appropriate selection of the time step Δt and steps along the space coordinates. The criterion obtained in one of the publications [8.14] for linearized equations was used as the first approximation. A numerical experiment established that in integrating the nonlinear system it is necessary to reduce the steps by a factor of 2-3.

To check the accuracy of the solutions obtained, we compared the computation results obtained by dividing the surface of the shell into different numbers of longitudinal and circumferential nodes. For example, for a fixed time corresponding to the instant of crossing of the lower end of the shell by the wave front, for grids having 20x20 and 36x36 nodes, the deflections differed by not more than 0.25%.

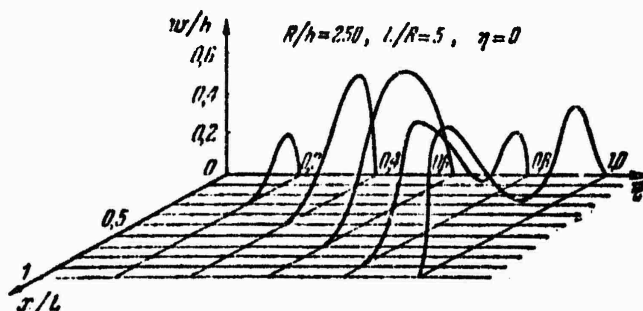


Figure 9.7. Wave formation shape of a shell for different instants of time.

Let us examine certain results of the computations. Figure 9.7 shows curves representing the change in the wave formation shape of a shell along the generatrix at different instants of time after the start of arrival of a wave front with a constant

pressure behind it. In the case of exponentially changing pressure behind the front ($n = 2$), for the same kind of shell, the transient process of deformations is even more complex in character. The wave formation shape was found to depend substantially on the magnitude of the incident wave front velocity, on the law of pressure variation behind the front, and also on the character of the initial imperfections of the shell. As before, the effect of increase in dynamic deflections along the length of the shell can be observed in the formulation discussed.

§99. Behavior of a Slightly Curved Cylindrical Panel Acted on by a Moving Load

We will now study the behavior of a slightly curved cylindrical panel hinged along the edges and acted on by a pressure wave propagating in the longitudinal direction.* Again we will assume that the panel is simultaneously subjected to the action of compressive or tensile longitudinal stresses.

The basic equations will be taken in the form of (1.40), (1.41); the pressure intensity will be taken according to formula (28), and the deflection function of the shell will be approximated by the expression

$$w(x, y, t) = f(t) \sin \gamma x \sin \psi y. \quad (9.38)$$

Here $\gamma = \pi/a$, $\psi = \pi/b$, and a and b are the length and width of the panel. We will assume that in the initial state, the panel has an initial deflection described by a relation analogous to (38). Omitting the intermediate operations, we will write down the equations of motion of the panel, obtained after applying the Bubnov-Galerkin method to relations (1.40), (1.41):

*The behavior of shells acted on by a lateral acoustic pressure wave was studied by E.I. Grigolyuk and A.G. Gorshkov (Scientific Transactions of the Mechanics Institute of Moscow State University, No. 2, 1970). They gave the solution of the problem for the case of a Longitudinal wave, obtained by E.D. Skurlatov [9.13].

$$\frac{d^2\zeta}{dt^2} + \mu \frac{d\zeta}{dt} + A_1\zeta^3 + A_2\zeta^2 + A_3\zeta + A_4(\zeta - \zeta_0) + A_5 = 0. \quad (9.39)$$

The coefficients A_i depend on the dimensions of the panel, initial irregularities, and characteristics of the shell material. θ designates the ratio p/p_u , where p_u is the upper critical static load in compression, and ϕ stands for the ratio q_f/q_u , where q_u is the upper critical static normal pressure for a shell of the same dimensions, see [1.11], $k = b^2/Rh$.

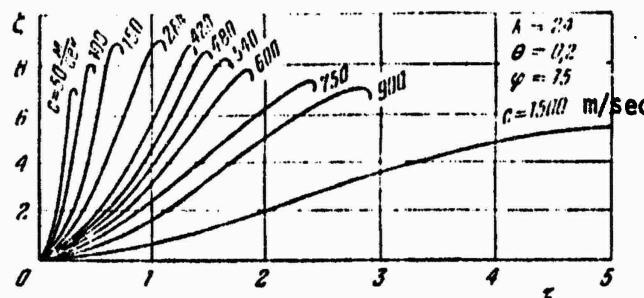


Figure 9.8. Change of the maximum dynamic deflections as a function of the incident load velocity.

The computations were carried out for square panels having different curvatures and thicknesses. Also variable were the traveling velocity of the wave front, pressure at the front, law of pressure decrease behind the front, axial forces, and damping coefficient.

Figure 9.8 shows curves of the change in dynamic deflection for the special case of an ideal shell ($\zeta_0=0$) at traveling velocities of a short pressure wave ranging from 50 to 1500 m/sec. By traveling velocity of the pressure wave is meant the traveling velocity of the front relative to the shell. The curvature of the panel and the parameters characterizing the load are marked on the graph.

It is evident from Figure 9.8 that as the traveling velocity of the wave rises to a certain value, the dynamic deflections increase. Exceeding this velocity, which we will again refer to as the first critical velocity, leads to a decrease of the deflections.

In contrast to the linearized problem, which leads to indefinitely increasing deflections, in solving the nonlinear problem one determines the maximum dynamic deflection, which, as in a real system, has a limited magnitude, and one also determines the value of the parameters of the "shell - impact wave" system at which snapping of the panel will take place.

Analysis of the computation results shows that the motion of a panel acted on by an incident pressure wave in air is vibratory in character, whereas in a heavy liquid the motion is close to aperiodic; this is naturally explained by the significant damping in the latter medium.

Judging from the character of the transient process for shells in air and vacuum, it may be concluded that the radiation pressure in air can be neglected; the error does not exceed a few percent.

It was found that, other things being equal, the dynamic deflections are higher the greater the curvature parameter of the panel. Analysis of data for various pressures at the wave front shows that raising the pressure leads to a more rapid increase of the deflections. At a pressure parameter $\phi = 200$, the deflection of the panel walls develops faster than at $\phi = 40$, and the transient process ends in damping vibrations around the new snapped position of equilibrium.

§100. Characteristics of the Behavior of a Nonlinear System Under a Moving Load

Let us examine certain aspects of the behavior of shells defined as linear or nonlinear systems. In Figure 9.9 a, b, the dashed lines represent the resonance curve for a linear system whose maximum dynamic deflections are reached at a certain traveling velocity of the front, referred to the critical velocity. At a traveling velocity of

the load greater or smaller than the critical velocity, the deflection decrease smoothly. In the same figures, the solid lines represent resonance curves for nonlinear systems with a soft (Figure 9.9 a) and hard (9.9 b) elastic response (see Chapters II-IV). The skeletal line separating the two branches of forced vibration amplitudes is straight in the linear case and bent (to the left or right) for the soft or hard nonlinear response. It may be concluded that for structures with a soft response, the dynamic deflections reach a maximum at a load displacement velocity lower than the critical velocity V_{cr} determined from the solution of the linear problem. For a system with a hard response, the largest deflections arise at a velocity higher than V_{cr} . As the pressure at the front increases, the maximum dynamic deflections develop at increasingly lower velocities of the moving load in the case of a soft response of the system and increasingly higher velocities in the case of a hard response. Figure 9.9 a, b gives three resonance curves corresponding to different pressures at the front ($q_{f_3} > q_{f_2} > q_{f_1}$) with constant damping.

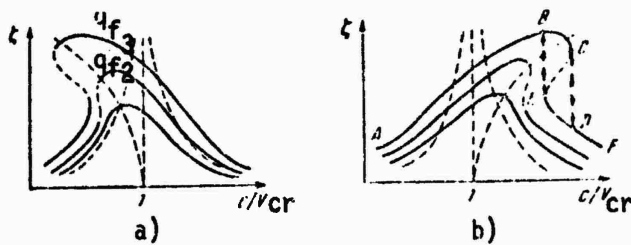


Figure 9.9. Resonance curves of systems with soft (a) and hard (b) response as a function of wave velocity c .

When static longitudinal axial compressive or tensile forces distributed over the edges of the shell are introduced, the resonance curves shift, respectively, toward lower or higher load displacement velocities. It is evident from Figure 9.9 a, b that at a certain traveling velocity of the front, two values of ξ can occur simultaneously. Which of these values actually prevails depends on the previous history of the motion. Let us consider, for example, the case of action on the shell of a wave that is characterized by a rapid decrease of the traveling velocity of the front along the structure. If we assume that the velocity of the front attenuates according to a linear law, the expression for the load (28) in the equations of motion must be replaced by the following:

$$q = \eta_0 c^{-\gamma} (ct - sl - x) / (cl - sl^2 - x),$$

where s is the acceleration of the wave front.

Let us examine the change in the vibration amplitude of the shell as a function of the traveling velocity of the front.* If at the initial instant the front moves at a velocity exceeding v_{cr} at point \bar{t} in Figure 9.9 b, then, as the velocity decreases, the vibrations of the shell take place with smoothly increasing amplitudes determined by the lower branch of the FDE resonance curve. At point E, the amplitude abruptly increases to a value corresponding to point B. Moreover, if there is no snapping of the shell, a further decrease in the velocity of the front leads to vibrations with smoothly decreasing amplitudes (motion along the upper branch of the resonance curve BA).

With increasing velocity, which at the initial instant is smaller than v_{cr} , there is an increase in the vibration amplitudes (line ABC), and at the instant when point C is passed, the amplitude changes abruptly to lower values (line CD), with subsequent motion along segment DF.

Let us note that in a certain range of variation of the geometric parameters of cylindrical panels, soft nonlinearity predominates at comparatively small deflections, which changes into hard nonlinearity at large deflections. The resonance curves for these cases have a more complex shape; when the incident velocity of the load changes smoothly, the existence of two amplitude discontinuity points turns out to be possible.

The problem of studying resonance regimes during the action of a moving load for shells considered from geometrically nonlinear points of view remains insufficiently studied.

*An analogous effect for the case of periodic external actions is discussed above in Chapter III.

§101. Behavior of a Cylindrical Panel Acted on by Moving Pulsating Pressure Shocks

Let us consider the behavior of a slightly curved cylindrical panel fixed in a rigid cylindrical screen (Figure 9.10 a) in the presence of oscillating compression shocks.* As a first approximation, the load on the outer surface of the panel, arising from the formation of compression shocks in subsonic flow, will be approximated by a step-shaped pressure wave whose front will move in the direction of the generatrix of the shell, simultaneously executing constant-frequency vibrations around a certain section [9.22]. The motion of the shell is described by a system of nonlinear equations of the theory of shallow shells (1.40), (1.41). The external load is then taken in the form

$$q = q_\phi H(B - x), \quad (9.40)$$

where

$$B = \phi + l \sin \omega t.$$

Here l and ω are the vibration amplitude and frequency of the front in the section defined by the coordinate $\phi = ct$, and B is the current coordinate of the front.

Approximating the deflection function in the form

$$w(x, y, t) = \sum_{m=1}^{\infty} \sum_{n=1}^{\infty} f_{mn} \sin \alpha x \sin \beta y, \quad (9.41)$$

where $\alpha = m\pi/a$, $\beta = n\pi/b$, and applying the Bubnov-Galerkin method to the equations

*This problem was investigated by E.D. Skurlatov and V.R. Solonenko (All-Union Symposium on Propagation of Elastic and Elastic-Plastic Waves, Alma-Ata, 1971); Problemy prochnosti (Strength problems), 1972, No. 6, 7-11.

of motion, we obtain a system of nonlinear differential equations in ordinary derivatives that can be integrated by means of a digital computer.

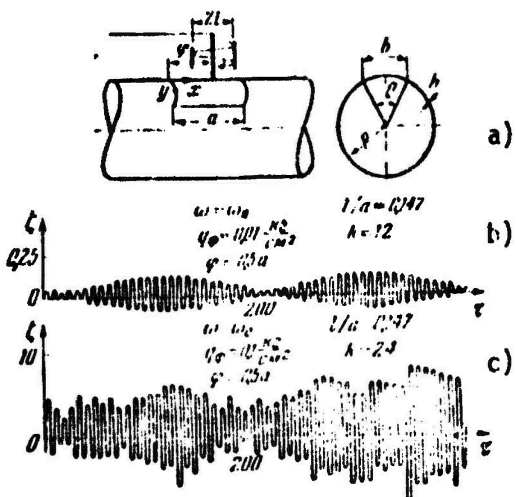


Figure 9.10. Cylindrical panel in the presence of oscillating compression shocks (a) and dynamic reaction for a panel with curvature parameter $k = 12$ (b) and $k = 24$ (c).

As a first approximation, we will study the behavior of the panel under the assumption that the pressure wave front executes vibrations around some fixed section defined by the coordinate $\phi = \text{const}$; in expansion (41), we will consider one term of the series. Then the equations of motion will be written as

$$\begin{aligned} \dot{\xi} &= \xi, \\ \ddot{\xi} &= A_1 \xi + A_2 \dot{\xi} + A_3 \xi^2 + A_4 \xi^3 + A_5, \end{aligned} \quad (9.42)$$

where the following dimensionless parameters were introduced:

$$\begin{aligned}
& \zeta = \frac{t}{h}, \quad \tau = \frac{ct}{a}, \quad A_1 = -\frac{2u}{c} e, \\
& A_2 = \frac{a^3}{c^3 p} \left[\frac{Eh^2 \pi^4}{12(1-\mu^2)} \left(\frac{1}{a^2} + \frac{1}{b^2} \right)^2 + \frac{E}{R^2 a^4 \left(\frac{1}{a^2} + \frac{1}{b^2} \right)^2} \right], \\
& A_3 = -\frac{4Eha^2}{Rc^2 p_0 b} \frac{1}{B - \frac{a}{2\pi} \sin \left(\frac{2\pi}{a} B \right)} \left\{ \frac{1}{a^2 b \left(\frac{1}{a^2} + \frac{1}{b^2} \right)^2} \left[-\frac{4}{3} + \frac{8}{3} \times \right. \right. \\
& \left. \left. \times \cos \left(\frac{\pi}{a} B \right) - \frac{4}{9} \cos^3 \left(\frac{\pi}{a} B \right) \right] + \frac{a}{4B} \left[-\frac{2}{3} \cos^3 \left(\frac{\pi}{a} B \right) + \cos \left(\frac{\pi}{a} B \right) - \frac{1}{3} \right] \right\}, \\
& A_5 = q_f \frac{8a^3}{\pi^3 h^3 c^2 p_0} \frac{1 - \cos \left(\frac{\pi}{a} B \right)}{B - \frac{a}{2\pi} \sin \frac{2\pi}{a} B}.
\end{aligned}$$

The dots denote derivatives with respect to time.

The numerical integration of the system of Eqs. (42) was carried out by means of a digital computer, using the Runge-Kutta method with an automatically selected time step. Results of the computations show that the vibrations of the shell have amplitudes of the order of several wall thicknesses, and the law of change of the amplitudes with time substantially depends on the curvature of the panel $k = b^2/Rh$, the coordinate of the average position of the front, the vibration amplitude l of the front, the vibration frequency w of the disturbing force, the pressure at the front q_f , and the damping coefficient e . At the same time, the dynamic coefficient K_d has large values; for example, for a panel of appreciable curvature, the value $K_d = 13$ was obtained for vibrations of the front at the midspan of the panel with a relative amplitude $l/a = 0.4$. Let us recall that the dynamic coefficient in this case is the ratio of the maximum deflection due to the action on the panel of a load with an oscillating front to the deflection due to a statically applied load. Thus, the deflections determined with and without allowing for the mobility of the load may differ appreciably.

The solution of the nonlinear problem also makes it possible to study the vibratory motions associated with snapping of the panel and constituting a danger in regard to the development of fatigue cracks (see Chapter X below). Figure 9.10 b, c presents the results of computations made for panels with curvature parameters $k = 12$ and $k = 24$; the other characteristics are shown in the figure. The natural

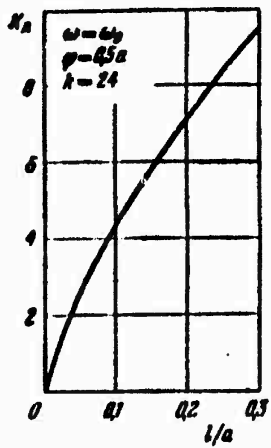


Figure 9.11. Dependence of dynamic coefficient on the vibration amplitude of a pressure shock.

vibration frequency of the panel corresponding to a given wave formation shape is denoted by ω_0 . We see that under the type of loading in question, for a shallow shell, vibrations around the fundamental stable position and vibrations covering the snapped and the fundamental position of equilibrium are possible. In this case, the dynamic coefficient may take the value $K_d = 9$. This is evident from Figure 9.11, where K_d is shown as a function of the parameter l/a .

§102. Experimental Study of the Behavior of Shells Acted on by Moving Pressure Waves

Let us consider certain results of experiments conducted with closed cylindrical shells.* The specimens were fixed with the aid of a special model consisting of a supporting bar at the upstream end of which was mounted a fairing of ogival shape. A pressure gauge was mounted on the cylindrical part of the fairing; a second pressure gauge was placed at the middle of the model. Two shells of the same radius

*These experiments were conducted by E.D. Skurlatov, see [9.13], [9.14], and also Problemy prochnosti, 1972, No. 9.

can be placed simultaneously on the model, while the lengths and thicknesses of the shells may be different. The shell located downstream may be loaded with static axial forces of tension or compression produced by a special device.

For each series of shells, safe values of the pressure at the front q_f and of the pulse J , by which is meant the magnitude of the shaded area in Figure 9.12 a, were chosen in the experiments. The shell was then subjected to the action of pressure waves with steadily increasing values of q_f and J until buckling of the shells occurred. Some results of the experiments are shown in Figure 9.12 a (steel shells) and Figure 9.12 b, c, d (Duralumin shells). Values of q_f and J for which no buckling took place are marked by open circles, and in the presence of buckling, by open triangles. The stability limit determined theoretically is represented by a solid line (see §98). The same graphs show the critical external static pressure q^* uniformly

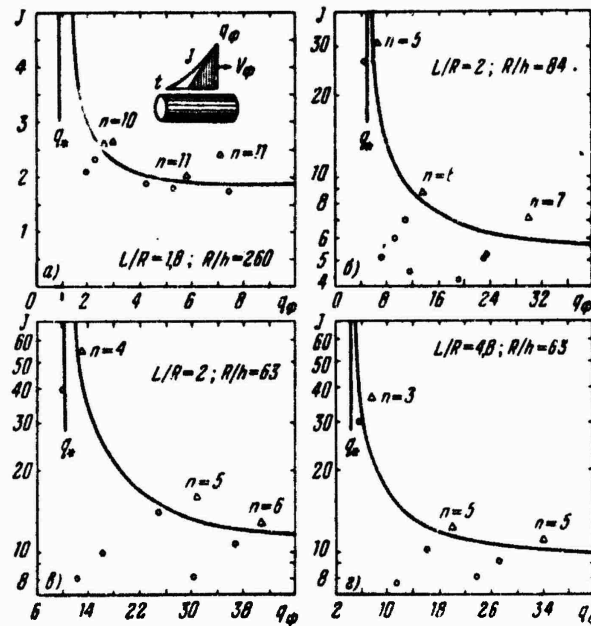


Figure 9.12. Stability limits for a) steel, b), c), d) Duralumin shells.

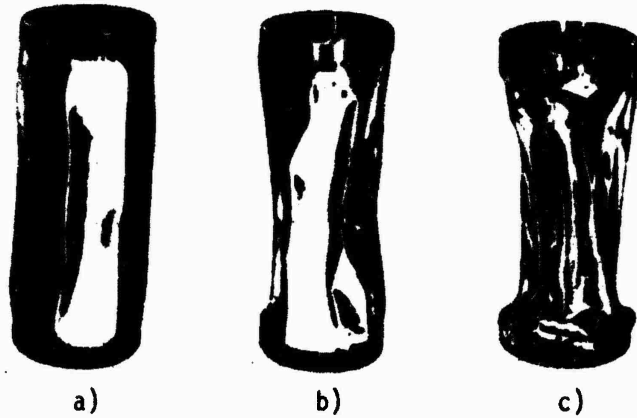


Figure 9.13. Typical wave formation shapes of shells; c) maximum residual strains are reached at the downstream ring frame support.

distributed over the lateral surface. For shells on which bulges formed, data pertaining to the wave formation shapes (n being the number of circumferential dents) are also noted. It is evident that for a pressure at the front slightly exceeding the critical static pressure (left-hand portion of limit) and large pulses (long wave), the shells lose stability in quasi-static form. As the pressure at the front increases and the action time of the load (right-hand portion of limit) decreases, buckling takes place in an increasingly higher form. Moreover, other things being equal, thinner and shorter shells have more circumferential bulges. Figure 9.13 shows typical wave formation shapes of cylindrical shells which buckled under an incident longitudinal pressure wave.

For sufficiently thick shells loaded by a wave with a high pressure at the front and a short-duration load action, an axisymmetric deformation of the shell takes place. As the pressure at the front rises further, such a shell receives residual axisymmetric strains on which nonaxisymmetric dents are superimposed.

In Figure 9.14, the solid line represents the stability limit for a cylindrical shell unstressed in the axial direction, and the dashed line with a black triangle shows the stability limit of the same shell compressed by an axial force amounting to 0.278 of the upper static critical load. It is evident that the unstressed shell buckles under a pulse 1.5 times greater than the compressed shell.

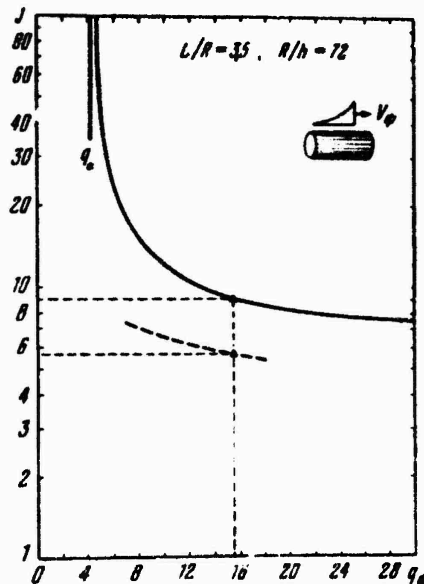


Figure 9.14. Stability limits for a shell unstressed in the axial direction (solid line) and a shell compressed by an axial force.

The buckling of shells subjected to combined loading is characterized by the formation of rhomboidal dents with smooth outlines. Figure 9.15 b shows a photograph of a shell that lost stability under combined loading, and for comparison the left side of the figure shows a shell of the same type which buckled under the action of the pressure wave only.

Another purpose of these experiments was to study the resonance phenomena and transient processes in shells simultaneously acted on by axial static forces and by the dynamic load produced by a moving wave. The pressure wave front was incident at right angles to the longitudinal axis of the shell. On the inner side of the shell near the ends, strain gauges were attached (Figure 9.16 shows the gauge numbers) that made it possible with the aid of a cathode oscillograph to record the dynamic strains of the shell walls. The incident velocity of the pressure wave front and the pressure at the front and behind it were also measured.



Figure 9.15. Characteristic buckling shape of a shell under: a) the action of a pressure wave only, b) combined loading.

Figure 9.16 shows oscillograms of strain ϵ of the shell for an incident pressure wave with velocities of 665 and 935 m/sec and axial compressive stresses amounting to 0.5 and 0.94 of the experimental value of the static critical stress. Comparison of oscillograms recorded for different sections of the shell shows that the dynamic strain increases along the shell and reaches its maximum value at the trailing edge (see §98). Comparing the oscillograms shown in Figure 9.16 a and 9.16 b, one can conclude that the strains of a shell compressed with axial stress amounting to $0.5 p_{cr}$ are much higher than the dynamic strains of a shell compressed with greater axial stresses, equal to $0.94 p_{cr}$; this shows an appreciable shift of the critical velocity for the given shell (see §§96, 98).

Considering the oscillograms shown in Figure 9.16, one can conclude that the dynamic strains of the shell acted on by a shock wave traveling at 935 m/sec are greater than the strains at 665 m/sec.

§103. Behavior of Closed Cylindrical Shells in a Short-Duration Gas Flow

Previously, we considered a moving pressure wave of a given profile, and it was assumed that the action of the pressure was normal to the surface of the shell and that the pressure on the surface of the shell was equal to the pressure in the incident wave. However, no account was taken of the fact that the pressure transmitted to the surface of the deformed shell will be somehow redistributed as a function of

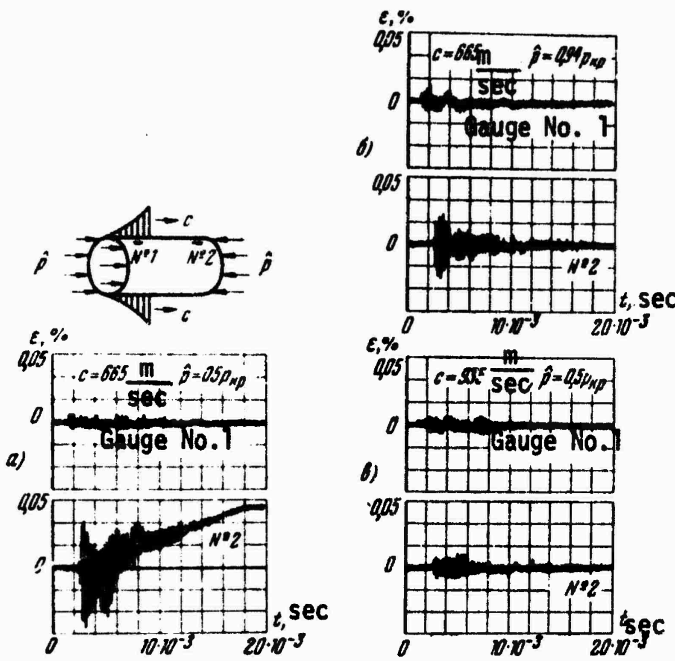


Figure 9.16. Oscillograms of dynamic strains of a shell for different compressive axial stresses and incident velocities of the pressure wave front.

the wave formation shape of the shell. As will be shown below, consideration of such forces produced by the incident flow gives rise to dynamic deflections substantially exceeding the deflections calculated by assuming that the flow is absent.* The wave formation shape also changes in this case [9.13].

We will consider the problem of the behavior of a closed circular cylindrical shell acted on by a wave of exponential profile and a gas wake flow of increased density incident on the shell along the generatrix.

*This solution was given by E.D. Skurlatov and the author [9.4]; see Theory of Plates and Shells, Nauka, Moscow, 1971, 29-33.

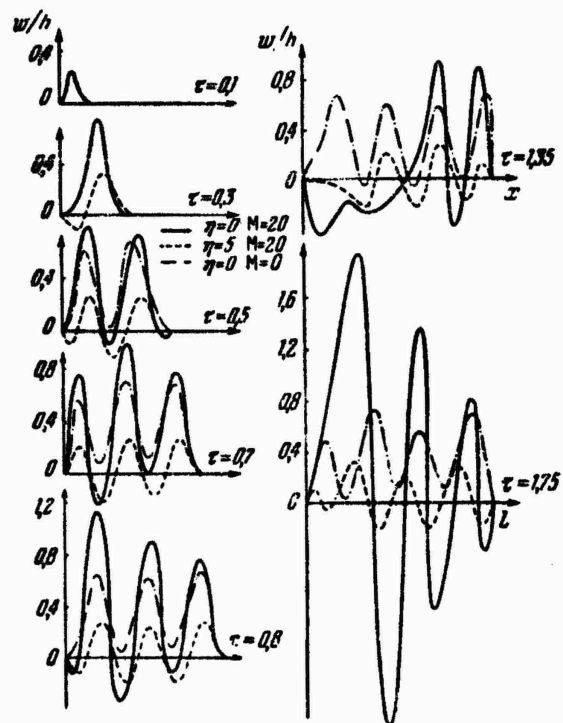


Figure 9.17. Distribution with time of dynamic deflections along a shell subjected to a pressure wave (dot-dash lines) and to pressure waves together with a wake flow (solid lines).

To solve this problem, nonlinear equations in displacements (1.27)-(1.29) were written.

The expression for the load intensity must include the pressure due to the traveling wave and the pressure caused by the incident gas flow, which will be considered supersonic. We will assume that the pressure and velocity of the gas behind the front also change exponentially. Then (see [0.6])

$$q = q_0 e^{-\eta(ct-x)} H(ct-x) + \\ + q_0 e^{-\eta(ct-x)} H(ct-x) \left[1 - \right. \\ \left. - \left(1 + \frac{x-1}{2} M \frac{\partial w}{\partial x} \right)^{\frac{2x}{x-1}} \right]. \quad (9.43)$$



Figure 9.18. Shape
of residual dents
and character of
failure of a panel
in a supersonic gas
flow.

where q_f is the pressure at the wave front, n is the exponential index determining the law of change of pressure behind the front, x is the polytropic index, M is the Mach number of the incident flow, and d is the velocity of the pressure wave front.

The equations of motion, represented in finite differences, were solved on a digital computer; the rectangular development of the shell surface was covered with a grid having from 30 to 60 nodes in the longitudinal and circumferential directions. Omitting the details of the computational scheme, let us consider some results.

For different instants of time, Figure 9.17 shows curves characterizing the distribution of dynamic deflections along a shell with parameters $L = 250$ mm, $R = 50$ mm, $h = 0.2$ mm, acted on by a long wave ($n = 0$) together with a flow (solid line) and by a pressure wave only (dot-dash line). For comparison, this figure also shows data obtained for a short wave ($n = 5$) together with a flow (dashed line). It was assumed that the pressure at the wave front was 10 atm, and the velocity of the gas particles behind the front corresponded to $M = 20$.

It is evident from the graphs that the influence of the flow on the transient process of deformation of the shell is significant and is manifested as early as the first few moments following the arrival of the wave front. With time, the vibration modes of the shell obtained by solving the problem with and without consideration of the flow differ increasingly; the shell past which the flow is moving executes intensive vibrations with amplitudes considerably exceeding the amplitudes caused by the pressure wave alone. The dimensionless time $t = ct/L$ is laid off on the graphs. Analysis of the distribution of the stresses set up in the middle surface of the shell leads to the conclusion that zones with stresses approaching the yield point in magnitude are formed in the shell. These zones are staggered and move in the direction of the flow while continually changing their outlines. The presence of such moving zones apparently explains the residual bulges covering the greater part of the surface of shells that have undergone flutter-type vibrations for a certain period of time.

Figure 9.18 shows a photograph of a part of the lateral surface of a cylindrical panel tested during the action of such a load. The dimensions of the dents increase toward the trailing edge; failure of the panel also begins at the trailing edge along the boundaries of the dents. A similar pattern occurs in "impulsive" flutter.

Comparing the data (see Figure 9.17) for a short and a long wave in the presence of the load produced by a flow, one can conclude that the amplitudes of the shell walls during a flow of shorter duration are much smaller.

§104. Experimental Study of the Behavior of Shells During Longitudinal Pulsating Compression Shocks

To study the behavior of flexible shells in the presence of pulsating compression shocks, a series of experiments with cylindrical shells were carried out.* The shell parameters were $L/R = 4$ and 7.4 ; $R/h = 250$.

*See the reference on p. 451).



Figure 9.19. Change of pressure with time at a point of the surface of the model in transonic flow.

To measure the normal pressure due to pulsating shocks, a piezoelectric gauge placed on the cylindrical part of the fairing was used. Measurement of dynamic deformations was carried out by means of a strain gauge stuck to the inner surface of the shell. Signals from both gauges were fed to a double oscillograph. The longitudinal axial forces remained unchanged during the experiment. The velocity of the incident flow changed from subsonic to supersonic.

The character of pressure variation with time at $M < 1$ is illustrated by the oscillogram shown in Figure 9.19. Evidently, the tested shell was subjected to compression shocks having an approximately constant vibration frequency. The pressure spikes on the oscillogram correspond to the instant when the shock front is located at the middle of the sensitive element of the gauge. As the front moves on along the flow, the pressure decreases, then increases again, since the surface of the gauge is reached by the next pulsating shock which has the same vibration frequency and maximum amplitude.

Results of high-speed photography also indicate that the shell is continually reached by series of shocks moving over the surface of the shell in the direction of the flow, while simultaneously executing vibrations around the middle position. The most vigorous vibrations occurred when the pulsation frequency of the compression shocks coincided with one of the natural frequencies of the shell; the frequency change was achieved by selecting a suitable magnitude of the compressive forces.

Failure of the walls usually began in the region of the surface located near the trailing edge of the shell, with the formation of cross-shaped cracks; three

to five seconds elapsed from the moment of formation of cracks to the complete failure of the shell.

Studies of the effect of moving pulsating compression shocks should be continued.

In conclusion, let us note that the behavior of shells acted on by pressure waves has been dealt with chiefly in the linear formulation by a number of authors: Carrier (Carrier, G.F., Techn. Rep. No. 4, Brown Univ., 1951), Mindlin and Bleich (Mindlin, R.D. and Bleich, H.H., J. Appl. Mech. 20, No. 2, 1953), V.V. Novozhilov (Prikl. matem. i mekhan. 23, No. 4, 1959), A.A. Il'yushin and P.M. Ogibalov (Elastoplastic deformation of hollow cylinders, Izd-vo Mosk. gosud. un-ta, 1960), A.P. Filippov [0.27], L.I. Balabukh [5.2], N.A. Kii'chevskiy [5.11 a], E.I. Grigolyuk, L.M. Kurshin, V.L. Prisekin (DAN SSSR 155, No. 1 (1964)), and others.

Chapter X

Problems of Statistical Dynamics

§105. Description of the Problems and Methods of Investigation

We will consider nonlinear problems in which the study of the behavior of plates and shells involves the use of the theory of random functions.

Below, emphasis will be placed on vibrations and stability of shells in an acoustic field. An essentially nonlinear character of the behavior of plates and shells during loading with sound pressure has been observed in a number of studies.* Most important is the study of nonlinear vibrations of structural elements tending to lose stability in the large. Acoustic vibrations in this case are characterized by significant deflections and may be accompanied by snapping of the shells, causing a rapid failure of the structure (see §41).

The present chapter will discuss the behavior of shells in similar cases of loading, account being taken of the random nature of the acoustic load. The objective is to obtain the probability characteristics of motion of a system with a tendency to snap.** The random process of change of acoustic pressure will be represented in the form of white noise. It was found that the acoustic radiation of motors is characterized by a nearly constant spectral density over a wide frequency range (see [10.27, 10.40, 10.65]). This characteristic makes it possible to approximate this type of acoustic pressure with white noise and to use the device of the theory of Markov processes in solving the problem. Application of nonlinear shell theory using the statistical approach makes it possible to analyze various types of shell vibrations.

*See the articles [3.11a], [10.32, 10.42, 10.44].

**The methods of solution of these problems in the determinate formulation for cases in which the acoustic pressure may be represented as changing according to the harmonic law are presented in Chapter III.

The most important probability characteristics of the behavior of a dynamic system can be obtained if the laws of distribution of the "output characteristics", i.e., generalized coordinates, are known. The device of the theory of Markov processes and Fokker-Planck-Kolmogorov type equations (FPK equations) permits the determination of the probability density for generalized coordinates on the basis of a general form of the corresponding equation of motion of the system. This method can also be applied in the case of a system with several equilibrium positions.*

As already stated, the discussion of the behavior of systems in an acoustic field with the aid of such methods is important for calculations of the strength and endurance of aircraft skin panels. Let us consider these practical applications in more detail.

As we know, the skin of an airplane body absorbs acoustic pressures produced by the jet of the engines, which is the source of loud noise. This leads in many cases to the fatigue failure of such structural elements of the plane as the trailing-edge assembly, flaps, ailerons, skin and ribs of the horizontal tail. In the presence of low-frequency pulsations, intense vibrations of whole assemblies, for example, the tail unit, may occur [10.38, 10.60].

Vibrations of parts of aircraft caused by acoustic pressure frequently disturb the operating conditions of various instruments and systems. For example, an inadmissible precession of the gyroscopes and breakdown of electronic equipment, hydraulic systems, etc. are possible. Damage due to acoustic loads can be very serious (see [10.60, 10.55]); this applies, for example, to the skin panels of the pressurized body of an airplane.

In recent years, problems in this area have become particularly important in aviation in connection with a more rapid increase in flying speed, weight, and overall

*The first investigations in this area with application to shells were carried out by I.I. Vorovich [10.10], V.M. Goncharenko [10.11] and M.F. Dimentberg [10.12].

dimensions of the structures. This involves, on the one hand, an increased thrust of the engines, and hence, an increased power of the jet. On the other hand, there is an increase in the acoustic pressures not directly connected with the engine and caused by pulsations in the turbulent boundary layer, pulsations of shock waves, etc.

An acoustic load level in excess of 150 decibels (dB) is considered dangerous for the strength of panels in existing airframes. However, judging from the data of [10.60], this value was exceeded back in the 1950's. The first reports of failures of skin sections under the influence of acoustic pressure appeared at that time. In 1970, this level was already in excess of 170 dB. Moreover, pressures up to 180 dB have been recorded in the acoustic near field.*

Acoustic pressures of high frequency reaching several thousand cycles may cause the destruction of structural members in a short time. Even when the stresses due to an acoustic load are comparatively small and below the endurance limit for a given material, they may substantially shorten the service life of individual members of the structures, particularly if repeated forces of a different origin are acting simultaneously.

The fact that acoustic loads have a very broad frequency spectrum seriously complicates the "detuning" of the structure relative to the resonant vibration mode by shifting the natural frequencies. Simulation of a real system acted on by an acoustic load is very complex. Costly full-scale tests of aircraft structures for acoustic strength are frequently conducted. Such experiments require prolonged operation of the engines at maximum power and the use of unique measuring equipment [10.39].

Another important factor causing vibrations of aircraft skin elements are pulsations in the turbulent boundary layer; the corresponding acoustic loads reach their highest intensity during flight under conditions of maximum dynamic head q_{\max} .**

*See Noise of Rockets in the Journal Space Aeronautics 44, No. 5, 1965.

**See V.S. Petrovskiy, Hydrodynamic Problems of Turbulent Noise, Sudostroyeniye, 1966.

Still another possible source of appreciable acoustic loads is the turbulent wake, located behind a moving vehicle. This wake has approximately the same structure as the wake of a jet engine. However, for the jet, the curve of additional velocities has a peak directed against the direction of flight, while for the wake, the peak is in the direction of flight [10.26, 10.33].

Fatigue failures for subsonic and supersonic aircraft are also called flow separation, for example, in the region of the wing-fuselage joint. This phenomenon may also take place when the jet from the engine compressor or pneumatic system is directed perpendicular to the flight velocity. The pressure fluctuations caused by the flow separation turn out to be so large that they can cause sharp vibrations of members located at a considerable distance from the separation site. Pressure fluctuations with an intensity of 160 dB at a relatively subsonic flight velocity have been observed. The character of the fatigue cracks formed in these cases is similar to that observed in the presence of acoustic pressures [10.26].

§106. Plate in an Acoustic Field. Law of Deflection Distribution

Let us consider the solution of problems of the behavior of plates acted on by acoustic radiation.* We will first discuss the case of a plate hinged along the contour. We will assume that in addition to an acoustic load, the plate is subjected to static axial compression forces. The plate is assumed to have initial deflections.

The initial equations of the theory of flexible plates will be taken in the form of (1.42a), (1.43a); here $q(t)$ is a random process of variation of acoustic pressure.

For the case of hinged support of the plate edges, we approximate the total and additional deflections by expressions (3.2), (3.3). Using the Bubnov-Galerkin method, we arrive at the expressions obtained in § 38 for $m = n = 1$. An equation of motion of the type of (3.5), will be written in the form (allowing for damping)

*The results given in §§ 106-114 are due to I.G. Kildibekov [10.15]; see also [10.9].

$$\frac{d^2\zeta}{dt^2} + 2\alpha \frac{d\zeta}{dt} + \omega_0^2 \left(1 - \frac{p^*}{p_0}\right) (\eta\zeta^2 - \beta\zeta^2 + a\zeta) - \xi_0 \omega_0^2 \frac{F^*}{p_0} = q^*(t), \quad (10.1)$$

where the acoustic pressure parameter in the case of uniform distribution over the plate surface

$$q^*(t) = \frac{16}{3\sqrt{E}} \left(\frac{\rho}{h}\right)^{1/2} q(t). \quad (10.2)$$

The quantities ω_0^2 , p_0^* , α , β , η entering into Eq. (1) are determined from the corresponding formulas of Chapter III for $m = n = 1$. We will study the vibrations of the plate on the assumption that $q^*(t)$ is white noise with a zero average value and a spectral density equal to S_0 .

In this and the subsequent sections, we will use an approach to the problem whereby the vibrations of a system acted on by white noise are represented in the form of some smoothed Markov type process. This assumption will be used below in determining the probability density of the extrema on the basis of a two-dimensional distribution function of the coordinate and velocity with the aid of Rice's formula [10.54]. This approach to the solution of the problem was taken by Lyon [10.46] in a discussion of a narrow-band process of vibrations of a system with a single position of stable equilibrium. In § 110, this method is applied to a system with snapping having two positions of stable equilibrium.* The deformation of the plate is represented in the form of a two-dimensional Markov process of change in deflection ζ and velocity $\dot{\zeta} = d\zeta/dt$.

We will cite certain facts from the theory of Markov processes that will be useful

*Another approach to the determination of the probability density of the coordinate for a system with snapping, requiring the knowledge of a three-dimensional distribution function of the coordinate, velocity, and acceleration, was given by M.F. Dimentberg [10.12].

below. A Markov process is one whose probability properties in the next time interval are determined by the value of the function at the given instant and are independent by the value of the function at the given instant and are independent of its former values. A process taking place in a physical system is referred to as a Markov process (process without aftereffect) if, the state of the system at time t_0 being known, the probability distribution of the states of the system for $t > t_0$ is independent of any information on the course of the change of its states up to time t_0 . Thus, a distinctive feature of a Markov process is the fact that a probabilistic estimation of the state of the system at the end of each time interval depends only on the characteristic of its state at the beginning of this interval and is independent of the previous history of the process.

A continuous process without aftereffect is characterized by the transition function $F(x, t|y, \tau)$, which expresses the probability Φ that at time t the value of some random function $\xi(t)$ will be below the level x if at time τ preceding time t the random function had the value y

$$\Phi[\xi_t < x | \xi_\tau = y] = F(x, t|y, \tau).$$

The probability density of the transition

$$f(x, t|y, \tau) = \frac{\partial F(x, t|y, \tau)}{\partial x}.$$

Let the random function change from the value y to the value x , not directly, but by assuming a certain intermediate value z at time s located in the interval between t and τ : $t < s < \tau$. The probability density of the transition from y to z , then to x , is expressed as a product of the densities for each transition, i.e., $f(x, t|z, s)f(z, s|y, \tau)$. The result of the integration of this expression over all z determines the probability density of the transition from the value y to the value x :

$$f(x, t|y, \tau) = \int_{-\infty}^{\infty} f(x, t|z, s)f(z, s|y, \tau) dz. \quad (10.3)$$

From this relation, known as the Chapman-Kolmogorov equation, the FPK equation is derived.* For a one-dimensional process, it has the form

$$\frac{\partial f}{\partial t} = - \frac{\partial}{\partial x} (Af) + \frac{1}{2} \frac{\partial^2}{\partial x^2} (Bf), \quad (10.4)$$

where

$$\left. \begin{aligned} A(z, t) &= \lim_{\Delta t \rightarrow 0} \frac{1}{\Delta t} \int_{-\infty}^{\infty} (x - z) f(x, t + \Delta t | z, t) dx, \\ B(z, t) &= \lim_{\Delta t \rightarrow 0} \frac{1}{\Delta t} \int_{-\infty}^{\infty} (x - z)^2 f(x, t + \Delta t | z, t) dx. \end{aligned} \right\} \quad (10.5)$$

Thus, the average displacement of a point during the interval Δt will be $A(z, t)\Delta t$, and the average dispersion of the displacement will be $B(z, t)\Delta t$. Let us denote the average value by M and represent (5) in the form

$$A(z, t) = \lim_{\Delta t \rightarrow 0} \frac{M(\Delta z)}{\Delta t}, \quad B(z, t) = \lim_{\Delta t \rightarrow 0} \frac{M((\Delta z)^2)}{\Delta t}. \quad (10.5a)$$

If one studies the change in the states of some system characterized by several random functions, an n -dimensional process be characterized by the parameters x_1, x_2, \dots, x_n . The probability density f for such a process will be the transition function $f(\bar{x}, t | \bar{y}, \tau)$. The FPK equation for this function takes the form

$$\frac{\partial f}{\partial t} = - \sum_{i=1}^{i=n} \frac{\partial}{\partial x_i} (A_i f) + \frac{1}{2} \sum_{i=1}^n \sum_{j=1}^n \frac{\partial^2}{\partial x_i \partial x_j} (B_{ij} f). \quad (10.6)$$

Here the coefficients A_i, B_{ij} will be functions of $A_i(\bar{x}, t), B_{ij}(\bar{x}, t)$; they are determined by relations of the type of (5)

*See for example the book [0.6], pp. 898-901.

$$\begin{aligned}
 A_{ij}(\bar{x}, t) &= \lim_{\Delta t \rightarrow 0} \frac{1}{\Delta t} \int_{-\infty}^{\infty} \dots \\
 &\quad \dots \int_{-\infty}^{\infty} (x_i - z_i) f(\bar{x}, t + \Delta t | \bar{x}, t) dx_1 dx_2 \dots dx_n, \\
 B_{ij}(\bar{x}, t) &= \lim_{\Delta t \rightarrow 0} \frac{1}{\Delta t} \int_{-\infty}^{\infty} \dots \\
 &\quad \dots \int_{-\infty}^{\infty} (x_i - z_i)(x_j - z_j) f(\bar{x}, t + \Delta t | \bar{x}, t) dx_1 dx_2 \dots dx_n.
 \end{aligned} \tag{10.7}$$

Expressions of the type of (5a) will be written

$$\left. \begin{aligned}
 A_i(\bar{x}, t) &= \lim_{\Delta t \rightarrow 0} \frac{M[\Delta z_i]}{\Delta t}, \\
 B_{ij}(\bar{x}, t) &= \lim_{\Delta t \rightarrow 0} \frac{M[\Delta z_i \Delta z_j]}{\Delta t}.
 \end{aligned} \right\} \tag{10.7a}$$

In the case of a stationary Markov process, $\partial f / \partial t = 0$. Equation (4) will be written as follows:

$$-\frac{\partial}{\partial x} [A(x)f(x)] + \frac{1}{2} \frac{\partial^2}{\partial x^2} [B(x)f(x)] = 0. \tag{10.4a}$$

For an n-dimensional process, instead of (6) we obtain

$$-\sum_{i=1}^n \frac{\partial}{\partial x_i} [A_i(\bar{x})f(\bar{x})] + \frac{1}{2} \sum_{i=1}^n \sum_{j=1}^n \frac{\partial^2}{\partial x_i \partial x_j} [B_{ij}(\bar{x})f(\bar{x})] = 0. \tag{10.6a}$$

We will set up an FPK equation for the plate under consideration. We will find the values of A_i , B_{ij} for this equation. The process $q^*(t)$ in Eq. (1), as was noted above, is considered as white noise with a zero average value and a spectral density S_0

$$M_{q^*} = 0, \quad M[q^*(t_1) q^*(t_2)] = 2\pi S_0 \delta(t_1 - t_2). \quad (10.8)$$

Further, we find

$$A_1 = \lim_{\Delta t \rightarrow 0} \frac{M[\Delta x_1]}{\Delta t} = x_2 = \dot{t}, \quad (10.9)$$

$$A_2 = \lim_{\Delta t \rightarrow 0} \frac{M[\Delta x_2]}{\Delta t}. \quad (10.10)$$

where Δx_2 is determined from the equation of motion of the shell (1). Then

$$A_2 = \lim_{\Delta t \rightarrow 0} \frac{M \left[-2e\dot{t} - \omega_0^2 \left(1 - \frac{p^*}{p_0} \right) (\alpha\zeta - \beta\zeta^2 + \eta\zeta^3) + \zeta_0 \omega_0^2 \frac{p^*}{p_0} \right] \Delta t}{\Delta t} + \\ + \lim_{\Delta t \rightarrow 0} \frac{M \left[\int_t^{t+\Delta t} q^*(u) du \right]}{\Delta t}, \quad (10.11)$$

Considering the first of conditions (8)

$$A_2 = -2e\dot{t} - \omega_0^2 \left(1 - \frac{p^*}{p_0} \right) (\alpha\zeta - \beta\zeta^2 + \eta\zeta^3) + \zeta_0 \omega_0^2 \frac{p^*}{p_0}, \quad (10.12)$$

$$B_{11} = \lim_{\Delta t \rightarrow 0} \frac{M[(\Delta x_1)^2]}{\Delta t} = 0, \quad (10.13)$$

$$B_{12} = B_{21} = \lim_{\Delta t \rightarrow 0} \frac{M[\Delta x_1 \Delta x_2]}{\Delta t} = 0, \quad (10.14)$$

$$B_{22} = \lim_{\Delta t \rightarrow 0} \frac{M[(\Delta x_2)^2]}{\Delta t}, \quad (10.15)$$

or

$$B_{22} = \lim_{\Delta t \rightarrow 0} \frac{1}{\Delta t} M \left\{ \left[-2e\dot{t} + \omega_0^2 \left(1 - \frac{p^*}{p_0} \right) (\alpha\zeta - \beta\zeta^2 + \eta\zeta^3) + \zeta_0 \omega_0^2 \frac{p^*}{p_0} \right] \Delta t + \int_t^{t+\Delta t} q^*(u) du \right\}^2 = \\ = \lim_{\Delta t \rightarrow 0} M \left\{ \left[-2e\dot{t} + \omega_0^2 \left(1 - \frac{p^*}{p_0} \right) (\alpha\zeta - \beta\zeta^2 + \eta\zeta^3) + \zeta_0 \omega_0^2 \frac{p^*}{p_0} \right]^2 \Delta t + \right. \\ \left. + 2 \left[-2e\dot{t} + \omega_0^2 \left(1 - \frac{p^*}{p_0} \right) (\alpha\zeta - \beta\zeta^2 + \eta\zeta^3) + \zeta_0 \omega_0^2 \frac{p^*}{p_0} \right] \int_t^{t+\Delta t} q^*(u) du + \right. \\ \left. + \frac{1}{\Delta t} \int_t^{t+\Delta t} \int_t^{t+\Delta t} q^*(u_1) q^*(u_2) du_1 du_2 \right\}. \quad (10.16)$$

On the basis of the properties of the load, from (8) we obtain

$$B_{22} = 2\pi S_0.$$

We now write the stationary FPK equation for the combined probability density $f(\zeta, \dot{\zeta})$ of the coordinate ζ and velocity $\dot{\zeta}$:

$$-\frac{\partial}{\partial \zeta} (A_1 f) - \frac{\partial}{\partial \dot{\zeta}} (A_2 f) + \frac{1}{2} \left[\frac{\partial^2}{\partial \zeta^2} (B_{11} f) + \frac{\partial^2}{\partial \zeta \partial \dot{\zeta}} (B_{12} f) + \frac{\partial^2}{\partial \dot{\zeta}^2} (B_{22} f) \right] = 0. \quad (10.17)$$

Substituting into this equation the values of the coefficients found above, we obtain

$$-\frac{\partial}{\partial \zeta} (\dot{U}) - \frac{\partial}{\partial \dot{\zeta}} \left\{ \left[-2e\dot{\zeta} - \omega_0^2 \left(1 - \frac{P^*}{P_0} \right) (\alpha_0^* - \beta_0^* \dot{\zeta} + \eta_0^* \ddot{\zeta}) + \zeta_0 \omega_0^2 \frac{P^*}{P_0} \right] f \right\} + \pi S_0 \frac{\partial^2 f}{\partial \dot{\zeta}^2} = 0. \quad (10.18)$$

This equation will be represented as follows:

$$\frac{\partial}{\partial \zeta} \left\{ \left[\omega_0^2 \left(1 - \frac{P^*}{P_0} \right) (\alpha_0^* - \beta_0^* \dot{\zeta} + \eta_0^* \ddot{\zeta}) - \zeta_0 \omega_0^2 \frac{P^*}{P_0} \right] f + \frac{\pi S_0}{2e} \frac{\partial f}{\partial \dot{\zeta}} \right\} + \left(-\frac{\partial}{\partial \dot{\zeta}} + 2e \frac{\partial}{\partial \zeta} \right) \left(\dot{U} + \frac{\pi S_0}{2e} \frac{\partial f}{\partial \dot{\zeta}} \right) = 0. \quad (10.19)$$

We will require that the combined probability density $f(\zeta, \dot{\zeta})$ satisfy the two equations obtained by equating to zero the corresponding parts of (19):

$$\left[\omega_0^2 \left(1 - \frac{P^*}{P_0} \right) (\alpha_0^* - \beta_0^* \dot{\zeta} + \eta_0^* \ddot{\zeta}) - \zeta_0 \omega_0^2 \frac{P^*}{P_0} \right] f - \frac{\pi S_0}{2e} \frac{df}{d\zeta} = 0, \quad (10.20)$$

$$\dot{U} + \frac{\pi S_0}{2e} \frac{df}{d\dot{\zeta}} = 0. \quad (10.21)$$

Hence we obtain for a stationary process

$$f(\zeta, \dot{\zeta}) = f(\zeta) f(\dot{\zeta}), \quad (10.22)$$

where the probability density of the coordinate will be

$$f(\zeta) = \frac{1}{C} \exp \left[-\frac{1}{S_0^*} \left(1 - \frac{P^*}{P_0} \right) \left(a_{\zeta}^{*2} - \frac{2}{3} \beta_{\zeta}^{*3} + \frac{1}{2} \zeta^4 \right) + \frac{2}{S_0^*} \frac{P^*}{P_0} \zeta \dot{\zeta} \right], \quad (10.23)$$

and the law of velocity distribution will be

$$f(\dot{\zeta}) = \frac{1}{C'} e^{-\frac{1}{S_0^* \omega_0^2} \dot{\zeta}^2}. \quad (10.24)$$

The following notation was used in (23) and (24):

$$S_0^* = \frac{\pi S_0}{e \omega_0^2}. \quad (10.25)$$

The quantity S_0^* is equal to twice the value of the mean square of the dimensionless bending deflection of an ideal linear system in the absence of compressive forces. The constants C and C' are determined from the normalization condition. The value of C is

$$C = \int_{-\infty}^{\infty} \exp \left[-\frac{1}{S_0^*} \left(1 - \frac{P^*}{P_0} \right) \left(a_{\zeta}^{*2} - \frac{2}{3} \beta_{\zeta}^{*3} + \frac{1}{2} \zeta^4 \right) + \frac{2}{S_0^*} \frac{P^*}{P_0} \zeta \dot{\zeta} \right] d\zeta. \quad (10.26)$$

The value of C' will be

$$C' = \int_{-\infty}^{\infty} e^{-\frac{1}{S_0^* \omega_0^2} \dot{\zeta}^2} d\dot{\zeta} = \omega_0 \sqrt{\pi S_0^*}. \quad (10.27)$$

We find the mean square of the deflection

$$\text{M}[\zeta^2] = \int_{-\infty}^{\infty} \zeta^2 f(\zeta) d\zeta. \quad (10.28)$$

§107. Distribution of Deflection Extremums for a Plate

We will now consider another characteristic of dynamic strength of a plate, related to the law of distribution of deflection extrema. The method employed here is based on the assumption that the vibratory process is a narrowband process. In this case, the expression for the probability density of the maxima and minima of the coordinate may be obtained by using the concept of the average relative frequency of crossings of a given level by the process. The average number per unit time of maxima located above a certain level ζ is equal to the average number of times per unit time v_{ζ}^+ that the process exceeds this level (crossovers of this level from the bottom upward) and is found from Rice's formula (see [0.6], p. 903)

$$v_{\zeta}^+ = \int_0^{\infty} f(\zeta, t) dt. \quad (10.29)$$

where $f(\zeta, t)$ is a two-dimensional distribution function found from the FPK equation. On the other hand, the average number v_m^* of all possible maxima is equal to the number of times v_{ζ}^+ that the process exceeds the initial level ζ_1

$$v_m^* = v_{\zeta_1}^+ = \int_0^{\infty} f(\zeta_1, t) dt. \quad (10.30)$$

The ratio of v_{ζ}^+ to v_m^* characterizes the relative frequency with which the process exceeds the given level

$$n = \frac{v_{\zeta}^+}{v_m^*}. \quad (10.31)$$

It is obvious that the value of n determines the probability $f(\zeta_{\max} > \zeta)$ that the maximum of the coordinate will exceed the level ζ :

$$f(\zeta_{\max} > \zeta) = n. \quad (10.32)$$

We now calculate the integral distribution function of the maxima

$$F(\zeta_{\max}) = F(\zeta_{\max} < \zeta) = 1 - \frac{v_{\zeta}^+}{v_{\zeta_1}^+}. \quad (10.33)$$

The expression for the probability density of the maxima takes the form

$$f(\zeta_{\max}) = -\frac{1}{v_{\zeta_1}^+} \frac{dv_{\zeta}^+}{d\zeta}. \quad (10.34)$$

We similarly obtain a formula for the probability density of the minima

$$f(\zeta_{\min}) = \frac{1}{v_{\zeta_1}^+} \frac{dv_{\zeta}^+}{d\zeta}. \quad (10.35)$$

The probability density of the extrema in the case of a system with a single equilibrium position will have the form

$$f(\zeta_{\max, \min}) = \mp \frac{1}{v_m} \frac{dv_{\zeta}^+}{d\zeta} = \mp \frac{1}{v_{\zeta_1}^+} \frac{dv_{\zeta}^+}{d\zeta}. \quad (10.36)$$

Calculating $f(\zeta_{\max})$, for a narrowband process we must consider only the region $\zeta > \zeta_1$, and in determining $f(\zeta_{\min})$, the region $\zeta < \zeta_1$; in the remaining regions, the corresponding densities will be equal to zero. Replacing in (36) the numbers v by their values from Rice's formula (29) and considering relation (22), we obtain

$$f(\zeta_{\max, \min}) = \mp \frac{1}{f(\zeta_1)} \frac{df(\zeta)}{d\zeta}. \quad (10.37)$$

Substituting (23) into the above, we arrive at the final formula

$$\begin{aligned} f(\zeta_{\max, \min}) &= \pm \frac{2(S_0^* C)^{-1} \left(1 - \frac{P^*}{P_0}\right)}{f(\zeta_1)} \left(\alpha \zeta - \beta \zeta^2 + \gamma \zeta^3 - \frac{\zeta_0}{\frac{P_0}{P^*} - 1} \right) \times \\ &\times \exp \left[-\frac{1}{S_0^*} \left(1 - \frac{P^*}{P_0}\right) \left(\alpha \zeta^2 - \frac{2}{3} \beta \zeta^3 + \frac{1}{2} \gamma \zeta^4 \right) + \frac{2}{S_0^*} \frac{P^*}{P_0} \zeta_0 \zeta \right]. \end{aligned} \quad (10.38)$$

§108. Acoustic Vibrations of a Cylindrical Shell. Model of a System with Many Degrees of Freedom

We will study the behavior of a closed circular cylindrical shell hinged at the ends, acted on by an external pressure q , including actions of the type of random processes and static axial compression forces p uniformly distributed over the end sections.*

Equations of the type of (1.40), (1.41) allowing for damping and external pressure will be

$$\frac{D}{h} \nabla^4 (w - w_0) = L(w, \Phi) + \frac{1}{R} \frac{\partial^2 \Phi}{\partial x^2} - p \frac{\partial^2 w}{\partial t^2} - 2\rho e \frac{\partial w}{\partial t} + \frac{q(x, y, t)}{h}, \quad (10.39)$$

$$\frac{1}{E} V^4 D = -\frac{1}{2} [L(w, w) - L(w_0, w_0)] - \frac{1}{R} \frac{\partial^2 (w - w_0)}{\partial x^2}. \quad (10.40)$$

The quantity q includes the static pressure q_0 and random processes $q_1(t)$, $q_2(t)$, having the character of white noise:

$$q(x, y, t) = [q_0 + q_1(t) \sin rx \sin sy + q_2(t) \sin^2 rx]. \quad (10.41)$$

As in § 29, the problem will be discussed for a design model in the form of a system with two degrees of freedom. For the additional and initial deflections, we will use expressions (2.159), (2.160).

A system of equations of the type of (2.163), (2.164) reduces to the form

$$\frac{d^2 \xi_1}{dt^2} + 2e_1 \frac{d\xi_1}{dt} + v_1 \frac{\partial U(\xi_1, \xi_2)}{\partial \xi_1} = q_1^*(t), \quad (10.42)$$

$$\frac{d^2 \xi_2}{dt^2} + 2e_2 \frac{d\xi_2}{dt} + v_2 \frac{\partial U(\xi_1, \xi_2)}{\partial \xi_2} = q_2^*(t). \quad (10.43)$$

*See the article [10.15, 1971].

Here $v_1 = 1$, $v_2 = 2/3$, $q_i^*(t) = q_i(t)V^2/Eh^2$, $V = \sqrt{Eg/\gamma}$. The expression for U will be

$$U = \left[C_1 \left(1 - \frac{p}{r_1} \right) + \bar{\alpha}_1 \right] \frac{\zeta_1^2}{2} + \frac{3}{2} \left[C_2 \left(1 - \frac{p}{r_2} \right) + \bar{\alpha}_2 \right] \frac{\zeta_2^2}{} + \\ + \beta \frac{\zeta_1^3}{3} + \chi \frac{\zeta_1^4}{4} - 0\zeta_1 \zeta_2 + x_6 \zeta_1^2 - \psi \frac{\zeta_1^2 \zeta_2}{2} + \\ + \psi \frac{\zeta_1^2 \zeta_2^2}{2} - C_1 \left(\frac{p}{r_1} \zeta_{1,0} + q_0 \right) \zeta_1 - \frac{3}{2} C_2 \frac{p}{r_2} \zeta_{2,0} \zeta_2; \quad (10.44)$$

where $\bar{q}_0 = q_0 V^2 / C_1 Eh^2$. The same notation and dimensionless parameters as in § 29 are used. The values of $\bar{\alpha}_1$, β , χ , θ , x , ϕ , ψ are determined via the corresponding values of these quantities from (2.171)-(2.178) taking the coefficient $\psi_1 h^2 V^2$ into account; $\bar{\alpha}_2 = \alpha_2 \psi_2 h^2 V^2$.

The function $q_1^*(t)$, $q_2^*(t)$ in (42), (43) will be represented in the form of white noise type random processes with spectral densities S_1 , S_2 . The average values, correlation functions and conditions of mutual correlation are

$$\left. \begin{aligned} M_{q_1^*} &= M_{q_2^*} = 0, \\ M[q_1^*(t) q_1^*(t + \tau)] &= 2\pi S_1 \delta(\tau), \\ M[q_2^*(t) q_2^*(t + \tau)] &= 2\pi S_2 \delta(\tau), \\ M[q_1^*(t) q_2^*(t + \tau)] &= 0. \end{aligned} \right\} \quad (10.45)$$

On the basis of the adopted assumptions regarding the loading conditions, the deformation of the shell is treated as a four-dimensional Markov process of variation in the parameters of deflection ζ_1 , ζ_2 and velocities $\dot{\zeta}_1$, $\dot{\zeta}_2$.

If the structure reduces to a design model in the form of a system with n degrees of freedom, a $2n$ -dimensional Markov process with parameters x_1 , x_2 , ..., x_n is studied. A system of equations of the type of (42), (43) will in this case have the form

$$\frac{d^2 \zeta_m}{dt^2} + 2e_m \frac{d\zeta_m}{dt} + v_m \frac{\partial U(\zeta_1, \zeta_2, \dots, \zeta_m)}{\partial \zeta_m} = q_m^*(t), \quad m = 1, 2, \dots, n. \quad (10.46)$$

For generalized forces

$$\begin{aligned} M_{q_m^*} &= 0, \\ M[q_m^*(t) q_m^*(t + \tau)] &= 2\pi S_m \delta(\tau), \\ M[q_m(t) q_k(t + \tau)] &= 0, \quad m \neq k. \end{aligned} \quad (10.47)$$

We will use the stationary FPK equation according to (6a) with $i = j = 2n$. The parameters of the process

$$x_m = \zeta_m, \quad x_{m+n} = \dot{\zeta}_m. \quad (10.48)$$

The characteristics of a Markov process according to (7a), using (46), (48) and taking (47) into account, will be

$$\left. \begin{aligned} A_m &= x_{m+n}, \quad A_{m+n} = -2e_m x_{m+n} - v_m \frac{\partial U}{\partial x_m}, \\ B_{mk} &= 0, \quad m \neq k; \quad B_{m+n, k+n} = 0, \quad m \neq k, \\ B_{mn} &= 0, \quad B_{m+n, m+n} = 2\pi S_m. \end{aligned} \right\} \quad (10.49)$$

Substituting into (6a) the values of the quantities from (49), we obtain

$$\sum_{m=1}^n \pi S_m \frac{\partial f}{\partial x_{m+n}^2} - \sum_{m=1}^n \frac{\partial}{\partial x_m} (f x_{m+n}) + \sum_{m=1}^n \frac{\partial}{\partial x_{m+n}} \left[\left(2e_m x_{m+n} + v_m \frac{\partial U}{\partial x_m} \right) f \right] = 0. \quad (10.50)$$

We represent this equation in the form

$$\sum_{m=1}^n \left[\frac{\partial}{\partial x_{m+n}} \left(v_m \frac{\partial U}{\partial x_m} f + \frac{\pi S_m}{2e_m} \frac{\partial f}{\partial x_m} \right) + \left(2e_m \frac{\partial}{\partial x_{m+n}} - \frac{\partial}{\partial x_m} \right) \left(f x_{m+n} + \frac{\pi S_m}{2e_m} \frac{\partial f}{\partial x_{m+n}} \right) \right] = 0. \quad (10.51)$$

Integration yields

$$f(x_1, x_2, \dots, x_{2n}) = \frac{1}{C} \exp \left[-\frac{1}{S_m} \left(\frac{1}{2} \sum_{m=1}^n \frac{x_{m+n}^2}{v_m} + \mu \right) \right]. \quad (10.52)$$

where

$$S_m = \frac{\pi S_m}{2v_m r_m} = G. \quad (10.53)$$

The velocities are eliminated by integrating again; then

$$f(x_1, x_2, \dots, x_n) = \frac{1}{C'} \exp\left(-\frac{U}{S_m}\right). \quad (10.54)$$

With reference to system (42), (43), we will have $i = j = 4$ in (6a); the parameters of the process are defined as

$$x_1 = \xi_1, \quad x_2 = \xi_2, \quad x_3 = \dot{\xi}_1, \quad x_4 = \dot{\xi}_2. \quad (10.55)$$

Expressions (47) become (45), and the values of A_i, B_{ij} in (6a) will be

$$\begin{aligned} A_1 &= \dot{\xi}_1, \quad A_2 = \dot{\xi}_2, \\ A_3 &= -2v_1 \dot{\xi}_1 - v_1 \frac{\partial U(\xi_1, \xi_2)}{\partial \xi_1}, \\ A_4 &= -2v_2 \dot{\xi}_2 - v_2 \frac{\partial U(\xi_1, \xi_2)}{\partial \xi_2}, \end{aligned} \quad \left. \right\} \quad (10.56)$$

$$\begin{aligned} B_{11} &= B_{12} = B_{21} = B_{22} = B_{33} = B_{44} = 0, \\ B_{30} &= 2\pi S_1, \quad B_{44} = 2\pi S_2. \end{aligned} \quad \left. \right\} \quad (10.57)$$

In accordance with relation (53), we have $S_1^* = S_2^*$, and

$$S_1^* = \frac{\pi S_1}{2v_1 r_1}. \quad (10.58)$$

The law of distribution of the deflection parameters is

$$f(\xi_1, \xi_2) = \frac{1}{C'} \exp\left[-\frac{U(\xi_1, \xi_2)}{S_1^*}\right]. \quad (10.59)$$

Expression (44) is substituted for U in (59), and C' is found from the normalization condition.

The mean square of the deflection parameters are:

$$M[\xi_1^2] = \int_{-\infty}^{\infty} \int_{-\infty}^{\infty} \xi_1^2 f(\xi_1, \xi_2) d\xi_1 d\xi_2, \quad (10.60)$$

$$M[\xi_2^2] = \int_{-\infty}^{\infty} \int_{-\infty}^{\infty} \xi_2^2 f(\xi_1, \xi_2) d\xi_1 d\xi_2. \quad (10.61)$$

§ 109. Cylindrical Panel. Probability Parameters of Deflection

We will now consider the case of a slightly curved circular cylindrical panel fixed at the edges and undergoing vibrations under the influence of acoustic pressure. As in the preceding sections, we will consider the action of static axial compression forces, and the acoustic action will be represented in the form of white noise. In the case at hand, nonlinear acoustic vibrations will be characterized by abrupt displacements of the shell from one position of stable equilibrium to another (snapping of the shell) and also by vibrations around the new stable equilibrium form.*

The main symbols will be taken from Figure 2.41. Using relations (1.40), (1.41) and approximating the total and additional deflection by expressions (3.2), (3.3), we arrive at the equation of motion (1)

$$\frac{d^2\xi}{dt^2} + 2\zeta \frac{d\xi}{dt} + \omega_0^2 \left(1 - \frac{P^*}{P_n}\right) (\eta \xi^3 - \beta \xi^2 + \alpha \xi) - \zeta_0 \omega_0^2 \frac{P}{P_n} = q^*(t); \quad (10.62)$$

where $q^*(t)$ as before is white noise characterized by a zero average value and a spectral density S_0 . The value of $q^*(t)$ is determined from (2).

*Formula (66) obtained below describes the behavior of a system with snapping. A dependence of this type for an ideal system was derived in a different way by M.F. Dimentberg (see footnote on p. 471); this involved a limiting transition from an exponentially correlated distributing process to white noise.

Integrating the FPK equation, we arrive at expressions of the structure of (22)-(24) by substituting p_u^* for p_0^* in them; the values of w_0^2 , α , β , η , p_u^* in formulas (23)-(25) for the case at hand are determined from (2.210), (2.211), (3.27), (3.28).

Figures 10.1-10.4 present data characterizing the influence of compressive axial forces p and of the initial camber parameter ζ_0 in the middle surface on the law of distribution of dynamic deflection according to (23). As an example, we use the case

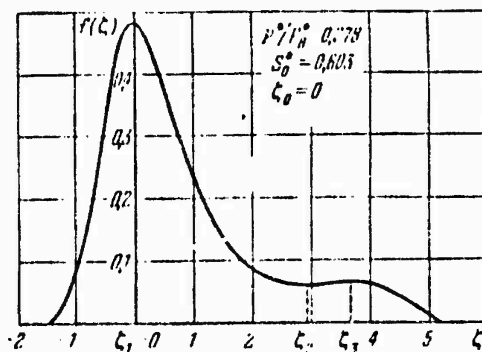


Figure 10.1. Probability density of dynamic deflection at the center of a cylindrical panel during nonlinear acoustic vibrations in the case of axial compression by stresses close to the lower critical value.

of a panel square in the plane ($\lambda = 1$) with a curvature parameter $k = 24$; the relations were plotted for cases in which the values of the parameter of compressive forces p^* were 5, 6, 9, 15. The load $p^* = 5$ was chosen near the lower critical value $p^* = 4.6$.

Let us first consider the case of an ideal panel for different values of compressive forces (solid curves in the graphs of Figures 10.1-10.4). We see that when $p^* = 5 = 0.278 p_u^*$ (Figure 10.1), the largest fraction of the probability corresponds to the region of deflection values around the principal stable position of equilibrium; when the load changes slightly near the lower critical value to $p^* = 6 = 0.333 p_u^*$ (Figure 10.2), the character of the distribution curve changes substantially; at the same time, there is an increase in the probability fraction of the interval of

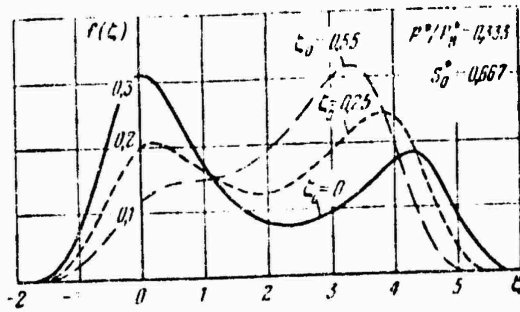


Figure 10.2. Law of deflection distribution for ideal and nonideal panels at another level of compressive forces near the lower critical value.

deflection values corresponding to the second stable state of the shell. As the compressive load increases to a value equal to one-half the upper critical value (Figure 10.3), there is a sharp increase in the probability of the region of deflection values that corresponds to the vicinity of the second equilibrium position. Finally, when $p^* = 15 = 0.832 p_u^*$ (Figure 10.4), the probability of the interval of deflection values in the vicinity of the principal equilibrium state of the shell is negligibly low.

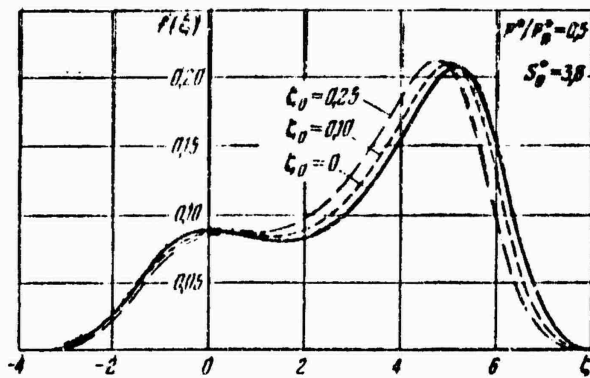


Figure 10.3. Deflection probability densities for ideal and nonideal shells under compressive forces amounting to one-half of the upper critical value.

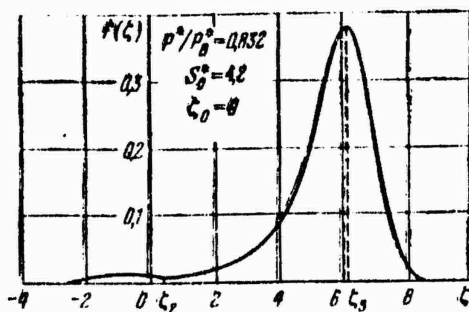


Figure 10.4. Law of deflection distribution during acoustic vibrations of the panel in the case of action of compressive forces close to the upper critical value.

Let us now turn to the influence of initial irregularities in the shape of the middle surface at various levels of compressive forces. When $p^* = 6$ and $\xi_0 = 0.25$ (Figure 10.2), there is a significant increase in the probability fraction of the interval of deflection values near the second stable position. As the initial deflection increases to $\xi_0 = 0.55$, the distribution function has a single extremum in the form of a maximum at the point $\xi = \xi_3$; in this case, the shell executes vibrations around the snapped equilibrium position. The influence of the values $\xi_0 = 0.1$ and $\xi_0 = 0.25$ when $p^* = 9$ is demonstrated by the graph of Figure 10.3. The effect of initial irregularities on the law of distribution of dynamic deflection proves considerable at a low level of compressive forces; as the parameter p^* increases, the effect of the initial camber weakens.

The dependence of the mean square of the deflection on the factors discussed is demonstrated below by the data of Table 10.1. Of decisive importance for this characteristic is the influence of the loading conditions; on the contrary, initial irregularities do not appreciably affect the value of the mean square of the deflection.

§ 110. Probability Density of Deflection Extremums for a System with Snapping

Above, we discussed a method of studying the probability density of deflection extrema in the analysis of a narrow-band vibration process of a system with one equilibrium position (§ 107). We will apply this method to a system with snapping,

when three types of vibrations become possible: around the main equilibrium position ζ_1 , around the second stable position ζ_3 , and when both of these states are included (Figure 10.5). It is assumed that the vibrations of the shell involve motions of only the three indicated types, involving crossings of the three characteristic deflection levels. The concept of narrow-bandedness is related to the character of the vibratory motions of each type.*

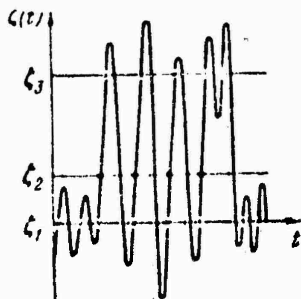


Figure 10.5. Determination of the average number of dynamic deflection extrema per unit time for a system with snapping.

We will denote by $v_{\zeta_1}^+$, $v_{\zeta_2}^+$, $v_{\zeta_3}^+$ the average number of times per unit time that each of the three levels of the equilibrium position of the shell is exceeded. Then, considering the above hypotheses on possible motions of only three types, the average number per time unit v_m^* of all possible maxima of the narrow-band vibratory process considered will be

$$v_m^* = v_{\zeta_1}^+ + v_{\zeta_2}^+ - v_{\zeta_3}^+. \quad (10.63)$$

Here the quantity $v_{\zeta_2}^+$ is taken with a minus sign, since in cycles of the third type (with snapings), one maximum involves the crossing of both levels of the stable

*This approach to the solution of the problem of determining the probability density of extrema in a system with snapping is due to I.G. Kif'dibekov.

position (Figure 10.5), while the number of direct snapplings (snapplings of the panel in the direction of the center of curvature) is equal* to $v_{\zeta_2}^+$. The term "cycle" applied to the motion of a given type is hereinafter used for a single crossing of some characteristic level in the course of this motion; by average frequency of cycles of a given type is meant the average number of such crossings per unit time. Returning to formula (36) and replacing v_m^* in the latter with the value from (63), we find the probability density of extrema for a system with snapping

$$f(\zeta_{\max, \min}) = \mp \frac{1}{v_{\zeta_1}^+ + v_{\zeta_2}^+ - v_{\zeta_3}^+} \frac{dv_{\zeta}^+}{d\zeta}. \quad (10.64)$$

The values of $f(\zeta_{\max})$ will be different from zero when $\zeta_1 < \zeta < \zeta_2$ and $\zeta > \zeta_3$, and the value $f(\zeta_{\min})$, in the region $\zeta < \zeta_1$ and $\zeta_2 < \zeta < \zeta_3$.

Using Rice's formula (29), we find

$$f(\zeta_{\max, \min}) = \mp \frac{1}{I(\zeta_1) + I(\zeta_2) - I(\zeta_3)} \frac{dI(\zeta)}{d\zeta}. \quad (10.65)$$

Considering that $f(\zeta)$ is determined from (23), we finally obtain

$$\begin{aligned} I(\zeta_{\max, \min}) = & \pm \frac{2(S_0 C)^{-1} \left(1 - \frac{P^*}{P_n}\right)}{I(\zeta_1) + I(\zeta_2) - I(\zeta_3)} \left(\alpha_0^* - \beta_0^* \zeta^2 + \gamma_0^* \zeta^3 - \frac{\zeta_0}{\frac{P^*}{P_n} - 1} \right) \times \\ & \times \exp \left[- \frac{1}{S_0} \left(1 - \frac{P^*}{P_n}\right) \left(\alpha_0^* \zeta^2 - \frac{2}{3} \beta_0^* \zeta^3 + \frac{\gamma_0^*}{2} \zeta^4 \right) + \frac{2}{S_0} \frac{P^*}{P_n} \zeta_0 \zeta \right]. \end{aligned} \quad (10.66)$$

We will determine one more important characteristic of the shell, the average number N of direct and reverse snaps per unit time. The quantity N is defined by Rice's formula (29) as the number of crossings of the level ζ_2

$$N = 2v_{\zeta_2}^+ = 2 \int_0^{\infty} f(\zeta_2, \zeta) d\zeta. \quad (10.67)$$

*This method applies to a system with three equilibrium positions. If $v_{\zeta_2}^+$ is not excluded, cycles of the first type will be considered twice.

Substituting (22) into the above and integrating, we get

$$\frac{N}{m_0} = \sqrt{\frac{s_0^2}{\pi}} f(t_c). \quad (10.68)$$

§111. Treatment of a Narrow-Band Process for a System with Snapping

Let us consider the case of a square panel with curvature parameter $k = 24$. Figures 10.6-10.9 show the results of computations of the probability density of extrema of the coordinate according to (66) for values of the compressive force parameter p^* equal to 5, 6, 9, and 15. These diagrams give a clear representation

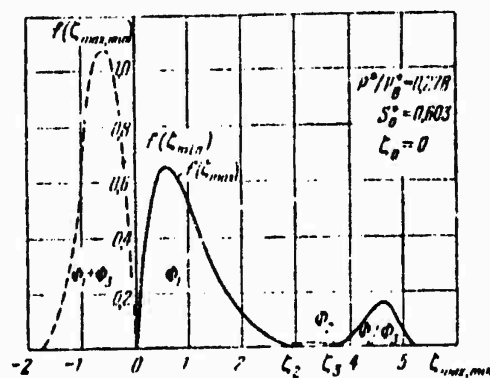


Figure 10.6. Probability densities of maxima and minima of dynamic deflection at the center of a cylindrical panel during acoustic vibrations and the action of compressive forces close to the lower critical value.

of the distribution of the vibratory process over possible cycles and illustrate the effect of compressive forces and initial irregularities in the shape of the shell on the relative repetition frequency of each type of cycles. Let us note that cycles of the third type are accompanied by dangerous snaps of the shell.

The total area under the distribution curve of the extrema consists of three parts. The area Φ_1 characterizes the probability level of vibratory motions around the main equilibrium position, and Φ_2 , around the snapped state. Φ_3 denotes the probability of extrema corresponding to vibrations encompassing the two positions of stable equilibrium.

Let us first consider the effect of compressive forces on the distribution of vibrations over possible cycles in the case of ideal panels. The values of Φ_1 , Φ_2 , Φ_3 are listed in Table 10.1. It is evident that in the case at hand, the probability Φ_3 refers to all possible crossings in which the level ζ_2 is exceeded.

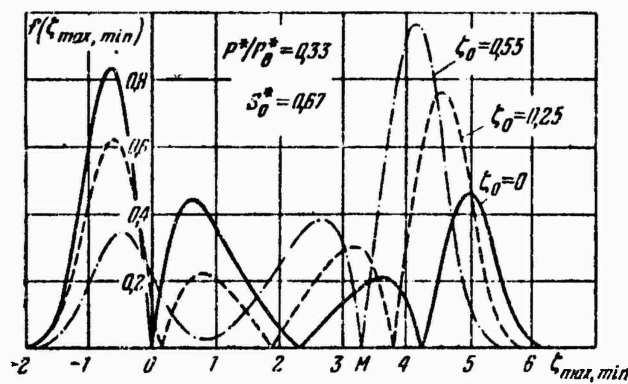


Figure 10.7. Laws of distribution of maxima and minima of dynamic deflection for ideal and nonideal panels at different levels of compressive forces near the lower critical value.

As is evident from the table and Figure 10.6, when $p^* = 5 = 0.278 p_u^*$, a significant probability $\Phi_1 = 0.867$ is displayed by the extrema of vibrations around the main equilibrium position. As the longitudinal load increases to the value $p^* = 0.333 p_u^*$, considerable changes take place in the behavior of the shell; there is an appreciable decrease in Φ_1 , and the probability of vibration cycles of the second and third types increases (Figure 10.7). When $p^* = 0.5 p_u^*$, the probability Φ_2 increases to 0.6. Cycles of the third type have a significant relative frequency $\Phi_3 = 0.37$ (Figure 10.8, Table 10.1). When $p^* = 15 = 0.83 p_u^*$, there is an almost zero probability of extrema of vibrations around the initial

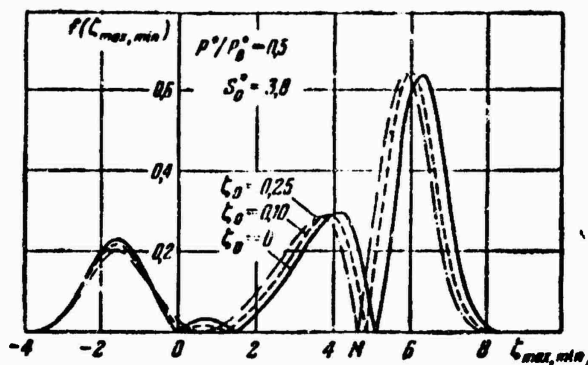


Figure 10.8. Laws of distribution of deflection extrema for ideal and nonideal shells under compressive forces amounting to one-half of the upper critical value.

equilibrium position, and a very low probability of vibration cycles encompassing the two stable equilibrium positions (Figure 10.9); the vibrations around the snapped position take place with an average relative frequency $\phi_2 = 0.962$.

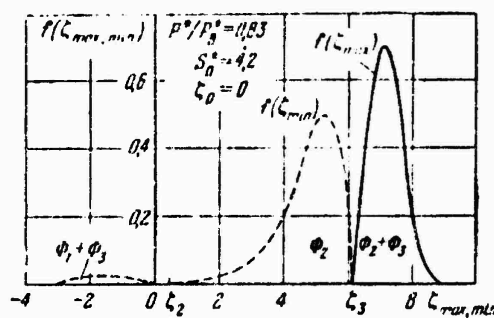


Figure 10.9. Probability densities of maxima and minima of dynamic deflections of a cylindrical panel during acoustic vibrations in the case of compression with forces close to the upper critical load.

Table 10.1 also gives the average number of snaps per unit time $N^* = 10^3 \cdot N/w_0$. It is evident that an increase in the compressive force to $p^* = 9 = 0.5 p_u^*$ leads to an increase in the frequency of snaps to the value $N^* = 85$; when $p^* = 15 = 0.83 p_u^*$, the average number of snaps per unit time declines; under this load, a significant

p^*	p^*/p_u^*	ζ_0^*	ζ_0	$M(G)$	Φ_1	Φ_2	Φ_3	$(N \text{ at } 10^6)$
5	0,28	0,693	0	2,1	0,867	0,005	0,124	27
6	0,333	0,67	0	6,6	0,55	0,25	0,2	38
			0,25	7,2	0,235	0,36	0,105	60
			0,55	7,1	0	1	0	0
9	0,5	3,8	0	15,2	0,03	0,6	0,37	85
			0,1	15,1	0,01	0,6	0,39	91
			0,25	11,3	0	1	0	0
15	0,83	4,2	0	32,8	0,0005	0,932	0,0375	17
			0,05	31,9	0	1	0	0

Table 10.1.

proportion of the vibratory process is due to motions around the snapped position.

Let us consider the influence of initial irregularities on the distribution of vibrations over the cycles and on the average number of snaps per unit time. The parameter ζ_0 has a significant effect at low values of the compressive stresses in comparison with the upper critical ones (Figures 10.7, 10.8, Table 10.1). It is evident from these data to what extent the fraction of cycles of the second and third types increases with rising ζ_0 . The initial irregularities characterized by the value $\zeta_0 = 0.25$ when $p^* = 0.333 p_u^*$ make this loading variant similar to the case of an ideal shell for a considerably greater value of p^* , equal to one-half the upper critical value: in both cases, cycles of the third type have a probability Φ_3 close to 0.4. The average number of snaps per unit time reaches the highest value $N^* = 91$ when $\zeta_0 = 0.1$ (Table 10.1).

§112. Description of the Stressed State of a Panel. Probability Density of Stresses

Let us determine the statistical characteristics of the stressed state of a shell. For a system with snapping, with application to the case of a circular

cylindrical panel discussed in the preceding sections, we will determine the probability densities of the stresses and their extrema, make a study of the possible cycles of stress variation, and establish the probability of occurrence of cycles of each type.* The characteristics pertaining to the probability density of stresses, to their extreme values and mean square, and to the analysis of the process of stress variation over possible cycles can be used in estimating the fatigue life of structures.

In the case under consideration, the stresses in the shell are composed of membrane stresses and bending stresses.

The stresses in the middle surface σ_x , σ_y acting along the generatrix and arc are found from formulas (1.30): $\sigma_x = \frac{\partial^2 \phi}{\partial y^2}$, $\sigma_y = \frac{\partial^2 \phi}{\partial x^2}$. The bending stresses σ_x , b , σ_y , b at any point of the shell surface ($z = h/2$) are ($w_1 = w - w_0$)

$$\sigma_{x,0} = -\frac{Eh}{2(1-\mu^2)} \left(\frac{\partial^2 w_1}{\partial x^2} + \mu \frac{\partial^2 w_1}{\partial y^2} \right),$$

$$\sigma_{y,0} = -\frac{Eh}{2(1-\mu^2)} \left(\frac{\partial^2 w_1}{\partial y^2} + \mu \frac{\partial^2 w_1}{\partial x^2} \right).$$

We will choose for the study of values of stresses acting at the point of maximum deflection, the center of the panel, where they reach their highest value. Using expressions (3.2), (3.3), (3.25) for the deflection and stress function in the middle surface, we obtain the membrane stresses at the center of the panel ($x = a/2$, $y = b/2$) (see Figure 2.41)

$$\sigma_x^* = \gamma_x (\zeta + \psi_x \zeta^2 - P_0), \quad \sigma_y^* = \gamma_y (\zeta + \psi_y \zeta^2), \quad (10.69)$$

where

*See the report of I.G. Kil'dibekov at the Kaunas All-Union Conference on Problems of Stability in Structural Mechanics, 1967, Abstracts of Papers, Vil'nyus, 1967.

$$\gamma_x = \frac{\xi_0 \pi^2}{20\lambda^2} - \frac{k\lambda^2}{5(1+\lambda^2)^2}, \quad \Phi_x = \frac{\pi^2}{10\lambda} \gamma_x, \quad P_0^* = \frac{P^*}{5V_x}. \quad (10.70)$$

$$\gamma_y = \frac{\xi_0 \pi^2}{20} - \frac{k}{5(1+\lambda^2)^2}, \quad \Phi_y = \frac{\pi^2}{10} \gamma_y. \quad (10.71)$$

The dimensionless stress parameters were introduced above by using the formulas

$$\sigma_x^* = \frac{\alpha_x h^2}{5Eh^2}, \quad \sigma_y^* = \frac{\alpha_y h^2}{5Eh^2}.$$

p

The bending stresses at the center of the panel are

$$\sigma_{x,0}^* = \gamma_{x,0} \xi, \quad \sigma_{y,0}^* = \gamma_{y,0} \xi, \quad (10.72)$$

$$\text{where } \gamma_{x,0} = \frac{\pi^2}{10\lambda^2(1-\mu^2)} + \frac{\mu\pi^2}{10(1-\mu^2)}, \quad \gamma_{y,0} = \frac{\pi^2}{10(1-\mu^2)} + \frac{\mu\pi^2}{10\lambda^2(1-\mu^2)}. \quad (10.73)$$

The total stresses σ_x^* , σ_y^* acting on the surface of the shell ($z = h/2$) at the center will be found by adding up the values found above for the membrane stresses and bending stresses:

$$\sigma_{x,0}^* = \gamma_{x,0} (\xi + \varphi_{x,0} \xi^2 - P^*), \quad \sigma_{y,0}^* = \gamma_{y,0} (\xi + \varphi_{y,0} \xi^2). \quad (10.74)$$

The quantities determining $\sigma_{x,t}^*$, $\sigma_{y,t}^*$ will be

$$\gamma_{x,0} = \frac{\pi^2}{10\lambda^2(1-\mu^2)} + \frac{\mu\pi^2}{10(1-\mu^2)} + \frac{\xi_0 \pi^2}{20\lambda^2} - \frac{k\lambda^2}{5(1+\lambda^2)^2}, \quad (10.75)$$

$$\varphi_{x,0} = \frac{\pi^2}{10\lambda^2 \gamma_{x,0}}, \quad P^* = \frac{P^*}{5V_{x,0}}. \quad (10.76)$$

The values of $\nu_{y,t}$ and $\phi_{y,t}$ are

$$\nu_{y,0} = \frac{\pi^2}{10(1-\mu^2)} + \frac{\mu\pi^2}{10\lambda^2(1-\mu^2)} + \frac{\pi^2 \xi_0}{20} - \frac{k}{5(1+\lambda^2)^2}, \quad \Phi_{y,0} = \frac{\pi^2}{10V_{y,0}}. \quad (10.77)$$

We will now determine the probability density for total stresses σ_x^* , t . The dependence σ_x^* , t (ζ) according to (74) for a square ideal panel at a level of compressive forces $p^* = 0.333 p_u^*$ is shown in Figure 10.10. On the basis of Eq. (74), we find

$$\dot{\sigma}_{x,u}^* = \gamma_{x,u} \dot{\zeta} (1 + 2\psi_{x,u} \zeta). \quad (10.78)$$

The transformations inverse of (74), (78) are two-valued and are determined as follows (the index for total stresses is omitted below):

$$U_{1,2}(\sigma_x^*) = \zeta_{1,2} = \frac{-1 \pm \sqrt{1 + \frac{4\varphi_x \sigma_x^*}{\gamma_x} + 4\varphi_x p^*}}{2\varphi_x}, \quad (10.79)$$

$$V_{1,2}(\sigma_x^*, \dot{\sigma}_x^*) = \dot{\zeta}_{1,2} = \mp \frac{\dot{\sigma}_x^*}{\gamma_x \sqrt{1 + \frac{4\varphi_x \sigma_x^*}{\gamma_x} + 4\varphi_x p^*}}, \quad (10.80)$$

where U_1 and U_2 correspond, respectively, to the left- and right-hand branches of the curve of Figure 10.10.

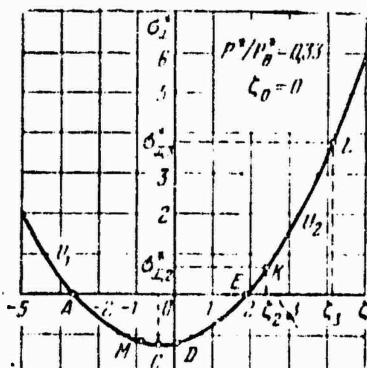


Figure 10.10. Dependence of total stresses at the center of a square ideal panel on deflection.

On the basis of expression (22) for $f(\zeta, \dot{\zeta})$, we determine the two-dimensional distribution function $f(\sigma_x, \sigma_x^*)$, using the well-known formula

$$f(\sigma_x^*, \dot{\sigma}_x^*) = \sum_{t=2}^n f(U_t, V_t) \left| \frac{\partial (U_t, V_t)}{\partial (\sigma_x^*, \dot{\sigma}_x^*)} \right|. \quad (10.81)$$

where

$$\frac{\partial (U_t, V_t)}{\partial (\sigma_x^*, \dot{\sigma}_x^*)} = \begin{vmatrix} \frac{\partial U_t}{\partial \sigma_x^*} & \frac{\partial U_t}{\partial \dot{\sigma}_x^*} \\ \frac{\partial V_t}{\partial \sigma_x^*} & \frac{\partial V_t}{\partial \dot{\sigma}_x^*} \end{vmatrix}.$$

The final expression for the combined probability density of total stresses σ_x^* , t and velocity $\dot{\sigma}_x^*$, t takes the form

$$f(\sigma_x^*, \dot{\sigma}_x^*) = \left[C w_0 Y_x^2 \sqrt{\pi S_0^2 \left(1 + \frac{4q_x \sigma_x^*}{Y_x} + 4q_x P^* \right)} \right]^{-1} \times \\ \times \{ \exp[x_1(\sigma_x^*)] + \exp[x_2(\sigma_x^*)] \} \exp \left[- \frac{\dot{\sigma}_x^{*2}}{S_0^2 w_0^2 Y_x^2 \left(1 + \frac{4q_x \sigma_x^*}{Y_x} + 4q_x P^* \right)} \right]; \quad (10.82)$$

where

$$x_1(\sigma_x^*) = - \frac{1}{S_0^2} \left(1 - \frac{P^*}{w_0} \right) \left(a U_1^2 - \frac{a}{3} b U_1^4 + \frac{a}{2} U_1^6 \right) + \frac{a}{S_0^2} \frac{P^*}{w_0} z_0 U_1, \quad (10.83)$$

The quantity $x_2(\sigma_x^*)c$ is similarly determined, U_1 being replaced by U_2 in expression (83). The values of U_1 and U_2 are determined from (79). Eliminating the velocities, we arrive at the following formula for the probability density:

$$f(\sigma_x^*) = \int_0^\infty f(\sigma_x^*, \dot{\sigma}_x^*) d\dot{\sigma}_x^* = \\ = \left(C Y_x \sqrt{1 + \frac{4q_x \sigma_x^*}{Y_x} + 4q_x P^*} \right)^{-1} \{ \exp[\beta_1(\sigma_x^*)] + \exp[\gamma_1(\sigma_x^*)] \}. \quad (10.84)$$

The laws of distribution of σ_y^* , t and stresses in the middle surface σ_x^* , σ_y^* are

similarly obtained; here the transformation of the law of distribution (22) is carried out according to (81) by taking expressions (74) and (69) into account for the cases under consideration.

For bending stresses $\sigma_{x,u}^*$, we obtain

$$f(\sigma_{x,u}^*, \sigma_{x,u}^*) = \frac{1}{C\omega_0 y_{x,u}^2 \sqrt{\pi S_0}} \exp \left[-\frac{1}{S_0} \left(1 - \frac{p^*}{p_u} \right) \left(\frac{a}{y_{x,u}^2} \sigma_{x,u}^{*2} - \frac{2}{3} \frac{p^*}{y_{x,u}^1} \sigma_{x,u}^{*3} + \frac{\eta}{2y_{x,u}^1} \sigma_{x,u}^{*4} \right) + \frac{2}{S_0} \frac{p^*}{p_u} \frac{\zeta_0}{y_{x,u}^1} \sigma_{x,u}^* \right] \times \exp \left(-\frac{\sigma_{x,u}^{*2}}{S_0^2 \omega_0^2 y_{x,u}^2} \right), \quad (10.85)$$

where $y_{x,u}$ is found from (73). Integrating (85) with respect to the velocity, we find

$$f(\sigma_{x,u}^*) = \frac{1}{C y_{x,u}} \exp \left[-\frac{1}{S_0} \left(1 - \frac{p^*}{p_u} \right) \left(\frac{a}{y_{x,u}^2} \sigma_{x,u}^{*2} - \frac{2}{3} \frac{p^*}{y_{x,u}^1} \sigma_{x,u}^{*3} + \frac{\eta}{2y_{x,u}^1} \sigma_{x,u}^{*4} \right) + \frac{2}{S_0} \frac{p^*}{p_u} \frac{\zeta_0}{y_{x,u}^1} \sigma_{x,u}^* \right]. \quad (10.86)$$

Results of computations of the integral distribution function of total stresses σ_x^* for an ideal square panel in the plane with curvature parameter $k = 24$ at a level of compressive forces $p^* = 6 = 0.333 p_u^*$ are shown in Figure 10.11.

We find the mean square of total stresses

$$M[\sigma_x^{*2}] = \int_{-\infty}^{\infty} \sigma_x^{*2} f(\sigma_x^*) d\sigma_x.$$

From results of computations for the case of an ideal shell for $k = 24$, $p^* = 0.333 p_u^*$, the mean square is equal to 6.28.

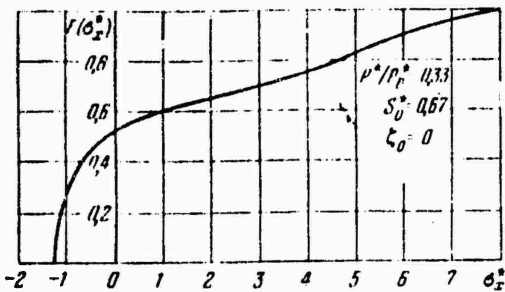


Figure 10.11. Integral distribution function of total stresses during acoustic vibrations of a panel with snapping.

3113. Law of Distribution of Stress Extremums for a System with Snapping. Analysis of Possible Cycles

We will now consider the possible cycles of variation of total stresses σ_x^* . In Figure 10.10, the points D, K, L are associated with the deflections $\xi_1 = \xi_D$, $\xi_2 = \xi_K$, $\xi_3 = \xi_L$, corresponding to the three possible equilibrium positions of the system. They are associated with the stresses $\sigma_{x,1}^* = \sigma_x^*, D$, $\sigma_{x,2}^* = \sigma_x^*, K$, $\sigma_{x,3}^* = \sigma_x^*, L$.

As is evident from the character of the dependence $\sigma_x(\xi)$ (Figure 10.10), the deflection maxima in the region $\xi > \xi_D$ give rise to the maxima of σ_x^* ; the possible deflection minima lying in this region are associated with minima of the stresses. The deflection minima in the interval of values pertaining to segment CD are associated with extremums of σ_x^* in the form of minima. In the region of the values $\xi_{\min} < \xi < \xi_C$, extremums of σ_x^* in the form of maxima correspond to the deflection extrema in the form of minima.

Thus, in a system with snapping, five types of cycles of stress variation are realized. They are shown in Figure 10.12. Here $\sigma_{x,C}^*$ denotes the level corresponding to point C in Figure 10.10, and values of total stresses $\sigma_{x,1}^*$, $\sigma_{x,2}^*$, $\sigma_{x,3}^*$ at the center of the panel, corresponding respectively to the first, second and third equilibrium positions of the shell are plotted. Cycles of stress variation around the

level σ_x^* , 1 are denoted by I and II: in the first case, we have simple cycles, and in the second, compound ones. Cycles of type III are realized around the level σ_x^* , 3, reached in the snapped position of the system. Cycles of types IV and V correspond to stress variations including the values σ_x^* , 1 and σ_x^* , 3: they will be called simple and compound cycles with snapping, respectively.

We see that the values of the extrema $\sigma_{x, \max}$ are confined to the region $\sigma_x^*, \max > \sigma_x^*, 3$ and correspond to branch U_1 of the $\sigma_x^*(\zeta)$ curve; maxima also represent the regions $\sigma_x^*, D < \sigma_x^*, \max < \sigma_x^*, 2$ and $\sigma_x^*, \max > \sigma_x^*, 3$ (portion U_2 in Figure 10.10). The minima of total stresses lie within the intervals $\sigma_x^*, C - \sigma_x^*, \min < \sigma_x^*, D$, $\sigma_x^*, 2 < \sigma_x^*, \min < \sigma_x^*, 3$, belonging to branch U_2 . The cycle of deflection variation with the minimum $\zeta < \zeta_C$ leads in the stresses to a cycle with two minima σ_x^*, \min equal to σ_x^*, C (compound cycles of types II and V in Figure 10.12).

We have studied a case pertaining to total stresses σ_x^* . Analogous cycles pertain to the stresses σ_y^* and also to the stresses in the middle surface.

The process of variation of bending stresses $\sigma_x^*, u = \sigma_y^*, u$ will include cycles of the same type as the process of deflection variation.

We will find an expression for the probability density of the extrema for the system at hand. We will determine the probability density of the maxima of total stresses $\sigma_{x, \max}$. For extrema corresponding to segments MA and DL (Figure 10.10), use may be made of the method employed in § 10 for the determination of the probability density of deflection extrema. The average number of maxima $\bar{v}_{\sigma_{x, \max}}^+$ of stresses per unit time exceeding the level σ_x^* in the range of values under consideration is obtained from Rice's formula

$$\bar{v}_{\sigma_{x, \max}}^+ = \int_0^\infty f(\sigma_x^*, \dot{\sigma}_x^*) \dot{\sigma}_x^* d\dot{\sigma}_x^*. \quad (10.87)$$

Substituting into the above formula expression (82) for the combined distribution of stresses σ_x^* and velocity $\dot{\sigma}_x^*$ and integrating, we arrive at a relation for $\bar{v}_{\sigma_{x, \max}}^+$:

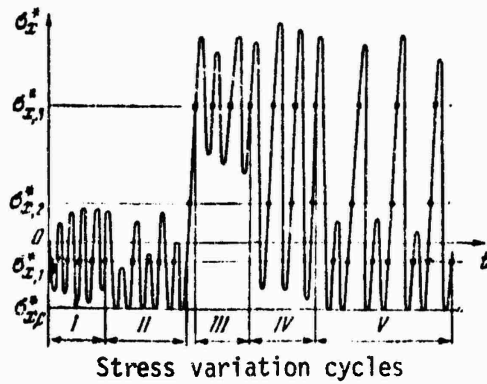


Figure 10.12. Possible cycles of stress variation in a system with snapping.

$$\bar{v}_{\sigma_{max}}^+ = \frac{\omega_0}{2C} \sqrt{\frac{S_0}{\pi}} \left\{ \exp[x_1(\sigma_v^*)]_{\sigma_v^* > \sigma_M^*} + \exp[x_2(\sigma_v^*)]_{\sigma_{x,1}^* < \sigma_v^* < \sigma_{x,2}^*, \sigma_v^* > \sigma_{x,3}^*} \right\}. \quad (10.88)$$

The average number $\bar{v}_{\sigma_{max}}^+$ per unit time for maxima corresponding to segment MC (Figure 10.10) is determined as the average number of minima of deflection ζ per unit time in the interval $\zeta_M < \zeta_{min} < \zeta_C$. Substituting the solution (22)-(24) and the expression for U_1 from (79) into (29), we arrive at the following expression:

$$\bar{v}_{\sigma_{max}}^+ = \frac{\omega_0}{2C} \sqrt{\frac{S_0}{\pi}} \left\{ \exp[x_1(\sigma_v^*)] \right\}_{\sigma_{x,C}^* < \sigma_v^* < \sigma_{x,M}^*}. \quad (10.89)$$

The general expression for the average number of maxima of total stresses per unit time exceeding a given level will be

$$v_{\sigma_{max}}^+ = \bar{v}_{\sigma_{max}}^+ + \bar{v}_{\sigma_{max}}^- + \frac{\omega_0}{2C} \sqrt{\frac{S_0}{\pi}} \left\{ \exp[x_1(\sigma_v^*)]_{\sigma_v^* > \sigma_{x,C}^*} + \exp[x_2(\sigma_v^*)]_{\sigma_{x,1}^* < \sigma_v^* < \sigma_{x,2}^*, \sigma_v^* > \sigma_{x,3}^*} \right\}. \quad (10.90)$$

The average number of extrema considered per unit time will be

$$v_{\sigma_{\max}^*}^* = \frac{\omega_0}{2C} \sqrt{\frac{S_0^2}{\pi}} \left\{ \exp[x_1(\sigma_x^*)]_{\sigma_x^* < \sigma_{x,C}} + \right. \\ \left. + \exp[x_2(\sigma_x^*)]_{\sigma_x^* > \sigma_{x,1}} + \exp[x_2(\sigma_x^*)]_{\sigma_x^* > \sigma_{x,3}} - \exp[x_2(\sigma_x^*)]_{\sigma_x^* > \sigma_{x,2}} \right\}. \quad (10.91)$$

We now find the integral law of distribution of stress maxima

$$F(\sigma_{x,\max}^*) = 1 - \frac{v_{\sigma_{\max}^*}^*}{v_{\sigma_{\max}^*}^*} = 1 - \left\{ \exp[x_1(\sigma_x^*)]_{\sigma_x^* < \sigma_{x,C}} + \right. \\ + \exp[x_2(\sigma_x^*)]_{\sigma_x^* > \sigma_{x,1}} + \exp[x_2(\sigma_x^*)]_{\sigma_x^* > \sigma_{x,3}} - \exp[x_2(\sigma_x^*)]_{\sigma_x^* > \sigma_{x,2}} \right\}^{-1} \times \\ \times \left\{ \exp \left[- \frac{1}{S_0^2} \left(1 - \frac{p^*}{p_n} \right) \left(\alpha U_1^2 - \frac{2}{3} \beta U_1^3 + \frac{\eta}{2} U_1^4 \right) + \right. \right. \\ \left. + \frac{2}{S_0^2} \frac{p^*}{p_n} \zeta_0 U_1 \right]_{\sigma_x^* < \sigma_{x,C}} + \\ + \exp \left[- \frac{1}{S_0^2} \left(1 - \frac{p^*}{p_n} \right) \left(\alpha U_2^2 - \frac{2}{3} \beta U_2^3 + \frac{\eta}{2} U_2^4 \right) + \right. \\ \left. \left. + \frac{2}{S_0^2} \frac{p^*}{p_n} \zeta_0 U_2 \right]_{\sigma_{x,1} < \sigma_x^* < \sigma_{x,2}, \sigma_x^* > \sigma_{x,3}} \right\}. \quad (10.92)$$

From this, the probability density of total stresses is determined.

The stress minima correspond to the deflection minima in the intervals corresponding to segments CD and KL (Figure 10.10). The minima along segment CD take place in simple cycles of the first and fourth types (Figure 10.12), and along segment KL, in stress variation cycles of the third type during vibrations of the shell around the snapped position. Thus, the average number of minima σ_x^* per unit time located above a given level is equal to the average number of deflection minima per unit time in the intervals of values $\zeta_C < \zeta_{\min} < \zeta_D$ and $\zeta_2 < \zeta_{\min} < \zeta_3$; it is also necessary to consider the minima by means of the quantity $\sigma_{x,C}^*$, minima occurring in the compound cycles of the second and fifth types (Figure 10.12) during vibrations of the shell around the fundamental equilibrium position and when both positions of stable equilibrium are included.

Using Rice's formula, the solution (22)-(24), and the expression for U_2 from (79), we find the repetition frequencies of the minima corresponding to the above-

indicated intervals. The final expression for the average number of stress minima per unit time located above a given level σ_x^* will be

$$v_{\sigma_{min}} = \frac{m_0}{2C} \sqrt{\frac{S_0}{\pi}} \left\{ \exp \left[-\frac{1}{S_0} \left(1 - \frac{p^*}{p_u^*} \right) \left(aU_2^2 - \frac{2}{3}\beta U_2^3 + \frac{\eta}{2} U_2^4 \right) + \frac{2}{S_0} \frac{p^*}{p_u^*} \zeta_0 U_2 \right] \right. \\ \left. + 2 \exp [\kappa_2(\sigma_x^*)]_{\sigma_x^* = \sigma_{x,C}} \right\}. \quad (10.93)$$

$\sigma_{x,C} < \sigma_x^* < \sigma_{x,1};$
 $\sigma_{x,2} < \sigma_x^* < \sigma_{x,3}$

We will determine the expression for the integral law of distribution of stress minima

$$F(\sigma_{x,min}) = \frac{\sqrt{\frac{S_0}{\pi}}}{\sigma_{min}} = \left\{ \exp [\kappa_1(\sigma_x^*)]_{\sigma_x^* = \sigma_{x,C}} + \exp [\kappa_2(\sigma_x^*)]_{\sigma_x^* = \sigma_{x,1}} + \exp [\kappa_2(\sigma_x^*)]_{\sigma_x^* = \sigma_{x,3}} - \exp [\kappa_2(\sigma_x^*)]_{\sigma_x^* = \sigma_{x,2}} \right\}^{-1} \left\{ \exp \left[-\frac{1}{S_0} \left(1 - \frac{p^*}{p_u^*} \right) \times \left(aU_2^2 - \frac{2}{3}\beta U_2^3 + \frac{\eta}{2} U_2^4 \right) + \frac{2}{S_0} \frac{p^*}{p_u^*} \zeta_0 U_2 \right] \right. \\ \left. + 2 \exp [\kappa_2(\sigma_x^*)]_{\sigma_x^* = \sigma_{x,C}} \right\}. \quad (10.94)$$

$\sigma_{x,C} < \sigma_x^* < \sigma_{x,1};$
 $\sigma_{x,2} < \sigma_x^* < \sigma_{x,3}$

From this one can also determine the probability density of the minima.

The distribution laws of extrema of total stresses σ_y^* and stresses in the middle surface $\sigma_x^*, 0, \sigma_y^*, 0$ are obtained in similar fashion. The corresponding expressions for bending stresses can be obtained by using the concept of average relative frequency of crossings of a given level by the process, on the basis of Rice's formula (87), using the two-dimensional distribution law according to (85).

Figure 10.13 shows a graph of the integral distribution function of extrema of total stresses σ_x^* ; as an example, we took the case of a cylindrical panel without initial deflection, square in the plane, at a level of compressive forces $p^* = 6 = 0.333 p_u^*$. The curvature parameter of the shell was taken as $k = 24$.

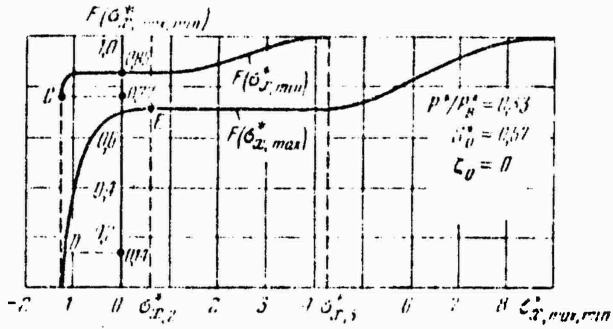


Figure 10.13. Graph of integral distribution function of total stress extrema during acoustic vibrations of a square ideal cylindrical panel with snapping.

The integral distribution function of the maxima determining the possible stress variation cycles are found from formula (92):

$$\begin{aligned} \Psi(\sigma_x^{\max}) &= 1 - \left\{ \exp[x_1(\sigma_x^*)]_{\sigma_x^*=\sigma_{x,1}} + \right. \\ &\quad \left. + \exp[x_2(\sigma_x^*)]_{\sigma_x^*=\sigma_{x,1}} - \exp[x_2(\sigma_x^*)]_{\sigma_x^*=\sigma_{x,2}} \right\}^{-1} \times \\ &\quad \times \exp \left[-\frac{1}{S_0} \left(1 - \frac{p^*}{p_s} \right) \left(aU_2^2 - \frac{2}{3} \beta U_2^3 + \frac{1}{2} U_2^4 \right) + \right. \\ &\quad \left. + \frac{2}{S_0} \frac{p^*}{p_s} \zeta_0 U_2 \right]_{\sigma_{x,1} < \sigma_x^* < \sigma_{x,2}}. \\ &\quad \sigma_x^* > \sigma_{x,2}. \end{aligned} \quad (10.95)$$

The corresponding expression for the distribution function of the minima will be

$$\begin{aligned} \Phi(\sigma_x^{\min}) &= \left\{ \exp[x_2(\sigma_x^*)]_{\sigma_x^*=\sigma_{x,1}} + \exp[x_2(\sigma_x^*)]_{\sigma_x^*=\sigma_{x,2}} - \right. \\ &\quad \left. - \exp[x_2(\sigma_x^*)]_{\sigma_x^*=\sigma_{x,2}} \right\}^{-1} \left\{ \exp \left[-\frac{1}{S_0} \left(1 - \frac{p^*}{p_s} \right) \left(aU_2^2 - \right. \right. \right. \\ &\quad \left. \left. \left. - \frac{2}{3} \beta U_2^3 + \frac{1}{2} U_2^4 \right) + \frac{2}{S_0} \frac{p^*}{p_s} \zeta_0 U_2 \right]_{\sigma_{x,2} < \sigma_x^* < \sigma_{x,1}} + \\ &\quad \left. + \exp[x_2(\sigma_x^*)]_{\sigma_x^*=\sigma_{x,1}} \right\}. \end{aligned} \quad (10.96)$$

We now turn to an analysis of the distribution of the stress variation process over the different cycles. The corresponding data are shown in Figure 10.14. It

was assumed that $k = 24$, $\lambda = 1$, $\zeta_0 = 0$, $p^*/p_u^* = 0.33$. Point C on this graph determines the total probability of compound cycles $\bar{\Phi}_1 + \bar{\Phi}_3$ ($\bar{\Phi}_1$ is the relative repetition frequency of compound cycles of the fifth type in vibrations with snapping of the system (Figure 10.12)). Point 1 defines the total probability of simple and compound cycles corresponding to vibrations associated with snaps of the shell. The probability level of cycles of the first and second type corresponds to point 2.

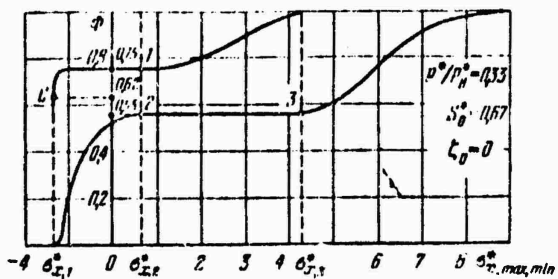


Figure 10.14. Probability distribution of cycles of different types in the process of stress variation during acoustic vibrations with snapping.

The distribution of the process of stress variation over possible cycles as a function of the level of compressive forces and initial irregularities in the shape of the middle surface of the shell is demonstrated by the data of Table 10.2. Here $\bar{\Phi}_1$, $\bar{\Phi}_3$ denote the probabilities of simple cycles. As is evident from the table, the vibration mode most unfavorable for the strength of the shell occurs in the presence of compressive forces amounting to one-half of the upper critical value. Cycles of the third type, associated with vibrations of the shell around the snapped position, occur at an average relative repetition frequency equal to 0.6; cycles of the fifth type have a significant probability.

§ 114. Shallow Shell

Finally, we will study the case of a shallow shell of arbitrary outline rectangular in the plane, assuming that in addition to an acoustic load $q(t)$, the shell is subjected to a static normal external pressure q_0 . The panel is assumed to be hinged

p^*	p^*/r_n^*	s_0^*	ζ_0	$\bar{\Phi}_0 + \Phi_0$	$\bar{\Phi}_0 + \Phi_0$	$\bar{\Phi}_0$	$\bar{\Phi}_0$	Φ_0	$\bar{\Phi}_0$	Φ_0
5	0.28	0.6	0	0.215	0.78	0.187	0.68	0.005	0.028	0.1
6	0.33	0.67	0	0.13	0.62	0.09	0.46	0.25	0.01	0.16
			0.25	0.337	0.303	0.121	0.111	0.36	0.213	0.192
			0.55	0.918	0.082	0	0	1	0.918	0.982
9	0.5	3.8	0	0.008	0.392	0.001	0.029	0.6	0.007	0.363
			0.1	0.026	0.3795	0.0005	0.0005	0.6	0.02	0.37
			0.25	0.654	0.316	0	0	0	0.654	0.346
15	0.83	4.2	0	0.0026	0.035	0	0.0005	0.962	0.0026	0.0315
			0.05	0.965	0.035	0	0	0	0.965	0.035

Table 10.2.

along the contour in the presence of free displacement of the points of its edges. The direction of the coordinate lines adopted in Figure 2.47 is retained. The shell will be assumed to have initial deviations in the shape of the middle surface corresponding to the shape of the additional deflection. The dimensions of the sides of the support contour are a , b . The principal curvatures k_x , k_y are assumed to be constant.

In the initial Eqs. (1.38), (1.39), the intensity of the transverse load will be

$$q(x, y, t) = -\rho h \frac{\partial^2 w}{\partial t^2} - 2\rho h e \frac{\partial w}{\partial t} + q_0 + q(t), \quad (10.97)$$

where $q(t)$ is approximated with white noise.

Using expressions (2.234) for the total and initial deflections, from Eq. (1.39) we will determine the stress function in the middle surface according to (2.235). The equation of vibrations of a shell of arbitrary shape, based on uniformly distributed static pressure, will be written

$$\frac{d^2\zeta}{dt^2} + 2\alpha \frac{d\zeta}{dt} + \omega_0^2(\alpha\zeta - \beta\zeta^2 + \eta\zeta^3) = q_0\omega_0^2 = q^*(t). \quad (10.98)$$

The same notation as in § 34 is used above. The square of the fundamental frequency of natural vibrations of an ideal panel for small deflections ω_0^2 is determined from formula (2.237), and the values of α , β , η are found from (2.240)-(2.242). The quantity \bar{q}_0 stands for

$$\bar{q}_0 = \frac{16}{\pi^2 \omega_0^2 E} \left(\frac{c}{h} \right)^2 q_0, \quad (10.99)$$

and the value of $q^*(t)$ corresponds to formula (2). As before, we assume that $q^*(t)$ is white noise with a zero average value and a spectral density equal to S_0^* , and the vibrations of the shell are represented in the form of a two-dimensional Markov process.

We find the quantities A_{ij} , B_{ij} entering into the Fokker-Planck-Kolmogorov equation (6a). On the basis of equation of motion (98), and taking the characteristics of acoustic pressure into account, we find

$$A_{11} = \dot{\zeta}, \quad A_{21} = -2\alpha\dot{\zeta} - \omega_0^2(\alpha\zeta - \beta\zeta^2 + \eta\zeta^3) + \bar{q}_0\omega_0^2, \quad (10.100)$$

$$B_{11} = B_{12} = B_{21} = 0, \quad B_{22} = 2\pi S_0^*. \quad (10.101)$$

The FPK equation assumes the form

$$\dot{\zeta} \frac{\partial f(\zeta, \dot{\zeta})}{\partial \zeta} = 2\alpha f(\zeta, \dot{\zeta}) + [2\alpha\dot{\zeta} + \omega_0^2(\alpha\zeta - \beta\zeta^2 + \eta\zeta^3) - \bar{q}_0\omega_0^2] \frac{\partial f(\zeta, \dot{\zeta})}{\partial \dot{\zeta}} + \pi S_0^* \frac{\partial^2 f(\zeta, \dot{\zeta})}{\partial \dot{\zeta}^2}. \quad (10.102)$$

The solution is obtained in the form of (22), where the deflection distribution law corresponds to the expression

$$f(\zeta) = \frac{1}{C} \exp \left[-\frac{1}{S_0^*} \left(\alpha\zeta^2 - \frac{2}{3}\beta\zeta^3 + \frac{\eta}{2}\zeta^4 \right) + \frac{2}{S_0^*} \bar{q}_0\zeta \right]. \quad (10.103)$$

and the velocity distribution law $f(\zeta)$ is determined from (24) with the corresponding value of w_0^2 . The symbol S_0^* denotes quantity (25); constant C and also c' from (24) are determined from the normalization conditions.

As an example, let us consider the case of a spherical panel; we will take the parameter $k^* = 48$, and $\lambda = 1$. The distribution laws of the shell deflection according to (103) as a function of the uniform pressure parameter \bar{q}_0 and initial irregularities in the shape of the middle surface are shown in Figures 10.15-10.19.

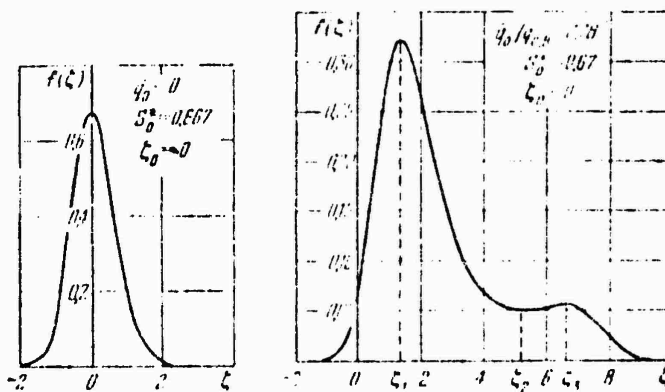


Figure 10.15. Deflection probability density at the center of a slightly curved panel during acoustic vibrations under conditions of absence of static external pressure.

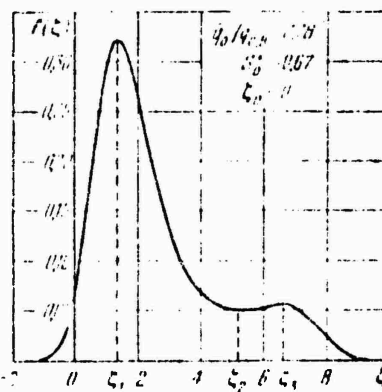


Figure 10.16. Deflection distribution law in the case of a shallow shell with snapping at the level of a static external load amounting to 0.78 of the upper critical value.

Let us turn to the results of computations in the case of an ideal shell (solid lines in Figures 10.15-10.19) for various conditions of loading with static external pressure. The upper critical pressure parameter for the shell under consideration $\bar{q}_0, u = 1.185$, and the lower critical value $\bar{q}_{0,1} = 0.874$ (see Figure 2.48). The values of \bar{q}_0 were chosen to be 0.92, 1.12, 1.3. The corresponding ratios $\bar{q}_0/\bar{q}_0, u$ were 0.78, 0.84, 0.95, 1.1.

In the absence of static pressure ($\bar{q}_0 = 0$), the shell executes vibrations around a single equilibrium position $\zeta_1 = 0$ (Figure 10.15). In the case of $\bar{q}_0 = 0.92 = 0.78 \bar{q}_0, u$, the shell has a second stable equilibrium state when the deflection $\zeta_3 = 6.6$; the deflection $\zeta_2 = 5.2$ corresponds to an unstable equilibrium position (Figure 10.16). As the parameter \bar{q}_0 increases to the value $\bar{q}_0 = 1 = 0.84 \bar{q}_0, u$, the probability of the interval of ζ values in the region of considerable deflections increases markedly (Figure 10.17). When the parameter $\bar{q}_0 = 1.12$, which is close to the upper critical value, the largest probability fraction corresponds to the region of deflection values in the vicinity of the second stable equilibrium position (Figure 10.18). Figure 10.19 corresponds to the case $\bar{q}_0 = 1.3$, when the shell has a single (snapped) equilibrium position: the distribution function covers the region of deflections which are equal to several shell thicknesses.

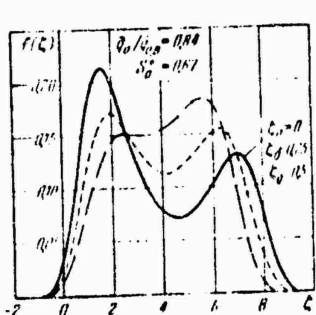


Figure 10.17. Increase in the probability of large deflections with increasing static external pressure. Effect of initial camber.

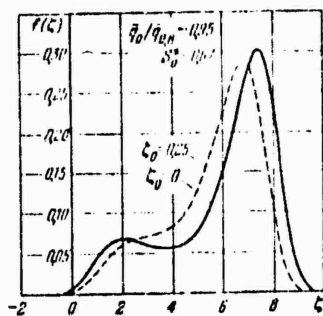


Figure 10.18. Probability densities of deflection at the center for an ideal and a nonideal shell during acoustic vibrations and in the presence of a static external pressure close to the upper critical value.

The influence of initial irregularities (dashed lines in Figures 10.17, 10.18) is more pronounced when the values of the static pressure parameter \bar{q}_0 are lower. As is evident from Figure 10.17, the transition from the case of an ideal shell to the variant $\zeta_0 = 0.25$ appreciably increases the probability of deflection values in the vicinity of the snapped equilibrium position. When $\bar{q}_0 = 1.12 = 0.945 \bar{q}_0, u$,

the shell with initial camber $\zeta_0 = 0.25$ executes vibrations around a single (snapped) equilibrium position: the distribution function has one maximum corresponding to the deflection $\zeta = 6.8$ (Figure 10.18).

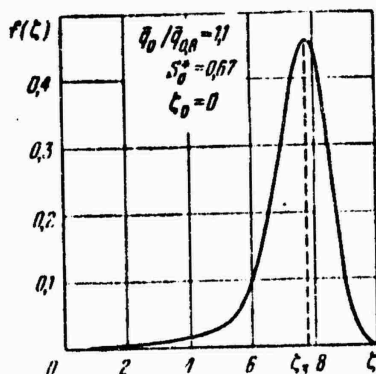


Figure 10.19. Law of distribution of dynamic deflection for a shallow shell during acoustic vibrations around snapped equilibrium.

a_n	$q_0/q_{0,n}$	ζ_0	S_0^*	$M(\zeta^2)$	Φ_1	Φ_2	Φ_3	$N^* = 10^3 N/mm$
0	0	0		0,4	1	0	0	0
0,92	0,78	0		10,9	0,833	0,021	0,116	22
		0		20,8	0,514	0,22	0,266	31
		0,1		21,0	0,127	0,212	0,361	41
1	0,81			21,0	0,265	0,195	0,51	53
		0,25	0,67	20,4	0,012	0,18	0,808	69
		0,5		30,9	0,013	0,781	0,176	25
		0		37,7	0,012	0,776	0,212	29
1,12	0,95	0,1		34,6	0	1	0	0
		0,25		55,6	0	1	0	0
1,3	1,1	0						

Table 10.3.

Data for the mean square of the deflection as a function of the factors considered are listed in Table 10.3. A change in loading conditions leads to an appreciable change of this characteristic. In the absence of static pressure, the mean square of the deflection amounts to 0.4. As the parameter \bar{q}_0 increases, this value increases rapidly; values of \bar{q}_0 equal to 0.92, 1, 1.12, 1.3 are associated with values of the mean square of the dynamic deflection equal to 10.9, 20.8, 39.9, 55.6 for an ideal shell. As is evident from the table, the dependence of the mean square of the deflection on the initial imperfections in the shape of the shell turns out to be unimportant.

We will use formulas (64), (65) to determine the expressions for the probability density of the extrema. Substituting in (65) the solution for $f(\zeta)$ from (103), we obtain

$$f(\zeta_{\max, \min}) = \frac{2(S_0^* C)^{-1}}{f(\zeta_1) + f(\zeta_2) - f(\zeta_3)} (\alpha_s^{*2} - \beta_s^{*2} + \alpha_s^* - \bar{q}_0) \times \\ \times \exp \left[-\frac{1}{S_0^*} \left(\alpha_s^{*2} - \frac{2}{3} \beta_s^{*2} + \frac{1}{2} \zeta^4 \right) + \frac{2}{S_0^*} \bar{q}_0 \zeta \right]. \quad (10.104)$$

The laws of distribution of deflection extrema for the case of a spherical shell with $k^* = 48$, $\lambda = 1$ as a function of the loading conditions and initial irregularities in the shape of the middle surface are shown in Figures 10.20-10.24. In Figures 10.20, 10.21, 10.24, solid lines indicate the probability densities of the maxima, and dashed lines, the probability densities of the minima. In Figures 10.22, 10.23, the solid lines correspond to the probability densities of the extrema for an ideal shell; the dashed and dot-dash lines, for shells with different parameters of initial irregularities.

Let us first consider the effect of the distributed pressure parameter \bar{q}_0 . In the absence of static pressure (Figure 10.20), the extrema cover a region of comparatively low deflection values in the vicinity of the equilibrium position $\zeta_1 = 0$. Figures 10.21-10.23 pertain to cases in which the shell has two stable equilibrium positions and executes vibrations of three types.

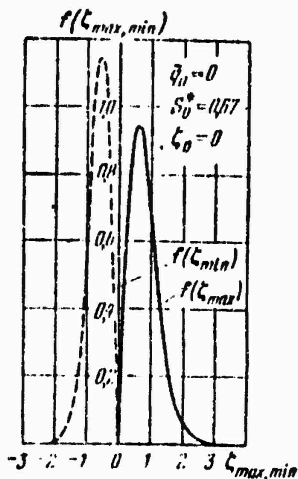


Figure 10.20. Probability densities of dynamic deflection maxima and minima for a shallow shell during acoustic vibrations under conditions of absence of static external pressure.

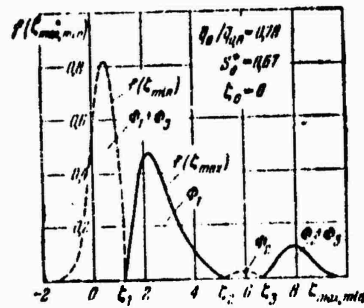


Figure 10.21. Laws of distribution of deflection maxima and minima in the case of a shallow shell with snapping at a level of static external pressure amounting to 0.78 of the upper critical value.

As before, we denote by ϕ_1 the probability of vibration cycles of the first type, and by ϕ_2 , ϕ_3 , those of the second and third types, respectively. The values of ϕ_1 , ϕ_2 , ϕ_3 are given in Table 10.3. When $\bar{q}_0 = 0.92 = 0.78 \bar{q}_{0,u}$, vibration cycles of the first type have a probability $\phi_1 = 0.83$; the relative repetition frequencies of cycles of the second and third types are $\phi_2 = 0.021$ and $\phi_3 = 0.146$, respectively (Figure 10.21, Table 10.3). Increasing the static pressure to $\bar{q}_0 = 1 = 0.84 \bar{q}_{0,u}$ leads to a sharp increase in the probability of cycles of the second type to the value $\phi_2 = 0.22$ (graph of Figure 10.22 for $\xi_0 = 0$), and when $\xi_0 = 0.25$, the relative frequency of cycles of the third type most dangerous for the shell strength increases to $\phi_3 = 0.54$ (Figure 10.22, Table 10.3). It is evident that in this loading variant, the shell with parameter $\xi_0 = 0.5$ is subjected to the most difficult vibration conditions: cycles with snaps occur with a probability $\phi_3 = 0.808$.

The average number of snaps of the shell per unit time is found from formula

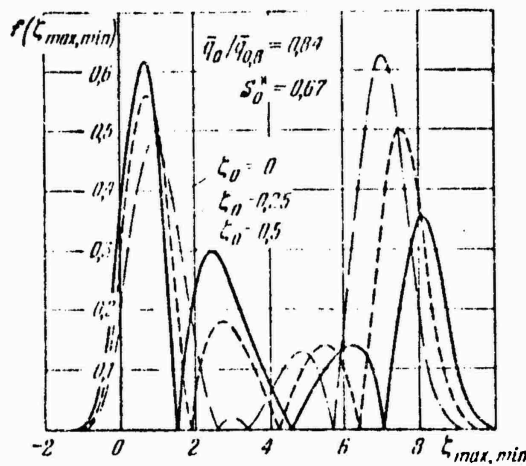


Figure 10.22. Probability densities of deflection extrema at the center for ideal and nonideal shells loaded with acoustic pressure and simultaneously acted on by a static pressure amounting to 0.84 of the upper critical value.

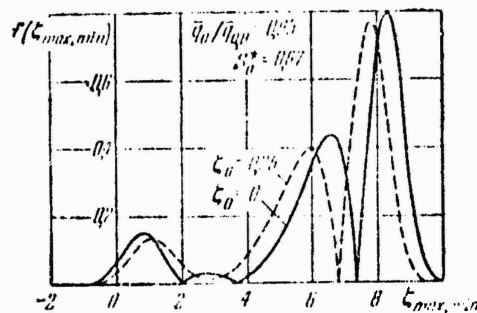


Figure 10.23. Laws of distribution of deflection maxima and minima for an ideal and nonideal shell during acoustic vibrations in the case of action of static external pressure close to the upper critical value.

(68). Values of the quantity $N^* = 10^3 N/w_0$ for a spherical shell with the parameters given above are listed in Table 10.3. It is evident that for an ideal shell, the highest value of this quantity, equal to 33.6, takes place at the level $\bar{q}_0 = 1 = 0.884 \bar{q}_0$, u

In the same case, we note a significant effect of the initial irregularities in the shape of the shell: when the parameter ζ_0 is equal to 0.1, 0.25, 0.5, vibratory regimes of the shell take place with an average number of snaps N^* per unit time equal to 41, 53, 69, respectively. As the value of \bar{q}_0 increases, the effect of initial imperfections decreases.

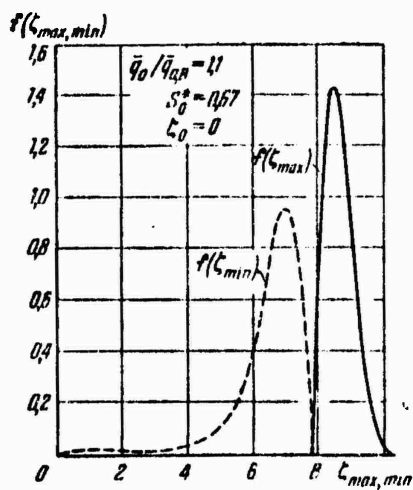


Figure 10.24. Distribution law of extrema for a shallow shell during acoustic vibrations around the snapped position.

Analysis of the probability characteristics of the stressed state may be carried out by using the method presented in the preceding section.

§ 115. Problems for Further Investigations

In conclusion, we will enumerate the problems which it would be desirable to consider in the next few years.

First of all, the general nonlinear theory of dynamic processes in shells and plates is awaiting further development. It is necessary to explain the limits of

application of different variants of basic equations and, in particular, Timoshenko-type theoretical variants. Dynamic equations pertaining to viscoelastic, elastoplastic, and viscoplastic shells, useful in practical applications, should be derived.

Particular attention should be given to the development of dynamic models for two-layer, many-layer and reinforced structures with consideration of possible deformations of different types for alternate layers. Physical and mathematical models for new composite materials of given structures should also be studied.

It is necessary to develop specific problems of natural, forced and parametric nonlinear vibrations of cylindrical, conical and spherical shells as systems with several degrees of freedom, considering the possibility of crossovers from one type of vibration mode to others. More detailed studies should be made of forced vibrations under random loads, caused by the noise of aircraft engines, pulsations in the turbulent boundary layer, atmospheric turbulence, gas flow separations, base pressure pulsations, and other related phenomena.

It is desirable to continue the study of transient processes in shells connected with their buckling, under dynamic and impact loads; this applies to shells of diverse shape and structure. The case of asymmetric deformation is important for spherical shells. The question of dynamic stability criteria should be investigated further.

Considerable attention should be given to the problems of aerohydroelasticity, including the problem of self-excited oscillations of shells in a supersonic gas flow, problems of the behavior of shells acted on by moving and pulsating loads, and cases of thermal shock.

In sufficiently studied remains the question of the effect of the conditions of fixing along the shell edges on nonlinear vibrations and on transient processes for shells of different configurations.

Thus far, there are no reliable data on the evaluation of the service life and supporting capacity of actual structures acted on by random loads at significant stress amplitudes.

The problems of optimum design of shells subjected to different types of dynamic loads remain important. It is desirable to study different variants of reinforcing elements, account being taken of their different orientations.

In connection with the development of numerical methods of solution of dynamic problems, a major importance is assumed by the development of rational computational algorithms and their application to digital computers.

Finally, new methods should be found for the experimental study of the behavior of shells under dynamic and impact loads, with the use of modern measuring instruments and more accurate methods of determination of the shell configuration at different instants of time.

Bibliography

- 0.1. Андронов А. А., Витт А. А., Хайкин С. Э., Теория колебаний, изд. 2-е, Физматгиз, Москва, 1959.
- 0.2. Бабаков И. М., Теория колебаний, изд. 3-е, «Наука», Москва, 1968.
- 0.3. Болотин В. В., Динамическая устойчивость упругих систем, Гостехиздат, Москва, 1956.
- 0.4. Болотин В. В., Неконсервативные задачи теории упругой устойчивости, Физматгиз, Москва, 1961.
- 0.4а. Болотин В. В., Некоторые новые задачи динамики оболочек, Доклад на Всесоюзном совещании по теории оболочек (Тарту, 1957), «Расчеты на прочность» 4, Машигиз, Москва (1959), 331—365; Современные направления в области динамики пластин и оболочек, Теория пластин и оболочек, Труды II Всесоюзной конференции по теории пластин и оболочек (Львов, 1961), Изд-во АН УССР, Киев, 1962, 16—32.
- 0.5. Бубнов И. Г., Труды по теории пластин, Гостехиздат, Москва, 1953.
- 0.6. Вольмир А. С., Устойчивость деформируемых систем, изд. 2-е, «Наука», Москва, 1967.
- 0.6а. Вольмир А. С., Устойчивость при ударе, сб. «Строительная механика», Стройиздат, Москва, 1966, 61—67; Актуальные задачи теории устойчивости оболочек, Механика твердого тела, Труды II Всесоюзного съезда по теоретической и прикладной механике (Москва, 1964) 3, «Наука», Москва, 1966, 95—115; Задачи теории устойчивости оболочек и пластинок, Труды VI Всесоюзной конференции по теории оболочек и пластинок (Баку, 1966), «Наука», Москва, 1966, 977—983; Современные проблемы устойчивости и динамики оболочек, Стройт. мех. и расчет соор., № 2 (1970), 32—37; Нелинейные задачи динамики оболочек, Расчеты на прочность 15, «Машиностроение», Москва (1971), 291—311.
- 0.7. Ворович И. И., Некоторые математические вопросы в теории пластин и оболочек, Механика твердого тела, Труды II Всесоюзного съезда по теоретической и прикладной механике (Москва, 1964) 3, «Наука», Москва, 1966, 116—136; Общие проблемы в теории пластин и оболочек, Труды VI Всесоюзной конференции по теории оболочек (Баку, 1966), «Наука», Москва, 896—903.
- 0.7а. Гольденблат И. И., Нелинейные проблемы теории упругости, «Наука», Москва, 1969.
- 0.8. Григорьев Э. И., Кабанов В. В., Устойчивость круговых цилиндрических оболочек, Итоги науки, Механика твердых деформированных тел 6 (1967), ВИНИТИ, Москва, 1969.
- 0.8а. Ильгамов М. А., Колебания упругих оболочек, содержащих жидкость и газ, «Наука», Москва, 1969.
- 0.9. Ильюшин А. А., Механика сплошной среды, Изд-во Моск. гос. ун-та, 1971.

- 0.10. Коповенко В. О. Колебательные системы с ограниченным возбуждением, «Наука», Москва, 1964.
- 0.10а. Крылов А. Н., Вибрация судов, ОГИИ, Ленинград, 1936.
- 0.11. Крылов И. М., Богоявленский И. И., Введение в нелинейную механику, Изд-во АН УССР, Киев, 1937.
- 0.12. Лурье А. И., Некоторые нелинейные задачи теории автоматического регулирования, Гостехиздат, Москва, 1951.
- 0.12а. Лурье А. И., Теория упругости, «Наука», Москва, 1970.
- 0.13. Малкин И. Г., Некоторые задачи теории нелинейных колебаний, Гостехиздат, Москва, 1956.
- 0.13а. Митропольский Ю. А., Метод усреднения в нелинейной механике, «Наукова думка», Киев, 1971.
- 0.14. Половников В. В., Основы нелинейной теории упругости, Гостехиздат, Москва, 1948.
- 0.15. Огibalov П. М., Колтунов М. А., Оболочки и пластинки, Изд-во Моск. гос. ун-та, 1969.
- 0.16. Оппенвиль О. Д., Некоторые динамические задачи теории оболочек, Изд-во АН СССР, Москва, 1957.
- 0.17. Наполко Я. Г., Основы прикладной теории упругих колебаний, изд. 2-е, «Машиностроение», Москва, 1967.
- 0.17а. Попомарев С. Д., Бидерман В. Л., Лихарев К. К., Макушкин В. М., Мозжин И. Н., Федосьев В. Н., Расчеты из прочности в машиностроении 1 (1950); 2 (1958); 3 (1959), Машгиз, Москва.
- 0.18. Попов Е. П., Пальтов И. И., Приближенные методы исследования нелинейных автоматических систем, Физматгиз, Москва, 1960.
- 0.19. Седов Л. И., Механика сплошной среды 1, 2, «Наука», Москва, 1970.
- 0.19а. Седов Л. И., К теории построения механических моделей сплошных сред. Труды Всесоюзного съезда по теоретической и прикладной механике (Москва, 1960), Изд-во АН СССР, Москва, 1962, 176–212.
- 0.20. Труды Международного симпозиума по нелинейным колебаниям 1–3, Изд-во АН УССР, Киев, 1953; Труды V Международной конференции по нелинейным колебаниям, 1–4, Изд-во АН УССР, Киев, 1970.
- 0.21. Филиппов А. И., Колебания деформируемых систем, изд. 2-е, «Машиностроение», Москва, 1970.
- 0.22. Vand D. R., Nonlinear dynamic elasticity, Waltham, 1969.
- 0.22а. Cunningham W. J., Introduction to nonlinear analysis, New York, 1958.
- 0.23. Den Hartog J. R., Mechanical vibrations, 4th ed., New York, 1956 (имеется русский перевод: Ден Гартог Дж., Механические колебания, Физматгиз, Москва, 1960).
- 0.24. Dynamics stability structures, Proc. of an Intern. confer. (ed. by Шеггини Г.), Oxford, 1967.
- 0.25. Flügge W., Statik und Dynamik der Schalen, Berlin, 1957 (имеется русский перевод: Флюгге В., Статика и динамика оболочек, Гостехиздат, Москва, 1961).
- 0.26. Hale J. K., Oscillations in nonlinear systems, New York, 1963 (имеется русский перевод: Хейл Дж., Колебания в нелинейных системах, «Мир», Москва, 1966).
- 0.27. Hayashi C., Forced oscillations in nonlinear systems, Osaka, 1953 (имеется русский перевод: Хаяси Т., Внужденные колебания в нелинейных системах, Изд-во иностр. лит., Москва, 1957); Nonlinear oscillations in physical systems, New York, 1964 (имеется русский перевод: Нелинейные колебания в физических системах, «Мир», Москва, 1968).
- 0.28. Kauderer H., Nichtlineare Mechanik, Berlin, 1958 (имеется русский перевод: Каудерер Г., Нелинейная механика, Изд-во иностр. лит., Москва, 1961).

- 0.29.** Koiter W. T. Устойчивость и практическое поведение упругих систем. Доклад на Всеобщем съезде по теоретической и прикладной механике (Москва, 1960), сб. «Механика», № 5 (1960). Изд-во иностр. лит., Москва; Elastic stability and postbuckling behavior, Proc. Symp. nonlinear problems (ed. by Langer R. E.), Madison, 1963; The effect of axisymmetric imperfections on the buckling of cylindrical shells under axial compression, Proc. Kon. Ned. Ak. Wet. **B66**, 1963; General equations of elastic stability for thin shells, Proc. Symp. in honor of L. H. Donnell (ed. by Muster D.), Univ. of Houston, 1966; On the nonlinear theory of thin elastic shells, Proc. Kon. Ned. Ak. Wet. **B69** (1966), 1—54; The nonlinear buckling problem of a complete spherical shell under uniform external pressure, I—IV, Proc. Kon. Ned. Ak. Wet. **B72**, 1969; On the foundations of the linear theory of thin elastic shells, I, II, Proc. Kon. Ned. Ak. Wet. **B73** (1970), 169—195; Error estimates for certain approximate solutions of problems in the linear theory of elasticity, J. Appl. Math. Phys. **21**, № 4 (1970), 534—538.
- 0.30.** Naghdi P. M. Foundations of elastic shell theory, «Progress in solid mechanics» (ed. by Sneddon I. N. and Hill R.) 4, Amsterdam, 1963, 1—90.
- 0.31.** Poincaré H. Les méthodes nouvelles de la mécanique céleste 1 (1892); 2 (1893); 3 (1899), Paris.
- 0.32.** Rayleigh, The theory of sound 1, 2, 2nd ed., London, 1929 (имеется русский перевод: Рэлей (Стретт Дж.), Теория звука 1, 2, изд. 2-е, Гостехиздат, Москва, 1955).
- 0.33.** Suttorp A. Nonlinear structural dynamics problems in aeronautics, Aeron. Res. Council Curr. papers, № 1048, 1969.
- 0.34.** Skudrinsk E. Simple and complex vibratory systems, Pennsylvania, 1968 (имеется русский перевод: Скудин Е., Простые и сложные колебательные системы, «Мир», Москва, 1971).
- 0.35.** Stoker J. J. Nonlinear vibrations in mechanical and electrical systems, New York, 1950 (имеется русский перевод: Стокер Дж., Нелинейные колебания в механических и электрических системах, Изд-во иностр. лит., Москва, 1953).
- 0.36.** Timoshenko S. P., Young D. H. Vibration problems in engineering, 3d ed., New York, 1955 (имеется русский перевод: Тимошенко С. П., Колебания в инженерном деле, изд. 2-е, «Наука», Москва, 1967).
- 0.37.** Zielinska S. Vibration analysis. Warszawa, 1970.

К главе I

- 1.1.** Айнола Л. Я. Нелинейная теория типа Тимошенко для упругих оболочек, Изв. АН Эст. ССР, сер. физ.-матем. и техн. наук, **14**, № 3 (1965), 337—344; Вариационные методы для нелинейных уравнений движения оболочек, Прикл. матем. и мех. **32**, № 1 (1968), 154—158.
- 1.2.** Айнола Л. Я., Шигул У. К. Волновые процессы деформации упругих пленок и оболочек, Изв. АН Эст. ССР, сер. физ.-матем. и техн. наук, **14**, № 1 (1965), 3—63.
- 1.3.** Алексеев С. А. Задачи статики и динамики мягких оболочек, Труды VI Всесоюзной конференции по теории оболочек (Баку, 1966), «Наука», Москва, 1966, 28—37.
- 1.4.** Алумияэ Н. А. О представлении основных соотношений нелинейной теории оболочек, Прикл. матем. и мех. **20**, № 1 (1956), 136—139.
- 1.5.** Амбаркумян С. А. Теория анизотропных оболочек, Физматгиз, Москва, 1961.
- 1.5а.** Амбаркумян С. А. Теория анизотропных пластин, «Наука», Москва, 1967.

- 1.6. Амизаде Ю. А., Теория упругости, 2-е изд., изд-во «Высшая школа», Москва, 1971.
- 1.7. Болотин В. В., О вариационных принципах теории упругой устойчивости, сб. «Проблемы механики твердого деформированного тела», «Судостроение», Ленинград, 1970, 83–88.
- 1.7а. Бондарь Н. Г., Исправленные автономные задачи механики упругих систем, «Будивельник», Киев, 1971.
- 1.8. Векуа П. Н., Об одном методе расчета призматических оболочек, Труды Тбилисского матем. института 21 (1955), 191–195.
- 1.9. Власов Б. Ф., Об уравнениях теории изгиба пластинок, Изв. АН СССР, Отдел. техн. наук, № 12 (1957), 57–60.
- 1.10. Власов В. З., Общая теория оболочек и ее приложения в технике, Гостехиздат, Москва, 1949.
- 1.11. Вольмир А. С., Глубокие пластины и оболочки, Гостехиздат, Москва, 1956.
- 1.12. Галеркин Б. Г., Упругие тонкие плиты, Госстройиздат, Ленинград, 1933; Собрание сочинений 1 (1952); 2 (1953). Изд-во АН ССР, Москва.
- 1.13. Гольденвейзер А. Л., Теория тонких упругих оболочек, Гостехиздат, Москва, 1953.
- 1.13а. Гольденвейзер А. Л., Развитие теории упругих тонких оболочек, Труды Всесоюзного съезда по теоретической и прикладной механике (Москва, 1960), Изд-во АН ССР, Москва, 1962, 339–357; Асимптотические методы исследования спектра частот собственных колебаний оболочек, Механика твердого тела, Труды II Всесоюзного съезда по теоретической и прикладной механике (Москва, 1964) 3, «Наука», Москва, 1966; Методы обоснования и уточнения теории оболочек, Прикл. матем. и мех. 32, № 4 (1968), 684–695; Некоторые вопросы общей линейной теории оболочек, Труды VII Всесоюзной конференции по теории оболочек и пластинок (Днепропетровск, 1969), «Наука», Москва, 1970, 749–755; Об ортогональности форм собственных колебаний тонкой упругой оболочки, сб. «Проблемы механики твердого деформированного тела», «Судостроение», Ленинград, 1970, 121–129.
- 1.13б. Капи С. Н., Стройная механика оболочек, «Машиностроение», Москва, 1966.
- 1.13в. Капитор В. Я., Исправленные задачи теории неоднородных пологих оболочек, «Наукова думка», Киев, 1971.
- 1.14. Кармишин А. В., Мяченков В. И., Методы решения задач теории устойчивости оболочек, Труды VII Всесоюзной конференции по теории оболочек и пластинок (Днепропетровск, 1969), «Наука», Москва, 1970, 794–807.
- 1.14а. Кармишин А. В., Лясковец В. А., Мяченков В. И., Репин А. А., Фролов А. Н., Единый метод решения задач прочности, устойчивости и колебаний оболочек и пластин, VIII Всесоюзная конференция по теории оболочек и пластин, Ростов-на-Дону, 1971.
- 1.15. Кильчевский Н. А., Основы аналитической механики оболочек, I, Изд-во АН УССР, Киев, 1963.
- 1.16. Кильчевский Н. А., Теория нестационарных динамических процессов в оболочках, Прикл. мех. 4, № 8 (1968), 1–18.
- 1.16а. Колкуоп Н. В., Основы расчета упругих оболочек, изд-во «Высшая школа», Москва, 1972.
- 1.16б. Кориншин М. С., Исправленные задачи теории пластин и оболочек и методы их решения, «Наука», Москва, 1964.
- 1.17. Королев В. И., Упруго-пластические деформации оболочек, «Машиностроение», Москва, 1971.
- 1.18. Лурье А. Н., Статика тонкостенных упругих оболочек, Гостехиздат, Москва, 1947.

- 1.19. **Москаленко В. Н.**, К применению уточненных уравнений изгиба пластинок к задаче о собственных значениях, Инжен. журн., № 3 (1961); Об учете ширин прращения и деформации сдвига в задачах о собственных колебаниях пластин, Теория пластин и оболочек, Труды II Всесоюзной конференции по теории пластин и оболочек, Львов, 1961, Изд-во АН УССР, Киев, 1962, 261—266.
- 1.20. **Муштари Х. М.**, Качественное исследование напряженного состояния упругой оболочки при малых деформациях и произвольных смещениях, Прикл. матем. и мех. 13, № 2 (1949), 121—134.
- 1.21. **Муштари Х. М., Гллимов К. З.**, Испинская теория упругих оболочек, Таткнигоиздат, Казань, 1957.
- 1.22. **Новожилов В. В.**, Теория тонких оболочек, Судпромгиз, Ленинград, 1951.
- 1.23. **Папкович П. Ф.**, Труды по строительной механике корабля 3 (1962), 4 (1963), Судпромгиз, Ленинград.
- 1.23а. **Селезов И. Т.**, Об уравнениях движения гибких пластинок, Прикл. мех. 5, № 4 (1959), 444—448.
- 1.23б. **Уфлиид Я. С.**, Распространение волн при пограничных колебаниях стержней и пластин, Прикл. матем. и мех. 12, № 3 (1948), 287—300.
- 1.24. **Черных К. Ф.**, Лицейская теория оболочек 1 (1962); 2 (1964), Изд-во Ленингр. ун-та.
- 1.24а. **Шмакский Ю. А.**, Справочник по строительной механике корабля 1, 2 (1958); 3 (1960), Судпромгиз, Ленинград.
- 1.25. **Bolle L.**, Contribution au problem lneutre de flexion d'une plaque elastique, Bulletin technique de la Suisse Romande 73, № 21 (1947), 281—285; № 22 (1947), 293—298.
- 1.26. **Green A. E., Adkins J. E.**, Large elastic deformations and nonlinear continuum mechanics, Oxford, 1960 (имеется русский перевод: Грин А., Адкинс Дж., Большие упругие деформации и нелинейная механика, атомной среды, «Мир», Москва, 1966).
- 1.27. **Habir L. M.**, Theory of elastic plates in the reference state, Intern. Journ. of solids and struct. 2, № 2 (1966), 157—166.
- 1.28. **Herrmann G., Mirsky J.**, Three dimensional and shell theory analysis of axially symmetric motions of cylinders, J. Appl. Mech. 23, № 4 (1956), 563—568.
- 1.29. **Huang T. C.**, Applications of variational methods to the vibration of plates including rotatory inertia and shear, Developments in mechanics I (1961), 61—72.
- 1.30. **Karman Th.**, Festigkeitsprobleme in Maschinenbau, Encycl. d. Math. Wiss. 4, № 4 (1910), 311—385.
- 1.31. **Lamb H.**, On waves in an elastic plate, Proc. of Royal Soc. A93, № 648 (1917), 114—128.
- 1.32. **Love A.**, Mathematical theory of elasticity, 1927 (имеется русский перевод: Лов А., Математическая теория упругости, Москва, 1935).
- 1.33. **Mindlin R. D.**, Influence of rotatory inertia, shear on flexural motions of isotropic elastic plates, J. Appl. Mech. 18 (1951), 31—38.
- 1.34. **Naghdi P. M., Cooper R. M.**, Propagation of elastic waves in cylindrical shells including the effects of transverse shear and rotatory inertia, J. Acoust. Soc. of Amer. 28, № 1 (1956), 56—63.
- 1.34а. **Nason W. A.**, Recent advances in the buckling of thin shells, Appl. Mech. Rev. 13, № 3 (1960), 161—164 (имеется русский перевод: Нэш У., Обзор новых исследований по устойчивости тонких оболочек, сб. «Механика», № 5 (1960), Изд-во иностран. лит., М., 111—119).
- 1.35. **Rayleigh**, On the free vibrations of an infinite plate of homogeneous isotropic elastic material, Proc. of Math. Soc. 10 (1889), 225—229.
- 1.36. **Reissner E.**, On transverse vibration of thin shallow shells, Quarterly of Appl. Math. 13, № 2 (1955), 169—170.

- 1.37. Timoshenko S. P., On the correction for shear of the differential equation for transverse vibration of prismatic bar, Philosophical Magazine 41, № 6 (1921), 744–746.
- 1.38. Timoshenko S. P., Woinowsky-Krieger S., Theory of plates and shells, 2nd ed., New York, 1959 (имеется русский перевод: Тимошенко С. П., Войновский-Кригер С., Пластины и оболочки, Физматгиз, Москва, 1963).

К главе II

- 2.1. Алфутов Н. А., Балабух Л. Н., О возможности решения задач устойчивости пластин без предварительного определения начального изгиженого состояния, Прикл. матем. и мех. 31, № 4 (1967), 716–722.
- 2.2. Биргер И. А., Колебания пластинок и оболочек, сб. «Прочность и динамика авиационных двигателей», 5, «Машиностроение», Москва, 1969, 5–27.
- 2.3. Болотин В. В., Краевой эффект при колебаниях упругих оболочек, Прикл. матем. и мех. 24, № 5 (1960), 831–842; Динамический краевой эффект при упругих колебаниях пластинок, Иж. сб. З1, Изд-во АН СССР, Москва (1961), 3–14; Асимптотический метод исследования задач о собственных значениях для прямоугольных областей, сб. «Проблемы механики сплошной среды», Изд-во АН СССР, 1961, 60–72; Асимптотический метод в теории колебаний упругих пластин и оболочек, Труды конференции по теории пластин и оболочек (Казань, 1960), Изд-во Казанского гос. ун-та, 1961, 21–26; Обобщение асимптотического метода решения задач о собственных значениях для прямоугольных областей, Иж. журн. 1, № 3 (1961), 86–92; О плотности частот собственных колебаний тонких упругих оболочек, Прикл. матем. и мех. 27, № 2 (1963), 362–364; Плотность собственных значений в задачах о колебаниях упругих пластин и оболочек, Труды VI Всесоюзной конференции по теории оболочек и пластинок (Баку, 1966), «Наука», Москва, 1966, 161–167.
- 2.4. Болотин В. В., Макаров Б. П., Мищенков Г. В., Шлейко Ю.Ю., Асимптотический метод исследования спектра собственных частот упругих пластинок, Расчеты на прочность 6, Машина, Москва, (1960), 231–253.
- 2.5. Болотин В. В., Москаленко В. Н., Колебания пластинок, в книге «Прочность, устойчивость, колебания» 3, «Машиностроение», Москва, 1968, 370–417; Колебания оболочек, там же, 418–467.
- 2.5а. Бреславский В. Е., О колебаниях цилиндрических оболочек, Иж. сб. 16, Изд-во АН СССР, Москва (1953), 109–118.
- 2.6. Вольмир А. С., Кильдибеков И. Г., О линейной теории устойчивости цилиндрических оболочек, Иж. журн. 4, № 2 (1961), 263–265.
- 2.7. Вольмир А. С., Кильдибеков И. Г., Изгиб пластинок, в книге «Прочность, устойчивость, колебания» 1, «Машиностроение», Москва, 1968, 526–586; Гибкие пластины и мембранны, там же, 597–614.
- 2.8. Вольмир А. С., Кильдибеков И. Г., Устойчивость пластинок, в книге «Прочность, устойчивость, колебания» 3, «Машиностроение», Москва, 1968, 91–126; Устойчивость оболочек, там же, 117–215.
- 2.8а. Вольмир А. С., Кильдибеков И. Г., Медведева С. В., Исследование собственных нелинейных колебаний пологих оболочек, Сборник, посвященный 100-летию со дня рождения И. Г. Бубнова, Судпромгиз, Ленинград, 1972.
- 2.8б. Вольмир А. С., Логинская А. А., Рогалевич В. В., Собственные нелинейные колебания оболочек, VIII Всесоюзная конференция по теории оболочек и пластинок, Ростов-на-Дону, 1971.

- 2.9. Гопткевич В. С., Собственные колебания пластинок и оболочек, «Наукова думка», Киев, 1964.
- 2.10. Григорюк Э. И., Нелинейные колебания и устойчивость пологих оболочек и стержней, Изв. АН СССР, Отдел техн. наук, № 3 (1955), 33—68; О колебаниях круговой цилиндрической панели, испытывающей конечные прогибы, Прикл. матем. и мех. 10, № 3 (1955), 376—382.
- 2.11. Калинин В. С., О расчете нелинейных колебаний гибких пластин и пологих оболочек методом малого параметра, Теория оболочек и пластин, Труды IV Всесоюзной конференции по теории оболочек и пластин (Ереван, 1962), Изд-во АН Арм. ССР, Ереван, 1964, 480—488; Нелинейные колебания стержней, пластин и пологих оболочек, Тезисы докладов на совещании по проблеме упругих колебаний механических систем (Рига, 1961), Изд-во АН Латв. ССР, Рига, 1961; Вынужденные нелинейные изгибные колебания однородного призматического стержня и песьма длиной прямоугольной пластинки, Всесоюзный съезд по теоретической и прикладной механике (Москва, 1960), анонс. докл., Изд-во АН СССР, Москва, 1960; Вынужденные нелинейные колебания гибридических стержней и вытянутых прямоугольных пластин под действием гармонической вибрации опор, «Судостроение», № 12 (1959), 11—16; Нелинейные колебания упругих тел, Третий Всесоюзный съезд по теоретической и прикладной механике, анонс. докл., «Наука», Москва, 1968.
- 2.12. Кильдибеков И. Г., Собственные нелинейные колебания круговой цилиндрической оболочки, VIII Всесоюзная конференция по теории оболочек и пластин, Ростов-на-Дону, 1971.
- 2.13. Лужин О. В., К вопросу о свободных колебаниях тонкой сферической оболочки, Стройт. мех. и расчет. сооруж., № 3 (1961), 32—36.
- 2.14. Метсавеэр Я. А., Нелинейные колебания прямоугольных пластин с жестким защемлением по контуру, Труды Таллинского политехн. ин-та А, № 257 (1967), 127—138.
- 2.15. Михлин С. П., Вариационные методы в математической физике, «Наука», Москва, 1970.
- 2.16. Морозов Н. Ф., Нелинейные колебания тонких пластинок с учетом шероховатости вращения, Дифф. уравн. 4, № 5 (1969), 932—937.
- 2.17. Пановко Я. Г., Основы теории колебаний механических систем, в книге «Прочность, устойчивость, колебания» 3, «Машгиз», Москва, 1968, 216—284.
- 2.18. Пановко Я. Г., Губанова Л. И., Устойчивость и колебания упругих систем, изд. 2-е, «Наука», Москва, 1967.
- 2.19. Рабинович Р. И., Динамический расчет пологих оболочек по нелинейной теории, сб. «Строительное проектирование промышленных предприятий» 5 (1965), 45—50; Свободные колебания гибких прямоугольных пластинок, Исп. высш. уч. зав., Стр-во и архитект., № 1 (1966), 63—69; Свободные колебания гибких пологих оболочек, Стройт. мех. и расчет сооруж., № 2 (1966), 38—41; О свободных колебаниях гибких пологих оболочек, Стройт. мех. и расчет. сооруж., № 4 (1968).
- 2.20. Образцов И. Ф., Вариационные методы расчета тонкостенных авиационных пространственных конструкций, «Машгиз», Москва, 1966.
- 2.21. Трапезин И. И., О малых колебаниях круговой тонкостенной конической оболочки, Расчеты на прочность 2, Машгиз, Москва (1958); О колебаниях круговой тонкостенной конической оболочки. Расчеты на прочность 4, Машгиз, Москва (1959), 367—373.
- 2.22. Федоров В. И., Об одном способе решения задач устойчивости деформируемых систем, Прикл. матем. и механика 27, № 2 (1963); Геометрически нелинейные задачи теории пластин и оболочек, Труды VI Всесоюзной конференции по теории оболочек и пластинок (Баку, 1966), «Наука», Москва, 1966, 971—976.

- 2.22a. Якушев Н. Э., Влияние больших амплитуд на частоты осесимметричных собственных колебаний круговой цилиндрической оболочки, Итоговая научная конф. Казанского гос. ун-та за 1962 г. (краткое содерж. докл.), секция прикл. матем. и мех., Изд-во Казанского гос. ун-та, 1963.
- 2.23. Akkas N., Bauld N. R., Buckling and initial post-buckling behavior of clamped shallow spherical sandwich shells, Intern. J. Sol. Struct. 7, № 9 (1971), 1237—1259.
- 2.24. Arnold R. N., Warburton G. B., The flexural vibrations of thin cylinders, Proc. Inst. Mech. Eng. 167, № 1 (1953).
- 2.25. Baran M. L., Bleich H. H., Tables for frequencies and modes of free vibration of infinitely long thin cylindrical shells, J. Appl. Mech. 21, № 2 (1954).
- 2.25a. Basuli S., Note on the large deflection of a circular plate under a concentrated load, Z. Angew. Math. Mech. 12 (1961), 357.
- 2.26. Berger H. M., A new approach to the analysis of large deflections of plates, J. Appl. Mech. 22 (1955), 465.
- 2.27. Chu H. N., Influence of large amplitudes of flexural vibrations of a thin circular cylindrical shell, J. Aerospace Sci. 28, № 8, (1961).
- 2.28. Chu H. N., Herrmann G., Free flexural vibrations of rectangular elastic plates, J. Appl. Mech. 23, № 4 (1956).
- 2.29. Collatz L., Eigenwertaufgaben mit technischen Anwendungen, Leipzig, 1963 (имеется русский перевод: Коллатц Л., Задачи на собственные значения, «Наука», Москва, 1968).
- 2.30. Cummings B. E., Large amplitude vibration and response of curved panels, AIAA Journ. 2, № 4 (1964).
- 2.31. Dowell E. H., On the nonlinear flexural vibrations of rings, AIAA Journ. 5 (1967), 1508—1509.
- 2.32. Dowell E. H., Ventres C. S., Modal equations for the nonlinear flexural vibrations of a cylindrical shell, Intern. J. Sol. Struct. 4, № 10 (1968).
- 2.33. Evensen D. A., Some observations on the nonlinear vibration of thin cylindrical shells, AIAA Journ. 1 (1963), 2857—2858.
- 2.33a. Forsberg K., A review of analytical methods used to determine the modal characteristics of cylindrical shells, NASA CR-613, 1966.
- 2.34. Fung Y. C., Barton M. V., Shock response of a nonlinear system, J. Appl. Mech. 29 (1962), 465—476.
- 2.35. Fung Y. C., Sechler E. E., Kaplan A., On the vibration of thin cylindrical shells under internal pressure, J. Aeronaut. Sci. 24 (1957), 650—660.
- 2.36. Gajendar N., Large amplitude vibrations of plates on elastic foundations, Intern. J. Nonlinear Mech. 2, № 2 (1967).
- 2.37. Greenspoon J. E., A simplified expression for the period of nonlinear oscillations of curved and flat panels, J. Aerospace Sci. 27, № 2 (1960).
- 2.37a. Hoff N. J., Thin shells in aerospace structures, Astronautics and aeronautics 5, № 2 (1967), 26—45.
- 2.38. Leissa A. W., Free vibrations of elastic plates, AIAA paper № 69—24, New York, 1969; Vibration of plates, Washington, 1969.
- 2.38a. Matsuzaki Y., Influence of the in-plane boundary conditions on the nonlinear characteristics of flexural vibration of rectangular plates, Presented at 12th Conf. Strength Struct., Japan Soc. Aero Space Sci. 1970; Influence of the in-plane boundary conditions on the natural frequency of cylindrically curved panels with simply supported edges, Intern. J. Sol. Struct. 7, № 11 (1971), 1555—1571.
- 2.39. Morley L. S., An improvement of Donnel's approximation for thin walled circular cylinders, Quart. J. Mech. Appl. Math. 12 (1959), 93.

- 2.40. Nash W. A., Modeer J. R., Certain approximate analysis of nonlinear behavior of plates and shallow shells, Proc. Symp. on the theory of thin elastic shells, Delft, 1959.
- 2.41. Nowinski J. L., Note on analysis of large deflections of rectangular plates, Appl. Sci. Res. A11 (1962), 85; Nonlinear transverse vibrations of orthotropic cylindrical shells, AIAA Journ. 1, (1964), 617—620.
- 2.42. Pal M. C., Large amplitude free vibrations of rectangular plates, J. Sci. and Engng Res. 11 (1967), 2.
- 2.43. Reissner E., On transverse vibrations of thin shallow elastic shells Quart. Appl. Math. 13 (1955), 169—176.
- 2.44. Sinha S. N., Large deflections of plates on elastic foundation, Proc. ASCE, J. Engng Mech. Div. EM1 (1963), 1—24.
- 2.45. Sun C. L., Lu S. Y., Nonlinear dynamic behavior of heated conical and cylindrical shells, Nuclear engineering and design 7, № 2 (1968).
- 2.46. Wahl Th., Large amplitude flexural vibrations of rectangular plates, Int. J. Mech. Sci. 5 (1963), 425; Vibration of circular plates on large amplitudes, Proc. ASCE, J. Engng Mech. Div. (1963), 1—15.
- 2.47. Weingarten V. I., Free vibration of thin cylindrical shells, AIAA Journ. № 4 (1964).
- 2.48. Yamaki N., Influence of large amplitudes on flexural vibrations of elastic plates, Zeitschr. für angew. Math. und Mech. 41, № 12 (1961).
- 2.49. Yang T. Y., A finite element procedure for large deflection analysis of plates with initial deflections, AIAA Journ. 9, № 8 (1971), 1468—1473.

К главе III

- 3.1 Алексеева Н. К., Нелинейные колебания пластин и пологих оболочек, канд. дисс., Москва, 1967; Вынужденные и параметрические колебания пластин конечного прогиба с учетом тангенциальных сил инерции, Расчет пространственных конструкций 12, «Машгостроение», Москва, (1969), 177—185.
- 3.2 Амбарумян С. А., Гуини В. Ц., О вынужденных колебаниях и динамической устойчивости трехслойных ортотропных пластинок, Изв. АН ССР, Отдел. техн. и. Механики и машиностроя, № 3 (1961), 117—123.
- 3.3 Багдасарян Ж. Е., Гуини В. Ц., Релаксация в вынужденных нелинейных колебаниях слоистых цилиндрических оболочек, Изв. АН Арм. ССР, серия физ.-матем. п. 14, № 1 (1961), 41—49.
- 3.4 Балабух Л. Н., Молчанов А. Г., Плоские колебания жидкости в прямоугольном упругом сосуде, Расчеты на прочность 13, «Машгостроение», Москва (1968), 231—250.
- 3.5 Балабух Л. Н., Молчанов А. Г., Об одной краевой задаче теории колебаний с граничными условиями, зависящими от параметра, Прикл. матем. и мех. 30, № 6 (1966), 1098—1102; Особенности колебаний сферической оболочки, частично заполненной жидкостью, Иж. журн. Механики тверд. тела, № 5 (1967), 56—61.
- 3.6 Буринстров Е. Ф., Нелинейные поперечные колебания ортотропных оболочек вращения, Иж. сб. 26, Изд-во АН ССР, Москва (1958), 5—20.
- 3.7 Верженко Е. П., Варвак П. М., Итенберг Б. З., Амплитуды нелинейных колебаний прямоугольных пластинок, сб. «Сопротивление и теория сооруж.» 7, «Будівельник», Київ (1968), 45—51.
- 3.8 Вольмир А. С., Кильдисеков Н. Г., Нелинейные акустические колебания цилиндрической оболочки, Изв. АН Арм. ССР, серия физ.-матем. п. 17, № 3 (1964), 65—70.
- 3.9 Диментберг М. Ф., Определение нелинейной диссипативной характеристики системы с одной степенью свободы на основе испытаний при

- вынужденных колебаниях, Изв. журн. Механ. тв. тела, № 2 (1968), 32–34.
- 3.10. Кап А. М., О вынужденных нелинейных колебаниях, Тр. Ленингр. индустрии ин-та, раздел физ.-матем. и. 3 (1939), 102–120.
- 3.11. Кильдибеков И. Г., Исследование нелинейных колебаний пластинок, Теория пластин и оболочек, Труды Всесоюзного симпозиума по теории оболочек и пластин (Казань, 1971), «Наука», Москва, 1971, 151–154.
- 3.11а. Кильдибеков И. Г., Мицюк А. А., Исследование несущей способности подкрепленных панелей в акустическом поле, Прикладная механика 7, № 12 (1971), 82–86.
- 3.12. Лурье А. Н., К задаче о вынужденных нелинейных колебаниях, Ученые зап. Ленингр. госуд. ун-та, серия матем. и., № 8 (1949), 25–33.
- 3.13. Минченков Г. В., О вынужденных нелинейных колебаниях упругих панелей, Изд. АН СССР, Отдел. технич. и. Механ. и машиностр., № 4 (1961), 97–103; Вынужденные колебания механической системы при наличии сухого трения и асимметричной квазипрергой характеристики, Изв. журн. 4, № 4 (1961), 759–764; К вопросу о взаимодействии параметрически возбуждаемых и вынужденных колебаний упругих панелей, Изд. АН Арм. ССР, серия физ.-матем. и., 18, № 1 (1965), 53–60.
- 3.14. Морозин И. Ф., Нелинейные колебания круглой пластинки, Тр. Ленингр. технол. ин-та целяса бум. пром. 17 (1965).
- 3.15. Несторов С. В., Нелинейные вынужденные колебания круглой пластинки, Акуст. журн. 11, № 1 (1965), 74–78.
- 3.16. Насетупкин В. Н., Установившиеся колебания пластинок и пологих оболочек из эластичных нелинейно-упругих материалов, Труды Моск. инж.-строит. ин-та 53 (1968), 185–201.
- 3.17. Соколова Г. А., Колебания типах трапециевидных пластинок, Труды Моск. инж.-строит. ин-та 53 (1968).
- 3.18. Сочинский С. В., Чулковский В. С., О нелинейных динамических деформациях прямоугольных пластин и цилиндрических оболочек, Труды конференции по теории пластин и оболочек (Казань, 1960), Изд-во Казанского гос. ун-та, 1961, 358–361.
- 3.19. Синхотов В. А., Nonlinear response of a circular membrane to sinusoidal acoustic excitation, J. Acoust. Soc. Amer. 36, № 1 (1964).
- 3.20. Ефсеу, Nonlinear vibration of beams and rectangular plates, Z. Angew. Mathem. und Phys. 15, № 2 (1964), 167–175.
- 3.21. Evensen D. A., Evans-Twawowski R. M., Dynamic response and stability of shallow spherical shells subject to time depended loading, AIAA Journ. 5, № 5 (1967).
- 3.22. Evensen D. A., Fulton R. E., Some studies of the nonlinear dynamic response of shell-type structures, в книге [0.21], 237–251.
- 3.23. Hassler J. E., Nowinski J. L., Non-linear transverse vibrations of a rectangular orthotropic panel, Proc. 5th Intern. Sympos. Space Technol. and Sci., 1963, Tokyo, 1964.
- 3.24. Herbert R. E., Random vibrations of plates with large amplitudes, Papers Amer. Soc. Mech. Engrs, 1965.
- 3.25. Kirchman E. J., Greenspoon J. E., Nonlinear response of aircraft panels to acoustic noise, J. Acoust. Soc. Amer. 29, № 7, 1957.
- 3.26. Nowinski J. L., Nonlinear transverse vibrations of circular elastic plates built at the boundary, Proc. 4th US Natl. Congr. Appl. Mech., Berkeley, Calif., 1962, I, Pergamon Press 1962; Nonlinear vibrations of elastic circular plates exhibiting rectilinear orthotropy, Z. angew. Math. und Phys. 14, № 2 (1963).
- 3.27. Tobols S. A., Nonlinear forced vibrations of a circular discs. An experimental investigation, Engineering 180, № 4818 (1958).

- 4.1. Амбарцумян С. А., Гурии В. Ц., Параметрические колебания пластинки в поле действия высоких температур, Изв. АН СССР, Отд. техн. н., Механика и машиностро., № 6 (1964).
- 4.2. Болотин В. В., Некоторые нелинейные задачи динамической устойчивости пластинок, Изв. АН СССР, Отд. техн. н., № 10 (1954), 47—59; Устойчивость тонкостенной сферической оболочки под действием гармонического давления, Расчеты на прочность, Машигиз, Москва 2 (1958), 284—289; Параметрические колебания упругих систем, в книге «Прочность, устойчивость, колебания» 3, «Машиностроение», Москва, 1968, 347—369.
- 4.3. Гурии В. Ц., К теории динамической устойчивости слоистых анизотропных оболочек, Изв. АН Арм. ССР, серия физ.-матем. н. 13, № 1 (1960), 47—58; О границах динамической неустойчивости оболочек, Труды по теории пластин и оболочек, Изд-во Казанского гос. ун-та, Казань, 1961, 117—123; О параметрических возбуждаемых колебаниях слоистых анизотропных гибких оболочек, Изв. АН Арм. ССР, серия физ.-матем. н. 16, № 3 (1962), 29—36.
- 4.3а. Нильгамов М. А., Сахабутдинов Ж. М., Параметрически возбуждаемые колебания цилиндрической оболочки, заполненной сжимаемой жидкостью или газом, Теория пластин и оболочек, «Наука», Москва, 1971.
- 4.4. Минеевков Г. В., О динамической устойчивости пологих упругих оболочек, Изв. журн. 1, № 2 (1961), 112—118.
- 4.5. Минеевков Г. В., Судомосов А. Д., Ефимов В. А., Электронное моделирование параметрических возбуждаемых колебаний в нелинейных системах, Сб. докл. научно-техн. конф. по итогам научно-исслед. работ за 1966—1967 гг., подсекция динамики и прочности машин, Моск. энергет. ин-т, 1967, 278—286.
- 4.6. Кана D. D., Craig R. R., Parametric oscillations of a longitudinally excited cylindrical shell containing liquid, J. Spacecraft and Rockets 5, № 1 (1968), 13—21.
- 4.7. Кана D. D., Dodge F. T., Bubble behavior in liquids contained in vertically vibrated tanks, J. Spacecraft and Rockets 3, № 5 (1966), 760—763.
- 4.8. Кана D. D., Gormley J. F., Longitudinal vibration of a model space vehicle propellant tank, J. Spacecraft and Rockets 4, № 12 (1967), 1585—1591.

К главе V

- 5.1. Амбарцумян С. А., Багдасарян Ж. Е., Флаттер' цилиндрической оболочки, находящейся в поле действия высоких температур, Изв. АН СССР, Отдел. техн. н., № 5 (1964), 77—82; Об устойчивости ортотропных пластинок, обтекаемых сверхзвуковым потоком газа, Изв. АН СССР, Отдел. техн. н., Механика и машиностр., № 4 (1961); Об устойчивости нелинейно-упругих трехслойных пластинок, обтекаемых сверхзвуковым потоком газа, Изв. АН СССР, Отдел. техн. н., Механика и машиностр., № 5 (1961).
- 5.1а. Багдасарян Ж. Е., Об устойчивости трехслойной ортотропной пластины в сверхзвуковом потоке газа, Изв. АН Арм. ССР, серия физ.-матем. н., 14, № 5 (1961).
- 5.2. Балабух Л. И., Взаимодействие оболочек с жидкостью и газом, Труды VI Всесоюзной конф. по теории оболочек и пластинок (Баку, 1966), «Наука», Москва, 935—943.

- 5.3. Болотин В. В., Колебания и устойчивость упругой цилиндрической оболочки в потоке сжимаемой жидкости, Изв. сб. 21 (1956), 3-16; К вопросу об устойчивости пластинок и панелей сжимаемого газа, «Вопросы прочности материалов и конструкций», Изд-во АН СССР (1959), 194-201; Некоторые новые задачи теории оболочек, Расчеты на прочность 4 (1959), 331-365; О применении метода Галеркина к задачам флаттера упругих панелей, Изв. вестн. уч. зав., Машиностроение, № 12 (1959), 25-32; Нелинейный флаттер пластин и оболочек, Изв. сб. 28 (1960), 55-75; О применении «закона плоских сечений» для определения аэродинамического давления на колеблющиеся оболочки, Изв. АН СССР, Отдел. техн. н., Механ. и машиностр., № 1 (1961), 159-162; Нестационарный флаттер пластин и пологих оболочек в потоке газа, Изв. АН СССР, Отдел. техн. н., Механ. и машиностр., № 3 (1962), 106-113; О поведении нагретых пластин и пологих оболочек в потоке газа, Изв. журн. 2, № 3 (1962), 119-125.
- 5.4. Болотин В. В., Гарялов Ю. В., Макаров Б. П., Швейко Ю. Ю., Нелинейные задачи устойчивости плоских панелей при больших сверхзвуковых скоростях, Изв. АН СССР, Отдел. техн. н., Механ. и машиностр., № 3 (1959), 59-64.
- 5.5. Болотин В. В., Макаров Б. П., Мишенков Г. В., Нагорнов Л. Н., Помацкис Л., Некоторые задачи динамической устойчивости упругих колец при интенсивном нагружении, Изв. вестн. уч. зав., Машиностроение, № 6 (1965), 76-82.
- 5.6. Болотин В. В., Попович Ю. Н., Вынуждение и установившийся флаттер термически сжатых панелей, находящихся в сверхзвуковом потоке, Изв. журн. 1, № 2 (1961), 82-96.
- 5.7. Болотин В. В., Попович Ю. Н., Швейко Ю. Ю., Теория аэрогидроупругости, в книге «Прочность, устойчивость, колебания» 3, «Машиностроение», Москва, 1968, 468-512.
- 5.8. Брусиловский А. Д., Мельникова Л. М., Швейко Ю. Ю., Колебания и устойчивость цилиндрической оболочки в потоке газа, Изв. журн. 6, № 1 (1966), 67-73.
- 5.8а. Вольмир А. С., Селезова Л. В., Поведение упругой цилиндрической панели в потоке производящего газа при действии магнитного поля, Прикл. мех., 7, № 5 (1971), 3-8.
- 5.9. Григорьев Э. И., Горшков А. Г., Взаимодействие слабых ударных волн с упругими конструкциями, Научные труды Ин-та механики Моск. гос. ун-та, № 2, 1970.
- 5.10. Григорьев Э. И., Лампер Р. Е., Шандаров Л. Г., Некоторые теоретические и экспериментальные исследования автоколебаний криволинейных панелей в потоке газа, Теория оболочек и пластин, Изд-во АН Арм. ССР, Ереван, 1961, 401-411; Флаттер панелей и оболочек, «Итоги науки», Механика, 1969, 31-90.
- 5.11. Григорьев Э. И., Михайлов А. П., Флаттер трехслойных цилиндрических оболочек, Изв. журн. 5, № 6 (1965), 1087-1091.
- 5.11а. Кильчевский И. А. (ред.), Механика систем оболочка — жидкость — нагретый газ, «Наукова думка», Киев, 1970.
- 5.12. Макаров Б. Н., О нелинейном флаттере закрепленных пластин, Теория пластин и оболочек, Изд-во Казанского гос. ун-та, Казань, 1960; Амплитуда установившегося флаттера защемленных панелей, Изв. вестн. уч. зав., Машиностроение, № 5 (1961).
- 5.13. Микишев Г. Н., Экспериментальное исследование автоколебаний квадратной пластины в сверхзвуковом потоке, Изв. АН СССР, Отдел. техн. н., Механ. и машиностр., № 1 (1959), 154-157.
- 5.14. Миси Е. Н., Перцев А. К., Гидроупругость оболочек, «Судостроение», Ленинград, 1970.

- 5.15. Новичков Ю. И., О решении уравнений установившегося флаттера цилиндрических панелей, Изв. журн. 2, № 4 (1962); Об устойчивости решений в задаче о флаттере панелей, Изв. АН СССР, Механика и машиностроение, № 4 (1962), 352—358; Устойчивость и автоколебания плоских и криволинейных панелей в потоке газа Труды III Всесоюзной конф. по теории пластин и оболочек, Кисловодск, 1962; О применении трехмерной аэродинамической теории к задачам вынуждения и флаттера панелей, Изв. АН СССР, Отдел. техн. и. Механика и машиностроение, № 3 (1963), 138—141; Неstationарный флаттер цилиндрических панелей, Труды IV Всесоюзной конф. по теории оболочек и пластин, Изд-во АН Арм. ССР, Ереван, 1964.
- 5.16. Скуратов Э. Д., Об устойчивости круговой цилиндрической оболочки в сверхзвуковом потоке газа, Сб. «Прочность и устойчивость элементов тонкостенных конструкций», 2, «Машиностроение», Москва (1967), 201—209; Понедение цилиндрических оболочек в сверхзвуковом потоке газа, Расчеты на прочность 15, «Машиностроение», Москва (1971), 356—365; Некоторые вопросы устойчивости цилиндрических оболочек в сверхзвуковом потоке, Переходные процессы деформации оболочек и пластин, Таллин, 1967, 173.
- 5.17. Смирнов А. Н., Сверхзвуковой флаттер трехслойных пластин, ДАН СССР 183, № 3 (1969), 540—543.
- 5.18. Швецко Ю. Ю., О влиянии сверхзвукового потока газа на нижнее критическое усилие для цилиндрических панелей, Изв. АН СССР, Студия техн. и. Механика и машиностроение, № 4 (1961), 14—19.
- 5.19. Anderson W. L., Experiments of the flutter of flat and slightly curved panels at Mach number 2, Rept. Calif. Inst. Tech. (1962); Oscillatory pressures in an idealized boundary layer with application to cylinder flutter, AIAA Journ. 4, № 5 (1966), 865—872.
- 5.20. Collahan J. A., Structural dynamics aspects of the Gemini program, J. Spacecraft and Rockets 4, № 1 (1967), 58—64.
- 5.21. Dzygadlo Z., Local analysis of nonlinear forced vibration of a plate of finite length in plane supersonic flow, Proc. vibr. Problems 4, № 11 (1970), 353—368.
- 5.22. Evensen D. A., Nonlinear flexural vibrations of thin circular rings, Calif. Inst. of Techn., 1964.
- 5.23. Faure G., Flottements de panneaux en tissussoalque, Rech. aeronaut., № 88 (1962).
- 5.24. Fung Y. C., Flutter of curved plates with edge compression in a supersonic flow, Proc. 3d Midwest. Conf. Solid Mech.; Ann. Arbor, 1957, 221—245; On two-dimensional panel flutter, J. Aeronaut. Sci. 26, № 3 (1958), 145—160; Some recent contributions to panel flutter research, AIAA Journ. 1, № 4 (1963), 898—909.
- 5.25. Garrick E. E., A survey of aerothermoelasticity, Aerospace Eng. 22, № 1 (1963), 110—147.
- 5.26. Hargrave N. F., Structural development of the Concorde, Aircraft Engineering 40, № 3 (1968), 21—25.
- 5.27. Harris G. Z., The problem of panel flutter with reference to the Blue Streak and Black Knight vehicles, ARC Current Papers, № 848, London (1966).
- 5.28. Iribesecu L., Statica si dinamica structurilor elastice anizotrope si heterogene, Bucuresti, 1969.
- 5.29. Iribesecu L., Malaiu E., Supersonic flutter of circular cylindrical heterogeneous orthotropic thin panels of finite length, J. Sound Vib. 8, № 3 (1968), 494—512.
- 5.30. Lock M. H., Fung Y. C., Comparative experimental and theoretical studies of the flutter of flat panels in a low supersonic flow, Calif. Inst. Tech. № 670 (1961).

- 5.31. Menkes E. G., Houboit J. C., Evaluation of aerothermoelasticity problems for unmanned Mars-entry vehicles, AIAA paper, № 68-283 (1968).
- 5.32. Olson M. D., Fung Y. C., Supersonic flutter of circular cylindrical shells subjected to internal pressure and compression, AIAA Journ. 4, № 5 (1966), 858-864; Comparing theory and experiment for the supersonic flutter of circular cylindrical shells, AIAA Journ. 6, № 10 (1967), 1849-1856.
- 5.33. Rayburn L. C., Shrouds for space payloads, Space Aeronaut. 47, № 2 (1967), 66-73.
- 5.34. Runyon H. L., Some research related to the structural dynamics of launch vehicles, Proc. of the 6th Intern. Symposium on Space Technology and Science, 1966, 421-430.
- 5.35. Sylvester M. A., Baker J. E., Some experimental studies of panel flutter at Mach number 1.3, NASA TN, № 3914 (1957).
- 5.36. Walker R. W., Rosecrans R., Deveikis W. D., Flutter investigation of strainwise oriented arrays of curved panels under compressive loading and aerodynamic heating, NASA TN-2910 (1965).
- 5.37. Young G., Shirokai T., Buffeting data obtained on Mercury-Atlas, NASA Rep. TDR 594 (1961).

К главе VI

- 6.1. Агакирин В. Я., Обзор исследований по устойчивости конструкций при импульсном нагружении. Рассчет пространственных конструкций 12, Стройиздат, Москва (1969), 186-200.
- 6.2. Алумиэ Н. А., Переходные процессы деформации упругих оболочек, Труды VI Всесоюзной конференции по теории оболочек и пластинок (Баку, 1966), «Наука», Москва, 1966, 883-889.
- 6.3. Болотин В. В., О понятии устойчивости в строительной механике. Проблемы устойчивости в строительной механике, Труды Всесоюзной конференции по проблемам устойчивости в строительной механике (Москва, 1963), Стройиздат, Москва, 1965, 6-27.
- 6.4. Вольмир А. С., Stability and post-buckling behavior of shells under dynamic loads, «Applied mechanics», Proc. Xth Intern. Congr. Appl. Mech., Amsterdam, 1962, 276-277.
- 6.5. Царевский В. М., Устойчивость оболочки при динамической нагрузке, Труды VII Всесоюзной конференции по теории оболочек и пластинок, «Наука», Москва, 1970, 224-229; еб. «Проблемы механики твердого деформированного тела», «Судостроение», Ленинград, 1970, 149-160.
- 6.6. Джайлз Г. Ю., Устойчивость упругих систем при динамических нагрузках, Проблемы устойчивости в строительной механике, Труды Всесоюзной конференции по проблемам устойчивости и строительной механике (Москва, 1963), «Наука», Москва, 1965, 68-81.
- 6.7. Лапрентьев М. А., Наганеский А. Ю., Динамические формы потери устойчивости упругих систем, ДАН СССР 64, № 6 (1949), 779-782.
- 6.8. Budiansky B., Dynamic buckling of elastic structures: criteria and estimates, в книге [0.24], 83-106; Notes on nonlinear shell theory, J. Appl. Mech. 35 (1968), 393-401.
- 6.9. Budiansky B., Hutchinson J. W., Dynamic buckling of imperfection-sensitive structures, Proc. XI Intern. Congr. Appl. Mech., Berlin, 1964, 636-651; A survey of some buckling problems, AIAA Journ. 4, (1966), 1505-1510.
- 6.10. Hoff N. J., Dynamic stability of structures, в книге [0.24], 7-41.

- 6.11. Hutchinson J. W., Initial post-buckling behavior of toroidal shell segments, *Intern. Journ. Sol. Struct.* 3 (1967), 97–115; Imperfection-sensitivity of externally pressurized spherical shells, *J. Appl. Mech.* 34 (1967), 49–56; Buckling and initial post-buckling behavior of oval cylindrical shells under axial compression, *J. Appl. Mech.* 35 (1968), 66–72.
- 6.12. Hutchinson J. W., Budiansky B., Dynamic buckling estimates, *AIAA Journ.* 4 (1966), 525–530.
- 6.13. Hutchinson J. W., Koiter W. T., Postbuckling theory, *Applied Mechanics Reviews* 23, № 12 (1970), 1353–1366 (имеется русский перевод: Хатчинсон Дж., Коитер В. Т., Теория послекритического поведения конструкций, сб. «Механика», № 4 (1971), Изд-во иностр. лит-ры, Москва, 129–149).
- 6.14. Stein M., Some recent advances in the investigation of shell buckling, *AIAA Journ.* 6, № 12 (1968).

К главе VII

- 7.1. Агамиров В. Л., Вольмир А. С., Поведение цилиндрических оболочек при динамическом приложении всестороннего давления и осевого сжатия, Изв. АН СССР, Отдел. техн. н., Механ. и машиностр., № 3 (1959), 78–83.
- 7.2. Биркгейс А. Ю., Вольмир А. С., Исследование динамической устойчивости пластинок с помощью электронных цифровых машин, ДАН СССР 135, № 5 (1960), 1083–1086.
- 7.3. Блажина А. Н., Динамическая устойчивость цилиндрической оболочки с начальным изгибом при заданной скорости сближения торцов, Инж. сб. 31 (1961), 196–201.
- 7.4. Болотин В. В., Бойченко Г. А., Макаров Б. П., Судакова Н. И., Швецко Ю. Ю., О потере устойчивости тонких упругих оболочек под действием импульсивной нагрузки, Стройт. мех. и расчет сооружений, № 2 (1959), 9–16.
- 7.5. Болотин В. В., Бойченко Г. А., Исследование процецирования тонких упругих оболочек под действием динамических нагрузок, Расчеты на прочность 5, Машига, Москва (1960), 259–272.
- 7.6. Вольмир А. С., Об устойчивости цилиндрических оболочек при динамическом нагружении, ДАН СССР, 123, № 5 (1958), 806–808.
- 7.6а. Вольмир А. С., Киладзе Б. А., Поведение цилиндрических оболочек при действии осевой динамической нагрузки и внутреннего давления, Сообщ. АН Груз. ССР 82, № 2 (1971), 373–376.
- 7.7. Вольмир А. С., Минеев В. Е., Экспериментальное исследование процесса выпучивания оболочки при динамическом нагружении, ДАН СССР 125, № 5 (1959), 1002–1003.
- 7.8. Вольмир А. С., Сметаппа Л. Н., Исследование динамической устойчивости стеклоизвестковых оболочек, Механика полимеров, № 1 (1968), 109–115; Об устойчивости цилиндрической ортотропной оболочки при продольном ударе, ДАН СССР 193, № 2 (1970), 306–308; Поведение оболочек из композиционных материалов при динамическом приложении осевого сжатия, Стройт. механ. и расчет соор., № 4 (1970), 34–37.
- 7.8а. Вольмир Е. А., Поведение упругой панели под действием ударной волны в жидкости, Изв. АН СССР, Механик тв. тела, № 1 (1969), 180–184; Поведение круговой цилиндрической панели, подвергающейся действию осевого динамического сжатия, ДАН СССР 201, № 6 (1971), 46–48; Выпучивание пластинок и цилиндрических панелей под действием осевого динамического сжатия, Изв. АН Арм. ССР 14, № 4 (1971), 48–50.

- 7.9. Ворович И. И., Зинялова В. Ф., Минакова Н. Н., Сребренник Л. И., Шенелева В. Г., О результатах математического исследования и численного анализа устойчивости некоторых типов изолотых и неподвижных оболочек, Третий Всесоюзный съезд по теоретической и прикладной механике, аннот. докл., «Наука», Москва, 1968.
- 7.9а. Герштейн М. С., К расчету на устойчивость пластин судового палуба, Изв. высш. уч. зав., Машиностроение, № 6 (1966), 10–15; Вынуждение прямоугольной пластины при динамическом сдвиге, Труды VII Всесоюзной конференции по теории оболочек и пластинок, «Наука», Москва, 1970, 177–180.
- 7.10. Григорьев Э. И., Сребренский А. Н., Тонкие круговые цилиндрические оболочки под действием импульса внешнего давления, Механ. тв. тела, № 3 (1968), 110–118.
- 7.11. Кадашевич Ю. И., Нерцек А. К., О потере устойчивости цилиндрической оболочки при динамическом нагружении, Изв. АН СССР, Отдел. техн. кн., Механик и машиностр., № 3 (1960), 30–33.
- 7.12. Карапишвили А. В., К устойчивости арок на упругом основании, Изв. журн. 1, № 2 (1961), 168–174.
- 7.12а. Кольман Э. Р., Устойчивость конической оболочки при динамическом нагружении равномерным давлением, Изв. высш. уч. зав., Машиностроение, № 4 (1968), 60–65.
- 7.13. Костылев В. В., Устойчивость круговых конических оболочек под действием динамического внешнего давления, сб. «Исследования по теории пластин и оболочек» 5, Казань (1967), 480–493.
- 7.14. Миллэля Г. З., Динамическая устойчивость многослойной ортотропной круговой цилиндрической оболочки, Изв. АН Арм. ССР 21, № 2 (1968), 42–52.
- 7.15. Панумоп К. А., Шапкин А. С., Динамическая устойчивость ортотропной конической оболочки, Труды Моск. ин-та радиотехники, электрон. и автоматики 38 (1969), 256–259.
- 7.16. Платонов Э. Г., Сленов Б. Н., Воздействие динамической нагрузки на полымкнутые сферические оболочки, сб. «Исследования по теории пластин и оболочек» 6, Казань (1967), 414–453.
- 7.16а. Риккарда Р. Б., Тетерс Г. А., Формы вынуждения оболочек из композитного материала при длительном нагружении, Механика полимеров, № 4 (1971), 697–703.
- 7.17. Салимков Г. М., К задачам динамической устойчивости тонкой конической оболочки, сб. «Исследования по теории пластин и оболочек» 3, Казань (1965); Устойчивость и колебания конической оболочки при комбинированных нагрузках, Изв. высш. уч. зав., Авиац. техн., № 4 (1966), 57–62; Динамическая устойчивость цилиндрических и конических оболочек кругового и некругового сечения при различных граничных условиях, сб. «Исследования по теории пластин и оболочек» 5, Казань (1967), 469–479.
- 7.18. Сметанина Л. Н., Нелинейная задача динамической устойчивости ортотропных оболочек при внешнем поперечном давлении, сб. лекции работ Веронежского лесотехн. ин-та 2 (1964).
- 7.19. Старцева Л. Н., Поведение трехслойной цилиндрической стеклоизолистиковой оболочки при действии осесимметричной динамической нагрузки, Труды Всесоюзного зооп. политехн. ин-та 52 (1969), 68–72; Оссесимметричная деформация трехслойных стеклоизолистиковых оболочек при динамическом нагружении, там же, 62–67.
- 7.20. Суркин Р. Г., Влияние симметричной начальной неправильности на значение критического внешнего давления равномерно нагруженной сферической оболочки, сб. «Исследования по теории пластин и оболочек» 3, Казань (1965), 18–23.

- 7.21. Суркин Р. Г., Зуев Б. М., Степанов С. Г., К вопросу об экспериментальном исследовании устойчивости металлических сферических сегментов при динамическом нагружении равномерным внешним давлением жидкости, Тезисы докт. юбилейной научн. конф., посв. двадцати летию Калужского физ.-техн. ин-та АН СССР, секц. мех.-матем. п., Калуга, 1966; Экспериментальное исследование динамической устойчивости сферических сегментов, Прикладная механика 3, № 8 (1967), 124—132; Об устойчивости сферических сегментов при ударном нагружении всесторонним внешним давлением жидкости, сб. «Исследования по теории пластин и оболочек» 5, Калуга (1967), 454—468.
- 7.22. Теребушко О. И., Устойчивость цилиндрической оболочки при быстрым нагружении осевой силой, Стройт. механ. и расчет соор., № 1 (1960), 10—12.
- 7.23. Федосеев В. И., Особенности эластичности сферической оболочки, Прикл. матем. и мех. 33, № 2 (1969), 280—286.
- 7.24. Шкутил Л. И., О критерии динамической устойчивости пологих оболочек вращения, Теория оболочек и пластин, Труды IV Всесоюзной конференции по теории оболочек и пластин (Ереван, 1962), изд-во АН Арм. ССР, Ереван, 1964, 1008—1013; Устойчивость упругих оболочек вращения при внесении приложенного давления, Проблемы устойчивости в строительной механике, Труды Всесоюзной конференции по проблемам устойчивости в строительной механике (Москва, 1963), Стройиздат, Москва, 1965, 347—354.
- 7.25. Шумик М. А., Устойчивость цилиндрических оболочек под действием динамического радиального давления, Труды VII Всесоюзной конференции по теории оболочек и пластин, «Наука», Москва, 1969, 625—628.
- 7.26. Abrahamson G. R., Goodier J. N., Dynamic plastic flow buckling of a cylindrical shell from uniform radial impulse, Proc. 4th U. S. National Congr. Appl. Mech., 1962, 939—950.
- 7.27. Archer R. R., Lang C. G., Nonlinear dynamic behavior of shallow spherical shells, AIAA Journ. 3, № 12 (1965), 2313—2317.
- 7.28. Baker W. E., Hu W. C., Jackson T. R., Elastic response of thin spherical shells to axisymmetric blast loading, J. Appl. Mech. 33, № 4 (1966), 809—806.
- 7.29. Blenck M. P., Fan T. C., Lackmann L. M., Dynamic stability of cylindrical shells, AIAA Journ. 4, № 3 (1966), 495—500.
- 7.30. Cheung M. C., Babcock C. D., Stability of a clamped shallow arch subjected to impulsive loading, AIAA Journ. 8, № 8 (1970), 1434—1439.
- 7.31. Budiansky B., Roth R. S., Axisymmetrical dynamic buckling of clamped shallow spherical shells, Collected papers on instability of shell structures, NASA TN D-1510 (1962), 597—606.
- 7.32. Coltris M. G., On the dynamic response of an orthotropic finite cylindrical shell to an arbitrary pressure field, Journ. of sound and vibration 7, № 1 (1968), 31—38.
- 7.33. Corra A. P., On the mechanism of buckling of a circular cylindrical shell under longitudinal impact Space sciences Laboratory, General Electric (1960).
- 7.34. Evensen H. A., Evans-Lwanowski R. M., Dynamic response and stability of shallow spherical shells subject to time-dependent loading, AIAA Journ. 6, № 5 (1967), 969—976.
- 7.35. Florence A. L., Buckling of viscoplastic cylindrical shells due to impulsive loading, AIAA Journ. 6, № 3 (1968), 532—537.
- 7.36. Fulton R. E., Dynamic axisymmetric buckling of shallow conical shells subjected to impulsive loads, J. Appl. Mech. 32, № 1 (1965), 129—134.
- 7.37. Goodier J. N., McIvor J. K., The elastic cylindrical shell under nearly uniform radial impulse, J. Appl. Mech. 31, № 2 (1964).

- 7.38. Humphreys J. S., On dynamic snap buckling of shallow arches, AIAA Journ. 4, № 5 (1966), 878-886.
- 7.39. Humphreys J. S., Bodner S. R., Dynamic buckling of shallow shells under impulsive loading, Journ. Engin. Mechanics, Division Proc. American Soc. Civil Engrs. 88, № 1 (1962), 17-36.
- 7.40. Humphreys J. S., Roth R. S., Zalters J., Experiments on dynamic buckling of shallow spherical shell under shock loading, AIAA Journ. 3, № 1 (1965), 33-39.
- 7.41. Humphreys J. S., Sve C., Dynamic buckling of cylinders under axial shock-tube loading, AIAA Journ. 4, № 8 (1966), 1177-1180.
- 7.42. Kapp W. A., Lemke D. G., Electromagnetic generation of high dynamic buckling pressures, AIAA Journ. 3, № 9 (1965), 1777-1779.
- 7.43. Koiter W. L., Over de stabiliteit van het elastisch evenwicht, Amsterdam, 1945; A consistent first approximation in the general theory of thin elastic shells, The theory of thin elastic shells, Proc. of the IUTAM Symposium (Delft, 1959), Amsterdam, 1960; Foundations and basic equations of shell theory, A survey of recent progress, The 2nd IUTAM Symposium, Copenhagen, 1967.
- 7.44. Konrad D. W., On the dynamic stability of eccentrically reinforced circular cylindrical shells, Syracuse Univ., 1967, Dissert. abstr. 28, № 4 (1967), 1556.
- 7.45. Kotnecki A., Dynamic stability of truncated conical shells under pulsating pressure, Journ. of Technology 4, № 1 (1966), 110-120.
- 7.46. Lindberg H. E., Buckling of a very thin cylindrical shell due to an impulsive pressure, J. Appl. Mech. 31, № 2 (1964), 267-272.
- 7.47. Lindberg H. E., Dynamic plastic buckling of a thin cylindrical shell containing an elastic core, J. Appl. Mech. 32, № 4 (1965), 803-812.
- 7.48. Lock M. H., The snapping of a shallow sinusoidal arch under a step pressure load, AIAA Journ. 4, № 7 (1966), 1249-1256.
- 7.49. Lock M. H., Snapping and buckling under dynamic pulse load, AIAA paper, № 69-22 (1969).
- 7.50. Love E. G., McEvor L. K., Effect of pressurization on the cylindrical shell under nearly uniform radial impulse, J. Appl. Mech. 33, № 2 (1966), 451-455.
- 7.51. Lyons W. G., Elastic and plastic buckling of cylindrical shells subjected to impulsive loads, Arch. Mech. Stosowanej 1, № 22 (1970), 111-121.
- 7.52. McEvor L. K., The elastic cylindrical shell under radial impulse, J. Appl. Mech. 33, № 4 (1966), 831-837.
- 7.53. O'Neill J. P., Dynamic loading of structural models by electrostatic forces, AIAA Journ. 3, № 3 (1965), 518-520.
- 7.53a. Ramsey H., Vaughan H., Dynamic elastic-plastic buckling of rectangular plates in sustained flow, Quart. Appl. Math. 28, № 4 (1971), 473-487.
- 7.54. Stephens W., Fulton R. E., Axisymmetric static and dynamic buckling of spherical caps due to centrally distributed pressures, AIAA Paper, № 68-69 (1969).
- 7.55. Strutler W., On the buckling of rings subjected to impulsive pressures, J. Appl. Mech. 32, № 3 (1965), 511-518.
- 7.56. Thurston G. A., A numerical solution of the nonlinear equations for axisymmetric bending of shallow spherical shells, J. Appl. Mech. 28, № 4 (1961), 557-562.
- 7.57. Vaughan H., Lindberg H. E., Dynamic plastic buckling of sandwich shells, J. Appl. Mech. 35, № 3 (1968), 539-546.
- 7.58. Wilkinson J. P., Kalinin A., On nonsymmetric dynamic problems of elastic spherical shells, J. Appl. Mech. 32, № 3 (1965), 525-532.

- 7.59. Witmer E. A., Pian T. H., Balmer H. A., Dynamic deformation and buckling of spherical shells under blast and impact loading, Collected Papers on Instability of shell structures, NASA TN D-1510, 1962.
- 7.60. Witmer E. A., Balmer H. A., Leech J. W., Pian T. H., Large dynamic deformations of beams, rings, plates and shells, AIAA Journ. 1, № 8 (1963), 1848–1857.
- 7.61. Wood L. D., Koval I. R., On the buckling of cylindrical shells under dynamic loads, AIAA Journ. 1, № 1 (1963), 2576–2582.

К главе VIII

- 8.1. Агамиров В. Л., Вольмир А. С., Об устойчивости цилиндрической оболочки при продольном ударе, ДАН СССР 157, № 2 (1964), 307–308; Поведение цилиндрических оболочек при продольном ударе, Проблемы устойчивости в строительной механике, Труды Всесоюзной конференции по проблемам устойчивости в строительной механике (Москва, 1963), Стройиздат, Москва, 1965, 143–152.
- 8.2. Амбариумян С. А., Некоторые вопросы развития теории анизотропных слоистых оболочек, Изв. АН Арм. ССР, серия физ.-матем. и. 17, № 3 (1964), 29–48; Специфические особенности теории оболочек из современных материалов, Изв. АН Арм. ССР, серия «Механика» 21, № 4 (1968), 3–19.
- 8.3. Багдоев А. Г., Мовсисян Л. А., К вопросу определения ударной волны в нелинейных задачах теории упругости, Изв. АН Арм. ССР, серия «Механика» 21, № 3 (1968).
- 8.3а. Божинский А. Н., Вольмир А. С., Попомарев А. Т., Устойчивость упругих стержней при тепловом ударе, Изв. высш. уч. зав., Машиностроение, № 4 (1966), 34–38.
- 8.4. Борисенко В. И., Клакова А. Н., Закритическая деформация цилиндрической оболочки при ударе, Прикл. механ. 2, № 10 (1966), 29–35.
- 8.5. Вольмир А. С., Кильдибеков И. Г., К исследованию поведения оболочек и пластинок при ударе, Изв. высш. уч. зав., Машиностроение, № 7 (1964), 26–30; Исследование процесса выпучивания стержней при ударе, ДАН СССР 167, № 4 (1966), 775–787.
- 8.6. Вольмир А. С., Попомарев А. Т., Динамическая устойчивость упругих систем при тепловом ударе, Доклад на Всесоюзной конф. по проблемам устойчивости в строит. мех. (Каунас, 1967); Устойчивость цилиндрических оболочек при тепловом ударе, ДАН СССР 192, № 4 (1970), 757–759; Поведение цилиндрических оболочек из композиционных материалов при израцином перегреве, Механика полимеров, № 2 (1971), 1289–1292; Поведение стержней и цилиндрических оболочек при распространении термоупругих волн, Доклад на V Всесоюзном симпозиуме по распространению упругих и упруго-пластических волн, Алма-Ата, 1971; Динамическая устойчивость оболочек при израцином нагреве, Проблемы механики, № 1 (1972), 3–9.
- 8.6а. Гордиенко Б. А., Экспериментальное исследование поведения стержней и цилиндрических оболочек при ударе, Труды VII Всесоюзной конф. по теории оболочек и пластин, «Наука», Москва, 1970, 190–193; Поведение стержней и цилиндрических оболочек при осевом ударе, канд. дисс., Москва, 1969; Выпучивание стержней при ударном нагреве, Изв. АН СССР, Механ. тв. тела, № 1 (1969).
- 8.7. Григорьев Э. И., Уравнения трехслойных оболочек с легким заполнителем, Изв. АН СССР, Отдел. техн. и., № 1, 1957, 77–84.
- 8.7а. Даревский В. М., Устойчивость цилиндрической оболочки при осевой динамической нагрузке, VIII Всесоюзная конференция по теории оболочек и пластин, Ростов н/Д, 1971.
- 8.8. Ильюшин А. А., Пластичность, Изд-во АН СССР, 1963.

- 8.9. Каптадзе О. И., Теоретическое и экспериментальное исследование ударного продольного изгиба, Труды Кутаинского с.-х. ин-та 1 (1957), 151—168; О продольном изгибе стержней при продольном ударе, Труды Грузинского ин-та субтроп. хоз-ва 5—6 (1961), 281—286; Влияние эксцентрикитета и предварительного прогиба на устойчивость стержней при продольном ударе, Труды Грузинского ин-та субтроп. хоз-ва 9—10 (1965), 417—423 (совместно с В. Д. Гогоберидзе); Об устойчивости стержней большой гибкости при продольном ударе, Стройл. механ. и расчет сооруж., № 4 (1969), 54—55; Об устойчивости стержней при динамическом нагружении продольной следящей силой, Стройл. механ. и расчет сооруж., № 2 (1970), 76—77.
- 8.9a. Кийко И. А., Гидравлическая оболочка, заполненная жидкостью, под действием осевой ударной нагрузки, Научные труды ин-та механики МГУ, № 8 (1971), 86—92.
- 8.9b. Корнеев В. М., О формах потери устойчивости упругого стержня при ударе, Журн. прикл. матем. и техн. физики, № 3 (1968).
- 8.10. Лурье А. И., Операционное исчисление и его применение к задачам механики, Гостехиздат, Москва, 1951.
- 8.11. Размадзе Г. И., Инженерные вопросы теории удара, Тбилиси, 1959; Устойчивость простой балки при синусоидальном распределении изгибающего момента, Труды Грузинского ин-та субтропич. хоз-ва 5—6 (1961), 225—230.
- 8.12. Размадзе Г. И., Каптадзе О. И., О проблеме ударной продольной устойчивости, Труды Кутаинского с.-х. ин-та 2 (1958), 381—386.
- 8.13. Рахматулин Х. А., Демьянов Ю. А., Прочность при интенсивных кратковременных нагрузках, Физматгиз, Москва, 1961.
- 8.14. Фельдштейн В. А., Упруго-пластические деформации цилиндрической оболочки при продольном ударе, Волны в неупругих средах, Кипинев, 1970, 199—204; Поведение упруго-пластической конической оболочки при продольном ударе, Труды VII Всесоюзной конф. по теории оболочек и пластинок, «Наука», Москва, 1970, 588—591.
- 8.15. Gerard G., Becker H., Column behavior under conditions of impact, J. Aeron. Sci. 19, № 1 (1952), 58—60.
- 8.16. Goldsmith W., Impact, London, 1960 (имеется русский перевод: Гольдшмит В., Удар, Стройиздат, Москва, 1965).
- 8.17. Jones I. P., Whitter J. S., Axially symmetric motions of a two-layered Timoshenko-type cylindrical shell, J. Appl. Mech. 33, № 4 (1966), 838—844.
- 8.18. Lindberg H. E., Impact buckling of a thin bar, J. Appl. Mech. 32, № 2 (1965), 315—322.

К главе IX

- 9.1. Бивин Ю. К., Исследование поведения цилиндрических и сферических оболочек при кратковременных нагрузках, Переходные процессы деформации оболочек и пластики, Татлити, 1967, 33—39.
- 9.2. Вольмир А. С., Нелинейные задачи теории переходных процессов деформации оболочек и проблема устойчивости, Переходные процессы деформации оболочек и пластики, Татлити, 1967, 51—66.
- 9.3. Вольмир А. С., Долгих Л. И., Скурлатов Э. Д., Соловьев В. Р., Поведение цилиндрических оболочек при действии по движущих нагрузок, Труды VII Всесоюзной конференции по теории оболочек и пластинок, «Наука», Москва, 1970, 153—155.
- 9.4. Вольмир А. С., Скурлатов Э. Д., Флаттер оболочек в кратковременном потоке газа, Теория пластики и оболочек, «Наука», Москва, 1971.

- 9.5. Григорюк Э. И., Горшков А. Г., Шкллярчук Ф. Н., Пронесение цилиндрической панели под действием ударной акустической волны давления, Иж. журн. Механ. тв. тела, 1967, № 5, 50–55; О воздействии ударной акустической волны на упругую цилиндрическую оболочку, Иж. журн. Мех. тв. тела, № 3 (1967), 60–65.
- 9.6. Замышляев Б. В., Яковлев Ю. С., Динамические нагрузки при подводном взрыве, «Судостроение», Ленинград, 1967.
- 9.7. Мисев Е. И., Перецов А. К., Динамическая реакция окруженной жидкостью цилиндрической оболочки при воздействии осесимметричных движущихся нагрузок, IV Всесоюзная конференция по прочности и пластичности, тезисы докл., Изд-во АН СССР, Москва, 1967.
- 9.8. Мисев Е. И., Реакция погруженной оболочки на волну давления, распространяющуюся со сверхзвуковой скоростью в направлении образующей, Иж. журн. Механ. тв. тела, № 3 (1968), 119–125.
- 9.9. Моргаевский А. Б., О критических скоростях и устойчивости сооружений, загруженных нагрузками, движущимися с большой скоростью, Проблемы устойчивости в строительной механике, Госстройиздат, Москва, 1965.
- 9.10. Моргаевский А. Б., О колебаниях пластины, несущей подвижную нагрузку, Прикладная механика 2, № 8 (1966), 64–70.
- 9.11. Перецов А. К., Кидашвили Ю. Н., Устойчивость погруженных в жидкость цилиндрических оболочек при кратковременных нагрузках, Труды конференции по теории пластики и оболочек, Казань, 1961, 271–277.
- 9.12. Розмадзе Г. Н., О флаттере панели в кратковременном потоке газа, Труды Груз. ин-та субтроп. хоз. 2 (1967), 413–419.
- 9.13. Скурлатов Э. Д., О воздействии цилиндрических панелей и оболочек, находящихся под действием набегающей волны давления, Теория пластики и оболочек, «Наука», Москва, 1971, 256–261.
- 9.14. Скурлатов Э. Д., Экспериментальное исследование устойчивости цилиндрических оболочек при действии подвижных нагрузок, VIII Всесоюзная конференция по теории оболочек и пластики, Ростов н/Д, 1971.
- 9.15. Слепян Л. И., Резонансные явления в пластинах и оболочках при бегущей нагрузке, Труды VI Всес. конференции по теории оболочек и пластиночек, «Наука», Москва, 1966, 690–696.
- 9.16. Старцева Л. Н., Расчет трехслойных стеклонапластиковых цилиндрических оболочек при действии движущихся нагрузок, Сб. трудов Всесоюзного звончного конгр., ин-та 62 (1969), 73–78.
- 9.17. Anderson D. L., Lindberg H. E., Dynamic pulse buckling of cylindrical shells under transient lateral pressure, AIAA Journ. 6, № 4 (1968).
- 9.18. Bhuta P. G., Transient response of thin elastic cylindrical shell to a moving shock wave, J. Acoustical Soc. Amer. 35, № 1 (1963), 25–30.
- 9.19. Burns J. L., Popelar C. L., Foral F. R., Experimental buckling of thin shells under transient pressure pulse loadings, Launch vehicles struc. and mater. conf., Arizona, 1962.
- 9.20. Chandramani K. L., Widnall S. E., Lyon R. H., Franken P. A., Structural response to inflight acoustic and aerodynamic environments, NASA CR (1966).
- 9.21. Condor E. M., Titan aerodynamic vibration analysis, The shock and vibration bull., № 35 1–7, Washington (1966).
- 9.22. Crocker M. I., Response of aerospace vehicle skin panels to oscillating shock waves, AIAA Paper, № 68–287 (1968).
- 9.23. Hedgepeth J., Widnall E., Dynamic and aeroelastic problems of lifting re-entry bodies, Aerospace Eng. 22, № 1 (1963), 148–153.
- 9.24. Henshall B. D., On some aspects of the use of shock tubes in aerodynamic research, ARS Rep. and Monogr., № 3044, London (1957).

- 9.25. Herrmann G., Baker E. H., Response of cylindrical sandwich shells to moving loads, *J. Appl. Mech.* **34**, № 1 (1967), 81–86.
- 9.26. Rayburn L., Shrouds for space payloads, *Space Aeronautics* **47**, № 2, 66–73.
- 9.27. Williams L., Terenak W., Noise level measurements for improved Delta Atlas, *The shock and vibration bulletin* **38** (1967).

К главе X

- 10.1. Айдропов А. А., Понtryagin Л. С., Витт А. А., О статистическом рассмотрении динамических систем, *Журн. эксперим. и теорет. физики* **3**, № 3 (1933), 165–180.
- 10.2. Болотин В. В., Статистические методы в строительной механике, изд. 2-е, Стройиздат, Москва, 1965.
- 10.3. Болотин В. В., Применение методов теории вероятностей к теории надежности в расчетах сооружений, Стройиздат, Москва, 1971.
- 10.4. Болотин В. В., Статистические методы в полнечастной теории упругих оболочек, Изв. АН СССР, Отдел. техн. н., № 3 (1958), 33–41; Некоторые обобщения теории суммирования усталостных повреждений и их применение к анализу долговечности при действии случайных сил, Изв. вестн. ун-та, Машиностроение, № 8 (1959), 27–40; Об оценке долговечности при стационарных случайных нагрузках, Изв. вестн. уч. зав., Машиностроение, № 9 (1959), 129–131; Долговечность конструкций при квазистационарных режимах напряжений, Изв. сб. **29** (1960), 30–36; «Прочность и накопление повреждений при случайных нагрузках, Расчеты на прочность» **7**, Машино, Москва (1961), 23–49; Об упругих колебаниях, подбужаемых случайными силами с широким спектром, Изв. вестн. уч. зав., Машиностроение, № 4 (1963), 14–31; Об оценке ресурса конструкций при действиях случайных нагрузок, Расчеты на прочность **9**, Машино, Москва (1963), 302–326.
- 10.5. Болотин В. В., О стационарных распределениях вероятностей в статистической динамике упругих систем, сб. «Вопросы динамики и динамической прочности» **10**, Изд-во АН Латв. ССР, Рига (1963), 57–67; Акустическая усталость и родственные вопросы, сб. «Вопросы механической усталости», «Машиностроение», Москва, 1961, 167–177; Применение методов теории вероятностей в теории пластин и оболочек, Теория оболочек и пластин, Труды IV Всесоюзной конференции по теории оболочек и пластин (Ереван, 1962), Изд-во АН Арм. ССР, Ереван, 1961, 15–63; Обзор исследований по статистической динамике упругих систем, Расчеты на прочность **10**, «Машиностроение», Москва (1964), 211–260.
- 10.6. Болотин В. В., Механика твердого тела и теория надежности, Механика твердого тела, Труды II Всесоюзного съезда по теоретической и прикладной механике (Москва, 1961) 3, «Наука», Москва (1966), 68–82; Стохастические краевые задачи в теории пластин и оболочек, Труды VI Всесоюзной конференции по теории оболочек и пластинок (Баку, 1966), «Наука», Москва, 996–1007; Statistical aspects in the theory of structural stability, в книге [0.24], 67–81; Статистическая динамика и теория надежности конструкций, Третий Всесоюзный съезд по теоретической и прикладной механике, анонс. докл., «Наука», Москва, 1968; Случайные колебания в упруго-акустических системах, Расчеты на прочность **13**, «Машиностроение», Москва (1968), 213–230; Планирование вибропримерений на конструкциях, испытывающих случайные колебания, Изв. АН СССР, Механика тв. тела, № 1 (1970), 19–27; Стохастические краевые эффекты при докритических деформациях упругих оболочек, Изв. АН СССР, Механика тв. тела, № 2 (1970), 94–99.

- 10.7. Болотин В. В., Диментберг М. Ф., Статистические задачи колебаний и устойчивости упругих систем, в книге «Прочность, устойчивость, колебания» З, «Машгизстроение», Москва, 1968, 513—546.
- 10.7а. Болотин В. В., Елишаков И. Б., Ефимцов Б. М., Москаленко В. Н., Шарый И. В., Методика расчета случайных акустических полей внутри подкрепленных оболочек, Сб. докл. науч.-техн. конф. Моск. энерг. ин-та, секция энергомашинстр., подсекция динамики и прочности машин, 1969.
- 10.8. Болотин В. В., Макаров Б. П., О приближенном решении некоторых задач статистической динамики, Изд. АН СССР, серия «Механика», № 3 (1965), 77—83; О корреляции перемещений в тонких упругих оболочках со случайными начальными неправильностями, Проблемы надежности в строительной механике, Материалы ко II Всесоюзной конференции по проблемам надежности в строительной механике, Вильнюс, 1968, 163—168; Корреляционная теория докритических деформаций тонких упругих оболочек, Прикл. матем. и механ. 32, № 3 (1968), 428—434.
- 10.8а. Болотин В. В., Москаленко В. Н., Случайные термоупругие напряжения в оболочках, Труды VI Всесоюзной конференции по теории оболочек, «Наука», Москва, 1966, 168—176.
- 10.9. Вольмир А. С., Кильдубеков И. Г., Вероятностные характеристики поведения цилиндрической оболочки при действии акустической нагрузки, Прикладная механика 1, № 3 (1965), 1—9; Нелинейные колебания и устойчивость пологой оболочки в акустическом поле, Проблемы надежности в строительной механике, Материалы ко II Всесоюзной конференции по проблемам надежности в строительной механике, Вильнюс, 1968, 169—174.
- 10.9а. Вольмир А. С., Даниленко А. Ф., Поведение цилиндрических панелей под влиянием порывов ветра, Стройт. механ. и расчет сооруж., № 4 (1971), 66—68; Нелинейные колебания цилиндрических панелей под действием атмосферной турбулентности, Стройт. механ. и расчет сооруж., № 2 (1972).
- 10.10. Борович И. Н., Статистический метод в теории устойчивости оболочек, Прикл. матем. и мех. 23, № 5 (1959), 885—892; Некоторые вопросы использования статистических методов в теории устойчивости пластин и оболочек, Теория оболочек и пластин, Труды IV Всесоюзной конференции по теории оболочек и пластин (Ереван, 1962), Изд-во АН Арм. ССР, Ереван, 1964, 64—94.
- 10.11. Гончаренко В. М., Об одном аспекте статистического метода в теории устойчивости оболочек, Теория пластин и оболочек, Труды II Всеобщей конференции по теории пластин и оболочек (Львов, 1961), Изд-во АН УССР, Киев, 1962, 368—371; Применение марковских процессов в статистической теории устойчивости оболочек, Укр. матем. журн. 14, № 2 (1962), 198—202; Исследование вероятности хлопка удлиненной цилиндрической панели под действием случайного давления, Прикл. матем. и мех. 26, № 4 (1962), 740—744; Пронескливание изнайд при наличии случайных силовых воздействий, Теория оболочек и пластин, Труды IV Всесоюзной конференции по теории оболочек и пластин (Ереван, 1962), Изд-во АН Арм. ССР, Ереван, 1964, 383—390; О динамических задачах статистической теории устойчивости упругих систем, Проблемы устойчивости в строительной механике, Труды Всеобщей конференции по проблемам устойчивости в строительной механике (Москва, 1963), Стройиздат, 1965, 210—216; О влиянии рассеяния энергии в материале на колебания упругого элемента при случайном возбуждении, Прикладная механика 2, № 11 (1968), 90—96; Колебания пластин из нелинейного упругого материала в однородном поле случайных давлений, Проблемы надежности в строительной механике, Ма-

- териалах к II Всесоюзной конференции по проблемам надежности в строительной механике, Вильнюс, № 8, 229—231.
- 10.11а. Гончаренко В. М., Егунова С. Н., Некоторые задачи о нелинейных колебаниях пластины при одновременном действии гармонической и случайной нагрузки, Труды VI Всесоюзной конференции по теории оболочек и пластинок (Баку, 1966), «Наука», Москва, 1966, 277—283.
- 10.12. Диментберг М. Ф., Вынужденные колебания пластины при нагрузке, представляющей собой пространственно-временной случайный процесс, Изв. журн. 1, № 2 (1961), 97—105; О низкой опенке долговечности при стационарных случайных напряжениях, Изв. АН СССР, Отдел. техн. и. Механ. и машиностр., № 5 (1962), 167—170; Вынужденные колебания панелей при случайных нагрузках. Теория пластины и оболочек, Труды II Всесоюзной конференции по теории пластины и оболочек (Львов, 1962), Изд-во АН УССР, К-ев, 1962, 270—273; Нелинейные колебания упругих панелей при случайных воздействиях, Изв. АН СССР, Отдел. техн. и. Механ. и машиностр., № 5 (1962); О нелинейных колебаниях упругих оболочек при случайных нагрузках. Теория оболочек и пластины, Труды IV Всесоюзной конференции по теории оболочек и пластины (Ереван, 1962), изд-во АН Арм. ССР, Ереван, 1964, 437—441; Некоторые задачи устойчивости оболочек, находящихся под действием случайных возмущений. Проблемы устойчивости в строительной механике, Труды Всесоюзной конференции по проблемам устойчивости в строительной механике (Москва, 1963), Стройиздат, Москва, 1965, 217—222; Колебания нелинейной системы с одной степенью свободы при действии периодической силы и изменении собственной частоты по периодическому закону, Изв. журн. Механ. тв. тела, № 4 (1965), 173—178; Исследование нелинейной стохастической системы методом регулируемых автоколебаний, Изв. журн. Механ. тв. тела, № 5 (1968).
- 10.13. Елишаков И. Б., О вычислении спектральных плотностей внешних сил для пластины и оболочек, Проблемы надежности в строительной механике, Материалы к III Всесоюзной конференции по проблемам надежности в строительной механике, Вильнюс, 1971, 37—44; Случайные колебания круговых цилиндрических оболочек, содержащих акустическую среду, VIII Всесоюзная конференция по теории оболочек и пластины, Ростов-на-Дону, 1971.
- 10.14. Елишаков И. Б., Хроматов В. Е., О колебаниях панелей в сверхзвуковом потоке при случайных воздействиях, Изв. АН СССР, Механ. тв. тела, № 1 (1971), 54—58; Влияние скорости набегающего сверхзвукового потока на поведение панелей, находящихся в поле случайных сил, Динамика и прочность машин, Труды Моск. ин-та 74, 1970.
- 10.15. Кильдибеков И. Г., Устойчивость и нелинейные колебания цилиндрической оболочки, находящейся под действием акустического давления, Всесоюзная конференция по проблемам устойчивости в строительной механике (Каунас, 1967), Тезисы докл., Вильнюс, 1967; Нелинейные колебания круговой цилиндрической оболочки при действии осевого сжатия и акустического давления, Проблемы надежности в строительной механике, Материалы к III Всесоюзной конференции по проблемам надежности в строительной механике, Вильнюс, 1971, 58—63.
- 10.16. Колмогоров А. Н., Об аналитических методах в теории вероятностей, Успехи матем. и. 5 (1938), 5—41.
- 10.16а. Левин Б. Р., Теоретические основы статистической радиотехники, 1, 2-е изд. (1969); 2 (1968), изд-во «Советское радио», Москва.
- 10.17. Ломакин В. А., Статистические задачи механики твердых деформируемых тел, «Наука», Москва, 1970.

- 10.18. Макаров Б. П., Применение статистического метода для анализа нелинейных задач устойчивости оболочек, Теория пластин и оболочек, Труды II Всесоюзной конференции по теории пластин и оболочек (Львов, 1961), Изд-во АН УССР, Киев, 1962, 363—367; Случайные несовершенства в тонких оболочках и их влияние на прочность и устойчивость, Третий Всесоюзный съезд по теоретической и прикладной механике, аннот. докл., «Наука», Москва, 1968; Статистический анализ устойчивости несовершенных цилиндрических оболочек, Труды VII Всесоюзной конференции по теории оболочек и пластинок (Днепропетровск, 1969), «Наука», Москва, 1970, 387—391; Последствия деформации неидеальных сферических оболочек, Проблемы надежности в строительной механике, Материалы к III Всесоюзной конференции по проблемам надежности в строительной механике, Вильнюс, 1971, 90—93.
- 10.18а. Макаров Б. П., Чеченев Н. А., О процессы в тонких упругих панелях при случайных импульсных нагрузках, Расчеты на прочность II, «Машгостроение», Москва (1965), 378—384.
- 10.19. Николаенко Н. А., Вероятностные методы динамического расчета машиностроительных конструкций, «Машгостроение», Москва, 1967.
- 10.20. Пугачев В. С., Теория случайных функций и ее применение к задачам автоматического управления, Физматгиз, Москва, 1960.
- 10.20а. Пугачев В. С., Статистические методы в технической кибернетике, изд-во «Советское радио», Москва, 1971.
- 10.21. Ржаницын А. Р., Статистический метод определения допускаемых напряжений при продольном изгибе, Госстройиздат, Москва, 1951; Определение коэффициента безопасности при изменяющихся во времени случайных нагрузках и прочности, Проблемы надежности в строительной механике, Материалы к III Всесоюзной конференции по проблемам надежности в строительной механике, Вильнюс, 1971, 143—150.
- 10.22. Федоров Ю. А., Колебания замкнутой цилиндрической оболочки в поле случайных акустических давлений, Изд. АН СССР, Отдел. техн. и. Механ. и машиностр., № 1 (1963); О нелинейных колебаниях прямоугольной пластины под воздействием случайных сил. Пиж. журн. 4, № 3 (1964), 523—532.
- 10.23. Arilaratnam S. T., Random vibrations of nonlinear suspensions, J. Mech. Eng. Sci. 2, № 3 (1960).
- 10.24. Ballantine J. R., Sonic proof testing B-58 weapons system, SAE preprint, № 355A, 1961.
- 10.25. Belcher P. M., Use of a high-intensity siren in fatigue testing of structures subjected to acoustic forcing, J. Acoust. Soc. Amer. 29, № 1 (1957), 176.
- 10.25а. Belcher P. M., Van Dyke J. D., Eshleman A. L., Development structure to withstand acoustic loads, Aero-Space engineering 18, № 6 (1969).
- 10.26. Bingman R. N., Resonant fatigue failures associated with noise, SAE preprint, № 164 B (1960).
- 10.27. Callaghan E. E., Howes W. I., Colls W. D., Near noise field of a jet engine exhaust I—Cross correlation of sound pressures, NASA TN 3764 (1956), Appl. Mech. Rev. 10 (1957), 919.
- 10.28. Caughey T. K., Derivation and application of the Focker-Planck equation to discrete nonlinear dynamic systems, subjected to white random excitation, J. Acoust. Soc. Amer. 35, № 11 (1963).
- 10.29. Clarkson B. L., Stresses produced in aircraft structures by jet engine, Journ. Roy. Aeronaut. Soc. 61, № 554 (1957); The effect of jet noise on aircraft structures, Aeronaut. Quart. 10, p. 2 (1959); Effects of noise on structures and human beings, Techn. aspects of sounds 3, Amsterdam, 1962; The design of structures to resist jet noise fatigue, J. Roy. Aeronaut. Soc. 66, № 622 (1962), 603—616 (имеется русский перевод).

- Кларксон В. Л. Проектирование конструкций, свободных от хорошо согласованных узкочастотных шумов ракетных двигателей, сб. «Механика», № 5 (1963), Изд-во инстр. лит., Москва, 25—61).
- 10.30. Clarkson B. L., Ford R. D., Random excitation of a tailplane section by jet noise, J. Roy. Aeronaut. Soc. 65, № 608 (1961); The response of a typical aircraft structure to jet noise, J. Roy. Aeronaut. Soc. 66, № 613 (1962).
- 10.31. Crandall S. H., Random vibration I (1958); 2 (1963); Massachusetts Institute of Technology, Cambridge, Случайные колебания систем с нелинейными восстанавливающими силами, Системы по нелинейным колебаниям, Ит-т матем. АН УССР, Киев, 1961; Random vibration of a nonlinear system with a set-up spring, Journ. Appl. Mech. 29, № 3 (1962), 477—482.
- 10.32. Dyer L., Estimation of sound-induced missile vibration, в книге [10.31], 9.1—9.50
- 10.33. Dyer L., Franken P. A., Ungar E. E., Noise environments of flight vehicles, Noise Control 6, № 1 (1960).
- 10.34. Franklin R. E., Space-correlations in the fluctuating pressure field near a jet engine, J. Roy. Aeron. Soc. 65, № 610 (1961).
- 10.35. Goodman L. E., Rattayya J. V., Review of panel flutter and effects of aerodynamic noise, p. II, Structural effects of aerodynamic noise, Appl. Mech. Rev. 13, № 2 (1960), 81—87 (имеется русский перевод: Гудман Л., Раттайя Дж., Обзор литературы по флаттеру панелей и влиянию аэродинамического шума, ч. II, Влияние аэродинамического шума на конструкцию, сб. «Механика», № 5 (1960), Изд-во инстр. лит., Москва, 135—152).
- 10.36. Hogan A. W., Acoustical fatigue facility, Missile design and development 6, № 10 (1959).
- 10.37. Hubbard H. H., Hess R. W., Some comparisons of the response of simple panels to random and discrete noise, J. Acoust. Soc. Amer. 29, № 1 (1957), 176.
- 10.38. Hubbard H. H., Maglieri D. J., Noise considerations in the design and operation of the supersonic transport, Noise Control 7, № 4 (1961).
- 10.39. Keast D. N., Measurement of rocket engine noise, Noise Control 7, № 2 (1961).
- 10.40. Kennard D. C., Sonic vibration as exemplified by the RB-66B airplane, J. Acoust. Soc. Amer., № 5 (1958).
- 10.41. Kowalewski J., On the relation between fatigue lives under random loading and under corresponding program loading, Full-scale fatigue testing of aircraft structures, Oxford, 1961.
- 10.42. Lassiter L. W., Hess R. W., Hubbard H. H., An experimental study of the response of simple panels to intense acoustic loading, J. Aeronaut. Sci. 24, № 1 (1957).
- 10.43. Lighthill M. J., On sound generated aerodynamically, Proc. Roy. Soc. A211, 1952; A222, 1954; Jet noise, АИАА Journ. 1, № 7 (1963), 1507—1517; Распространение теории шума струй на струи, в том числе ракетные, при больших сверхзвуковых скоростях, Второй Всесоюзный слезд по теоретической и прикладной механике, зинот. докл., «Наука», Москва, 1964.
- 10.44. Lin Y. K., Response of a nonlinear flat panel to periodic and randomly-varying loadings, Journ. Aerospace Sci. 29, № 9 (1962), 1029—1033; Probability distributions of stress peaks in linear and nonlinear structures, АИАА Journ. 1, № 5 (1963), 1133—1138.
- 10.45. Lin Y. K., Probabilistic theory of structural dynamics, 1967.